Anatomy and evolution of the Galápagos marine iguana, *Amblyrhynchus cristatus* (Squamata, Iguanidae), with a new phylogeny of Iguania and considerations about aquatic adaptations in extant and fossil lizards

by

Ilaria Paparella

A thesis submitted in partial fulfillment of the requirements for the degree of

Doctor of Philosophy

in

Systematics and Evolution

Department of Biological Sciences
University of Alberta

ABSTRACT

*Amblyrhynchus cristatu*s, the marine iguana, is unique amongst the ~7000 species of living limbed lizards as it has successfully evolved adaptations that allow it to live in both terrestrial and marine environments. This species is endemic to the Galápagos Archipelago and has evolved a specialized feeding behaviour, consuming primarily the algae that grow on the rocky seafloor. The intriguing questions arising around the evolution of the marine iguana concerns the use of exaptations of terrestrial features for aquatic and specifically marine adaptations. However, the lack of fundamental information about its anatomy currently prevents us from understanding how it became adapted to such a peculiar lifestyle in comparison to all other iguanids. Here I present a comprehensive anatomical description and review of the skeletal anatomy of *Amblyrhynchus* in order to perform a revision of the morphological characters used to assess phylogenetic relationships across iguanians and to investigate its origins in the larger context of iguanian evolution.

Iguanian lizards are a highly diverse clade of squamates that, in addition to the common iguanas, include also anoles, dragon lizards, and chamaeleons. They are roughly divided into two main lineages, the Acrodonta and Pleurodonta, and represented by over 2000 living species and a fairly extensive fossil record, with the earliest undisputed iguanians known from the early Late Cretaceous of Gondwana. In this study, I perform a new phylogenetic analysis of Iguania based on a combined dataset of morphological and molecular data. I include representatives from all modern clades as well as the largest sampling of fossil iguanians ever tested in a phylogeny before. I analysed the data primarily using Bayesian inference methods and performing both calibrated and uncalibrated analyses of the combined and separate data matrices.

With the new phylogenetic hypothesis presented here, I was able to revise long-standing issues in the classification of Iguania, to propose a new taxonomic scheme that better encompasses the diversity of the iguanian fossil record, and to address questions about the evolutionary and biogeographic history of both crown and fossil lineages. For example, I suggest limiting the use of the

high-level taxa Acrodonta and Pleurodonta to crown lineages, and to account for the sister-group relationship between Pleurodonta and its fossil relatives, I established the new clade Iguaniformes, in parallel to the existing Chamaeleontiformes that includes Acrodonta and the fossil clade Priscagamidae. Acrodonta and Pleurodonta were defined based on the macroscopic differences in tooth-jaw geometries found between most of the members of the two groups. Acrodont implantation, used to indicate that the teeth are positioned apically along the jaw bone, appears in most crown chamaeleontiforms; pleurodont implantation, which refers to the teeth being located on the lingual side of the jaw, characterises all iguaniforms and some chamaeleontiforms. However, recent studies on amniote dental anatomy show how superficial this dualistic interpretation can be. With my revised morphological characters, I shift the attention to the single features that contribute to determine an overall acrodont or pleurodont appearance, and provide a re-interpretation of these conditions in living and fossil iguanians based on the new knowledge.

Finally, I discuss the origins and radiation of the Galápagos iguanas and other similar cases of disjointed distribution within Iguania. I argue that iguanids may have colonized ancient Galápagos Islands as long as 20-25 Ma via a dispersal event from the Caribbean plate. The initial dispersal was followed by constant short-range hopping from older to newer islands that continued to emerge during the activity of the Galápagos Hotspot, until the archipelago reached its current position. This scenario is consistent with both the sister-relationships of the Galápagos iguanids and the unusually old divergence time estimates that are persistently inferred in phylogenetic studies. Persistence of long-lasting lineages rather than more recent dispersal events is presented as the most plausible explanation also for the presence of iguaniform oplurids in Madagascar and the iguanid *Brachylophus* in the Fiji and Tonga Archipelagos.

PREFACE

The content of this thesis contains my original work as well as results of collaborative research that was led by myself with contributions from my supervisor, Dr. Michael W. Caldwell, and other collaborators.

A version of Chapter 2 is currently under review as Paparella I. and Caldwell M.W., Cranial anatomy of the Galápagos marine iguana *Amblyrhynchus cristatus* (Squamata: Iguanidae). *The Anatomical Record*: submitted on July 20th, 2021. I was responsible for the study design, data collection, analysis, and description, analytical work, and manuscript composition. M.W. Caldwell was the supervisory author and contributed toward manuscript editing.

A version of Chapter 3 has been published as Paparella I., Palci A., Nicosia U., and Caldwell M.W. (2018). A new fossil marine lizard with soft tissues from the Late Cretaceous of southern Italy. *Royal Society Open Science*, 5(6):172411. https://doi.org/10.1098/rsos.172411. I was responsible for the study design, analysis and description of the study material, performed the analytical work, and drafted the manuscript. M.W. Caldwell was the supervisory author, was involved with the study design, and contributed to manuscript edits. A. Palci assisted with the data collection and contributed toward manuscript editing. U. Nicosia contributed to the study design and part of the analytical work.

A version of Chapter 4 has been published as Paparella I., LeBlanc A.R.H., Doschak M.R., and Caldwell M.W. (2020). The iliosacral joint in lizards: an osteological and histological analysis. *Journal of Anatomy*, 236(4): 668-687. https://doi.org/10.1111/joa.13132. I was responsible for the project design, data collection and interpretation, analytical work, and manuscript composition. A.R.H. LeBlanc help designing the study, contributed to the data collection and interpretation, and contributed to manuscript edits. M.W. Caldwell was the supervisory author and contributed toward manuscript editing. M.R. Doschak provided access to laboratory equipment, contributed to data collection, and provided edits to the final manuscript.

ACKNOWLEDGEMENTS

Firstly, I'd like to express my thanks to my supervisor, Michael Caldwell, who has supported me throughout this research project and beyond. I am extremely grateful for our friendship, time spent talking, discussions on research, adventures around the world, and for the endless encouragement and inspiration.

A very special thanks to the members of my supervisory committee, Alison Murray and Randall Nydam, for their mentorship and guidance during these years. Both you helped me to stay focus on my goals and I am grateful for all your feedback and advise on my research and academic career.

Thank you to my examining committee members, John Acorn and Chris Bell, for being part of this final sprint of my journey as a PhD. I am very grateful for your feedback and the time you dedicated to help improve my work.

I would like to say a special thank you to the following people, not just for sharing with me their time and passion as fellow researchers and brilliant minds, but for their friendship above all: Katherine Bramble, Meghan Dueck, Aaron LeBlanc, Audrey Reid, Oksana Vernygora, Paulina Jiménez-Huidobro, Tiago Simões, Fernanda Campello, Javier Luque, Kecia Kerr, Al Lindoe.

Many thanks to my lab mates, other fellow paleo-grads, and fellow researcher that I had the pleasure to share time with during the course of my PhD: Hallie Street, Michelle Campbell Mekarski, Sydney Mohr, Mark Powers, Catie Strong, Yan-yin Wong, Matthew Rhodes, Angelica Torices, Victoria Arbour, Stephanie Blais, Gavin Bradley, Sinjini Sinha, Rebekah Vice, Michael Hudgins, Aaron Dyer, Greg Funston, Sam Hamilton, Annie McIntosh, Michael Burns.

My sincere gratitude also to the following people for the helpful discussions, intellectual inputs, and general interactions that have influenced my development as a scientist in the last few years: Takuya Konishi, Alessandro Palci, Vladimir Alifanov, Dmitry Grigoriev, Joshua Lively, Erin Maxwell, Hans Larsson, Eva Koppelhus, Philip Currie, Rob Holmes, Corwin Sullivan.

I also owe a special thanks to several people from the UofA-BioSci team for various reasons that ranges from technical support, bureaucratic assistance, all things teaching, etc.: Braden Barr, Christianne Nylund, Shelley Scott, Dean Wilson, Mark Wolansky, Arlene Oatway, Dianne Payeur.

Finally, I am deeply grateful to all the curators and other people that have welcomed and assisted me during my collection visits around the world: Vladimir Alifanov, Andrey Sennikov (PIN); Dmitry Grigoriev, Alexander Averianov, Nikolay Zverkov; Kevin Seymour, David Evans (ROM); Jolanta Kobylinska (ZPAL); Brandon Strilisky (TMP); Emily Lindsey (UCMP); Juan Abella (Universidad Estatal Península de Santa Elena, Ecuador); Lauren Vonnahme, David Kizirian, Carl Mehling, Mark Norell, Emanuel Tschopp (AMNH); Coleman Sheehy, David Blackburn, Ed Stanley, Zackary Randall, Jason Bourque (UF).

INSTITUTIONAL ABBREVIATIONS

AMNH, American Museum of Natural History, New York, New York, USA.

BSPG, Bayerische Staatssammlung für Paläontologie und historische Geologie, Munich, Germany.

CP, CENPALEO, Universidade do Contestado, Mafra, Santa Catarina State, Brazil.

DGM, Museu de Ciencias da Terra, Companhia de Pesquisa de Recursos Minerais, Rio de Janeiro, Rio de Janeiro State, Brazil.

FMNH,Field Museum of Natural History, Chicago, Illinois, USA.

GM, Geiseltalmuseum, Martin-Luther-Universität, Halle-Wittenberg, Germany.

GSI, Geological Survey of India Central Palaeontological Repository Unit, Kolkata, India.

GU/RSR/VAS, Garhwal University, Srinagar, Uttarakhand, India.

HLMD, Hessisches Landesmuseum, Darmstadt, Germany.

IGM, Institute of Geology, Mongolian Academy of Sciences, Ulaanbaatar, Mongolia.

IITR/SB/VLM, Vertebrate Paleontology Laboratory, Department of Earth Sciences, Indian Institute of Technology, Roorkee, India.

IPS, Institut de Paleontologia de Sabadell, Catalonia, Spain.

IVPP, Institute of Vertebrate Paleontology and Paleoanthropology, Beijing, China.

LPM, Liaoning Paleontological Museum, Shenyang Normal University, Shenyang, Liaoning Province, China.

LSUMZ, Louisiana State Museum of Natural History, Baton Rouge, Louisiana, USA.

MCZ, Museum of Comparative Zoology, Harvard University, Cambridge, Massachusetts, USA.

MN, Museu Nacional/UFRJ, Rio de Janeiro, Rio de Janeiro, Brazil.

MNHN, Muséum National d‘Histoire Naturelle, Paris, France.

MNZ, Museum of New Zealand Te Papa Tongarewa, Wellington, New Zealand.

MOR, Museum of the Rockies, Bozeman, Montana, USA.

MPUR, Museo Paleontologico dell‘Universitá di Roma, Rome, Lazio, Italy.

MVZ, Museum of Vertebrate Zoology, University of California, Berkeley, California, USA.

PIN, Paleontological Institute, Russian Academy of Sciences, Moscow, Russia.

PZO, Museo di Scienze Naturali dell'Alto Adige, Sudtirol, Bolzano, Italy.

ROM, Royal Ontario Museum, Toronto, Ontario, Canada.

SMF, Senckenberg Forschungsinstitut und Naturmuseum, Frankfurt, Germany.

TMP, Royal Tyrrell Museum of Palaeontology, Drumheller, Alberta, Canada.

TNHC, Texas Memorial Museum, Austin, Texas, USA.

UALP, University of Arizona Laboratory of Paleontology, Tucson, Arizona, USA.

UALVP, University of Alberta Laboratory for Vertebrate Paleontology, Edmonton, Alberta, Canada.

UAMZ, University of Alberta Museum of Zoology, Edmonton, Alberta, Canada.

UCL, Zoology Department, University College London, London, UK.

UCMP, University of California Museum of Paleontology, Berkeley, California, USA.

UF, Florida Museum of Natural History, Gainesville, Florida, USA.

USNM, National Museum of Natural History, Smithsonian Institution, Washington D.C., USA.

USTL, Université Montpellier 2, Sciences et Techniques du Languedoc, Montpellier, France.

UWBM, Burke Museum of the University of Washington, Seattle, Washington, USA.

VPL,University of Jammu, Geology Department collections, Jammu, India.

YPM, Peabody Museum of Natural History, Yale University, New Haven, Connecticut, USA.

ZFMK, Zoological Research Museum Alexander Koenig, Bonn, Germany.

ZPAL, Institute of Palaeobiology, Polish Academy of Sciences, Warsaw, Poland.

TABLE OF CONTENTS

LIST OF FIGURES

LIST OF TABLES

CHAPTER 1

General Introduction

Iguanian lizards are a highly diverse clade of squamates, including common iguanas, anoles, dragon lizards, and chamaeleons among others. They are represented today by ~2000 living species (Uetz et al. 2020) and characterized by a quite extensive fossil record (Alifanov 1989; Alifanov 1993b; Alifanov 2000; Alifanov 2013; Apesteguía et al. 2005; Apesteguia et al. 2016; Borsuk-Bialynicka 1996; Borsuk-Bialynicka & Alifanov 1991; Borsuk-Bialynicka & Moody 1984; Conrad & Norell 2007; DeMar et al. 2017; Estes & Price 1973; Gao & Norell 2000; Gao & Fox 1996; Gao & Hou 1995; Gilmore 1928; Gilmore 1943; Nava & Martinelli 2011; Simões et al. 2015). Traditionally, iguanians have been interpreted as the most basal squamates based on morphological data (e.g., Conrad 2008; Estes et al. 1988; Gauthier et al. 2012; Lee 2005). However, more recent phylogenetic studies using molecular or combined molecular and morphological evidence recover Iguania as more closely related to anguimorphs and snakes, occupying a more nested position in the squamate tree of life (Burbrink et al. 2020; Pyron 2017; Reeder et al. 2015; Simões et al. 2018; Vidal & Hedges 2009).

The taxonomic history of Iguania is complex and its internal classification still open to debate (e.g., Burbrink et al. 2020; Conrad 2008; Daza et al. 2012; de Queiroz 1987; Estes et al. 1988; Etheridge & de Queiroz 1988; Frost & Etheridge 1989; Frost et al. 2001; Gauthier et al. 2012; Townsend et al. 2011). Historically, the suborder Iguania was divided into the three main families Agamidae, Chamaeleonidae (or Chamaeleontidae), and Iguanidae, each including several subfamilies (e.g., Estes et al. 1988; Etheridge & de Queiroz 1988; Gauthier et al. 1988;

McDowell & Bogert 1954). As our knowledge about the diversity of these lizards grew and cladistic methods were implemented to assess phylogenetic relationships, this long-standing classification was finally challenged by Frost & Etheridge (1989). These authors acknowledged the limitations of the three-family system for Iguania, and focused in particular on reorganizing the status of Iguanidae. Their revised taxonomy of Iguania relied on nomenclature that was already established in the older literature (Camp 1923; Cope 1864; Duméril & Bibron 1837; Gilmore 1928; Gilmore 1943; McDowell & Bogert 1954), and two main lineages of modern iguanians were proposed: the Pleurodonta, with a New World distribution, and the Acrodonta, with an Old World distribution (Evans 2003; Frost & Etheridge 1989; Frost et al. 2001; Myers et al. 2021). Exceptions to this biogeographic separation between Pleurodonta and Acrodonta are represented by the pleurodontan oplurids found in Madagascar, and the pleurodontan iguanids occupying some of the South Pacific islands (i.e., Galápagos, Melanesia, and Polynesia) (e.g., Bell 1825; Cope 1864; Cope 1886; Darwin 1845; Duméril & Bibron 1837; Fitzinger 1843; Gibbons 1981; Pregill & Steadman 2004).

The terms Acrodonta and Pleurodonta were coined by Cope (1864), based on the difference in the geometric relationship between the teeth and jaw bone observed among iguanians: *acrodont*, meaning ‗tooth at the top', and *pleurodont* meaning literally ‗tooth to the side'. What Cope (1864) included in Acrodonta and Pleurodonta was quite different from the current assignments, and the two taxonomic categories were slowly refined to their modern use which essentially follows Frost et al. (2001). Most of these taxonomic revisions were limited to extant iguanians and further complexity was added to the picture when fossil taxa started to be considered.

Phylogenetic studies including fossil iguanians increased substantially in the last two decades and limitations with the unstable definitions of both higher and lower level clades became apparent, especially regarding the formal use of Acrodonta and Pleurodonta (Alifanov 1996; Alifanov 2009; Apesteguia et al. 2016; Borsuk-Bialynicka 1996; Borsuk-Bialynicka & Alifanov 1991; Borsuk-Bialynicka & Moody 1984; Conrad 2008; Conrad & Norell 2007; Daza et al. 2012; Gauthier et al. 2012; Norell & de Queiroz 1991; Simões et al. 2015; Smith 2009). Modern taxonomic definitions are based on cladistic analyses and the traditional Linnaean ranking system has become hardly applicable to the multitude of clade names that have been coined over the last several decades. The lack of inclusivity of fossil taxa in the traditional taxonomic classification was approached slowly and mostly by isolated studies focused on the description of new fossils (Apesteguia et al. 2016; Conrad 2015; Conrad & Norell 2007; Daza et al. 2012; DeMar et al. 2017; Simões et al. 2015). Larger phylogenetic revisions of Iguania, when not based exclusively on molecular data, were typically limited in their fossil taxon sampling (Conrad 2008; Daza et al. 2012). Conrad (2008) recognized at least the sister-group relationship between fossil taxa of the family Priscagamidae and modern Acrodonta, which he formally defined as clade Chamaeleontiformes. Similarly, fossil iguanians of the clade Gobiguania defined by (Conrad & Norell 2007) are usually recovered at the stem of Pleurodonta; however, this sister-group relationship has never been definitively addressed, and the use of Pleurodonta as formalised by Frost et al. (2001) has not been consistently applied in recent phylogenetic studies, especially those based on morphological evidence (Daza et al. 2012; Gauthier et al. 2012).

Earliest iguanians date back at least to the early Late Cretaceous (Cenomanian-Turonian) of Gondwana, with fragmentary but diagnostic remains from Patagonia and Northwest Africa (Apesteguía et al. 2005; Apesteguia et al. 2016). Older fossils have been reported from Jurassic

and Triassic deposits of Gondwana, but either their age or classification were later revised in the literature. For example, *Bharatagama* from the Early-Middle Jurassic of India was originally described as a primitive acrodont iguanian (Evans et al. 2002) but later re-acknowledged as a sphenodontian (Jones et al. 2013). *Tikiguana*, a well-preserved dentary from a Late Triassic outcrop of India (Datta & Ray 2006), is generally recognized as an acrodontan iguanian but its stratigraphic age was shown to be the result of recent sediment infiltration (Hutchinson et al. 2012). A diverse and abundant fossil fauna is better known from the Late Cretaceous of the Gobi Desert, with numerous fossil taxa that show affinities to either acrodontan or pleurodontan iguanians (e.g., Alifanov 1989; Alifanov 1993b; Alifanov 2000; Alifanov 2013; Borsuk-Bialynicka 1996; Borsuk-Bialynicka & Alifanov 1991; Borsuk-Bialynicka & Moody 1984; Conrad & Norell 2007; Gao & Norell 2000; Gao & Hou 1995; Gilmore 1943). Deposits in the Gobi Desert (Mongolia and China) continues upward into the Cenozoic, with more fossil iguanians reported mostly from Paleogene deposits (Alifanov 2012; Alifanov 2009; Dong et al. 2016; Hou 1976); however, the relationships of these taxa have never been assessed in a phylogenetic analysis thus far. Finally, the presence of fossil iguanians, both from the Mesozoic and Cenozoic, has been reported also from several localities across North and South America, Europe, and Africa (as just mentioned above) (Apesteguía et al. 2005; Apesteguia et al. 2016; Bolet & Evans 2013; DeMar et al. 2017; Dollion et al. 2015; Estes & Price 1973; Gao & Fox 1996; Georgalis et al. 2016; Gilmore 1928; Hillenius 1978a; Hillenius 1978b; Nava & Martinelli 2011; Rieppel et al. 1992; Simões et al. 2015). Considering the abundance and quality of the iguanian fossil record, it is rather surprising that a more inclusive phylogenetic and taxonomic revision of extant and fossil iguanians is still not available.

1.1 The marine iguana of the Galápagos: an introduction

Frost & Etheridge (1989) focused in particular on revising the internal classification of former Iguanidae and its subfamilies (cf. Camp 1923; Estes et al. 1988; McDowell & Bogert 1954; Romer 1956). At the end of their study, they elevated all the subfamilies to the family rank, thus causing an overlap between the former subfamily Iguaninae *sensu* Etheridge & de Queiroz (1988), and the new Iguanidae *sensu* Frost & Etheridge (1989). This was solved by Frost et al. (2001) that replaced the old Iguanidae with the use of Pleurodonta. The newly defined Iguanidae *sensu* Frost & Etheridge (1989) includes the genera: *Iguana* Linnaeus, 1758; *Cyclura* Harlan, 1824; *Amblyrhynchus* Bell, 1825; *Ctenosaura* Wiegmann, 1828; *Brachylophus* Cuvier, 1829; *Conolophus* Fitzinger, 1843; *Dipsosaurus* Hallowell, 1854; *Sauromalus* Duméril, 1856.

Iguanids have by far one of the most disjointed biogeographic distribution among iguanians, being found across North and South America, as well as on several South Pacific islands, including the Galápagos, Fiji, and Tonga Archipelagos (Buckley et al. 2016; Etheridge 1982; Frost & Etheridge 1989). However, how modern iguanids were able to colonized the Pacific islands is still highly debated, with most hypotheses calling for multiple long-distance and fairly recent dispersal events from South America to the Pacific (e.g., Bartholomew 1987; Keogh et al. 2008; Macey et al. 1997; Noonan & Sites Jr 2009; Rassmann 1997; Rassmann et al. 1997a; Townsend et al. 2011).

Two genera and four species of iguanids currently inhabit the Galápagos Islands: *Conolophus* (*C. subcristatus*, *C. pallidus*, *C. marthae*) and *Amblyrhynchus* (Myers et al. 2021; Uetz et al. 2020). The two Galápagos iguanas are persistently recovered as sister-taxa in phylogenetic analyses, but there are different hypotheses regarding their divergence from the other iguanids (e.g., Miralles et al. 2017; Rassmann 1997; Rassmann et al. 1997a; Wiens &

Hollingsworth 2000). Phylogenetic reconstructions based on morphology tend to recover either *Sauromalus* (Norell & de Queiroz 1991) or *Iguana* (Etheridge & de Queiroz 1988) as sister-taxon to the Galápagos iguanids, while based on molecular and combined evidence they share a more recent common ancestor with *Ctenosaura* (Wiens & Hollingsworth 2000). The lack of a solid phylogenetic hypothesis for the relationships among iguanids limits our understanding of the evolutionary history of the Galápagos iguanas and prevents a proper reconstruction of how the iguanids were able to colonize these islands. It was even suggested that land and marine iguanas of the Galápagos may have been introduced to the islands by humans quite recently and independently, due to the fact that immunological data indicate a low level of differentiation within the two genera (Wyles & Sarich 1983). However, this seems to be extremely unlikely since the two taxa are reported to still hybridize, as further evidence of their close phylogenetic relationships (Rassmann et al. 1997b). Hypotheses to explain the presence of these two iguanids on the Galápagos remain quite vague. The general view is that at some point their ancestor arrived via dispersal from South America with no clear explanation for the timing and mode of this colonization event (Bartholomew 1987).

*Amblyrhynchus cristatu*s, the marine iguana, is unique amongst the ~7000 species of living limbed lizards adapted to bestride successfully between terrestrial and marine environments. This species is endemic to the Galápagos Archipelago and has evolved a specialized feeding behaviour, consuming primarily the seawater algae that grow on the rocky seafloor of the intertidal and subtidal zones surrounding the islands. The intriguing questions arising around the evolution of the marine iguana concerns the use of exaptations of terrestrial features for aquatic and specifically marine adaptations. However, the lack of fundamental

information about its anatomy currently prevents us from understanding how it became adapted to such a peculiar lifestyle in comparison to all other iguanids.

1.2 Functional adaptations in living and fossil marine lizards: the marine iguana as a model

To understand how the Galápagos marine iguana became adapted to such a unique lifestyle, we certainly need more information about its anatomy. The unique cranial morphologies displayed by the marine iguanas seem to be mostly associated with the modified configuration of the snout and specialized feeding behaviour. Since *Amblyrhynchus* is the only non-ophidian squamate currently adapted to spend part of its life in the ocean, I used comparisons to fossil marine lizards such as mosasauroids and dolichosaurids to properly discuss some of its most distinctive features.

Comparisons between the modern marine iguana and fossil marine lizards are actually beneficial in both directions, because *Amblyrhynchus* represents a unique source of information in the development of aquatic adaptations that can help to better understand the earliest stages of the transition from land to water that characterized some fossil lineages. Despite its fairly conservative body plan, the marine iguana is a capable swimmer, able to dive in the ocean for almost an hour before returning ashore, and to stay submerged for up to 30 minutes before re-emerging for breathing (Bartholomew & Lasiewski 1965; Boersma 1983; Dawson et al. 1977). The adaptation to swimming in *Amblyrhynchus* was clearly driven by the exploitation of a new food source – i.e., marine algae – that is quite uncommon across iguanids and squamates in general. The most evident aquatic adaptations in the marine iguana are represented by the long and laterally compressed tail used as the main propelling organ, and the use of the hindlimbs as paddles (while the forelimbs remain mostly tackled to the body during the swim). However,

marine iguanas overall spend most of their time on land, for basically any other vital function that is not feeding and especially for thermoregulatory reasons (Bartholomew et al. 1976; Bartholomew & Lasiewski 1965; Boersma 1983; Carpenter 1966).

The basics adaptations to a partial (or facultative) life in water displayed by the marine iguana are comparable to those found in some extinct lizards typically interpreted as secondarily aquatic, and more in general in secondarily aquatic marine reptiles (Caldwell 2002; Lee et al. 2016; Motani 2009; Motani & Vermeij 2021). By comparing the skeletal configuration of certain structures between the marine iguana and a new specimen of dolichosaurid from the Late Cretaceous of Southern Italy, I discuss how these fossil lizards were likely adapted to a semi-aquatic lifestyle rather than being fully aquatic like their close relatives and more derived mosasauroids (Paparella et al. 2018; Simões et al. 2017b). *Primitivus manduriensis* Paparella et al., 2018 displays a fairly conservative and more primitive anatomy in comparison to other dolichosaurids in terms of adaptive features to the aquatic environment. While the laterally compressed tail, axial elongation of the neck and tail, and paddle-like limbs clearly suggest that the new dolichosaur was adapted to swim, more terrestrial-like features includes: 1) a limited axial elongation of the trunk that typically characterizes dolichosaurids; 2) a limited reduction of the limb elements that in *Primitivus* retain a configuration that is fairly similar to terrestrial lizards (Caldwell 2000; Caldwell 2003; Caldwell 2006; Caldwell & Palci 2010; Evans et al. 2006; Lee & Scanlon 2002a; Lee & Caldwell 2000; Palci & Caldwell 2007; Paparella et al. 2018; Pierce & Caldwell 2004).

The most important indication of the retention of the ability to move on land in *Primitivus*, and potentially all dolichosaurids, is the persistence of a functional contact between the pelvic girdle and the sacral region of the column (also present in other dolichousaurs but not

in mosasauroids). The coexistence of more terrestrial-like features and aquatic adaptations suggests that in fact *Primitivus* and possibly all dolichosaurs were still able to move on land and may have conducted a semi-aquatic lifestyle, similarly to the modern marine iguana. The contact between the pelvic girdle and the sacral region of the vertebral column is referred to as the iliosacral joint. The development of the iliosacral joint in tetrapods represented a crucial step in the evolution of terrestrial locomotion. This structure is responsible for transferring forces between the vertebral column and appendicular skeleton, thus supporting the bodyweight on land (e.g., Carroll et al. 2005; Wolff 1990). Most research dealing with the water-to-land transition and biomechanical studies in general have focused exclusively on the articulation between the pelvic girdle and femur, and our knowledge about the contact between the pelvic girdle and vertebral column at a tissue level is restricted so far to human anatomy, with little to no information available on other tetrapods (e.g., Arnold et al. 2014; Pierce et al. 2012; Tsai et al. 2018). To compensate for this lack of data, I performed a survey across limbed lizards of the variability of the structures associated with this important articulation, i.e., sacral ribs and ilium, and described this joint both osteologically and histologically. The absence and presence of certain features of the ilium in particular, as well as the geometrical relationships between the ilium and vertebral column show interesting trends in lizards adapted to specific lifestyle. In some of these aspects, the marine iguana is better comparable to fossil marine lizards like dolichosaurids and basal mosasauroids rather than to its closest relatives (Paparella et al. 2020).

1.3 Organization of the dissertation

My dissertation is focused on the study of the Galápagos marine iguana with the goal of providing new information on its unique anatomy and to investigate its origins in the larger

context of iguanian evolution. In Chapter 2 I present a detailed description of the cranial anatomy of *Amblyrhynchus* that is based on the examination of several individuals through a series of growth stages. I include comparisons with all other modern members of the family Iguanidae and discuss some morphologies that seem to be strongly affected by the marine lifestyle of this unique lizard. As there are no other secondarily marine adapted lizards amongst modern squamates, insights on the marine iguana skeletal adaptations can be derived from proxies in the fossil record. Chapter 3 is a description and analysis of the anatomy and aquatic adaptations of a new Late Cretaceous marine dolichosaurid from Southern Italy that served as a proxy for the investigation of some skeletal adaptations in secondarily marine lizards.

An analysis of the articulation between the pelvic girdle and sacral vertebrae across living and fossil lizards is presented In Chapter 4, where I investigate this contact from both an osteological and histological perspectives. In this aspect, the marine iguana shares clear similarities with fossil marine lizards, such as dolichosaurids, and differs instead from its closest iguanids relatives. This and other data and comparisons, strongly suggest that variability for the components of this articulation correlates directly with type of locomotion.

For Chapter 5, I used the analysis of the anatomy of *Amblyrhynchus* to revise the morphological characters typically used to assess phylogenetic relationships for all iguanians. Here I present the results of a new phylogeny of Iguania based on combined morphological and molecular evidence and including both living and fossil iguanian species. The newly formulated phylogenetic hypothesis of iguanian interrelationships has important implications for the origins and radiation of the modern clades, the status of some high-level taxonomic categories, and for reconstructing the evolutionary and biogeographic history of both extant and extinct iguanian lineages.

CHAPTER 2

Cranial anatomy of the Galápagos marine iguana *Amblyrhynchus cristatus* (Squamata: Iguanidae)

A version of Chapter 2 is currently under review as Paparella I. and Caldwell M.W., Cranial anatomy of the Galápagos marine iguana *Amblyrhynchus cristatus* (Squamata: Iguanidae). *The Anatomical Record*: submitted on July 20th, 2021.

2.1 Introduction

Marine iguanas are iconic organisms that inhabit the Galápagos Archipelago and feed primarily in the ocean, consuming algae that are found in the intertidal and subtidal zones (e.g., Boersma 1983; Dawson et al. 1977; Trillmich & Trillmich 1986). Within Squamata, they belong to the highly diverse clade Iguania, which includes over 1900 living species (Uetz et al. 2020). Based on recent phylogenetic analyses, Iguania includes two major lineages, the Acrodonta and Pleurodonta. Both names date back to Cope (1864), though modern use follows Frost et al. (2001). The taxonomic history of Iguania is quite complicated as its internal classification has been revised multiple times, with familial and subfamilial ranks being frequently changed by various authors (e.g., Daza et al. 2012; de Queiroz 1987; Estes et al. 1988; Etheridge & de Queiroz 1988; Frost & Etheridge 1989; Frost et al. 2001; Gauthier et al. 2012).

*Amblyrhynchus cristatu*s Bell, 1825, the marine iguana, is part of the Iguanidae *sensu* Frost & Etheridge (1989) – equivalent to the Iguaninae *sensu* de Queiroz (1987) – together with

the land iguana of the Galápagos *Conolophus* Fitzinger, 1843, and the rest of the iguanine genera: *Ctenosaura* Wiegmann, 1828; *Brachylophus* Cuvier, 1829; *Cyclura* Harlan, 1824; *Dipsosaurus* Hallowell, 1854; *Iguana* Linnaeus, 1758; *Sauromalus* Duméril, 1856. The modern distribution of these taxa includes the south-western United States, eastern Mexico, and south to Southern Brazil and Paraguay, including also the Antilles, Galápagos and the Fiji-Tonga Archipelagos.

When Thomas Bell formally named the marine iguana, he erroneously described *Amblyrhynchus* as coming from Mexico as that is where the first specimens were shipped from (Bell 1825). Bell was a British zoologist that described many of the species that Charles Darwin collected during his expedition with the Beagle. It was not until 1836, when more specimens were brought back by Darwin, that the mistake regarding the provenance of *Amblyrhynchus* was rectified (Darwin 1845). Both Bell and Darwin in their original descriptions of the taxon emphasized the peculiarity of *Amblyrhynchus* with its short, truncated, and broad head, which was in contrast to the long and pointed snout of other large iguanas from Central and South America (i.e., *Iguana* and *Ctenosaura*).

The two Galápagos iguanas, *Amblyrhynchus cristatu*s and *Conolophus* spp., are persistently recovered as sister-taxa in phylogenetic reconstructions, but hypotheses regarding their divergence show substantial differences (e.g., Miralles et al. 2017; Rassmann et al. 1997a; Rassmann et al. 1997b; Wiens & Hollingsworth 2000). Moreover, evidence of hybridization between *A. cristatu*s and *C. subcristatus* has also been reported (Rassmann et al. 1997b). According to Wyles & Sarich (1983), the divergence between the two taxa (based on immunological data) would date back at least to 15-20 Ma. The modern Galápagos Islands are not older than 5 My (Morgan 1971), however, a study by Christie et al. (1992) found out that the

activity of the Galápagos Hotspot may have started as long as 80-90 Ma, and during this time different islands have emerged and sank continuously. Moreover, the possibility of older eastern Pacific connections between the Galápagos and American mainland, as well as the presence of a single large Galápagos Island between the latest Cretaceous and Eocene, have been proposed by several authors and supported by both geological and biological evidence (e.g., Croizat 1952; Croizat 1958; Grehan 2001). Taken together, it is possible to imagine that Galápagos iguanas evolved on older islands and then migrated to younger islands as they emerged, leaving open the possibility of a continental origin for these lizards with subsequent occupation of the modern Galápagos Archipelago (at least by the ancestor of *Amblyrhynchus* and *Conolophus*) due to vicariance rather than dispersal (cf. Cox 1983; Geist et al. 2014; Grehan 2001; MacLeod et al. 2015; Merlen 2014; Peck 1996).

Amblyrhynchus represents a unique example of the acquisition of marine adaptations amongst iguanian lizards, and one of the few amongst living squamates in general. Marine iguanas can dive in the ocean for up to 50 minutes, however, they are bound to land for thermoregulation and most other vital functions, such as reproduction (Bartholomew & Lasiewski 1965; Boersma 1983; Dawson et al. 1977). They spend most of their time on land and they nest in deep burrows on the shores or close to the island volcanoes. They occasionally feed on carcasses and feces of other animals, with a noticeable shift in diet from juveniles to adults, and they tend to supplement their algae diet with beach plants especially during El Niño oscillations (Boersma 1983; Laurie 1989; Nagy & Shoemaker 1984; Wikelski & Trillmich 1994). In response to a drastic food shortage, they are also able to slow their growth and shrink their size in order to increase survivorship (Wikelski & Wrege 2000).

As fascinating as they are with their peculiar lifestyle, marine iguanas are still poorly understood from an osteological point of view. Most of the studies on this species have focused on physiology or molecular biology to assess phylogenetic relationships (e.g., MacLeod et al. 2015; Miralles et al. 2017; Rassmann 1997; Rassmann et al. 1997a; Rassmann et al. 1997b). There are virtually no studies on the cranial anatomy of *Amblyrhynchus*, with the few studies available on skeletal adaptations being limited to the post-cranium (Hugi & Sánchez-Villagra 2012; Paparella et al. 2020). To date, the best source of information on the anatomy of *Amblyrhynchus* is probably that of de Queiroz (1987), which included a thorough description of the morphological characters he used to assess the relationships among iguanids (i.e., iguanines in his work).

Here I provide the first ever detailed osteological description of the skull, mandible, and hyoid of *Amblyrhynchus*, and include comparisons with other iguanids. I identify several potential autapomorphies that distinguish *Amblyrhynchus* from all other iguanids, which should be further assessed in future phylogenetic analyses. Some of these features can certainly be interpreted as adaptations to the marine environment and linked to the peculiar feeding behaviour that make the marine iguana so unique among lizards.

2.2 Material and Methods

As *Amblyrhynchus* is a monotypic genus, I refer to this taxon simply by its generic epithet. All descriptions and comparisons are based on direct analysis of the material and personal observations for all the taxa mentioned in this study. The description of *Amblyrhynchus* is based on several specimens, spanning different ontogenetic stages, both sexes, and various locations across the Galápagos Archipelago. A list of all the specimens analysed and compared

for this study is provided in Appendix 2.1. Part of the material is illustrated in Figures 2.1-2.35 and additional figures are provided in Appendix 2.2.

The anatomical terminology is based on Oelrich (1956) and Evans (2008). In most cases, I also added topological references (e.g., anterior, posteromedial, lateral, ventral, etc.) to the traditional terms, in order to improve clarity with regards to the identification of structures (e.g., angular process of the articular = medial process of the articular). This is helpful especially when there are multiple names for the same structure in the literature.

Several cranial features show late ontogenetic development and to explain their variation during growth, I made reference to the relative size as well as skeletal maturity of the specimens (note: sexual maturity is unknown for all the specimens examined). As lizards are characterized by continuous growth, fusions between skeletal elements have variable timings and as described by Maisano (2002), there is significant inter- and intraspecific variation. I agree with this study based on my observations and in order to better pinpoint variation of certain characteristics during ontogeny, I coupled the relative size of each specimen with indicators of skeletal maturity. Fusion between epiphyses and diaphyses are not reliable indicators in this case, as in iguanian lizards these elements mostly remain unfused throughout ontogeny (e.g., Estes et al. 1988; Gans et al. 2008). Fusion of basicranial elements instead is completed quite early in ontogeny, with the lines of suture visible only in small to medium size individuals. Hence, the braincase represents a better indicator of skeletal maturity, and is in agreement with the data recorded by Maisano (2002).

The illustrations included in this work are mostly based on segmentation of x-ray micro-Computed Tomography (μCT) scans of specimen UF 41558 (Figs. 2.1-2.31, 2.33, 2.35). Raw μCT data were downloaded from the Morphosource database. The scans were generated and

made available by the Florida Museum of Natural History‘s Herpetology collections and they can be found at https://www.morphosource.org/concern/biological_specimens/0000S9994. The same specimen was also photographed to show the external anatomy of *Amblyrhynchus* (Fig. 2.32A, C). Segmentation and imaging were generated by the authors using Dragonfly Version 2.0 and Version 2020.2 for Windows (Object Research Systems Inc, Montreal, Canada, 2016 and 2020); software available at http://www.theobjects.com/dragonfly.

2.3 Results

2.3.1 General remarks

Amblyrhynchus is a fairly large iguanid with a mandible length of up to 10 cm in the largest specimens, while in average size adults it is commonly around 8 cm. The typical blunt profile of its skull – which was the inspiration for its generic name: *ambly*-, „blunt“ and -*rhynchus*, „snout“ (Bell 1825; Darwin 1845) – distinguishes the overall appearance of the marine iguana from all other iguanids. The skull and mandibles of *Amblyrhynchus* are visibly shortened even when compared to its sister taxon the land iguana of the Galápagos, *Conolophus* spp. (de Queiroz 1987; Etheridge & de Queiroz 1988; Frost & Etheridge 1989; MacLeod et al. 2015; Rassmann 1997). This trend affects in particular the snout region, as reflected for instance by the verticalization of the nasal process of the premaxilla and the septomaxillae, the presence of deep concavities along the anteroventral margin of the frontal, and a relatively low dentary-mandible length ratio. In fact, the dentigerous portion of the dentary in *Amblyrhynchus* makes up less than half of the length of the entire mandible, while in other iguanids it usually occupies more than half of the mandible. Moreover, the tooth-bearing portions of both the maxilla and dentary are

deeply scooped and the teeth have unique shaped cusps, which are wide and rounded instead of tapering as in other iguanians (and squamates) with mesio-distal cusps.

Specific observations related to ontogenetic variation are included in the description of each cranial element. It is noteworthy to mention that there is a strong difference in ontogenetic trends observed for *Amblyrhynchus* in contrast to other iguanids. While ontogenetic variation is evident in taxa like *Ctenosaura*, *Iguana*, and *Dipsosaurus*, *Amblyrhynchus* displays its most unique features beginning early in ontogeny. Young *Iguana iguana* and *Ctenosaura pectinata* specimens tend to be more similar to each other than to their adults, and do not display some of the distinguishing features that characterize each species later in ontogeny. Instead, a juvenile marine iguana can be already identified when the frontoparietal fontanelle is still open and the braincase elements are not fully fused. The trend in *Conolophus* appears similar to *Iguana* and *Ctenosaura*, and overall young specimens of *Conolophus* have more similarities with *Ctenosaura* than *Amblyrhynchus*, starting with the shape of the tooth cusps, the lack of verticalization of the premaxilla and septomaxilla, and the earlier appearance of a parietal mid-sagittal crest. A parietal crest is formed only in larger sized specimens of *Amblyrhynchus*, while small and average size individuals lack one. These and other aspects of its osteology are described in greater detail below.

2.3.2 Skull

Premaxilla – The premaxilla is a single element, with a flattened anterior surface and a dorsally oriented nasal process (Fig. 2.2). The nasal (or posterodorsal) process is larger at the base and its lateral margins gently tapers throughout, giving the element a roughly triangular shape. The cross-section of the nasal process is triangular, with tapering lateral surfaces and a

crested posterior surface (Fig. 2.2D). The posterior end of the nasal process angles and inserts in between the two nasals. Hence, this portion of the nasal process is not exposed in articulation as it is covered by the nasals. Two marked facets are present on each side of the posterior nasal process, separated by a sharp dorsal crest (where the nasals make contact) (Fig. 2.2A). The anterior surface of the premaxilla is pierced by at least three foramina: a smaller one along the midline and two on the sides of the nasal process, close to the contact with the maxilla (Figs. 2.2, A2.1F). Based on their position, the two lateral openings represent the foramina for the passage of the ethmoidal nerves. Whether the median foramen is an additional ethmoidal foramen is unclear. Ethmoidal foramina can be present as a single or double pair, but an odd number of foramina for the ethmoidal nerves has never been reported so far, and I could not find a similar number in any other iguanid species analysed for this study. Oelrich (1956) described a double pair of ehthmoidal foramina as occasionally present in *Ctenosaura*. Moreover, in some specimens of *Amblyrhynchus*, one or more additional and smaller foramina can be present below the level of the three main ones just described, without following a consistent pattern of distribution. Some of these openings most likely represent mental/nutritional foramina. The maxillary (or anterolateral) process is weakly developed and is found lateral to the base of the nasal process, extending towards the maxilla (Fig. 2.2A). This process is generally weakly developed in iguanids in comparison to other iguanian lizards, however only in *Amblyrhynchus* it is highly reduced. The ventral surface of the premaxilla bears 7 teeth, with the median teeth being smaller than the lateral ones (Fig. 2.2B). Behind the dentigerous portion, there is a well-developed incisive process, which projects anteriorly and consists usually of a single lobe. In some smaller sized individuals, the incisive process appears bilobed, but this is likely due to their earlier ontogenetic stage and thus ongoing fusion of the premaxillae. Projecting posteriorly

relative to the incisive process, there is another median flange, which is known in the literature as the vomerine process. This flange overlaps the anterior tip of the vomers and is visible only in the largest specimens, suggesting a fairly late ontogenetic development of the flange. A palatal process (or flange) of the premaxilla is absent in *Amblyrhynchus*, while typically found in other iguanids (including *Conolophus*). In *Amblyrhynchus*, the ventral surface of the premaxilla is narrower and its lateral margins taper posteriorly more abruptly than for instance in *Ctenosaura* and *Conolophus*, due to the lack of a palatal flange. There are multiple foramina on the ventral surface of the premaxilla (i.e., premaxillary foramina). Two of these foramina are slightly larger than the others and mirroring on each side of the incisive foramen (Fig. 2.2B). Smaller foramina can be found around the main ones, and show variation in number across the different specimens.

Maxillae – The maxilla is approximately as long as it is tall and possess a well-developed facial process (Figs. 2.3; A2.1F). The premaxillary (or anterior) process is expanded in *Amblyrhynchus* in comparison to *Iguana* and similar to *Conolophus*, and is well-sutured to the anterior portion of the septomaxilla (Fig. A2.1F). The process is bifurcated, with both tips pointing medially, one along the internal (lingual) anterior margin and one more external (or labial) to that (Fig. 2.3B-E). The medial lappet of the two premaxillary processes of the maxillae contact each other between the premaxilla and septomaxillae, though do not form a sutural contact. The facial (or nasal or mid-dorsal) process of the maxilla is vertical for most of its extension, while its dorsal end is medially deflected and well-exposed in dorsal view (Figs. 2.1; 2.3; A2.1). The anterior margin of the facial process, bordering the external narial opening, is deeply concave, with its dorsal tip protruding anteriorly and sutured to the anterolateral margin

of the nasal. The internal surface of the medially deflected portion of the nasal process bear a flat facet for the nasal, while along its posterior margin, there is a large facet for the articulation of the prefrontal. The facet for the lacrimal is set along a gentle notch at the transition between the facial and posterior processes of the maxilla, while a sinusoidal and long facet for the jugal occupies the medial surface of the posterior process (Fig. 2.3B, D). The palatal (or supra-alveolar) shelf of the maxilla bears from 16 to 23 teeth; the most posterior teeth are always the smallest, while all the others are of a similar size (Fig. 2.3F). The lateral surface of the labial wall of the maxilla is quite convex relative to the rest of the bone. On the dorsomedial side of the palatal shelf, the superior alveolar canal opens anteriorly with a small foramen and groove, while posteriorly the canal opens in a large and elongated fossa (Fig. 2.3D). A tongue-shaped facet on the posterior end of the palatal shelf represents the articular facet for the ectopterygoid, right above the two terminal teeth. The number of mental foramina along the lateral surface of the maxilla varies from 6 to 10, depending on the size of the specimens (Figs. 2.3A; A2.1E, F). There are also additional small foramina, irregularly distributed across the same surface, with a higher concentration on the facial process. These smaller openings match a pattern of random foramina found also on the nasals and anterior frontal, and to a minor extent on the prefrontal (see descriptions below).

Nasals – The two nasals are sutured to each other medially for most of their length (Figs. 2.1; 2.4; A2.1). The suture between the two nasals is highly irregular, non-interdigitated, but strongly sinusoidal and consistently asymmetrical across all specimens (Fig. 2.4A). The anterior margins of the nasals contribute to the posterior borders of the external narial openings. The anteromedial processes of the nasals diverge anteriorly to accommodate the nasal process of the

premaxilla, which they overlap dorsally (Fig. 2.4A, B). There is no nasal anterolateral process as in *Iguana*; a blunt and broad mid-lateral process mediates the contact with the anteromedial portion of the prefrontal and the facial process of the maxilla. The anterior margin of the mid-lateral process bears a transversally oriented and concave surface for the articulation of the facial process of the maxilla (Fig. 2.4A, C, E). The contact with the prefrontal extends from the most lateral tip of the mid-lateral process to the posterior end of the lateral margin. An articular facet for the prefrontal is located along the posterior border of the mid-lateral process, while the rest of the contact between nasal and prefrontal is fairly straight. The dorsal surface of the nasals becomes gently rugose in adults, but never heavily sculptured as in *Conolophus* (see description of integumentary ossifications). There are several foramina on each nasal that are randomly distributed and variable in size and number. Some of these foramina fully pierce the bones and are visible both in dorsal and ventral views, while others are incomplete and simply notch the dorsal surface. In ventral view, the contacting surfaces (i.e., median margins) of the two nasals form two median sagittal crests (one on each nasal) (Fig. 2.4B, D, F). Most of the ventral surface is occupied by a double concavity (= orbitonasal concavity of the nasals): the anterior portion of this concavity roofs the anterior nasal capsule, while its posterior portion roofs the orbitonasal membrane (cf. Oelrich 1956). A blunt anteromedial-to-posterolateral ridge marks the separation between the nasal capsule concavity and orbitonasal concavity, located above the level of the septomaxillae (Fig. 2.4B, D). The posterior margin of the orbitonasal concavity is formed by a sharp ridge, known as conchal ridge (e.g., Oelrich 1956), with an anterolateral-to-posteromedial orientation. The posterior margin of the nasals is characterized by an interdigitated suture with the frontal. Similarly to *Conolophus* and *Iguana*, *Amblyrhynchus* lacks the triangular posterior process that is present in *Ctenosaura* and *Cyclura*.

Septomaxillae – In *Amblyrhynchus* the septomaxillae are verticalized, appearing L-shaped in mediolateral view, unlike in any other iguanid (Figs. 2.1E; 2.5; A2.1F). Only the most anterior portion of the septomaxilla is horizontally oriented (parallel to the vomer), while the rest of the bone is dorsally oriented and about parallel to the nasal process of the premaxilla. Each septomaxilla is pierced by several small foramina, randomly distributed across the two bones. These foramina are more numerous in small/young individuals, and decrease in number in more skeletally mature specimens. The anterior margin is triangular, with a notch present at the anteromedial tip of the bone, where it makes contact with the premaxillary process of the maxilla (Fig. 2.5A, E). A prominent dorsolateral process is visible on the anterior portion. This process is notched about midway along its dorsal margin and its lateral surface is slightly concave. The two dorsolateral processes of the septomaxillae accommodates medially the nasal capsule (cf. Oelrich 1956). The horizontal anterior region of the septomaxillae roofs the vomeronasal (or Jacobson‘s) organ, while the verticalized posterior portion separates the nasal capsule from the orbitonasal system. The ventral surfaces of the septomaxillae are fairly flat and bear posteriorly a diagonally oriented nasal septum which divides the paired vomeronasal organs (Fig. 2.5B, D). The posterior surface of the septomaxilla is deeply concave and separated from the ventral surface by the crested nasal septum. The posterior concavities of the two septomaxillae mirror the concavities on the frontal and are quite unique amongst iguanids. Together with the nasals, frontal, and prefrontals, the septomaxillae border the orbitonasal chamber (or nasal capsule), which includes the lacrimal and olfactory systems (Oelrich 1956).

Prefrontals – The anterior margin of the prefrontal is sinusoidal, with its main portion contacting the posterior border of the facial process of the maxilla, and its posteroventral corner in contact with the lacrimal and jugal (Figs. 2.1; 2.6; A2.1). There is a fairly large and shallow facet on the anterodorsal surface of the bone that underlies the facial process of the maxilla (Fig. 2.6A). Numerous small foramina pierce the dorsal surface of the prefrontals, most of which are concentrated close to the posteromedial margin. A single boss (or tuberosity) is present on the dorsolateral surface of the prefrontal and is particularly well-developed and prominent in larger specimens. The medial margin contacts the nasal for its entire length. This suture is quite irregular and slightly sinusoidal in large specimens, while it is straight and smooth in small individuals. The posteromedial surface of the prefrontal contribute to the lateral wall of the orbitonasal chamber and it is characterized by a deep double concavity that is partially split by an incomplete and blunt ridge (Fig. 2.6B). The internal surface of the prefrontal is deeply concave and multiple foramina of various sizes pierce its most medial region (dorsal to ventral). The palatine process (Oelrich 1956) or orbitonasal flange (Evans 2008) represents a ventral expansion of the posterior margin that contacts the palatine and forms the anteromedial border of the orbital opening. The ventrolateral corner of the palatine foramen is well-sutured to the jugal and contacts the lacrimal along its anterior surface (Fig. 2.6A, B). The lateral region of the prefrontal palatine process partially overlaps the medial region of the lacrimal, thus contributing to the border of the lacrimal duct foramen when the elements are articulated. The posterior border of the prefrontal contacts the frontal, forming an indented suture, or tongue-and-groove suture as defined in Oelrich (1956). The anterolateral process of the frontal inserts onto a grooved facet located in the middle of the prefrontal posterior margin. The posterodorsal region of the prefrontal, contributing to the anterodorsal margin of the orbit and overlapping the frontal

in ventral view, is pierced by a foramen (Fig. 2.6A, C). The foramen appears to match the large pair of foramina found on the anterior region of the frontal. The function of these foramina is unclear. A similar foramen is present in *Conolophus* while in *Iguana* there is no opening in small to medium size specimens, but a notch is found in larger individuals in the same position. No foramen or notch is present in *Ctenosaura* and *Cyclura*.

Lacrimals – The lacrimal is minimally exposed in lateral view and is largely overlapped by the maxilla anteroventrally and the jugal posteriorly, while contacting the prefrontal dorsally (Fig. 2.7). The lateral surface of the lacrimal is mostly occupied by the facet for the maxilla, and posterodorsally by the facet for the jugal suborbital ramus (Fig. 2.7A). The anterior margin is highly irregular, with a squared process projecting towards the maxilla (anterior process), and a superior process projecting dorsally, with a deep notch separating the two processes (Fig. 2.7A, B). The ventral margin is gently concave, while the dorsal margin is sinusoidal. The posterior margin is also irregular, with three tubercular projections interlocking with the anteromedial surface of the jugal. On the medial side, the lacrimal fully encloses the foramen for the lacrimal duct (Fig. 2.7C, D). The lacrimal duct foramen in *Amblyrhynchus* becomes increasingly smaller in larger specimens and overall is relatively smaller in comparison to other iguanids, where it is usually quite elongated (e.g., *Iguana iguana*). In some larger specimens of *Amblyrhynchus*, there are two small openings instead of a single large lacrimal foramen. Posterior to the lacrimal duct foramen, a sharp sagittal ridge marks the contact with the palatine process of the prefrontal and reaches up to the anterior margin of the jugal, being separate from the lateral wall of the lacrimal bone by a shallow groove (Fig. 2.7C).

Jugals – The jugal has a sub-rectangular anterior (or suborbital) ramus, most of which is covered in lateral view by the posterior portion of the maxilla when the elements are articulated (Fig. 2.8A, B). An oblique ridge on the lateral face of the suborbital ramus marks the limit of the maxillary facet, and the maxilla contacts the full length of the anteroventral margin of this process. The most anterior tip of the suborbital ramus contacts the lacrimal dorsally and posteriorly. On the medial side of the suborbital ramus, there is a short process forming an interdigitating contact with the lacrimal and palatine process of the prefrontal anteriorly, the palatine medially, and the ectopterygoid posteriorly (Fig. 2.8B-D). This medial process is pierced by a small foramen for the passage of the maxillary nerve (cf. Oelrich 1956). Along the ventral margin of the suborbital ramus a blunt process is visible that projects laterally between the articular facets for the maxilla and ectopterygoid (Fig. 2.8C, D). The lateral surface of the jugal is fairly concave and a prominent suborbital shelf borders the dorsal margin of the bone in large specimens. The shelf is weakly developed in small to medium size individuals. Across the lateral surface of the jugal, on both the suborbital and postorbital rami, there are multiple small foramina (i.e., suborbital foramina *sensu* Oelrich 1956), which are evident in young individuals but harder to discern in adults. The postorbital (or posterodorsal) ramus of the jugal tapers posterodorsally and bears the facet for the postorbital (Fig. 2.8C). The postorbital facet is quite elongate, making up more than half of the length of the posterodorsal ramus. In articulation, the posterodorsal ramus of the jugal never fully contact the anteroventral process of the squamosal: the two elements are close, but a small gap remains in between in all the specimens examined here (Figs. A2.1E; A2.2B).

Frontal – The frontal in *Amblyrhynchus* is uniquely configurated in comparison to all other iguanids. The bone is short, much wider posteriorly at the contact with the parietal, and abruptly constricted at the level of the orbits, while its lateral margins flares anteriorly (Figs. 2.1; 2.9; A2.1, A2.2). The anterior margin forms an irregular interdigitating suture with the nasals and prefrontals. During late ontogenetic development, the line of suture between the frontal and nasals-prefrontals becomes faint and difficult to discern in the largest individuals examined. A fairly long orbitonasal projection (or anteromedial process) from the anterior margin of the frontal inserts underneath the nasals, and it is not visible when the bones are in articulation (Fig. 2.9A, B, E, F). The orbitonasal projection is relatively longer in younger individuals and bears two narrow groves on its sides for the articulation of the nasals. On the ventral surface, a sharp mid-sagittal crest runs from the tip of the orbitonasal projection to about mid-length of the frontal table. I refer to this crest as the anteroventral crest (of the orbitonasal projection), which among iguanids is only found in *Amblyrhynchus*. This crest contributes to the median margins of the nasal concavities that open along the anteroventral margin of the frontal (Fig. 2.9C). These concavities are bordered on the sides by tall lateral walls and posteroventrally by a narrow and short lappet of bone. The subolfactory canal in *Amblyrhynchus* is made of calcified cartilage and never ossifies, as in all other iguanian lizards. Two specular and narrow grooves are visible on the mid-ventral surface of the frontal table where the cartilaginous element makes contact, posterior to the anteroventral crest of the frontal (Fig. 2.9B). Two short and pointed lateral processes project from the anterior corners of the frontal table, bearing ventral facets for the articulation of the prefrontals. These anterolateral processes are shorter than the orbitonasal projection and overlap the mid-posterior margin of the prefrontals (Fig. 2.9A, B, G). The anterolateral margins of the frontal have two V-shaped notches where they contact the

posterolateral processes of the prefrontals (Fig. 2.9G). The dorsal surface of the frontal is quite flat, with a shallow posteromedian concavity present at the contact with the parietal that is better defined in smaller individuals. This surface becomes gently sculptured in large specimens, but never as rugose as in *Conolophus* where numerous regular tubercles are visible on the snout-skull roof region of medium to large specimens (Fig. 2.32E, F). Multiple foramina of variable sizes are present on the dorsal surface of the frontal, and quite often these foramina are not symmetrical between right and left sides. Two paired and large foramina are present in the anterior region of the frontal table in UF 41558, close to the contact with the nasals and prefrontals (Figs. 2.9A, B; A2.1A; A2.2C). These foramina are found in all specimens but in different number and size. Some specimens have up to five such foramina spread along the anterior margin of the frontal (AMNH 29938). As described for the prefrontal – which bears a dorsal opening matching the lateral foramina on the frontal – their function is unclear. While the prefrontal foramen is present also in *Conolophus*, the anterior foramina of the frontal are unique to *Amblyrhynchus* among iguanids. The posterior margin of the frontal is fairly convex. The suture with the parietal becomes interdigitated in larger specimens, though it is straight and smooth in small-to-medium sized individuals. Along the midline of the posterior margin there is a notch that makes up the anterior border of the pineal foramen (Fig. 2.9). I noticed some variability related to the changeable position of the pineal foramen and consequently to the presence and/or extension of this notch on the frontal (see description of the pineal foramen for further details). The posterolateral corners of the frontal bear facets for the articulation of the postfrontal and postorbital. The facets for the postfrontals are oriented anteriorly, with a visible concavity on the anterior surface of the frontal posterolateral corners (Fig. 2.9B, D). The

postorbitals contact the frontal via a small and flat surface located on its posterolateral corners (Fig. 2.9F, G).

Parietal – The parietal consists of a triangular dorsal table, tall lateral flanges (or walls), supratemporal processes, and a posterior wall bearing a nuchal fossa (Figs. 2.1; 2.10; A2.1; A2.2). There are two distinct facets for the articulation of the frontal on both sides of the parietal anterior border(Fig. 2.10C). Overall, the anterior margin of the parietal is slightly concave and eventually forms an interdigitating suture with the frontal during ontogeny (in young specimens, this margin is fairly smooth) (Fig. 2.11A; A2.1C). In most cases, the parietal anterior margin contributes to the posterior border of the pineal foramen; in some specimens the foramen can be exclusively surrounded by either the frontal or the parietal (Fig. 2.11) (see description of the pineal foramen for further details). The anterolateral corners of the parietal bear facets for the articulation of the postorbitals. In lateral view, these facets are semicircular in shape and quite concave, and in dorsal view are gently sinusoidal. The dorsal surface of the parietal is pierced by several foramina of variable size. Some of these foramina are aligned to the sides of the triangular table, while others are irregularly distributed, and not all are fully open. The number of foramina is greater in larger specimens, though their size tends to decrease in comparison to the foramina in smaller specimens. The posterior dorsal surface of the parietal is characterized by a mid-sagittal crest, commonly present amongst iguanids. The mid-sagittal crest of the parietal in *Amblyrhynchus* is not as prominent as in other iguanids (e.g., *Conolophus*) and is present only in medium-to-large specimens (Fig. A2.2E). Variability for this structure is quite high, as different specimens of the same size may or may not have a defined parietal crest. The mid-sagittal crest is located between the main parietal table and the bifurcation of the two supratemporal (or

posterolateral) processes. The supratemporal processes are quite tall and laterally flattened, and they bear facets for the articulation of the supratemporal bone on both the lateral and medial surfaces (Fig. 2.10A, B, E). Close to the posterior corner of the supratemporal process, on its lateral surface, there is a concavity/fossa for muscle attachment; this feature appears to be unique to *Amblyrhynchus* as none of the other iguanids have a similar structure (Fig. A2.2B, E). Attachment for the adductor musculature on the lateral surface of the parietal supratemporal process is present in all iguanids, but only in *Amblyrhynchus* is there such a well-developed fossa for muscle insertion. The posterior end of the supratemporal processes in *Amblyrhynchus* do not contact the paroccipital processes of the otoccipitals as they do in *Iguana*. The lateral walls (or flanges) or the parietal are constricted at the level of the mid-supratemporal fenestra (Fig. 2.10A, B). A small triangular flange is present along the ventral border of the lateral wall for the articulation of the epipterygoid, and this contact is mediated by a significant amount of cartilage (Figs. 2.10A, E; A2.2E). This flange, however, is absent in smaller specimens, where there is instead a small facet mediating the contact with the epipterygoid at the level of the temporal constriction. The posterior wall of the parietal is also quite tall and with a flaring dorsal margin. Along the midline of the posterior wall, a defined nuchal fossa develops quite late in ontogeny, well after the bones of the braincase are fully fused, and it is only visible in specimens of medium to large size (Figs. 2.1D; 2.10D, F; A2.2A). Small to medium specimens only display a shallow median concavity on the posterior wall. In larger specimens the nuchal fossa is deep and large, and divided by a vertical septum. The septum starts forming from the dorsal border of the posterior wall and in some specimens appears incomplete. A well-defined and complete septum is found only when the nuchal fossa is fully developed. Two shallow crests border the lateral margins of the fossa, and these are visible before the nuchal fossa is formed. The ventral surface

of the parietal is slightly concave in small specimens, while flat in larger ones. Two shallow grooves are found along the medial side of the lateral walls and are slightly deeper at the level of the temporal constriction. The posterior margin of the ventral surface is characterized by the presence of the parietal fossa, where the supraoccipital processus ascendens of the synotic tectum makes contact (cf. Evans 2008; Oelrich 1956) (Fig. 2.10B, D, F). The parietal fossa bears a distinct anterior margin, while it is open posteriorly, with two lateral lappets bordering its sides. The posterior opening of the parietal fossa along the midline of the bone (right below the nuchal fossa) is barely exposed in dorsal view, due to the vertical orientation of the posterior wall of the parietal (Fig. A2.1A, C; A2.2C).

Pineal foramen – With the exception of *Dipsosaurus*, where the pineal foramen pierces exclusively the frontal, in iguanids, the pineal foramen is usually located at the fronto-parietal suture. This is the case in most of the specimens of *Amblyrhynchus* analysed in this study as well; however, I recorded a great deal of variability associated with this structure (Fig. 2.11). The most frequent condition is that the pineal opening is located along the suture between the frontal and parietal, with the anterior margin of the parietal usually concave at the midline, matched by a blunt posterior convexity along the posterior margin of the frontal (Figs. 2.11A, B; A2.1A; A2.2E). In some specimens, the pineal foramen is fully enclosed by either the frontal or parietal, and there is variation in the contribution to the opening by the two bones when the foramen is located along the suture (Figs. 2.11; A2.1A, C; A2.2C, E). The less frequent condition is that the pineal foramen pierces only the parietal (with no contribution from the frontal), which I only observed in one specimen. The frontal contribution to the pineal opening is usually represented by two posteromedian indentations on the parietal. These posterior projections from the margin of the frontal tend to eventually contact and enclose the pineal foramen entirely, or only in either

dorsal or ventral view. These patterns of variation related to the pineal foramen do not seem to follow any specific trend in ontogeny, nor do they appear dimorphic, nor are they linked to island distributions, based on the specimens examined in this study. A larger sample number and more detailed information about location, sex, and life stage of the specimens is necessary to further assess a trend in such variability, if any in particular.

Postfrontals – The postfrontal and postorbital are separate elements as in all other iguanids. The postfrontal has a thick and rounded anterior margin and a deep notch along its dorsal margin for the articulation of the frontal (Fig. 2.12). Posteriorly, the postfrontal bears a v-shaped indentation for the insertion of the posterolateral corner of the frontal (Fig. 2.12C, D). The lateral (or distal) margin is well-rounded and partially contributes to the supraorbital boss that mostly extends onto the postorbital (Fig. 2.12C). The posterolateral surface of the postfrontal contacts most of the anterior margin of the postorbital. The articular facet for the postorbital is bordered ventrally by a lappet of bone which partially overlaps the postorbital dorsal ramus (Fig. 2.12D, E).

Postorbitals – The postorbital is a triradiate bone with a dorsal, posterior, and anteroventral ramus (Fig. 2.13). The dorsal ramus is flat anteriorly, where it bears a large facet for the postfrontal, and rounded posteriorly (Fig. 2.13A, B, E). Along its medial margin, there is a groove for the insertion of the parietal, with small tubercles all around the margin (Fig. 2.13B, C). At the junction between the three rami, there is a prominent boss (i.e., supraorbital boss) with a crest extending more ventrally along the lateral surface of the bone (Fig. 2.13A). The anteroventral ramus is narrow and fairly long, and it overlaps the posterior process of the jugal

for most of its length (Fig. 2.13D, F). The posterior ramus contacts the squamosal and is distally forked (Fig. 2.13C, D). A medially deflected flange extending from the posterior to the dorsal ramus bears a deep fossa right behind the supraorbital boss (Figs. 2.13A-C; A2.1A; A2.2B, E). This fossa is absent in all other iguanids and fits with the pattern of increase muscle attachments found in many areas of the skull and mandibles in *Amblyrhynchus*. The area of the dorsal fossa is frequently pierced by multiple tiny foramina, along both its lateral and medial walls.

Squamosals – The squamosal has an overall trapezoidal shape (Fig. 2.14). Its anterior margin is sloped and interlocks with the postorbital, with a small gap between the two bones at the level of the squamosal anteroventral process (Figs. 2.14A, B; A2.1E; A2.2B). A short posterodorsal process overlaps the lateral surface of the supratemporal and reaches up to the parietal supratemporal process. The posterior margin is fairly flat and contacts mostly the supratemporal; in larger specimens there is also a minimum contact with the supraoccipital process of the otoccipital. The posteroventral (or quadrate) process is well-developed and tubular, inserting firmly into the dorsal notch of the quadrate (Figs. 2.14; A2.1A, E; A2.2B).

Supratemporals – The supratemporal clasps around the supratemporal process of the parietal, contacting the latter ventrally, medially, and laterally, with a much greater exposure in medial view (Figs. 2.15; A2.2A, E). The bone consists of lateral and medial rami, separated by a sagittal sulcus. The medial surface of the lateral ramus and lateral surface of the medial ramus both bear a large and flat facet for the articulation of the supratemporal process of the parietal (Fig. 2.15A). The lateral ramus is much shorter, has a fairly flat dorsal margin and does not extend for the full length of the supratemporal. The medial ramus is taller and longer and

prevents the parietal from contacting the paroccipital process of the otoccipital. The medial surface of the medial ramus is characterized by a shallow posteroventral concavity, likely for muscle insertion (Fig. 2.15B). The posterior end of the supratemporal is knob-shaped and it sits between the paroccipital process of the otoccipital medially, the squamosal laterally, the supratemporal process of the parietal dorsally, and the quadrate ventrally. The posterior end is crested dorsally and an incomplete foramen pierces its medial side (Fig. 2.15B, D).

Quadrates – The quadrate is oriented about vertically when articulated and has a broad dorsal end that is mostly occupied by the cephalic condyle (Figs. 2.16; A2.1E; A2.2B). The large squamosal notch is located along the posterior margin of the dorsal end, lateral to the cephalic condyle and suprastapedial process (Fig. 2.16A, D, F). This position for the squamosal notch is by far the most common amongst iguanids, with the only exception being *Iguana iguana*, where the notch is located instead along the lateral margin of the quadrate head. A large foramen is visible on the dorsal surface of the bone anterior to the squamosal notch; this is particularly well-developed in smaller sized specimens, and less noticeable in large individuals (Fig. 2.16E, F). The anterior surface is relatively flat, with a shallow fossa located in the dorsomedial region. The cephalic condyle is oriented posteromedially underlying the squamosal and supratemporal. A lappet of bone from the cephalic condyle extends beyond the level of the quadrate posterior pillar forming a suprastapedial process (Figs. 2.16A-D; A2.2B). The suprastapedial process almost contacts the paroccipital process of the otoccipital distally, but for a small gap between the two elements, which is filled by fibres and cartilage. The quadrate conch is not very deep, while the tympanic crest is thick, especially more dorsally. The pterygoid lappet typically found in iguanids along the medial margin of the quadrate is not very prominent (Fig. 2.16E). In

Amblyrhynchus, the pterygoid lappet contacts the dorsolateral margin of the quadrate process of the pterygoid, while in *Conolophus* and *Iguana* the pterygoid lappet makes contact with the pterygoid along the ventrolateral surface of the quadrate process. The ventral end of the quadrate, contacting the articular, is saddle-shaped and has one medial and one lateral condyle (Fig. 2.16G). The quadrate foramen is particularly small, and barely noticeable in young individuals. In anterior view, it is visible on the lateral side, right above the saddle of the ventral end of the bone, while in posterior view the foramen pierces the base of the posterior pillar medially (Fig. 2.16D). Another foramen is present above the quadrate foramen, piercing the quadrate pillar at the level of the pterygoid lappet. On the medial side of the posterior surface, an elongate notch is visible between the posterior pillar and the pterygoid lappet (Fig. 2.16C, D): this notch corresponds to the mandibular groove described by Oelrich (1956), for the passage of the mandibular artery.

Epipterygoids – The epipterygoid has the typical columnar shape found in most squamates (Fig. 2.17). The dorsal half is slightly larger and mediolaterally compressed, while the ventral half is anteroposteriorly compressed. The anterior and lateral surfaces are smooth and continuous, while the posteromedial side has a v-shaped fossa at about mid-height, with a posterior crest on its lateral margin (Fig. 2.17B). The dorsal end is rounded and separated from the epipterygoid process of the parietal by a fairly large gap; this gap is larger in small size specimens, and decreases in relative size later in ontogeny. The ventral process of the epipterygoid has a square shape and inserts into a deep notch on the dorsal margin of the quadrate process of the pterygoid (Fig. 2.17).

Vomers – The two vomers contact each other for most of their length, diverging posteriorly where the anteromedial processes of the palatines interpose (Figs. 2.1C; 2.18; A2.1B, D). The anterior end of the vomer is pointed and inserts behind the incisive process of the premaxilla. It lacks an anteromedial (or premaxillary) process that is present for example in *Conolophus* and *Cyclura* and that branches medially from the anterior end of the vomer. The anterolateral margin contributing to the fenestra vomeronasalis is deeply concave and a shallow lacrimal groove is visible along its ventral surface (Fig. 2.18A, D). The dorsal surface is gently concave, with slightly crested lateral and medial margins: the medial margin crest is sharper, while the lateral margin crest is quite blunt. The ventral surface is characterized by the presence of an anterolateral crest, mirroring in direction the concavity bordering the fenestra vomeronasalis (Fig. 2.18A, D, E). The anterolateral crest borders the lacrimal groove medially, while medial to the crest there is a small foramen. This is different from the vomerine foramen *sensu* Oelrich (1956) which is located posterior to the anterolateral crest (Fig. 2.18A, B). The vomerine foramen is very large in UF 41558, which is a medium size individual; the opening appears relatively much smaller in larger size specimens (Fig. A2.1A, B). In *Amblyrhynchus*, there is no lateral expansion of the main body of the vomer posterior to the lacrimal groove and the contribution of the fenestra vomeronasalis (e.g., *Conolophus* and *Iguana*). The condition in *Amblyrhynchus* is similar to *Ctenosaura* where the mid-to-posterior lateral margin is straight throughout. In ventral view, the posterior end overlaps a portion of the anterior ramus of the palatine (Fig. 2.18B). The posterior border is quite irregular and it varies from overall blunt in shape in smaller specimens to slightly pointed in larger individuals.

Palatines – The palatine has three main rami: an anterior one, also known as vomerine process, a lateral one or the maxillary process, and a posterior one or the pterygoid process (Figs. 2.19; S1B, D). The anterior ramus is narrow and tapers anteromedially into a single tip that borders part of the posterior end of the vomer (Fig. 2.19A, B). It is dorsally deflected relative to the rest of the bone and it partially overlaps the vomer in dorsal view. The medial margin of the anterior ramus is crested and sharp, with the dorsal surface deeply concave. Its lateral margin is more blunt, following the trend described for the vomer. The lateral (or maxillary) process bears articular facets for the maxilla and jugal laterally, and the posteroventral process of the prefrontal dorsally (Fig. 2.19C). A large infraorbital foramen pierces this process between the maxilla and jugal contact (Fig. 2.19E, F). Another smaller foramen is present medial to the infraorbital one, piercing the lateral process in ventral view, while opening more centrally on the palatine dorsal surface (Fig. 2.19E). This foramen is known as the palatine or maxillo-palatine foramen and in dorsal view its opening is marked by the presence of a fairly large but short transverse groove. Some small foramina are present on the posterior process and aligned along a shallow, sagittal palatine groove (Fig. 2.19B). Overall, the posterior (or pterygoid) process is flat both dorsally and ventrally. A long and sub-triangular facet for the pterygoid is present on its ventral surface, along the medial margin (Fig. 2.19D). The posterior border is irregular and bears small incisions and tubercles along the suture with the pterygoid (Fig. 2.19F). The most posterior end of the process also appears bifurcated, with both medial and lateral lappets being quite short.

Pterygoids – The pterygoid is a large element composed of a main body and three long processes: the palatine process anteriorly, the transverse process laterally, and the quadrate process posteriorly (Fig. 2.20). The palatine (or anterior) process borders the palatine medially

for most of its length; the two palatine processes of the two pterygoids get very close along the midline of the skull but never make contact (Fig. A2.1B, D). The anterior end of the palatine process tapers to a single point, though in *Ctenosaura* and *Cyclura* the process is distinctly bifurcated. The anterior end of the palatine process is pierced by a foramen that is not known from any other iguanid (Fig. 2.20C, D). This foramen matches the two small foramina found piercing the anteromedial end of the palatine, within the articular groove for the pterygoid (Fig. 2.19F). Along its lateral margin and ventral surface, the palatine process bears the articular facet for the posterior process of the palatine. This articular facet is elongate and fairly grooved, and extends up to the base of the palatine process, almost reaching the transverse process. The dorsal surface of the palatine process is concave and its medial margin appears bluntly crested. A marked groove on the dorsal surface of the palatine process and main body of the pterygoid is present close to the medial margin, where the palatine makes contact (Fig. 2.20A). The transverse process is engraved dorsally by a v-shaped facet for the ectopterygoid, and has a tall, sub-triangular ventral flange (Fig. 2.20A). Close to the mid-lateral margin of the pterygoid, immediately anterior to the quadrate process, a deep fossa for the articulation of the epipterygoid is present on the dorsal surface. This is referred to as the columellar fossa in Oelrich (1956), and posterior to it there is a crested process that extends onto the quadrate process. The ventral surface of the pterygoid main body is flat and, closer to the medial margin, there are usually 3 to 5 small teeth set in a groove with sockets (Figs. 2.20B; 2.34; A2.1B, D) (see the dentition section for further details). A broad and rounded posteromedial flange is present at the contact with the basipterygoid process of the basisphenoid. The flange partially overlaps the head of the basipterygoid process and underlines the concavity present at the transition between the main body of the pterygoid and quadrate process where the basipterygoid process articulates. The

quadrate process is tall and laterally compressed. Its lateral surface is smooth, while the medial side is excavated by a deep sagittal groove (serving for the insertion of *m. protractor pterygoideus*: cf. Oelrich 1956).

Ectopterygoids – The ectopterygoid is characterized by a fan-shaped lateral process and a vertical and bifurcated medial process with a dorsal and ventral ramus (Fig. 2.21). The lateral process has a bluntly bifurcated posterior lappet contacting the jugal, while its anterior portion contacts both the jugal and maxilla (Fig. 2.21A, B, E). In lateral view, the process is roughly triangular and gently concave; a small foramen pierces its lateral surface at the level of the anterior lappet, which is covered by the jugal when the elements are articulated. The main body and medial process of the ectopterygoid bear a large v-shaped facet on the posterior surface for the articulation of the pterygoid transverse process (Fig. 2.21C). The dorsal ramus of the medial process overlaps the pterygoid and extends anteriorly towards the contact between the pterygoid and palatine. The ventral ramus underlies the pterygoid, reaching down to the corner of the ventral flange of the transverse process of the pterygoid (Fig. 2.21C, D). Both the dorsal and ventral rami of the medial process are pierced by a small foramen, close to the (Fig. 2.21B, E) edge of the medial margin.

Orbitosphenoids – The orbitosphenoid is a small ossified and paired element. The two orbitosphenoids are suspended in the orbital region by cartilage, and connected via cartilage to the subolfactory canal (Figs. 2.1A; 2.22). The element is fairly compressed, with all three processes (superior, posterior, and inferior) being quite flat. The dorsal margin, connecting the superior and posterior processes, is gently convex in small to medium size specimens (e.g., UF

41558: Fig. 2.22), while it is roughly v-shaped in the largest specimens. In both young and adult individuals, the ossified portion of the dorsal margin is capped by a thick layer of cartilage. The anterior margin, connecting the superior and inferior processes, is concave, while the posterior margin, between the posterior and inferior processes, is more sinusoidal. The ventral margin of the inferior process is flat, with fairly sharp corners.

Supraoccipital – The dorsal head of the supraoccipital is narrow and fan-shaped, with a foramen piercing its posterior surface (Figs. 2.1D; 2.23; A2.2A). In younger individuals, this opening appears as a v-shaped notch along the dorsal margin and is closed by bone dorsally later in ontogeny (Figs. 2.1D; 2.23C; A2.2A). The sides are flared in an anterolateral direction. There is a blunt median (or mid-sagittal) crest along the posterior surface that appears incomplete in smaller sized specimens but extends down to the ventral margin in large individuals. A dorsolateral ridge is present on each side of the mid-sagittal crest (on the flared sides) that does not reach the ventral margin of the supraoccipital. Two lateral ridges are also present along the anterior surface, on the sides of the notch for the attachment of the processus ascendens of the synotic tectum (PAST). The PAST is cartilaginous in small to medium size specimens and ossified only in the largest specimens. I found a similar trend in *Iguana*, while in *Ctenosaura* and *Cyclura*, the PAST seems to remain cartilaginous throughout life, though some may be partially ossified (Oelrich 1956). The position and orientation of the PAST in *Amblyrhynchus* is quite different in comparison to *Iguana* and *Ctenosaura* and is located well in front of the fan-shaped mid-dorsal margin of the supraoccipital, projecting anteriorly instead of dorsally (Fig. 2.23A, B, D, E). When the supraoccipital is articulated to the parietal, the PAST is fully covered in posterior view, inserting into the parietal fossa. The ventral margin of the supraoccipital roofing

the foramen magnum is smooth and concave (Figs. 2.23C; A2.2A). The suture lines between the supraoccipital and otoccipital are faint but still visible even in larger specimens.

Basioccipital – The dorsal surface of the basioccipital is concave and bears a median, broad groove which disappears posteriorly before the occipital condyle. The ventral surface of the basioccipital is slightly concave and a median septum extends from the occipital condyle to the level of the sphenoccipital tubercles, but does not reach the suture with the basisphenoid (Fig. 2.23F). The sphenoccipital tubercles are broad and gently flare distally. Between the basioccipital tubercles and the basisphenoid tubercles, there is a marked groove that runs transversally and remains within the extension of the basioccipital (right posterior to the suture with the basisphenoid) (Figs. 2.23F; A2.1B). The distal end of the sphenoccipital tubercles have a rough surface and are covered by a cartilage cap.

Sphenoid (basisphenoid + parasphenoid) – The basisphenoid has a deep concavity on its ventral surface, anterior to the suture with the basioccipital (Figs. 2.23F; A2.1B). This concavity is separated from the more gentle one found on the basioccipital by a raised transverse margin that runs from one sphenoccipital tubercle to the other, and unlike the basioccipital, the basisphenoid concavity is single and not divided by a septum. The crista trabecularis bears a broad ossified cultriform process that projects anterodorsally and is sutured to the parasphenoid rostrum (Fig. 2.23D, F). The carotid canal is marked by a blunt median crest on the dorsum sella (Fig. 2.23A, D). Two parallel foramina are visible on the anterior surface of the dorsum sella, entering the main body of the basisphenoid. The crista sellaris (along the dorsum sella) is thick and blunt and the two alar processes are somewhat rounded, with a slightly concave tip (Fig.

2.23A, B, D). A foramen for the abducens canal perforates the anterior surface in correspondence to each alar processes and is located above the level of the median carotid foramina. The openings for the vidian canal start as a groove on the dorsal surface of the basipterygoid processes and then pierce the basisphenoid on both sides of the crista trabecularis (Fig. 2.23A). The two basipterygoid processes are thick and broad at the base; they flare distally into an asymmetrical end and the posterior lappet is longer than the anterior one. The basipterygoid processes are capped by cartilage and insert underneath the posteromedian flanges of the pterygoid and thus are covered in ventral view (Fig. 2.23A, B, D). The parasphenoid rostrum is quite short and fully fused to the cultriform process of the basisphenoid. In *Amblyrhynchus*, it is relatively shorter than in any other iguanid, is dorsoventrally compressed, and tapers anteriorly displaying an overall triangular shape (Fig. 2.23).

Prootics – The prootic is a triradiate element, fully sutured to the supraoccipital, otoccipital, and basisphenoid in all the specimens of *Amblyrhynchus* examined in this study (Fig. 2.23). The prootic alar process has a short extension along its anterodorsal margin, known as the crista alaris (cf. Oelrich 1956). The crista alaris is anterior to the anterior semicircular canal and in *Amblyrhynchus* it is short and has a straight anterior margin, unlike in *Ctenosaura* where it is convex and more pronounced (Fig. 2.23D). The parietal process of the prootic is flat and squared and raised above the level of the alar process (Fig. 2.23A, B, D). Posterior to the parietal process, a concave surface connects the prootic to the supraoccipital. The suture between the two bones is completely obliterated in all the specimens examined. Anteriorly, the parietal process is separated from the anterior margin of the crista alaris by a notch and a small lateral tubercle. The supratrigeminal process is short and develops from a crest along the medial surface of the prootic

just above the level of the foramen ovale (Fig. 2.23A, D). In lateral view, the supratrigeminal process is barely visible, projecting anteriorly above the trigeminal notch. The inferior process at the contact with the basisphenoid is fairly cylindrical, with a gently concave anterior surface. In *Amblyrhynchus*, the crista prootica is straight and blunt (Fig. 2.23B, D), unlike in *Iguana* where the crista has a well-developed descending ventral lappet about mid-length. The medial surface of the lateral wall is convex posteriorly, where the tympanic bulla is formed, partially involving the contact margin with the exoccipital and supraoccipital (Fig. 2.23D). Anterior to the tympanic bulla, the lateral wall is pierced by several foramina, likely the passage for the external semicircular canal and the facial foramen more ventrally (see description of braincase foramina below).

Otoccipitals (opisthotic + exoccipital) – The otoccipital is a compound element deriving from the fusion of the opisthotic and exoccipital, and in *Amblyrhynchus* it is quite distinct from all other iguanids. The posterior surface of the otoccipital is pierced by the foramen for the vagus nerve (X) and two to three hypoglossal foramina on each side of the foramen magnum (Figs. 2.23C; 2.24D, F). The occipital condylar processes of the exoccipital are well-exposed posteriorly, underlie the foramen magnum, and do not contact each other along the midline, as they do in most chamaeleonids. The paroccipital processes flare laterally and their expanded ends bear a cap of cartilage distally where they contact the supratemporal anterolaterally and the parietal dorsally (Figs. 2.23; A2.2A). In the largest specimens, the distal end of the paroccipital process is close to the contact with the suprastapedial process of the quadrate, though the gap between the two is filled with fibrous tissue. The ventral margin of the paroccipital process is crested. A defined occipital recess is missing in *Amblyrhynchus*, as there is no crista

interfenestralis, which typically makes up the anterior wall of the recess (Oelrich 1956). This is different from the condition found in other iguanids, including *Conolophus*. Because of the absence of a crista interfenestralis, the lateral aperture of the recessus scalae tympani (LARST) is exposed on the posterolateral wall of the otoccipital (Fig. 2.23B). Posterior to the LARST, there is a thick and broad crista tuberalis, which typically makes up the posterior margin of the occipital recess. The lateral margin of the crista tuberalis is concave and merges ventrally to the sphenoccipital tubercle of the basioccipital.

Stapes – The stapes (or columella) is a slender bone with fairly cylindrical extremities and an anteroposteriorly compressed mid-shaft (Figs. 2.1C, D; A2.2A). Instead of being straight as in *Iguana* and *Ctenosaura*, the stapes in *Amblyrhynchus* is slightly angled ventrally along the shaft approaching the lateral tip. The lateral (or distal) end is more expanded than the medial (or proximal) one. Distally, the stapes attaches to the cartilaginous extracolumella, which contacts the tympanic membrane on the medial side of the quadrate (Fig. 1C). The medial end contacting the basicranium is knob-shaped and there is a small foramen piercing its posterior margin. No medial footplate or stapedial foramen is present.

Foramina of the braincase – The Vidian (or pterygoid) canal serves as the passage for the homonymous nerve, artery (carotid?), and vein, opens anteriorly on the basisphenoid, and bears a foramen on each side of the crista trabecularis and at the base of the retractor pit (Fig. 2.24A, D). The canal runs through the side of the dorsum sella alongside the basisphenoid-prootic contact. The posterior opening of the Vidian canal is partially covered in lateral view by the initial portion of the crista prootica. A small but deep notch is also found below and lateral to the level

of the posterior opening of the Vidian canal at the onset of the crista prootica (Fig. 2.24B). The function of this notch is unclear: it does not bear a full foramen piercing through the lateral wall of the Vidian canal, and its position is slightly inferior to the level of the canal. This structure may not be related to the Vidian system and rather serves for ligament or muscle insertions. Further analysis of the associated soft tissues will be necessary to determine its function with certainty. On the upper part of the basisphenoid retractor pit, a small foramen pierces the anterior surface of the bone. This represents the passage for the abducens (VI) nerve (Oelrich 1956). Two more foramina are visible at the base of the basisphenoid dorsum sellae and dorsal to the crista trabecularis; they serve to transmit the branches of the internal carotid artery (Fig. 2.24A, C). The canals opened by these two foramina merge into the larger Vidian canals that run just below and along the lateral regions of the basisphenoid (Oelrich 1956). The main branch of the facial (VII) nerve pierces the medial surface of the prootic very close to the dorsal surface of the basisphenoid and below the supratrigeminal process (Fig. 2.24E). This small foramen is located in a shallow recess, visible behind and ventral to the supratrigeminal process of the prootic. In the same recess, another small foramen is present dorsal to the facial foramen, identifiable as the anterior foramen for the acoustic nerve (cf. Oelrich 1956). The posterior foramen that transmits the acoustic nerve is found more medially and slightly higher than the anterior one, being also much larger in size (Fig. 2.24E). Above both foramina for the acoustic nerve, another tiny opening can be identified as the aperture for the endolymphatic duct (Fig. 2.24E). It pierces the medial wall of the prootic at the level of a rounded prominence that represents the cavum capsularis (cf. Oelrich 1956). Piercing the ventrolateral wall of the prootic and covered in lateral view by the crista prootica, there are two more foramina representing the palatal branch (more dorsal) and hyomandibular branch (more ventral) of the facial nerve (Fig. 2.24B, D). These

foramina are located about midway between the posterior opening of the Vidian canal and the larger foramen for the jugular vein that opens towards the posterior end of the crista prootica (close to the paroccipital process of the otoccipital). Below the jugular foramen and close to the crista tuberalis and occipital recess, another aperture represents the fenestra ovalis (also referred to as the foramen ovale or vestibular fenestra) (Evans 2008; Oelrich 1956). The fenestra ovalis pierces the otoccipital above the lever of the occipital recess and the opening of the recessus scalae tympani, with no bony separation between the two foramina, due to the lack of a crista interfenestralis (Fig. 2.24B, D). In *Amblyrhynchus*, the occipital recess as defined by Oelrich (1956) is only delimited posteriorly by the crista tuberalis, appearing as a shallow elongate notch on the posterolateral surface of the otoccipital (Fig. 2.24C). The recess is fully open anteriorly, as a crista interfenestralis is missing, so the LARST is exposed in both lateral and anterior view (Fig. 2.24B). The LARST is flanked by another much smaller opening for the perilymphatic duct that transmits the glossopharyngeal (IX) nerve (Oelrich 1956). Marking the passage of the branches of the hypoglossal nerve (XII), there are three foramina on the medial surface of the otoccipital and three more apertures on the otoccipital posterior surface; these are located beside and below the exit for the vagus nerve (Fig. 2.24D-F). On each side of the foramen magnum, on the posterior surface of the otoccipital, there is a fairly large opening for the passage of the vagus nerve (Fig. 2.23C; Fig. 2.24D). The vagus foramen pierces the otoccipital posteriorly and also medially, being visible in medial view as a smaller opening above the three hypoglossal foramina (Fig. 2.24E, F).

2.3.3 Mandibles

Dentaries – The dentary is relatively shorter and taller than in other iguanids, consistent with the shortening trend of the snout in *Amblyrhynchus* (Figs. 2.25; 2.26). The anterior margin of the dentary is rounded dorsally at the symphyseal contact (i.e., where the two dentaries articulate), while the remainder is fairly straight (Fig. 2.26A, B). This condition is typical of pleurodontan iguanians, where the symphyseal surface is limited to the most dorsal region of the anterior margin of the dentary. In acrodontan iguanians the contact between the two dentaries extends dorsoventrally along most of the anterior margin of the two dentaries. The lateral surface is fairly flattened and pierced by a variable number of mental foramina closer to the ventral margin (Figs. 2.25A; 2.26A). Amongst the specimens examined here, the number of mental foramina varies from 5 to 8 and shows an increase with size. The Meckel‘s canal opens anteromedially into a large oval-shaped foramen (Figs. 2.25C; 2.26A, B, F). The canal runs through to the dentary below the teeth and is enclosed medially by a short subdental shelf. Anteriorly, the Meckelian canal merges with the inferior alveolar canal, while the two canals are separate more posteriorly along the dentary (Fig. 2.26G). The posterior margin is characterized laterally by a posterolateral and a posteroventral process, and dorsomedially by a short, tapering posteromedial process (Fig. 2.26A, C, E, F). *Amblyrhynchus* lacks a coronoid (or dorsolateral) process that is typical of some acrodontan iguanians, and present but reduced in iguanids like *Ctenosaura* and *Conolophus*. A large facet for the anterolateral process of the coronoid is visible on the dorsal region of the posterior end of the dentary (Fig. 2.26A). The ventral margin of this facet is roughly sinusoidal and excavates the dentary below the level of the terminal teeth.

Coronoids – The coronoid is characterized by a fairly tall dorsal process, outlined posteromedially by a sharp adductor crest (Figs. 2.25; 2.27; A2.1E; A2.2D). In dorsal view, this process is transversally oriented relative to the sagittal axis of the mandible and extends posterior to the tooth row (Fig. A2.2D). The anterior margin of the coronoid bears two process: an anterolateral process and an anteromedial process, which together wrap around the posterodorsal end of the dentary (Fig. 2.27). The anterolateral process is shorter and about square in shape, overlapping the lateral surface of the dentary, above its posterolateral process (Fig. 2.25A, B). The anteromedial process of the coronoid is fairly long and tapers anteriorly, bearing an elongate facet for the articulation of the splenial (Fig. 2.27C). A large foramen pierces the mid-medial surface of the anteromedial process of the coronoid (Fig. 2.27C). This represents the anterior alveolar foramen and its status as fully enclosed by the coronoid is quite unique. In fact, the anteromedial process of the coronoid usually just contributes only slightly to the posterior border of the anterior inferior alveolar foramen in all other iguanids. When the bones of the mandible are articulated, the splenial also contributes to the ventral edge of the anterior inferior alveolar foramen, overlapping in medial view onto a part of the coronoid anteromedial process (Fig. 2.25C, D). Two posterior processes, one lateral and one medial, border the anterior margin of the mandibular fossa (Fig. 2.27C-E). The posterolateral process is wider and shorter, and lies on the dorsal surface of the surangular, posterior to the anterior surangular foramen (Fig. 2.25A, B). The posteromedial process of the coronoid projects ventrally and bears the terminal portion of the adductor crest, which extends from the top of the dorsal process (Fig. 2.27C, D). Ventrally, the posteromedial process has a marked facet for the articular-prearticular, which inserts below the coronoid and lateral to the splenial (Fig. 2.25C, D).

Splenials – The splenial has a fairly straight and flat ventral margin and a semicircular and irregular dorsal margin, and the bone overall tapers both anteriorly and posteriorly (Fig. 2.28). The anterior tip is shorter and blunt, while posteriorly it tapers into a sharp end that inserts between the articular and angular (Figs. 2.25C, D; 2.28A, B). The facet for the articulation of the dentary extends onto the medial surface of the splenial, both anteriorly and ventrally. The facet for the articulation of the angular is also located along the ventral margin, starting more posteriorly, well beyond the level of the mylohyoid foramen (Fig. 2.28A-C). The anterior mylohyoid foramen pierces the splenial about mid-length, proximate to the ventral margin. A notch along the anteroventral margin marks the contact of the splenial with the Meckelian cartilage (Fig. 2.28A, B). This notch is overlapped by the dentary in medial view (Fig. 2.25C, D). Another notch, more square in shape and located along the dorsal margin, represents the contribution of the splenial to the anterior alveolar foramen (Fig. 2.28A, B).

Angulars – The angular is a narrow and elongate bone, tapering both anteriorly and posteriorly, and pierced about mid-length by the posterior mylohyoid foramen (Figs. 2.25C, D; 2.29). The ventral surface is gently convex and a v-shaped facet for the dentary is present on most of the anterior half of the bone (Fig. 2.29A). The surangular overlaps part of the posterolateral margin of the angular, while the articular makes contact along the posteromedial margin. A groove marked by two raised margins is present on the anterodorsal surface of the angular, where the anterior portion of the articular-prearticular articulates (Fig. 2.29B, E).

Surangulars – The surangular has a bifurcated anterior end that inserts into the dentary up to about its mid-length (Fig. 2.30). Hence, a great portion of the surangular is covered in lateral

view, and a broad facet for the articulation of the dentary is present on its lateral surface (Fig. 2.25A, B). The dorsal lappet of the bifurcation bears a flat facet for the contact with the dentary, followed more posteriorly by the insertion of the coronoid (Fig. 2.30A, D). Along the dorsomedial surface of the bone, a groove marks the facet for the articulation of the coronoid: it is a fairly deep and narrow groove, which posteriorly opens into a wider triangular facet, exposed medially, where the ventral portion of the anterolateral process of the coronoid articulates (Fig. 2.30A). Ventral to the coronoid facet, a flat medial process bears another articular facet for the prearticular (Fig. 2.30A, D). The anterior surangular foramen opens about mid-length along the dorsal margin of the bone, above the posterolateral process of the dentary and right behind the anterolateral process of the coronoid (Fig. 2.30C). The facet for the articular extends along most of the posteromedial and ventral region of the surangular, with a marked posterodorsal concavity sitting below the level of the articular-quadrate contact (Fig. 2.30A, D). A sharp crest is present on the posterolateral surface of the surangular, known in the literature as the lateral adductor crest, which serves for the insertion of the *musculus adductor mandibularis externus* (Oelrich 1956). The crest departs from the posterodorsal margin and runs down and anteriorly to fade away close to the ventral border of the bone (Fig. 2.30C). About mid-length along the ventral margin, a sub-triangular lappet, marked above by the presence of a shallow crest on the medial side, bears the facet for the articulation of the angular (Fig. 2.30C, D).

Articular + Prearticular – The articular and prearticular are fused into a single element, of which the prearticular makes up part of the medial surface (Fig. 2.31) (see Evans 2008). Though the two bones are tightly sutured to each other, a faint line of suture underlying the outline of the prearticular is visible in some specimens, especially more posteriorly in front of the

angular process. The articular tapers anteriorly and has a concave lateral surface, topped by a dorsal lappet along which are present an elongate facet for the articulation of the surangular and a shorter triangular face for the coronoid (Fig. 2.31A). More ventrally, on the lateral side and anterior half of the bone, a long and narrow groove marks the position of the Meckel‘s cartilage (at the level of the mandibular fossa) (Figs. 2.25C, D; 2.31D). A well-developed retroarticular process, with tapering sides in dorsal view, projects posteriorly into a knob-shaped end. The dorsal surface of the retroarticular process is gently and homogenously concave, with both a lateral and medial tubercle at the border with the quadrate articular facet. A shallow and narrow notch is visible along the ventrolateral surface of the retroarticular process, close to its posterior end (Fig. 2.31B, D). The facet for the articulation of the quadrate is saddle-shaped, with a raised median ridge and two concavities on the sides. In lateral view, abundant cartilage is visible along this surface, and particularly anterior to the saddle (Fig. 2.31D, F). The angular process projects medially between the articular surface of the quadrate and the retroarticular process. The process is quite thick, its dorsal surface is smooth, and the ventral surface is slightly convex. The ventral surface of the articular is characterized by a long and fairly flat facet for the articulation of the angular, that takes up most of this surface. A mild ventral crest is present at the level of the retroarticular process, running parallel to the angular process, and continuing anteriorly to disappear about midway along the medial surface of the bone (Fig. 2.31B, C). This crest likely marks part of the suture between the articular and prearticular.

2.3.4 Integumentary ossifications

While the presence of osteoderms in *Amblyrhynchus* has been reported in previous studies (de Queiroz 1987), I was not able to corroborate their presence in any of the skeletonized

specimens analysed in this study or via the available CT-scans. “Hard” structures on the snout are clearly present in the two wet specimens UF 41558 and 41424, and they are similar in shape and position to the osteoderms reported by de Queiroz (1987) (Fig. 32A, C). On the other hand, large specimens of *Conolophus* (e.g., ROM R 112, AMNH R 131308) have obvious integumentary ossifications fused to the underlying bones of the snout that are visible in skeletonized specimens (Fig. 2.32E, F). These osteoderms are present in all fairly large specimens of *Conolophus* examined, though they are absent in smaller individuals (AMNH R 147847, 147849). It appears that *Amblyrhynchus* possesses similar osteoderms but these apparently do not fuse to the underlying bones to the extent that they can be found on skeletonized material (Fig. 2.32B, D). From the analysis of the wet specimens, osteoderms of different shape and size are present on most of the snout and skull roof, and on parts of the lateral side of the skull, at the level of the postorbital region (Fig. 2.32C). The largest osteoderms are located at the level of the nasals; they are roughly pyramidal in shape and quite tall, but all are slightly different in length and width (Fig. 2.32A, C). Anteriorly on the snout, at the level of the prefrontal-maxilla-premaxilla, there are smaller, almost flat osteoderms, varying from pentagonal to hexagonal in shape. On the rest of the skull roof, shapes and sizes become more irregular, with some taller osteoderms present at the back of the skull. A myriad of smaller and frequently pointed osteoderms covers the postorbital region (Fig. 2.32C).

2.3.5 Dentition

Marginal teeth – All marginal teeth in *Amblyrhynchus* are tricuspid with the cusps oriented mesio-distally (i.e., parallel to the jaw wall) (Figs. 2.1A, E; 2.2A, B; 2.3A, B, F; 2.25; 2.26; 2.33B, F; A2.1B, D, E; A2.2D). The cusps are all similarly sized, with the median one

being slightly taller than the other two. The number of cusps never varies along the tooth row in *Amblyrhynchus*, unlike in *Conolophus* spp. where an additional smaller cusp is added mesially about halfway along the posterior tooth row. The teeth are loosely attached to the lingual side of the labial wall of the dentary and maxilla, and they are easily removed without breakage after the soft tissues are gone. *Amblyrhynchus* has an *Iguana*-type tooth attachment *sensu* LeBlanc et al. (2020b). All marginal teeth are highly asymmetric in shape, with the labial side of the root lacking a dentine wall (Fig. 2.33D-F). The short labial wall of the tooth is restricted to the crown and attaches to the apex of the labial wall of the jaw, while the taller lingual side of the tooth (crown + root) attaches to the jaw bone at the base (i.e., to the top of the subdental shelf of the dentary, and the ventral surface of the supralveolar shelf of the maxilla) (Figs. 2.3B, F; 2.26C-E; 2.33A, C, D). The resorption pits associated with the tooth replacement form ventrolingually to the functional teeth (Figs. 2.3F; 2.26B, C), as in *Iguana iguana* (LeBlanc et al. 2020b). From the µCT-scans of UF 41558, up to three tooth generations are visible for at least two tooth positions on the maxilla and three tooth positions on the dentary (Figs. 2.3F; 2.26C, D; 2.33A, C; A2.2D). Soft tissues usually cover most of the lingual side of the tooth row, so the replacement teeth remain hidden till the functional tooth is shed. In UF 41558, the replacement tooth erupts when the resorption pit extends apically to invade the crown, just below the three cusps. And in some cases, another replacement tooth is already present at the base of the replacing one while the functional tooth is still in place.

Palatal teeth – Pterygoid teeth in *Amblyrhynchus* are variably present and reduced in number in comparison to *Iguana iguana*. Some specimens lack pterygoid teeth completely while others can have few teeth only on one side of the skull. Most specimens have no more than 3 to 5

teeth on each pterygoid (Figs. 2.20B, C; 2.34). Their crown is conical in shape instead of cuspate like the marginal teeth, and they are set in small sockets or grooves along the ventromedial margin of the pterygoid, at the level of the transverse process (Figs. 2.21B; 2.34D).

2.3.6 Hyoid

The hyoid is characterized by a tapering processus lingualis that projects anteriorly from the basihyoid (Fig. 2.35). The basihyoid is roughly square in shape and the two second ceratobranchials project posteriorly from its margin and are parallel to each other. No evidence of the second epibranchials can be found in any of the skeletonized specimens, nor the μCT - scans. The first ceratobranchial articulates with the basihyoid laterally and immediately behind the hyoid cornu. The head of the first ceratobranchial is squared and flat, with a rounded, cartilaginous condylar surface that is not completely fused (Fig. 2.35). A short and distally tapering first epibranchial is present and attached to the posterior end of the first ceratobranchial I. The hyoid cornu, articulating to the anterolateral corner of the basihyoid, is broad and rounded proximally and tapers distally where it contacts the epihyal. The epihyal is long and slender, and it is characterized by an extremely thin anteromedial flange. This flange is often damaged in skeletonized specimens and barely captured in the μCT-scans, likely due to its low density (Fig. 2.35).

2.4 Discussions

The Galápagos marine iguana has a unique lifestyle amongst squamates. In my description, I was able to identify several unique anatomical features that distinguish this lizard

from any other squamate, including its most closely related taxon *Conolophus*, the land iguana of the Galápagos.

Episodes of hybridization between marine and land iguana of the Galápagos are clearly reported in the literature, where male individuals of *Amblyrhynchus* can interbreed with females of *Conolophus subcristatus* (e.g., Rassmann et al. 1997b). Interestingly, the offspring appears to follow the marine iguana lifestyle though it is unclear at this point if the offspring are fertile or not. This may suggest that the divergence between these two species is still ongoing. However, from an osteological point of view there are many dissimilarities between these two iguanids, with *Conolophus* lacking the features associated with the shortening of the skull, i.e., the nasal concavities on the frontal and verticalized premaxilla and septomaxillae. In fact, when comparing features of the skull roof, postorbital region, and dentition, *Conolophus* shares more similarities with some species of *Ctenosaura* rather than *Amblyrhynchus*.

2.4.1 Unique morphologies

Autapomorphic traits in *Amblyrhynchus* are all associated with the modified nasal capsule system and shortening of the snout, which can in turn be linked to its peculiar feeding strategy. The diet of *Amblyrhynchus* consists almost exclusively of algae that they graze from rocks underwater. Together with their food, they tend to ingest large amounts of seawater and previous studies have also reported large volumes of rock particles in their stomachs as well as larger gastroliths (Mackie et al. 2004; Nagy & Shoemaker 1984; Shoemaker & Nagy 1984). As a consequence of the environment they are adapted to, the morphology and physiology of these iguanas are highly specialized. While there are several studies regarding their physiology, the

descriptions and details presented here are first attempt to thoroughly analyse the cranial anatomy of the marine iguana.

As Bell (1825) mentioned in his first description of the taxon, the marine iguana lacks the conventional elongate snout that characterizes other iguanids such as *Iguana* and *Ctenosaura*. As a consequence, the bones surrounding the orbitonasal chamber in *Amblyrhynchus* are quite unique in shape and arrangement. The premaxilla and septomaxillae are both verticalized, with the nasal process of the premaxilla being about parallel to the main body of the septomaxillae (Figs. 2.1E; 2.2; 2.5; 2.32D; A2.1F). The septomaxillae are L-shaped in lateral view, with the anteroventral region parallel to the vomers, as is more typical across lizards, while the rest of the bone is abruptly deflected dorsally. Each septomaxilla bears a deep concavity posteriorly that makes up the anterior wall of the nasal chamber. The nasal septum, located at the base of the posterior concavity of the septomaxilla, creates a division between the nasal chamber and the vomeronasal (or Jacobson‘s) organ, which is partially roofed by the anterior portion of the septomaxilla (Fig. 2.5). The nasals and frontal roof the nasal chamber, while the prefrontals and lacrimals form its later walls. The shape and features of the nasal and prefrontal are more comparable to other iguanids, and less affected by the modified arrangement of the snout. The only noticeable traits are associated with the greater depth of the concavities marking the position and contact of the nasal capsule along the posteroventral surface of the nasal and the posteromedial surface of the prefrontal (Figs. 2.4, 2.6).

On the other hand, the frontal of *Amblyrhynchus* is extremely unique. Two concavities – that I named here the orbitonasal concavities – are present along the anteroventral margin of the frontal and they form most likely as a consequence of the shortening of the snout, causing the nasal capsule to invade the anterior portion of the skull roof. I presume that this space is

occupied by enlarged salt glands, the presence of which has been hinted at in previous studies (Dunson 1969; Schmidt-Nielsen & Fange 1958). The nasal capsule forms well before the ossification of the snout and skull roof starts and thus the ossification of the frontal would be constricted by the position of the nasal capsule, resulting in its unique shape and features (cf. Oelrich 1956). Elements of the mandible are also affected by the shortening of the snout, causing significant differences between *Amblyrhynchus* and other iguanids. The toothed portion of the dentary is relatively shorter in *Amblyrhynchus*, occupying less than half of the entire mandible; in all other members of Iguanidae, the tooth row is relatively longer and makes up for more than half the mandible. The anterior inferior alveolar foramen is located entirely on the coronoid, piercing its anteromedial process, and it is underlined by the splenial when the bones are in articulation because the splenial overlaps part of the coronoid in medial view (Fig. 2.25). This position of the anterior inferior alveolar foramen in *Amblyrhynchus* is also unusual amongst iguanids, where usually this foramen is found between dentary and splenial, sometimes with a limited contribution from the anterior tip of the coronoid anteromedial process (cf. Evans 2008; Oelrich 1956). This difference is clearly consistent with the trend of shortening of the snout in *Amblyrhynchus*, with the shifted position of some structures.

2.4.2 Foramina of the snout

Another aspect to consider is the unusual number and random pattern of foramina found across the snout in *Amblyrhynchus*. Virtually every bone of the anterior half of the skull has additional openings that cannot be compared to other iguanids, nor to other squamates. A large number of random foramina are concentrated on the nasals and anterior frontal, and a few extra openings can be found also on the medial half of the prefrontal and the facial process of the

maxilla. The matching foramina that I identified on the prefrontal and frontal may represent passages for ducts connected to the nasal capsule. A variable number of fairly large foramina are present in the anterior region of the frontal table, and the most lateral of these openings also pierce the dorsal portion of the prefrontal. Similarly, the two nasals are pierced by multiple foramina of variable sizes that are spread across the two elements with no regular pattern. The increased number of openings is localized in the surroundings of the nasal chamber. I consider that at least some of these foramina are connected to the nasal chamber and possibly serving as exits for fluid collecting ducts branching from the nasal glands. This system would facilitate the excretion of the extra salt ingested with the consumption of seawater and marine algae and could explain the formation of salt crusts typically covering the snout of *Amblyrhynchus*. With the current data, it is premature to precisely identify which of the additional foramina may serve this function and which are simply related to vascularization, but considering their position, it is fairly reasonable to interpret them as part of the complex nasal capsule system that the marine iguana has developed to sustain its highly specialized diet. Dunson (1969) analysed the marine iguana salt glands by collecting samples from within the nostrils and from cloacal excretions of several specimens of marine iguana. He concluded that marine iguanas have a higher secretory capacity in comparison to most reptiles, and they can excrete solutions with high concentrations of both Na and K ions. He also hypothesized that *Amblyrhynchus* must have a large salt gland above the orbit, similar to that observed in many sea-going birds, with a connecting duct between the gland and the nasal capsule. Based on my analysis of the skull bones, I find it more likely that enlarged salt glands are set within the orbitonasal chamber, extensively invading the anterior portion of the frontal (Fig. 2.9). The excretion of the extra salt would be facilitated by the increased number of foramina found all over the snout, in addition to the sneezing through the

external nares. This would also explain the constant formation of salt crystals on the head of *Amblyrhynchus*, which tend to cover the large osteoderms located at the level of the fronto-nasal region (Fig. 2.32A, C). New investigations on the soft tissue anatomy of the marine iguana are necessary to elucidate more about its modified nasal capsule, and in particular the salt glands and complete system of salt excretion. Systematic dissections and CT-scans of marine iguana skulls with contrasting agents will be required to further corroborate my hypothesis.

2.4.3 Nasal capsule, salt excretion, and integument

Further study is also required regarding the interaction between the modified nasal capsule system and the integument of the skull. If at least some of the additional foramina I identified on the snout of *Amblyrhynchus* are there for the excretion of excess salt, the integument must certainly play a role in osmoregulation. This may explain the difference I observed in integumentary ossifications between the marine and land iguanas of the Galápagos (Fig. 2.32). In *Conolophus subcristatus* there are large extra ossifications found on the outer surface of several skull roof bones that are particularly well-developed in specimens of medium and large sizes; in skeletonized specimens of *Amblyrhynchus* the same bones are all fairly smooth, with few exceptions (i.e., the prefrontal boss, some mild bumps on the anterior frontal, and the postorbital boss). However, in wet specimens of *Amblyrhynchus* well developed integumentary structures are visible all over the head. These osteoderms have also been previously reported in *Amblyrhynchus* by de Queiroz (1987). The difference in osteoderms between *Amblyrhynchus* and *C. subcristatus* seems to be similar to what has been described for *Heloderma suspectum* and *Varanus komodoensis* in terms of relationship with the underlying bones (Maisano et al. 2019). While both *H. suspectum* and *V. komodoensis* have cephalic

osteoderms, only in *H. suspectum* do they fuse to the underlying bones; in *V. komodoensis* the osteoderms are never fused to the cranial bones. When osteoderms fuse to the underlying bones, the superficial structure of those bones is deeply altered. The sutures between bones can be obliterated as the osteoderm pattern does not necessarily match the geometry of the underlying bones. The lack of fusion of the integumentary ossifications to the skull bones in *Amblyrhynchus* could be related to its modified nasal system and the need to maintain an effective osmoregulation between the internal nasal capsule and the outside environment for the excretion of the excessive salt. To date, there are virtually no data available about integumentary ossifications in my study organism or iguanids in general. Additional histological analyses and μCT-scans of specimens are necessary to collect more data.

2.4.4 Feeding mechanics

The feeding mechanics in *Amblyrhynchus* are clearly linked to unique adaptations of muscle attachments on the skull as well as the peculiar shape of its teeth. As described for the first time by Carpenter (1966), the marine iguana twists its head sideways while feeding, to graze algae off the rocks with its bluntly cusped teeth. The teeth are all similar in size, with three rounded cusps on their crowns (Fig. 2.33). The crown as a whole is concave lingually, while gently convex labially. The teeth can be detached from the jaw when the soft tissues are removed with not much effort which means the attachment is weak. In fact, most of the specimens I analysed lost numerous teeth during the skeletonization process, or they fell out while manipulating the material for study. Blunt cusps and the greater role of soft tissues in tooth attachment in *Amblyrhynchus* make sense considering its feeding style. The rocks from which marine iguanas scrape the algae are an incredibly hard substrate and pointed cusps would be

easily damaged; a significant amount of soft tissues involved in attachment of the dentition would serve well for shock absorption while the teeth are grinding against the hard substrate. From a macroscopic point of view, *Amblyrhynchus* has all the features expected in an *Iguana*-type of tooth implantation *sensu* LeBlanc et al. (2020b). While proper histological studies will be necessary to uncover more details regarding tooth attachment in the marine iguana, it is reasonable to expect some variation in the arrangement or composition of the attachment tissues due to the animal specialized feeding behaviour.

I found evidence of increased musculature attachment in several bones of the skull in *Amblyrhynchus*, and some of these structures are autopomorphic. The postorbital dorsal fossa is one of the most obvious (Figs. 2.13A, C; A2.1A; A2.2B, F). Nothing resembling this fossa can be found in any other closely related iguanid or iguanians in general. The dorsal flange of the postorbital is deflected medially offering a large area for the fossa to be formed and to serve as an aponeurotic surface. Muscle anatomy for iguanas is largely based on dissections of *Iguana iguana* and *Ctenosaura pectinata*, neither of which has a similar structure on the postorbital. Another aponeurotic attachment that represents a unique structure in *Amblyrhynchus* is located on the posterolateral wall of the parietal supratemporal process (Figs. A2.1A; A2.2B, F). It is a squared shaped concavity close to the posterior corner of this process that develops fairly late in ontogeny, as smaller size specimens do not display it. This differs from the postorbital fossa that is present even in the youngest individuals. Based on topology, it seems likely that the muscles involved with the postorbital fossa and the parietal supratemporal concavity are the *m. adductor mandibularis externus* and/or the *m. pseudotemporalis*, both of which play a major role in the movement of the jaws (cf. Oelrich 1956; Oldham & Smith 1975; Wilken et al. 2019). There are features associated with muscle attachment in the mandible as well, which are particularly well-

developed in *Amblyrhynchus* but commonly present across iguanids. These include for instance the adductor crest on the lateral surface of the surangular, the angular process of the articular, and the adductor crest on the coronoid. All together these characteristics contribute to a robust and powerful cranium that is functional to a highly specialised feeding system unique to *Amblyrhynchus*. The shortened snout facilitates the scraping of algae from the rocks in a high energy intertidal zone. Such a blunt shape is greatly advantageous in allowing for a larger toothed portion of the skull to be in contact with the rock surface while the head keeps moving from side to side to scrape and tear off the algae.

2.4.5 Crista interfenestralis

Another difference that stands out between *Amblyrhynchus* and all other iguanids is the absence of the crista interfenestralis of the otoccipital (Figs. 2.23B; 2.24B, D, F). When present, the crista interfenestralis makes up the anterior wall of the occipital recess, located on the lateral side of the braincase (Oelrich 1956). The occipital recess is lined posteriorly by the crista tuberalis and prevents the exposure of the LARST in lateral and anterior view. In *Amblyrhynchus*, the crista tuberalis is well-developed but there is no crista interfenestralis (and occipital recess), and as a result the LARST is fully exposed (Fig. 23B). In *Conolophus* the occipital recess is well-defined and the LARST is not exposed in either anterior or lateral view. Interestingly, a crista interfenestralis can be absent in some other marine lizards such as the extinct mosasaurids.

The halisaurine *Phosphorosaurus ponpetelegans* has a well-preserved and complete braincase and there is no additional crest between the crista prootica and the crista tuberalis (cf. Konishi et al. 2015). As a result, there is no occipital recess and the LARST is exposed in

anterior and lateral view, similarly to *Amblyrhynchus*. Rieppel & Zaher (2000) describe a crista interfenestralis in *Platecarpus* sp., however, in their reconstruction they label the exposed LARST as the occipital recess (Rieppel & Zaher 2000: Fig. 2). The two structures are not the same. The occipital recess is a large opening that is formed by the crista interfenestralis anteriorly and the crista tuberalis posteriorly, and only present if both crests are present. The LARST is an exit foramen on the lateral wall of the exoccipital, which cannot be seen directly if an occipital recess is formed by the two crests (Oelrich 1956). I personally analysed a variety of mosasaurid specimens and a crista interfenestralis is indeed present for instance in *Platecarpus* (AMNH 1820). The crest is poorly developed and not large enough to form an occipital recess with the crista tuberalis, so the LARST is exposed in lateral view similarly to *Amblyrhynchus* and *Phosphorosaurus*. Cuthbertson et al. (2015) described the braincase in *Plioplatecarpus peckensis*: the crista interfenestralis is not mentioned in the study, however, it is clear from the figures that the condition is similar to *Platecarpus* (AMNH 1820) (i.e., the crista interfenestralis is weakly developed) (see Cuthbertson et al., 2015: Figs. 2.2C, 2.3E). Overall, the crista interfenestralis is either absent or weakly developed in mosasaurids and this suggests that the loss or reduction of this structure may be a functional adaptation to the marine environment.

A crista interfenestralis is absent also in most chamaeleonids (pers. obs.). However, this seems to be a result of the miniaturization and complete rearrangement of the basicranial, suspensorial, and temporal regions of the skull. In other miniaturized lizards, such as *Anolis* (iguanian), *Ablepharus* (skink), and *Sphaerodactylus* (gecko), the crista is weakly developed (cf. Daza et al. 2008; Handschuh et al. 2019; pers. obs.).

The crista interfenestralis serves for the attachment of the columellar fold *sensu* Oelrich (1956), which plays a role in the auditory system. The columellar fold represents an extension of

the tympanic membrane and divides the tympanic cavity into a medial and lateral chamber. The lack of the crista interfenestralis may reflect the lack of a columellar fold and hence of a separation of the tympanic cavity and overall reduction of the tympanic membrane in swimming animals. An inconspicuous or reduced tympanic membrane makes the difference for instance in the auditory system of sea turtles in comparison to terrestrial turtles (Hetherington 2008). The function of the tympanic membrane is to produce vibrations when sound waves reach the ear, and the transmission of sound waves underwater is significantly lower than land (Hetherington 2008; Manley 1972; Saunders et al. 2000). In marine turtles the membrane is reduced and hardened, and Hetherington (2008) relates this to the fact that underwater, bone conduction of vibrations becomes more effective than resonance via a soft membrane. Limiting sound reception to an undivided tympanic cavity mostly made by bone would be beneficial, as it better resonates vibrations in an environment where sound localization is more difficult. As there are no specific studies on the tympanic system of neither living or fossil marine squamates, I do not have enough data to further speculate on the topic. However, it is interesting that *Amblyrhynchus* shares the lack of a crista interfenestralis with other marine lizards, while closely related iguanids have a well-developed crest, hinting strongly that this absence is linked to the unique lifestyle of the marine iguana.

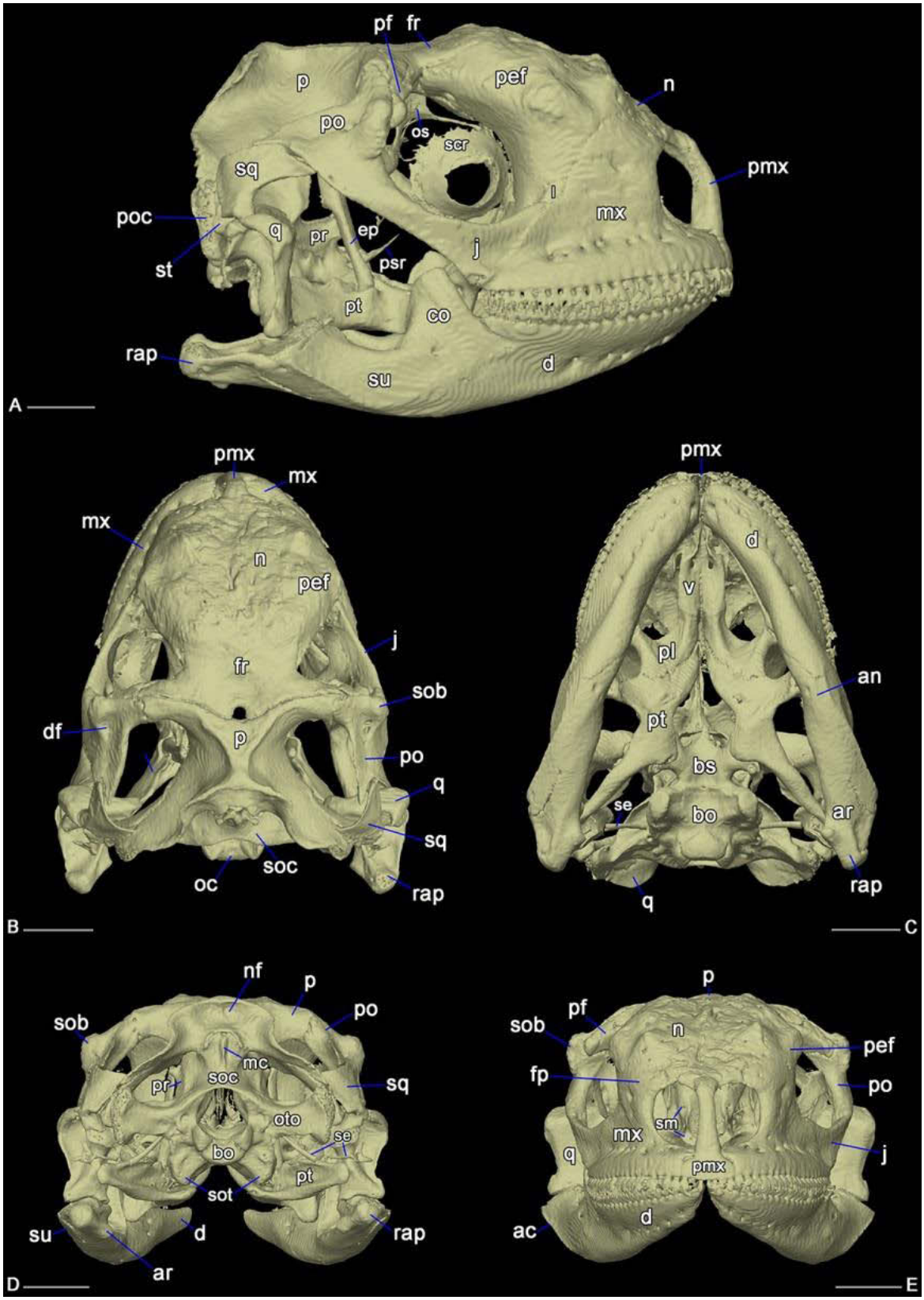
pf
fr
p
pef
n
po
os
scr
sq
pmx
l
mx
poc
q
pr
ep
j
st
psr
pt
co
rap
su
d
A
pmx
mx
mx
n
pef
j
fr
sob
df
p
po
q
sq
soc
oc
rap
B
pmx
d
v
pl
an
pt
bs
se
bo
ar
q
rap
C
nf
p
po
sob
mc
pr
soc
sq
oto
se
bo
pt
sot
su
d
rap
ar
D
p
pf
sob
n
pef
fp
po
sm
mx
q
j
pmx
d
ac
E

Figure 2.1. Overview of the cranium of *Amblyrhynchus* UF 41558 in lateral (A), dorsal (B), ventral (C), posterior (D), and anterior (E) views. Abbreviations: a, anterior; ac, adductor crest of the surangular; an, angular; ar, articular; bo, basioccipital; bs, basisphenoid; co, coronoid; d, dentary; df, dorsal fossa of the postorbital; ep, epipterygoid; fp, facial process of the maxilla; fr, frontal; j, jugal; l, lacrimal; mc, mid-sagittal crest of the supraoccipital; mx, maxilla; n, nasal; nf, nuchal fossa of the parietal; oc, occipital condyle; os, orbitosphenoid; oto, otoccipital; p, parietal; pef, prefrontal; pf, postfrontal; pmx, premaxilla; po, postorbital; poc, paroccipital process of the otoccipital; pr, prootic; psr, parasphenoid rostrum; pt, pterygoid; q, quadrate; rap, retroarticular process; scr, sclerotic ring; se, stape; sob, supraorbital boss of the postorbital; soc, supraoccipital; sot, sphenoccipital tubercle; sq, squamosal; st, supratemporal; su, surangular. Scale bars: 1 cm.

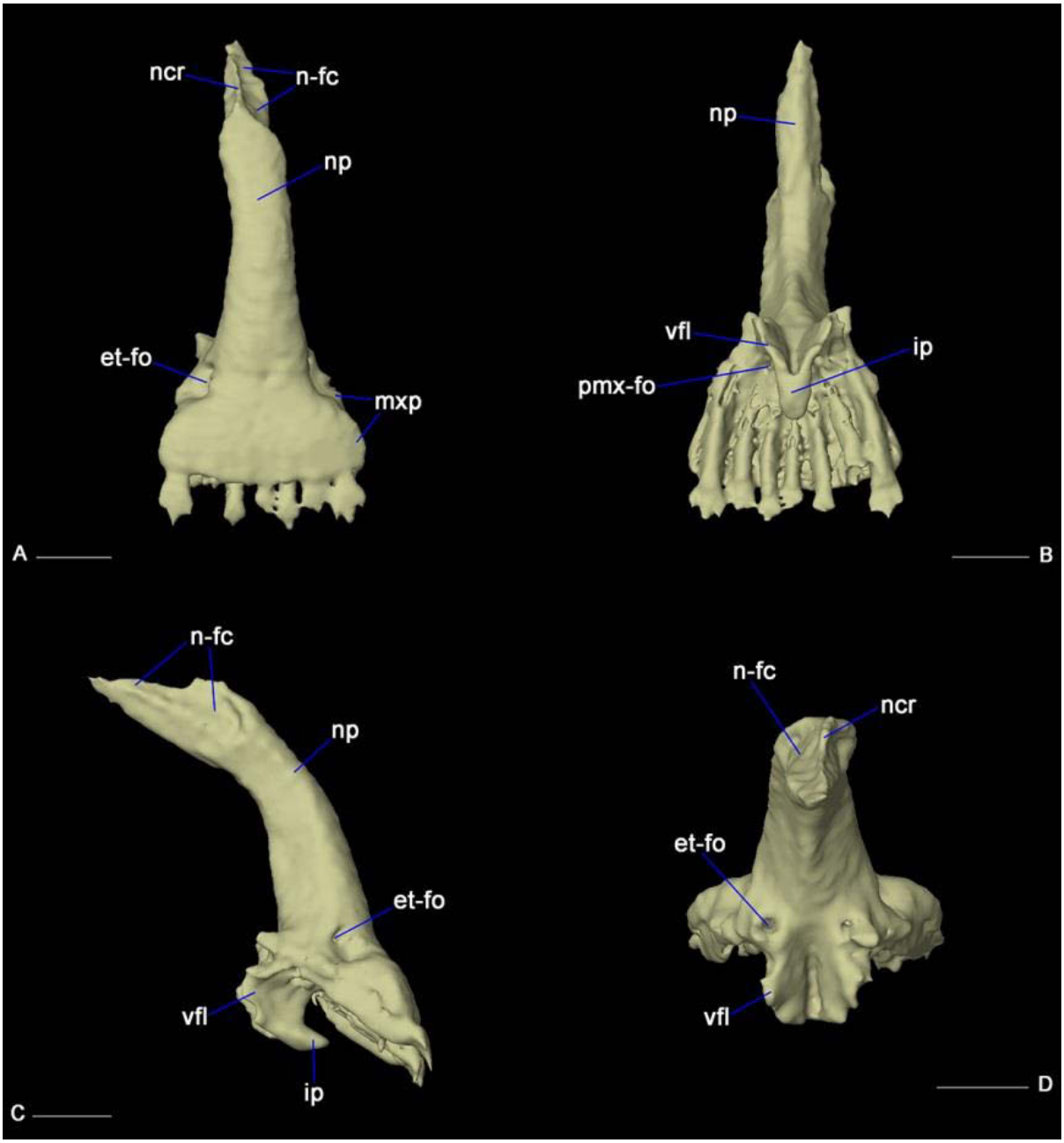

Figure 2.2. Premaxilla of *Amblyrhynchus* UF 41558 in anterior (A), posteroventral (B), lateral (C), and posterodorsal (D) views. Abbreviations: et-fo, ethmoidal foramina; ip, incisive process; mxp, maxillary (lateral) process; ncr, nasal crest; n-fc, facet for nasal; np, nasal (posterodorsal) process; pmx-fo, premaxillary foramen; vfl, vomerine flange.

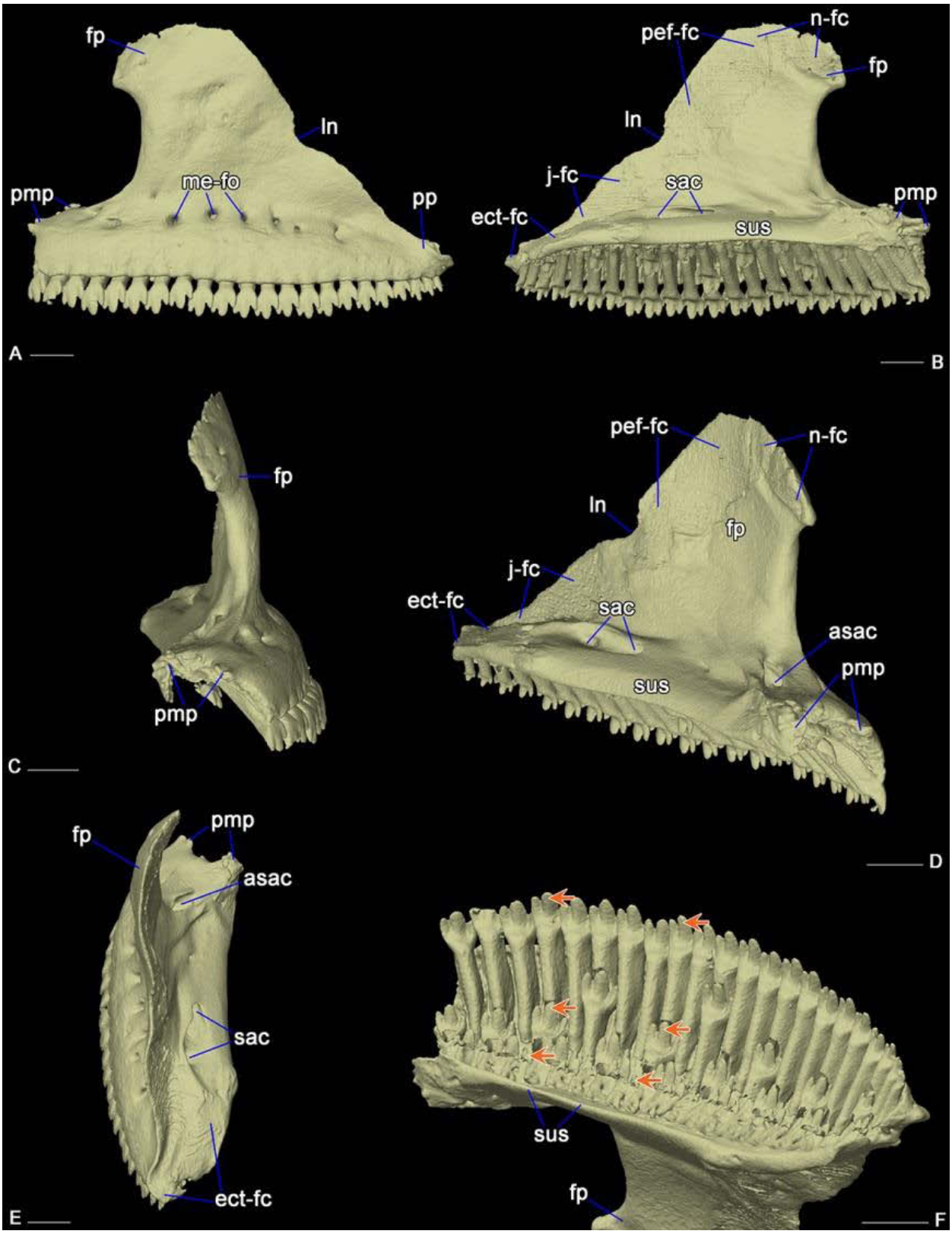
fp
ln
pmp
me-fo
pp
A
pef-fc
n-fc
fp
ln
j-fc
sac
pmp
ect-fc
sus
B
fp
pmp
C
pef-fc
n-fc
ln
fp
j-fc
ect-fc
sac
asac
pmp
sus
D
fp
pmp
asac
sac
ect-fc
E
sus
fp
F

Figure 2.3. Maxilla of *Amblyrhynchus* UF 41558 in lateral (A), medial (B), anterior (C), anteromedial (D), dorsal (E), and posterolingual (F) views. The orange arrows point at the mesial cusp of the crown of different tooth generations. Abbreviations: asac, anterior opening of supralveolar canal; ect-fc, facet for ectopterygoid; fp, facial (mid-dorsal) process; j-fc, facet for jugal; ln, lacrimal notch; me-fo, mental foramina; n-fc, facet for nasal; pef-fc, facet for prefrontal; pmp, premaxillary (anteromedial) process; pp, posterior process; sac, superior alveolar canal; sus, supralveolar (or palatal) shelf. Scale bars: 5 mm.

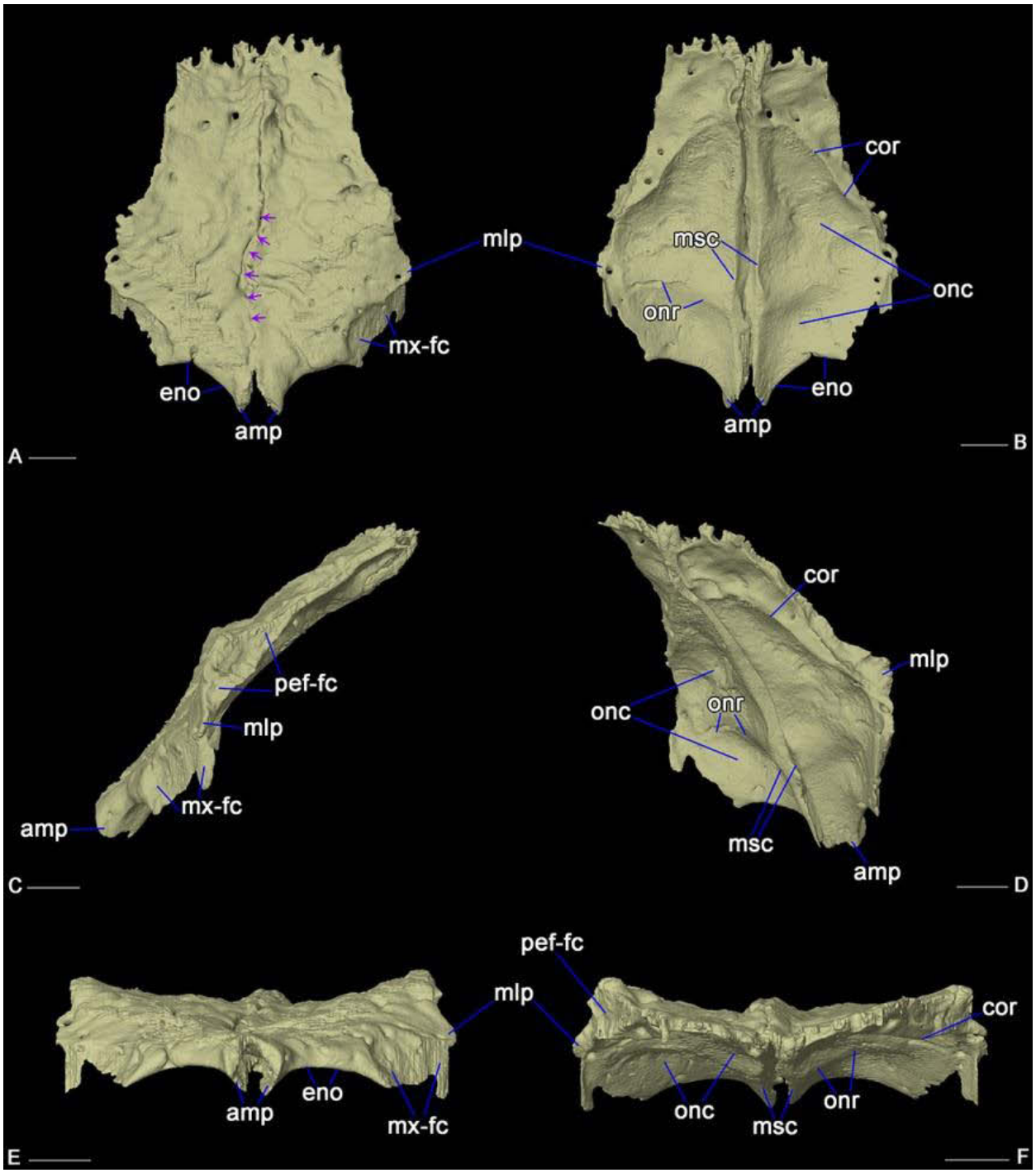

Figure 2.4. Nasals of *Amblyrhynchus* UF 41558 in anterodorsal (A), posteroventral (B), lateral (C), posterolateral (D), ventral (E), and dorsal (F) views. The purple arrows point at the irregular suture between the two nasals. Abbreviations: amp, anteromedial process; cor, conchal ridge; eno, external narial opening margin; mlp, mid-lateral process; msc, mid-sagittal crest; mx-fc,

facet for maxilla facial process; onc, orbitonasal concavities; onr, orbitonasal ridge (between anterior and posterior concavities); pef-fc, facet for prefrontal. Scale bars: 5 mm.

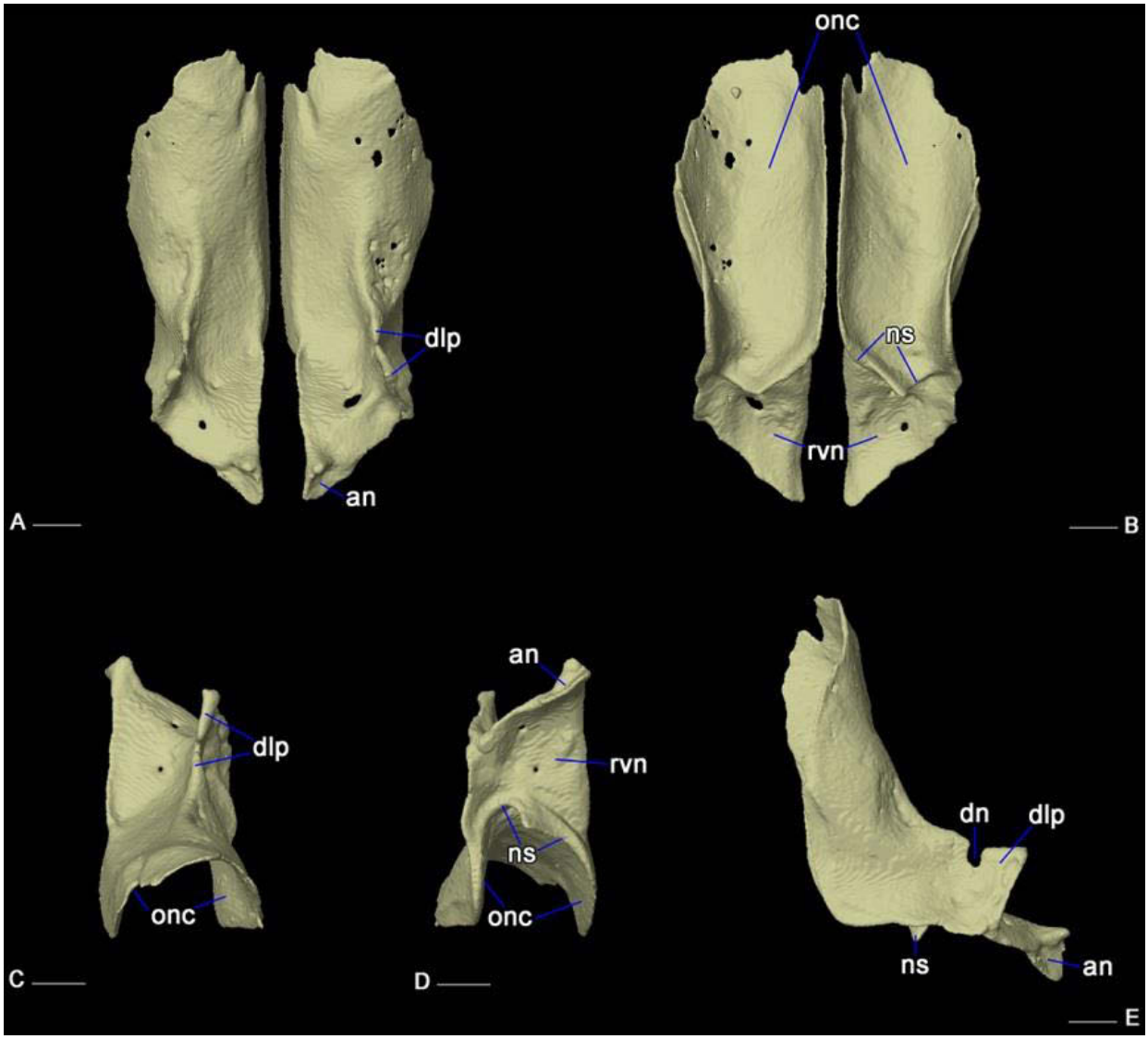

Figure 2.5. Septomaxilla of *Amblyrhynchus* UF 41558 in anterior (A), posterior (B), dorsal (C), ventral (D), and lateral (E) views. Abbreviations: an, anterior notch; dlp, dorsolateral process; dn, dorsal notch; ns, nasal septum; onc, orbitonasal concavity; rvn, roof of vomeronasal organ.

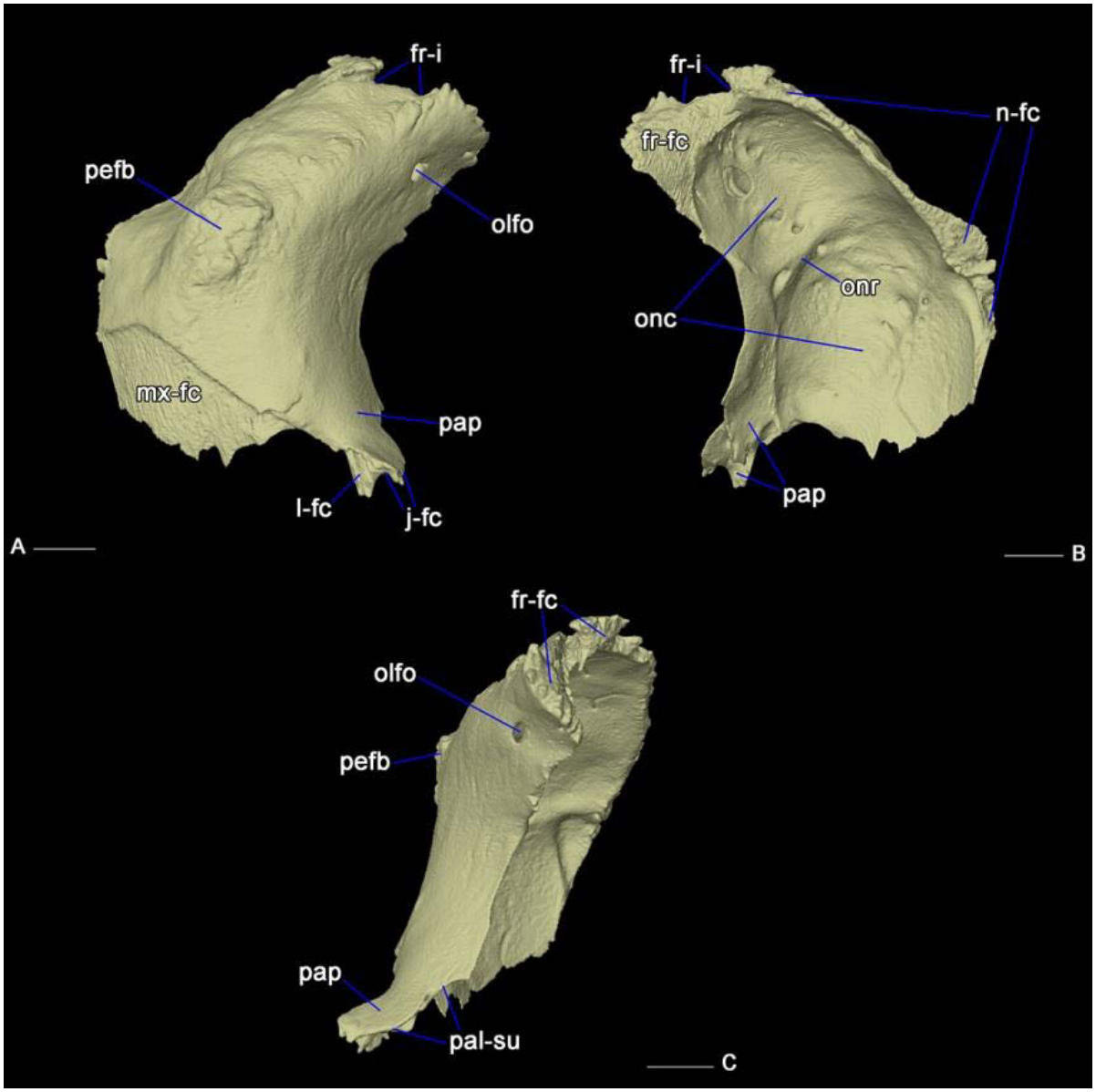

Figure 2.6. Prefrontal of *Amblyrhynchus* UF 41558 in lateral (A), medial (B), and posterior (C) views. Abbreviations: fr-fc, facet for frontal; fr-I, frontal indentation; mx-fc, facet for facial process of maxilla; j-fc, facet for jugal; l-fc, facet for lacrimal; n-fc, facet for nasal; olfo, olfactory foramen; onc, orbitonasal concavities; onr, orbitonasal ridge; pal-su, suture with the palatine; pap, palatine (posteroventral) process; pefb, prefrontal boss. Scale bars: 5 mm.

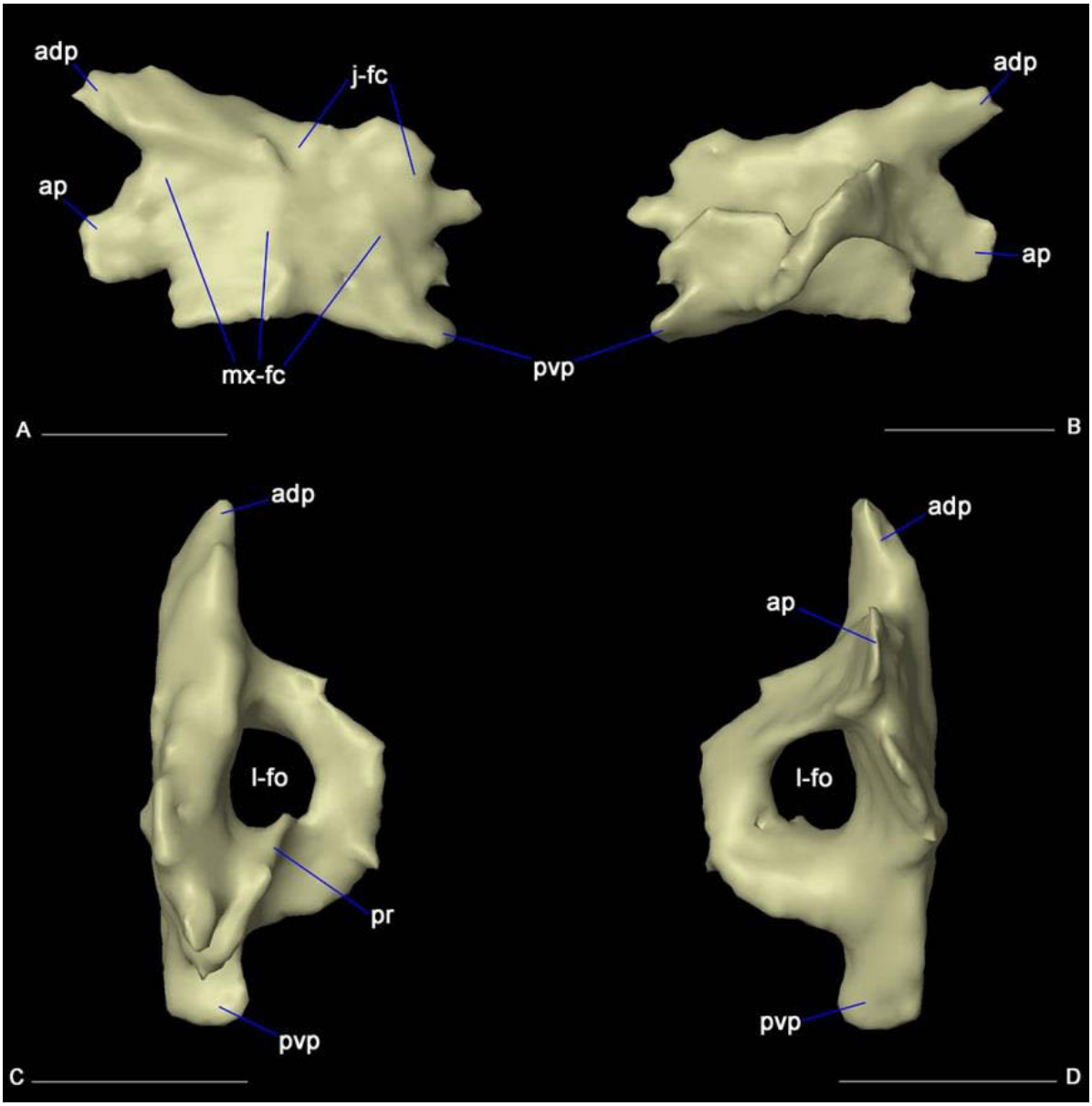

Figure 2.7. Lacrimal of *Amblyrhynchus* UF 41558 in lateral (A), medial (B), dorsal (C), and ventral (D) views. Abbreviations: adp, anterodorsal process; ap, anterior process; j-fc, facet for jugal; l-fo, lacrimal foramen; mx-fc, facet for maxilla; pr, posterior ridge; pvp, posteroventral process. Scale bars: 5 mm.

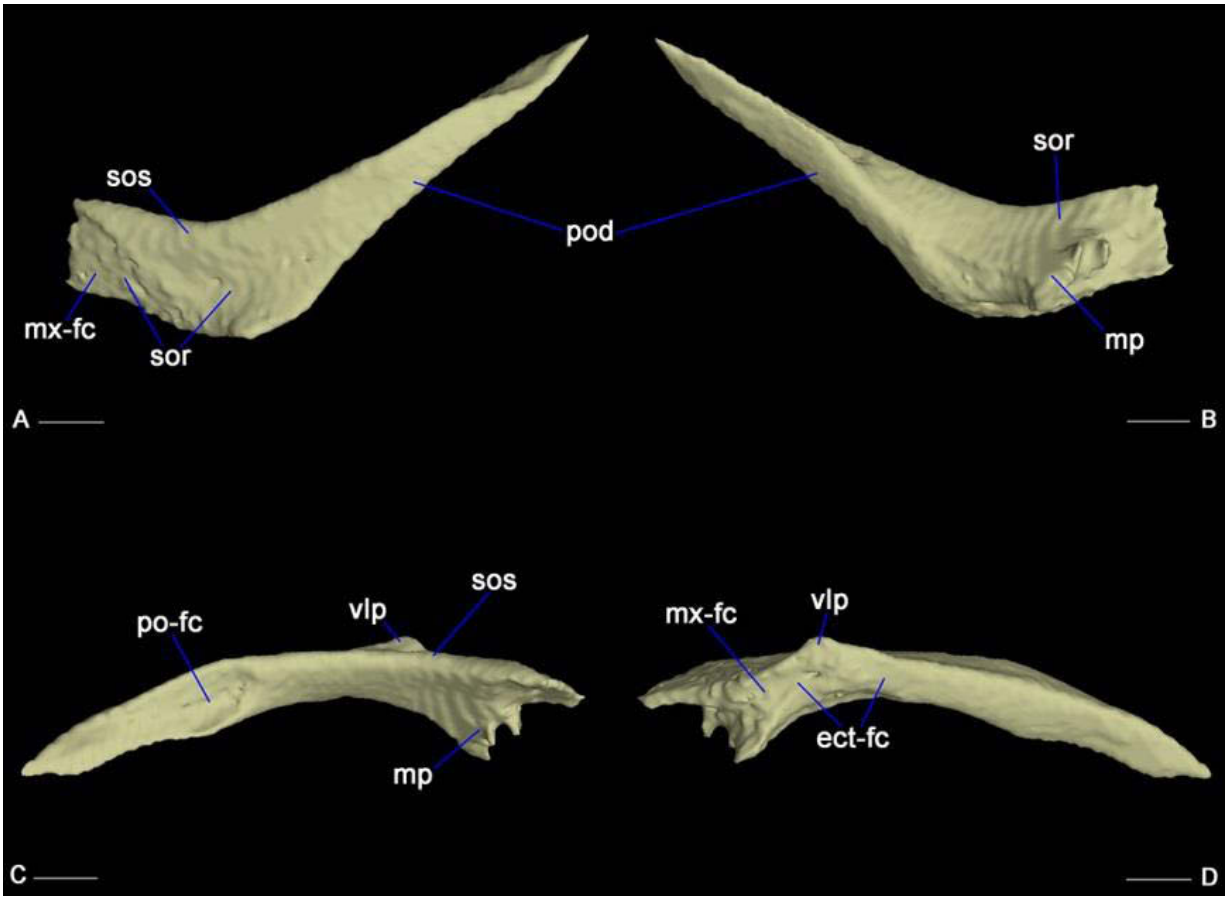

Figure 2.8. Jugal of *Amblyrhynchus* UF 41558 in lateral (A), medial (B), dorsal (C), and ventral (D) views. Abbreviations: ect-fc, facet for ectopterygoid; mp, medial process; mx-fc, facet for maxilla; pod, posterodorsal (or postorbital) process; sor, suborbital ramus; sos, suborbital shelf; vlp, ventrolateral process. Scale bars: 5 mm.

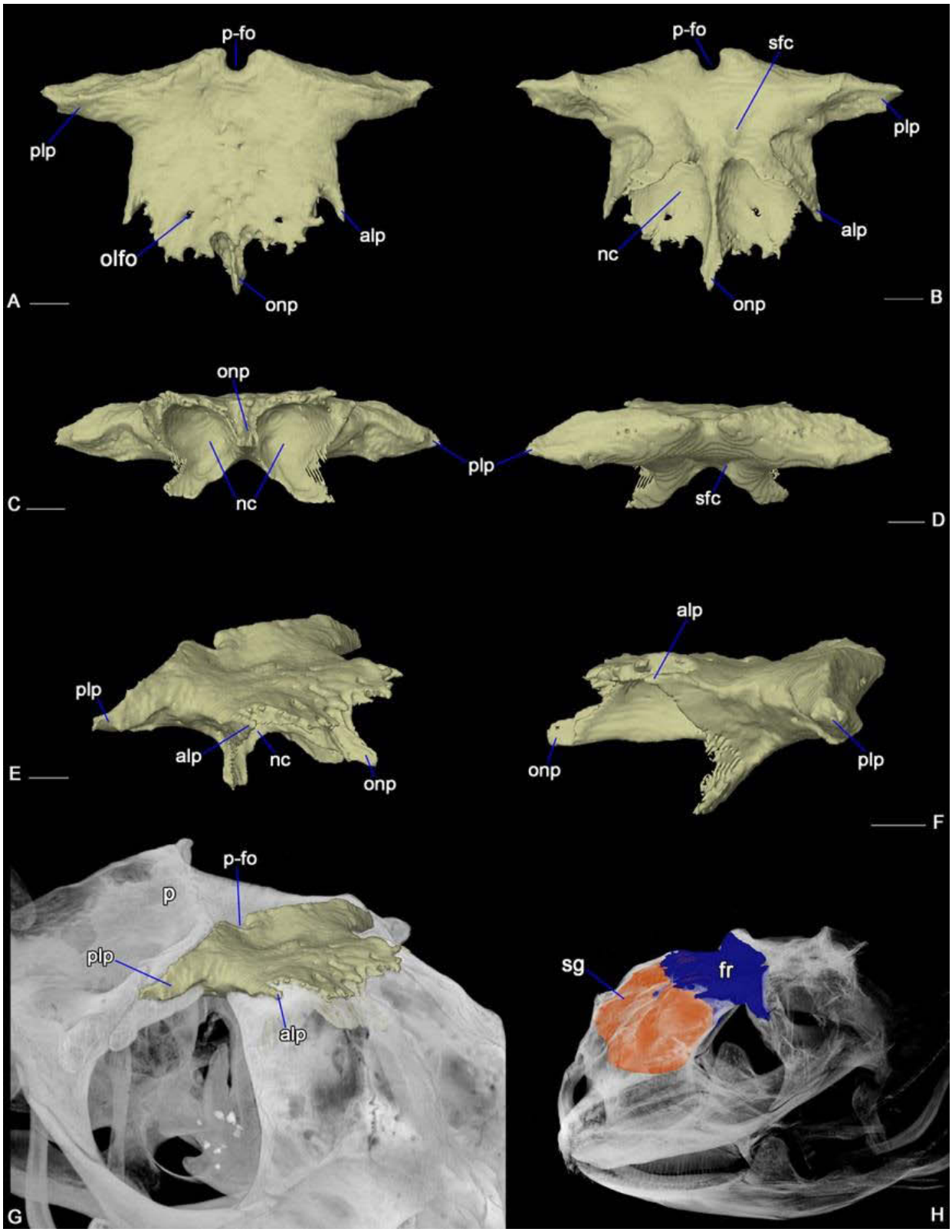
p-fo
plp
olfo
alp
onp
A
p-fo
sfc
plp
nc
alp
onp
B
onp
plp
nc
C
plp
sfc
D
plp
alp
nc
onp
E
alp
onp
plp
F
p-fo
p
plp
alp
G
sg
fr
H

Figure 2.9. Frontal of *Amblyrhynchus* UF 41558 in dorsal (A), ventral (B), anterior (C), posterior (D), dorsolateral (E), and lateral (F) views; position of the frontal and extension of the nasal chamber in dorsolateral view (G, H). Abbreviations: alp, anterolateral process; fr, frontal; nc, nasal concavity; olfo, olfactory foramina; onp, orbitonasal (or anteromedial) process; p, parietal; p-fo, pineal foramen; plp, posterolateral process; sfc, groove for the articulation of the subolfactory canal; sg, space available for enlarged salt glands in the nasal chamber. Scale bars: 5 mm.

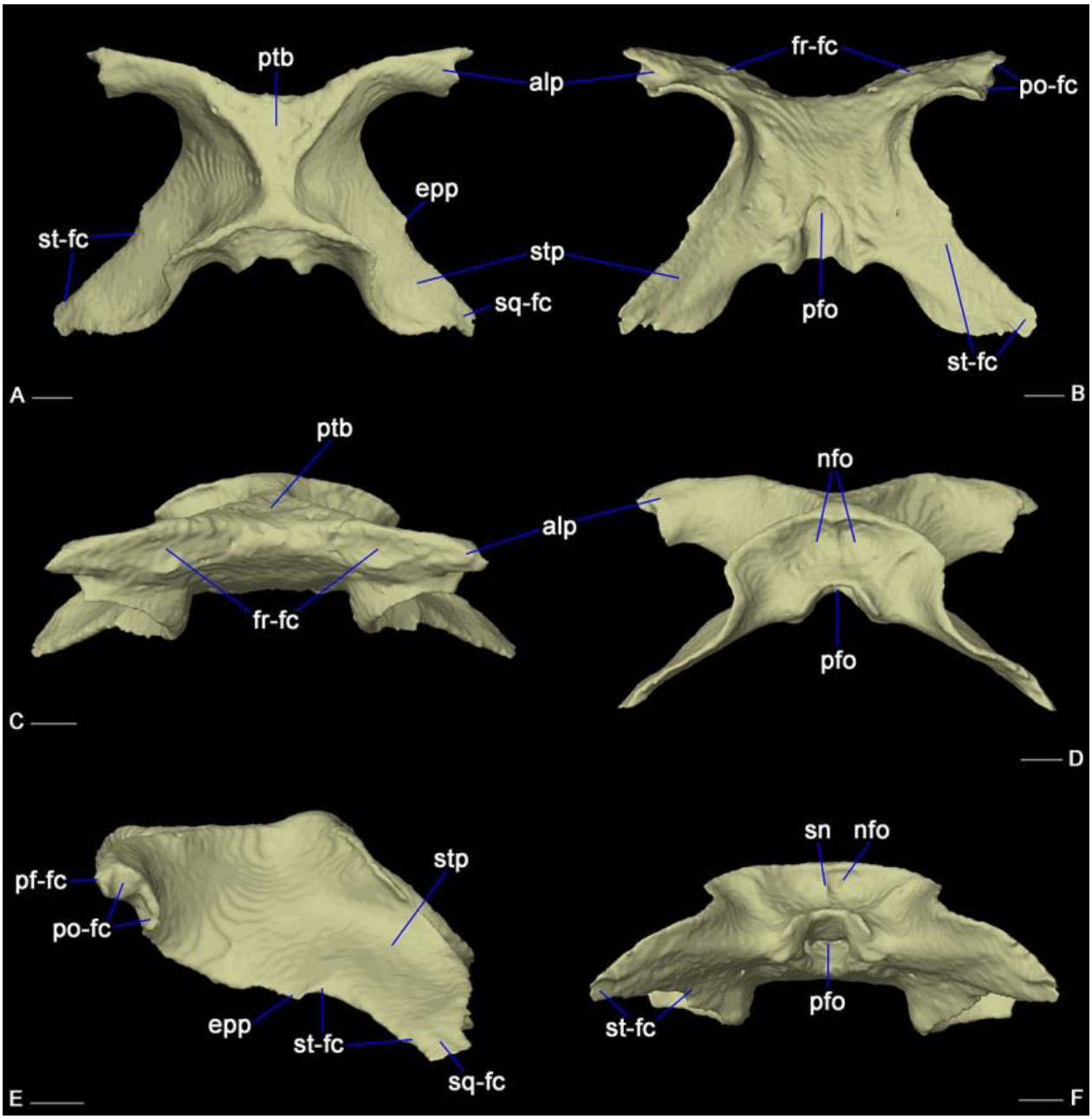

Figure 2.10. Parietal of *Amblyrhynchus* UF 41558 in dorsal (A), ventral (B), anterior (C), posterior (D), lateral (E), and posteroventral (F) views. Abbreviations: alp, anterolateral process; epp, epipterygoid process; fr-fc, facet for frontal; nfo, nuchal fossa; pf-fc, facet for postfrontal; pfo, parietal (ventral) fossa; po-fc, facet for postorbital; ptb, parietal table; sn, septum dividing the nuchal fossa; sq-fc, facet for squamosal; st-fc, facet for supratemporal; stp, supratemporal (posterolateral) process. Scale bars: 5 mm.

Figure 2.11. Variability of the position of the pineal foramen in *Amblyrhynchus*: AMNH 114491 (A), AMNH 29937 (B), and AMNH 29938 (C). All specimens in dorsal view. Abbreviations: fr, frontal; p, parietal. Scale bars: 1 cm.

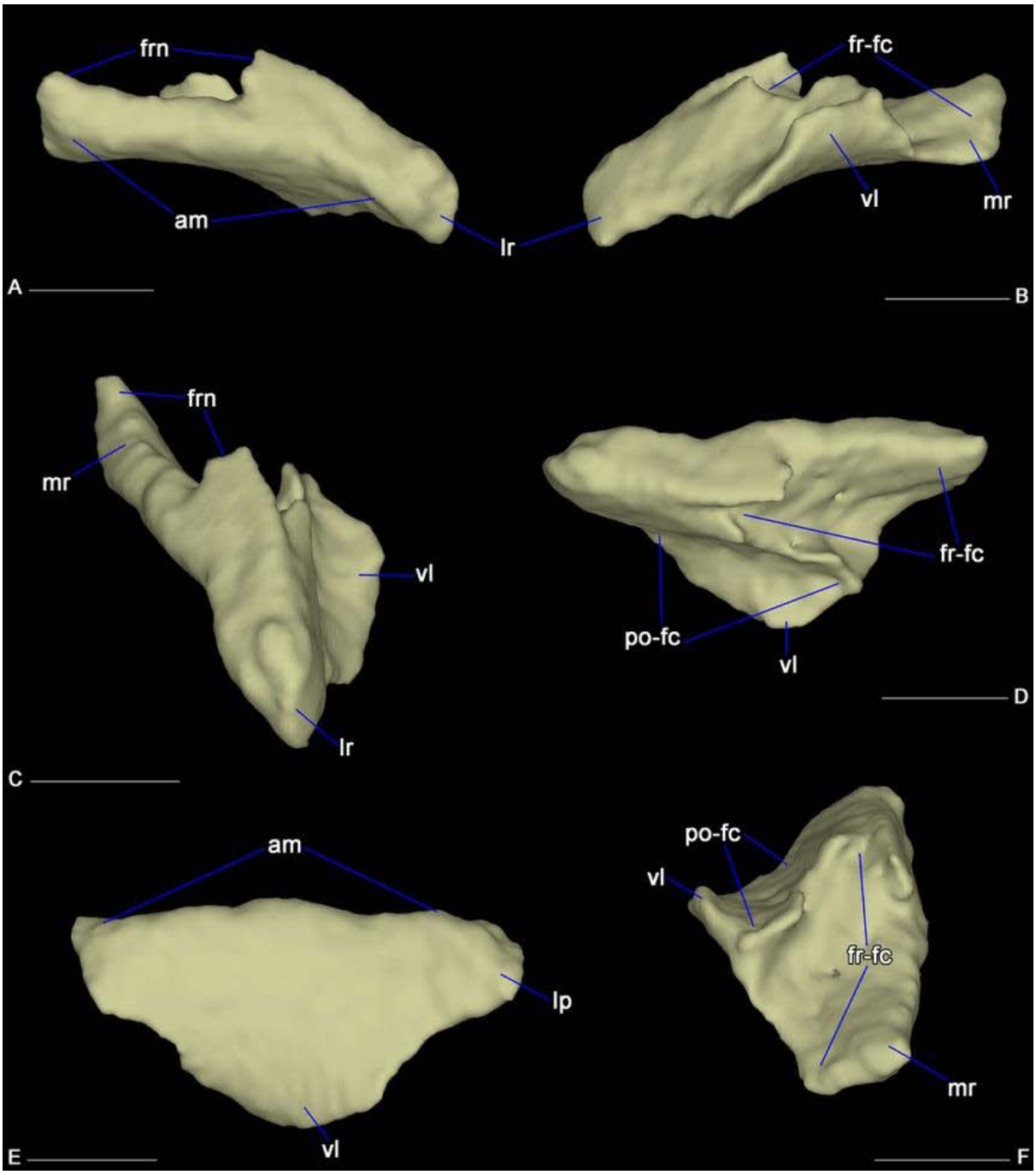

Figure 2.12. Postfrontal of *Amblyrhynchus* UF 41558 in anterior (A), posteroventral (B), dorsolateral (C), posterior (D), ventral (E), and medial (F) views. Abbreviations: am, anterior margin; fr-fc, facet for frontal; frn, frontal notch; lr, lateral ramus; mr, medial ramus; po-fc, facet for postorbital; vl, ventral lappet. Scale bars: 5 mm.

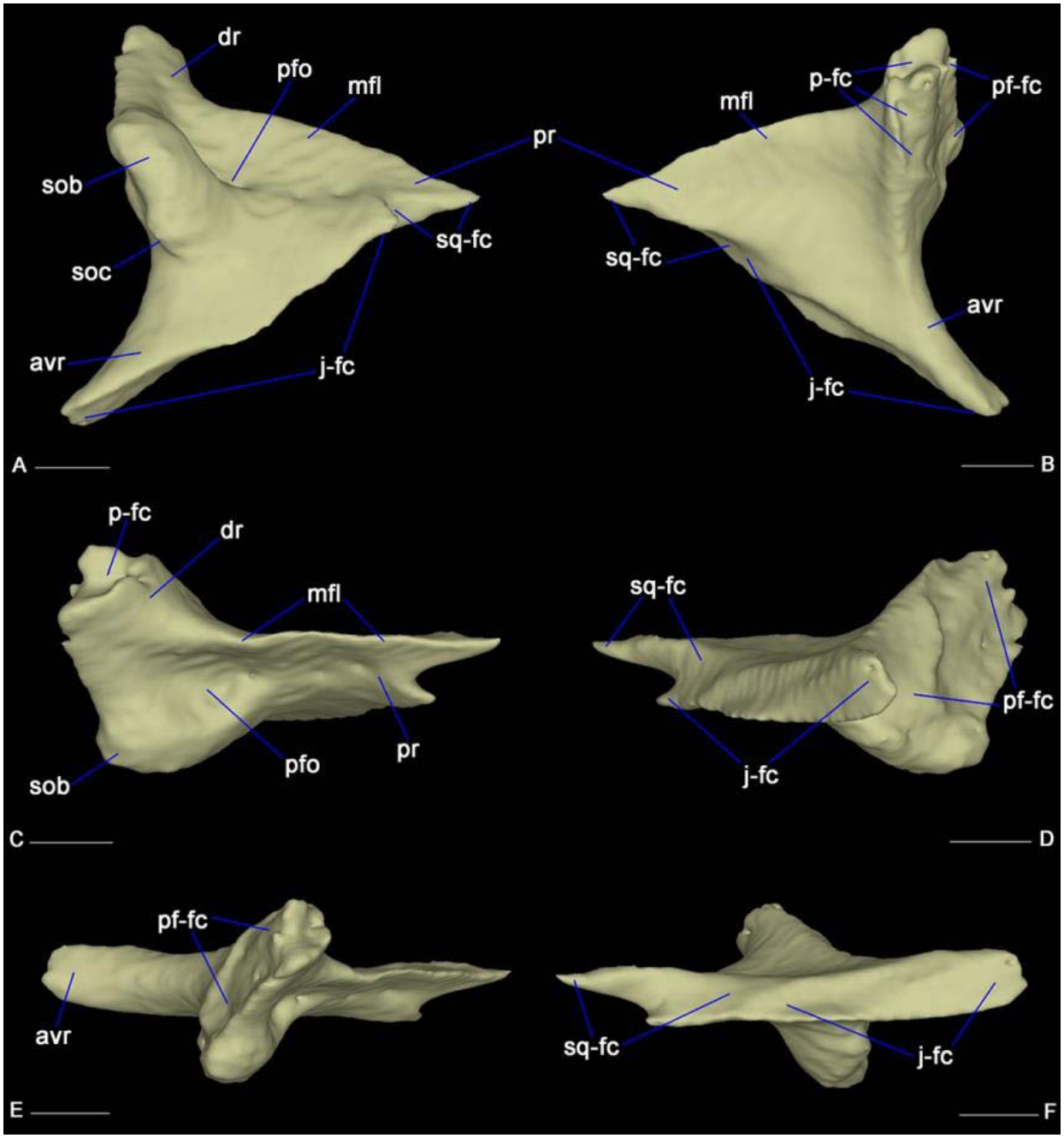

Figure 2.13. Postorbital of *Amblyrhynchus* UF 41558 in lateral (A), medial (B), dorsomedial (C), ventral (D), anterodorsal (E), and posteroventral (F) views. Abbreviations: avr, anteroventral ramus; dr, dorsal ramus; j-fc, facet for jugal; mfl, medially deflected dorsal flange; p-fc, facet for parietal; pf-fc, facet for postfrontal; pfo, postorbital fossa; pr, posterior ramus; sob, supraorbital boss; soc, supraorbital crest; sq-fc, facet for squamosal. Scale bars: 5 mm.

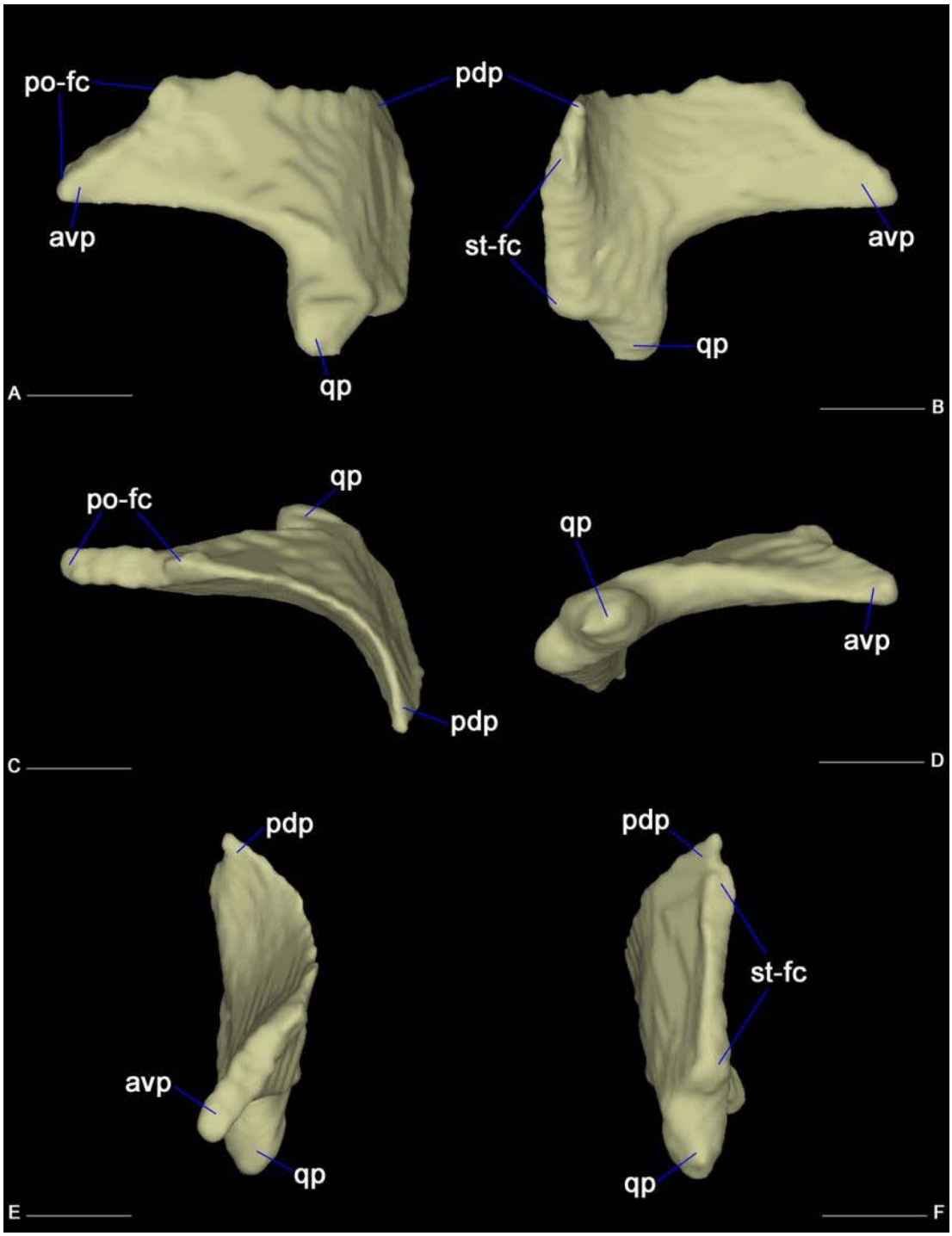

Figure 2.14. Squamosal of *Amblyrhynchus* UF 41558 in lateral (A), medial (B), dorsal (C), ventral (D), anterior (E), and posterior (F) views. Abbreviations: avp, anteroventral process; pdp, posterodorsal process; po-fc, facet for postorbital; qp, quadrate (ventral) process; st-fc, facet for supratemporal. Scale bars: 5 mm.

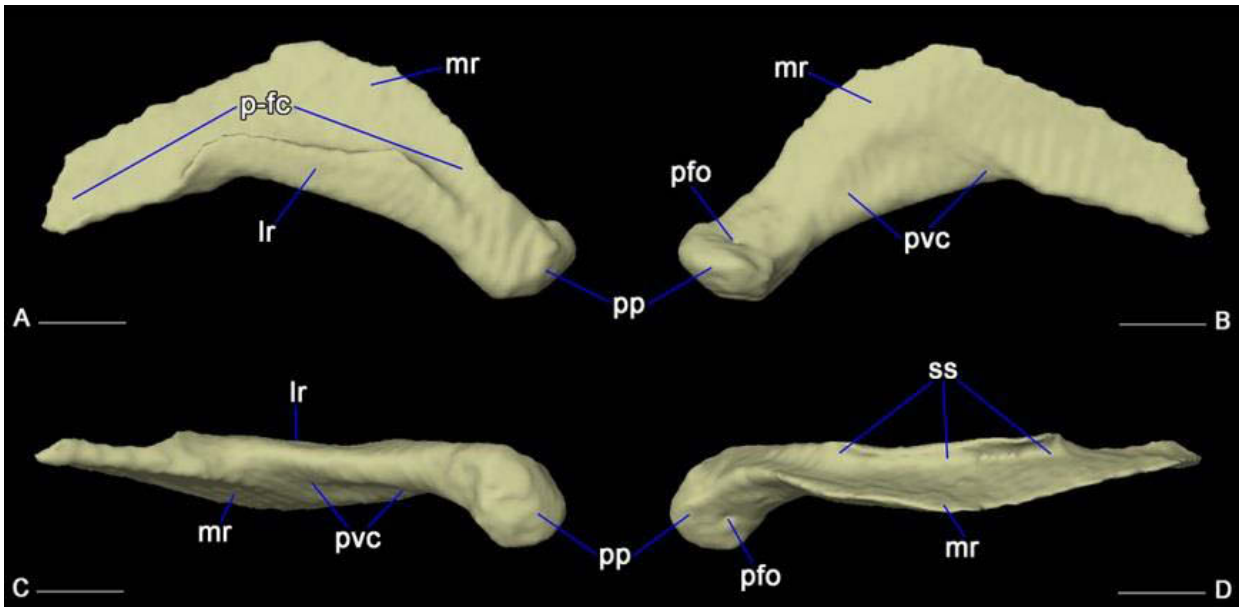

Figure 2.15. Supratemporal of *Amblyrhynchus* UF 41558 in lateral (A), medial (B), ventral (C), and dorsal (D) views. Abbreviations: lr, lateral ramus; mr, medial ramus; p-fc, facet for parietal supratemporal process; pfo, posterior foramen; pp, posterior process; pvc, posteroventral concavity. Scale bars: 5 mm.

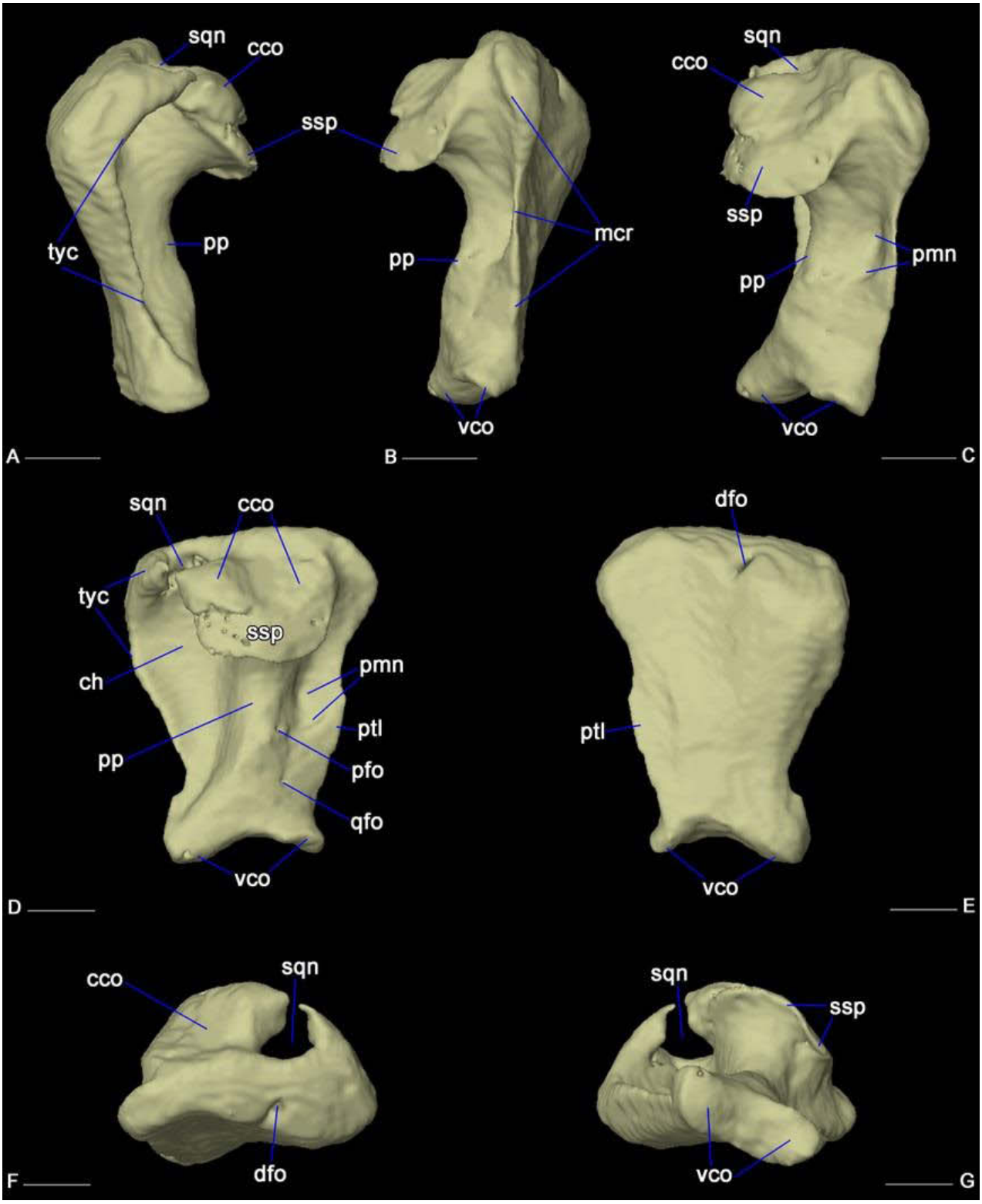

Figure 2.16. Quadrate of *Amblyrhynchus* UF 41558 in lateral (A), medial (B), posteromedial (C), posterior (D), anterior (E), dorsal (F), and ventral (G) views. Abbreviations: cco, cephalic

(dorsal) condyle; ch, conch; dfo, dorsal foramen; mcr, medial crest; pfo, posterior foramen; pmn, posteromedial notch; pp, posterior pillar; ptl, pterygoid lappet; qfo, quadrate foramen; sqn, squamosal notch; ssp, suprastapedial process; vco, ventral condyles. Scale bars: 5 mm.

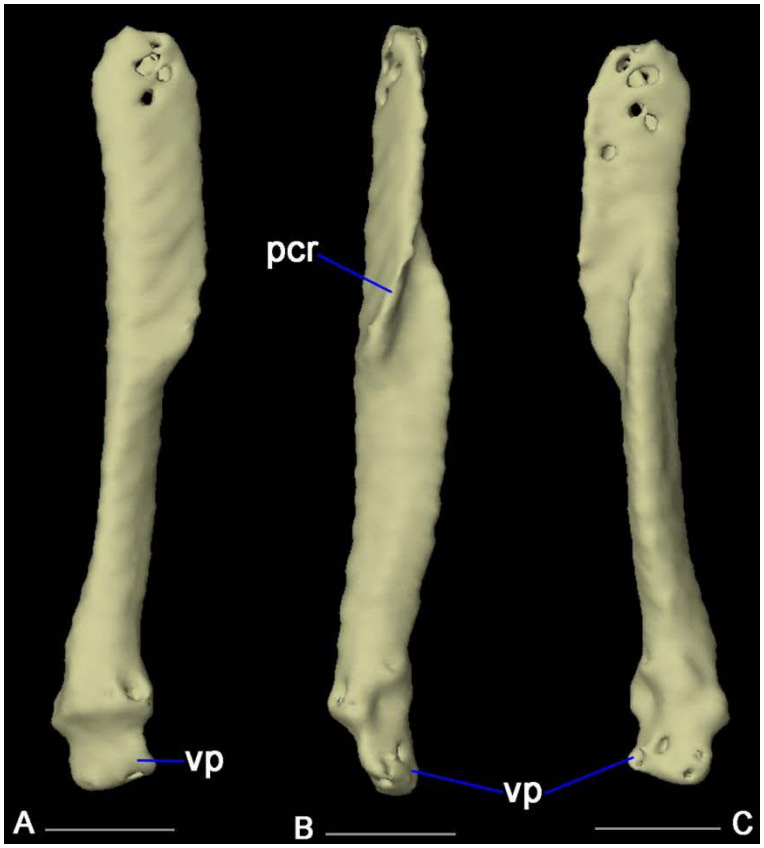

Figure 2.17. Epipterygoid of *Amblyrhynchus* UF 41558 in lateral (A), posterior (B), and medial (C) views. Abbreviations: pcr, posterior crest; vp, ventral process. Scale bars: 5 mm.

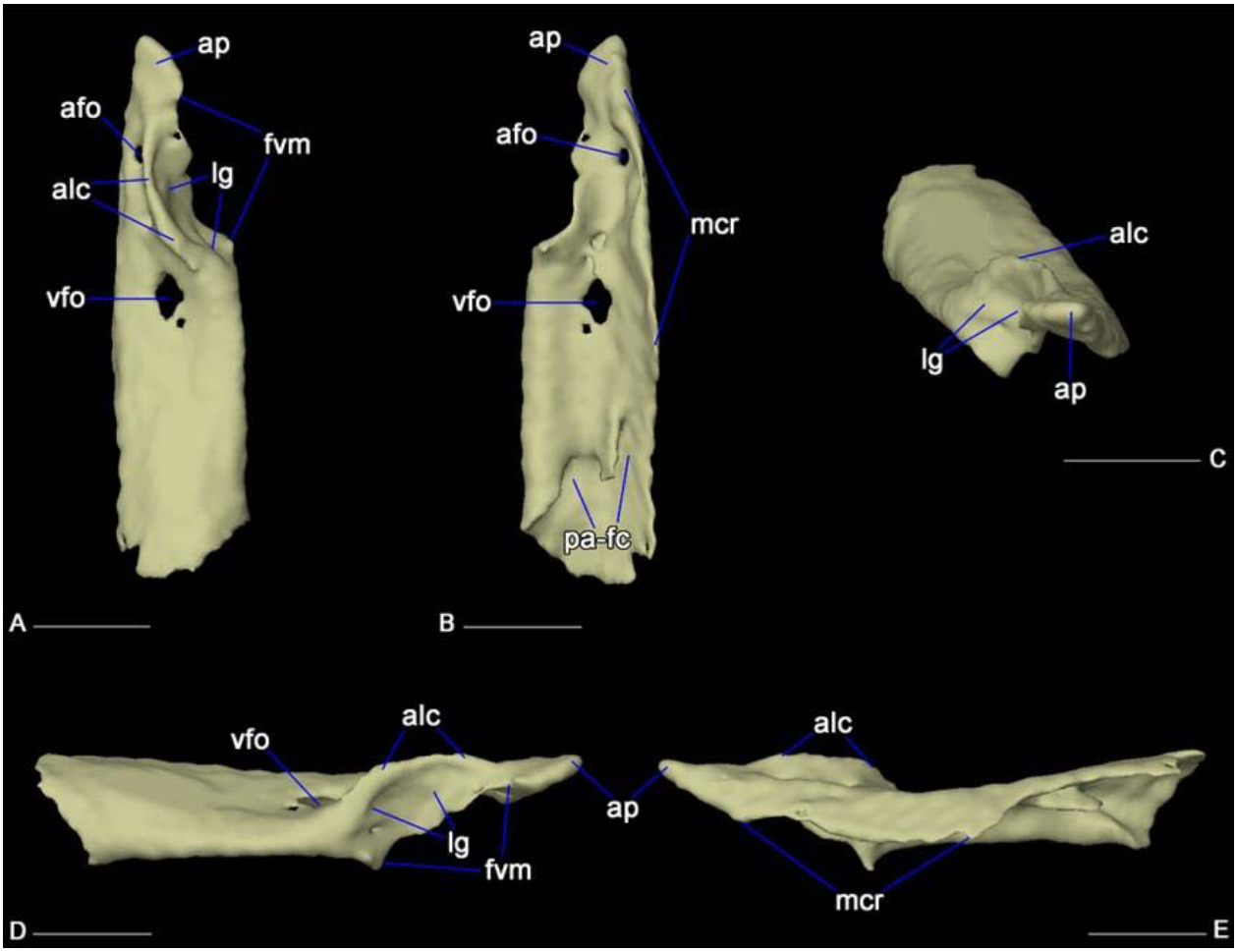

Figure 2.18. Vomer of *Amblyrhynchus* UF 41558 in ventral (A), dorsal (B), anterior (C), lateral (D), and medial (E) views. Abbreviations: afo, anterior foramen; alc, anterolateral crest; ap, anterior process; fvm, fenestra vomeronasalis margin; lg, lacrimal groove; mcr, medial crest; vfo, vomerine foramen. Scale bars: 5 mm.

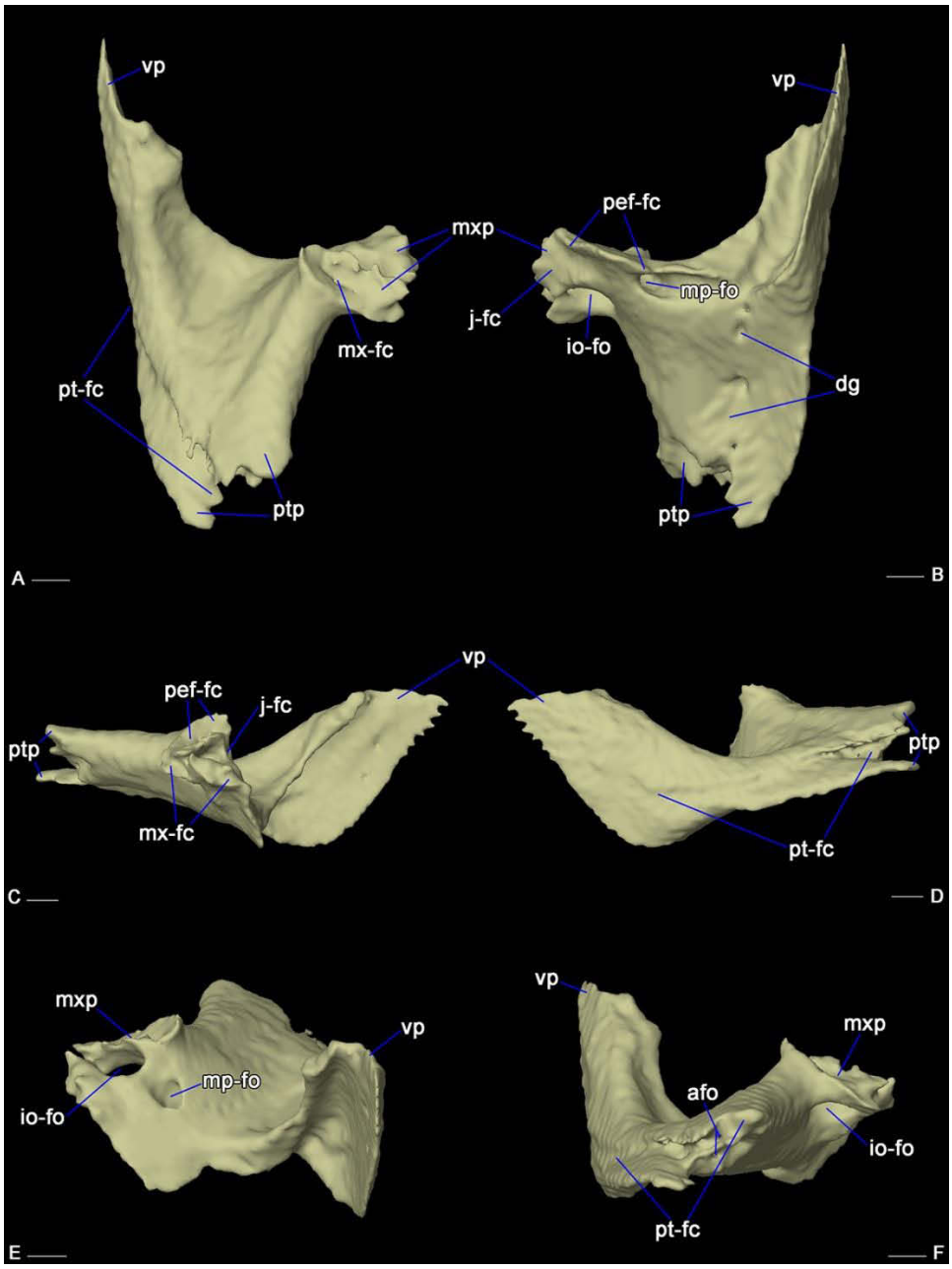

Figure 2.19. Palatine of *Amblyrhynchus* UF 41558 in ventral (A), dorsal (B), lateral (C), medial (D), anterior (E), and posterior (F) views. Abbreviations: afo, anterior foramina; dg, dorsal palatine groove (with aligned foramina); io-fo, infraorbital foramen; j-fc, facet for jugal; mp-fo, maxillo-palatine foramen; mx-fc, facet for maxilla; mxp, maxillary (lateral) process; pt-fc, facet for pterygoid; ptp, pterygoid (posterior) process; vp, vomerine (anterior) process. Scale bars: 5 mm.

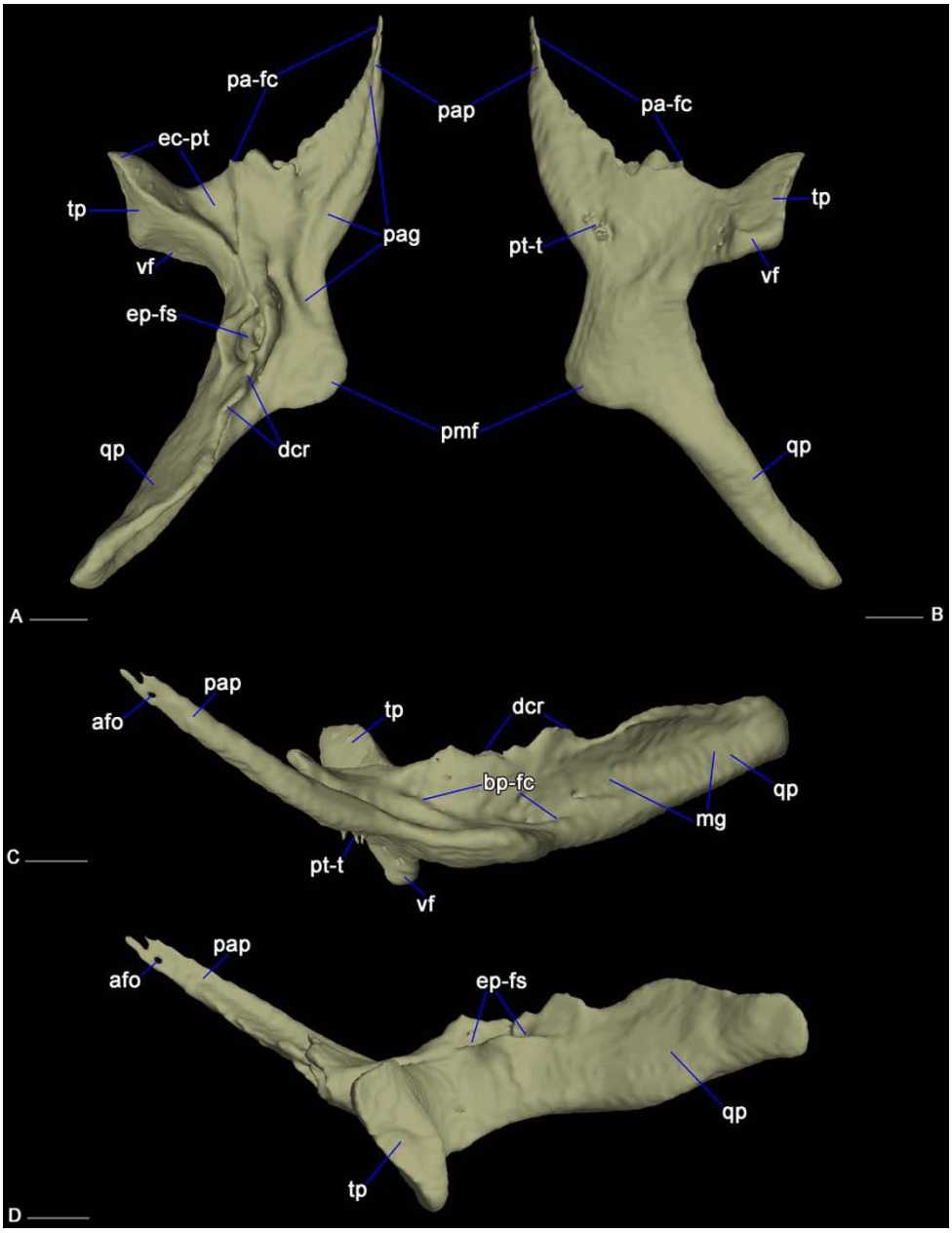

Figure 2.20. Pterygoid of *Amblyrhynchus* UF 41558 in dorsal (A), ventral (B), medial (C), and lateral (D) views. Abbreviations: afo, anterior foramen; bp-fc, facet for basipterygoid process; dcr, dorsal crest; ep-fs, deep fossa for the articulation of the epipterygoid; mg, medial groove of quadrate process; pa-fc, facet for palatine; pag, groove for the articulation of the palatine; pap, palatine process; pmf, posteromedial flange; pt-t, pterygoid teeth; qp, quadrate process; tp, transverse process; vf, ventral flange. Scale bars: 5 mm.

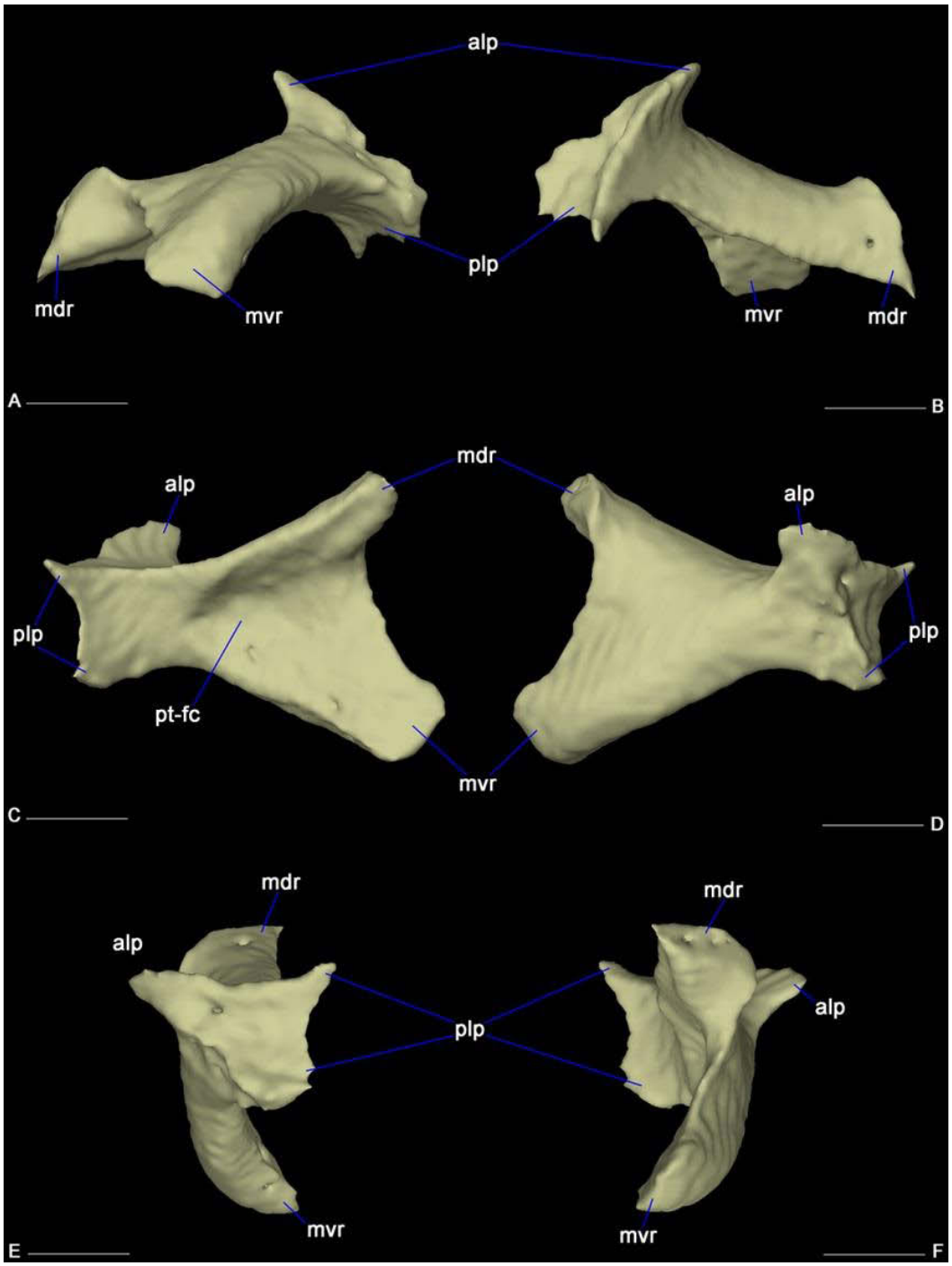

Figure 2.21. Ectopterygoid of *Amblyrhynchus* UF 41558 in ventral (A), dorsal (B), posterolateral (C), anteromedial (D), dorsolateral (E), and posteromedial (F) views. Abbreviations: alp, anterolateral process; mdr, dorsal ramus of the medial process; mvr, ventral ramus of the medial process; plp, posterolateral process; pt-fc, pterygoid facet. Scale bars: 5 mm.

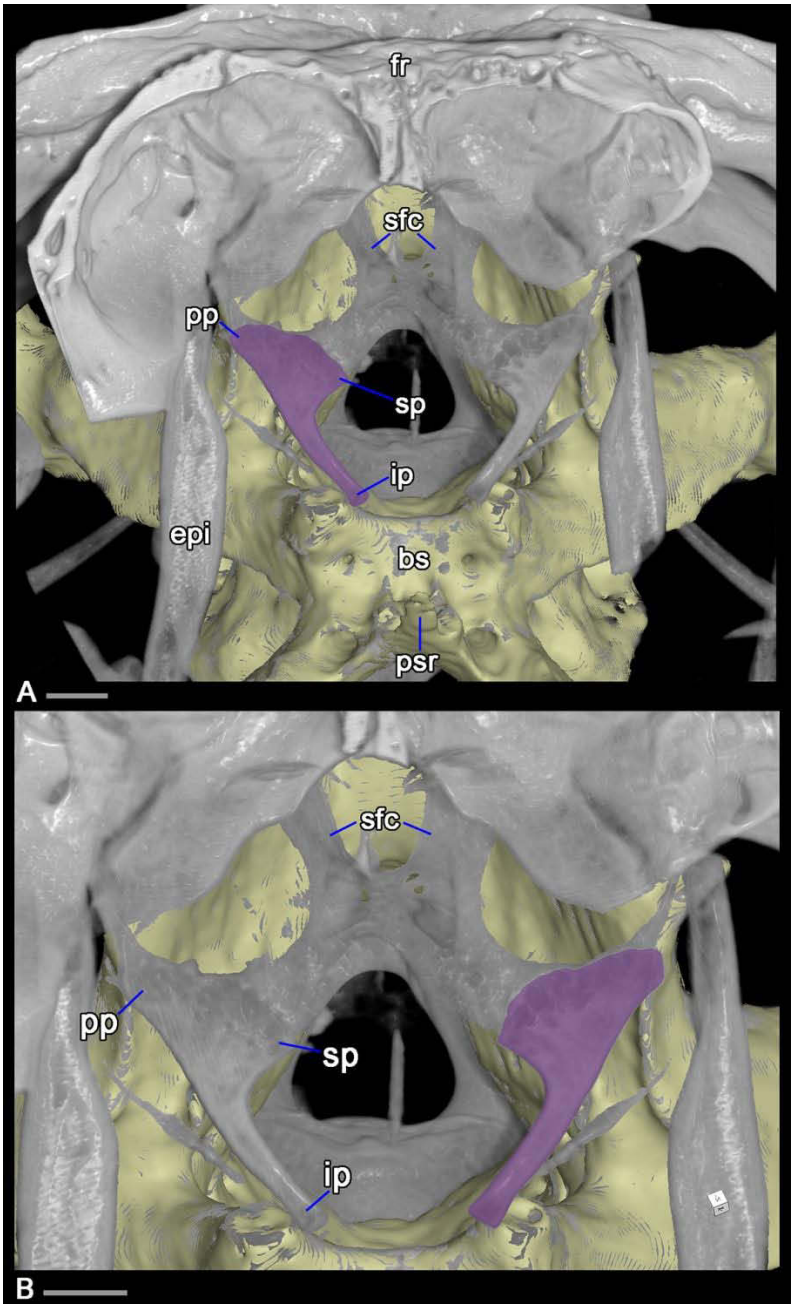

Figure 2.22. Orbitosphenoid of *Amblyrhynchus* UF 41558 in anterior view (A, B). Abbreviations: bs, basisphenoid; epi, epipterygoid; fr, frontal; ip, inferior process; pp, posterior process; psr, parasphenoid rostrum; sfc, cartilaginous walls of the subolfactory canal; sp, superior process. Scale bars: 2 mm.

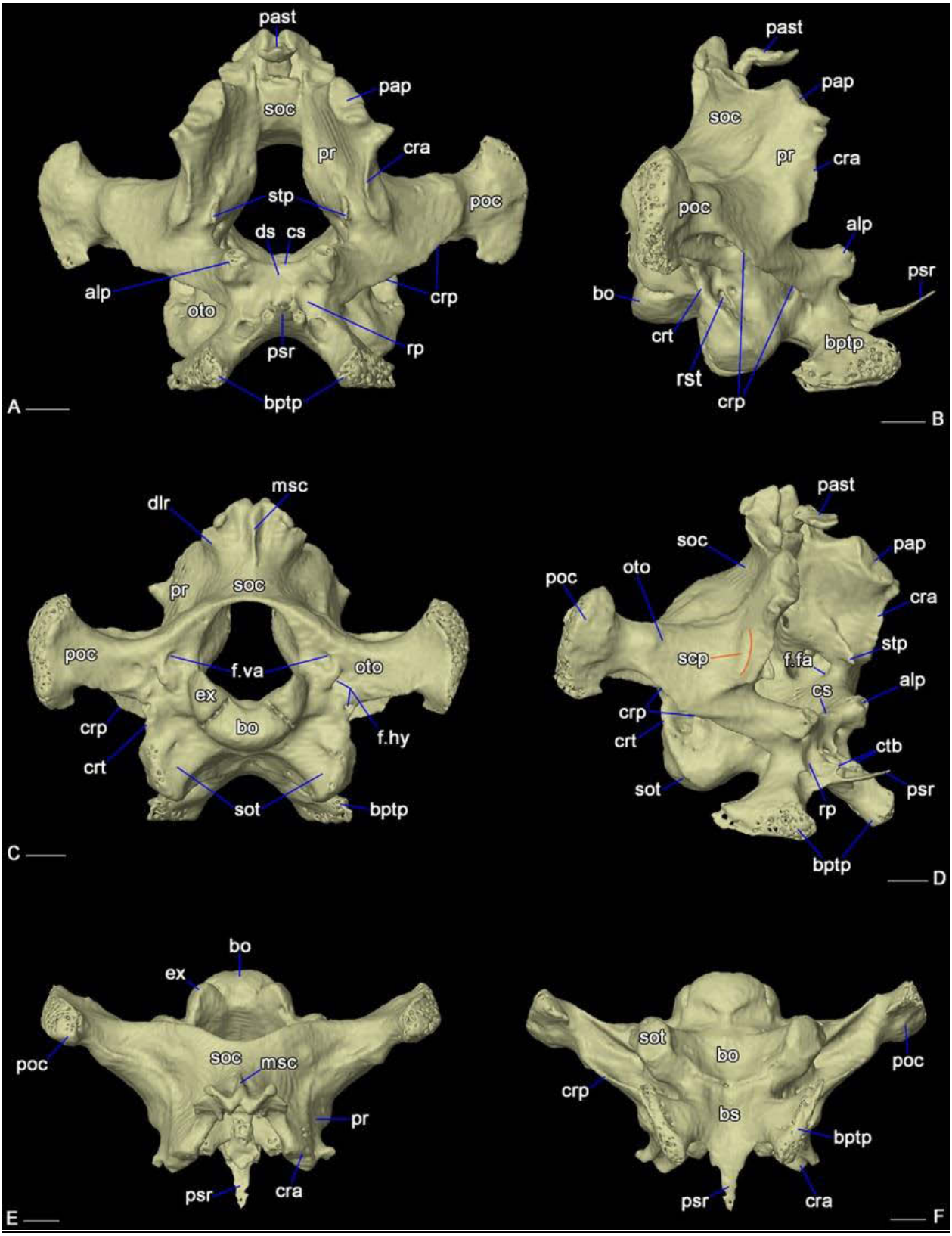
past
pap
soc
pr
cra
stp
poc
ds cs
alp
crp
oto
psr
rp
bptp
A
past
pap
soc
pr
cra
poc
alp
psr
bo
crt
bptp
rst
crp
B
msc
dlr
pr
soc
poc
f.va
oto
ex
bo
f.hy
crp
crt
sot
bptp
C
past
soc
pap
poc
oto
cra
scp
f.fa
stp
cs
alp
crp
crt
ctb
sot
psr
rp
bptp
D
bo
ex
poc
soc
msc
pr
psr
cra
E
sot
bo
poc
crp
bs
bptp
psr
cra
F

Figure 2.23. Braincase of *Amblyrhynchus* UF 41558 in anterior (A), right lateral (B), posterior (C), anterolateral (D), dorsal (E), and ventral (F) views. Abbreviations: alp, alar process; bo, basioccipital; bptp, basypterygoid process of the basisphenoid; bs, basisphenoid; cra, crista alaris; crp, crista prootica; crt, crista tuberalis; cs, crista sellaris; ctb, crista trabecularis; dlr, dorsolateral ridge of the supraoccipital; ds, dorsum sellae; ex, exoccipital (fused with the opisthotic to form the otoccipital); f.fa, facial foramen; f.va, vagus foramen; f.hy, foramina for hypoglossal (XII) nerve; msc, mid-sagittal crest of the supraoccipital; or, occipital recess; oto, otoccipital; pap, parietal process; past, processus ascendens of the synotic tectum; poc, paroccipital process of the otoccipital; pr, prootic; psr, parasphenoid rostrum; rp, retractor pit; rst, lateral aperture of the recessus scalae tympani; scp, semicircular canal passage (on prootic); soc, supraoccipital; sot, sphenoccipital tubercle; stp, supratrigeminal process. Scale bars: 5 mm.

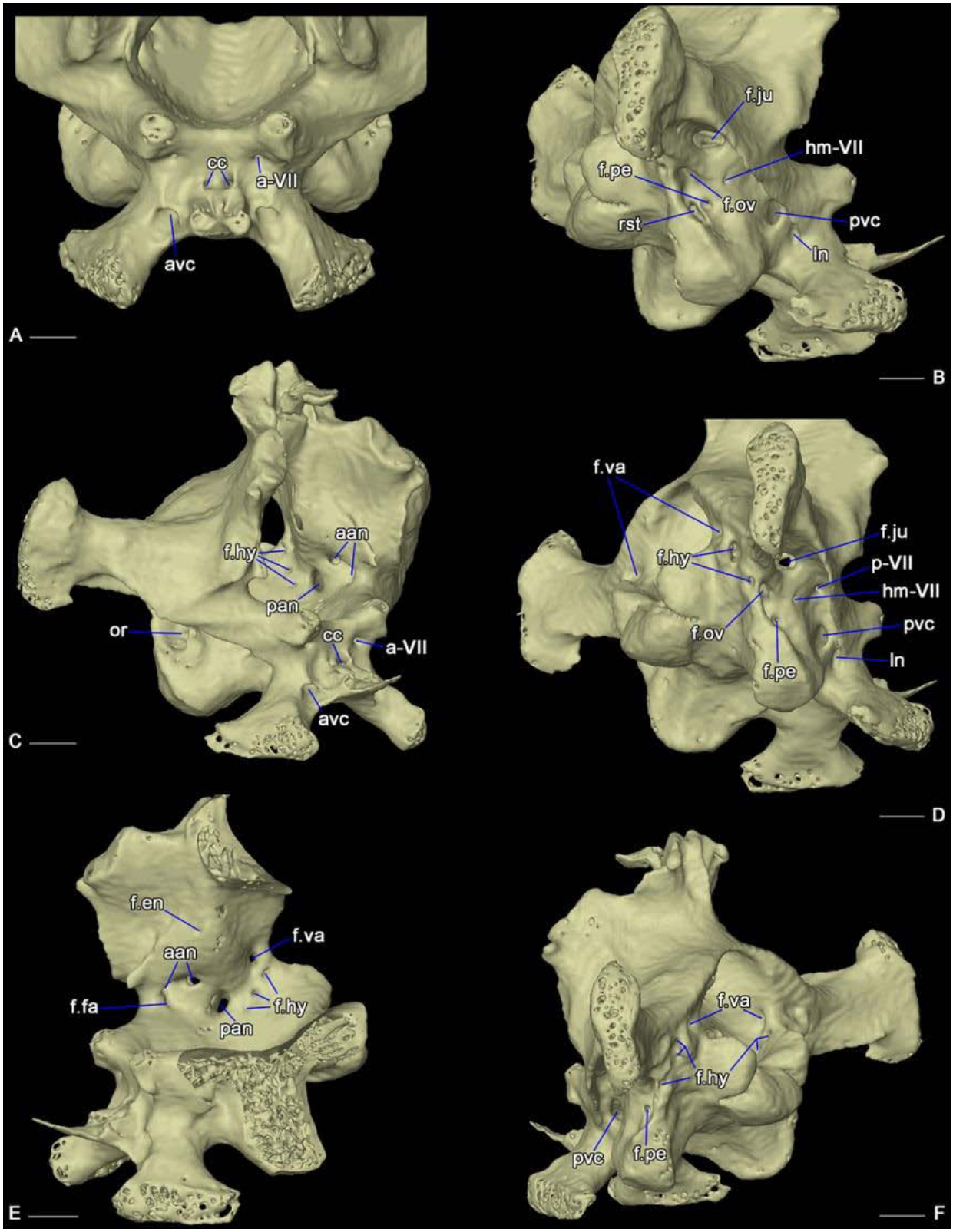
cc
a-VII
avc
A
f.ju
hm-VII
f.pe
f.ov
rst
pvc
ln
B
f.hy
aan
pan
or
cc
a-VII
avc
C
f.va
f.ju
f.hy
p-VII
hm-VII
f.ov
pvc
f.pe
ln
D
f.en
f.va
aan
f.fa
f.hy
pan
E
f.va
f.hy
pvc
f.pe
F

Figure 2.24. Foramina of the braincase in *Amblyrhynchus* UF 41558 in anterior (A), right lateral (B), anterolateral (C), posteroventral (D), medial (E), and posterolateral (F) views. Abbreviations: a-VII, foramen for abducens nerve VI; aan, anterior foramen for acoustic nerve; avc, anterior opening of vidian canal; cc, carotid canal; f.en, endolymphatic foramen; f.fa, facial foramen; f.ju, jugular foramen; f.ov, foramen ovale/fenestra ovalis; f.pe, perilymphatic foramen; f.va, vagus foramen; hm-VII, foramen for hyomandibular branch of facial nerve; f.hy, foramina for hypoglossal (XII) nerve; ln, lateral notch (beside the posterior opening of the vidian canal); or, occipital recess; p-VII, foramen for palatal branch of facial nerve; pan, posterior foramen for acoustic nerve; pvc, posterior opening of vidian canal; rst, lateral aperture of the recessus scalae tympani. Scale bars: 5 mm.

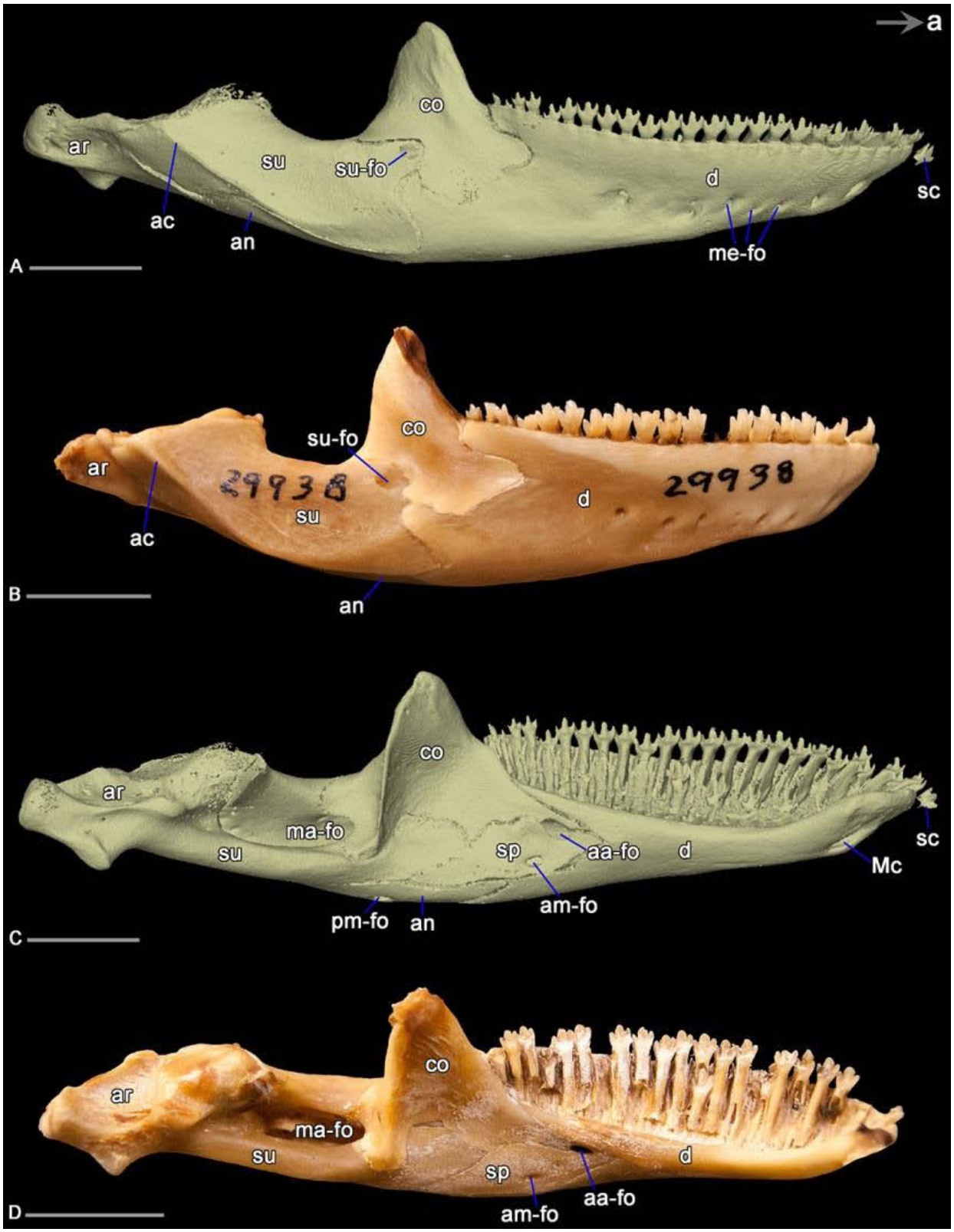
a
co
ar
su
su-fo
d
sc
ac
an
me-fo
A
su-fo
co
ar
29938
29938
d
su
ac
B
an
co
ar
ma-fo
su
sp
aa-fo
d
sc
Mc
am-fo
pm-fo
an
C
co
ar
ma-fo
su
sp
d
aa-fo
am-fo
D

Figure 2.25. Overview of the mandible of *Amblyrhynchus* UF 41558 in lateral (A-B) and medial (C-D) views. Abbreviations: a, anterior; aa-fo, anterior inferior alveolar foramen; ac, adductor crest; am-fo, anterior mylohyoid foramen; an, angular; ar, articular; co, coronoid; d, dentary; ma-fo, mandibular fossa (or foramen); Mc, Meckel‘s canal; me-fo, mental foramina; p, posterior; pm-fo, posterior mylohyoid foramen; sc, shedding crown of tooth; sp, splenial; su, surangular; su-fo, anterior surangular foramen. Scale bars: 1 cm.

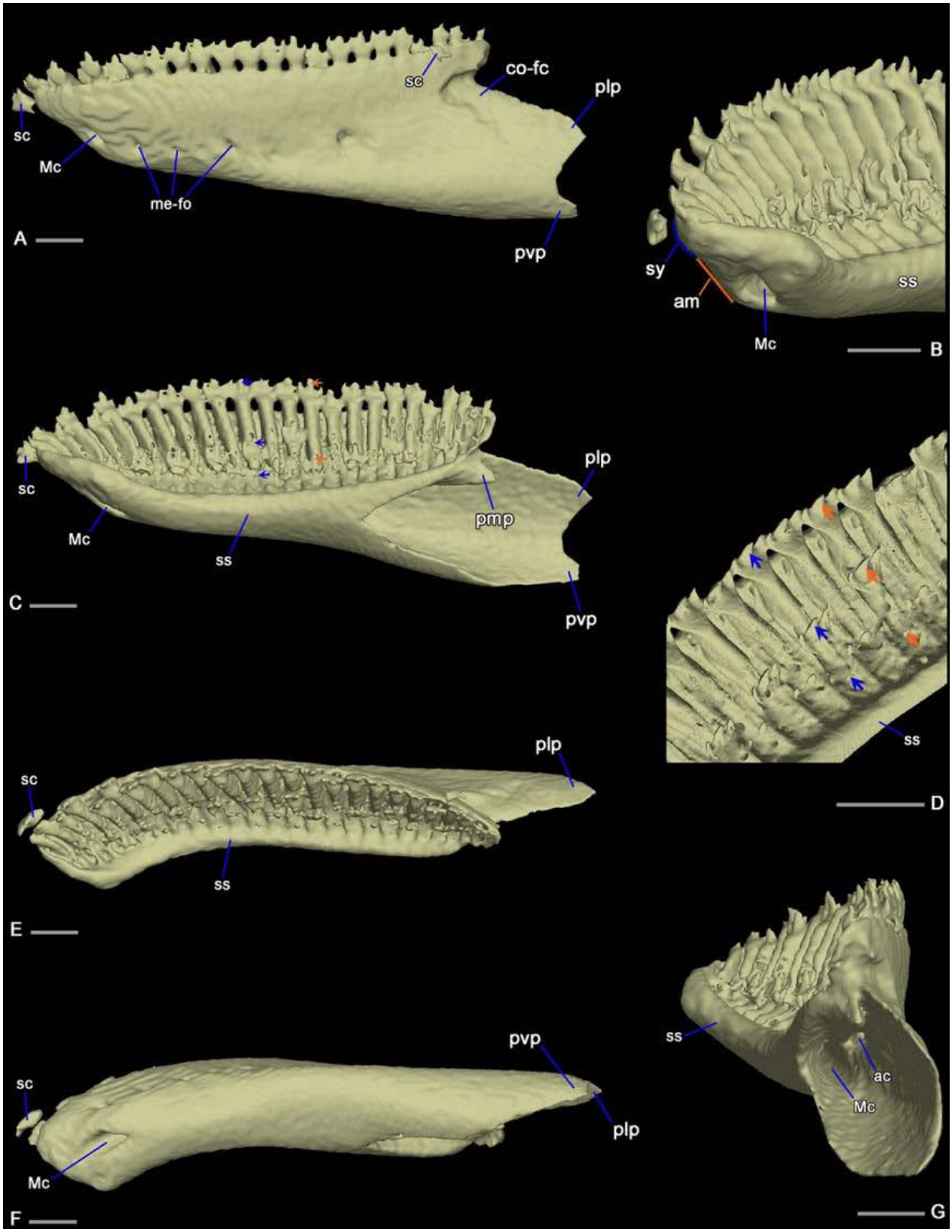
sc
co-fc
plp
sc
Mc
me-fo
A
pvp
sy
ss
am
Mc
B
plp
sc
pmp
Mc
ss
C
pvp
ss
D
plp
sc
ss
E
pvp
sc
plp
Mc
F
ss
ac
Mc
G

Figure 2.26. Dentary of *Amblyrhynchus* UF 41558 in lateral (A), anteromedial (B), medial (C), dorsomedial (D), dorsal (E), ventral (F), and posterior (G) views. The orange and blue arrows point at the crowns of different tooth generations. Abbreviations: a, anterior; ac, inferior alveolar canal; am, anterior margin; co-fc, coronoid facet; Mc, Meckel‘s canal; me-fo, mental foramina; p, posterior; plp, posterolateral process; pmp, posteromedial process; pvp, posteroventral process; sc, shedding crown of tooth; ss, subdental shelf; sy, symphysis. Scale bars: 5 mm.

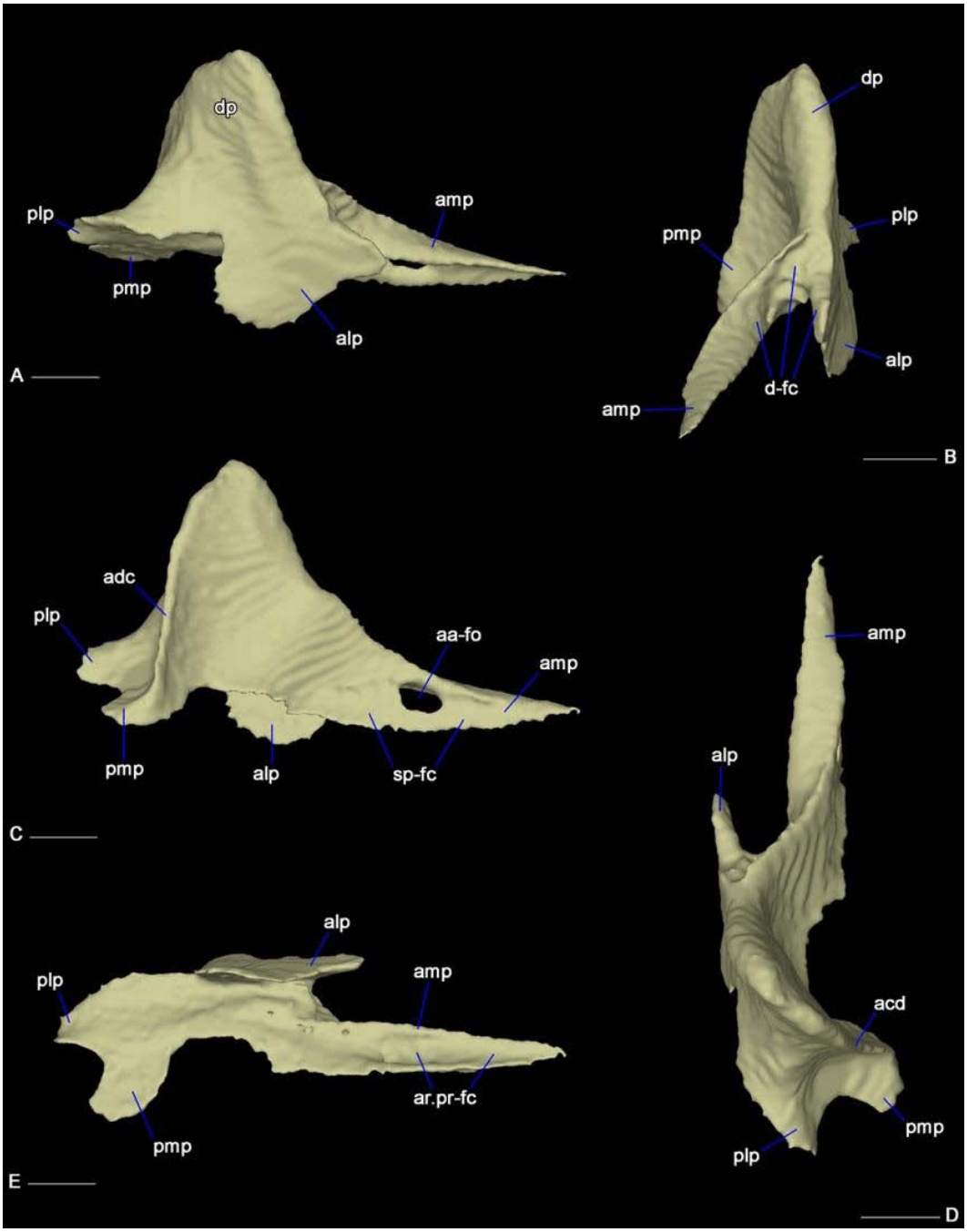

Figure 2.27. Coronoid of *Amblyrhynchus* UF 41558 in lateral (A), anterior (B), medial (C), dorsal (D), and ventral (E) views. Abbreviations: a, anterior; aa-fo, anterior inferior alveolar foramen; adc, adductor crest; alp, anterolateral process; amp, anteromedial process; ar.pr-fc, articular-prearticular facet; dp, dorsal process; p, posterior; plp, posterolateral process; pmp, posteromedial process; sp-fc, splenial facet. Scale bars: 5 mm.

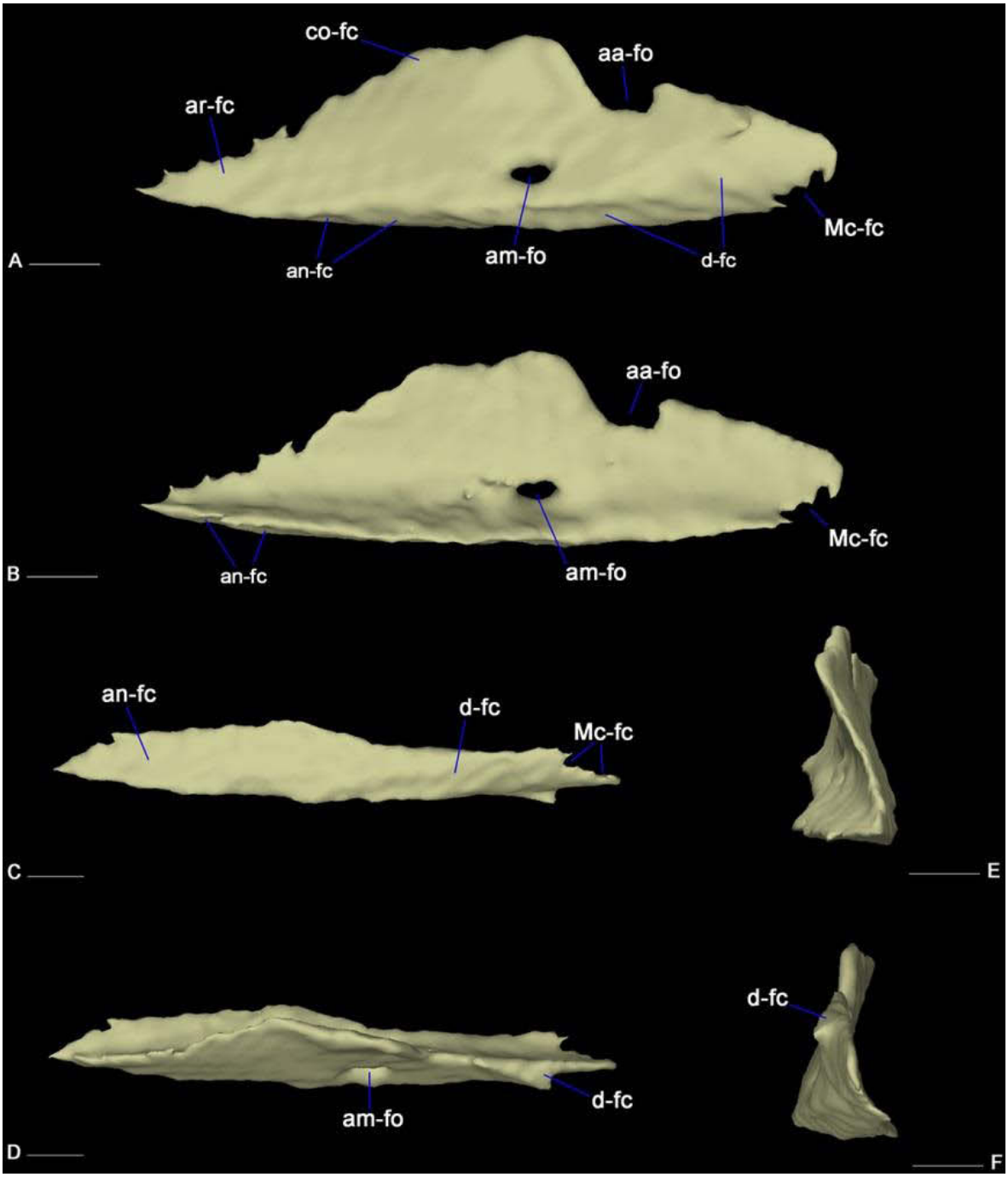

Figure 2.28. Splenial of *Amblyrhynchus* UF 41558 in medial (A), lateral (B), ventral (C), dorsal (D), anterior (E), and posterior (F) views. Abbreviations: a, anterior; aa-fo, anterior inferior alveolar foramen; am-fo, anterior mylohyoid foramen; d-fc, dentary facet; Mc-fc, facet for Meckel‘s canal; p, posterior. Scale bars: 5mm.

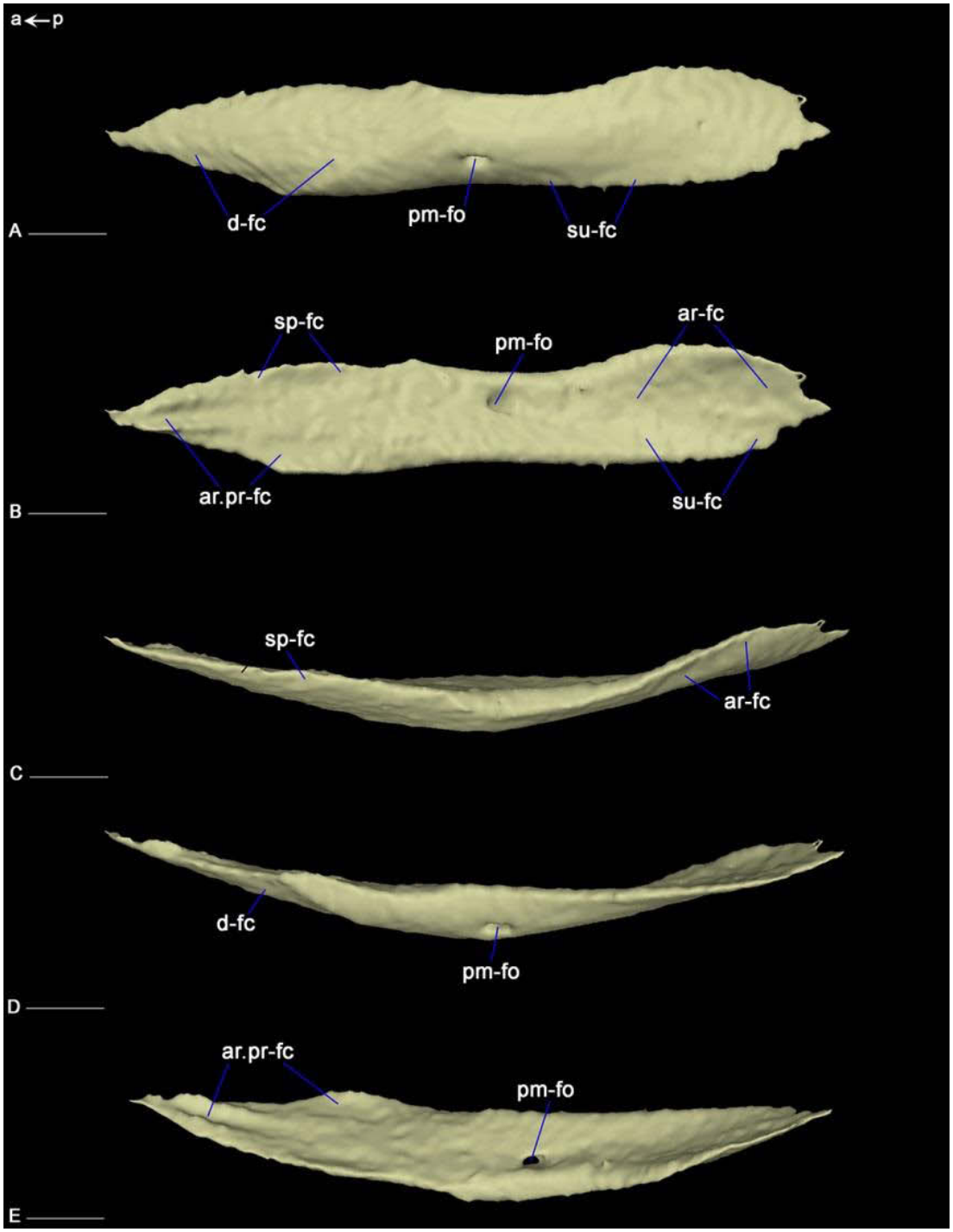

Figure 2.29. Angular of *Amblyrhynchus* UF 41558 in ventromedial (A), dorsal (B), medial (C), lateral (D), and dorsolateral (E) views. Abbreviations: a, anterior; ar-fc, articular facet; ar.pr-fc, articular-prearticular facet; d-fc, facet for dentary; p, posterior; pm-fo, posterior mylohyoid foramen; sp-fc, splenial facet; su-fc, surangular facet. Scale bars: 5 mm.

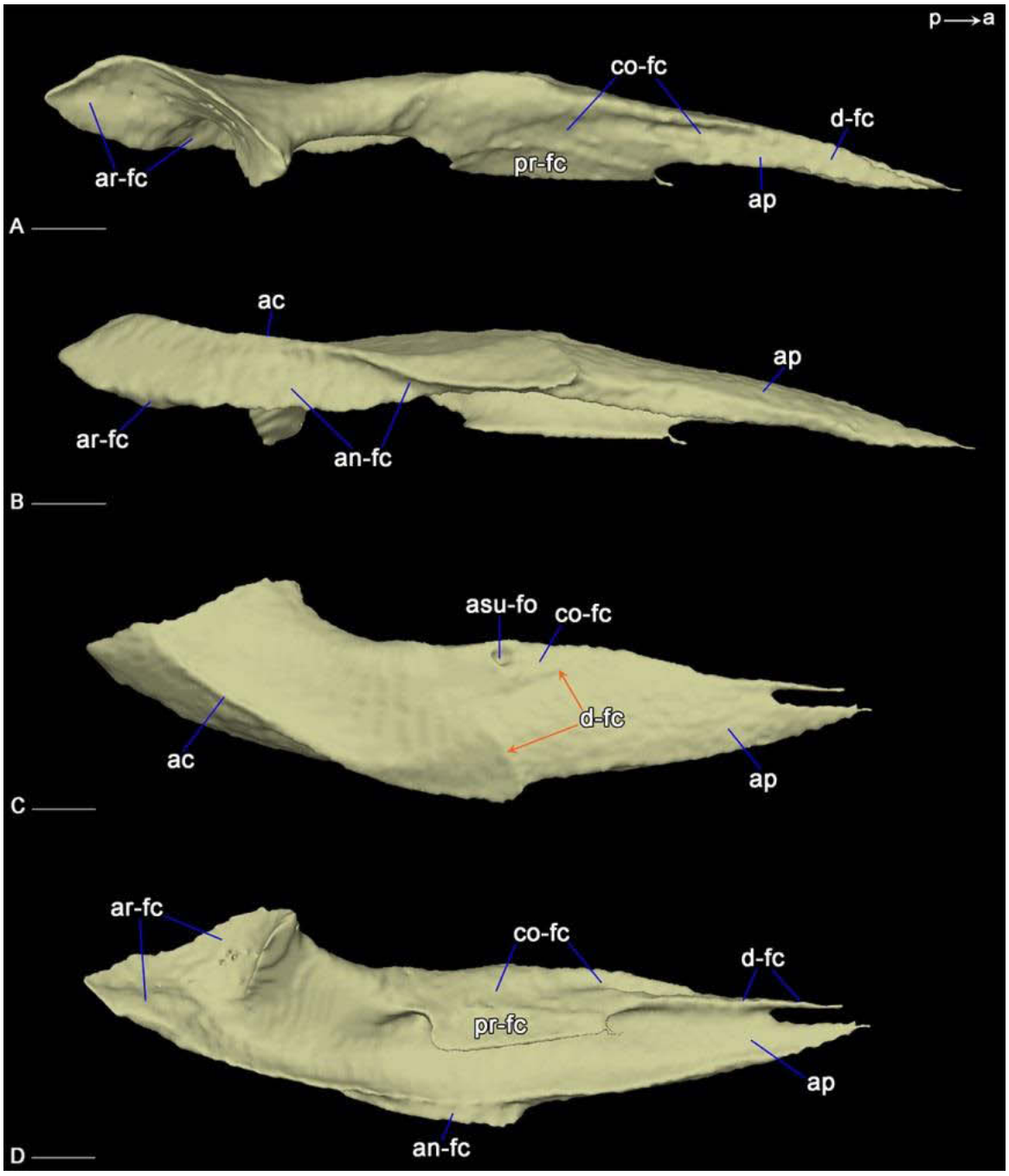

Figure 2.30. Surangular of *Amblyrhynchus* UF 41558 in dorsal (A), ventral (B), lateral (C), and medial (D) views. The orange arrows point to the posterior margins of the dentary facet on the surangular lateral surface. Abbreviations: a, anterior; ac, adductor crest; an-fc, angular facet; ar-fc, articular facet; asu-fo, anterior surangular foramen; co-fc, coronoid facet; d-fc, dentary facet; p, posterior; pr-fc, prearticular facet. Scale bars: 5 mm.

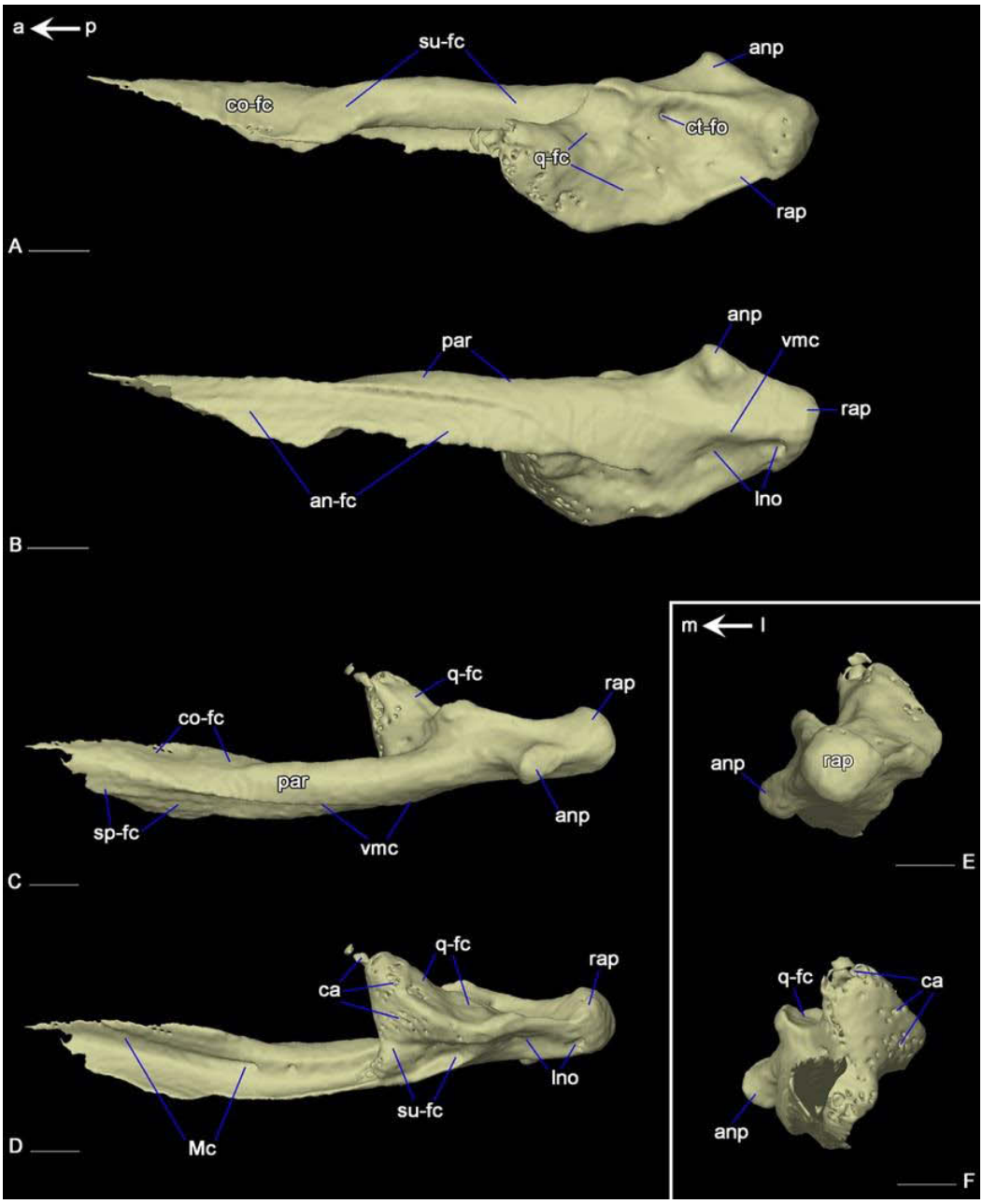

Figure 2.31. Articular-prearticular of *Amblyrhynchus* UF 41558 in dorsal (A), ventral (B), medial (C), lateral (D), posterior (E), and anterior (F) views. Abbreviations: a, anterior; an-fc, angular facet; anp, angular process; ap, anterior process; co-fc, coronoid facet; ct-fo, foramen for the chorda tympani nerve; l, lateral; lno, lateral notch; m, medial; Mc, Meckel‘s canal; p, posterior; par, prearticular; q-fc, quadrate facet; rap, retroarticular process; sp-fc, splenial facet; su-fc, surangular facet; vmc, ventromedial crest. Scale bars: 5 mm.

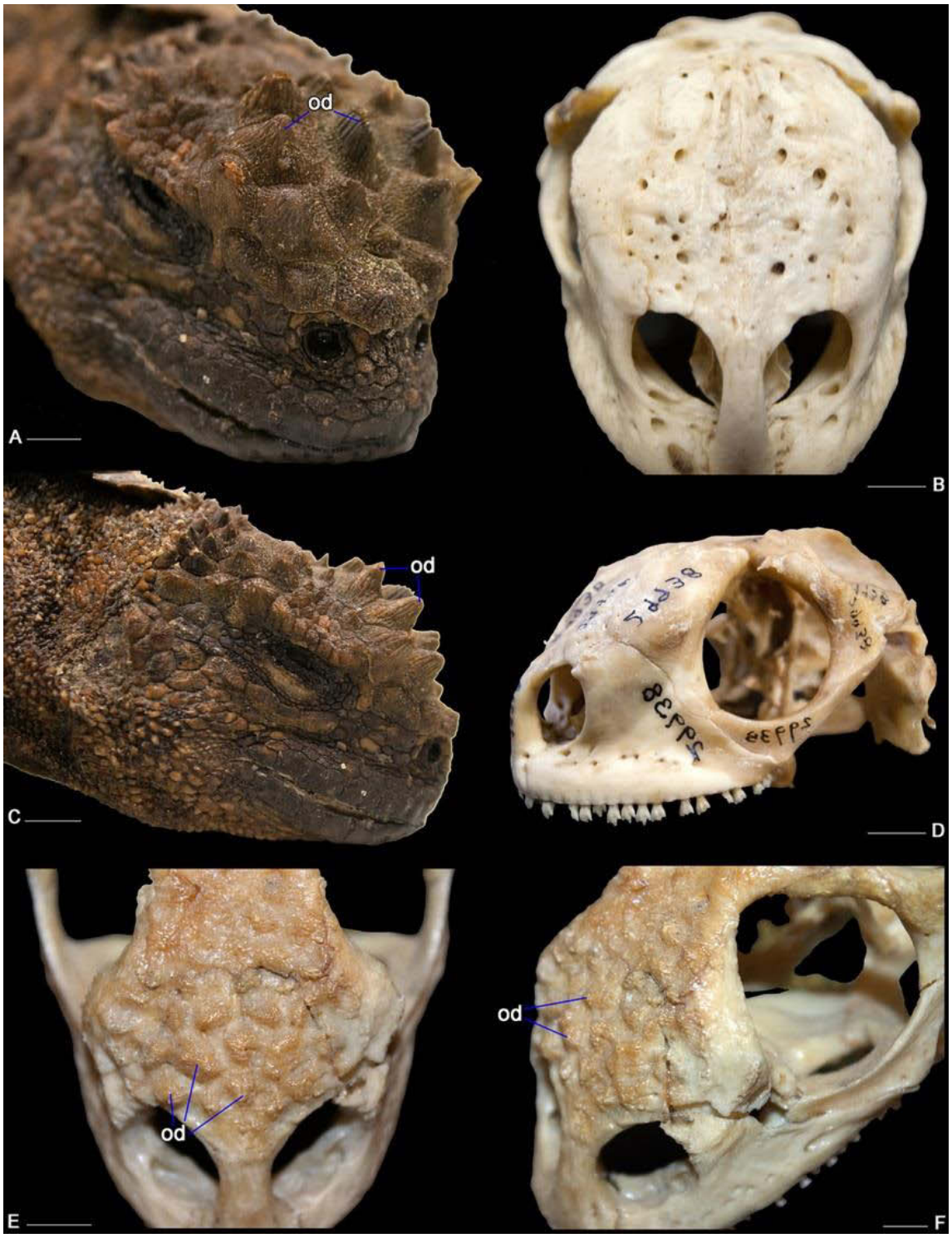

Figure 2.32. View of the snout region of *Amblyrhynchus* (A-D) and *Conolophus* (E, F), showing the differences related to integumentary ossifications: UF 41558 (A, C), AMNH 114492 (B), AMNH 29938 (D), ROM R 112 (E, F). Abbreviations: od, osteoderms. Scale bars: 1 cm.

Figure 2.33. Marginal dentition of *Amblyrhynchus* UF 41558: transverse section of maxilla (A, C), isolated marginal teeth in lingual (B), labial (E), anterior (F) views, and coronal section of maxilla (D). The yellow arrows point at different tooth generations. Abbreviations: a, anterior; att, apex point of attachment of the tooth to the lingual side of the jaw bone; c-r, limit between crown (upper part) and root (lower part); cs, cusp; Ft, functional tooth; Lb, labial side; mc, median cusp; mx, maxilla; pc, pulp cavity; pmx, premaxilla. Scale bars: 2 mm.

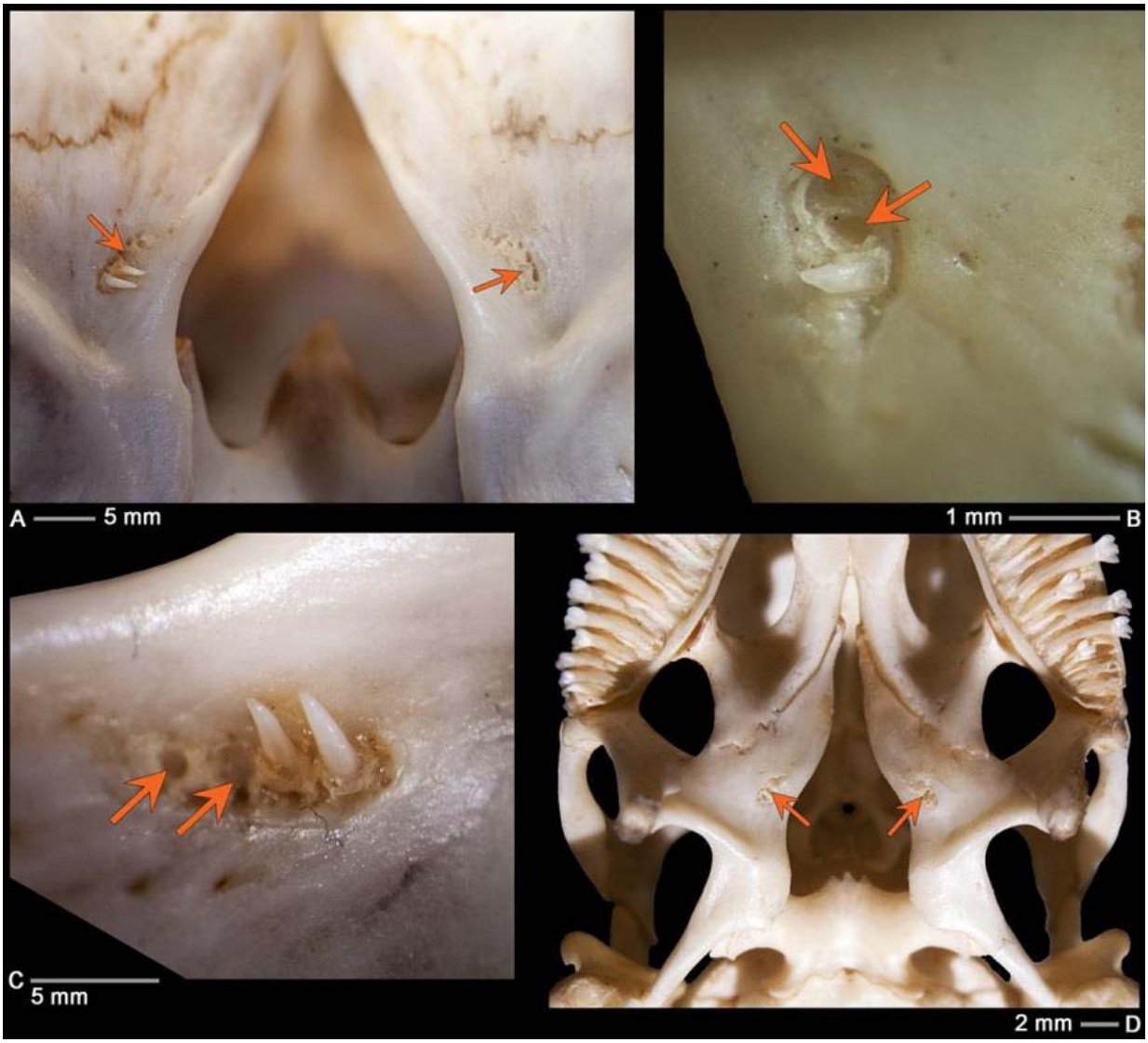

Figure 2.34. Pterygoid teeth in *Amblyrhynchus*: AMNH 114492 (A, C), AMNH 76197 (B, D). All specimens are in ventral view. The orange arrows point to tooth positions where the actual tooth is missing.

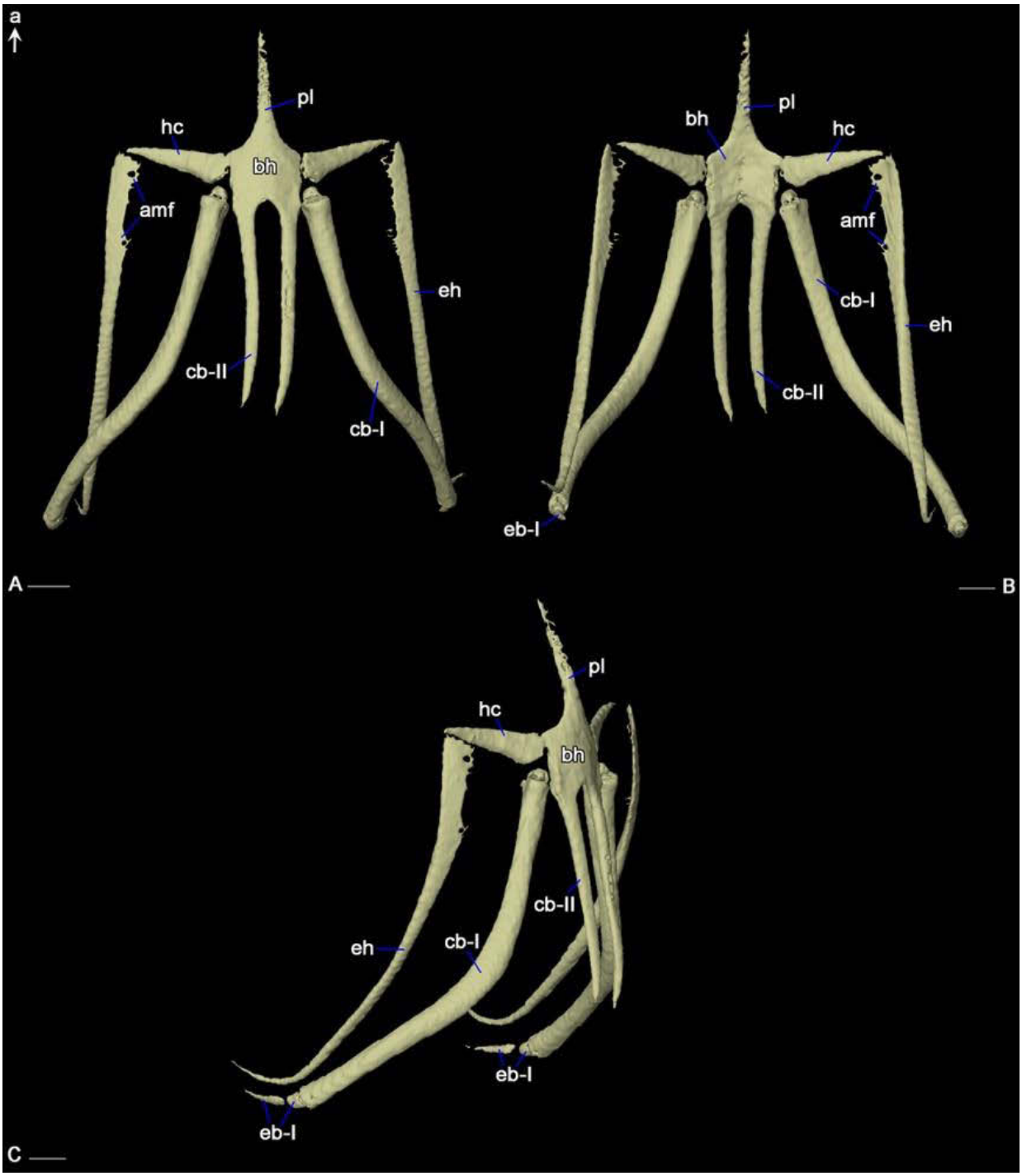

Figure 2.35. Hyoid of *Amblyrhynchus* UF 41558 in ventral (A), dorsal (B), and ventrolateral (C) views. Terminology for the hyoid is based on Tanner & Avery (1982). Abbreviations: a, anterior; bh, basihyoid; cb-I, first ceratobranchial; cb-II, second ceratobranchial; eb-I, first epibranchial; eh, epihyal; hc, hyoid cornu; p, posterior; pl, processus lingualis. Scale bars: 5 mm.

APPENDIX 2.1 – List of specimens used in this study.

Amblyrhynchus cristatus: AMNH 29937; AMNH 29938; AMNH 36230; AMNH 36231; AMNH 43228; AMNH 46270; AMNH 75942; AMNH 76197; AMNH 78979; AMNH 89841; AMNH 114491; AMNH 114492; AMNH 123309; AMNH 147810; UAMZ 384; UF 41424; UF 41558 (http://www.morphosource.org/Detail/MediaDetail/Show/media_id/20786); UF 49137; UF 49138; UF 54782; UF 57134; http://www.morphosource.org/Detail/MediaDetail/Show/media_id/9055 (MVZ 67721); http://www.morphosource.org/Detail/MediaDetail/Show/media_id/9056 (UCMP 137167). *Brachylophus fasciatus*: AMNH 29033; AMNH 29034; AMNH 121274; UF 37578; http://www.digimorph.org/specimens/Brachylophus_fasciatus/ (FMNH 210158). *Conolophus pallidus*: AMNH 147847; AMNH 147848; AMNH 147849. *Conolophus subcristatus*: AMNH 50797; AMNH 50798; AMNH 89845; AMNH 110168; AMNH 114493; AMNH 131308; ROM 112; UF 11583. *Ctenosaura pectinata*: ROM 1046; ROM 6709; UF 48333; UF 55461; UF 56553; UF 56619; http://digimorph.org/specimens/Ctenosaura_pectinata/. *Ctenosaura similis*: AMNH 147860; AMNH 147861; UF 48750; UF 67496; UF 67525; UF 67707. *Cyclura carinata*: UF 30425; UF 67232. *Cyclura cornuta*: AMNH 93182; AMNH 147865; AMNH 147865: UF 52004; UF 57134; UF 99016; UF 99017; UF 99056. *Dipsosaurus dorsalis*: AMNH 73058; AMNH 75603; AMNH 141110; AMNH141115; ROM 875; ROM 4279; UF 42777; http://digimorph.org/specimens/Dipsosaurus_dorsalis/ (YPM 14376). *Iguana iguana*: AMNH 81871; AMNH 88423; AMNH 94167; AMNH 154811; ROM 294; ROM 346; ROM 373; ROM 401; ROM 426; ROM 428; ROM 441; 7716; UAMZ 951; UF 142724; UF 146560; UF 149744. *Sauromalus obesus*: ROM R 335; ROM R 9335; UF 11691.

APPENDIX 2.2 – Supplementary figures for Chapter 2.

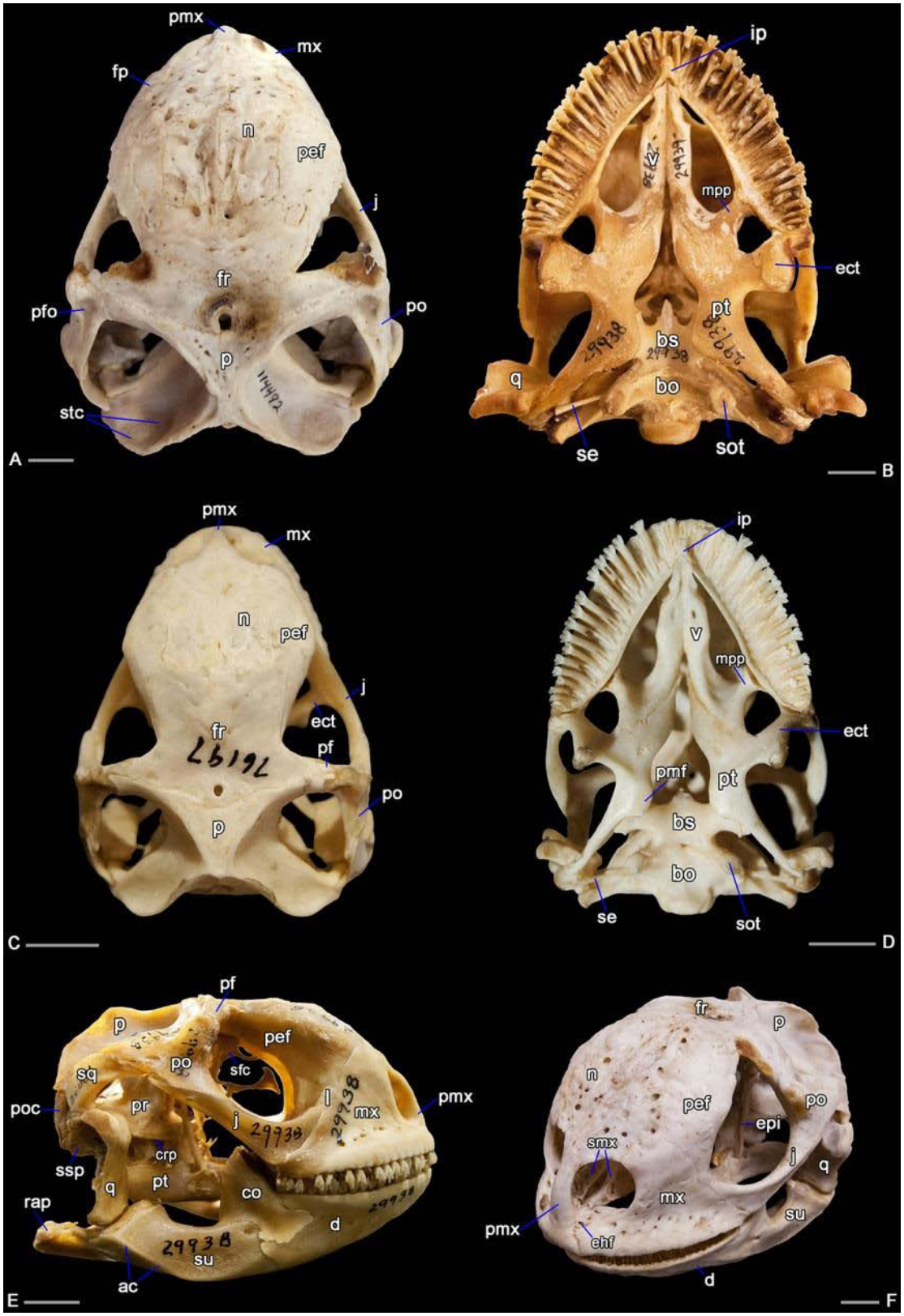

Figure A2.1. Overview of cranial features in specimens of *Amblyrhynchus* in dorsal (A, C), ventral (B, D), lateral (E), and anterolateral (F). Specimens: AMNH 114492 (A, F), AMNH 29938 (B, E), AMNH 76197 (C, D). Abbreviations: co, coronoid; crp, crista prootica; d, dentary; ect, ectopterygoid; ehf, ethmoidal foramen; epi, epipterygoid; fp, facial (mid-dorsal) process of maxilla; fr, frontal; ip, incisive process of premaxilla; j, jugal; l, lacrimal; mx, maxilla; mpp, maxillary (lateral) process of palatine; n, nasal; p, parietal; pef, prefrontal; pf, postfrontal; pfo, postorbital fossa; pmf, posteromedial flange of pterygoid; pmx, premaxilla; po, postorbital; poc, paroccipital process of otoccipital; pr, prootic; pt, pterygoid; q, quadrate; rap, retroarticular process; se, stape; sfc, cartilaginous walls of the subolfactory canal; smx, septomaxilla; sot, spheno-occipital tubercle; sq, squamosal; ssp, suprastapedial process of quadrate; stc, supratemporal concavity of parietal; su, surangular; v, vomer. Scale bars: 1 cm.

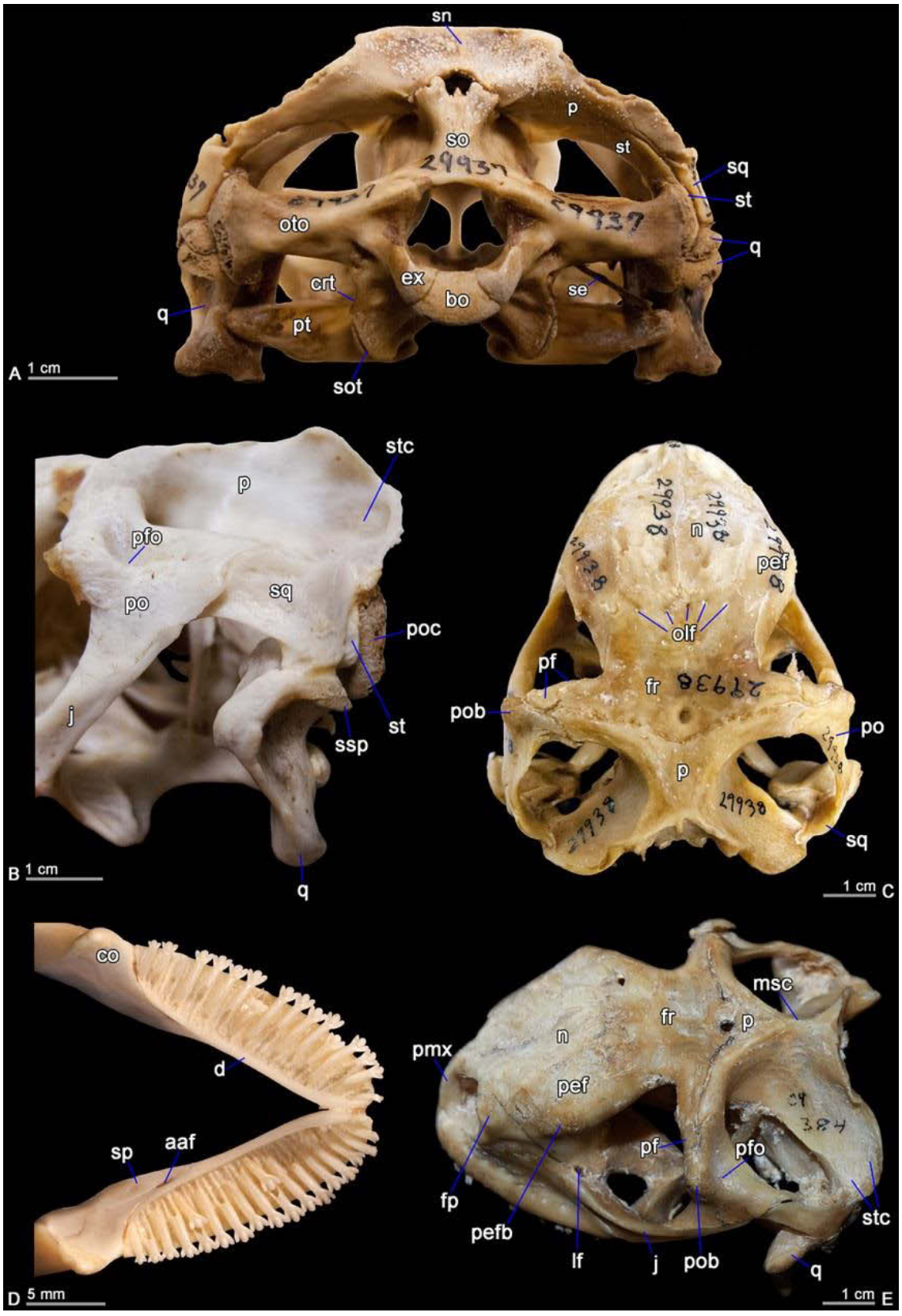
sn
p
so
st
sq
st
oto
q
crt
ex
bo
se
q
pt
A 1 cm
sot
stc
p
pfo
po
sq
poc
j
st
ssp
q
B 1 cm
n
pef
olf
pf
fr
pob
po
p
sq
1 cm C
co
d
sp
aaf
D 5 mm
msc
fr
p
n
pmx
pef
pf
pfo
fp
pefb
lf
j
pob
stc
q
1 cm E

Figure A2.2. Overview of cranial features in specimens of *Amblyrhynchus* in posterior (A), lateral (B), dorsal (C, D), and dorsolateral (E). Specimens: AMNH 29937 (A), AMNH 114492 (B), AMNH 29938 (C), AMNH 75942 (D), UAMZ 384 (E). Abbreviations: aaf, anterior alveolar foramen; bo, basioccipital; co, coronoid; crt, crista tuberalis; d, dentary; ex, exoccipital; fp, facial (mid-dorsal) process of maxilla; j, jugal; lf, lacrimal foramen; n, nasal; olf, olfactory foramina; oto, otoccipital; p, parietal; pef, prefrontal; pefb, prefrontal boss; pf, postfrontal; pfo, postorbital fossa; po, postorbital; pob, postorbital boss; poc, paroccipital process of otoccipital; se, stape; sn, septum dividing the nuchal fossa; sot, sphenoccipital tubercle; sp, splenial; sq, squamosal; ssp, suprastapedial process of quadrate; st, supratemporal; stc, supratemporal concavity of parietal.

CHAPTER 3

A new fossil marine lizard with soft tissues from the Late Cretaceous of Southern Italy

A version of this chapter has been published as Paparella I., Palci A., Nicosia U., and Caldwell M.W. (2018). A new fossil marine lizard with soft tissues from the Late Cretaceous of southern Italy. *Royal Society Open Science*, 5(6):172411. https://doi.org/10.1098/rsos.172411.

3.1 Introduction

Pythonomorpha (mosasauroids, ‗dolichosaurs' and snakes) is a clade including both extinct and extant squamates. While both snakes (Ophidia) and mosasauroids (Mosasauroidea) are recognized as monophyletic groups, dolichosaurs are typically reconstructed as a paraphyletic assemblage basal to mosasauroids (Lee 2005; Pierce & Caldwell 2004; Reeder et al. 2015). The earliest fossil record of non-ophidian pythonomorphs dates back to the Early Cretaceous (Valanginian-Hauterivian) (Evans et al. 2006), while the latest discovery in non-marine deposits is reported from the late Campanian – early Maastrichtian of Spain (Houssaye et al. 2013). By the Cenomanian-Turonian, non-ophidian pythonomorphs are found in marine deposits around the Mediterranean area, in western Europe, North America, and possibly Australia (Bardet et al. 2008; Bell et al. 1982; Caldwell 1999; Caldwell 2000; Caldwell 2006; Caldwell & Dal Sasso 2004; Dutchak & Caldwell 2006; Dutchak & Caldwell 2009; Houssaye 2010; Lee & Scanlon 2002a; Palci & Caldwell 2010; Pierce & Caldwell 2004; Scanlon & Hocknull 2007), testifying to

an ongoing radiation of these aquatic lizards at the beginning of the Late Cretaceous (Bardet et al. 2008). Of all non-ophidian pythonomorphs, only the more derived fully-aquatic forms (Mosasauridae), survived up to the end of the Cretaceous, while aigialosaurs and dolichosaurs have insofar been considered extinct by the Santonian (Bardet et al. 2008).

Here, I present new data from an extremely well preserved specimen, including soft tissue remains, of the first dolichosaur from the latest Cretaceous of Southern Italy (Puglia), recovered from a new *Lagerstätte*-quality locality. This new finding not only fills a palaeogeographic gap in the Mediterranean Tethys for this group, being the first record from the Apulian Platform, but it also extends the range of dolichosaurs *sensu* Nopcsa (Nopcsa 1903) by about 10 million years (from the Santonian to the upper Campanian – lower Maastrichtian). The new taxon may well represent a Tethyan relict of its clade, a group that was presumed to be extinct much earlier in the Late Cretaceous. It also testifies to the survival of a quite conservative morphology (in terms of axial elongation and other aquatic adaptations) for marine non-ophidian pythonomorphs up to the late Campanian – early Maastrichtian. Moreover, the astonishing preservation of the soft tissues provides an unprecedented source of information to help us better understand the morphology of pythonomorphs and their interrelationships.

3.2 Material and Methods

3.2.1 Specimen and images

The new specimen is housed at the Museum of Palaeontology of the "Sapienza" University of Rome (MPUR, Museo Paleontologico dell'Università di Roma), Lazio, Italy. Natural light photos were taken using a Canon EOS 1000D digital single-lens reflex camera. A Nikon D3100 digital single-lens reflex camera was used for UV light photography. A Nikon

Coolpix S3600 compact digital camera was used for dissecting scope photomicrography. Line drawings were made by hand using photographs of the material at both natural and ultraviolet light, and by direct observation of the specimen. Digitizing and figure construction were accomplished using Adobe® Photoshop® (outlines and colouring) and Adobe® Illustrator® (labelling and final production), both version CC 17 (2013 release).

3.2.2 Spectroscopic analysis

Scanning Electron Microscopy (SEM) using Energy Dispersive X-ray (EDX) microanalysis was performed on selected samples of cortical bone, muscles, gut contents and sediment in order to verify the composition of both hard and soft tissues, and to understand what factors might have led to such outstanding preservation. The samples were mounted on aluminium stubs using double-sided carbon tape, and examined with a SEM FEI Quanta 400 under low vacuum and uncoated (analysis time of 60 s at 20 KeV) (see Fig. 3.9 and Appendix 3.2, Fig. A3.10).

3.2.3 Ultraviolet radiation

Bones and matrix are of about the same colour under natural light; the distinction between preserved bone and molds, as well as between soft and hard tissues, was facilitated by the use of ultraviolet (UV) radiation. The UV lamp used to analyse the specimen is a double-wavelength model that can radiate both short (254 nm) and long (365 nm) waves: the short waves highlight the different elements of the specimen in the grey spectrum of colours, while the long waves work in the scale of the colour purple (see Figs. 3.1-3.6; Appendix 3.2, Figs. A3.2, A3.6-A3.7 for further details). When exposed to UV light, the bony tissues (cartilage and bone)

appear white, in high contrast to the coloured soft tissues (grey range with short waves, purple range with long waves). While the bones assume an off-white colour, the cartilaginous elements usually appear more bright white, though they are mostly undistinguishable from the matrix under natural light. The contrast in colours is related to the presence of original phosphorous (P) (bone and cartilage = white range), and replacement P (soft tissues = pink-purple range) that replaces the original composition of both muscles and integument; from the SEM/EDX analyses we know that both hard and soft remains consist of calcium phosphate, interpreted as replacement calcium phosphate (Briggs et al. 1993; Briggs 2003; Trinajstic et al. 2007).

3.2.4 Phylogenetic procedures

To assess the phylogenetic position of MPUR NS 161, I added character scores to a modified version of the dataset of Palci & Caldwell (Palci & Caldwell 2010). The updated list of characters, as well as other details about the results of our analyses, are included in Appendices 3.3-3.6. Terminal taxa were modified to perform a mostly species-level analysis (except for *Adriosaurus* and *Aigialosaurus* scored as genera); all scorings are based on personal observation of the terminals. *Tetrapodophis amplectus* was also added to the data matrix, again with scorings based on personal observations (MWC). The final dataset consists of 27 taxa and 129 characters, with the anguid *Diploglossus millepunctatus* as outgroup. The data matrix was generated with Mesquite 3.04 (Maddison & Maddison 2018).

Parsimony – I performed both an equal-weight maximum parsimony (MP) and an implied weighting maximum parsimony (IWMP) analysis using TNT 1.5-beta (Goloboff et al. 2008a; Goloboff et al. 2008b; Goloboff et al. 2017). The MP heuristic search was run using the

tree-bisection-reconnection (TBR) algorithm, considered the best option for small datasets (27 taxa in our study) as per Goloboff et al. (Goloboff et al. 2008b), with the number of maximum trees set to 99,999 and all the characters processed as unordered and unweighted. For the MP analysis, I ran a first round with starting Wagner trees calculated from 1,000 replicates of additional random sequences, and a successive round swapping trees from RAM (i.e., using the Wagner trees calculated from the first round), in order to increase the chance to find the actual shortest trees. Two optimal trees were retained after removing all the suboptimals, and the strict consensus topology is presented with relative supports in Figure 3.6a (both optimal trees are included in Fig. A3.11). Following Goloboff et al. (Goloboff et al. 2008a; Goloboff et al. 2017), I also performed an IWMP with K set to 3, and adopting the same steps described for the MP analysis. The IWMP resulted in a single optimal tree and the topology is presented in Figure 3.6b (see also Fig. A3.12). The link to download the nexus file used to run the analyses is provided in Appendix 3.6.

Bayesian Inference – The Bayesian Inference (BI) analysis was performed with MrBayes 3.2.6 (Ronquist et al. 2012c), under the Mk(V) model for variable characters (Lewis 2001). Since MrBayes does not handle polymorphic scorings, all the polymorphisms were converted in the dataset used to run the parsimony analysis into uncertainties using Mesquite 3.04 (Maddison & Maddison 2018). I used a gamma distribution for rate heterogeneity and treated the data as a single partition. Generations were set to 10 000 000, frequency of sampling to 1 000, burn in fraction to 0.25, and the temperature parameter to 0.010 (which gave the best chain mixing values). I checked the optimality of the parameters for convergence and effective sample size from both MrBayes log file, and Tracer 1.6 (Rambaut et al. 2014). LogCombiner (Rambaut &

Drummond 2016a) and Tree Annotator (Rambaut & Drummond 2016b) were used to estimate the posterior tree (maximum clade credibility tree (MCCT)). The link to download the nexus file used to run the BI is provided in Appendix 3.6.

3.3 Results

3.3.1 Geological aspects and age

The specimen was found near Nardò (Lecce, Puglia), a small town located on the Salento Peninsula (Southern Italy) (Fig. A3.1). This locality is particularly famous for its fossiliferous limestones containing abundant fossil fish remains (Medizza & Sorbini 1980; Sorbini 1981). The limestones are part of the informal geological unit ‗Calcari di Melissano' (Cenomanian – Maastrichtian), that was deposited in a shallower portion of the inner lagoon of the Apulian Carbonate Platform (Bossio et al. 2006). The age of the limestones outcropping in the area of Nardò is considered to be upper Campanian – lower Maastrichtian based on nannofossils (Medizza & Sorbini 1980; Sorbini 1978; Sorbini 1981). The specimen is preserved in a finely laminated (submillimetric laminae) carbonate mudstone that is light hazel in colour (Fig. 3.1). Spectroscopic analysis indicates that the carbonate is a Mg-rich calcite, i.e., dolomite (see also Fig. A3.10). The macroscopic lamination results from small differences in the recrystallization of the mudstone into euhedral nannometric crystals (dolomitization process); the thickest lamina is 2 mm thick, and darker than the other laminae, suggesting hypoxic conditions at the sediment-water interface. Neither bioclasts nor microfossils are present in the sediment, and the only evidence of bioturbation is represented by one U-shaped tubular burrow (cf. *Terebellina*) preserved next to the specimen (Fig. 3.1a, top right). The densely packed laminae, the lack of

microfossils and bioclasts, and the limited presence of bioturbation, are consistent with deposition within anoxic to dysoxic waters in a tropical, semiarid environment.

3.3.2 Systematic Palaeontology

Reptilia Linnaeus, 1758

Squamata Oppel, 1811

Pythonomorpha Cope, 1869

DOLICHOSAURIDAE Gervais, 1852

Definition. Dolichosauridae is here defined as the group including all taxa sharing a more recent common ancestor with *Dolichosaurus longicollis* than with *Aigialosaurus* sp. In our study, this includes the following genera: *Dolichosaurus*, *Pontosaurus*, *Primitivus* gen. nov., *Adriosaurus*, *Acteosaurus*, and *Aphanizocnemus* (cf. Nopcsa (Nopcsa 1903) and Conrad (Conrad 2008)).

Diagnosis. Dolichosauridae is here defined as the group of non-ophidian pythonomorphs characterised by the following combination of features: non-sutural contact between premaxilla and maxilla; jugal lacking large posterior process; postorbital portion of postfrontal + postorbital forming half or more of posterior orbital margin; hypapophyses/hypapophyseal peduncles extending to the tenth presacral/precloacal vertebra or beyond (10-12 cervical vertebrae); 32-40 presacral/precloacal vertebrae; reduced scapula and coracoid; tail deep, laterally compressed (cf. Pierce & Caldwell 2004; Caldwell 2000; 2006; Palci & Caldwell 2010).

Primitivus manduriensis gen. et sp. nov.

Etymology. The genus is named after the famous red wine grape varietal, ‗Primitivo', native to and grown in great quantities in the Salento Peninsula (Puglia, Southern Italy). The species name has been chosen to honour the full name of the wine, ‗Primitivo di Manduria', which is not only produced around the town of Manduria (Taranto, Puglia), but also in other localities of the Salento Peninsula, including Nardò where the specimen was found.

Holotype. MPUR NS 161, an almost complete skeleton mostly in articulation, exposed in dorsal view, partially embedded in the rock, and lacking the terminal portion of the tail and some elements of the skull. Together with the skeleton, there are abundant soft tissues preserved, including permineralized muscle fibers and integument (Figs. 3.1-3.8; Appendix 3.2, Figs. A3.2-A3.9).

Locality and Stratigraphy. Nardò, Lecce (Puglia, Southern Italy); higher portion of the informal geological unit ‗Calcari di Melissano', Apulian Carbonate Platform (Bossio et al. 2006; Medizza & Sorbini 1980; Sorbini 1978; Sorbini 1981).

Age. Upper Campanian – lower Maastrichtian, based on microfossils (Medizza & Sorbini 1980; Sorbini 1978; Sorbini 1981).

Diagnosis. The new taxon can be distinguished from other dolichosaurids by the following unique combination of features: contact between frontal and prefrontal limited in dorsal view; sutural contact between septomaxilla anterolateral margin and maxilla; septomaxilla posterolateral margin in contact with nasal; 10 cervical vertebrae + 22 dorsal vertebrae (32 presacrals); bowtie-shaped astragalus (with both a dorsal and a ventral notch); calcaneum with proximal concavity for articulation with fibula; deeply imbricated, small subcircular scales on lateral sides of trunk and limbs; larger diamond-shaped scales on trunk dorsal region; transversally expanded subcaudal scales.

3.3.3 Description

Cranial skeleton – The skull is dorsoventrally crushed and exposed in dorsal view (Figs. 3.2; A3.2). Many elements are fragmentary and preserved in part as impressions, as portions of the bones were lost with the unknown counterpart. This is the case for the parietal and frontal, both of which are preserved as impressions in the area adjacent to the fronto-parietal suture. The occipital region is badly crushed, and the cavities for the semicircular canals are partially exposed as the posterodorsal portion of the braincase (i.e., part of the otoccipitals) is missing. The limit between the basioccipital and the atlas is clear, and on the right side of the atlas, forming a 45° angle with its longitudinal axis, is a thin and long bone projecting posteriorly, that is part of the hyoid apparatus and most likely represents the first ceratobranchial. Both quadrates can be easily identified: the right quadrate is better preserved and almost complete; the left is mostly present as an impression on the matrix. On the right side, about all the original contacts for the quadrate are preserved both dorsally (with the skull roof) and ventrally (with pterygoid and mandible). The anterior portions of both the lower and upper jaws are hard to differentiate, while posteriorly the mandibular elements are easier to recognize at least as impressions, with the retroarticular process being particularly well-developed. The anterior portion of the skull preserves the septomaxillae and portions of the nasals and premaxilla.

The three large foramina on each side at the back of the braincase are most likely areas where the cavity of the inner ear (semicircular canals) is exposed due to the breakage and removal of the dorsal portions of the otoccipitals) (Fig. A3.2a). The anterior and posterior cavities correspond to coronal sections through the anterior and posterior semicircular canals, respectively; the largest and more medially placed cavity most likely represents a section through the crus commune, i.e., the portion of the inner ear where anterior and posterior semicircular

canals meet dorsally. Between these foramina is a trapezoidal element that is likely a dorsoventrally flattened supraoccipital. Anterior to the semicircular canals, in what is likely a portion of prootic, a distinct foramen is visible on the right side, and is interpreted here as an opening for the VII cranial nerve (facial nerve). These identifications are based on braincase descriptions in Russell (1967), Rieppel & Zaher (2000), Bever et al. (2005), and Head et al. (2009). Posterior to the otooccipital, the occipital condyle is partially exposed and its articulation with the atlas is visible as a slightly convex line (Fig. A3.2a).

The parietal is very fragmentary, especially anteriorly, but a general outline of this bone can be resolved in dorsal view on the left side, where the posterior process is broken but almost complete, and as an impression of its ventral surface on the right side (Fig. A3.2a). The parietal table is broadly trapezoidal, while the posterolateral process (visible on the left side) is slender and triangular in dorsal view. It is not clear whether a large gap between parietal and supraoccipital represents the equivalent of the space for the *processus ascendens tecti synotici* or is an artefact of preservation. The fronto-parietal suture is preserved mostly as an impression, but it is clear that it was fairly straight, similar to that observed in aigialosaurs or even modern monitor lizards. The outline of the pineal foramen, located anteriorly in the parietal table, can be easily recognized, and anterior to it is a distinct mid-sagittal line that divides the left and right sides of the parietal. The posterior portion of the parietal, still mostly represented by bone, indicates that the bone was divided only anteriorly (parietal notch) as is typical of juvenile monitor lizards (Palci et al. 2016) and was not paired, an adult feature observed among extant lizards only within gekkotans (Gauthier et al. 2012). The incomplete ossification of left and right counterparts of the parietal can be interpreted as either a juvenile feature or a delay in ossification, a phenomenon common in aquatic forms (see discussion).

On the right side of the skull, in front of the prootic and lying along the right side of the parietal table, is a rod-like element that is interpreted here as the epipterygoid, which must have rotated 90° due to the dorsoventral diagenetic compression of the skull.

The frontal is a very elongated unpaired element, much wider posteriorly at the suture with the parietal, then strongly constricted between the orbits, and finally tapering anteriorly between the nasals. As in pontosaurs and coniasaurs, the posterior end is much more broadly expanded than the anterior one (Caldwell 1999; Caldwell 2006; Pierce & Caldwell 2004). The posterior half of the frontal is mostly preserved as an impression, whereas anteriorly some fragments of the bone are still present, and the most anterior fragment (tip of the frontal) is located slightly anterior to the mid-point of the prefrontal. On the impression of the posterior ventral surface of the frontal, it is possible to recognize the natural mould of the olfactory canal (Figs. 3.2; A3.2a). Whether or not the canal was completely enclosed by descending flanges of the frontal anteriorly cannot be determined.

Laterally and in front of the orbits, the frontal articulates with the prefrontals. A fragment of bone sandwiched between the frontal and right prefrontal may represent the posterior end of the right nasal. The extension of the impression of the premaxillary internarial bar suggests that originally it came in contact with the anterior tip of the frontal posteriorly (Figs. 3.2; A3.2a).

A fragment of the left postorbitofrontal is preserved on the left side of the skull. It clasps the fronto-parietal suture, forms the posterodorsal margin of the orbit, and has a distinct squamosal ramus projecting posteriorly (Fig. A3.2a). The squamosal ramus is cracked longitudinally, but its slender, distally tapering shape can nonetheless be inferred. Posterolateral to the squamosal ramus of the postorbitofrontal is the impression of a pointed and slightly

recurved element that must be the anterior portion of the squamosal. The impression can be followed posteriorly as it connects to a series of thin rod-like fragments.

Medial to the head of the right quadrate, and partially overlapping it, there is another rod-like element that I interpreted as a fragment of the right squamosal. This element can be followed anteriorly into a series of other fragments and impressions that together taper into a point, very similar in thickness and length to its left counterpart (Fig. A3.2a).

The supratemporal is preserved on the left side as a small element inserted between the otoccipital and the posterior end of the squamosal. Its right counterpart can be identified in a similar position on the opposite side of the skull, where most of it is exposed due to breakage and displacement of the posterior end of the right squamosal (Fig. A3.2a). The extension of the contact between the supratemporal and the quadrate seems to be greater than the contact between the quadrate and the squamosal, and also to prevent the contact between the quadrate and the paroccipital process (at least in dorsal view).

Both quadrates are preserved in their articular position: the right one is quite complete and exposed in posterolateral view, whereas the left quadrate is present mostly as an impression of its medial face. The anterior outline of the quadrate is quite convex, and there is a distinct, posteriorly projecting suprastapedial process that is well-preserved on the right quadrate. Details of the tympanic ala and tympanic crest cannot be resolved, but a distinct lateral conch is visible anterior to the suprastapedial process (Figs. 3.2; A3.2a). Anterodorsally, the quadrate head is still in articulation with a rod-like element that likely represents a fragment of the squamosal (more than the supratemporal); the rest of the dorsal-posterodorsal contact was likely occupied by the parietal ramus (which in the right side of the skull is missing, but it is present on the left half), and then with at least one elongated element that projects farther more posteriorly than the

quadrate itself, interpreted here as the supratemporal. This last bone seems also to prevent the contact between the quadrate and the paroccipital process, the position of which is indicated by the semicircular canal openings (Fig. A3.2a). The right quadrate overlaps the posterior process (quadrate ramus) of the pterygoid, to which is in contact medially. It is interesting to note that according to the geometric relationship that the quadrates and mandibles have as compressed on the slab, the quadrates would turn to be almost vertical in lateral view, more similar to the condition seen in mosasaurs, aigialosaurs, or even most iguanians, rather than for instance in varanids (Lee 2005; pers. obs.).

Only the right pterygoid is partially exposed in dorsal view, and part of it is only preserved as an impression (Fig. A3.2a). The quadrate ramus consists of a robust, plate-like bone, posteriorly recurved towards the quadrate condyle (i.e., with the concavity facing laterally). The termination of the quadrate ramus does not taper significantly posteriorly, and terminates in a blunt, subrectangular end. On the left side the quadrate ramus is not exposed, but anteriorly a bone that could be interpreted as the ectopterygoid process is exposed in dorsal view, and forms the floor to the anterior portion of the orbit.

On the right side of the skull is a natural mould of the prefrontal, located just in front of the orbit; the element is rotated medially, so that what we see is the mould of its lateral and posterior walls. The left counterpart instead is not clearly identifiable among a mass of bone fragments. Due to poor preservation, nothing can be said about the contact between the prefrontal and the maxilla. The contact between frontal and prefrontal appears to have been very limited, and must have occurred at the posterior end of the external naris. The lateral wall of the prefrontal tapers anteriorly, and has a straight lateral margin, while posteriorly it is both dorso-ventrally deeper and medio-laterally wider. No indication of a lacrimal foramen or notch can be

observed. The posterior wall shows a gently sinusoidal ventral margin, and a weak median concavity that is facing posteriorly, while its dorsal margin is smoothly rounded (Figs. 3.2; A3.2a).

The premaxilla is missing, and only impressions and fragments of the internarial bar are visible between the two septomaxillae, and extending posteriorly towards the anterior tip of the frontal (Fig. A3.2a). Close to the tip of the snout, two sub-triangular and paired elements are identified as the septomaxillae. The left septomaxilla is fractured, and only its medial portion is preserved. The right septomaxilla is complete, and its shape in dorsal view is extremely similar to that of *Coniasaurus gracilodens* (Caldwell 1999). The anterolateral margin shows a sutural contact with the maxilla, while posterolaterally it was at least in contact with the nasal (Fig. A3.2a): this sutural contact between septomaxilla and maxilla likely prevented the maxilla from moving independent of the rest of the skull (pers. obs.). The external naris must have been framed by: the septomaxilla anteriorly; the medial margins of maxilla and prefrontal laterally; the internarial bar of the premaxilla and the nasals medially; and must have terminated posteriorly in a tapering point where prefrontal, nasal, and possibly the frontal met.

Two paired elements, very narrow and pointed anteriorly, are identified as fragments of the anterior ends of the nasals, and are very similar in shape and topographical location to those of *P. kornhuberi* (Caldwell 2006). A subtriangular fragment at the posterior end of the external naris, between prefrontal and frontal, is also interpreted here as a fragment of the right nasal (posterior end); this is because of its shape, size, position, and the presence of an impression in the sediment that connects this element to the anterior tip of the nasal described above. If this fragment is in its natural position, then the frontal may have been excluded from the posterior margin of the external naris by nasals and prefrontals.

Only fragments of the left and right maxillae are present. The left maxilla is the most complete, and appears to be preserved in dorsal view. The top portion has been sheared off and displaced medially, so that the canal for the second branch of the trigeminal nerve (V_2) is exposed. Anteriorly, and located on the course of the canal for the above-mentioned nerve, is the section through a large tooth alveolus. Only one small tooth is preserved anteriorly on the maxilla. Just under the maxilla, and exposed only anteriorly, where a portion of the latter is missing, a fragment of the dentary can be observed. It bears one large tooth, complete with the root. Small fragments of dentary are also visible on the right side of the skull, but not much can be said about the general shape of this bone, except that it was probably extending posteriorly below the orbit.

Most of the lower jaws are preserved only as impressions (Figs. 3.2; A3.2a). The condylar region appears to be exposed in dorsolateral view, as suggested by the shape of the retroarticular processes, but anteriorly the jaws are twisted somewhat more medially. On the impression of the right mandible, it is possible to identify one extensive suture line running antero-posteriorly, and starting in front of the condylar region: considering that the impression is that of the lateral face of the jaw, this suture is most likely that between the surangular and the angular (Fig. A3.2a). On the left side this same suture can be observed dividing posterior fragments of surangular and angular. The retroarticular processes are preserved only as impressions, but it is possible to infer their size and shape very clearly. The retroarticular processes were broad and sub-rectangular, similar in shape and extension to those of *Pontosaurus* spp. and *Adriosaurus suessi* (Caldwell 2006; Lee & Caldwell 2000; Pierce & Caldwell 2004).

Scleral ossicles are visible inside both orbits, but an almost complete scleral ring is only visible on the right side. The shape of the individual ossicles cannot be established due to poor preservation, and a count of the number of elements is also not possible.

A jugal is not preserved, but the posterior extent of the orbit can be estimated by observing the posterior extension of the sclerotic ring. The orbits must have been antero-posteriorly elongate and relatively quite large, though not as much as in *Pontosaurus* (orbit diameter to skull length = 0.13; in *P. kornhuberi* = 0.19; in *P. lesinensis* = 0.19) (see Table A3.1 for measurements of the specimen).

As mentioned above, only two marginal teeth are preserved in association with the skull elements (Fig. A3.3). They are both located towards the anterior end of the skull, and point in opposite directions. The most anterior of the two, lacking the root and pointing laterally in dorsal view, is interpreted as a maxillary tooth; while the other one, almost complete and pointing medially, probably belongs to a fragment of the left dentary. Both teeth are conical, with no apparent lateral compression, and are slightly recurved posteriorly. The tooth crowns have multiple longitudinal facets separated by thin ridges (Fig. A3.3a, b).

A slender and elongated element coming out from below the base of the skull, and exposed on the right side of the atlas and axis, is the first ceratobranchial (Figs. 3.2; A3.2a). It is broken in two sections at mid-length and the posterior half is slightly displaced medially. This element terminates in a blunt end posteriorly, to which a thin rod of calcified cartilage is attached. The cartilaginous portion is preserved in a displaced position, and its longitudinal axis forms an angle of about 60° with that of the ossified portion of the ceratobranchial.

Axial skeleton – Both vertebrae and ribs show some degree of pachyostosis, which is, *sensu stricto* a thickening of the perichondral bone – as defined by Ricqlès & Buffrénil (Ricqlès & Buffrénil 2001). The mode of preservation of most of the skeleton facilitates the observation of the thicker walls (of vertebrae and ribs especially) and the brittle-like internal organization of the bony tissue. Unfortunately, without sectioning the bones it is not possible to verify if osteosclerosis had developed in the inner bone tissue (Houssaye 2009; Houssaye et al. 2008; Houssaye et al. 2016; Rage et al. 2016).

Both the cervical and dorsal vertebrae are elongate, and roughly rectangular in shape, while the sacral and caudal vertebrae are shorter and more square (see measurements in Table A3.1). The dimensions of the vertebrae are in general quite different from typical ophidiomorph squamates, in which cervicals and dorsals are quite short relatively to their width.

The precaudal vertebral column is complete, though for the tail the most distal part is missing. The boundary between cervical and dorsal series – as defined by Hoffstetter & Gasc (Hoffstetter & Gasc 1969): the first dorsal vertebra bears the first rib that articulates to the sternum – can be determined due to some preserved costal cartilages (Fig. 3.5d). There are four well-preserved costal cartilages on the right side of the body, which although partially covered by dorsal ribs can be highlighted using UV light. The third of these costal cartilages still preserves its articulation with one of the ribs. By following a rib to its articulation with the corresponding vertebra, it is possible to determine that the latter must represent the third dorsal, and that therefore there are 10 cervical and 22 dorsal vertebrae. The atlas is identified as the shorter element articulating with the basioccipital condyle, just before the first cervical vertebra with a rib (i.e., the axis) (Fig. A3.2a). The number of presacral vertebrae is very different from *Pontosaurus*, in which the number of dorsals is above 26, and in general from most

ophidiomorphs that have a presacral vertebral count greater than 35 (39 in *Pontosaurus kornhuberi*) (Caldwell 2006; Caldwell & Dal Sasso 2004; Palci & Caldwell 2007; Pierce & Caldwell 2004). The presacral vertebral count in *Primitivus* is 32, just slightly higher than *Aigialosaurus dalmaticus*, where there are only 7 cervicals, followed by 22 dorsals like in *Primitivus*, for a total of 29 presacral vertebrae.

The dorsal vertebrae in MPUR NS 161 are all broken through the neural arch or slightly ventral to it (Figs. 3.1, 3.5). Their centra are cylindrical and robust, slightly expanded anteriorly and bear well-developed, laterally projecting synapophyses. The last dorsal bears a pair of very small ribs.

There are two sacrals, with the sacral ribs still in articulation with the posterior iliac blade. The first pair of sacral ribs is directed laterally, while the second pair is somewhat recurved anteriorly. The distal bony end of the second sacral rib bears an indentation on the posterior margin, which on both the left and right side is occupied by cartilage (Figs. 3.3c-d; A3.4b). Such a morphology of the second sacral rib is similarly present in some iguanians, such as *Iguana* sp., *Agama* sp., *Physignathus* sp., while in other lizards, such as *Gecko* sp., *Varanus* sp. and *Heloderma* sp., the distal bony margin of the second sacral rib appears quite square, and the posterior margin of the second sacral rib is about straight (pers. obs.). In the case of *Iguana* sp. or *Agama* sp., it looks like the posterior margin of the second sacral rib has a bony projection located about mid-length; in the case of MPUR NS 161 or *Physignathus* sp., this bony projection is located more distally, looking more like an indentation of the posterior distal corner of the sacral rib.

Posterior to the sacrals, there are several vertebrae with long distally-tapering transverse processes that point laterally, but from about the tenth caudal vertebra the orientation of the

transverse processes changes, becoming slightly posteriorly oriented. There are 19 caudal vertebrae preserved in dorsal view after the sacrum, then the tail rotates about 90° (between caudals 17th and 21st) and the following caudals are exposed in left lateral view (Figs. 3.1, 3.6g-h, 3.7). The transverse processes are well developed in the first ten caudal vertebrae, then reduce in size between the 11th and 16th vertebra, where the tail begins to turn. After the curvature, there is no more evidence of transverse processes, although this might be due to preservation bias (these vertebrae are preserved in lateral view and the transverse processes may have broken off). In the portion of the tail exposed in lateral view, long haemal arches (or chevron bones) can be recognized between the 22nd and the 27th caudals (Figs. 3.6g-h, 3.7). After the 27th caudal vertebra, there is a gap due to matrix covering the specimen, followed by at least seven more caudals. In total, there are 37 caudals preserved, but considering that the last vertebrae present on the slab show no significant reduction in size, the tail was likely much longer. The chevron bones are slightly flattened against the vertebral centra, and most of them are disarticulated; their length is greater than the corresponding neural spines, at least for all the caudals preserved in lateral view (Fig. 3.6g-h). The caudal vertebral centra bear posteriorly a distinctive pedestal (haemapophysis) to which the chevron articulates, so the haemal arches are not fused to the haemapophyses, and the articular facet is posteroventrally oriented. Moreover, between two of the caudal vertebrae preserved in lateral view, it is possible to observe a zygosphene-zygantrum supplementary articulation (Fig. 3.6h).

The caudal neural spines in lateral view are inclined posteriorly about 45°, and narrow anteroposteriorly. Some scales preserved as both mineralizations and impressions in lateral view along the caudal region, assist in determining the outline of the tail (Fig. 3.6f-h). The hypaxial portion is greatly dorsoventrally deepened in comparison to the epaxial portion, however, it is

also clear that the epaxial portion of the tail must have extended dorsally beyond the neural spines. Indeed, along the dorsal edge of the tail, the scales impressed on the matrix indicate that there was some sort of caudal fin, similar to that of some modern sea snakes and sea kraits (e.g., *Hydrophis platurus*, *Laticauda colubrina*), or the water monitor *Varanus salvator*. The width of the anterior portion of the tail, as inferred from the extension of the transverse processes, is quite remarkable, and is consistent with attachment for powerful caudofemoralis muscles. The depth of the posterior part of the tail suggests that it must have served as an excellent propelling organ during swimming.

Fragments of cervical ribs are preserved along the neck, but most of these ribs are either not fully exposed or too fragmentary to allow proper description. As was mentioned above, the limit between the neck and the trunk is recognizable thanks to the preservation of four sternal cartilages on the right side of the body, one of which (the third) retains its connection to one of the ribs, which in turn is articulated to one of the vertebrae (the third dorsal vertebra).

All the ribs are single-headed. The proximal head is flared, and there is no neck-like constriction. The ribs have a thick, pachyostotic shaft, and taper distally towards the end, but expand again just before the tip, probably to form a surface for the attachment of a cartilaginous termination (Fig. 3.5d). The anterior dorsal ribs are uniformly recurved similarly to *Pontosaurus lesinensis* or *Dolichosaurus longicollis*, and unlike *Pontosaurus kornhuberi* or *Mesoleptos zendrinii*, where the distal portion of the ribs is very straight (Caldwell 2000; Caldwell 2006; Caldwell & Dal Sasso 2004; Lee & Scanlon 2002a; Palci & Caldwell 2010; Pierce & Caldwell 2004). Some of the trunk ribs preserved as impressions on the slab also show a weak longitudinal groove, closer to the anterior margin of the shaft. The longest dorsal rib is about 81.5 mm, which indicates that the trunk must have been fairly deep compared to other squamates, as can be

expected in an animal adapted to swimming (Motani et al. 1996) (Table A3.1). Finally, in MPUR NS 161 there are five terminal dorsal ribs considerably shorter and straight in comparison to the rest of the thoracic series. This anatomy differs from that of mosasaurids where there is a much longer series of short presacral ribs, and similarly to more basal non-ophidian pythonomorphs where this feature can be observed. In *Pontosaurus kornhuberi* there are at least four shortened presacral ribs, while in *Adriosaurus* spp. the decrease in size is quite gradual, with the last two posterior dorsal ribs being significantly shorter. The condition is variable instead in aigialosaurs, since in *Aigialosaurus dalmaticus* all the presacral ribs are generally shorter and decrease in length gradually as in *Adriosaurus* spp., whereas *Aigialosaurus bucchichi* is similar to MPUR NS 161.

Appendicular skeleton – With respect to *Pontosaurus kornhuberi*, *Acteosaurus tommasinii*, and *Adriosaurus suessi*, the contrast in length between forelimbs and hindlimbs in MPUR NS 161 is not as pronounced, being more similar to the condition in both *Aigialosaurus* species. Following Palci & Caldwell (Palci & Caldwell 2010), this can be quantified through the humerus and femur to mean dorsal vertebra length (mdv) ratio: the humerus mdv ratio in MPUR NS 161 is up to 2.3, against a value of 1.3 in *Acteosaurus*, 2.0 in *P. kornhuberi*, and between 1.6 and 2.2 in *Adriosaurus suessi*, and a similar value of 2.3 for *Aigialosaurus* spp.; for the femur to mdv ratio instead, the value in MPUR NS 161 is 2.9, slightly higher than both *Aigialosaurus* spp. (2.6-2.7) and *Acteosaurus* (2.7), and much lower in comparison to *P. kornhuberi* (3.3) and *Adriosaurus suessi* (3.3-3.6).

Only the right pectoral girdle is clearly recognizable on the skeleton as exposed, and this is partially overlapped by the ribs at the cervical-dorsal series transition, which are now lost but

have left impressions on the surface of the bones (Figs. 33a-b; A3.4a). Of the left pectoral girdle, only a large cartilaginous element is visible on the left side of the trunk, and this most likely represents the suprascapular cartilage (Figs. 3.1, 3.5a-b).

The scapula and coracoid are single elements, and are not fused together. Under UV light, cartilage is identified in several places around both the scapula and coracoid (Figs. 3.3a-b; A3.4a). Overall, the pectoral girdle is quite reduced in comparison to the rest of the body, a feature typical of pythonomorphs, and its morphology resembles very much the condition seen in *Carsosaurus marchesetti* and *Dolichosaurus longicollis*.

The scapula is hourglass-shaped, much smaller than the coracoid and with both ends about the same width. This is different from the condition identified for instance in *Adriosaurus skrbinensis*, and more similar instead to that of *Dolichosaurus longicollis*, *Carsosaurus marchesetti*, and *Coniasaurus gracilodens*.

The coracoid is crescent-shaped, similar to that of *Aigialosaurus bucchichi* and *Carsosaurus marchesetti*. There seems to be no emargination on the anterior margin of the coracoid, while a scapulocoracoid fenestra seems to be present close to the glenoid fossa, as in *C. marchesetti*. Presence of a coracoid foramen cannot be confirmed, due to extensive cartilage material covering the median portion of the bone (epicoracoid cartilage), surrounding both the coracoid and the scapula, and likely in contact with the suprascapula (which is also preserved as cartilage).

The forelimbs are preserved pressed to the body and pointing posteriorly, so that the hand is in ventral view (flexor aspect). The overall morphology of the humerus resembles that of *Carsosaurus marchesetti*, rather than either *Pontosaurus* or *Aigialosaurus*. The bone is hourglass-shaped but still quite elongated in comparison to the pectoral girdle elements and the

presacral column, while in both *Pontosaurus* and *Aigialosaurus* the propodial is clearly shortened relatively to the overall length of the limb (see measurements in Table A3.1). The distal end surface of the humerus is damaged, and the bone does not show the presence of either the ectepicondylar or the entepicondylar foramina. Although lack of an entepicondylar foramen is expected, as it is an autapomorphy of Squamata (Estes et al. 1988), lack of the ectepicondylar foramen may be preservational. The epiphyses are present on both humeri, but are not fully ossified, as observed when the skeleton is exposed to the UV light (Figs. 3.3-3.4; A3.4-A3.7).

The radius and ulna are best preserved on the left side. It is not possible to resolve their proximal epiphyses on either side of the body, however, on the left forelimb, distal unfused epiphyses (slightly disarticulated) are clearly visible on both bones. The two bones are close together proximally, contacting each other at the articulation with the distal margin of the humerus, then strongly diverge distally, although part of the divergence is artificial, because the ulna is no longer in articulation with the ulnare and its distal end is located dorsal to the pisiform (Figs. 3.4a-d; A3.6). Divergent epipodials are also characteristic of other non-ophidian pythonomorphs, and are considered to be associated with an aquatic lifestyle (Caldwell et al. 1995; Carroll & de Braga 1992; Lee & Caldwell 2000; Pierce & Caldwell 2004; Russell 1967). The radius is a rod-like bone, slightly hourglass-shaped, with its posterior margin more prominently recurved than the anterior one; both its proximal and distal ends are only weakly enlarged in comparison to the thin shaft. The distal end has an oblique surface to which the distal epiphysis is attached. The ulna has a more evidently constricted shaft, with a more symmetrical anterior proximal end, and a posterior proximal end characterized by a distinct olecranon process.

In both fore and hind limbs the autopodium is much longer than the epipodial portion, consistent with the tendency of reduction of the proximal elements of the limb found in other non-ophidian pythonomorphs; however, in MPUR NS 161 this tendency is not as strong as in both *Pontosaurus* and *Aigialosaurus* for the propodials, even if the autopodial length is more than twice the length of the epipodials.

The right manus is very poorly preserved, so the following description is based on the left, which is complete, although surface preservation is not excellent (most of the perichondral bone has been sheared off) (Figs. 3.4a-d; A3.6). In the left manus only the proximal carpals are readily recognizable, while of the distal carpals only the large fourth distal carpal can be seen close to the proximal end of the metacarpal IV.

The proximal carpals consist of a large square radiale, located between the epiphysis of the radius and metacarpals I and II; a large round central element (likely the lateral centrale), located postaxial to the radiale; a large oval ulnare, postaxial to the lateral centrale; and a small, comma-shaped pisiform, sandwiched between the ulnare and the distal epiphysis of the ulna (therefore, the distal end of the ulna is clearly disarticulated and shifted somewhat postaxially).

All metacarpals are hourglass-shaped (Figs. 3.4a-d; A3.6). Metacarpal I is the shortest and broadest of the metacarpals, followed by metacarpal V, while metacarpal III is the longest.

The phalangeal formula for the manus is 2-3-4-5-3. Shape and size of all the phalanges (excluding the unguals) are similar in all digits with a flared proximal head and a less expanded distal condyle (Fig. A3.6b). Most ungual phalanges are quite well preserved on both manus and pes, making up a distinct claw, posteriorly recurved and bearing two tubercles for attachment of the flexor musculature: a larger one located ventroproximally, and a smaller one located on the ventral margin (Fig. A3.8).

All the unguals appear mediolaterally compressed and taper anteriorly into a blunted distal tip. On some ungual phalanges the articulation for the penultimate phalanx is also visible, and this facet appears slightly sinusoidal in lateral view. On the dorsolateral surface of the ungual phalanges there are two foramina: one is located more proximally, and the other one more anteriorly, at about the mid-length of the dorsal margin leading to the distal tip of the ungual. Below this second foramen, running longitudinally along the tapering distal end of the ungual phalanges, there are some parallel grooves that do not reach the proximal end of the ungual (Fig. A3.8).

The pelvic girdle is flattened on the slab and both sides are exposed in medial view, with the individual bones still in articulation or just slightly dislocated (Figs. 3.3c-d; A3.4b). All the pelvic elements are preserved: pubes and ischia are complete, while the ilia are present part as actual bone and part as an impression in the matrix. Although tightly connected, the individual pelvic elements are not fused together.

In dorsomedial view, the ilium is characterized by an elongated and well developed rod-like, posteriorly oriented process – here referred to as the posterior iliac or postiliac process – and a long, thin anteroventrally oriented preacetabular process overlapping the pubis (Fig. A3.4b). The ilium is still connected to both sacral ribs, and this articulation is visible on the medial aspect of the right postiliac process, although most of the iliac process is preserved only as an impression. The contact between the second sacral rib and the ilium is particularly intact, with a strip of cartilage completing the termination of the rib onto the posterior iliac process (Figs. 3.3c-d; A3.4b). The posterior end of the postiliac process is blunt in mediolateral view, and on the left side it partially overlaps the left transverse process of the first caudal (pygal?) vertebra. The presence of the dorsoanteriorly oriented supracetabular process found in many

terrestrial lizards (e.g., varanoids, iguanians) as well as mosasaurids, cannot be verified due to preservational factors: both left and right anterior iliac portions are flattened against the head of the femur, and their dorsal margin, where the supracetabular anterior iliac tubercle might be, is not clearly exposed. The two facets for articulation with the pubis and the ischium on the iliac head have about the same length: the right ilium is still weakly articulated to the ischium more posteriorly, while the left ilium is still articulated to the pubis but only partially with the ischium.

The left pubis is particularly well-preserved, with a broad proximal head that is greatly expanded posteriorly in lateral view (resulting in the typical hatchet-like shape for this bone) (Figs. 3.3c-d; A3.4b). The distal end of the right pubis is hidden underneath the last dorsal vertebra, and only its proximal head remains visible. Due to the poor preservation of the bony surface, it is not possible to determine the location or presence of a pubic foramen. The anterior pubic process (or tubercle) is very inconspicuous, and appears only as a swollen eminence along the anterior margin of the proximal head of the pubis, not far from the acetabulum. The articular facet for the ilium occupies most of the dorsal and posterodorsal margin of the pubis in medial view; while the facet for the ischium is located posteriorly on the pubic head. The ventromedially directed pubic shaft is significantly narrower than the proximal head, and ends distally in a square termination, quite weakly expanded; still attached to the distal end, there is also a fragment of cartilage that is most likely part of the pubic symphysis. On the medial side of the pubic shaft, there is a well-preserved and dorsoventrally elongated, teardrop-shaped surface for the attachment of muscle tissues: considering the position (medial view), the surface was likely for the insertion of the *Musculus puboischiofemoralis internus* (Snyder 1954) (Figs. 3.3c-d, 3.5e-f; A3.4b).

The ischium is the shortest element of the hip. Both ischia are a bit dislocated from their original position in connection with the other pelvic bones, and are partially covered by the sacral vertebrae and ribs (Fig. A3.4b). The ischium is strongly recurved along its anterior margin, and its proximal head is narrower than the distal end. The ischial expansion opens posteriorly right below the ischial neck to form a steep angle and then continues along the posterior margin of the ventromedially directed shaft, almost until the distal end. The distal termination of the ischium, where the element would contacts its counterpart along the midsagittal plane, is fairly straight and at least twice the size of the distal extremity of the pubis. The proximal head of the ischium articulates with the pubis along an anterior facet, and with the ilium along its dorsal margin.

Unlike in *Aigialosaurus* spp., in MPUR NS 161 the femur is still quite long relative to the axial skeleton, and the morphology of the pes is not significantly modified in comparison to a terrestrial lizard, as observed in *Pontosaurus* (Caldwell 2006; Caldwell & Dal Sasso 2004; Pierce & Caldwell 2004). However, the epipodials in the hindlimbs, similar to those described for the forelimbs, are strongly divergent distally, a feature that is associated with swimming (Lee & Caldwell 2000; Pierce & Caldwell 2004).

As in the humerus, the epiphyses of the femur are not completely ossified (Figs. 3.3c-d; A3.5b). The shaft of the femur is quite long and robust, almost twice the length of the epipodials (Table A3.1). The proximal epiphyses are partially overlapped by the anterior portions of the ilia. The proximal head of the femur is expanded, but less than the distal end; a gently rounded condyle for articulation with the pelvic girdle is visible at least on the left femur, especially when the element is exposed to UV light. On both sides of this condyle, in posterior view, there are two weak trochanters, with the internal one being slightly lower than the external (Figs. 3.3c-d;

A3.4b; A3.5b). For the articulation with the tibia and fibula, the distal femoral end in posterior view bears a more prominent mesial (tibiofibular) condyle, and a less prominent but wider lateral (tibial) condyle.

As a result of the flattening of the hindlimbs, with most of the axial skeleton visible in dorsal view, both pairs of epipodials are exposed on the slab in posterolateral view (Fig. A3.5b). The epiphyses of both the tibia and fibula are not fully ossified, nor fused to the diaphyses. They are in close contact proximally, at the articulation with the femur, but then diverge distally, as described for the radius and ulna.

The tibia is more robust than the fibula, and its proximal head is larger than the distal end (Fig. A3.5b). On the right tibia, both medial and lateral condyles can be recognized, and still contacting the articular cartilage of the distal end of the femur. The distal end of the tibia is fan-shaped, and articulates with both the astragalus and a small preaxial element that is identified as part of the tibial epiphysis. The tibial shaft is strongly constricted at mid-length and its internal margin is more prominently recurved than the external one.

The fibula is preserved mostly as an impression on both sides (only proximal and distal extremities are represented by bone). It is more gracile than the tibia, and both proximal and distal terminations are about half as wide than those of the latter bone (Fig. A3.5b). The internal articulation of the left fibula with the medial condyle of the tibia is particularly well-preserved, showing the close proximal contact of the two bones. The distal end of the fibula is somewhat irregular, due to the greatly expanded articular cartilage, and it contacts both the calcaneum (distally) and the astragalus (preaxially).

The mesopodium of MPUR NS 161 is by far the most complete ever found in any dolichosaur (Figs. 3.4e-f; A3.7). Both distal and proximal rows of tarsals are preserved on the

hindlimbs, though better exposed in the right pes, which is not overlapped by the tail. The proximal row consists of a bowtie-shaped astragalus, and a trapezoidal calcaneum, which shows a weak proximal concavity for articulation with the fibula (Fig. A3.7b). The two bones are clearly not fused together. The astragalus articulates proximally with the epipodials, and postaxially with the calcaneum.

In the right pes, distal to the astragalus and calcaneum, a large centrale and four distal tarsals are preserved. The first three distal tarsals increase gradually in size postaxially, while the fourth is the smallest (Fig. A3.7). There is no fifth distal tarsal. The centrale, which lies between the astragalus and the fourth distal tarsal is a large trapezoidal element, roughly as large as the calcaneum.

In all metatarsals the epiphyses are poorly ossified, especially distally (Figs. 3.4e-h; A3.7). Metatarsal I and V are shorter and stouter in comparison to the elongated and slender metatarsals II to IV (Table A3.1). Metatarsal I is the only element of the metapodium with a distal termination that is smaller than the proximal one, and it also has a greatly recurved preaxial margin. Metatarsal IV is the longest element of the metapodium, and like metatarsal II and III, is characterized by a relatively thin shaft. Metatarsal V is broadly expanded proximally, and slightly hooked.

Common to both metatarsals and phalanges is the presence of a flexor groove on the ventral aspect: this structure is visible on the distal half of the autopodial elements of the right pes that are preserved as impressions in the matrix (Figs. 3.4e-f; A3.7).

The phalangeal formula for the pes shows the typical primitive condition seen in lepidosaurs, corresponding to 2-3-4-5-4, so there is no reduction of the fifth digit, contrary to what is observed in aigialosaurs and mosasaurs. The overall shape of the phalanges of the pes is

similar to that of the same elements in the manus: they have a broad square proximal end, a constricted shaft and a smaller distal end (Fig. A3.7b). The terminal phalanges consist of well-developed claw-like unguals, and the same description given for the ungual phalanges of the manus also applies to the pes (Fig. A3.8).

Cartilage – With the use of UV light, it was possible to distinguish between bone and cartilage, and even identify cartilaginous elements that are not readily visible under natural light. These elements include: tracheal and bronchial rings, calcified sternal ribs, epicoracoid and suprascapular cartilages, and all the un-ossified appendicular epiphyses (Fig. 3.5). On the right side of the neck, starting from the fifth cervical vertebra – at the beginning of the bend in the neck – a set of tracheal half-rings are visible under UV light (Fig. 3.5c). Unlike *Pontosaurus kornhuberi*, where complete rings are preserved, in MPUR NS 161 only incomplete rings are present, and they appear as narrow rod-like fragments of cartilage compressed against the cervical vertebrae. The rings disappear next to the eighth cervical, where the cartilaginous portion of the pectoral girdle covers up most of the right side of the anterior region of the trunk. Under UV light, beneath both the ribs and vertebrae of the anterior trunk, several cartilaginous elements are observed (Fig. 3.5d). These include both the cartilaginous sternal ribs and the bronchial rings. The bronchial rings are well-exposed along the right side of the trunk: they appear as tiny rod-like fragments amongst the anterior dorsal ribs, and extend anteriorly up to a point just posterior to the right coracoid. Four pairs of cartilaginous sternal ribs, each formed by at least two segments, can be recognized, and are especially evident on the right side of the body. The sternal ribs can be distinguished from the other trunk ribs because of their greatly expanded distal ends. The third cartilaginous rib still retains its articulation with one of the dorsal ribs

(articulating with the 13th presacral vertebra). On the left side of the trunk, close to the proximal head of the left humerus, another broad cartilaginous element was UV illuminated that I interpreted as the suprascapula (Fig. 3.5a-b). The element is trapezoidal in shape, with the distal margin greatly expanded. Under UV light, the epicoracoid cartilage appears preserved in connection with the coracoid on the right side, and surrounds most of the scapula (Figs. 3.3a-b; A3.4a). This cartilage was crushed underneath some trunk ribs and the rest of the pectoral girdle; it is hard to tell if the right suprascapula is preserved, however the cartilaginous portion visible along the anterior margin of the scapula is quite extensive, so it is likely that the epicoracoid cartilage and suprascapula were in contact. With regard to the appendicular skeleton, all the epiphyses are unossified: the lack of ossification becomes more evident when the bones are exposed to UV radiation and the epiphyses are emphasized in a much brighter white colour, in comparison to the diaphysis, indicating a contrast in density and mineralization (Figs. 3.1-3.4; A3.4-A3.7).

Integument – Different types of squamation are recognizable together with the skeletal remains. Even accounting for some post-mortem flattening of the body during compaction of the sediments, the scales appear to be preserved in their original position (Figs. 3.1, 3.6). However, the external morphology of the scales is not preserved anywhere along the body, suggesting that it is not the outer layer of the epidermis (keratinized stratum corneum) that is preserved, but rather an inner layer of the integument, resulting in the reproduction of the scale outlines (here referred to as ―scale ghosts‖) and not the actual epidermal scales.

Deeply imbricated, small subcircular scale ghosts are visible on both sides of the specimen next to the trunk and limbs (Fig. 3.6a-e). Between the right forelimb and the trunk, the

permineralized integument follows the bend of the anterior portion of the skeleton, so that the scales look compressed against each other, highlighting the position of the original body outline. These small scales must have covered the sides and part of the belly of the animal, at least from the pectoral girdle to the sacral region (Fig. 3.6c). Larger diamond-shaped scales are preserved between the trunk ribs, and in particular on the left side of the posterior trunk region (Fig. 3.6c-d). These scales most likely covered the dorsal region of the body, since they appear to overlap the ribs (where present) and are abruptly interrupted where the bone is missing leaving only natural molds. Diamond-shaped scales are also present in lateral view along the tail, where in the ventral region there are at least four rows of rhomboidal scales before the beginning of the broader, transversely expanded, subcaudal scales. Dorsal caudal scales are also preserved, but are not as clear as the subcaudals (Fig. 3.6g). Impressions of rhomboidal scales are clearly visible above the neural spines of the caudals in lateral view (Fig. 3.6f), suggesting the presence of a fin-like dorsal expansion along the top of the tail, likely similar to that of modern sea snakes and sea kraits (e.g., *Hydrophis platurus* and *Laticauda colubrina*), or the water monitor *Varanus salvator*. One of the most important features characterizing the new marine lizard is the presence of transversally expanded scales, visible along the ventral margin of the last preserved caudal vertebrae, where the tail is exposed in left lateral view (Figs. 3.1, 3.6g-h, 3.7). The only extant squamates possessing such scales are some snakes (Lee & Scanlon 2002b), while amongst fossils a similar squamation has been found in another basal pythonomorph, *Pontosaurus kornhuberi* (Caldwell 2006; Caldwell & Dal Sasso 2004). Lee & Scanlon (2002b), and Lee (2005) refer to these scales as subcaudal scales – or simply subcaudals – and in snakes they can be present as single (i.e., one row) or paired (i.e., two adjacent rows). In MPUR NS 161, either the tail is exactly in left lateral view, with the scales visible along the ventral edge representing part of the

right-side counterparts (like the paired condition in snakes), or due to twisting and compression of the soft tissues – as suggested by the irregularity of the tail base outline – the long scales represent complete, transversally expanded ventral scales (like the single condition in snakes). According to this second interpretation, the partially exposed scale ghosts along the ventral edge would belong to the other flank (right) of the tail (Figs. 3.6g-h, 3.7). The subcaudals in MPUR NS 161 are antero-posteriorly shorter than the caudal centra, and the length of one centrum corresponds to that of about two scales, similar to *Pontosaurus kornhuberi*; in snakes this ratio is highly variable. The scale ghosts are preserved thanks to permineralization of the integument, or as impressions in the sediment. Being only the outline of the scales present, it is difficult to determine if the scales were smooth or keeled, as in the mosasauroids *Tylosaurus proriger* and *Ectenosaurus clidastoides*, or in *Pontosaurus kornhuberi* (Caldwell 2006; Lindgren et al. 2011; Snow 1878). In MPUR NS 161, the most complete scales are found in the posterior trunk region and around the hindlimbs (Fig. 3.6c-e), but even in these cases the permineralization of the soft tissue does not allow full assessment of their original external morphology. Finally, in some parts of the specimen there are extensive portions of permineralized soft tissues where no distinct squamation is recognizable. Here the scale ghosts are not discernible, and there is no fibre-like arrangement either, suggesting that no mineralized muscle fibres are present: what is exposed may be the dermis (with the epidermal layer being degraded) or even the superficial fascia (or hypodermis), which lies between the integument and the external musculature (Fig. 3.6a, b).

Muscles – Portions of permineralized epaxial and hypaxial musculature are preserved along the trunk and tail (Figs. 3.1, 3.5e-f, 3.8). Collagen fibres and muscle bundles are visible around the pelvic girdle and in close association with the anterior caudal vertebrae. To assess the

identity of the muscles in MPUR NS 161 I made comparisons with studies on the musculature of several squamates (Bhullar 2009; Gans et al. 2008; Moritz & Schilling 2013; Ritter 1996; Snyder 1954; Zaaf et al. 1999). On the right lateral posterior region of the trunk, where the body curves, small portions of permineralized muscles are preserved between the last dorsal ribs (Fig. 3.5e-f), with the fibers being obliquely oriented relative to the vertebral column. These muscles must have been part of the more internal layers, since they attach to the lateral surface of the vertebral centra, and seem to arise from the ventrolateral aspect of the trunk (hypaxial musculature), and are overlapped by both ribs and vertebrae. Based on their position, they may be part of the *musculus* (*m*.) *obliquus internus*, or of the *m. transversus abdominis* (Bhullar 2009; Ritter 1996). More muscle tissue is visible along the anterior margin of the ischia: these muscle fibers are so well-preserved that the single myomeres can be easily distinguished with the naked eye (Figs. 3.3c-d, 3.8a-c). Considering that the hips are visible in medial view, and the muscles appear to attach to the anterolateral surface of the ischia, most likely they represent a mineralized portion of the *m. puboischiofemoralis externus*, which usually originates from the lateral surface of the ischium and inserts onto the proximal portion of the shaft of the femur (Snyder 1954; Zaaf et al. 1999). Along the anterior caudal region, before the tail bend, a large portion of permineralized muscle tissue is preserved on the left side of the vertebral column (Figs. 3.8d-g; A3.9). This part of the tail is exposed in dorsal view, and according to the relationship between vertebrae and soft tissues, and the changes in orientation and organization of the muscle fibers, it is possible to identify at least two different types of fascicles likely belonging to different epaxial muscles: 1) antero-posteriorly oriented, thin and tubular-like fibres overlapping the transverse processes of some caudal vertebrae, interpreted as part of the *m. transversospinalis* (Figs. 3.8d, f, g); 2) bundles of broad and flat muscle sheets, positioned more laterally than the previous type (further

away from the vertebrae), and oriented obliquely relative to the long axis of the body, interpreted to be part of the *m. iliocaudalis* (Moritz & Schilling 2013; Ritter 1996; Snyder 1954) (Fig. 3.8d-e).

Gastric and gut contents – In the posterior trunk region, near the transition to the sacrum, a large mass of permineralized soft tissue is preserved that is not observable under natural light (Figs. 3.1, 3.5e-f). Under UV light, some parts of this mass acquire a pink-to-purple colouring, typically assumed by the soft tissues, but most of the mass remains white, indicating the large presence of bony material in the gut (Fig. 3.5f). Several tiny, rod-like fragments of bones are visible under UV light, and although their identity cannot be clearly assessed, this suggests that the animal was feeding on small vertebrates (e.g., fish). More anteriorly, on the left side of the mid-trunk, a small bone is visible between the dorsal ribs of the specimen (Fig. 3.6d): the small and slightly recurved element does not seem to be consistent with the rest of the skeleton, since its shape and size does not match any other bones from this body region, and it is clearly overlapped by a trunk rib. Considering its position in the trunk, and its etched surface, this element can be confidently interpreted to be a partially digested bone (possibly from a fish) that was present in the stomach at the time of death.

3.4 Discussions

3.4.1 Taphonomy

The spectra resulting from the SEM/EDX analyses of the soft tissues, bones, and sediment are presented in Figure 3.9, and Appendix 3.2 Figure A3.10. Both bony and soft tissues are rich in phosphorous (P), and display a very similar composition, while there is no P in the

embedding sediment. The soft tissues have been permineralized with calcium phosphate and thus preserved. According to Briggs (2003), the replication of the original morphology of the soft tissues, resulting in exceptional preservation, is dependent upon rapid authigenic mineralization due to the steep geochemical gradients generated by microbes associated with decomposition. The mineralization of the soft tissues is not bacterially controlled but can be bacterially induced, since bacterial decay contributes to establishing the conditions for the retention of high concentrations of P during fossilization (Trinajstic et al. 2007). Two requirements have been proved to co-occur for the permineralization of soft tissues: reducing conditions in the surroundings of the carcass to slow decay, and the establishment of environmental isolation, either physical or chemical (Briggs et al. 1993; Briggs 2003; Briggs & Kear 1993; Wilby et al. 1996). After such conditions are established, the availability of P ions is fundamental, and sources can be internal (from the animal‘s decay), or even external (other decaying organisms releasing P into the microenvironment) (Briggs & Kear 1993; Dornbos 2010; Wilson et al. 2016). The establishment of an anoxic environment and a drop in the pH of the microenvironment around the specimen, would inhibit the precipitation of calcium carbonate from the surrounding sediment, and the abundance of P would favour instead precipitation of calcium phosphate to permineralize hard and soft tissues (Briggs et al. 1993; Briggs & Kear 1993; Wilby & Briggs 1997; Wilson et al. 2016). In our specimens there are signs of at least partial decay of the carcass, as the outer layer of the epidermis (i.e., the keratinized stratum corneum) is not preserved: the integument is found in multiple areas of the body, but not perfectly preserved, and is lacking where the muscle fibers are more extensively exposed, suggesting that decomposition had started to some extent (Figs. 3.1, 3.6). The permineralization of the soft tissues happened at the “expense” of internal sources of P, such as bony tissue, and

possibly muscle fibers (Briggs 2003; Wilson et al. 2016): the P was first trapped and then re-used, in order to permineralize both integument and muscles. While the integument was greatly affected by decomposition, the muscles are almost perfectly replicated in three-dimensions; this should be related to both the fact that the muscle fibers are a source of the —recycled" P themselves, and that the sediment burial had prevented the degradation to penetrate deep into the carcass. The lack of interaction between the carcass and the sediment – i.e., release of P ions from the carcass into the sediment – which is suggested by the lack of P into the surrounding matrix (see Fig. A3.10), must be related to the formation of a film around the internal sources of P produced by bacteria (Fig. 3.9d-e: cf. Cosmidis et al. 2013). Films are accretions of bacteria that concentrate and attach to a surface, usually at an interface solid-liquid, producing in the process a substance matrix (Hall-Stoodley et al. 2004). Looking at the way the abdominal region of the specimen is preserved, with some of the posterior trunk ribs missing or poorly impressed on the matrix, it is possible that gaseous rupture of the body also occurred before the carcass was completely covered by the sediment (Figs. 3.1, 3.5e-f). However, due to the lack of evidence of scavenging, the great degree of skeletal articulation, and the preservation of abundant soft tissues, likely only a short amount of time passed between the death of the animal, the floating phase, sinking, and burial after landing on the seafloor. At that point, the microbial film (with bacteria related to the initial decay and possibly internal gut bacteria (Briggs 2003; Butler et al. 2015), together with the sediment cover established anoxic to dysoxic conditions in the microenvironment surrounding the corpse, triggering the process that led to such exceptional preservation (Briggs & Kear 1993; Trinajstic et al. 2007). The fact that the spectroscopic analysis found the same composition for both the skeletal elements and soft tissues, coupled with the complete lack of P in the surrounding sediment, corroborates the diagenetic hypothesis above.

3.4.2 Phylogenetic Relationships

Based on anatomical comparisons, *Primitivus* was identified here as a non-ophidian pythonomorph, and assessed its phylogenetic relationships using an updated version of the dataset of Palci & Caldwell (Palci & Caldwell 2010) (Appendix 3.3). The main difference between the results of the MP and IWMP analyses centers on the resolution of the resulting trees, greater in the IWMP (see also Appendix 3.4). Final topologies for both MP (strict consensus of two optimal trees) and IWMP (single optimal tree) agree in recovering a monophyletic Pythonomorpha, with snakes (Ophidia) as sister group to the clade *Tetrapodophis* + Mosasauroidea + Dolichosauridae (i.e., non-ophidian pythonomorphs) (Fig. 3.10). In the parsimony analysis, *Tetrapodophis* is recovered at the stem of a monophyletic mosasauroids + dolichosaurs grouping, and although its placement with the other non-ophidian pythonomorphs is poorly supported by Bremer and bootstrap values on a relatively long branch, it is consistent in both MP strict consensus and IWMP optimal tree (Fig. 3.10). The Bayesian Inference analysis offers instead a different scenario (Fig. 3.11): Pythonomorpha is still monophyletic, but *Primitivus* is recovered as the sister taxon to all other pythonomorphs which consists of Mosasauroidea + Ophidiomorpha *sensu* Palci & Caldwell (2007). In the model-based topology, *Tetrapodophis* is more deeply nested as sister taxon to *Aphanizocnemus* and together they represent the sister clade to *Adriosaurus* + (*Acteosaurus* + Ophidia).

A monophyletic Dolichosauridae, as recovered in our parsimony analysis, includes most of the taxa traditionally assigned to the family by Nopcsa (Nopcsa 1903) – i.e., *Dolichosaurus*, *Pontosaurus*, *Adriosaurus*, and *Acteosaurus* –with the addition of *Aphanizocnemus*, already placed within Dolichosauridae by Conrad (Conrad 2008) – and the new taxon *Primitivus*. The different placement of *Primitivus* between the model-based and parsimony-based topologies can

be interpreted as consistent with our observations based of its anatomy. The new specimen shares numerous similarities with *Pontosaurus*, and in particular with *P. lesinensis* , as emphasized in the description, and this is reflected in the MP and IWMP trees (Fig. 3.10). However, it also displays some conservative traits in terms of aquatic adaptations that make it comparable to both aigialosaurs and dolichosaurs (see description), and this justifie the results of the BI (Fig. 3.11). *Primitivus* may well represent an early-diverging pythonomorph, maintaining a more conservative body plan (e.g., limited axial elongation, poorly modified paddle-like limbs) in contrast to more derived forms such as obligatory aquatic mosasauroids or even greatly elongated adriosaurs and snakes. Its persistence until the end of the Cretaceous was likely favoured by the relatively isolated conditions of the Apulian Platform (see discussion about palaeobiogeography and palaeoecology below).

Unlike previous phylogenies (Caldwell 2006; Palci & Caldwell 2010), our results suggest the genus *Pontosaurus* is not monophyletic, with *P. kornhuberi* forming a clade with *Adriosaurus* (as sister taxon in the IWMP optimal tree), *Aphanizocnemus* and *Acteosaurus*, while *P. lesinensis* is grouped with *Primitivus* (its sister taxon in the IWMP topology) and *Dolichosaurus* (Fig. 3.10). Although *P. knornhuberi* shares several anatomical features with *P. lesinensis*, details of the anatomy reveal a closer affinity with *Adriosaurus*. These include a fused postorbital and postfrontal (separated in *P. lesinensis*); a wider parietal table (reduced to a thin mid-sagittal crest posteriorly in *P. lesinensis*), and pachyostotic ribs that are straight distally (uniformly recurved in *P. lesinensis*).

Ophidia is recovered as a monophyletic in both model-based and parsimony results, as sister group of *Tetrapodophis* + (Mosasauroidea + Dolichosauridae) in the MP and IWMP trees, and sister to *Acteosaurus* in the MCCT (Figs. 3.10-3.11). In the parsimony-based topologies, the

two extant taxa *Typhlops* and *Leptotyphlops* are sister taxa and together form the sister group to the rest of the snakes included in our phylogeny; the Upper Cretaceous snakes (*Dinilysia*, *Pachyrhachis*, *Haasiophis*, *Eupodophis*) are part of a clade with *Yurlunggur* (Oligo-Miocene) (Scanlon 2006), and the extant taxa *Anilius*, *Lampropeltis*, and *Python*. The South American fossil snake *Dinilysia* represents the most basal member of this latter clade, while the Middle Eastern taxa *Pachyrhachis*, *Haasiophis*, and *Eupodophis* are more deeply nested, as the sister group to modern macrostomatan snakes *Lampropeltis* + *Python*. The phylogenetic placement of the hind-limbed pachyophiids (*Pachyrhachis*, *Haasiophis* and *Eupodophis*) as the sister group to modern macrostomatan snakes is consistent with their skull morphology (adaptation for large gape), while their retention of well-developed hind limbs would suggest that these have been independently reduced in snakes such as *Anilius* and *Python* (or more unlikely that pachyophiids re-evolved some distal limb elements). In the BI topology, *Pachyrhachis*, *Haasiophis* and *Eupodophis* form a clade that is the sister group to the modern taxa, while *Dinilysia* and *Yurlunggur* occupy the most basal branches of Ophidia (Fig. 3.11). Importantly, in this topology scolecophidians (*Typhlops* and *Leptotyphlops*) are no longer placed at the base of Ophidia, but are nested above all fossil forms.

The oldest known snake is Middle Jurassic in age (Caldwell et al. 2015), while non-ophidian pythonomorphs seems to make their first appearance in the Lower Cretaceous (Evans et al. 2006). This means that the divergence between the ophidian and non-ophidian lineages within Pythonomorpha happened, or is older than, the Middle Jurassic, and the longer branch leading to the non-ophidian pythonomorph clade in the parsimony-based topologies or the longer branch leading to Ophidia in the model-based tree, can be likely shortened by including the earliest

snakes, and hopefully more complete specimens of early dolichosaurids (e.g., *Kaganaias hakusanensis*).

3.4.3 Ontogeny and Lifestyle

Because secondary adaptations to an aquatic lifestyle often lead to reduced or delayed ossification in the limb bones (Caldwell 2002), in aquatic animals it is not always straightforward to separate juveniles from adults. The reduced ossification observed in the limbs of *Primitivus* is an example of this problem. Characters such as the unossified bony epiphyses, unfused epiphyses, or unfused hip elements, can all be interpreted as either indicative of an earlier ontogenetic stage (Maisano 2002), or as the retention of paedomorphic traits linked to adaptations to an aquatic lifestyle (Rieppel 1989; Rieppel et al. 2008). The final interpretation relies upon the combination of these morphologies to other relevant characters that instead are not affected by a similar dualistic explanation. The presence of an open parietal notch, with the parietal table apparently divided in two halves anterior to the parietal foramen, is a typical juvenile feature in different groups of lizards (Palci et al. 2016). This character suggests that the specimen most likely represents a sub-adult. On the other hand, features like the elongated neck (increased number of cervical vertebrae, as well as an elongated cervical centrum), the reduced pectoral girdle, distally diverging epipodials on both fore and hindlimbs, the elongated autopodium (phalanges long and slender), and the laterally flattened tail (tail much taller than wide, emphasized by the presence of the scaled caudal fin), are all indicative of aquatic adaptations. Another important aspect to consider in order to reconstruct the lifestyle of *Primitivus* is the morphology of the sacral region. *Primitivus* retains a functional sacrum, preserving a firm connection between the pelvic girdle and the sacral vertebrae, similarly to other

dolichosaurs. The terrestrial-like configuration of the articulation between the posterior process of the ilium and the two sacral ribs together with the configuration of the limbs, suggest that this lizard was likely still capable of moving about on land, and not obligatorily aquatic like mosasaurs (Fig. 12).

3.4.4 Palaeobiogeography and Palaeoecology

Despite the possession of more derived traits such as the increased number of cervical vertebrae and reduced ossification of both axial and appendicular elements, *Primitivus* displays a low degree of axial elongation in the trunk region in comparison to most other non-mosasauroid pythonomorphs, possessing only 22 dorsal vertebrae, for a total of 32 presacrals. Moreover, there is no evident reduction of the forelimbs in the new specimen as instead in most dolichosaurids, and the hindlimbs clearly retain a more terrestrial-like configuration (similar to *Pontosaurus* spp.). Whether *Primitivus manduriensis* represents a relict form that survived until the latest Cretaceous in an isolated area of the Mediterranean Tethys, or is just the first evidence of a more diverse and long-lived dolichosaur fauna, will need further investigation. As suggested by Citton et al.(Citton et al. 2015), the Southern Italian Carbonate Platforms (e.g., the Apulian Platform), must have had an archipelago-like arrangement of small, short-lived, but continuously alternating emerged lands throughout the Late Jurassic to Late Cretaceous. In such a framework, the dispersal of terrestrial faunas was highly limited (Citton et al. 2015), but for aquatic/semi-aquatic animals feeding on fish and small invertebrates (e.g., molluscs) – that were clearly abundant in the area (Cestari & Sirna 1987; Medizza & Sorbini 1980; Schlüter et al. 2008; Sorbini 1978; Sorbini 1981) – this environment might have offered a favourable refuge, guaranteeing a longer survivorship to groups that instead were facing extinction elsewhere.

Further corroboration for the hypothesis that *Primitivus manduriensis* is a relict taxon representative of a clade that was declining (or presumed to be extinct in the uppermost Cretaceous) may rely on the collection of additional evidence from these poorly explored and quite promising deposits of the southern-east Mediterranean realm.

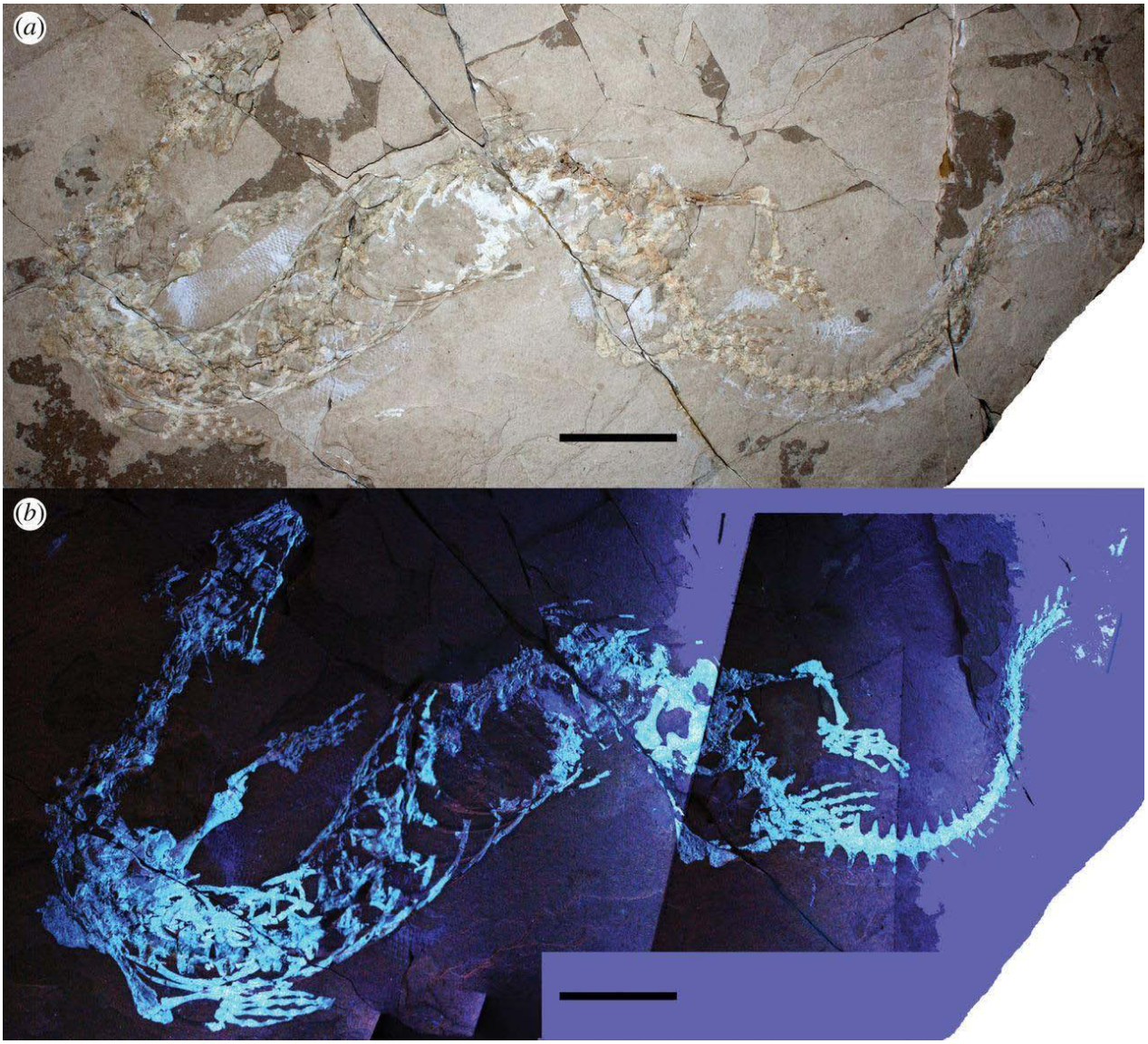

Figure 3.1. Holotype of *Primitivus manduriensis* gen. et sp. nov. (MPUR NS 161) at natural (a) and UV (b) light as exposed from the matrix in dorsal view. The imaging under UV radiations is a composite of two pictures, finalized with Adobe® Photoshop® CC 17 (2013 release). Scale bars: 5 cm.

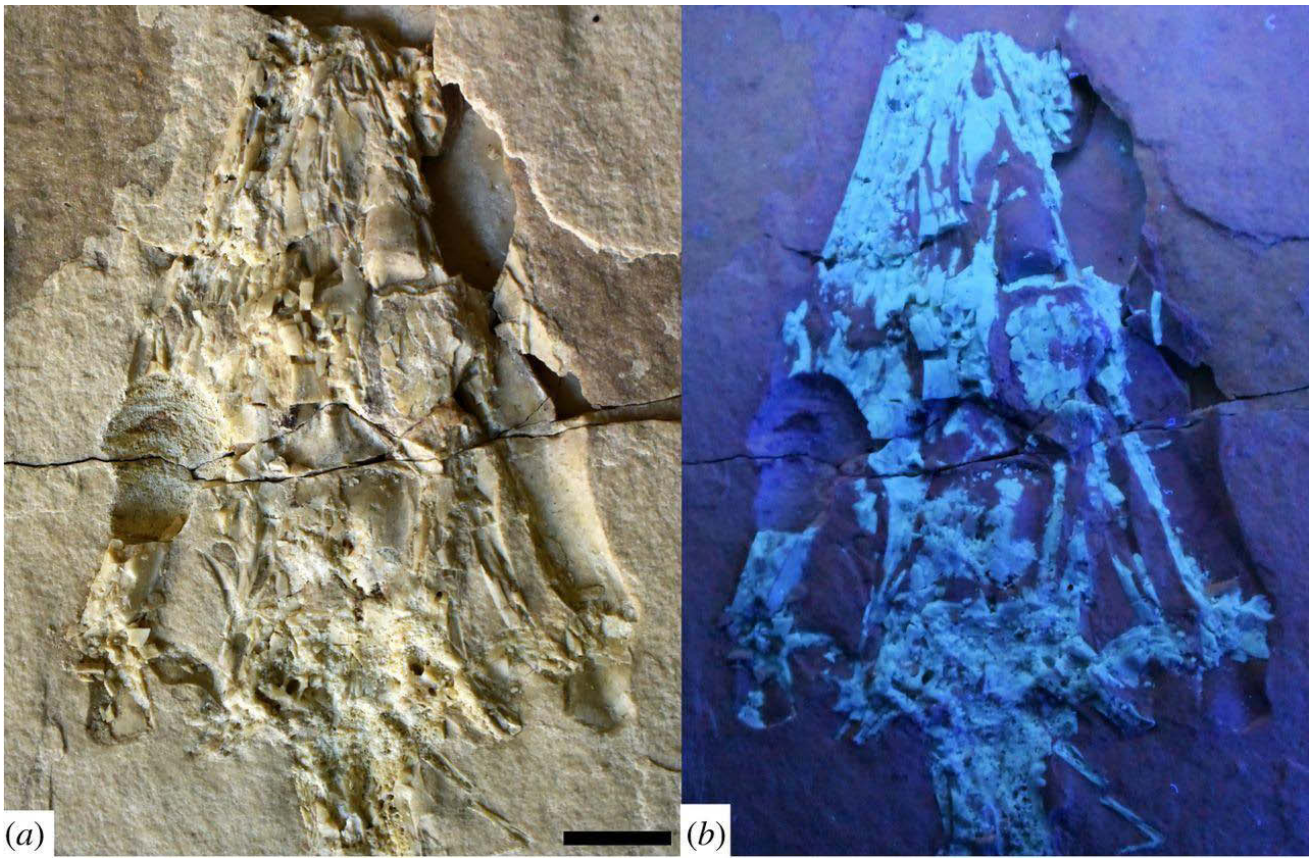

Figure 3.2. *Primitivus manduriensis* MPUR NS 161 imaging of the skull at natural (a) and UV (b) light. The skull of the holotype is deeply crushed (a), and part of the elements are only preserved as impressions on the matrix, as observed under UV light (b), where the bone material still preserved is bright white. Reconstruction and interpretation of the cranial skeleton is presented in SM1 (Fig. S2). Scale bar: 1 cm.

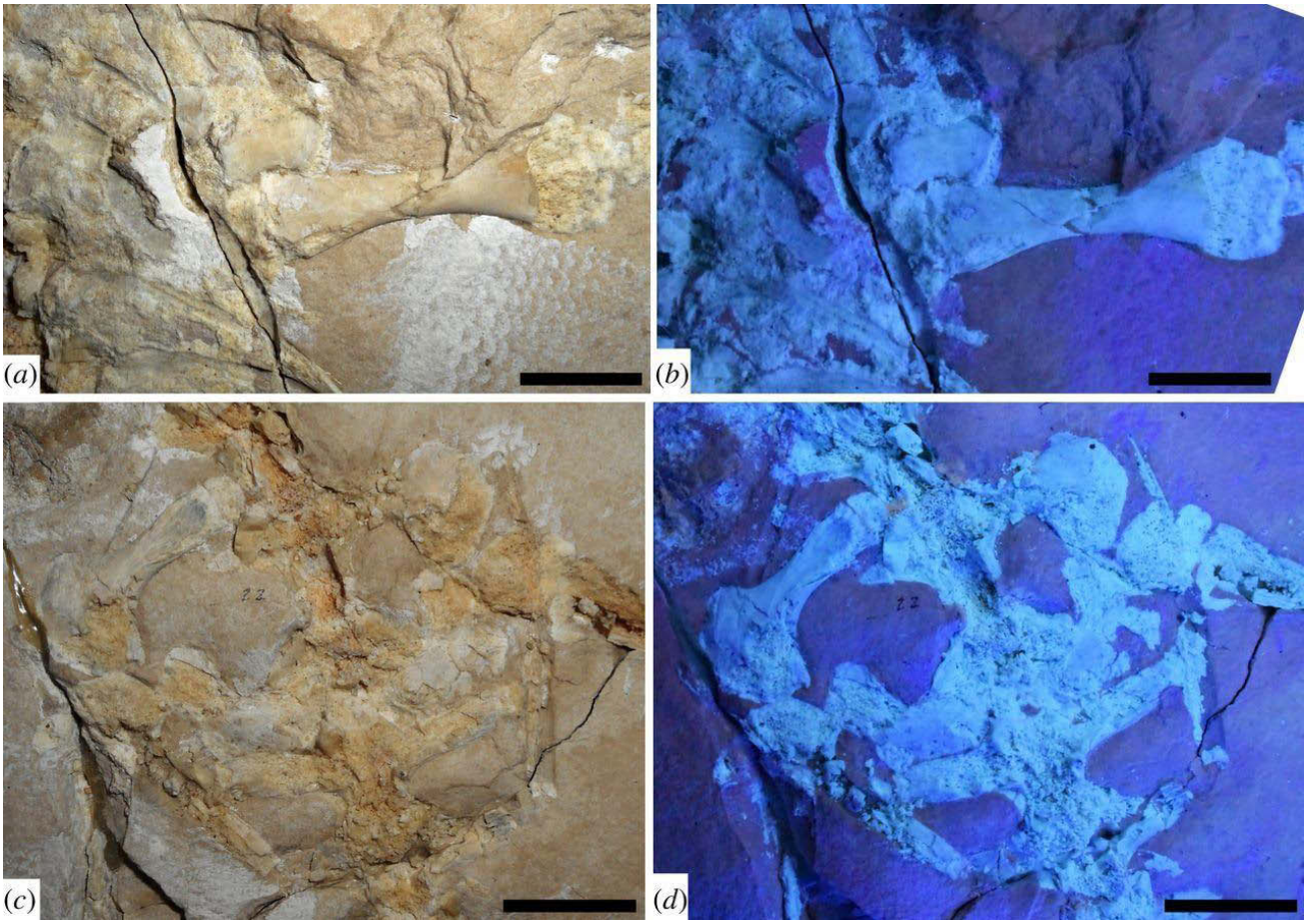

Figure 3.3. *Primitivus manduriensis* MPUR NS 161 imaging of pectoral and pelvic girdles at natural (a, c) and UV (b, d) light. As visible from the photographs under UV radiation, the pectoral region is extensively covered by cartilage (b), surrounding both right scapula and coracoid, up to the humeral proximal epiphyses, which are invisible under natural light. For the sacral region, the white material visible under natural light anteriorly to both ischia and first sacral rib becomes purple when exposed to the UV radiation, as well as the scales on both sides of the hips. Reconstruction of both pectoral and pelvic girdles is provided in SM1 (Fig. S4). Scale bars: a-b, 1 cm; c-d, 2 cm.

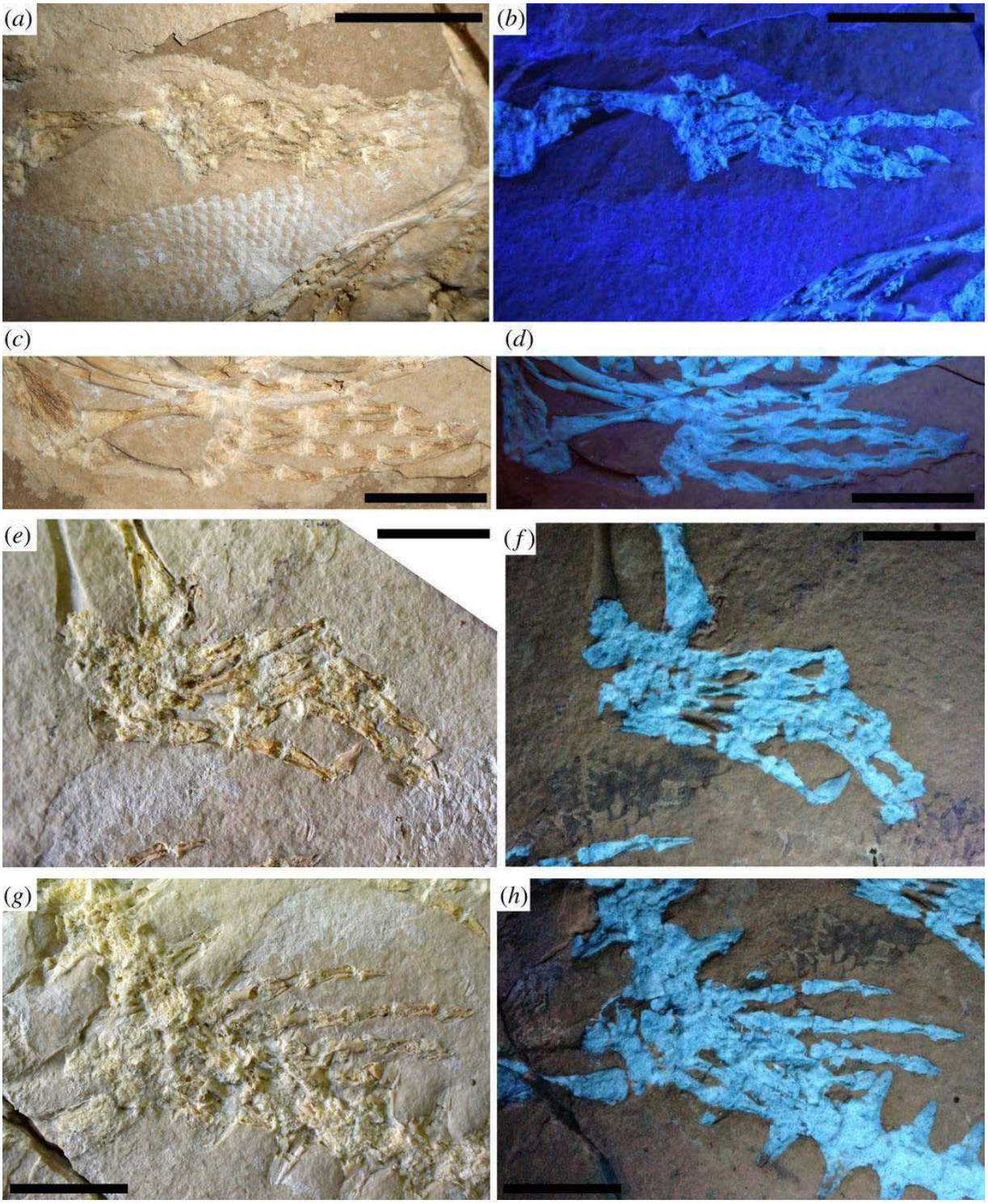

Figure 3.4. *Primitivus manduriensis* MPUR NS 161 imaging of appendicular elements at natural (a, c, e, g) and UV (b, d, f, h) light. Both manus and pes, as well as most of the limb bones are preserved and mostly articulated. The forelimb autopodium is pictured here at both natural (a, c)

and long-wave UV radiations (b, d), where the soft tissues are differentiated by a pink-purple colour range. For the hindlimb autopodium (e-h), the images are taken under short-wave UV radiations (f, h), with the soft tissues spanning a grey colour scale. Reconstruction of the limbs is presented in SM1 (Figs. S5-S8). Scale bars: 2 cm.

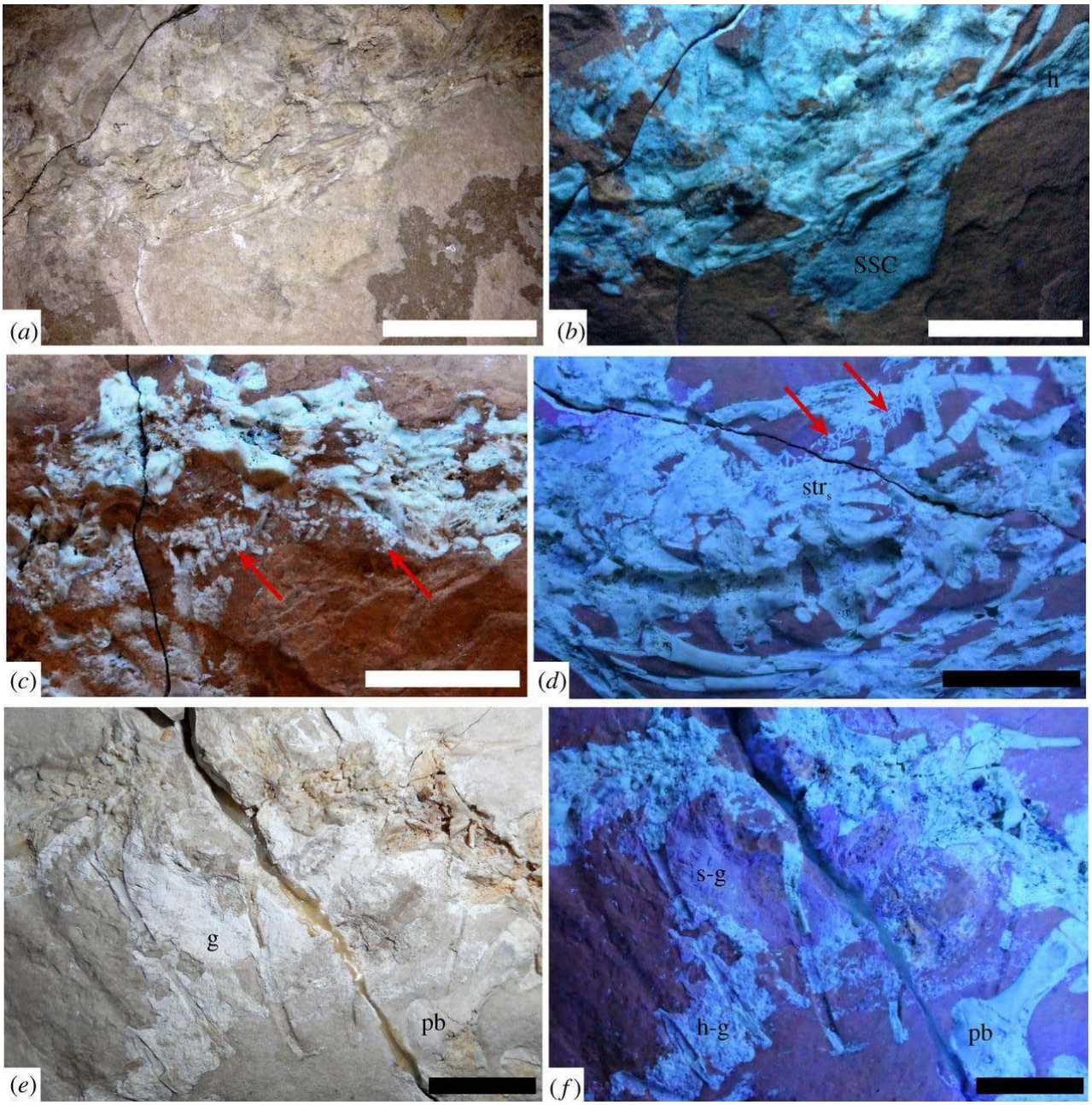

Figure 3.5. Cartilages and gut content preserved in MPUR NS 161. Cartilaginous elements, like suprascapula (a, b), tracheal rings (arrows in c), bronchial rings (arrows in d), and sternum (d) are also preserved in the specimen, and their assessment was possible thanks to the use of UV radiations (b, c, d, f). For the gut content (e, f), under UV light is possible to differentiate between a hard tissue component (emphasized in white), and a soft tissue component (emphasized in pink-purple). Scale bars: 2 cm. Abbreviations: g, gut content; h, humerus; h-g,

hard tissue component in the gut; pb, pubis; s-g, soft tissue component in the gut; ssc, suprascapula; str_s, sternal ribs.

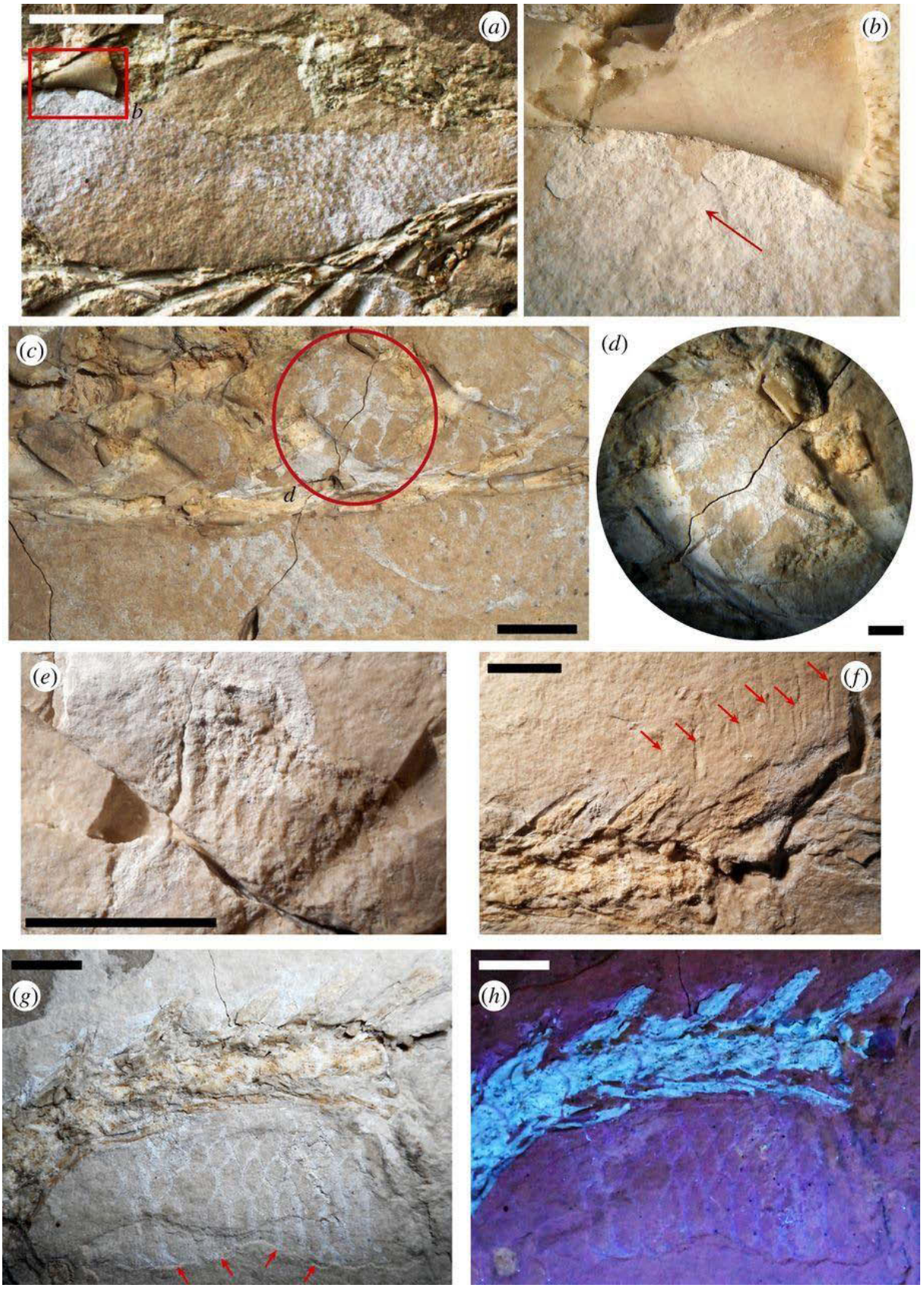
(a)
b
(b)
(c)
d
(d)
(e)
(f)
(g)
(h)

Figure 3.6. Different types of scales preserved in *Primitivus manduriensis*. Integument and scale impressions are present on both sides of the trunk (a-d), around the limbs (e), and along the tail (f-h). The different types of dorsal scales vary from polygonal (a, c, e, g, h) to diamond-shaped (d), but in the subcaudal region of the tail they are transversally elongated (g, h). Among extant squamates, only snakes possess transversally elongated belly or subcaudal scales, while among fossils, similar scales are found in *Pontosaurus kornhuberi*. Arrows: b, pointing at inner layer of the integument (dermis or hypodermis); f, pointing at scales of the caudal fin impressed on the matrix; g, pointing at body outline. Scale bars: a, 2 cm; c, e-h, 1 cm; d, 5 mm.

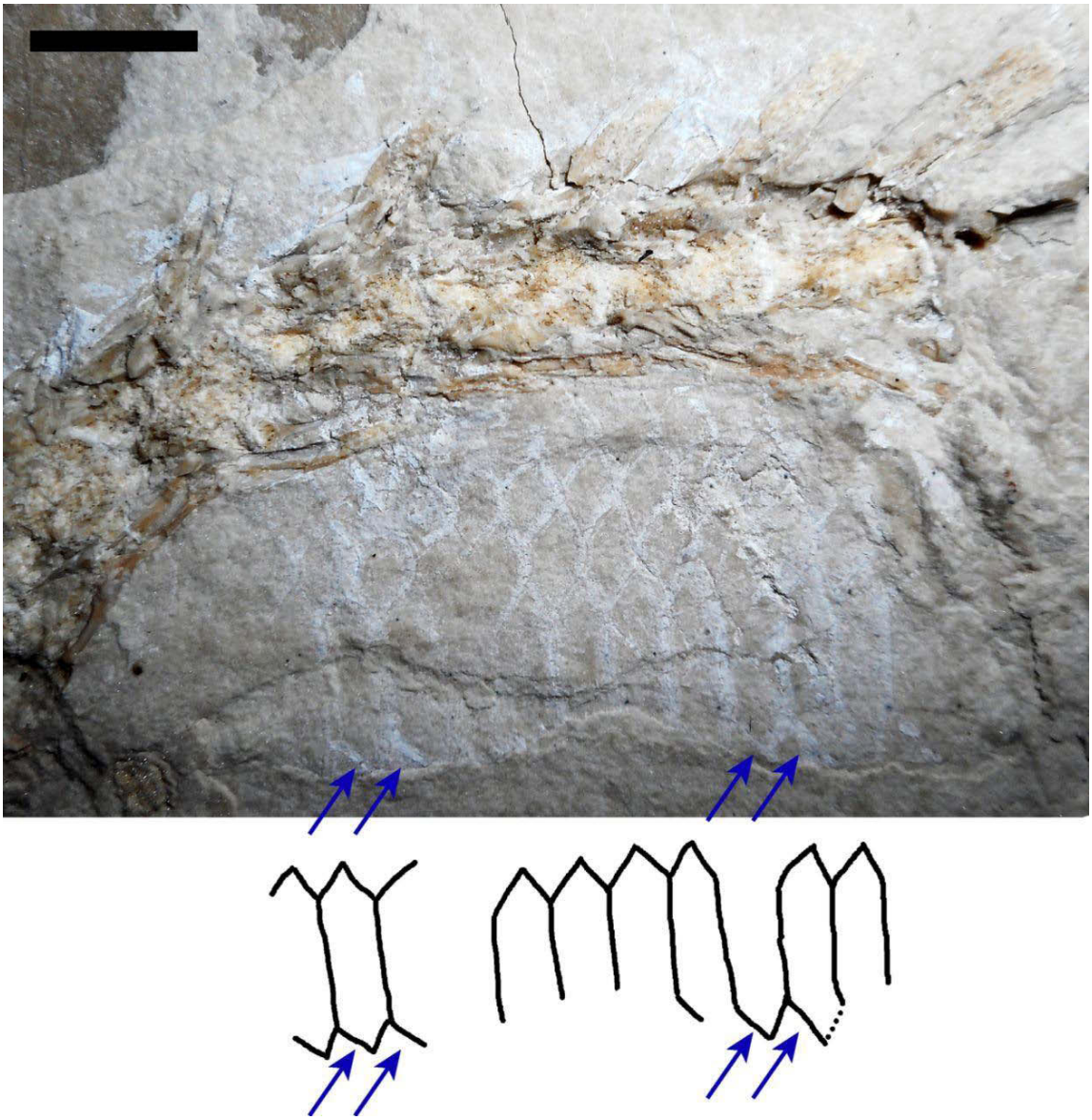

Figure 3.7. *Primitivus manduriensis* MPUR NS 161 subcaudal scales detail. The proximal portion of the tail is exposed in dorsal view like the rest of the body, but at some point the tail rotates about 90° and the second part of the caudal column is exposed in left lateral view. Right after the torsion of the tail is where the transversally expanded ventral caudal scales (or subcaudals), similar to snakes, are visible. In snakes these scales can be present in a single row or as two adjacent rows; in MPUR NS 161, considering that this portion of the tail seems to be slightly twisted and compressed, both interpretations can be plausible. Scale bar: 1 cm.

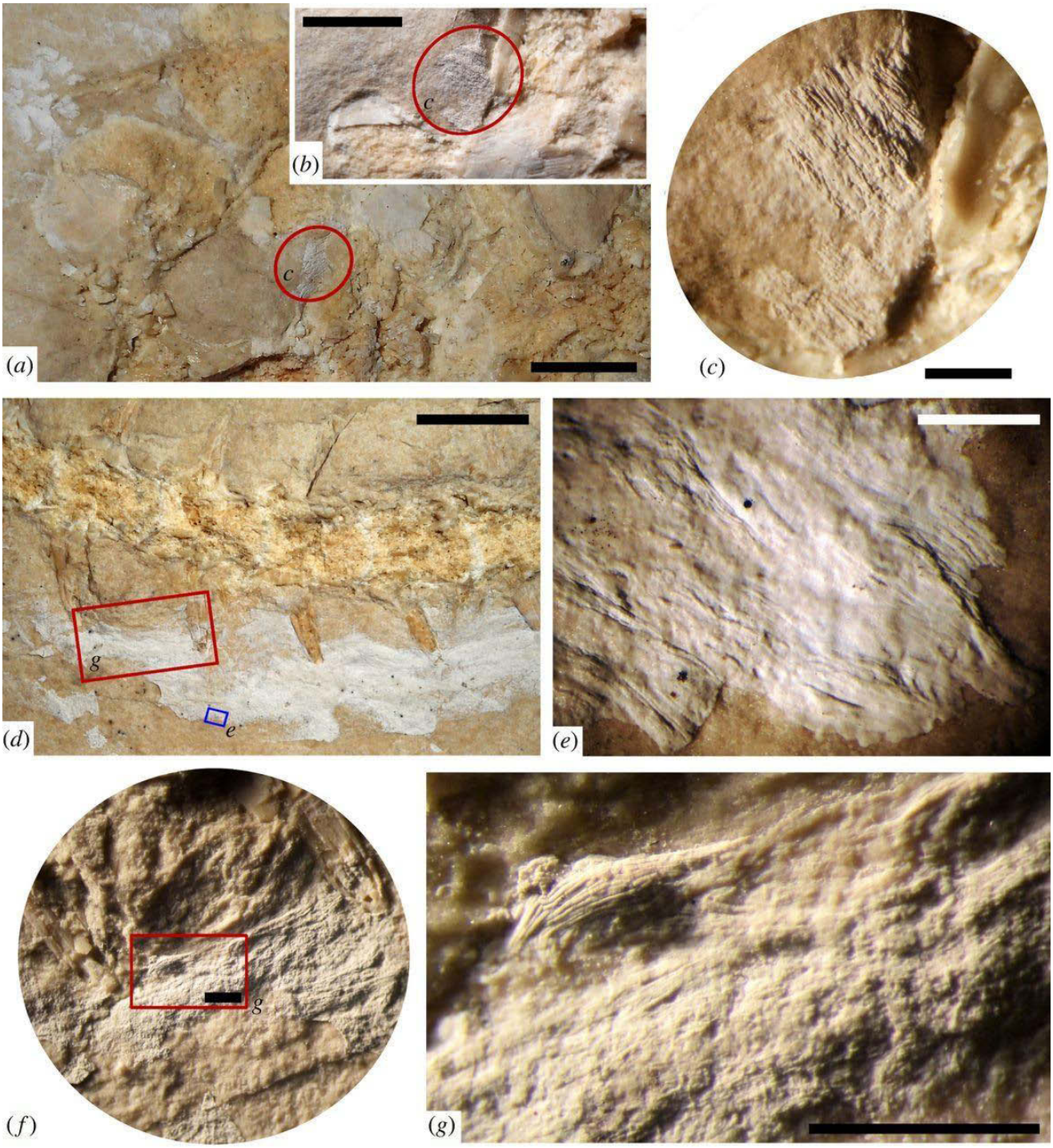

Figure 3.8. Mineralized epaxial and hypaxial muscles preserved in *Primitivus manduriensis*. Muscle fibers and bundles are well-recognizable along the posterior trunk, the pelvic girdle and the tail, even at naked eye. Muscle fibers preserved between the first sacral vertebra and the left ischium (a-c) are about 30-35 μm in diameter; the size of the muscle fibers along the anterior

caudal region (d, f, g) are in the order of 10-15 μm. Under a compound microscope the single myomeres can in some instances also be distinguished (e). Scale bars: a, d, 1 cm; b, 5 mm; c, e-g 1 mm.

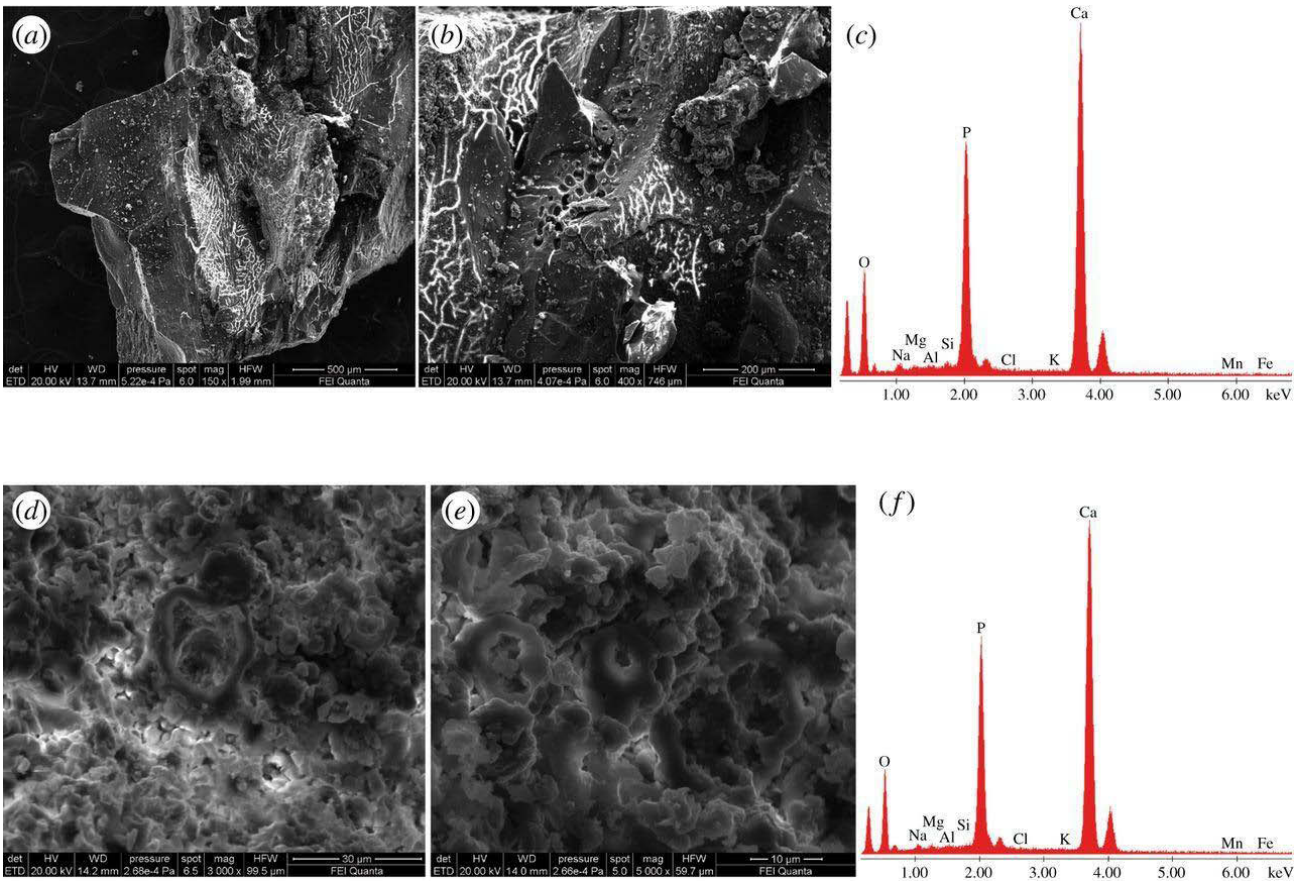

Figure 3.9. Results of SEM/EDX analyses for bony and soft tissues. Samples of hard and soft tissues have been selected in order to find their composition: a fragment of cortical bone from a trunk rib (a-c), and a sample from the muscles preserved along the trunk (d-f). Results for additional samples from the sediment and the gut content are reported in SM1 Fig. S10. From the two spectra (c, f) is clear that both bony and soft tissues have been permineralized with calcium phosphate, presenting the same composition. By comparison with Cosmidis et al. (68), the spherical forms visible in (d) and (e) can be interpreted as presence of fossil bacteria. Bone vascularization is also perfectly preserved as visible on the bone fragment (a), and the diameter of the blood vessels is between 3.5 µm and 5 µm.

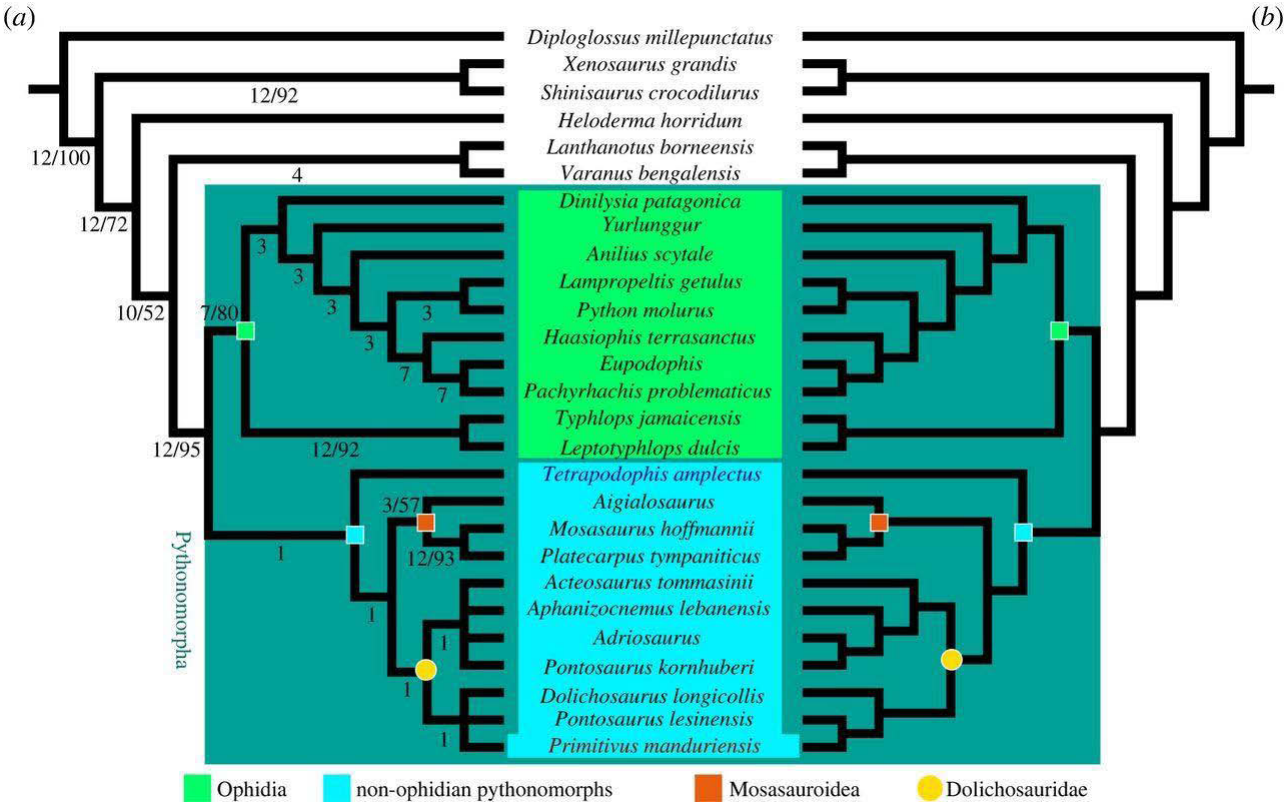

Figure 3.10. *Primitivus manduriensis* phylogenetic relationships based on parsimony. Phylogenetic hypotheses on the interrelationships of the new taxon are based on equal-weight maximum parsimony (a), and implied weighting maximum parsimony (b).

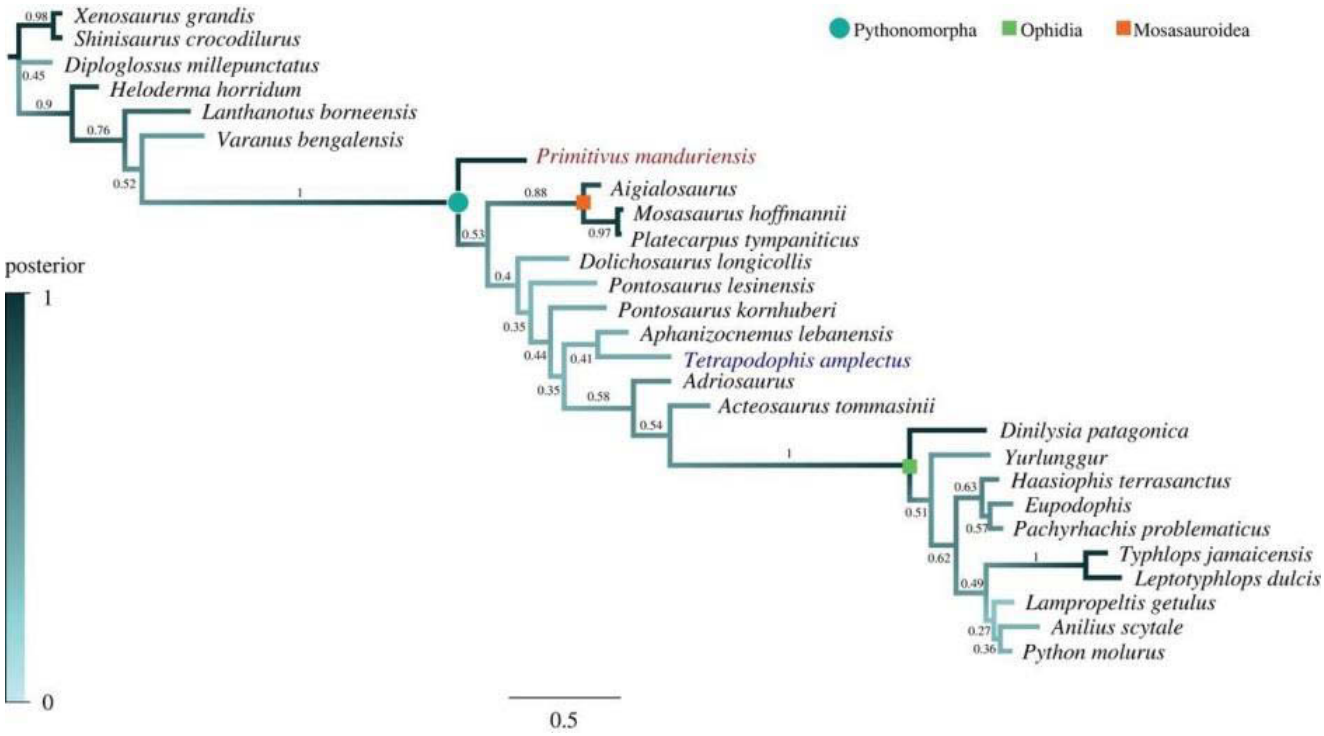

Figure 3.11. *Primitivus manduriensis* phylogenetic relationships based on Bayesian Inference. The MCCT resulting from our model-based analysis recovers the new taxon as basal to all other pythonomorphs. The gradient colour of the branches is based on values of the posterior probabilities (numbers on each branch).

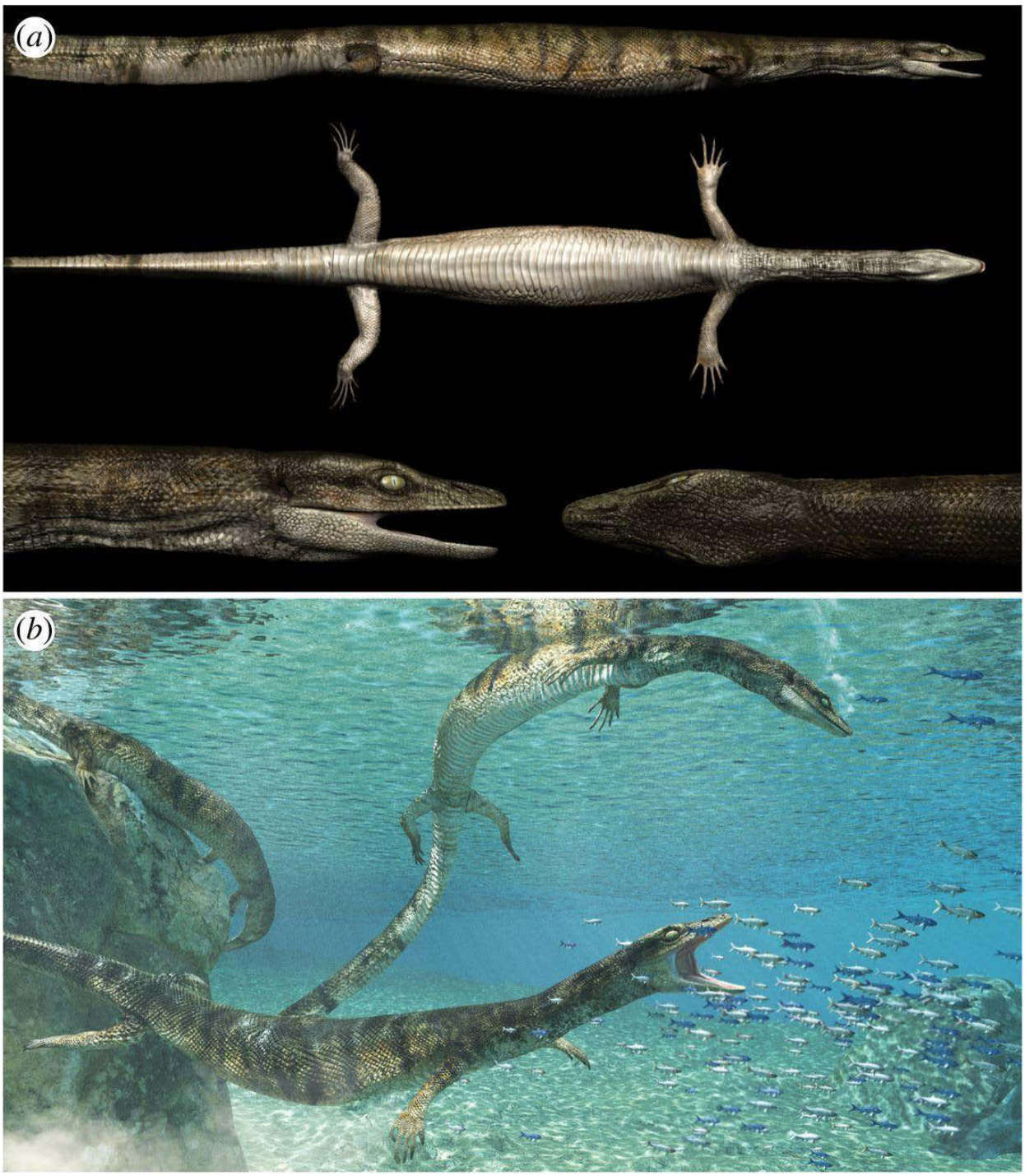

Figure 3.12. *Primitivus manduriensis* 3D model and life reconstruction. The specimen is preserved in sediments deposited in the shallower portion of an inner lagoon of the Apulian Carbonate Platform, and is inferred to have a semi-aquatic lifestyle. Three-dimensional model (a) and life reconstruction (b) created by Fabio Manucci.

Appendix 3.1 – Provenance of the specimen.

In 2014, the specimen was presented to Prof. Umberto Nicosia (UniRome), after which it was transferred to the Museum of Paleontology of the University of Rome „Sapienza“ (MPUR). The exact finding place for the specimen was unclear, and the only associated data mentioned a small outcrop of limestones in the town of Nardò (Lecce, Puglia, Southern Italy). During subsequent fieldwork in the area to collect rock samples, and to prospect possible outcrops of interest, we identified the outcrop as a long abandoned quarry that had previously been reported as a site of paleontological excavations: the so called ―Cavǻ locality in Sorbini (Sorbini 1981), and Guidotti *et al*. (Guidotti et al. 1993). We are currently conducting a project reassessing the geology and stratigraphy of the area based on the macro (e.g., rudists) and nannofossil content in order to refine the age of the strata (upper Campanian – lower Maastrichtian (Medizza & Sorbini 1980; Sorbini 1978; Sorbini 1981)), and further explore these potential *Lagerstätte*-type beds (Cipriani et al., work in progress). Uncovering more material from this site represents a unique opportunity to not only improve our knowledge about such poorly sampled deposits, but especially to study the peculiarity of the faunas of the Apulian Platform that could represent the key for understanding the radiation and dispersal of at least non-ophidian pythonomorphs in the Mediterranean Tethys.

Appendix 3.2 – Supplementary figures and table of measurements.

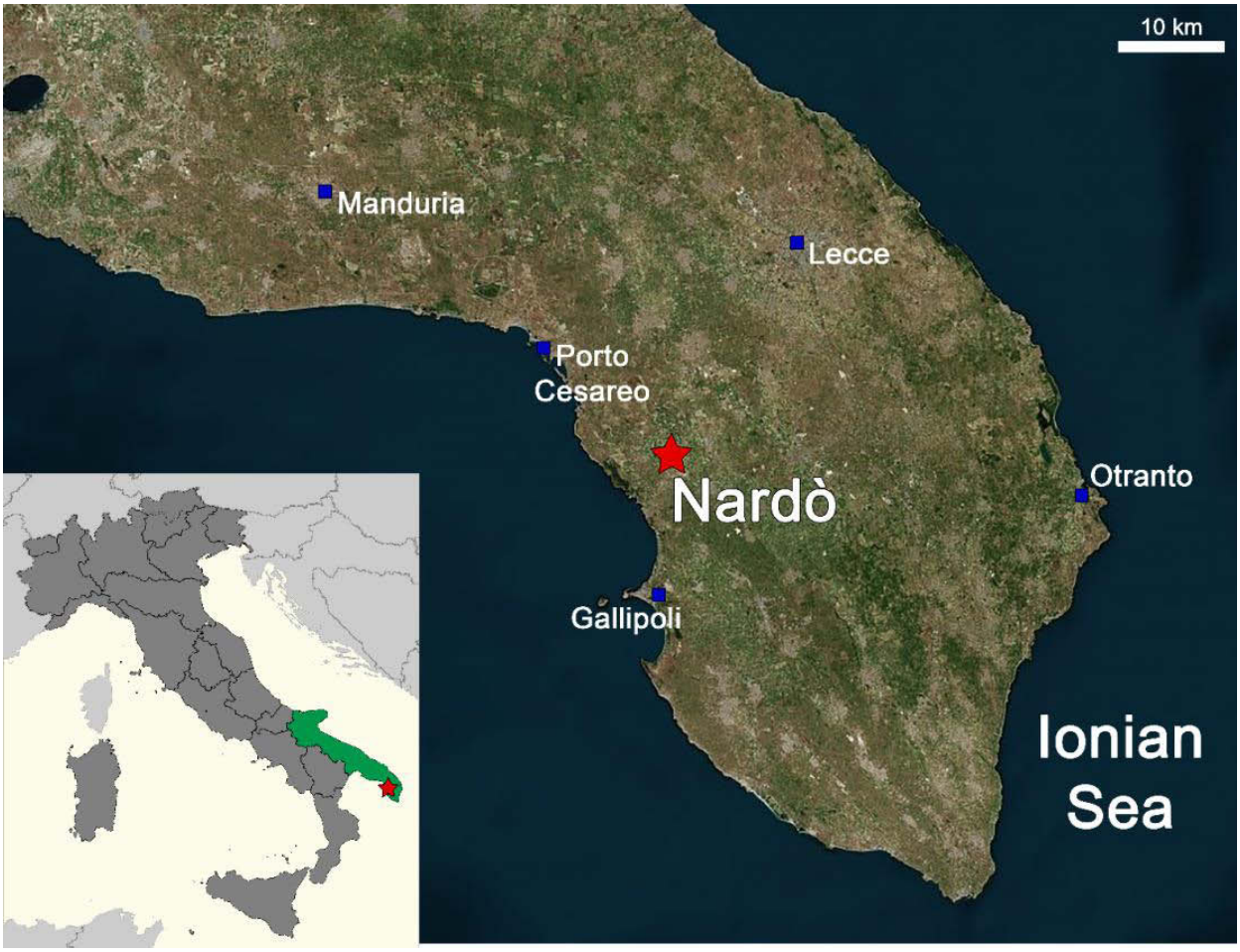

Figure A3.1. Map illustrating the position of the town of Nardò (Lecce, Puglia), finding locality of *Primitivus manduriensis*, MPUR NS 161. The specimen was found in deposits of the upper Campanian – lower Maastrichtian of the Apulian Platform, which makes *Primitivus manduriensis* the latest dolichosaurid up to date. The satellite image was retrieved and modified from Zoom Earth (www.zoom.earth; accessed 10 Nov. 2016), whereas the map of Italy was retrieved and modified from Wikimedia Commons (www.commons.wikimedia.org/wiki/File:Italy_location_map.svg; accessed 9 Nov. 2016).

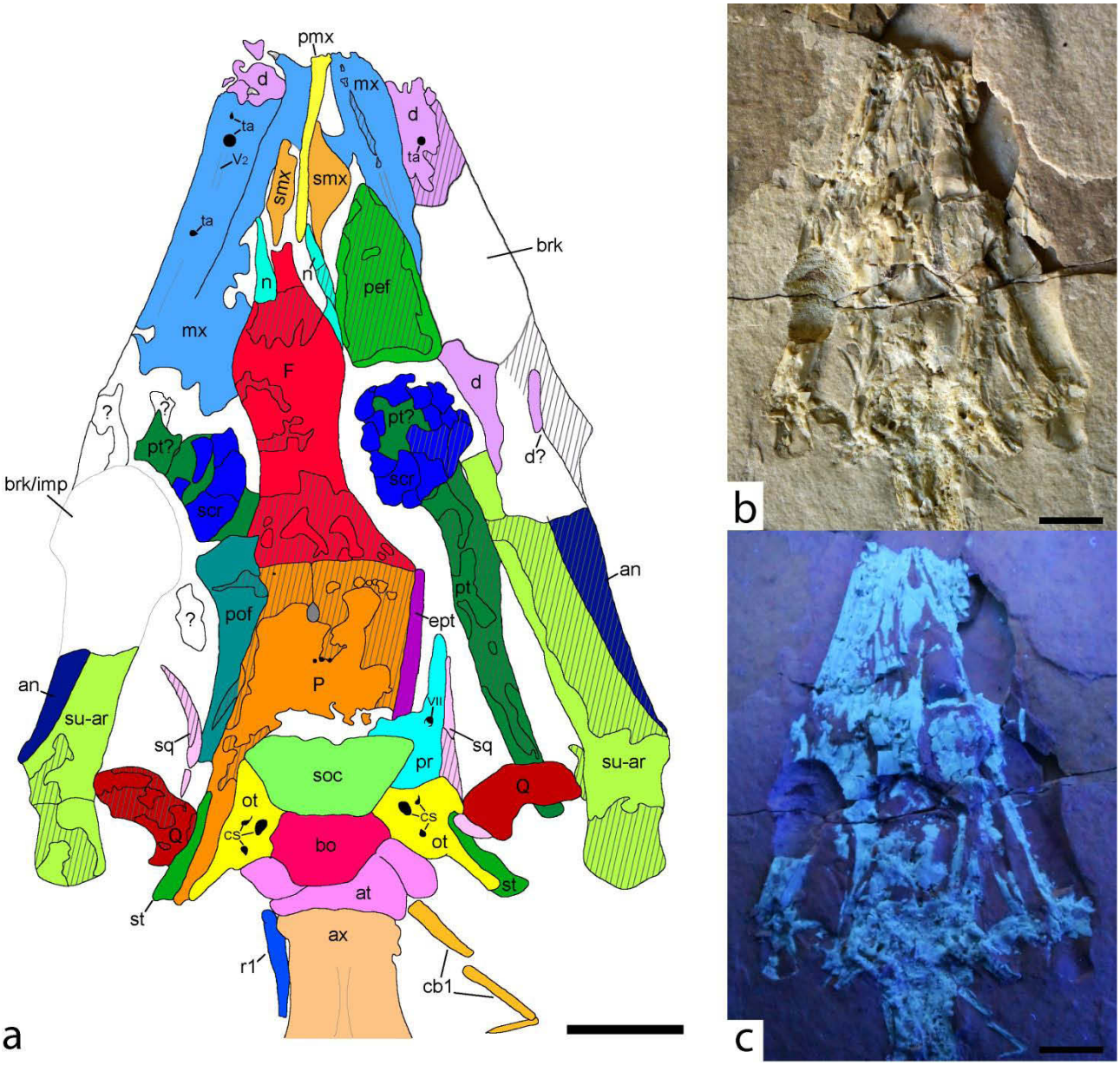

Figure A3.2. Interpretation of the cranial skeleton of *Primitivus manduriensis*, MPUR NS 161. Reconstruction (a) of the cranium of the holotype, realised by combining the observations under natural (b) and UV (c) light. Striped areas indicate where the elements are only preserved as impressions. Scale bars: 1 cm. Abbreviations: an, angular; at, atlas; ax, axis; bo, basioccipital; brk, breakage; cb1, first ceratobranchial; cs, canalis semicircularis; d, dentary; ept, epipterygoid; F, frontal; imp, impression; imp, impression on the matrix; mx, maxillary; n, nasal; ot,

otoccipital; P, parietal; pef, prefrontal; pmx, premaxilla; pof, postorbitofrontal; pr, prootic; pt, pterygoid; q, quadrate; r1, first cervical rib; su-ar, surangular-articular; smx, septomaxilla; soc, supraoccipital; sq, squamosal; scr; sclerotic ring ossicles; st, supratemporal; ta, tooth alveolus; V_2, canal for the maxillary branch of the trigeminal nerve; VII, facial nerve foramen; ?, unidentified element.

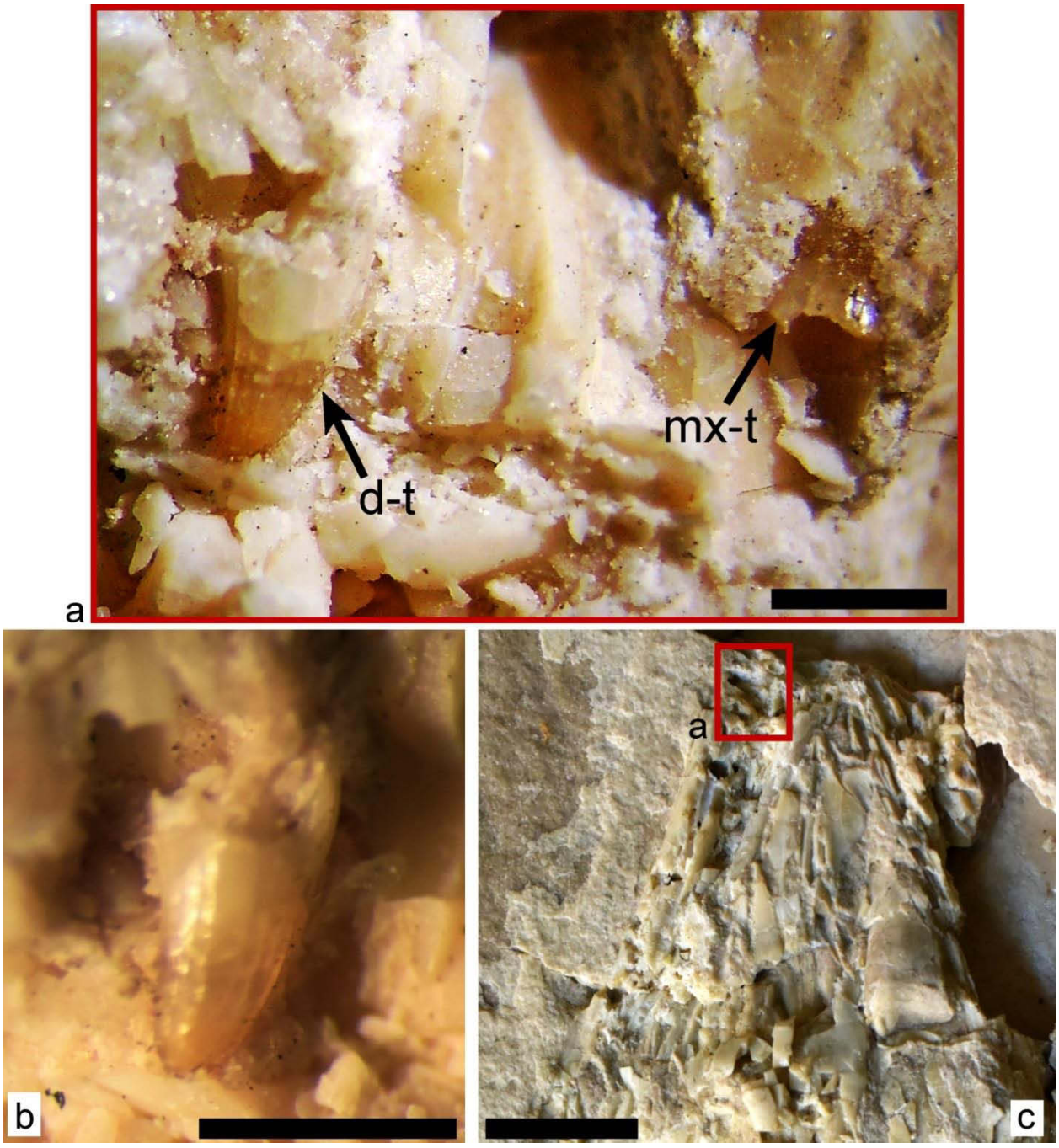

Figure A3.3. Teeth of *Primitivus manduriensis*, MPUR NS 161. Maxillary (a) and dentary (a, b) teeth preserved on the anterior left portion of the skull, pictured under a compound microscope. Both teeth are conical in shape and slightly posteriorly recurved, with multiple longitudinal facets along the tooth crown. Scale bars: a, b, 1 mm; c, 3 cm. Abbreviations: d-t, dentary tooth; mx-t, maxillary tooth.

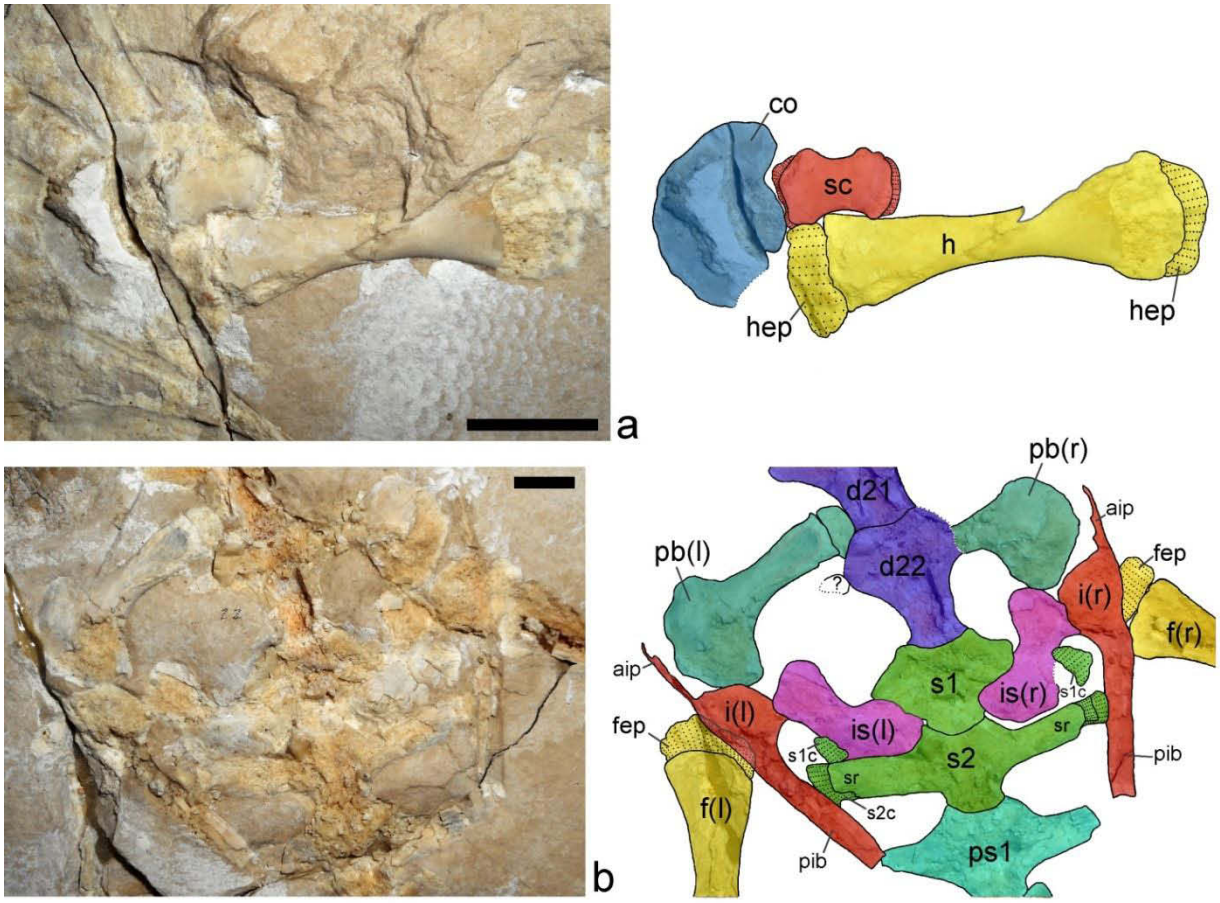

Figure A3.4. Interpretation of *Primitivus manduriensis* pectoral and pelvic regions. Both coracoid and scapula (a), are preserved for the right limb: the elements are reduced and unfused as typical for non-ophidian pythonomorphs. The elements of the pelvic girdle (b) are unfused as well, although the elements must have been tightly articulated together in anatomical position, similarly to _dolichosaurs‘ and plesiopelvic mosasauroids. The articulation between the posterior iliac blade and the second sacral rib is quite well preserved, with the contact mediated by cartilage (dotted areas). Scale bars: 1 cm. Abbreviations: aip, anterior preacetabular process of the ilium; co, coracoid; d, dorsal vertebra; f, femur; fep, epiphysis of the femur; h, humerus; hep, epiphysis of the humerus; i, ilium; is, ischium; (l), left; pb, pubis; pib, posterior iliac blade; ps, post-sacral vertebra; (r), right; s, sacral vertebra; s1c, cartilaginous end of the first sacral rib; s2c, cartilaginous end of the second sacral rib; sc, scapula; sr, sacral rib.

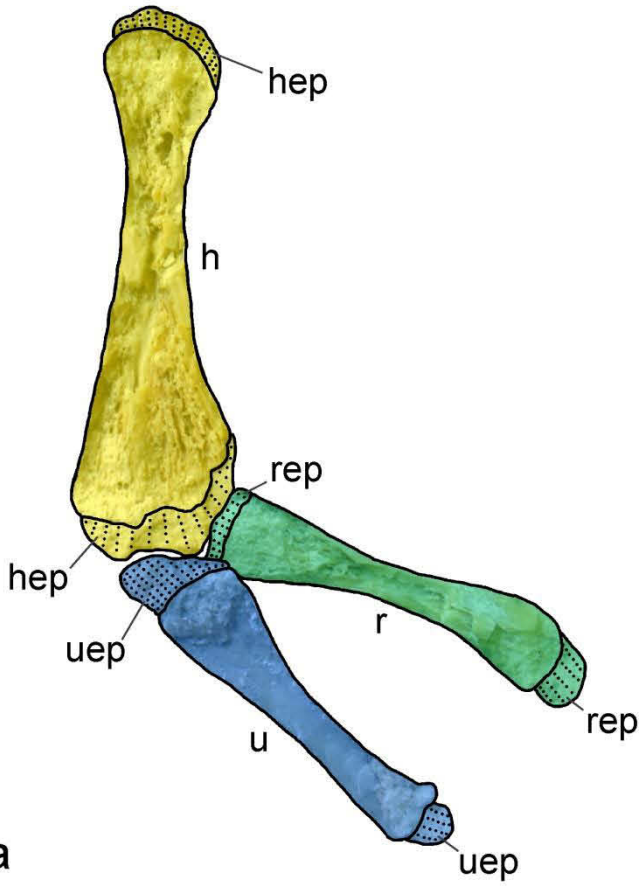
hep
h
rep
hep
uep
r
rep
u
uep

a

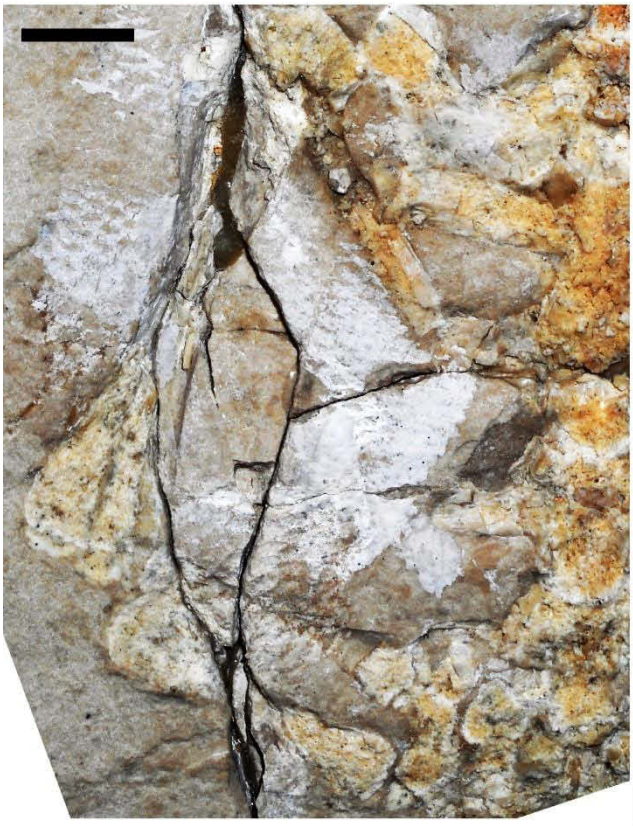

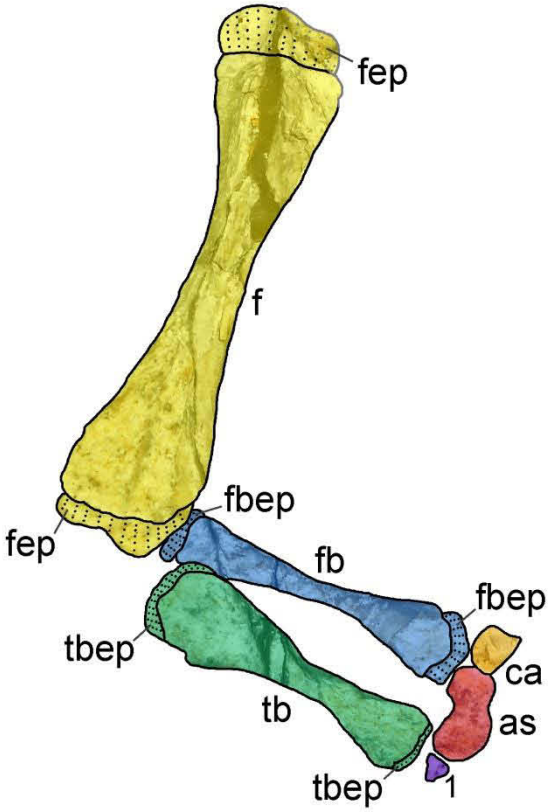
fep
f
fbep
fep
fb
fbep
tbep
ca
tb
as
tbep
1

b

Figure A3.5. Interpretation of *Primitivus manduriensis* fore and hind limb elements. Reconstruction of the left forelimb propodial and epipodials (a), and of the left hindlimb propodial, epipodials and tarsals (b), emphasizing the presence of incompletely ossified and unfused epiphyses (dotted areas) of the long bones and distally divergent epipodials. Scale bars: 1 cm. Abbreviations: as, astragalus; ca, calcaneum; f, femur; fb, fibula; fep, epiphysis of the femur; fbep, epiphysis of the fibula; h, humerus; hep, epiphysis of the humerus; r, radius; rep, epiphysis of the radius; tb, tibia; tbep, epiphysis of the tibia; u, ulna; uep, epiphysis of the ulna; 1, first distal tarsal.

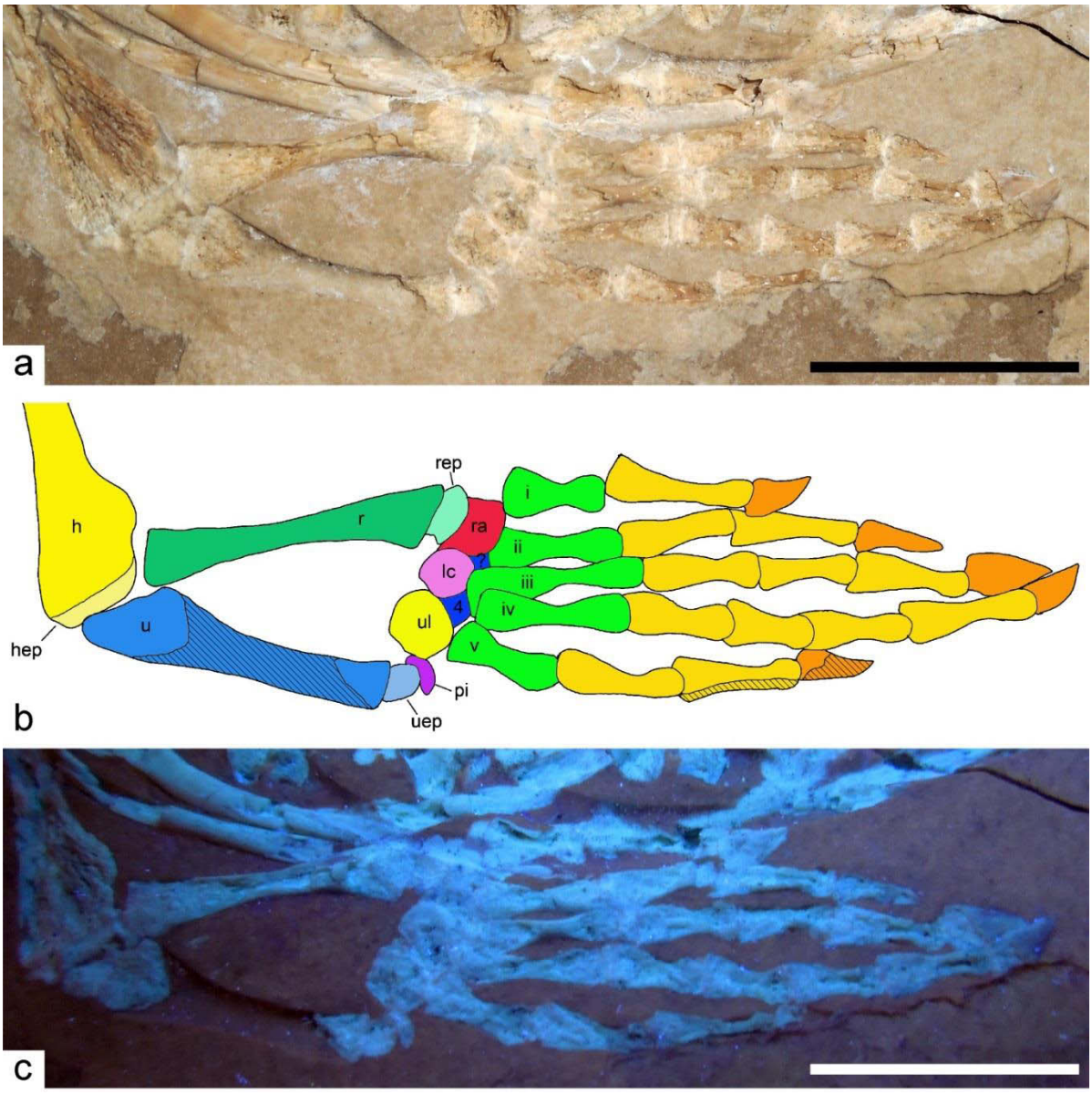

Figure A3.6. Interpretation of the zeugopodial and autopodial elements of *Primitivus manduriensis* forelimb. Reconstruction (b) of the epipodials and manus of the new specimen realised by combining the observations under natural (a) and UV (c) light. Portion preserved only as impressions on the matrix are indicated by stripes. Scale bars: 2 cm. Abbreviations: h, humerus; hep, epiphysis of the humerus; lc, lateral centrale; pi, pisiform; r, radius; ra, radial; rep, epiphysis of the radius; u, ulna; uep, epiphysis of the ulna; ul, ulnar; 4, fourth distal carpal; i-v, first to fifth metacarpals; ?, unidentified distal carpal.

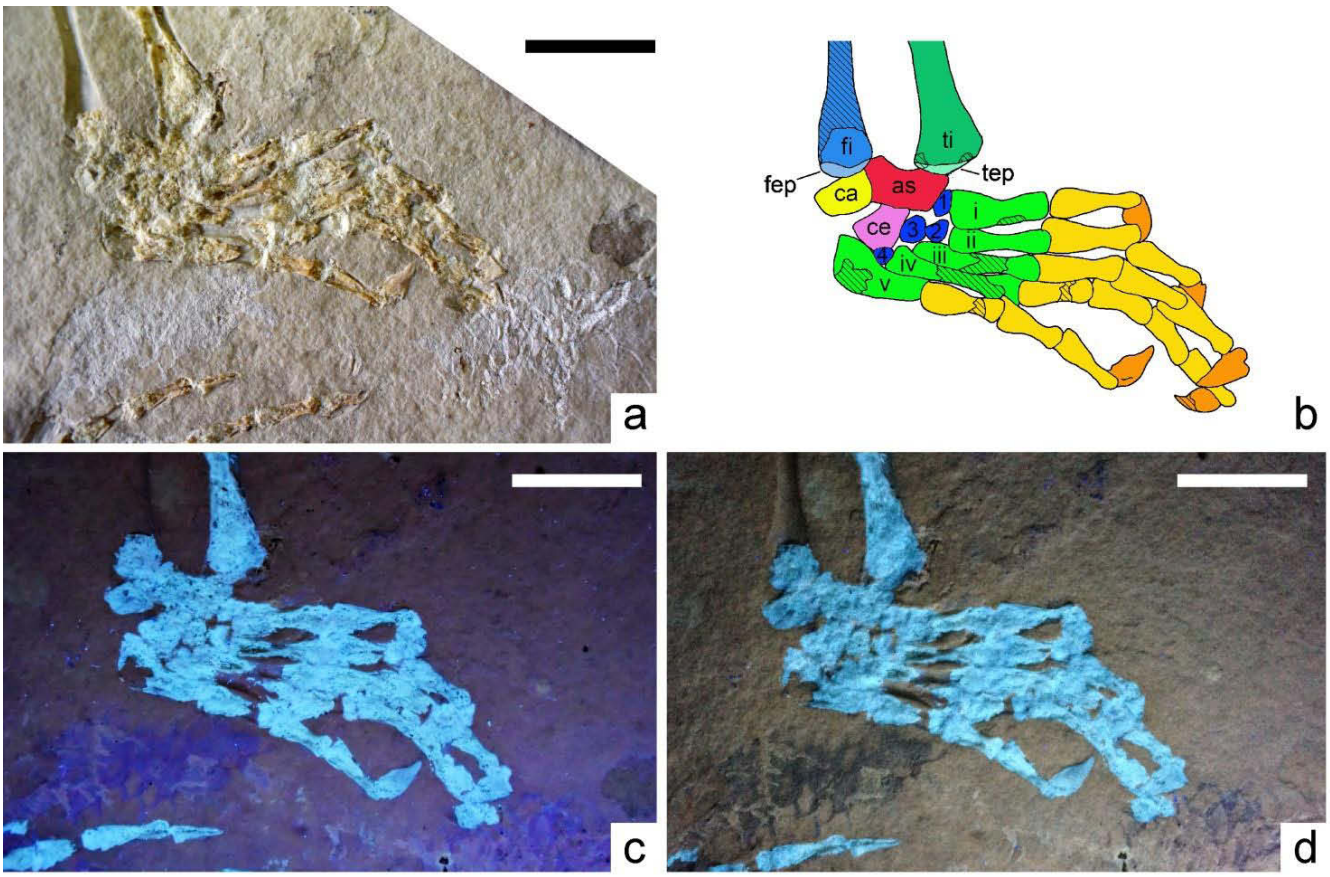

Figure A3.7. Interpretation of the zeugopodial and autopodial elements of *Primitivus manduriensis* hindlimb. Reconstruction (b) of the epipodials and manus of the new specimen realised by combining the observations under natural (a) and UV (c, d) light. The UV lamp used for analysing the specimen can radiate both short (254 nm) and long (365 nm) waves, and the difference is in the resulting spectrum of colours: grey for the short waves (d), and purple of the long waves (c). Striped areas indicate where the bones are only preserved as impressions. Scale bars: 1 cm. Abbreviations: as, astragalus; ca, calcaneum; ce, centrale; fep, epiphysis of the fibula; fi, fibula; tep, epiphysis of the tibia; ti, tibia; 1-4, first to fourth distal tarsals; i-v, first to fifth metatarsals.

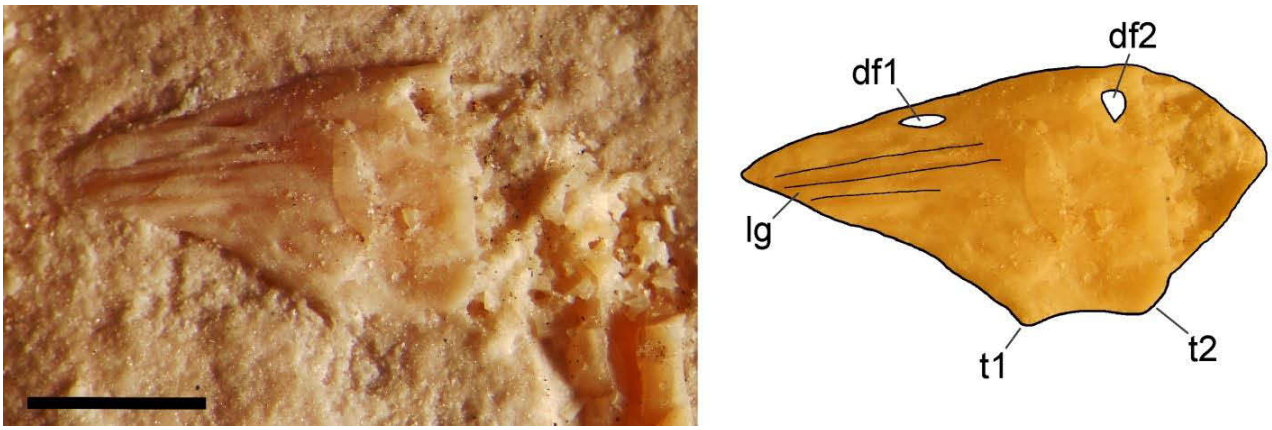

Figure A3.8. Interpretation of the ungual phalanx of *Primitivus manduriensis* pes. Illustration of the anatomical details preserved for one of the claw-like ungual phalanges of MPUR NS 161. Scale bar: 2 mm. Abbreviations: df, dorsal foramen; lg, longitudinal grooves; t, tubercle.

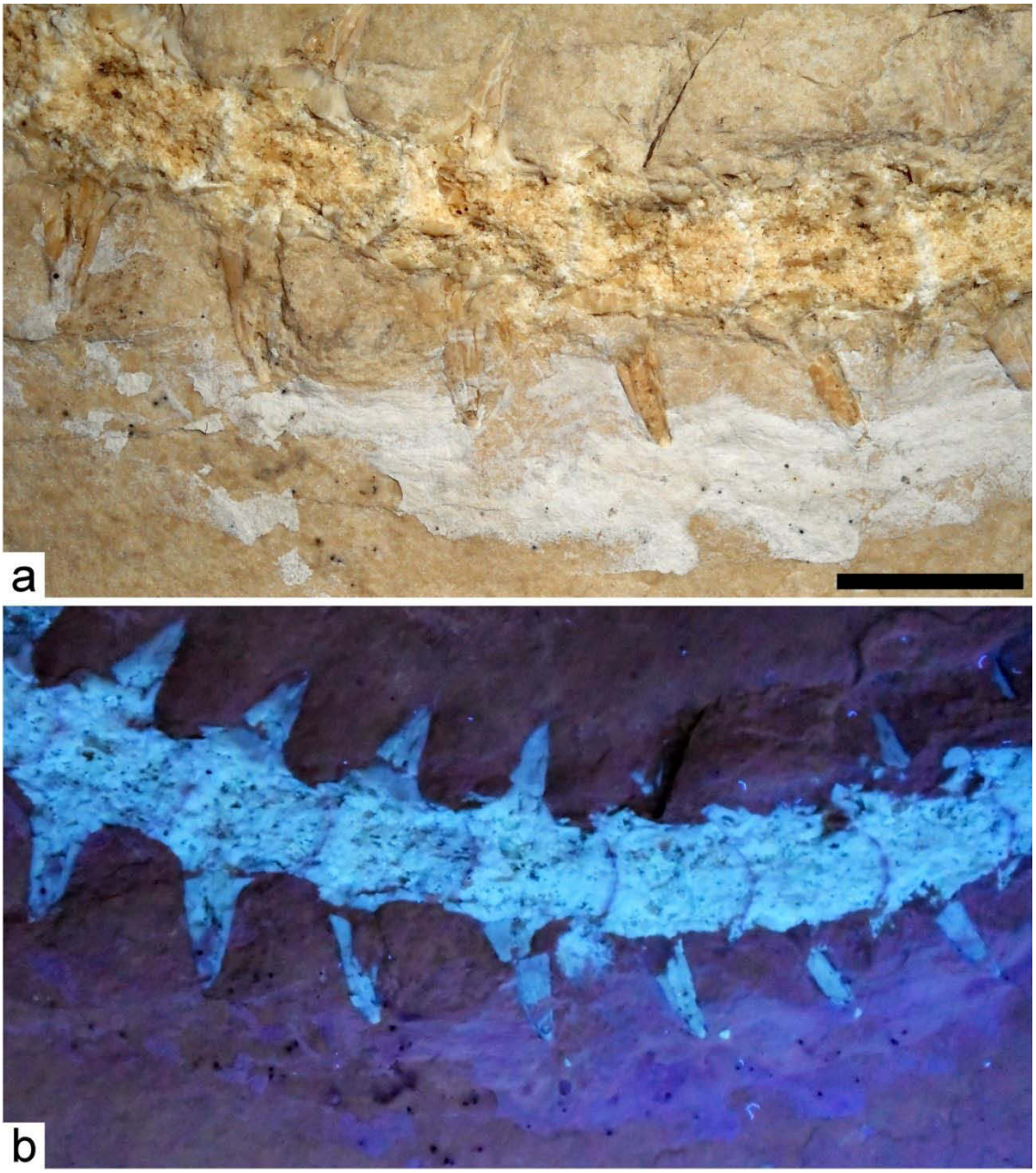

Figure A3.9. *Primitivus manduriensis* MPUR NS 161 imaging of anterior portion of the tail at natural (a) and UV (b) light. Anterior portion of the tail is exposed in dorsal view, and an extended portion of muscle bundles (dark purple in b) is visible on the left side of the column. According to the position and difference in fibers and bundles orientation and size, I identified these muscles as part of the *musculus transversospinalis* and *musculus iliocaudalis* (see also Figure 8d-g). Scale bar: 1 cm.

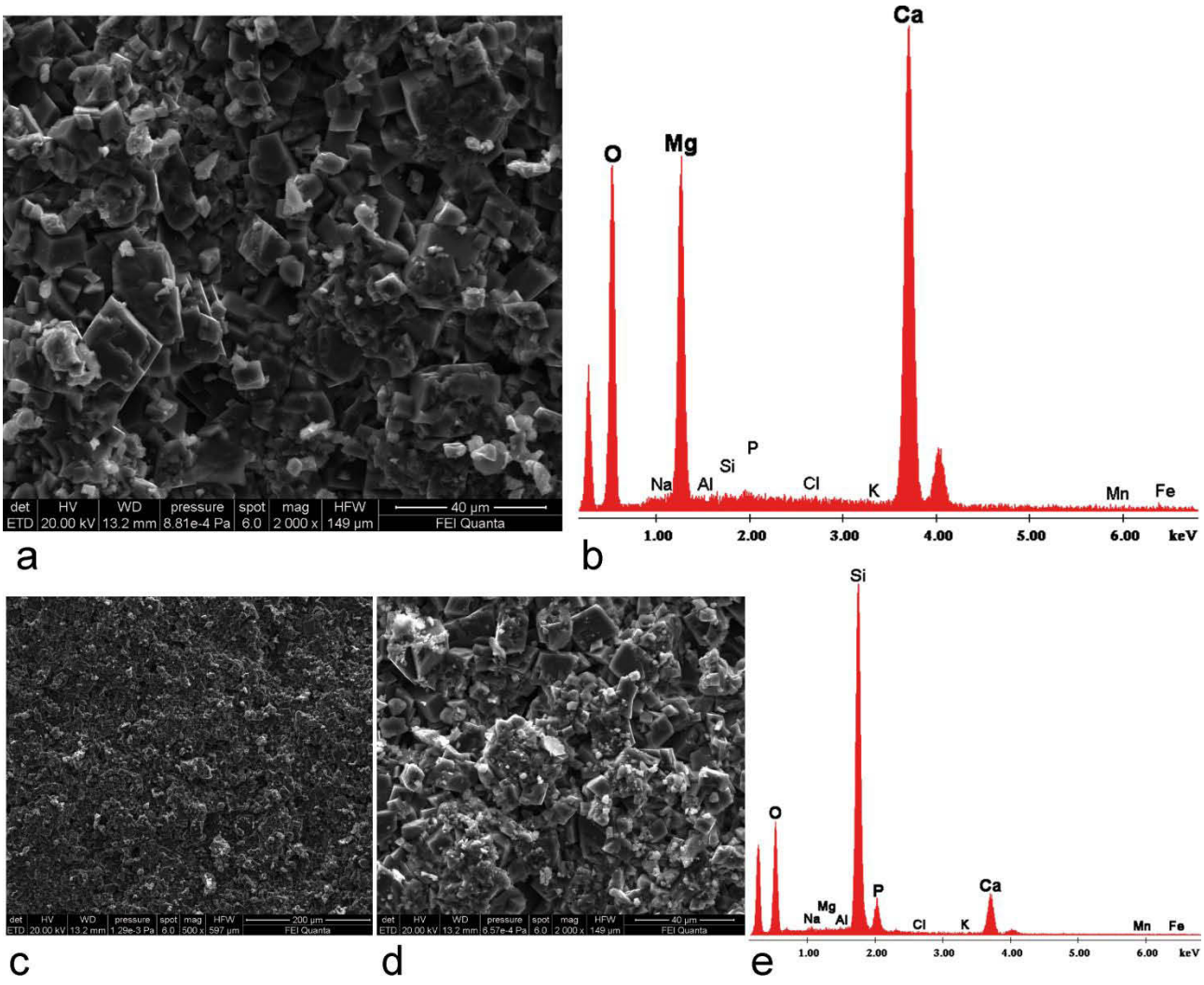

Figure A3.10. Results of the EDX analyses for sediment (a-b) and gut contents (c-e). As shown in Figure 9 for the bony and soft tissues, the composition for the material preserved in the posterior trunk region consists of replacement calcium phosphate (rich in Ca and P), while the sediment is rich in Ca and Mg, but there is no significant content of P. The high peak of silicon (Si) in the gut content spectrum must be related to the substrate bearing the sample which is made of silica-glass.

Table A3.1. Measurements and counts for *Primitivus manduriensis*, MPUR NS 161. Values reported for each vertebral series are average measurements. Abbreviations: d, diameter; dist, distal; H, height; L, length; max, maximum; min, minimum; mc, metacarpal; mt, metatarsal; n., number of; prox, proximal; seg., segment; W, width.

Element	Measurement (mm) or count	Element	Measurement (mm) or count
skull L	~70	ulna W(prox)	5.76
skull W	42.51	ulna W(mid-shaft)	2.67
mandible L	62	ulna W(dist)	4.23
postorbital L	25	mc–I L	9.59
orbit d(antero-posterior)	9	mc–I W	2.71
orbit d(transversal)	6.5	mc–II L	9.39
parietal foramen d(antero-posterior)	3.6	mc–II W	2.5
parietal foramen d(transversal)	1.9	mc–III L	9.78
n. cervicals	9-10	mc–III W	2.5
n. dorsals	22	mc–IV L	10.12
n. sacrals	2	mc–IV W	2.5
n. caudals (postsacral vertebrae)	>40	mc–V L	8.34
cervical centrum L	13.29	mc–V W	2.5
cervical centrum W	11.05	manus phalangeal formula	2-3-4-5-3
dorsal centrum L	15.09	hindlimb L	138
dorsal centrum W	11.92	hindlimb W(prox)	13.01
sacral centrum L	17.3	hindlimb W(dist)	17.42

sacral centrum W	19.08	femur L	43.23
anterior caudal centrum L	10.38	femur W(prox)	13.01
anterior caudal centrum W	12.48	femur W(mid-shaft)	5.41
mid-caudal centrum L	8.45	femur W(dist)	9.72
mid-caudal centrum H	5.67	tibia L	28.1
mid-caudal centrum W	9.14	tibia W(prox)	8.04
mid-caudal neural spine H	10.85	tibia W(mid-shaft)	3.27
mid-caudal neural spine W	2.93	tibia W(dist)	6.93
longest trunk rib L	81.5	fibula L	23.91
trunk rib W (head)	4.02	fibula W(prox)	4.21
tail H	38	fibula W(mid-shaft)	1.98
precaudal L	571.85	fibula W(dist)	5.59
forelimb L	107.5	mt–I L	9.35
forelimb W(prox)	8.72	mt–I W	2.11
forelimb W(dist)	16.5	mt–II L	10.53
humerus L	34.74	mt–II W	1.46
humerus W(prox)	8.72	mt–III L	12.19
humerus W(mid-shaft)	4.62	mt–III W	1.69
humerus W(dist)	11.5	mt–IV L	10.94
radius L	22.83	mt–IV W	2
radius W(prox)	5.34	mt–V L	10.37
radius W(mid-shaft)	2.25	mt–V W	2.96
radius W(dist)	5.48	pes phalangeal formula	2-3-4-5-4
ulna L	21.13		

Appendix 3.3 – List of morphological characters used in the phylogenetic analyses. Description of characters used to assess the phylogenetic relationships of the new taxon in the parsimony (MP and IWMP) analyses. All scorings are based on personal observation on relevant fossil and extant specimens, the literature, or images available on the Digimorph online database (www.digimorph.org). Most of the characters are taken or modified from Palci & Caldwell[1]; some of the characters are new, as indicated in the remarks. A list of cited literature is provided at the end of the character list.

Institutional Abbreviations – **HUJ-Pal**, Hebrew University of Jerusalem, Palaeontology Collections, Jerusalem, Israel; **MACN**, Museo Argentino de Ciencias Naturales ―Bernardino Rivadavia," Buenos Aires, Argentina; **MLP**, Museo de La Plata, La Plata, Argentina; **NHML**, Natural History Museum, London, England; **QM**, Queensland Museum, Brisbane, Queensland, Australia.

1. Premaxilla: does not contact frontals (0) / contacts frontals (1).
2. Premaxilla with median palatal ramus bearing foramina: absent (0) / present (1).
3. Premaxillary lateral foramina: absent (0) / present (1). *Yurlunggur* was rescored from state 1 to state 0[2]; *Pontosaurus kornhuberi* was rescored from unknown (?) to state 0[3].
4. Premaxilla-maxilla contact: immobile and sutural (0) / mobile and non-sutural (1).
5. Posterior process of maxilla: long, reaching or extending past middle of ventral margin of orbit (0) / short, not reaching middle of ventral margin of orbit (1).
6. Lacrimal: present, either permanently separate or fusing with prefrontal during ontogeny (0) / absent, never present as a discrete element (1).
7. Lacrimal foramen: single opening (0) / double opening (1).

8. Jugal: does not extend anteriorly past orbit (0) / extends anteriorly past orbit (1).
9. Jugal: with large posterior process (0) / without large posterior process (1). *Xenosaurus* and *Shinisaurus* were rescored from state 1 to state 0[4, 5]; *Lanthanotus* and *Varanus* were rescored from state 0 to state 1[4]; *Eupodophis* was rescored from inapplicable (-) to unknown (?); *Pachyrhachis* was rescored from state 0 to unknown (?). *Eupodophis* and *Pachyrhachis* do have a jugal, but it is not clear whether the posteroventral corner of the bone represents a posterior process homologous to that of lizards (point of attachment of quadratojugal ligament) or simply the posterior end of the expanded articular surface beteween jugal and maxilla.
10. Jugal: lacking dermal sculpture (0) / with dermal sculpture (1).
11. Nasals: large (0) / greatly reduced or absent (1).
12. Nasals: paired elements (0) / single median element (1).
13. External naris: not retracted, prefrontal and frontal both excluded from posterior narial margin by nasal and maxilla (0) / slightly retracted, prefrontal (but not frontal) enters posterior narial margin (1) / greatly retracted, prefrontal and frontal enter posterior narial margin (2).
14. Frontals: single median element (0) / paired elements (1).
15. Frontal: enters orbital margin, prefrontal does not contact postfrontal or postorbital (0) / excluded from orbital margin, prefrontal contacts postfrontal or postorbital (1). *Aigialosaurus* has been rescored from state 0&1 to state 0[6, 7]; *Pachyrhachis* has been rescored from state 1 to unknown (?). The skull reconstruction of *Pachyrhachis* in Caldwell [8] suggests that the frontal was excluded from the orbital margin (state 0),

however, due to poor preservation, disarticulation, and crushing of the only known skull of *Pachyrhachis* this character is best left as unknown (?).

16. Frontoparietal suture: in dorsal view, simple straight transverse contact (0) / in dorsal view, complex curved or interdigitating contact (1).

17. Postfrontal (or dorsomedial portion of single posterior orbital bone): forked medially, with an anterior process along the frontal and a posterior process along the parietal (0) / not forked medially, does not extend a long distance along frontal or parietal (1). *Heloderma* was rescored from state 1 to state 0 [4]; *Haasiophis* was rescored from state 1 to state unknown (?) (a postfrontal cannot be clearly identified in *Haasiophis*, the homology of the element preserved dorsal to the orbit in the type and only specimen is dubious [8]).

18. Palpebral (superciliary) ossifications on dorsal margin of orbit: present (0) / absent (1). *Aigialosaurus* was rescored from unknown (?) to state 1. No palpebral is known in *Aigialosaurus* [6, 7].

19. Postorbital: present (0) / absent (1). *Dinilysia, Eupodophis, Haasiophis*, *Pachyrhachis* and *Yurlunggur* were rescored from state 0 to state 1 [9].

20. Postorbital ventral process: small, forming less than half of posterior orbital margin, postorbital primarily a temporal bone (0) / prominent, forming half or more of posterior orbital margin, postorbital primarily an orbital bone (1). *Dinilysia, Eupodophis, Haasiophis* and *Pachyrhachis* were rescored from state 1 to inapplicable (-). *Yurlunggur* was rescored from state 0 to inapplicable (-). All these snakes lack a postorbital.

21. Pineal foramen: present (0) / absent (1).

22. Parietal table and jaw adductor muscles: parietal table very wide, jaw adductors restricted entirely to ventral surface of parietal (0) / parietal table much narrower posteriorly, jaw

adductors extend onto lateral margin of parietal (1) / parietal table tapers posteriorly into a sagittal crest (2). Modified from Palci & Caldwell[1].

23. Suspensorial ramus (posterolateral process) of parietal: well developed (0) / extremely short or absent (1).

24. Upper temporal arch: complete, upper and lower temporal fenestrae separated (0) / incomplete, upper and lowertemporal fenestra confluent (1). *Haasiophis* and *Yurlunggur* were rescored from inapplicable (-) to state 1 [2, 8].

25. Temporal arch: without canthal crest (0) / with canthal crest (1).

26. Dorsal process of squamosal: absent (0) / present (1). *Pachyrhachis* was rescored from state 0 to unknown (?). *Pachyrhachis* lacks a squamosal, what has been tentatively identified as a possible squamosal e.g., [10] may also be the shaft of the stapes or part of the hyoid apparatus.

27. Supratemporal: in deep position, on ventrolateral surface of parietal (0) / in superficial position, on dorsolateral surface of parietal (1). *Yurlunggur* was rescored from unknown (?) to state 1 (AP pers. obs. on QMF45391); *Adriosaurus* was rescored from state 1 to unknown (?) (AP pers. obs. on NHML R2867); *Pontosaurus lesinensis* was rescored from state 1 to state 0 [11].

28. Supratemporal: confined to skull roof (0) / forms part of paroccipital process and/or braincase (1).

29. Supratemporal: present (0) / absent (1).

30. Supratemporal-prootic contact: absent (0) / present (1). *Haasiophis* was rescored from state 0 to state 1 (AP pers. obs. on HUJ-Pal. EJ 695); *Yurlunggur* was rescored from unknown (?) to state 1 (AP pers. obs. on QMF45391).

31. Quadrate suspension: mobile, articulates dorsally with squamosal, supratemporal and opisthotic (0) / mobile, articulates dorsally with supratemporal, little or no contribution from other elements (1) / mobile, articulates dorsally with opisthotic, little or no contribution from other elements (2). *Pontosaurus kornhuberi* was rescored from state 0 to unknown (?); *Pontosaurus lesinensis* was rescored from unknown (?) to state 0 [3, 11].

32. Quadrate: tympanic crest (outer conch) directed laterally and a well-developed wall (0) / tympanic crest directed laterally but a low ridge (1) / distinct tympanic crest absent and external surface of quadrate only weakly concave (2).

33. Quadrate suprastapedial process: directed mostly posteriorly (0) / recurved posteroventrally (1) / absent (2). As examples, *Varanus bengalensis* represents state 0, while *Mosasaurus hoffmannii* represents state 1. Modified from Palci & Caldwell[1].

34. Mandibular articulation of quadrate: saddle-shaped, with lateral and medial condyles (0) / flat, a single continuous condyle (1). *Aigialosaurus* was rescored from state 1 to unknown (?), because the articulation is not visible in either *A. bucchichi* or *A. dalmaticus* [6, 7]; *Dinilysia* was rescored from unknown (?) to state 0 (AP pers. obs. on MACN-RN 1013); *Pontosaurus lesinensis* was rescored from state 1 to unknown (?) because the articulation is not visible [11].

35. Ventromedial processes of frontals: not contacting anything below olfactory tracts (0); abutting or sutured with each other below olfactory tracts (1); contacting each other and parabasisphenoid below olfactory tracts (2). *Dinilysia* was rescored from states 0&1 to state 2 [12]. Modified from Palci & Caldwell[1].

36. Parietal downgrowths: absent or weakly developed ridges (0) / prominent flanges (1). *Pontosaurus lesinensis* was rescored from state 0 to unknown (?). This feature is not clear in the type and only specimen [11].

37. Parietal downgrowths: not sutured to prootic (0) / sutured to prootic (1).

38. Parietal downgrowths: not contacting parabasisphenoid or orbitosphenoid (0) / contacting parabasisphenoid (1). *Haasiophis* was rescored from unknown (?) to state 1 (AP pers. obs. on HUJ-Pal. EJ 695).

39. Optic foramina: not enclosed in bone (0) / enclosed partly or entirely by frontals (1). *Pachyrhachis* was rescored from state 1 to unknown (?) because the optic foramen is not exposed in *Pachyrhachys* [8].

40. Trigeminal foramen or foramina: anterior margin not enclosed in bone (0) / anterior margin enclosed by descending flange of parietal and/or prootic (1). *Pachyrhachis* was rescored from state 1 to unknown (?) (the trigeminal foramen is not exposed in *Pachyrhachys* [8]).

41. Crista prootica (ridge on lateral surface of the prootic, overhanging foramen pro nervi facialis): well-developed lateral flange (0) / reduced to weak ridge, or absent (1). *Yurlunggur* was rescored from state 0 to state 1 (AP pers. obs. on QMF45111).

42. Foramen pro nervi facialis: single (0) / double (1) /exit confluent with trigeminal opening (2). *Yurlunggur* was rescored from unknown (?) to state 0 (AP pers. obs. on QMF45111). Modified from Palci & Caldwell[1].

43. Basipterygoid process: long, i.e., projecting far anterolaterally beyond the body of the basisphenoid (0) / short, i.e., not projecting very far beyond the body of the basisphenoid (1). *Aigialosaurus*, *Pontosaurus lesinensis* and *Pachyrhachis* were rescored from state 1 to unknown (?) because the processes are not visible in any of the available specimens for

these taxa [6, 7, 8, 11]; *Haasiophis* was rescored from unknown to state 1 (AP pers. obs. on HUJ-Pal. EJ 695).

44. Basal tubera: posteriorly located, very near to occipital condyle (0) / anteriorly located, well away from occipital condyle (1). *Yurlunggur* was rescored from state 1 to unknown (?). *Yurlunggur* lacks proper basal tubera, and has instead an elongate crest directed posterolaterally.

45. Posterior opening of vidian canal: at basisphenoidprootic suture (0) / situated within basisphenoid (1).

46. Posterior opening of vidian canal: situated anteriorly, well in front of the posterior end of the basisphenoid (0) / situated posteriorly, near the posterior end of the basisphenoid (1).

47. Opisthotic sub-horizontal flange posterior to basal tubera: weak or absent, with most of the stapes exposed in ventral view (0) / wide, extending posterolaterally from basal tubera, and obscuring much of the stapes in ventral view (1). *Eupodophis* was rescored from state 0 to unknown (?). All known specimens of *Eupodophis* are too porly preserved to score for this character [13, 14]. Modified from Palci & Caldwell[1].

48. Supraoccipital: does not contact parietal, unossified gap persists between the two elements (0) / abuts parietal, the two elements meet but contact is non-sutural, and a tiny gap might remain between the two elements along part of the dorsal edge of the supraoccipital (1) / sutural contact with parietal, entire anterodorsal edge of supraoccipital contacts parietal (2).

49. Supraoccipital: situated ventral or posteroventral to parietal, does not form part of posterior skull roof (0) / situated posterior to parietal, forms part of posterior skull roof (1).

50. Postemporal fenestra: present as an opening (0) / completely closed via sutural contact of the skull roof and otic region of braincase (1). *Aigialosaurus* was rescored from state 0 to

unknown (?) because the posterior region of the skull is not visible in either *A. bucchichi* or *A. dalmaticus* [6, 7]; *Haasiophis* was rescored from unknown (?) to state 1 because the position of the parietal on the skull roof and the lack of paroccipital processes in *Haasiophis* exclude the possibility that a postemporal fenestra was present [15].

51. Septomaxilla-maxilla contact: rigid, septomaxilla extensively sutured to the dorsal surface of the palatal flange of the maxilla (0) / septomaxilla not sutured to maxilla (1). *Dolichosaurus* and *Pachyrhachis* were rescored from 1 to unknown (?). The septomaxilla is unknown in both taxa [8, 16].

52. Median flange of septomaxilla: short, not reaching level of prefrontal (0) / long, extends posteriorly to reach level of prefrontal (1). *Yurlunggur* was rescored from state 1 to state 0 (AP pers. obs. on QMF45391).

53. Opening of Jacobson‘s organ: enclosed fully by maxilla and vomer, sometimes with a tiny contribution from the septomaxilla, not confluent with choana (0) / enclosed partly by maxilla and vomer, confluent posteriorly with choana (1) / enclosed fully by vomer and septomaxilla only, not confluent with choana (2). *Pachyrhachis* was rescored from state 2 to unknown (?) as the vomeronasal opening is not visible in *Pachyrhachys* [8]; *Yurlunggur* was rescored from state 0 to state 2 (AP pers. obs. on QMF45391).

54. Palatine-vomer contact: immobile, sutural contact (0) / mobile, non-sutural contact (1). *Dinilysia* was rescored from unknown (?) to state 0 [12]; *Eupodophis* was rescored from unknown to state 1 as a long tapering choanal process of the palatine of *Eupodophis* suggests that this element must have had a loose mobile connection with the vomer [14]; *Pachyrhachis* was rescored from state 1 to unknown (?) because the vomer is not visible in *Pachyrhachis* [8].

55. Palatine anterior dentigerous process: absent (0) / present (1).

56. Ectopterygoid: does not enter cheek (0) / enters cheek as a sliver sandwiched between maxilla and jugal (1). *Pachyrhachis* was rescored from state 0 to unknown (?). Because of disarticulation and compression it is not clear whether the ectopterygoid of *Pachyrhachys* would have entered the cheek region or not [8].

57. Ectopterygoid-palatine contact: absent, maxilla enters suborbital fenestra (0) / present, maxilla excluded from suborbital fenestra (1). *Pachyrhachis* was rescored from state 0 to unknown (?). The contact between ectopterygoid and palatine is not visible in this taxon [8].

58. Interpterygoid vacuity (‗pyriform recess' of Estes et al.[17]): open and wide (0) / open and narrow (1).

59. Pterygoid: anterior (palatine) process merges gradually, in a gentle curve, with the lateral (ectopterygoid) process (0) / anterior process distinctly set off from lateral process, the two portions meeting at a distinct ‗corner' (1). *Pontosaurus lesinensis* was rescored from state 0 to unknown (?). The region of interest is not exposed in the skull of *P. lesinensis* [11].

60. Mandibular symphysis: rigid anterior tips of dentary with a distinct flat symphysial area (0) / mobile anterior tips of dentary smoothly rounded and without distinct symphysial area (1). *Yurlunggur* was rescored from unknown (?) to state 1 (AP pers. obs. on QMF45391).

61. Mental foramina on lateral surface of dentary: three or more foramina (0) / two or fewer foramina (1). *Pachyrhachis* was rescored from state 1 to state 0 [9]; *Pontosaurus lesinensis* was rescored from state 1 to unknown (?) because no mental foramina are visible in the type and only specimen [11].

62. Dentary: curved in lateral view, with concave dorsal (alveolar) edge (0) / straight in lateral view, with straight dorsal edge (1). *Haasiophis* was rescored from state 0 to state 1 because

its dentary is curved medially, but in lateral view its dorsal margin would appear quite straight [15].

63. Dentary: with small posterodorsal extension onto anterolateral part of coronoid process (0) / does not cover lateral surface of coronoid process (1). *Dolichosaurus* was rescored from state 1 to unknown (?): the only dentary known for *Dolichosaurus longicollis* is too fragmentary to be scored for this character [16].

64. Anterior (symphysial) end of Meckel‘s canal: extends along ventral margin of lower jaw (0) / confined to medial surface of lower jaw (1). *Dolichosaurus* was rescored from state 1 to unknown (?): the only dentary known for *Dolichosaurus longicollis* is too fragmentary to be scored for this character [16].

65. Subdental shelf: large (0) / weakly developed (1) / absent (2). Modified from Palci & Caldwell (2010). For example the shelf is large in *Platecarpus tympaniticus* (state 0), weakly developed in *Shinisaurus crocodilurus* (state 1) and absent in *Anilius scytale* (state 2). *Dinilysia* and *Yurlunggur* were rescored from state 2 to state 0 [2, 12]; *Haasiophis* was rescored from unknown (?) to state 2 (AP pers. obs. on HUJ-Pal. EJ 695); *Pachyrhachis* was rescored from state 2 to unknown (?) because the medial aspect of the dentary is partially exposed only in the paratype, HUJ-Pal 3775, but the condition of the subdental shelf is unclear [8]; *Dolichosaurus* was rescored from state 1 to unknown (?) as the only dentary known for *Dolichosaurus longicollis* is too fragmentary to be scored for this character [16].

66. Posterior margin of lateral surface of dentary: no notch present (0); shallow notch present (1); deep notch present (2). For example, the notch is absent in *Platecarpus tympaniticus* (state 0), shallow in *Shinisaurus crocodilurus* (state 1), and deep in *Python molurus* (state

2). *Yurlunggur* was rescored from state 0 to state 2 (AP pers. obs. on QMF45391); *Dolichosaurus* was rescored from state 1 to unknown (?) as the only dentary known for *Dolichosaurus longicollis* is too fragmentary to be scored for this character [16]. Modified from Palci & Caldwell[1].

67. Dentary-postdentary articulation: extensive overlap (0) / reduced overlap (1). *Yurlunggur* was rescored from state 2 to state 1 (although a postdentary is not known in *Yurlunggur*, the articular surface on the dentary indicates that the connection between these two bones was fairly loose and overlap was reduced; AP pers. obs. on QMF45391).
68. Splenial: large, extending anteriorly past middle of tooth row (0) / small, only reaching middle of tooth row (1).
69. Splenial: extends posteriorly onto postdentary bones, past apex of coronoid process (0) / extends posteriorly onto postdentary bones but does not reach level of apex of coronoid process (1) / does not substantially overlap postdentary elements (2).
70. Anterior tip of splenial: on ventral edge of dentary (0) / on medial surface of dentary (1). *Dinilysia* was rescored from state 0 to unknown (?) (due to proximity of the anterior tip of the splenial to the ventral edge of the dentary and uncertainty in the original orientation of the dentary this character cannot be confidently assessed); *Eupodophis* was rescored from unkown (?) to state 1 [14]; *Haasiophis* was rescored from state 0 to state 1 [15].
71. Splenial-dentary contact: extensive bony contact (0) / reduced bony contact, much intervening connective tissue (1).
72. Splenial-angular contact: in medial view, overlapping, irregular, and with limited mobility (0) / inmedial view, abutting, straight (vertical), and highly mobile (1). *Lanthanotus* was rescored from state 0 to state 1 [18].

73. Splenial-angular contact: not, or very slightly, exposed in lateral view (0) / greatly exposed in lateral view (1).

74. Anteromedial process of coronoid: long, extensive overlap on medial surface of dentary in front of coronoid process (0) / short, coronoid does not greatly overlap medial surface of dentary in front of coronoid process (1). *Pontosaurus lesinensis* was rescored from state 1 to state 0 [11].

75. Anterolateral process of coronoid: present, overlapping lateral surface of dentary (0) / absent, coronoid does not overlap lateral surface of dentary (1). *Dolichosaurus* was rescored from state 0 to unknown (?) as the only dentary known for *Dolichosaurus longicollis* is too fragmentary to allow evaluation of this character [16].

76. Coronoid: anteromedial margin contacts splenial (0) / anteromedial margin does not contact splenial (1). *Haasiophis* was rescored from state 1 to state 0 [15]; *Pachyrhachis* was rescored from state 1 to unknown (?) because, although the medial aspect of the lower jaw is partially exposed only in the paratype, HUJ-Pal 3775, it is unclear whether the splenial would have been in contact with the coronoid or not in an undistorted jaw [8].

77. Coronoid: ventral margin of medial surface concave (0) / ventral margin of medial surface straight or convex (1).

78. Subcoronoid fenestra on medial surface of the mandible: fenestra present as distinct gap between coronoid and prearticular, surangular exposed in medial view (0) / fenestra absent, prearticular expands dorsally and contacts the entire ventral edge of the coronoid, surangular covered by these elements in medial view (1). *Dolichosaurus* was rescored from state 1 to unknown (?) as this character cannot be evaluated in *Dolichosaurus* [16]; *Pontosaurus lesinensis* was rescored from state 1 to state 0 [11].

79. Surangular: does not form large portion of articular cotyle (0) / forms half of articular cotyle (1).

80. Angular: not exposed, or exposed as only a very narrow splint, on the medial surface of the mandible (0) / with wide exposure on medial surface of the mandible (1). *Dinilysia* was rescored from state 0 to state 1 [12]; *Yurlunggur* was rescored from unknown (?) to state 1 (AP pers. obs. on QMF45391).

81. Prearticular (in medial view with dentary and splenial removed): extends well anterior to coronoid process, past posterior teeth (0) / extends only a short distance in front of coronoid process, not past posterior teeth (1).

82. Adductor fossa: faces dorsomedially (0) / faces dorsally (1). *Pachyrhachis* was rescored from state 1 to unknown (?) because the fossa is not exposed in either of the available specimens [8].

83. Prearticular: not fused with surangular (0) / fused with surangular (compound bone) (1). Modified from Palci & Caldwell[1].

84. Retroarticular process size: short, shorter than articular cotyle (0) / intermediate, between 1 and 2 times articular cotyle (1) / long, over 2 times longer than articular cotyle (2). Modified from Palci & Caldwell[1].

85. Retroarticular process: not tapering, broad distally (0) / tapering, narrow distally (1). Note: not applicable for taxa with a very short retroarticular process. *Dinilysia* was rescored from unknown (?) to inapplicable (-).

86. Marginal teeth: pleurodont, teeth set in a continuous groove (0) / thecodont, teeth ankylosed in discrete alveoli and separated by well-developed interdental plates (1). *Aigialosaurus* was rescored from state 1 to state 0 because, although tooth implantation

cannot be assessed in *A. dalmaticus* due to lack of exposure, in *A. bucchichi* the roots of the teeth are clearly exposed medially and there are no interdental plates [6, 7]; *Dolichosaurus* was rescored from state 1 to unknown (?) as no marginal dentition is known for this taxon [16]; *Pontosauurs kornhuberi* was rescored from state 0 to unknown (?) because tooth attachment cannot be evaluated due to lack of exposure in the only specimen [3].

87. Marginal teeth: without high pedestals (0) / with high pedestals (1).

88. Resorption pits: at base of teeth (0) / on bony tooth pedicel (1) / absent (2). *Aigialosaurus* and *Dolichosaurus* were rescored from state 2 to unknown (?) as these states cannot be evaluated in either *Aigialosaurus* [6, 7] or *Dolichosaurus* [16] material.

89. Orientation of replacement teeth: erupt upright, growing straight upwards into functional position (0) / erupt horizontally, and then rotating through ninety degrees about the base into functional position (1). *Dolichosaurus* was rescored from state 1 to unknown (?) as this character cannot be evaluated for this taxon [16].

90. Premaxillary teeth: 6 or more (0) / 2–5 (1) / none (2). *Aigialosaurus* was rescored from state 1 to unknown (?) as a premaxilla is not preserved in either *A. dalmaticus* or *A. bucchichi* [6, 7]; *Eupodophis* and *Haasiophis* were rescored from state 2 to unknown (?) because the premaxilla is not visible in either taxon [9, 13, 14]; *Pachyrhachis* and *Adriosaurus* were rescored from state 1 to unknown (?) because, although a premaxilla is preserved for both taxa, it cannot be determined how many tooth positions were present on its ventral surface [8, 19].

91. Premaxillary teeth (apart from median tooth): similar size or larger than anterior maxillary teeth (0) / distinctly smaller than anterior maxillary teeth (1). *Adriosaurus* was rescored from state 1 to state 0 [19].

92. Palatine teeth: absent (0) / present (1). *Heloderma* was rescored from states 0&1 to state 0 (AP pers. obs. on *H. horridum*); *Dinilysia* was rescored from unknown (?) to state 1 (AP pers. obs. on type specimen MLP 26-410).

93. Palatine teeth: small conical denticles (0) / similar in size to marginal teeth (1).

94. Pterygoid teeth: present (0) / absent (1). *Heloderma* was rescored from state 0 to state 1 (while this state does appear to be polymorphic in *Heloderma suspectum*, in the specimens of *Heloderma horridum* examined there were no pterygoid teeth).

95. Pterygoid teeth: small conical denticles (0) / similar in size to marginal teeth (1). *Xenosaurus* and *Heloderma* were rescored from state 0 to inapplicable (-).

96. Zygosphenes and zygantra: absent (0) / present (1). *Aigialosaurus* was rescored from state 1 to unknown (?) as the presence or absence of these accessory intervertebral articulations cannot be evaluated in either *A. dalmaticus* or *A. bucchichi* [6, 7].

97. Hypapophyses/hypapophyseal peduncles: only extending to the posterior end of the ninth presacral-precloacal vertebra at most (0) / extending to the tenth presacral/precloacal vertebra or beyond (1).

98. Transverse processes of cervicals: on anterior end of centrum (0) / on middle of centrum (1). *Yurlunggur* was rescored from state 1 to state 0 (AP. pers. obs. on QMF45391).

99. Cervical (anterior) intercentra (excluding atlas and axis) as individual ossifications: present (0) / absent (1). For example, intercentra are present as individual ossifications in the anterior (cervical) vertebrae of *Platecarpus tympaniticus*, but are fused to the centrum in *Diploglossus millepunctatus*. Modified from Palci & Caldwell[1].

100. Pachyostosis of mid-dorsal vertebrae and ribs: absent (0) / present (1). *Yurlunggur* was rescored from unknown (?) to state 0 (AP. pers. obs. on QMF45391).

101. Ventral surface of caudal vertebrae: has facets for articulation with intercentra (chevron bones; V- or Y-shaped ossifications) (0) / lacks facets for articulation with intercentra (intercentra absent) (1) / lacks facets for articulation with intercentra (intercentra absent) but has long paired processes (2).

102. Trunk ribs: smoothly curved (0) / middle and distal regions of ribs totally straight (1). In state 0, the body results in a more rounded shape, while state 1 accounts for the laterally compressed condition of the body. *Dinilysia* was rescored from unknown (?) to state 0 (AP pers. obs. on MACN-RN 976); *Pontosaurus lesinensis* was rescored from state 1 to state 0 [11]. Modified from character 107 (‗Body shape') of Palci & Caldwell[1].

103. Ribs: begin from third (or more anterior) cervical vertebra (0) / begin from fourth (or more posterior) cervical vertebra (1).

104. Distally forked cloacal ribs (‗‗lymphapophyses''): absent (0) / present (1). *Yurlunggur* was rescored from unknown (?) to state 1 (AP pers. obs. on QMF45391).

105. Tail: cylindrical or only slightly lateral compressed, transverse processes well-developed, chevrons and neural spines not elongated (0) / very laterally compressed, transverse processes reduced anteriorly and absent posteriorly, chevrons and neural spines elongated (1). *Pachyrhachis* was rescored from state 1 to unknown (?) as only the base of the tail is known in *Pachyrhachys* so it is not possible to determine whether the mid and distal portions of the tail were compressed or not [8].

106. Neural spines of posterior caudal vertebrae: projecting dorsally or posterodorsally (0) / projecting almost horizontally, highly inclined posteriorly (1). *Yurlunggur* was rescored from unknown (?) to state 0 (AP pers. obs. on QMF45391).

107. Scapulocoracoid: present and large (0) / present but reduced (1) / absent (2).

108. Anterior (primary) coracoid emargination: present (0) / absent (1).

109. Clavicle: present (0) / absent (1). *Dolichosaurus* was rescored from unknown (?) to state 0[16].

110. Interclavicle: present (0) / absent (1). *Dolichosaurus* was rescored from state 1 to unknown (?)[16].

111. Interclavicle: cross-shaped, with lateral processes (0) / simple rod, without lateral processes (1).

112. Calcified sternum: present (0) / absent (1). *Aigialosaurus* was rescored from state 0 to unknown (?) because a calcified sternum is not preserved in either *A. dalamticus* or *A. bucchichi*[6, 7].

113. Number of rib attachment points to sternum: five pairs (0); four pairs (1); three pairs (2); two pairs or fewer (3). *Aigialosaurus* was rescored from state 2 to unknown (?) because the number of attachment points for ribs on the sternum cannot be determined in either *A. dalamticus* or *A. bucchichi*[6, 7]. Modified from Palci & Caldwell[1].

114. Forelimbs: large (0) / small, humerus as long as or shorter than two dorsal vertebrae (1) / absent (2). *Yurlunggur* was rescored from state 2 to unknown (?): although it is likely that *Yurlunggur* lacked forelimbs, their presence cannot be excluded from disarticulated remains only.

115. Ectepicondylar foramen of humerus: present (0) / absent (1).

116. Pelvis: present and large (0) / present and small (1) / absent (2).

117. Supracetabular iliac process: has the size of a tubercle or spine, being short to very reduced (0) / is elongated and rod-like (1). The supracetabular iliac process departs from the anterodorsal margin of the iliac shaft; state 0 accounts for the condition seen in most extant

terrestrial lizards (e.g., *Varanus*, *Xenosaurus*, *Shinisaurus*) and basal mosasauroids (e.g., *Tethysaurus*, *Pannoniasaurus*) while state 1 accounts for the modified condition in derived mosasaurids (e.g., *Mosasaurus*, *Platecarpus*) where the anterodorsal process is elongated and more or less cylindrical (in some mosasaurid taxa not included in this dataset the process can also be dorsoventrally compressed, like for example in *Tylosaurus*). *Aigialosaurus* is scored as ?, because the presence of a supracetabular tubercle cannot be verified due to the way the ilium is exposed; the anteroventrally extended process visible in *A. dalmaticus* and described by Dutchak & Caldwell[6] is instead the preacetabular process departing from the anterior margin of the iliac shaft and not homologous to the supracetabular tubercle (both processes are present in most extant lizards, like for instance *Varanus* and *Iguana*) (IP pers. obs.). New character.

118. Pubis: without expanded plate-like proximal end (0) / with expanded plate-like proximal end (1). For example, *Varanus bengalensis* has state 0, while *Acteosaurus tommasinii* has state 1. Modified from Palci & Caldwell[1].
119. Hindlimbs: present (0) / absent or vestigial (i.e., only femur clearly recognizable inside rib cage) (1).
120. Distal end of tibia: with notch fitting into a ridge on astragalocalcaneum (0) / gently convex for astragalocalcaneal articulation (1).
121. Astragalus and calcaneum: co-ossified (0) / separate (1).
122. Fifth metatarsal: hooked (0) / not hooked (1). *Pachyrhachis* was rescored from state 1 to unknown (?) as no metatarsals are preserved for this taxon [20].

123. Dorsal body osteoderms: present (0) / absent (1). *Yurlunggur* was rescored from state 1 to unknown (?): although it is likely that *Yurlunggur* lacked osteoderms, their presence cannot be excluded from the available disarticulated material.
124. Separable cranial osteoderms: present over entire skull table (0) / absent (1).
125. Scleral ossicles: present (0) / absent (1).
126. Epiphyses on skull and axial skeleton: present (0) / absent (1).
127. Epiphyses on appendicular skeleton: present (0) / absent (1). In *Tetrapodophis* the absence of epyphises is possibly due to its likely early ontogenetic stage; therefore this taxon was conservatively scored as unknown (?) for this character.
128. Posterodistal process of fibula: weakly developed to absent (0) / strongly developed, triangular process extends posteriorly beyond calcaneum (1).
129. Opening for trigeminal nerve: not subdivided for exits of V2 and V3 branches of trigeminal nerve (0) / subdivided for exits of V2 and V3 branches of trigeminal nerve (laterosphenoid bridge present) (1). New character.

Literature Cited in Appendix 3.3

1. Palci A, Caldwell MW. Redescription of *Acteosaurus tommasinii* von Meyer, 1860, and a discussion of evolutionary trends within the clade Ophidiomorpha. *J Vert Paleontol* **30**, 94-108 (2010).
2. Scanlon JD. Skull of the large non-macrostomatan snake Yurlunggur from the Australian Oligo-Miocene. *Nature* **439**, 839-842 (2006).
3. Caldwell MW. A new species of *Pontosaurus* (Squamata, Pythonomorpha) from the Upper Cretaceous of Lebanon and a phylogenetic analysis of Pythonomorpha. *Memorie della*

Società Italiana di Scienze Naturali e Museo Civico di Storia Naturale di Milano **34**, 1-43 (2006).

4. Gauthier JA, Estes R, de Queiroz ET. A phylogenetic analysis of Lepidosauromorpha. In: *Phylogenetic Relationships of the Lizard Families* (ed^(eds Estes R, Pregill G). Stanford University Press (1988).
5. Conrad JL. Postcranial skeleton of *Shinisaurus crocodilurus* (Squamata: Anguimorpha). *J Morphol* **267**, 759-775 (2006).
6. Dutchak AR, Caldwell MW. Redescription of *Aigialosaurus dalmaticus* Kramberger, 1892, a Cenomanian mosasauroid lizard from Hvar Island, Croatia. *Can J Earth Sci* **43**, 1821-1834 (2006).
7. Dutchak AR, Caldwell MW. A redescription of *Aigialosaurus* (= *Opetiosaurus*) *bucchichi* (Kornhuber 1901)(Squamata: Aigialosauridae) with comments on mosasauroid systematics. *J Vert Paleontol* **29**, 437-452 (2009).
8. Caldwell MW. Snake phylogeny, origins, and evolution: the role, impact, and importance of fossils (1869–2006). *Major Transitions in Vertebrate Evolution Indiana University Press, Bloomington and Indianapolis, Indiana*, 253-302 (2007).
9. Palci A, Caldwell MW, Nydam RL. Reevaluation of the anatomy of the Cenomanian (Upper Cretaceous) hind-limbed marine fossil snakes *Pachyrhachis*, *Haasiophis*, and *Eupodophis*. *J Vert Paleontol* **33**, 1328-1342 (2013).
10. Lee MSY, Caldwell MW. Anatomy and relationships of *Pachyrhachis problematicus*, a primitive snake with hindlimbs. *Philos Trans R Soc Lond, Ser B: Biol Sci* **353**, 1521-1552 (1998).

11. Pierce SE, Caldwell MW. Redescription and phylogenetic position of the Adriatic (Upper Cretaceous; Cenomanian) dolichosaur *Pontosaurus lesinensis* (Kornhuber, 1873). *J Vert Paleontol* **24**, 373-386 (2004).
12. Zaher H, Scanferla CA. The skull of the Upper Cretaceous snake Dinilysia patagonica Smith-Woodward, 1901, and its phylogenetic position revisited. *Zool J Linn Soc* **164**, 194-238 (2012).
13. Rage J-C, Escuillié F. Un nouveau serpent bipède du Cénomanien (Crétacé). Implications phylétiques. *Comptes Rendus de l'Académie des Sciences-Series IIA-Earth and Planetary Science* **330**, 513-520 (2000).
14. Rieppel O, Head JJ. *New Specimens of the Fossil Snake Genus" Eupodophis" Rage & Escuillié, from Cenomanian (late Cretaceous) of Lebanon*. Società italiana di scienze naturali (2004).
15. Rieppel O, Zaher H, Tchernov E, Polcyn MJ. The anatomy and relationships of *Haasiophis terrasanctus*, a fossil snake with well-developed hind limbs from the mid-Cretaceous of the Middle East. *J Paleontol* **77**, 536-558 (2003).
16. Caldwell MW. On the aquatic squamate *Dolichosaurus longicollis* owen, 1850 (Cenomanian, Upper Cretaceous), and the evolution of elongate necks in squamates. *J Vert Paleontol* **20**, 720-735 (2000).
17. Estes R, de Queiroz K, Gauthier JA. Phylogenetic relationships within Squamata. In: *Phylogenetic Relationships of the Lizard Families* (ed^(eds Estes R, Pregill G). Stanford University Press (1988).
18. McDowell SB, Bogert CM. The systematic position of Lanthanotus and the affinities of the anguinomorphan lizards. *Bull Am Mus Nat Hist* **105**, (1954).

19. Lee MSY, Caldwell MW. *Adriosaurus* and the affinities of mosasaurs, dolichosaurs and snakes. *J Paleontol* **74**, 915-937 (2000).

20. Caldwell MW, Lee MSY. A snake with legs from the marine Cretaceous of the Middle East. *Nature* **386**, 705-709 (1997).

Appendix 3.4 – Additional topologies resulting from the phylogenetic analyses.

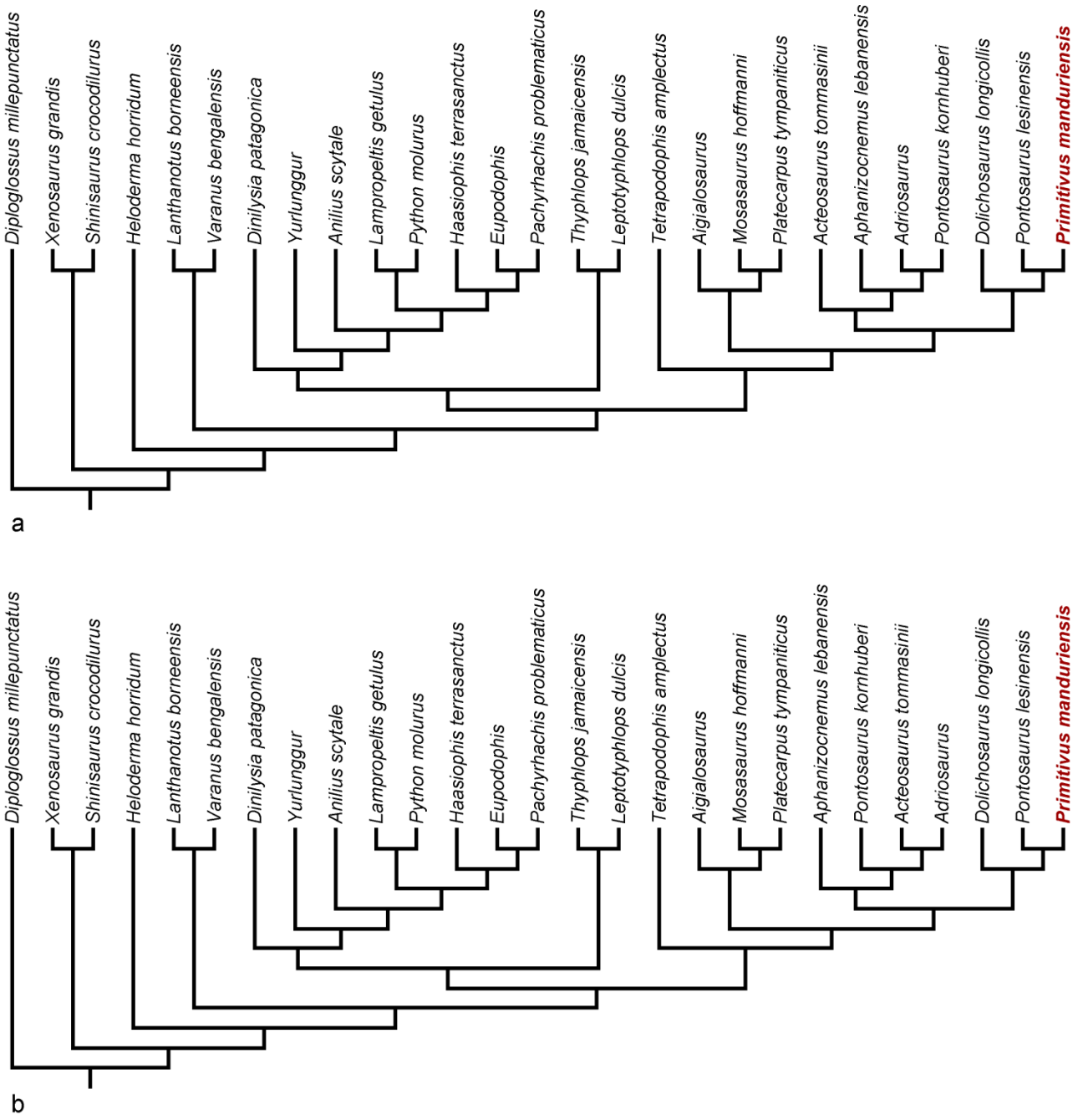

Figure A3.11. Optimal trees resulted from the MP analysis. The heuristic search for the MP analysis was performed using the TBR algorithm, and applying two successive rounds of tree searching and swapping. The first round resulted in 967 suboptimal trees (or simply suboptimals), while the second round overflowed the number of Max Trees (99,999). After

removing the suboptimals, two optimal trees were retained, and the only difference between them is the arrangement of the clade *Aphanizocnemus* + *Pontosaurus kornhuberi* + *Acteosaurus* + *Adriosaurus*: in one case, *Adriosaurus* and *P. kornhuberi* are sister taxa, with *Aphanizocnemus* at their base, and *Acteosaurus* as the most basal member of the clade (a); alternatively, *Aphanizocnemus* is recovered as the most basal taxon, and *Acteosaurus* + *Adriosaurus* as the most deeply nested, with *P. kornhuberi* in sister relationship to them (b). The length of the two optimal trees is equal to 283 steps, with a consistency index (CI) of 0.53497 and a retention index (RI) of 0.80149.

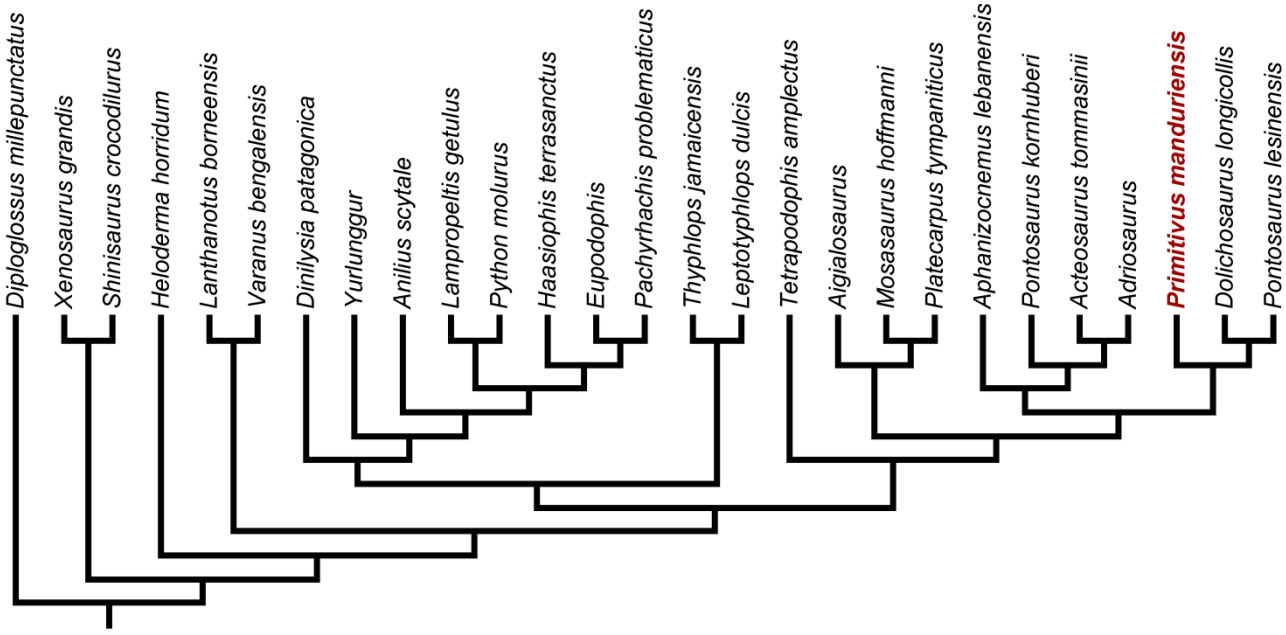

Figure A3.12. Single optimal tree resulted from the IWMP analysis. For the IWMP analysis I implemented the same procedure as the MP method, enabling the implied weighting option (under K = 3) before running the TBR heuristic search. 271 suboptimal trees were found with the first round of TBR, while the successive swapping of these trees overflowed the limit of 99,999

Max Trees. Only one shortest tree is retained after removing all the suboptimals, corroborating with a better resolution the hypothesis offered by the MP strict consensus of *Primitivus* forming a clade with *Dolichosaurus* and *P. lesinensis*, and *Tetrapodophis* at the stem of a clade consisting of Mosasauroidea (aigialosaurs + mosasaurids) + Dolichosauridae.

Appendix 3.5 – List of synapomorphies derived from the equal-weight maximum parsimony analysis (strict consensus tree). The corresponding number of the character is given in brackets, and the node numbers are given in the figure below.

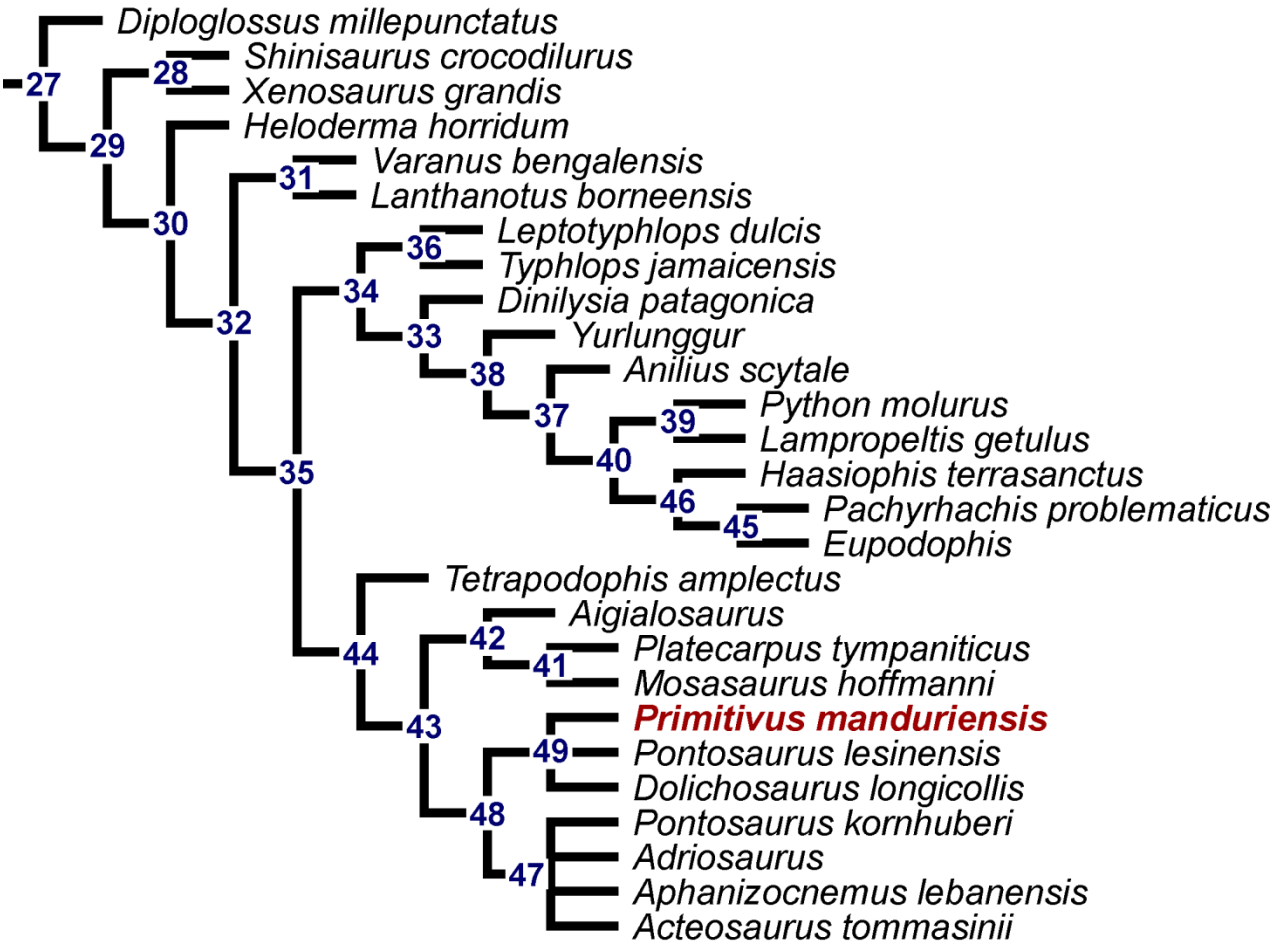

Diploglossus millepunctatus: No autapomorphies.

Xenosaurus grandis: squamosal_dorsal_proc. (26): 0 --> 1; post.opening_vidian_canal_1 (45): 0 --> 1.

Shinisaurus crocodilurus: parietal-jaw_muscles (22): 0 --> 1; pterygoid_teeth (94): 1 --> 0.

Heloderma horridum: frontal-orbit (15): 0 --> 1; frontal_ventromedial_proc. (35): 0 --> 1; splenial_size (68): 0 --> 1; coracoid_anterior_emargination (108): 0 --> 1; interclavicle_shape (111): 0 --> 1.

Lanthanotus borneensis: frontal-orbit (15): 0 --> 1; splenial_size (68): 0 --> 1; palatine_teeth (92): 0 --> 1; pterygoid_teeth (94): 1 --> 0.

Varanus bengalensis: pineal_foramen (21): 1 --> 0; frontal_ventromedial_proc. (35): 0 --> 1; crista_prootica (41): 1 --> 0; opisthotic_flange (47): 0 --> 1

Dinilysia patagonica: basipterygoid_proc. (43): 1 --> 0; Meckel's_canal (64): 1 --> 0; anteromedial_coronoid-splenial (76): 0 --> 1; adductor_fossa (82): 0 --> 1.

Typhlops jamaicensis: palatine-vomer (54): 0 --> 1; angular (80): 1 --> 0; Retroarticular_proc._size (84): 0 --> 2.

Leptotyphlops dulcis: pmx_foramina (3): 0 --> 1; nasals_fused/unfused (12): 0 --> 1; dentary_mental_foramina (61): 0 --> 1; splenial_size (68): 0 --> 1; splenial-angular_2 (73): 0 --> 1; anteromedial_coronoid-splenial (76): 0 --> 1; marginal_teeth_implantation (86): 1 --> 0.

Anilius scytale: parietal_post.rami (23): 1 --> 0; dentary_dorsal_margin (62): 1 --> 0; dentary-coronoid_proc. (63): 1 --> 0; ventral_coronoid (77): 1 --> 0; caudal_vertebrae (101): 0 --> 1.

Lampropeltis getulus: adductor_fossa (82): 0 --> 1; pelvis_size (116): 1 --> 2.

Python molurus: frontal-orbit (15): 0 --> 1.

Mosasaurus hoffmanni: frontal-orbit (15): 0 --> 1.

Platecarpus tympaniticus: No autapomorphies.

Aigialosaurus: tympanic_crest (32): 0 --> 1; marginal_teeth_implantation (86): 1 --> 0; coracoid_anterior_emargination (108): 0 --> 1; pelvis_size (116): 1 --> 0.

Eupodophis: Meckel's_canal (64): 1 --> 0.

Haasiophis terrasanctus: nasals_size (11): 0 --> 1.

Pachyrhachis problematicus: No autapomorphies.

Yurlunggur: external_naris (13): 1 --> 2; frontal-orbit (15): 0 --> 1; opisthotic_flange (47): 0 --> 1; smx_median_flange (52): 1 --> 0.

Acteosaurus tommasinii: post.caudal_neural_spines (106): 1 --> 0; clavicle (109): 0 --> 1; sternum (112): 0 --> 1.

Aphanizocnemus lebanensis: No autapomorphies.

Adriosaurus: frontal_fused/unfused (14): 0 --> 1; pachyostosis_vertebrae_&_ribs (100): 0 --> 1; clavicle (109): 0 --> 1.

Dolichosaurus longicollis: nasals_size (11): 1 --> 0.

Pontosaurus kornhuberi: retroarticular_proc._size (84): 1 --> 2; pachyostosis_vertebrae_&_ribs (100): 0 --> 1.

Pontosaurus lesinensis: supratemporal (29): 0 --> 1; pachyostosis_vertebrae_&_ribs (100): 0 --> 1; sternum (112): 0 --> 1.

Primitivus manduriensis: supraoccipital-parietal_1 (48): 2 --> 0; forelimbs (114): 1 --> 0; pelvis_size (116): 1 --> 0.

Tetrapodophis amplectus: splenial_posterior_extension (69): 2 --> 0; splenial-dentary (71): 1 --> 0; ribs_curved/straight (102): 0 --> 1; post.caudal_neural_spines (106): 0 --> 1.

Node 28 (*Shinisaurus* + *Xenosaurus*): pmx_foramina (3): 0 --> 1; jugal_dermal_sculpture (10): 0 --> 1; frontal_fused/unfused (14): 1 --> 0; palpebral_ossification (18): 1 --> 0; pineal_foramen (21): 1 --> 0; temporal_arch_crest (25): 0 --> 1; ectopterygoid-cheek (56): 0 --> 1.

Node 29 ((*Shinisaurus* + *Xenosaurus*) + (*Heloderma* + ((*Varanus* + *Lanthanotus*) + Pythonomorpha))): No synapomorphies.

Node 30 (*Heloderma* + ((*Varanus* + *Lanthanotus*) + Pythonomorpha)): dentary-coronoid_proc. (63): 0 --> 1; subdental_shelf (65): 1 --> 2; dentary-postdentary (67): 0 --> 1; splenial-dentary (71): 0 --> 1; angular (80): 0 --> 1; Retroarticular_proc._size (84): 2 --> 1 resorption_pits (88): 0 --> 2; pmx_teeth_size (91): 0 --> 1.

Node 31 (*Varanus* + *Lanthanotus*): pmx_foramina (3): 0 --> 1; lacrimal_foramen (7): 0 --> 1; posterior_jugal (9): 0 --> 1; nasals_fused/unfused (12): 0 --> 1; palpebral_ossification (18): 1 --> 0; prearticular_medial_view (81): 0 --> 1.

Node 32 ((*Varanus* + *Lanthanotus*) + Pythonomorpha): pmx-palatal_ramus (2): 0 --> 1; external_naris (13): 0 --> 2; post.opening_vidian_canal_1 (45): 0 --> 1; anterolateral_coronoid (75): 0 --> 1.

Node 33 (*Dinilysia* + (*Yurlunggur* + (*Anilius* + ((*Python* + *Lampropeltis*) + (*Haasiophis* + (*Pachyrhachis* + *Eudophis*)))))): pmx-mx (4): 0 --> 1; palatine_teeth (92): 0 --> 1; pterygoid_teeth (94): 1 --> 0; hypapophyses (97): 0 --> 1.

Node 34 (Ophidia): lacrimal (6): 0 --> 1; external_naris (13): 2 --> 1; frontal-parietal (16): 0 --> 1; parietal_post.rami (23): 0 --> 1; frontal_ventromedial_proc. (35): 0 --> 2; parietal_flange-parabasisphenoid (38): 0 --> 1; optic_foramina (39): 0 --> 1; trigeminal_foramen (40): 0 --> 1; postemporal_fenestra (50): 0 --> 1; Prearticular_surangular (83): 0 --> 1; Retroarticular_proc._size (84): 1 --> 0; forked_cloacal_ribs (104): 0 --> 1; Scapulocoracoid

(107): 0 --> 2; clavicle (109): 0 --> 1; interclavicle (110): 0 --> 1; sternum (112): 0 --> 1; hindlimbs (119): 0 --> 1; sclerotics (125): 0 --> 1; appendicular_epiphyses (127): 0 --> 1.

Node 35 (Pythonomorpha): supratemporal-prootic (30): 0 --> 1; quadrate_shape (33): 0 --> 1; parietal_flanges (36): 0 --> 1; parietal_flange-prootic (37): 0 --> 1; basipterygoid_proc. (43): 0 --> 1; smx_median_flange (52): 0 --> 1; mandibular_symphysis (60): 0 --> 1; dentary_dorsal_margin (62): 0 --> 1; Meckel's_canal (64): 0 --> 1; subdental_shelf (65): 2 --> 0; ventral_coronoid (77): 0 --> 1; marginal_teeth_implantation (86): 0 --> 1; zygosphenes_&_zygantra (96): 0 --> 1; ribs_begin (103): 1 --> 0; pelvis_size (116): 0 --> 1; distal_tibia (120): 0 --> 1; astragalus-calcaneum (121): 0 --> 1; skull-axial_epiphyses (126): 0 --> 1.

Node 36 (*Leptotyphlops* + *Typhlops*): supratemporal (29): 0 --> 1; quadrate-mandible (34): 0 --> 1; post.opening_vidian_canal_1 (45): 1 --> 0; post.opening_vidian_canal_2 (46): 0 --> 1; caudal_vertebrae (101): 0 --> 1.

Node 37 (*Anilius* + ((*Python* + *Lampropeltis*) + (*Haasiophis* + (*Pachyrhachis* + *Eudophis*)))): subdental_shelf (65): 0 --> 2; separation_ov_V2_and_V3 (129): 0 --> 1.

Node 38 (*Yurlunggur* + (*Anilius* + ((*Python* + *Lampropeltis*) + (*Haasiophis* + (*Pachyrhachis* + *Eudophis*))))): palatine-vomer (54): 0 --> 1; palatine_medial_proc. (55): 0 --> 1; dentary_mental_foramina (61): 0 --> 1; palatine_teeth_size (93): 0 --> 1.

Node 39 (*Python* + *Lampropeltis*): splenial_size (68): 0 --> 1; caudal_vertebrae (101): 0 --> 2.

Node 40 ((*Python* + *Lampropeltis*) + (*Haasiophis* + (*Pachyrhachis* + *Eudophis*))): quadrate_shape (33): 1 --> 2; anteromedial_coronoid (74): 1 --> 0; pterygoid_teeth_size (95): 0 --> 1.

Node 41 (*Mosasaurus* + *Platecarpus*): frontal-parietal (16): 0 --> 1; squamosal_dorsal_proc. (26): 0 --> 1; interclavicle_shape (111): 0 --> 1; appendicular_epiphyses (127): 0 --> 1.

Node 42 (Mosasauroidea): mandible_subcoronoid_fenestra (78): 0 --> 1; surangular-articular_cotyle (79): 0 --> 1; adductor_fossa (82): 0 --> 1; marginal_teeth_pedestals (87): 0 --> 1; cervical_transv.proc. (98): 0 --> 1.

Node 43 (Mosasauroidea + Dolichosauridae): splenial_anterior_tip (70): 0 --> 1; retroarticular_proc_end (85): 1 --> 0; tail_compression (105): 0 --> 1.

Node 44 (*Tetrapodophis* + (Mosasauroidea + Dolichosauridae)): pmx-frontal (1): 0 --> 1.

Node 45 (*Pachyrhachis* + *Eudophis*): ribs_curved/straight (102): 0 --> 1.

Node 46 (*Haasiophis* + (*Pachyrhachis* + *Eudophis*)): pmx-palatal_ramus (2): 1 --> 0; cervical_intercentra (99): 1 --> 0; pachyostosis_vertebrae_&_ribs (100): 0 --> 1; hindlimbs (119): 1 --> 0.

Node 47 (*Pontosaurus kornhuberi*, *Adriosaurus*, *Aphanizocnemus*, *Acteosaurus*): ribs_curved/straight (102): 0 --> 1; post.caudal_neural_spines (106): 0 --> 1; posterodistal_fibula (128): 0 --> 1.

Node 48 (Dolichosauridae): pmx-mx (4): 0 --> 1; posterior_jugal (9): 0 --> 1; postorbital_ventral_proc. (20): 0 --> 1; hypapophyses (97): 0 --> 1; Scapulocoracoid (107): 0 --> 1.

Node 49 (*Primitivus*, *Pontosaurus lesinensis*, *Dolichosaurus*): retroarticular_proc._size (84): 1 --> 2; coracoid_anterior_emargination (108): 0 --> 1.

Appendix 3.6 – The two nexus files including the dataset for the MP and BI analyses are available online with the paper Paparella et al. (2018) –A new fossil marine lizard with soft tissues from the Late Cretaceous of southern Italy" at https://royalsocietypublishing.org/doi/10.1098/rsos.172411. The files have also been uploaded to the Dryad Digital Repository at https://doi.org/10.5061/dryad.6t4f27g.

CHAPTER 4

The iliosacral joint in lizards: an osteological and histological analysis

A version of this chapter has been published as Paparella I., LeBlanc A.R.H., Doschak M.R., and Caldwell M.W. (2020). The iliosacral joint in lizards: an osteological and histological analysis. *Journal of Anatomy*, 236(4): 668-687. https://doi.org/10.1111/joa.13132.

4.1 Introduction

In the water to land transition, a crucial change that made the *bauplän* of tetrapods suitable for terrestrial locomotion involves the establishment of an articulation between the pelvic girdle and the vertebral column via a sacral rib (e.g., Carroll et al. 2005). While most research has focused so far on the articulation between the pelvic girdle and the femur (i.e., the hip joint) (e.g., Arnold et al. 2014; Pierce et al. 2012; Tsai & Holliday 2015; Tsai et al. 2018), comparatively little attention has been given to the connection between the axial skeleton and the pelvic girdle in tetrapods. The iliosacral joint (ISJ) is the weight-bearing structure that transfers the force of gravity between the appendicular and axial skeletons (e.g., Carroll et al. 2005; Wolff 1990). The axial component of the ISJ consists of modified vertebrae (sacrals) with elaborated ribs that extend to meet the pelvic girdle. In human anatomy, the sacrum is the single bony complex resulting from the fusion of sacral vertebrae located between the right and left pelves, however, the vertebrae may not fuse in other tetrapods (Gray 1878; Hoffstetter & Gasc 1969; Romer 1956). The evolution of the ISJ allowed early tetrapods to shift towards hindlimb-

powered locomotion (Boisvert 2005; Coates et al. 2002). In amniotes, the ISJ consists of multiple rib-bearing sacral vertebrae attached to the ilium, increasing from the single vertebral attachment in early tetrapods; this evolutionary increase in the number of sacral vertebrae is probably correlated with changes in locomotory habits and lifestyle of terrestrial amniotes (e.g., Boisvert 2005; Coates et al. 2002). For example, mammals, dinosaurs, and birds can have more than two sacral vertebrae in contact with the pelvic girdle (Romer 1956). In secondary aquatic amniotes instead, as a consequence of their ~~re~~turn" to life in water, the ISJ is either reduced or lost – as in ichthyosaurs, mosasaurs and cetaceans (e.g., Bejder & Hall 2002; Caldwell & Palci 2007; Gingerich et al. 1994; Motani et al. 1998) –, or there is a significant increase in the number of sacral ribs contacting the ilium – as in plesiosaurs and nothosaurs (e.g., Cheng et al. 2004).

Most squamates, with the exclusion of limbless and obligatory aquatic forms, have two sacral vertebrae that articulate with the posterior process of the ilium (e.g., Caldwell & Palci 2007; Hoffstetter & Gasc 1969; Snyder 1954). Moreover, instead of being completely fused together to form a sacrum, only the distal portions of the sacral ribs in squamates form a sutural contact with each other, whereas the vertebrae themselves are in most cases unfused (Hoffstetter & Gasc 1969). Despite possessing a small number of unfused sacral vertebrae and a relatively slender ilium, the ISJ in squamates displays considerable variation in: 1) the positions of the sacral facets on the medial surface of the ilium (Borsuk-Białynicka 2008); 2) the orientation of the posterior iliac process in relation to the vertebral column (Borsuk-Białynicka 2008); and 3) the greater development of the supracetabular process of the ilium in facultatively bipedal lizards (Snyder 1954). How this variation relates to muscle attachment, joint mobility, locomotory habits, and phylogeny have not been explored in most amniotes. Considering the key role that the ISJ played in the colonization of the terrestrial environment by tetrapods (Carroll 1988;

Carroll et al. 2005), and the fact that squamates have been able to adapt to many different environments and locomotion styles, repeatedly evolving aquatic habits, bipedal posture, or limblessness, I decided to characterize the anatomical details of this structure and to discuss its potential role in the evolutionary plasticity of this group.

Histological studies on the ISJ are not available for any amniote group, with the exception of humans (e.g., Forst et al. 2006; Rupert et al. 2009; Vleeming et al. 2012). Our study therefore aims to describe the ISJ in limb-bearing lizards, and to define the anatomical details of the elements involved in this structure (i.e., ilium and sacral ribs) using osteology, histology, and micro-Computed Tomography (μCT).

4.2 Material and Methods

Specimens of iguanians were used to perform the histological analyses and μCT, whereas osteological comparisons are made across several groups of extant and fossil lizards in order to fully understand the complexity of this structure. A detailed list, with relative methodology applied to each specimen, is presented in Table 4.1. As different authors tend to use different terminology, especially when referring to the iliac processes, the anatomical nomenclature adopted in this study is illustrated in Figure 4.1.

Specimens were scanned using a Bruker-SkyScan 1076 micro-CT scanner (Bruker-SkyScan, Kontich, Belgium) at the Pharmaceutical Orthopaedic Research Lab (University of Alberta). Samples were scanned at 18 μm resolution, with the cathode ray tube voltage / current set to 100 kV / 100 μA, with low energy X-rays removed in all samples using a 1.0 mm aluminum filter. Three scan projections were averaged per step, through the 180° of rotation at 0.5° step increments with exposure times of 1180 ms for *I. iguana* UAMZ R951 and *P. vitticeps*

UAMZ R952, and 885 ms for *Phrynosoma* sp. UAMZ R953. The two-dimensional raw image projections were reconstructed using a modified Feldkamp back-projection algorithm, with the cross-section to image conversion values set to 0.0 - 0.05 for *I. iguana* UAMZ R951 and *P. vitticeps* UAMZ R952, and 0.0 – 0.1 for *Phrynosoma* sp. UAMZ R953, using bundled vendor software (NRecon, version 1.7.0.4, Skyscan NV, Belgium). These settings allow for the capturing of bone and calcified cartilage, while unmineralized cartilage remains transparent. Three-dimensional reconstructions as well as additional two dimensional images from the µCT scans were generated using Dragonfly (ver. 2.0 for Windows; Object Research Systems (ORS) Inc, Montreal, Canada, 2016).

Iguana iguana UAMZ R951 was µCT-scanned and then partially dissected, removing the skin and superficial musculature in order to extract the ISJ for serial histology. *Pogona vitticeps* UAMZ R952 was completely dissected after being µCT-scanned, in order to observe ligaments and muscle attachments, following Snyder (1954). *Phrynosoma* sp. UAMZ R953 was µCT-scanned and skeletonized. This specimen represents a subadult stage (incomplete skeletal maturity based on basicranial sutures) and shows evidence of partial mummification that caused the capturing of both unmineralized and mineralized cartilage during the scans (cf. Panzer et al. 2015). This resulted in an usually thick cartilaginous layer at the distal end of the sacral ribs of UAMZ R953 (visible both in the scan frames and three dimensional reconstructions). All the other specimens listed in Table 4.1 were used to collect anatomical data on the skeletal elements involved in the ISJ (i.e., pelvic girdle and sacral region of the column), looking at both articulated and disarticulated bones.

For the serial histology, the joint samples were prepared using first a hand-saw and then a low-speed wafering saw (Buehler IsoMet). The samples were fixed in 10% formalin for 3 days,

and then decalcified in solutions of Cal-Ex (Fischer Scientific, 5.5% Hydrochloric acid and 0.12% EDTA, pH = 2.0) for 17 to 28 days (according to the size of the sample). To speed up the decalcification process, the solution was replaced every 24 hours and the samples were placed on a mechanical shaker for 8 hours every day. Samples were rinsed in running tap water after the decalcification was completed, stored back in fixative for several hours, and then placed overnight in a tissue processor for clearing and paraffin infiltration. Finally, the samples were embedded in blocks of paraffin wax and placed on ice for about an hour before starting sectioning. The serial sections were cut at 5 μm using a rotary microtome (Leica 2025) and mounted on charged glass slides (Fisherbrand, Superfrost Plus). Sections for the right sacrum of the *Iguana iguana* sample were cut axially (i.e., transverse or cross sections), anterior to posterior, and posterior to anterior, in order to capture the articulation of each sacral rib with the ilium separately. The left sacrum of the same *Iguana iguana* specimen was used to cut longitudinal or coronal sections (ventral to dorsal), in order to capture the two sacral ribs in articulation with the ilium at the same time. I then applied Masson‘s trichrome staining, following the protocol in Appendix 4.1.

The thin sections were imaged using a Nikon DS-FI3 camera mounted on a Nikon Eclipse E600 POL microscope, and Nikon NIS Elements (ver. 4.60) imaging software. Images of the thin sections were captured in plane and cross-polarized light.

4.3 Results

4.3.1 Osteology

The two sacral vertebrae in lizards bear ribs that tend to converge distally and form a contact between the posterior/posteroventral margin of the first sacral rib (sr-I) and the

anterior/anterodorsal margin of the second sacral rib (sr-II). The extent of this contact never exceeds the distal half of the two ribs, and in general seems to vary from species to species. The two sacral ribs never fuse completely to the extent that the suture between them is obliterated in any of our study specimens (Table 4.1; Figs. 4.1-4.3, 4.5, 4.7-4.12), as reported for some lizards by Hoffstetter & Gasc (1969). In fact, the μCT scans of *I. iguana*, *P. vitticeps* and *Phrynosoma* sp. show that both sacral ribs have separate, finished margins, and sometimes even a small gap between them (Figs. 4.3, 4.7-4.8).

The contact between sr-I and sr-II is more extensive in the extant *I. iguana*, *C. pallidus*, *A. cristatus*, and the fossil taxa *Macrocephalosaurus* and *Saichangurvel* (Figs. 4.1-4.3, 4.5, 4.10-4.11). In *Phrynosoma* sp. and *P. vitticeps*, sr-I overlaps the anterodorsal margin of sr-II, but in terms of length, the contact is limited to the very distal ends of the two ribs (Figs. 4.7-4.8). The contact is limited to the most distal tip of the two ribs also in *B. basiliscus*, *H. suspectum*, *P. draconoides*, and *V. albigularis* (Figs. 4.1, 4.9, 4.12).

In general, sr-I is larger than sr-II in terms of distal expansion and/or dorso-ventral thickness, or at most they are similar in size (e.g., *Macrocephalosaurus* and *Saichangurvel*: Fig. 4.2). The difference is quite emphasized in some taxa, such as *B. basiliscus*, and *P. draconoides*. In lateral view, sr-I is characterized by a C-shaped termination that forms most of the articulation with the ilium , and sr-II posteriorly (Figs. 4.1, 4.9-4.10, 4.12). As a consequence of the greater dorso-ventral thickness of sr-I, and its C-shaped distal end, the contribution to the ISJ by sr-II is mostly ventral or posteroventral; dorsally, the first sacral rib forms the entire contribution to the ISJ.

The ilium in lizards is characterized by the presence of three main processes: 1) the posterior process – often referred to as the posterior iliac blade or postiliac blade (cf. Borsuk-

Białynicka 2008; Gans et al. 2008; Snyder 1954) – projecting posterodorsally from the iliac shaft, and bearing the facets for articulation of the sacrals; 2) the preacetabular process, located anteriorly to the acetabulum and overlapping the pubic head; and 3) the supracetabular process – often referred to as the iliac tubercle or spine – located above the acetabulum, and anterodorsally oriented relative to the iliac shaft (Figs. 4.1-4.2, 4.7-4.11). All three iliac processes vary in shape and extent, and a correlation with the posture and locomotion abilities has been found at least for the supracetabular process (Snyder 1954).

The posterior process is the only one of the iliac processes directly involved in the ISJ, being the part that articulates with the sacral ribs. In the specimens examined here, the main differences in the posterior iliac process regard its orientation in relation to the vertebral column (and to the ischium and pubis) and its shape and thickness in cross section. Borsuk-Białynicka (2008) described how this process is almost perpendicular to the vertebral column in the non-squamate lepidosaur *Sphenodon*, and is greatly tilted posteriorly in lizards. I found that in the marine iguana, *A. cristatus*, the posterior iliac process is almost horizontal and parallel to the vertebral column (Fig. 4.10). A similar condition occurs in the water monitor *V. albigularis*, and *H. suspectum*, though to a lesser degree, with the posterior iliac process slightly more posterodorsally oriented in relation to the vertebral column (Figs. 4.1B, 4.9). The process clearly forms a much greater angle with the column in *P. vitticeps*, *I. iguana*, *B. basiliscus*, *Phrynosoma*, and the fossil taxa, *Macrocephalosaurus* and *Saichangurvel* (Figs. 4.1-4.2, 4.7-4.8). The main portion of the posterior iliac process is fairly cylindrical in *V. albigularis*, and *H. suspectum* (although quite narrow and elongated only in the latter) (Figs. 4.1, 4.9, 4.12), while it is more elliptical in most iguanian specimens (*Amblyrhynchus*, *P. vitticeps*, *I. iguana*, and *Saichangurvel*: Figs. 4.1-4.3, 4.7-4.8, 4.10-4.11). The process is quite laterally flattened in *B. basiliscus*,

Phrynosoma, and *Macrocephalosaurus*, even taking into account that taphonomic processes may have emphasized the condition in the fossil specimen ZPAL Mg R I-23 (Figs. 4.1, 4.2, 4.7).

For the preacetabular and supracetabular iliac process, the terminology in the literature is inconsistent: what here is called the preacetabular process can be hard to discern when there is complete fusion of the three pelvic bones, and authors tend to not address this process and often use ‗preacetabular' for the iliac tubercle (i.e., the supracetabular process) (Borsuk-Białynicka 2008; Snyder 1954; Snyder 1962). I prefer to use an anatomical terminology that best reflects the topology of these processes, taking into account their relative position to one another, and to the iliac shaft. The preacetabular process is particularly long in *B. basiliscus* (especially visible in the disarticulated specimen ROM R 5583: Fig. 4.1C, E), and exceptionally long in the dolichosaur *P. manduriensis* (Fig. 4.2A, D). The degree of development of this process is fairly similar amongst the rest of the specimens here examined.

The supracetabular process changes in the length, width and shape of its distal end. Specimens of *Basiliscus* and *Pogona* have relatively longer and more slender processes that taper distally to pointed tips (Figs. 4.1, 4.8). In *Varanus albigularis*, the supracetabular process is overall wider and remains cylindrical throughout (Figs. 4.1B, 4.12A). In *I. iguana*, *Saichangurvel*, *Phrynosoma*, and *Macrocephalosaurus* this process is relatively broad proximally, quite elliptical in cross section, and only weakly tapers distally, ending in a fairly rounded tip (Figs. 4.1, 4.2, 4.7). A short process, quite broad across the dorsoventral axis, and fairly blunt distally characterizes *Amblyrhynchus* (Fig. 4.10), while in *Heloderma* it is basically absent, with barely a tiny spur remaining (Fig. 4.9).

4.3.2 Histology

Results from the serial histology are illustrated in Figures 4.4-4.6. The presence of a large gap between the ilium and sacral ribs is apparent in the μCT scans of the *I. iguana*, *Phrynosoma* sp., and *P. vitticeps* specimens (Figs. 4.3, 4.5, 4.7, 4.8). From the serial histology of the *I. iguana* sample, it is possible to see that this space is partially occupied by articular cartilage, fibrocartilage, and dense connective tissue, which are variably present at the edges of the bones (Figs. 4.4-4.6). However, a gap in our thin sections is present between the distal ends of the sacral ribs and the medial surface of the ilium throughout both transverse and longitudinal series, and it is continuous even when transitioning from sr-I to sr-II (Fig. 4.4). The gap becomes narrower close to the transition from sr-I to sr-II, as visible in Figure 4.4E-F.

Articular cartilage is found at the distal ends of the sacral ribs, connected to the subchondral bone via a conspicuous layer of calcified cartilage (Figs. 4.4-4.6A). The transitional zone of the articular cartilage is particularly thick in comparison to both the radial and tangential zones (Fig. 4.6A). Both transverse and longitudinal series of thin sections of the *I. iguana* ISJ show that the large cap of articular cartilage is continuous between the two ribs, which join to form a single structure for articulation with the posterior process of the ilium. Fibrocartilage surrounds the articular cartilage on both sacral ribs virtually in all our thin sections (Figs. 4.4B-C, E-F; 4.5; 4.6A). The distinction between articular (hyaline) cartilage and fibrocartilage is particularly evident under cross-polarized light, which emphasizes the typical arrangement of the cross-laid collagen fibres of the latter (Fig. 4.5D).

In comparison to the sacral ribs, the ilium has a smaller amount of articular cartilage, which is not found throughout the extent of the ISJ in the serial sections. This is not completely unexpected, as the portion of the posterior process of the ilium that contacts the sacrals seems to

be limited to the outline of the articular facets for sr-I and sr-II. This outline is often visible macroscopically on the posterior process of the ilium (medial surface), marked usually by the presence of cartilage and/or a convexity on the bone (Figs. 4.1, 4.3, 4.8-4.12). Fibrocartilage is more frequent on the ilium, surrounding often the periosteum directly, and associated to the presence of dense connective tissue (externally) and Sharpey‘s fibres into the bone (fibrous bone) (Figs. 4.4E-F; 4.6B-D).

The collagen fibre bundles bordering the ilium and sacral ribs anchor into the bones and form Sharpey‘s fibres around the ISJ and along the contact between sr-I and sr-II (Figs. 4.4E-F; 4.5C-D; 4.6B, D). The Sharpey‘s fibres are particularly dense in correspondence to the ligament connecting the ilium to the sacral ribs; they are all parallel to each other, and with the same orientation of the ligament fibres anchoring to the bone.

Finally, another smaller gap is visible in the μCT scans of the *I. iguana* sample at the contact of the two sacral ribs (Figs. 4.3, 4.5B). In thin section, this space is filled with dense collagen fibres that are interrupted distally by the articular cartilage capping sr-I and sr-II (Fig. 4.5). The fibres seems to either attach directly to the cortical bone of the two sacral ribs (more proximally) or to a layer of calcified cartilage present on both sides of this contact (more distally) (Fig. 4.5C-D).

4.4 Discussions

4.4.1 The ISJ in lizards is a synovial joint

Micro-CT imaging of the iguanian ISJ region revealed large gaps between the sacral ribs and the ilium, but the type of joint can only be determined using histological techniques. There are two major categories of joints: 1) diarthroses (synovial joints), which are the type of joints

that allow for greater mobility; and 2) synarthroses, which provide no or limited mobility (e.g., Barnett et al. 1961; Kardong 2006). Synovial joints are characterized by four main histological features: 1) a cavity filled with synovial fluid; 2) a membrane encasing the cavity and secreting the fluid; 3) articular cartilage at the edges of the contacting bones; and 4) a multilayered dense fibrous tissue surrounding the membrane and forming the capsule bordering the entire structure (Archer et al. 2003; Barnett et al. 1961; Kardong 2006; Martin et al. 1998b). Articular cartilage is a special type of hyaline cartilage that lacks a perichondrium and is characterized by a specific internal zonation of collagen fibres and chondrocytes (e.g., Hall 2005; Lambert 1938; Martin et al. 1998a). Articular cartilage persists in skeletally mature individuals, even after hyaline cartilage has been fully replaced by bone during growth (e.g., Archer et al. 2003; Bilezikian et al. 2008).

Synarthroses lack a cavity and articular cartilage, and are subdivided into: 1) synostoses, where the contact is bone to bone; 2) synchondroses, where the contact is lined by intervening cartilage; and 3) syndesmoses, where fibrous connective tissue intervenes between the contacting elements (Barnett et al. 1961; Kardong 2006). Among synarthroses, mobility is found in syndesmotic joints, where the fibrous connective tissue allows for some movement between the articulating elements. Cartilage is less rigid than bone and typically functions as a cushion between the articulating elements; however, its shock absorbing properties are more limited compared for instance to fibrous connective tissue (Bilezikian et al. 2008; Hall 2005; Martin et al. 1998b).

According to the results of our serial histology, the contact between the sacral ribs and the ilium is characterized by the presence of articular cartilage and/or fibrocartilage, and a cavity surrounded by dense fibrous connective tissue (Figs. 4.4-4.6). These elements together clearly

define the ISJ as a synovial joint. Although fibrocartilage is not always found in synovial joints and it is not considered to be a defining feature for this type of joint, it has been observed in some human joints, such as the knee joint (e.g., Martin et al. 1998b), in form of fibrocartilaginous disks (or menisci), as well as in the hip joint of several extant sauropsids (Tsai & Holliday 2015). Our results are consistent with those of Tsai & Holliday (2015) for lepidosaurs, where thick layers of fibrocartilage cap or partially border the articular cartilage at the proximal epiphysis of the femur, similarly to crocodylians and in contrast to birds and turtles, for which much thinner layers or small patches of fibrocartilage are involved in the same joint.

Wolff (1990) defined the acetabulum (i.e., the junction of the three pelvic bones: ilium, ischium, and pubis) as the joint cavity for the femoral head, and in a very similar mode, the distal ends of the two sacral ribs join together to form a joint cavity for articulation with the posterior process of the ilium. This comparison between the ISJ and the hip joint can be directly observed also in our thin sections (Fig. 4.4A) and μCT scans (Fig. 4.7A), where both articulations are visible. This arrangement is consistent with the fact that the distal cap of articular cartilage and the cavity between the sacral ribs and the ilium are continuous from sr-I to sr-II in the *I. iguana* sample (Fig. 4.5A). Moreover, the suture between sr-I and sr-II being interrupted by this articular cartilage, further demonstrates that the two sacral ribs converge to form a single contacting surface for the ilium (Fig. 4.5).The position of the articular surface for the sacral ribs along the posterior process of the ilium varies interspecifically (see also below), and in our thin sections articular cartilage is found on the ilium only in a limited area of the contact with the distal margins of the sacral ribs (Fig. 4.4A). More frequently, in the serial histology of the *I. iguana* sample, fibrocartilage or simply dense connective tissue is present and separating the bone of the ilium from the joint cavity formed by sr-I and sr-II (Figs. 4.4; 4.5A; 4.6B-D).

Among all the specimens analysed here, a joint cavity formed by the two sacral ribs for articulation with the ilium is always present and macroscopically visible in skeletonized specimens (Figs. 4.1D, F, H-I; 4.2B, E-F; 4.7E-F; 4.8F-G; 4.9C; 4.10A-C; 4.11C-D; 4.12), suggesting that potential variation in the different limbed lizards is not in the type of joint, but in the features of the bones involved and possibly the associated musculature. A certain variability is observed for the shape of the two articular surfaces across the analysed taxa (Table 4.1). I determined that the two sacral ribs join together distally to form an articular cavity (for the contact with the ilium), and its concave shape is easily observed in the ct-scans (Figs. 4.3; 4.5B; 4.7A-D; 4.8A-B, E) or in lateral views (Figs. 4.1H; 4.10C; 4.12B, D) of some of the specimens. However, for the ilium, the shape of the articular facet for the joint cavity formed by the two sacral ribs is not always round. For instance, the medial surface of the posterior iliac process is fairly flat in *Basiliscus*, *Phrynosoma*, *Macrocephalosaurus*, and *Conolophus* (Figs. 4.1E; 4.2B; 4.7H; 4.11B). This variation in shape of the articular surface of the ilium most likely affects the mobility of the ISJ.

Interestingly, a study on paralyzed chicken embryos conducted by Drachman & Sokoloff (1966) demonstrated how the lack of muscle contractions during the development of the embryo can prevent the formation of typically synovial joints (e.g., knee and ankle joints), affecting the morphogenesis of the articular surfaces. In their experiments, paralyzed embryos either completely failed to develop a cavity between the contacting bones or only a partial cavity developed, with the joint space being filled by fibrous or cartilaginous connective tissue. The articular surfaces of the contacting bones were also flat and distorted rather than forming a ball-and-socket joint typical of the articulations under analysis (Drachman & Sokoloff 1966). This study reveals that: 1) synovial cavities cannot form if there is lack of skeletal muscle contractions

during embryonic development, and 2) lack of muscle contractions (i.e., lack of movement) alters the surface morphology of the developing articular surfaces. By comparison, it is possible to infer that the ISJ in limbed lizards, as a synovial joint, must have some mobility, and more so in those taxa where the concavity formed by the two sacral ribs is in contact with a fairly rounded posterior process of the ilium (e.g., *I. iguana*, *V. albigularis*, *P. vitticeps*).

Despite the rounded shape of the facet for articulation of the sacral ribs on the medial surface of the posterior iliac process, the rest of this process is elongate and sandwiched between the dorsal and ventral margins of the cavity formed by the two sacral ribs. This configuration would prevent a translation or a complete rotation of the ilium, as it does happen for instance for the femur within the acetabulum (cf. Irschick & Jayne 1999; Oldham & Smith 1975; Snyder 1954). However, during the dissections of *I. iguana* UAMZ R951 and *P. vitticeps* UAMZ R952, I noticed that the ilium can be twisted while still in articulation with the sacral ribs. A limited torsion (or axial rotation) of few degrees about parallel to the vertebral column, for instance when lizards abduct the hip during locomotion, would certainly be possible. The presence of fibrocartilage within the lizard ISJ suggests that while the hindlimb is being protracted or retracted, the ISJ may also serve a shock-absorbing function, similar to what occurs with the joint disks in the knee or ankle articulations (cf. Carey 1922; Drachman & Sokoloff 1966; Irschick & Jayne 1999; Martin et al. 1998b).

The shape of the articular surface on the posterior process of the ilium is more complex in taxa such as *Amblyrhynchus* and *Heloderma*, where the contacting surface with the joint formed by the sacral ribs is crested (Figs. 4.9A; 4.10E). Further observations would be necessary to assess how this shape can affect the movement at the ISJ, but it is reasonable to assume that a crested surface would be less favourable to either rotation or translation in comparison to any

smooth, rounded surface. In taxa where the posterior process of the ilium is flattened, an overall decrease in mobility of the ISJ is observed, due possibly to a reduced muscle activity during the embryogenesis of these structures, as showed by Drachman & Sokoloff (1966) for chickens.

As there are no histological studies available for the condition of the ISJ in mammals other than humans, and in amniotes in general, drawing comparisons with other groups is rather difficult. Adaptation to a bipedal lifestyle in humans involved a great deal of evolutionary change in comparison to quadrupedal forms (cf. Vleeming et al. 2012). The human sacrum is the result of the fusion of the three sacral vertebrae, and sometimes of the last lumbar vertebra (e.g., Forst et al. 2006; Fortin 1993; Vleeming et al. 2012); the human ISJ is more typically formed between the first two sacral vertebrae and the ilia, and is considered a unique combination of a synarthrosis – dorsally, in correspondence of the first sacral vertebra – and a synovial joint – for the middle and ventral portion (fide Vleeming et al. 2012). Because of its composite nature, the mobility of the ISJ in humans has been highly debated in the literature, and not all authors agree on its full mobility or even on what type of movements are possible (e.g., Forst et al. 2006; Fortin 1993; Rupert et al. 2009; Vleeming et al. 2012). The most recent interpretation of the ISJ in humans is that limited motion is possible in all three planes of the joint (i.e., frontal, transversal and sagittal), consisting essentially of a combined rotation–translation displacement (Vleeming et al. 2012). In comparison to humans, the ISJ of limbed squamates is far less complex, having only two sacral vertebrae contributing to form a single joint cavity for articulation with the ilium. At the macroscopical level, the overall configuration of the ISJ in crocodiles and most quadrupedal tetrapods seems to be similar to that of limbed lizards. However, this does not necessarily means that the ISJ is similarly a synovial joint in these groups, something that will need to be further investigated through histological studies. As for

birds and their highly specialized *bauplän*, the condition of the ISJ may well be more comparable to humans than to lizards, considering that in combination with their flying abilities, they are also adapted to a bipedal lifestyle. Birds are characterised by having a synsacrum, a structure that results from the fusion of vertebrae from the posterior thoracic, lumbar, sacral and occasionally caudal regions (e.g., Kardong 2006). The synsacrum then fuses to the pelvic girdles, creating a single solid structure, implying that the nature of the ISJ in birds is likely synarthrotic. Again, in the absence of histological studies, a conclusive comparison of the ISJ across different amniote groups is unfortunately very limited at this point.

4.4.2 The joint between the two sacral ribs

The two sacral ribs in the specimens analysed here are distally sutured, to a greater or less extent depending on the different species. All our μCT-scanned specimens show a small gap at the confluence of sr-I and sr-II, excluding already the possibility of a synostosis (i.e., bone-to-bone contact) (Figs. 4.3; 4.5B; 4.7A-D; 4.8A-E). With our thin sections, I was able to determine that this space, however, is filled by dense fibres and no gap persists between the two bones (Fig. 4.5). As explained above, a fibrous-based contact is indicative of a syndesmosis, which allows for limited mobility (Barnett et al. 1961; Kardong 2006). The presence of calcified cartilage, more distally along the margins of the sacral ribs, interposed between the subchondral bone and the fibres, suggests that this contact transitions to a synchondrosis towards the ISJ, similarly to what is described by Bailleul & Holliday (2017) for some cranial joints of modern alligators.

The cushioning properties of cartilage have been abundantly discussed in the literature (e.g., An & Martin 2003; Bilezikian et al. 2008; Cormack 2001; Hall 2005; Levangie & Norkin 2005; Martin et al. 1998a). Considering that our findings imply that the ISJ is fairly mobile, a

non-rigid suture between the two sacral ribs may serve as a shock-absorber (cf. Bilezikian et al. 2008; Martin et al. 1998b). Moreover, limited translation in the transversal plane (perpendicularly to the vertebral column) cannot be excluded at least along the fibrous-only portion. However, I suspect that the nature of this contact may be more variable across limbed lizards, as previous studies have shown that during ontogeny the line of suture between the two sacral ribs can disappear completely in some taxa (e.g., geckos), with the two elements becoming fully fused to one another (Hoffstetter & Gasc 1969). In this case, the joint between the two sacral ribs would certainly become immobile in older individuals.

4.4. 3 Distinguishing between sacral ribs, diapophyses, and lymphapophyses

One important issue regarding the homology of the elements involved in the ISJ system, is represented by the confusion frequently found in the literature between sacral ribs and sacral transverse processes. In general, a vertebra can be defined as sacral when its rib mediates the contact between the vertebral column and the pelvic girdle (e.g., Hoffstetter & Gasc 1969; Romer 1956). The plesiomorphic number of sacrals in lizards is two, and both sacral vertebrae have distally expanded ribs bearing an articular surface at their tip. The undifferentiated use of ‗sacral transverse processes' instead of ‗sacral ribs' is incorrect as ‗transverse process' (or diapophysis) should be limited to the projection from the vertebral neural arch that articulates with the rib tuberculum (one of the two heads of a rib: see Romer 1956). Moreover, the ribs and transverse processes of the sacrals have two separate centres of ossification, meaning that in fact they are two separate elements (Malashichev 2001; Winchester & Bellairs 1977). A line of fusion between the transverse process proper and the ribs is usually visible early in ontogeny in most lizards, while in some groups of amniotes, such as ichthyosaurs and sauropterygians, the

ribs never fuse to the vertebra (e.g., Cheng et al. 2004; Malashichev 2001; Motani et al. 1998; Romer 1956).

The sutured sacral ribs form what can be defined as a sacrum located between the two pelves (even though the two sacral vertebrae not always fuse completely in lizards – see Hoffstetter & Gasc (1969). Our histological series of the *Iguana iguana* ISJ shows that the contact between the two sacral ribs is mostly fibrous-based, with some calcified cartilage found at the distal edges of the two bones (a syndesmotic-synchondrotic joint) (Fig. 4.5). When the contact between the sacral vertebrae and the pelvic girdle is lost – as for instance in snakes – the distally expanded ribs do not bear an articular facet for an osseous contact with the ilium anymore, but in proximity of the pelvic elements it is usually possible to identify distally grooved or forked ribs for the support of the lymph hearts (i.e., cloacal vertebrae with lymphapophyses) (Hoffstetter & Gasc 1969; Romer 1956; Salle 1880; Sood 1948; Woltering 2012). I noticed that in some extant lizards, post-sacral vertebrae with distally grooved ribs can also be present: one in *Varanus albigularis* (UAMZ R947), two in *Conolophus pallidus* (AMNH R-147848), and up to three in *Ctenosaura pectinata* (ROM R6709) (Figs. 4.11-4.12). These grooved ribs likely are supporting the lymph hearts and should be considered homologous to the cloacal vertebrae in snakes. This would also suggest that the presence of vertebrae with lymphapophyses is independent from the presence/absence of sacral vertebrae. Interestingly, Malashichev (2001) shows in his study an anomalous specimen of *Lacerta vivipara*, with an asymmetry in the sacrals (and consequently in their contact with the ilium), where the right sacral ribs have shifted posteriorly by one vertebra. This results in the second sacral rib on the right side being paired with a left counterpart that is in fact distally forked, and not in contact with the ilium (i.e., a lymphapophysis). As was explained for the sacrals, the lymphapophyses

are indeed ribs, and not elongated diapophyses, since they also have a separate centre of ossification, and only at some point during development do they fuse completely to the vertebral diapophyses (Malashichev 2001).

In conclusions, sacral vertebrae in lizards can be defined as such if they possess all of the following features: 1) distally expanded ribs (fused to the diapophyses) converging to form a synovial cavity; 2) consecutive ribs forming a sutural (synarthrotic) contact between the posterior/posteroventral distal end of the first sacral rib and the anterior/anteroventral distal end of the next sacral rib (a structure that can be defined as a sacrum); and 3) ribs contacting the ilium via a synovial cavity.

4.4.4 Variability of the iliac processes and their implications for locomotion

Snyder (1954) analysed the anatomical differences between quadrupedal and facultative bipedal lizards, and recognised that bipeds have a narrower interacetabular width, a longer posterior process of the ilium, as well as a longer supracetabular process of the ilium. Moreover, in bipedal lizards there seems to be a greater distal fusion between the two sacral ribs, and the second sacral slopes forward favouring a more even distribution of the stress resulting from the body weight between the sacral vertebrae and the limb (Snyder 1954). In addition to these aspects, I found that the following features also change across lizards with different locomotion habits: 1) the orientation of the posterior process of the ilium relative to the vertebral column from almost vertical to almost horizontal; and 2) the shape of the supracetabular process – together with its length, as already emphasized by Snyder (1954) – from pointy and long (as in *Basiliscus*, and *Pogona*: Figs. 1c-e; 8h-i), to blunt and short (as in the marine iguana, *A. cristatus*: Fig. 4.10d-e), to basically absent (as in *Heloderma*: Fig. 4.9b, d).

Furthermore, I noted a variability in the length of the preacetabular process of the ilium, which is particularly elongate in taxa such as the extinct marine dolichosaurid *Primitivus manduriensis* (Fig. 4.2A, D). However, the preacetabular process of the ilium extends ventrally to overlap onto the pubis head anteriorly, so that when the three pelvic bones fuse together its identity is blended with the anterior portion of the pubis, and thus it does not seem to have a specific function on its own. Considering that in terrestrial lizards this process becomes indiscernible when the ilium and pubis fuse completely, its relevance in terms of function is arguable, and this variation may be more related to phylogenetic relationships. For example, *P. manduriensis* is described as a semi-aquatic lizard in which the fusion of the pelvic bones is never complete during ontogeny (Paparella et al. 2018). In this case, a greatly extended preacetabular process may be a character shared with a terrestrial ancestor. A similar condition is also found in *Aigialosaurus dalmaticus* (Dutchak & Caldwell 2006), and aigialosaurs and dolichosaurs are hypothesized to share a common ancestor (e.g., Caldwell 2006; Conrad 2008; Lee & Caldwell 2000; Paparella et al. 2018). In fact, in obligatory aquatic forms such as mosasauroids, where the ilium, ischium and pubis do not fuse during ontogeny, the preacetabular process is either reduced or completely lost (pers. obs.: cf. Bardet et al. 2003; Jiménez-Huidobro et al. 2018; Konishi et al. 2012; Makádi et al. 2012; Street & Caldwell 2017).

Both posterior and supracetabular process of the ilium play a role as muscle and ligament attachments. The supracetabular process of the ilium represents the site of attachment of the iliopubic ligament, and both the *musculus* (*m*.) *iliocostalis* and the *m*. *quadratus lumborum* also extend to this process, respectively on its dorsal margin and medial surface (Oldham & Smith 1975; Snyder 1954). These muscles function to assist the *m*. *longissimus dorsi* in raising the trunk. From the dorsomedial side of the ilium, the *m*. *quadratus lumborum* attaches to the ventral

surface of the sacral ribs, helping in stabilizing the spine and ribs (Carrier 1989; Moritz & Schilling 2013; Snyder 1954). A longer supracetabular process means not only a longer surface for the attachment of these muscles, but also these muscles extending more anteriorly with respect to the rest of the body. This would likely have an effect on the centre of gravity of the body during locomotion, and thus being relevant to the possibility of a bipedal posture in some lizards, as described by Snyder (1954). The superficial *m. iliocaudalis dorsalis* and *m. iliocaudalis ventralis* anchor to the posterior process of the ilium, as well as the ilioischiadic ligament (Ali 1948; John 1971; Snyder 1954). Both the *m. iliocaudalis dorsalis* and *ventralis* run posteriorly from the ilium respectively above and below the posterior surface of the sacral ribs and transverse processes of the caudal vertebrae, until the end of the tail. Their function is to abduct the tail, or stiffen the tail when contracted (Ali 1948; John 1971). The preacetabular process of the ilium, that extends ventrally to overlap onto the pubis head anteriorly, is not a primary surface of muscle or ligament attachment. Muscles such as the *m. puboischiofemoralis externus* and *m. puboischiofemoralis internus*, which anchor respectively to the lateral and medial side of the pubis, and are involved in the movements of the femur, can potentially reach up to the preacetabular process when the three pelvic bones are fused together (Oldham & Smith 1975; Snyder 1954). However, it is the development of the anterior process of the pubis that is most relevant to these muscles.

Movement at a joint occurs due to the action of muscles and ligaments on the skeletal elements. Previous embryological studies have shown that muscle movements are necessary to trigger the formation of synovial cavities (Carey 1922; Drachman & Sokoloff 1966). It is reasonable to assume that development of the ISJ as a synovial cavity in limbed lizards similarly happens early in ontogeny and the contact is then predisposed for mobility. Variations in the type

of movements and arrangement of the muscles must have an effect in the growth and development of the joint systems throughout life. Limbed lizards can have either exclusively quadrupedal posture or also facultative bipedal posture (e.g., Irschick & Jayne 1999; Snyder 1954; Snyder 1962), and in both situations a series of joints between the appendicular and axial skeletons are involved during locomotion. The ISJ mobility must be highly dependent on the movements happening at the hip joint and involving the hindlimb in general. The modification of the bones as sites of soft tissue attachment is strongly indicative of variation in the locomotion habits of an animal. In forms such as *Amblyrhynchus* and *Heloderma*, with a semi-aquatic lifestyle, the use of limbs during swimming is limited, because they adopt an anguilliform style driven by lateral undulations of the vertebral column. In this case, the axial musculature plays the most important role, and it makes sense that attachments for the appendicular musculature, like the iliopubic ligament that anchors to the supracetabular process of the ilium, undergoes reduction. At the same time, however, these animals still require a weight-bearing ISJ that allows them to keep moving on land, so the maintenance of this contact between the sacrum and the pelvic girdle remains necessary for efficient locomotion outside the water. This is consistent with the conclusions of Snyder (1954) that facultative bipedality in some iguanian lizards is related to the greater development of the supracetabular process, offering a larger site of attachment to the iliopubic ligament and appendicular musculature.

As seen above, the ISJ system is surrounded by both axial and appendicular muscles that are involved respectively in motion or stabilization of the trunk and tail, and various type of movements of the shank (e.g., Oldham & Smith 1975; Snyder 1954; Snyder 1962). In this framework, the mobility of the ISJ during locomotion can be a direct or indirect effect of the action of any of the associated muscles. We know that soft tissues (muscles and ligaments) are

responsible for the development of joints (Carey 1922; Drachman & Sokoloff 1966) and we can assume that any rearrangement of those soft tissues can trigger anatomical variation of the structures involved with consequences on the type of possible movements, and hence locomotion style.

4.5 Conclusions

At the osteological level, the elements involved in the ISJ (i.e., ilium and sacral ribs) across limb-bearing squamates display variability in a certain number of features. The iliac processes can vary in extension, cross-section and orientation in relation to the vertebral column, as well as to the other pelvic bones (pubis and ischium). The sacral ribs vary in the extension of their sutural contact, and their relative size and contribution to the joint cavity for the articulation with the ilium.

The presence of a joint cavity (i.e., concave articular surface) formed by the convergence of the two sacral ribs is consistent across all the limb-bearing lizards analysed in this study. Histological analysis of the ISJ in *Iguana iguana* revealed this contact to be a synovial joint. The undivided cartilage cap that encompasses both sacral ribs makes clear that these two elements join together distally to form a single cavity for articulation with the posterior process of the ilium. As synovial joints develop in the embryo only if there is contraction of muscles, mobility seems to be a factor and not just a consequence for such structures. I hypothesize that the mobility of the ISJ in limbed lizards is tightly correlated to the movement of the hindlimb, and most likely limited to partial torsion (parallel to the vertebral column) of the ilium, together with absorption of the mechanical forces acting during compression and extension of the femur.

The nature of the contact between the two sacral ribs is syndesmotic, or possibly a mix of a syndesmosis and a synchondrosis, being characterized by the presence of extensive collagen fibres holding the two bones together for most of the contact, with some calcified cartilage present on both elements more distally. Syndesmoses are contacts where limited mobility is allowed between the elements involved, and in the case of the two sacral ribs of limbed lizards I attribute to this joint a shock-absorbing function during locomotion.

Muscles can increase as much as restrict the mobility at a joint, and in order to understand the changes in locomotory abilities that are consequential to the anatomical differences found in the ISJ apparatus, further research on the variation of the soft tissues is necessary.

As histological analyses of the ISJ in other tetrapods are not currently available (except for humans), in order to understand if this joint as synovial is unique to squamates or rather common within Tetrapoda, a thorough study of this structure across the entire clade will need to be carried out.

Table 4.1. List of specimens used in this study. The last column specifies for which method each specimen was used.

Taxon	Specimen	Preservation	Method
Iguana iguana	UAMZ R951 (adult)	frozen	dissection, μCT, 3D rendering, serial histology
	ROM R 441 (subadult)	skeletonized	comparative osteology
Basiliscus basiliscus	ROM R 5539 (adult)	skeletonized	comparative osteology
	ROM R 5583 (subadult)	skeletonized	comparative osteology
Phrynosoma sp.	UAMZ R953 (subadult)	frozen	μCT, 3D rendering
	TMP 1997.030.0321 (adult)	skeletonized	comparative osteology
	TMP 1997.030.0324 (adult)	skeletonized	comparative osteology
Pogona vitticeps	UAMZ R952 (adult)	frozen	dissection, μCT, 3D rendering, comparative osteology
	ROM 8514 (adult)	skeletonized	comparative osteology
Physignatus cocincinus	TMP 1990.007.0347 (adult)	skeletonized	comparative osteology
Amblyrhynchus cristatus	AMNH R-29937 (adult)	skeletonized	comparative osteology
	AMNH R-114492 (adult)	skeletonized	comparative osteology

	AMNH R-114491 (young)	skeletonized	comparative osteology
Conolophus subcristatus	AMNH R-131308 (adult)	skeletonized	comparative osteology
	AMNH R-110168 (subadult)	skeletonized	comparative osteology
Conolophus pallidus	AMNH R-147848 (adult)	skeletonized	comparative osteology
Heloderma suspectum	TMP 1990.7.27 (young)	skeletonized	comparative osteology
	TMP 90.7.357 (subadult)	skeletonized	comparative osteology
Varanus albigularis	UAMZ R947 (adult)	skeletonized	comparative osteology
Varanus timorensis	UAMZ R901 (hatchling)	skeletonized	comparative osteology
Macrocephalosaurus chulsanensis	ZPAL Mg R I-21 (adult)	fossil	comparative osteology
	ZPAL Mg R I-23 (adult)	fossil	comparative osteology
Saichangurvel davidsoni	IGM 3-858 (adult)	fossil	comparative osteology
Primitivus manduriensis	MPUR NS 161 (subadult)	fossil	comparative osteology

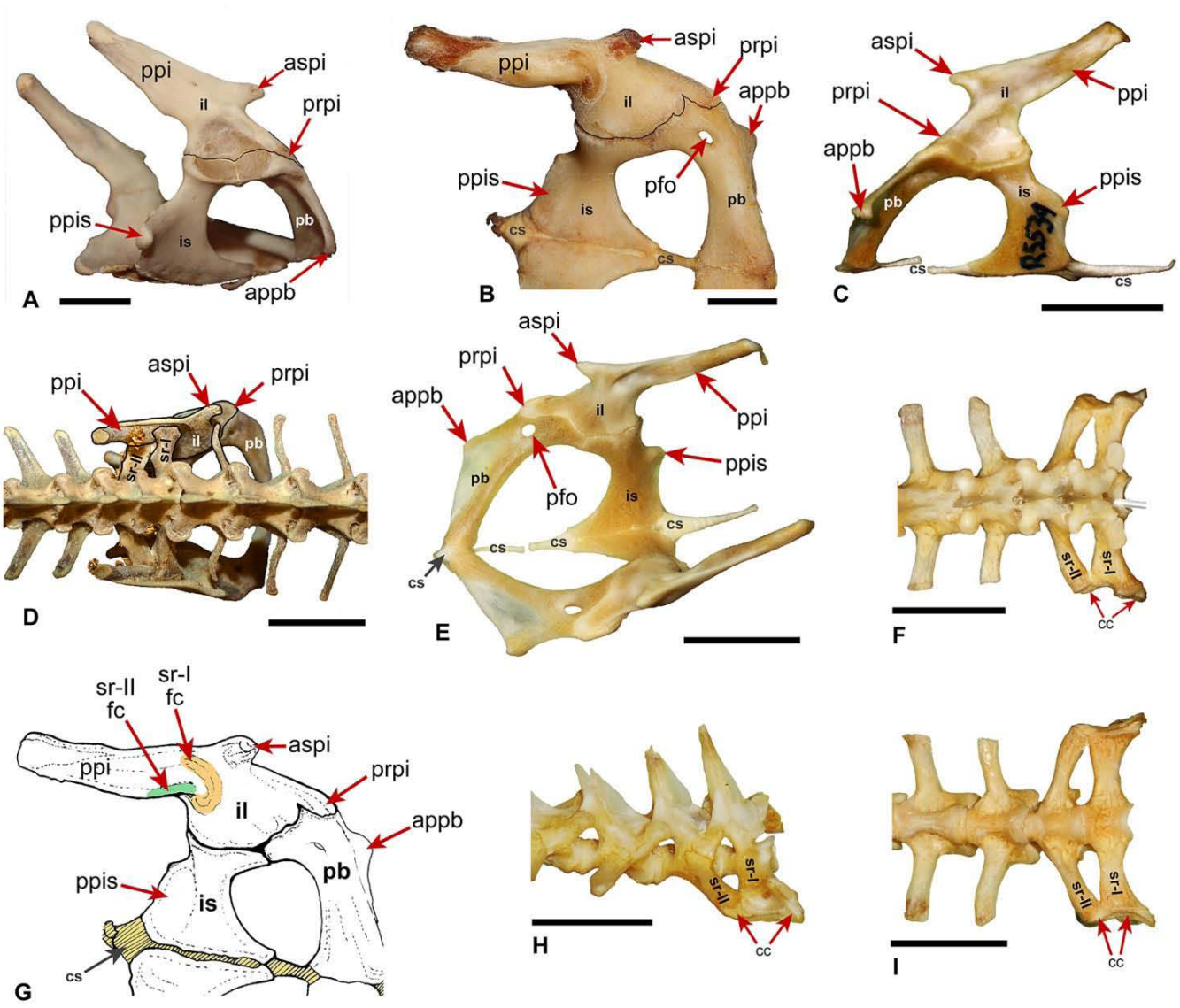

Figure 4.1. Lizard ISJ osteological terminology and examples: *Iguana iguana* (ROM R 441 (a, d)), *Varanus albigularis* (UAMZ R947 (b, g)), and *Basiliscus basiliscus* (ROM R 5539 (c, e, f, h, i)). (A) Right pelvic girdle of *I. iguana* in lateral view showing the three pelvic bones (ilium, pubis, and ischium) and relative processes. (B) Left pelvic girdle of *V. albigularis* in medial view showing the three pelvic bones (ilium, pubis, and ischium) and relative processes. (C) Left pelvic girdle of *B. basiliscus* in lateral view showing the three pelvic bones (ilium, pubis, and ischium) and relative processes. (D) Dorsal view of the sacral region and ISJs of *I. iguana*. (E) Right pelvic girdle of *B. basiliscus* in medial view showing the three pelvic bones (ilium, pubis, and

ischium) and relative processes. (F) Dorsal view of the sacral region and ISJs of *B. basiliscus*. (G) Diagram of the left pelvic girdle of *V. albigularis* in medial view showing the facets for the articulation of the two sacral ribs on the posterior process of the ilium. (H) Lateral view of the right sacral ribs of *B. basiliscus* showing the joint surface of articulation that they form to contact the posterior process of the ilium. (I) Ventral view of the sacral region and ISJs of *B. basiliscus*. Scale bars: 1 cm. **appb**, anterior process of the pubis; **aspi**, anterior supracetabular process of the ilium; **car**, cartilage; **cs**, symphyseal cartilage; **fc**, facet; **fe**, femur; **il**, ilium; **is**, ischium; **pb**, pubis; **pfo**, pubic foramen; **ppi**, posterior process of the ilium; **ppis**, posterior process of the ischium; **prpi**, preacetabular process of the ilium; **sr-I**, first sacral rib; **sr-II**, second sacral rib.

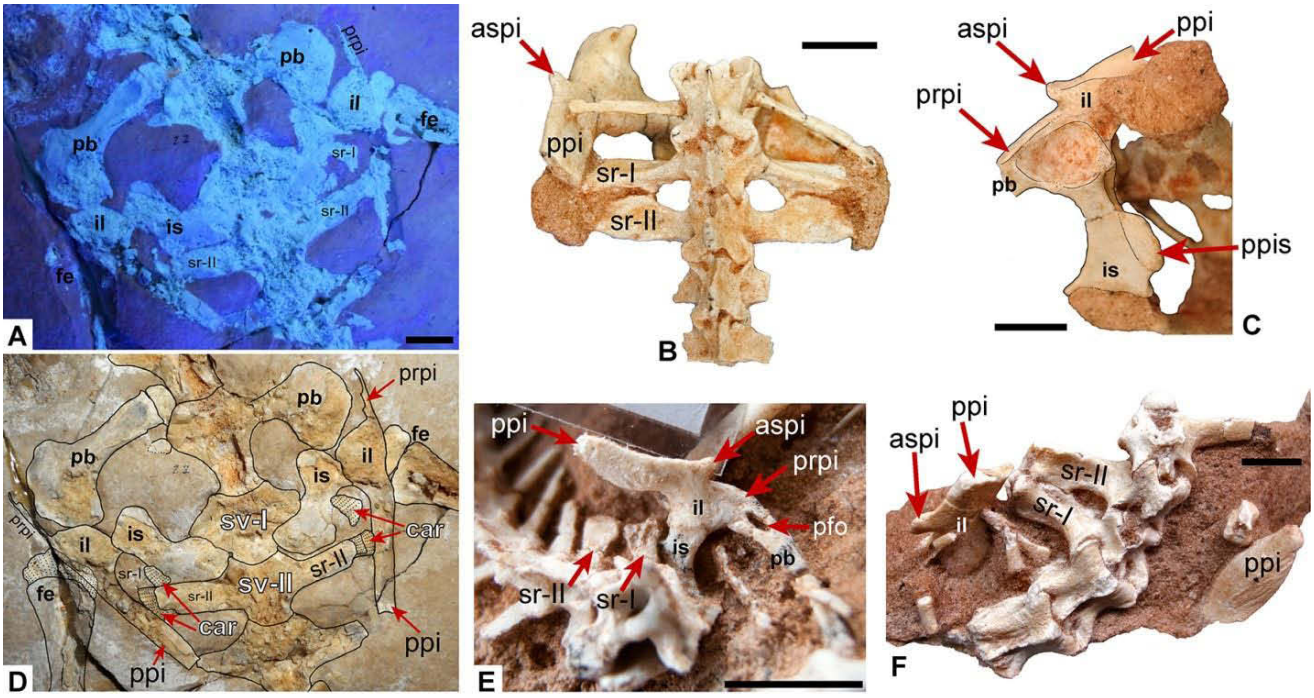

Figure 4.2. Osteology of the ISJ in some fossil lizards: *Primitivus manduriensis* (MPUR NS 161 (a, d)), *Macrocephalosaurus chulsanensis* (ZPAL Mg R I-23 (b, c) and ZPAL Mg R I-21 (f)), *Saichangurvel davidsoni* (IGM 3-858 (e)). (A) Sacral region and ISJs of *P. manduriensis* in dorsal view, exposed to ultra-violet light and showing the preservation of cartilage at the distal ends of the sacral ribs. (B) Sacral region and left ISJ of *M. chulsanensis* in dorsal view. (C) Pelvic girdle of *M. chulsanensis* in lateral view. (D) Sacral region and ISJs of *P. manduriensis* in dorsal view photographed at natural light. (E) Left pelvic girdle in medial view and sacral region of *S. davidsoni*. (F) Disarticulated pelvic girdles and sacral region of *M. chulsanensis* in dorsal view. Scale bars: 1 cm. **aspi**, anterior supracetabular process of the ilium; **car**, cartilage; **fe**, femur; **il**, ilium; **is**, ischium; **pb**, pubis; **pfo**, pubic foramen; **ppi**, posterior process of the ilium; **prpi**, preacetabular process of the ilium; **sr-I**, first sacral rib; **sr-II**, second sacral rib; **sv-I**, first sacral vertebra; **sv-II**, second sacral vertebra.

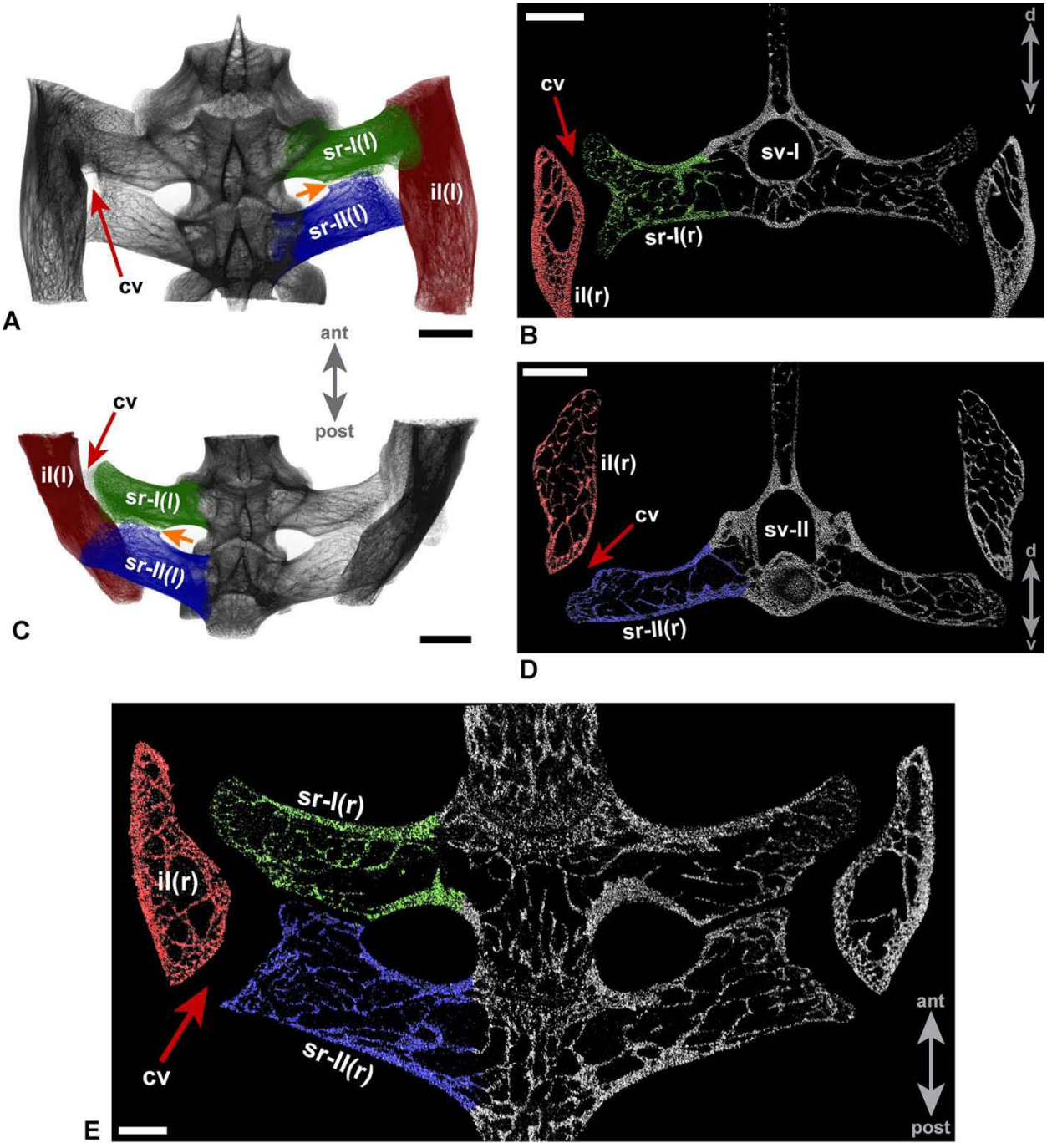

Figure 4.3. Micro-computed tomography of the ISJ of *Iguana iguana* (UAMZ R951). (A) Three dimensional reconstruction of the ISJ from the µCT scans showing a dorsal view of the structure. (B) Frame of the ISJ from the µCT scans showing the ilium and first sacral rib in cross section. (C) Three dimensional reconstruction of the ISJ from the µCT scans showing the structure in

ventral view. (D) Frame of the ISJ from the μCT scans showing the ilium and second sacral rib in cross section. (E) Frame of the ISJ from the μCT scans showing an overview of the articulation in longitudinal section. The orange arrows in (A) and (C) point at the gap between the two sacral ribs that the histological sections revealed to be a syndesmotic suture (Fig. 4C-D). Scale bars: 1 cm. **ant**, anterior; **cv**, cavity; **il**, ilium; **l**, left; **post**, posterior; **r**, right; **sr-I**, first sacral rib; **sr-II**, second sacral rib.

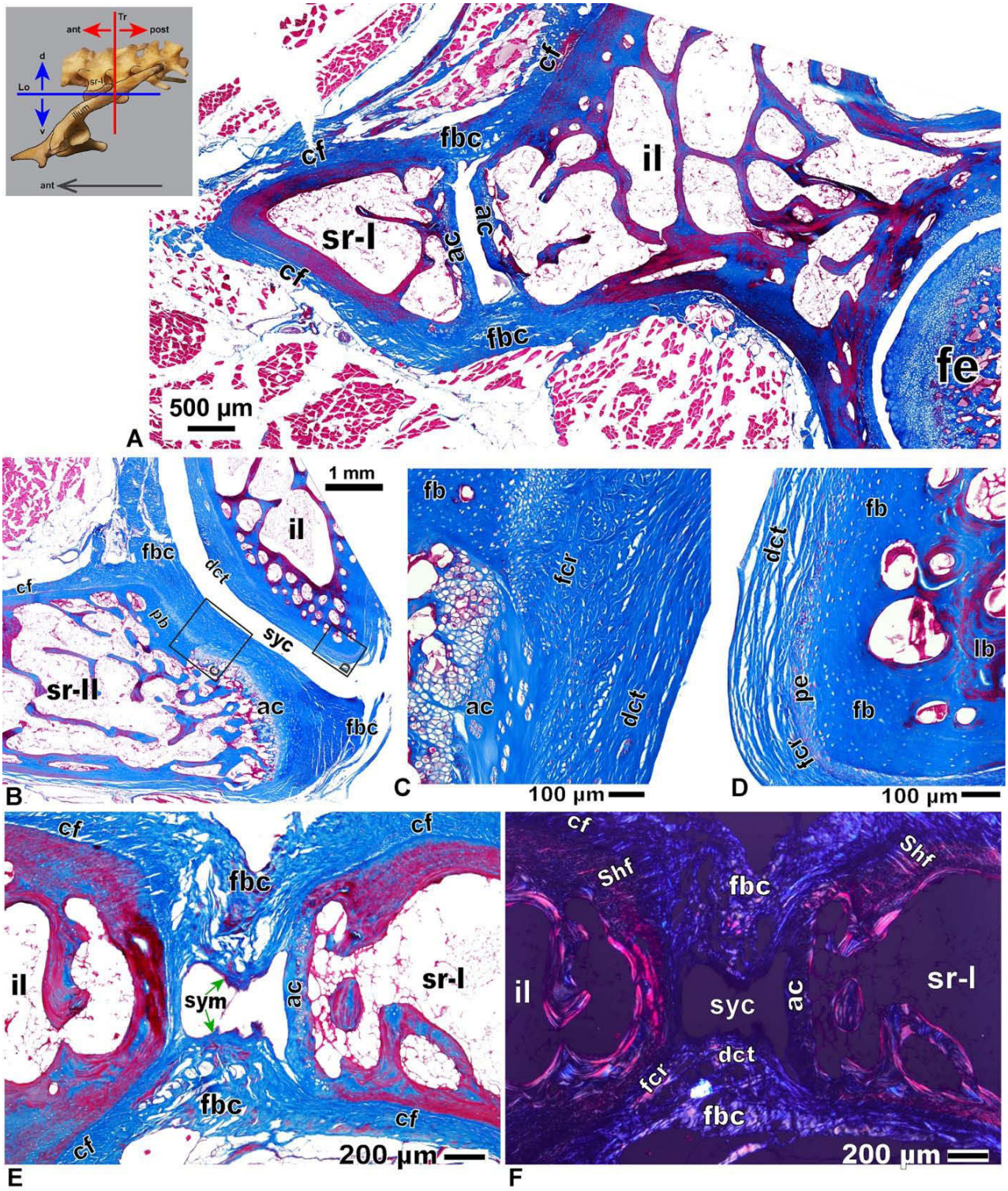

Figure 4.4. Histology of the ISJ of *Iguana iguana* (UAMZ R951). (A) Transverse section of the ISJ, showing an overview of the contact between the first sacral rib and the ilium, with also the

hip joint (between the acetabulum and femur) visible on the right. (B) Overview of the contact between sacral ribs and the ilium in transverse section (close to the transition to sr-II). (C) Close-up of the articular surface of sr-II. (D) Close-up of the articular surface of the ilium. (E) Close-up of the contact between the first sacral rib and the ilium at plane-polarized light. (F) Close-up of the contact between the first sacral rib and the ilium at cross-polarized light. The thin sections pictured in (B), (C), (E), and (F) are cut close to the transition from sr-I to sr-II. In (E)-(F) the ISJ cavity reaches its narrowest point recorded throughout the transverse section series. **ac**, articular cartilage; **ant**, anterior; **cf**, collagen fibres; **d**, dorsal; **dct**, dense connective tissue; **fb**, fibrous bone; **fbc**, fibrous capsule; **fcr**, fibrocartilage; **fe**, femur; **il**, ilium; **lb**, lamellar bone; **Lo**, longitudinal plane of sectioning; **pe**, periosteum; **post**, posterior; **r**, right; **Shf**, Sharpey‘s fibres; **sr-I**, first sacral rib; **sr-II**, second sacral rib; **syc**, synovial cavity; **sym**, synovial membrane; **Tr**, transversal plane of sectioning; **v**, ventral.

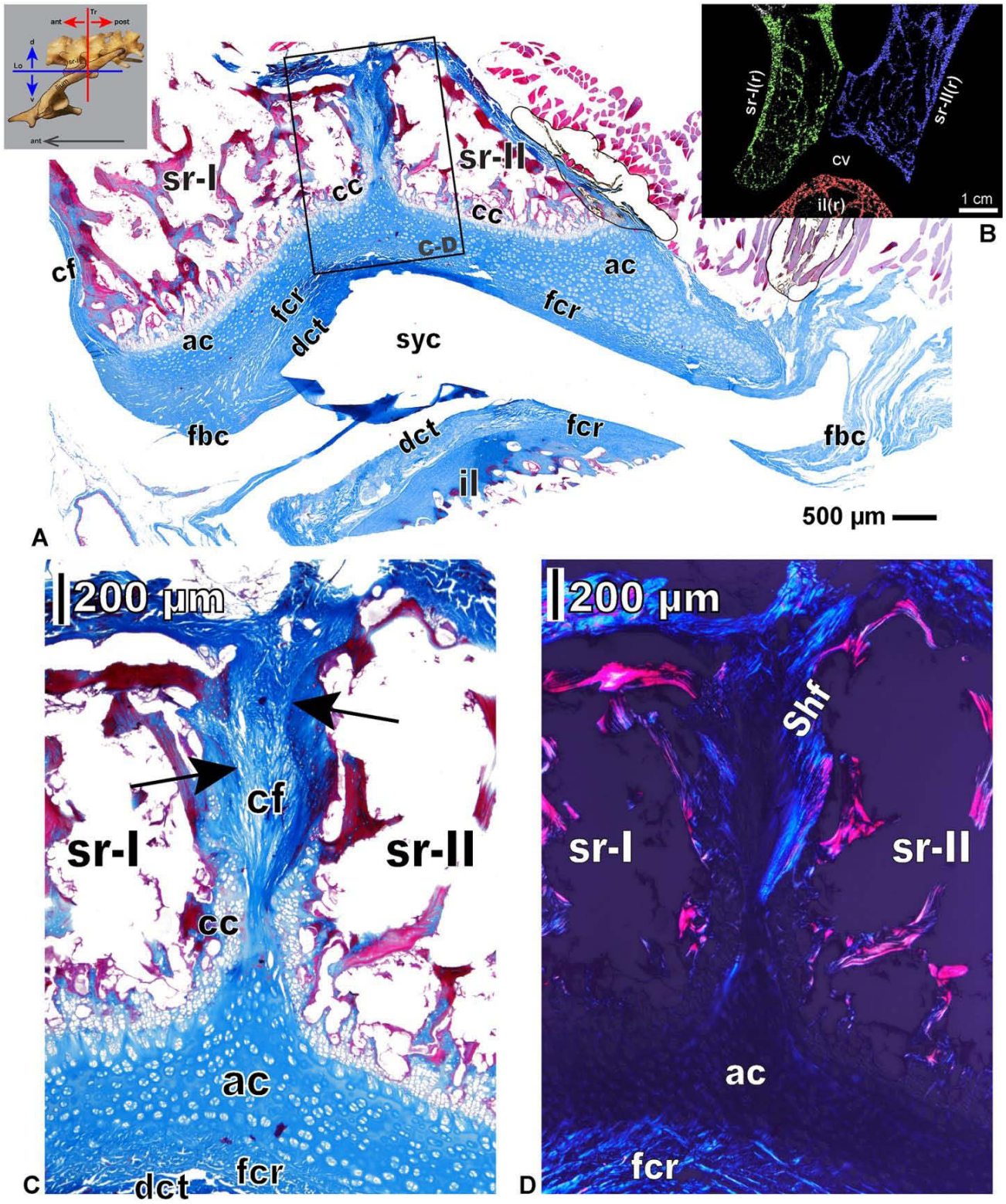

Figure 4.5. Histology of the ISJ of *Iguana iguana* (UAMZ R951). (A) Longitudinal section of the ISJ, showing the contact between the two ribs and the ilium close to the ventral edge of the

structure. (B) Frame of the right ISJ from the µCT scans showing the gap between the sacral ribs and the ilium for comparison with the histological section in (A). (C) Longitudinal section of the suture between sr-I and sr-II at plane-polarized light. (D) Longitudinal section of the suture between sr-I and sr-II at cross-polarized light. The black arrows in (C) point at the edge between the bone and collagen fibres at the suture between the two sacral ribs, while closer to the articular cartilage cap these fibres are contacting a layer of calcified cartilage. **ac**, articular cartilage; **ant**, anterior; **cc**, calcified cartilage; **cf**, collagen fibres; **d**, dorsal; **dct**, dense connective tissue; **fbc**, fibrous capsule; **fcr**, fibrocartilage; **fe**, femur; **il**, ilium; **Lo**, longitudinal plane of sectioning; **post**, posterior; **r**, right; **Shf**, Sharpey‘s fibres; **sr-I**, first sacral rib; **sr-II**, second sacral rib; **syc**, synovial cavity; **Tr**, transversal plane of sectioning; **v**, ventral.

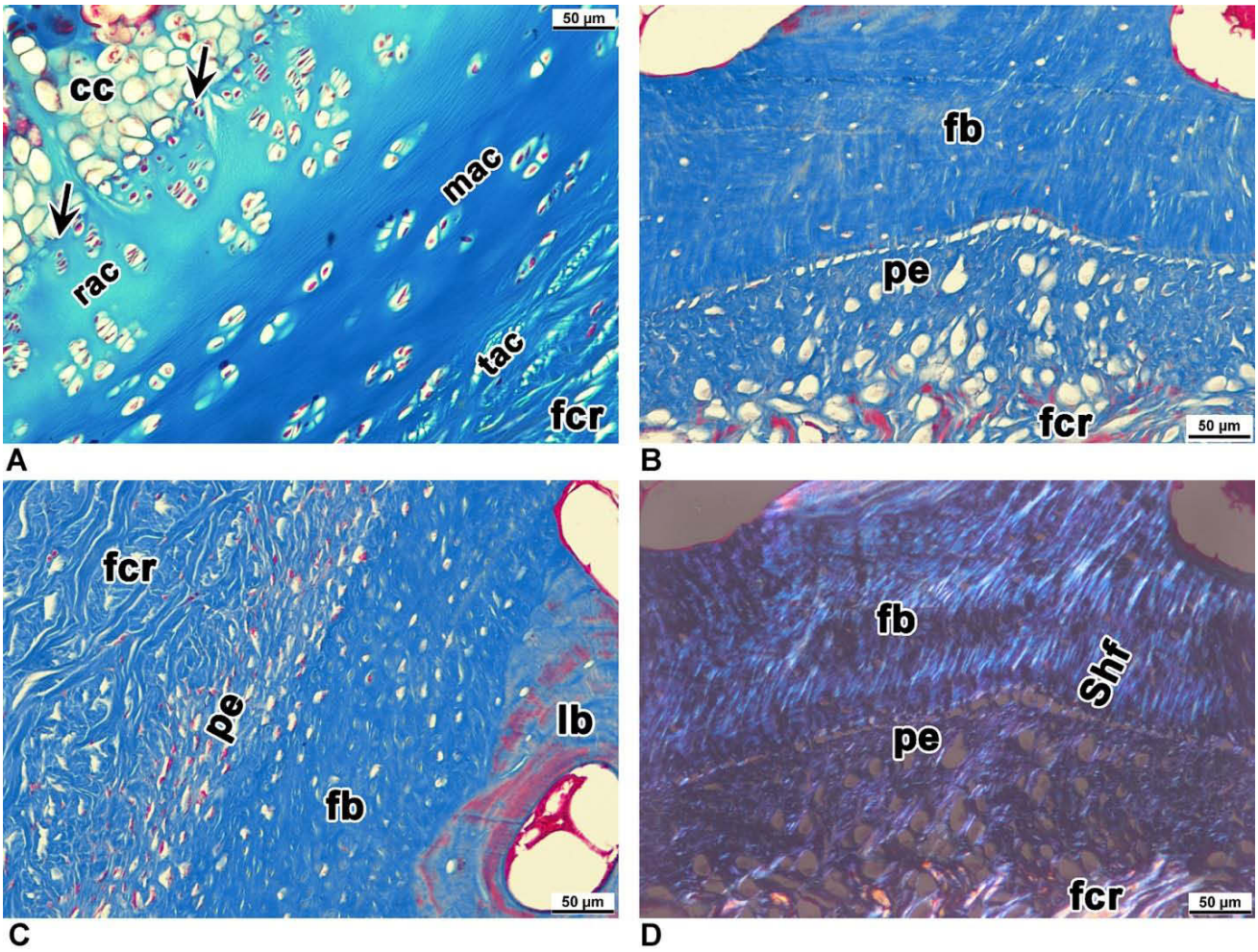

Figure 4.6. Detail of the tissues of the ISJ elements of *Iguana iguana* (UAMZ R951) from the transverse section series. (A) Close-up of the distal edge of the first sacral rib at plane-polarized light. (B) Close-up of the tissues along the medial margin of the ilium, away from the contact with the sacral ribs (at plane-polarized light). (C) Close-up of the ilium in correspondence of the articular facet for the first sacral rib. (D) Same thin section captured in (B) but with cross-polarized light. Secondary osteons (lamellar bone) are found more internally on the ilium, at the transition towards the trabecular region of the bone(C). Instead, closer to the periosteal region of the ilium the bone shows abundance of Sharpey‘s fibres and small lacunae (fibrous bone). Fibrocartilage is overlying the periosteum on the ilium (B-D), while surrounding the articular cartilage in the sacral ribs (A). The different zones of the articular cartilage on the sacral ribs are

visible in (A), including the tidemark (black arrows) between the calcified cartilage and radial zone. **cc**, calcified cartilage; **fb**, fibrous bone; **fcr**, fibrocartilage; **lb**, lamellar bone; **mac**, middle (or transitional) zone of the articular cartilage; **pe**, periosteum; **rac**, radial (or deep) zone of the articular cartilage; **Shf**, Sharpey‘s fibres; **tac**, tangential (or superficial) zone of the articular cartilage.

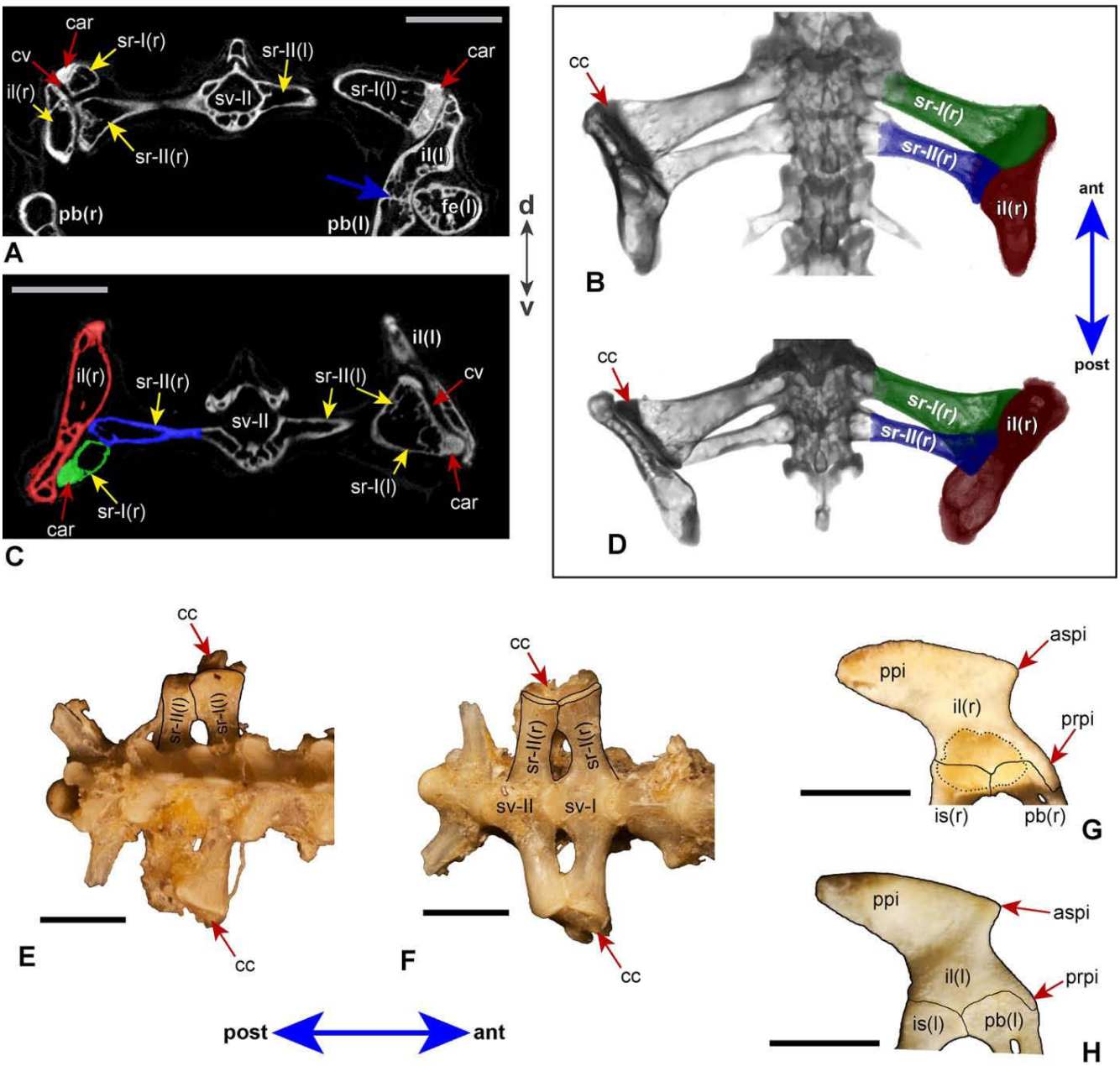

Figure 4.7. Osteology and micro-computed tomography of the ISJ of *Phrynosoma*: UAMZ R953 (A-D), TMP 1997.030.0324 (Bennett et al.), and TMP 1997.030.0321 (G-H). (A) Cross section of the sacral region and ISJs from the µCT scans of UAMZ R953. (B) Three dimensional reconstruction of the sacrum and ISJs from the µCT scans of UAMZ R953 in dorsal view. (C) Cross section of the sacral region and ISJs from the µCT scans of UAMZ R953 close to the contact between sr-I and sr-II. (D) Three dimensional reconstruction of the sacrum and ISJs from

the μCT scans of UAMZ R953 in ventral view. (E) Sacral region of the vertebral column of specimen TMP 1997.030.0324 in dorsal view. (F) Sacral region of the vertebral column of specimen TMP 1997.030.0324 in ventral view. (G) Right ilium of specimen TMP 1997.030.0321 in lateral view. (H) Left ilium of specimen TMP 1997.030.0321 in medial view. The blue arrow in (a) indicates the position of the suture between the ilium and the pubis. Scale bars: 1 cm. **ant**, anterior; **aspi**, anterior supracetabular process of the ilium; **car**, cartilage; **cc**, calcified cartilage; **cs**, symphyseal cartilage; **cv**, cavity; **d**, dorsal; **fe**, femur; **il**, ilium; **is**, ischium; **l**, left; **pb**, pubis; **post**, posterior; **ppi**, posterior process of the ilium; **prpi**, preacetabular process of the ilium; **r**, right; **sr-I**, first sacral rib; **sr-II**, second sacral rib; **sv-I**, first sacral vertebra; **sv-II**, second sacral vertebra; **v**, ventral.

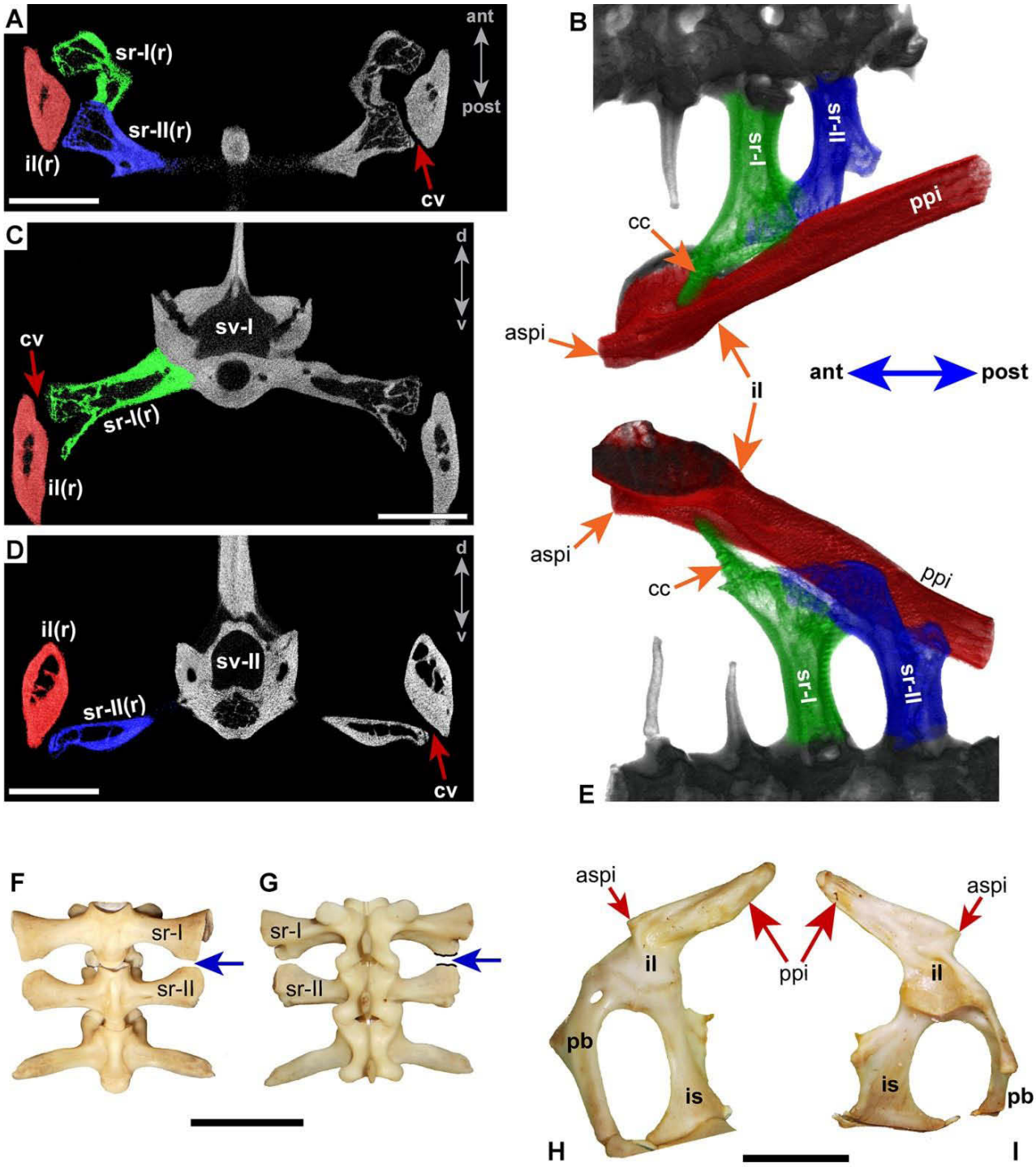

Figure 4.8. Osteology and micro-computed tomography of the ISJ of *Pogona vitticeps*, specimens UAMZ R952 (Pees et al.), and ROM 8514 (f-i). (A) Longitudinal section of the sacral region and ISJs from the µCT scans of UAMZ R952. (B) Three dimensional reconstruction of

the left sacrum and ISJ from the μCT scans of UAMZ R952 in dorsal view. (C) Cross section of the sacral region and ISJs from the μCT scans of UAMZ R952 at the contact between the first sacral rib and the ilium. (D) Cross section of the sacral region and ISJs from the μCT scans of UAMZ R952 at the contact between the second sacral rib and the ilium. (E) Three dimensional reconstruction of the left sacrum and ISJ from the μCT scans of UAMZ R952 in ventral view. (F) Sacral region of the vertebral column of ROM 8514 in ventral view. (G) Sacral region of the vertebral column of ROM 8514 in dorsal view. (H) Right ilium of ROM 8514 in medial view. (I) Right ilium of ROM 8514 in lateral view. The two sacral ribs in (F) and (G) are distally disarticulated and show the finished margin of both ribs at the level of their contact. Scale bars: 1 cm. **ant**, anterior; **aspi**, anterior supracetabular process of the ilium; **cc**, calcified cartilage; **cs**, cartilage symphysis; **cv**, cavity; **d**, dorsal; **fe**, femur; **il**, ilium; **is**, ischium; **l**, left; **pb**, pubis; **post**, posterior; **ppi**, posterior process of the ilium; **r**, right; **sr-I**, first sacral rib; **sr-II**, second sacral rib; **sv-I**, first sacral vertebra; **sv-II**, second sacral vertebra; **v**, ventral.

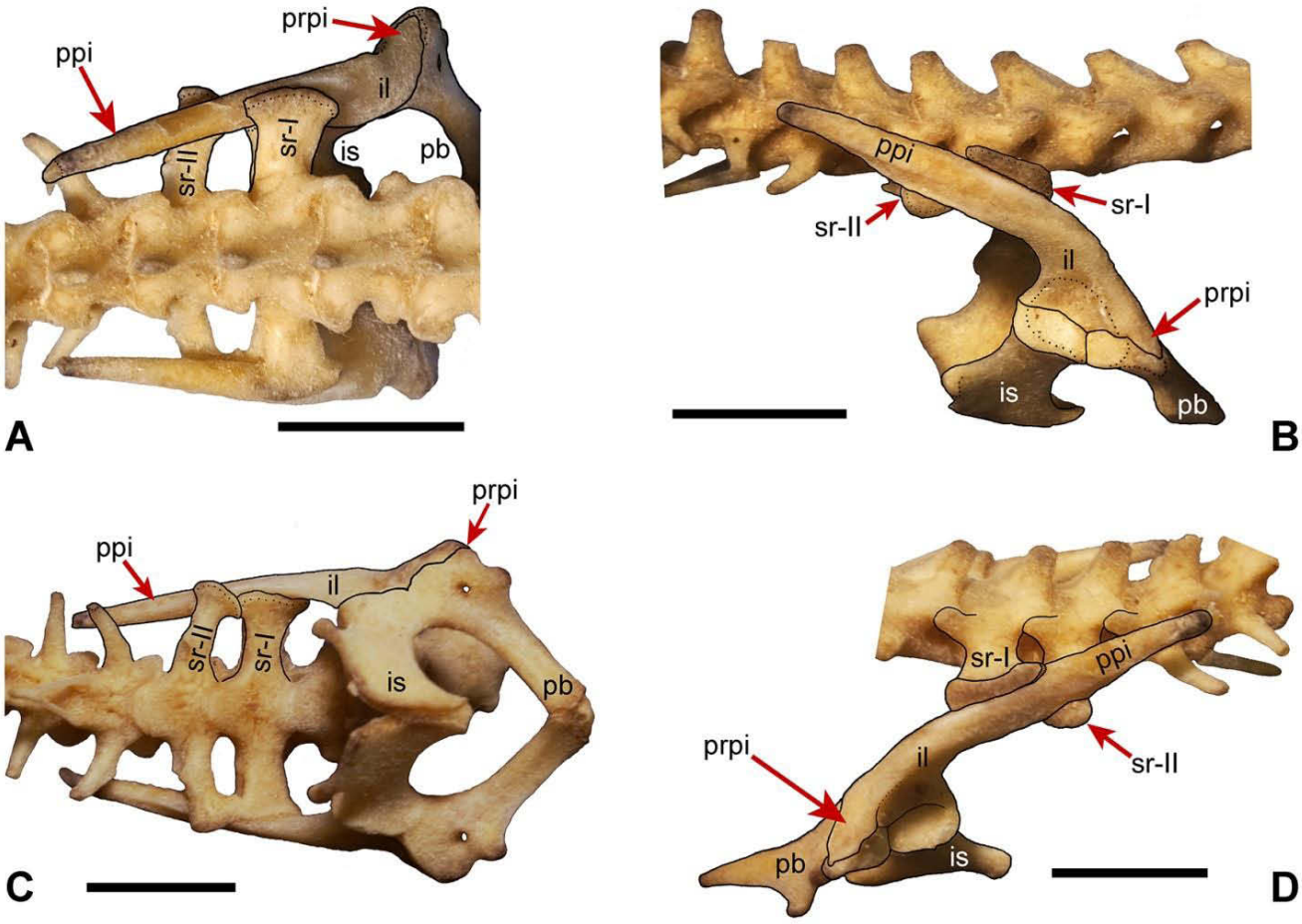

Figure 4.9. Osteology of the ISJ of *Heloderma suspectum* (TMP 90.7.357). (A) Sacral region and ISJs in dorsal view. (B) Sacral region and right pelvic girdle in lateral view. (C) Sacral region and ISJs in ventral view. (D) Sacral region and left pelvic girdle in lateral/anterolateral view. Noticeable is the absence of the supracetabular process of the ilium on its anterodorsal margin (cf. Fig. 1). Scale bars: 1 cm. **il**, ilium; **is**, ischium; **pb**, pubis; **ppi**, posterior process of the ilium; **prpi**, preacetabular process of the ilium; **sr-I**, first sacral rib; **sr-II**, second sacral rib.

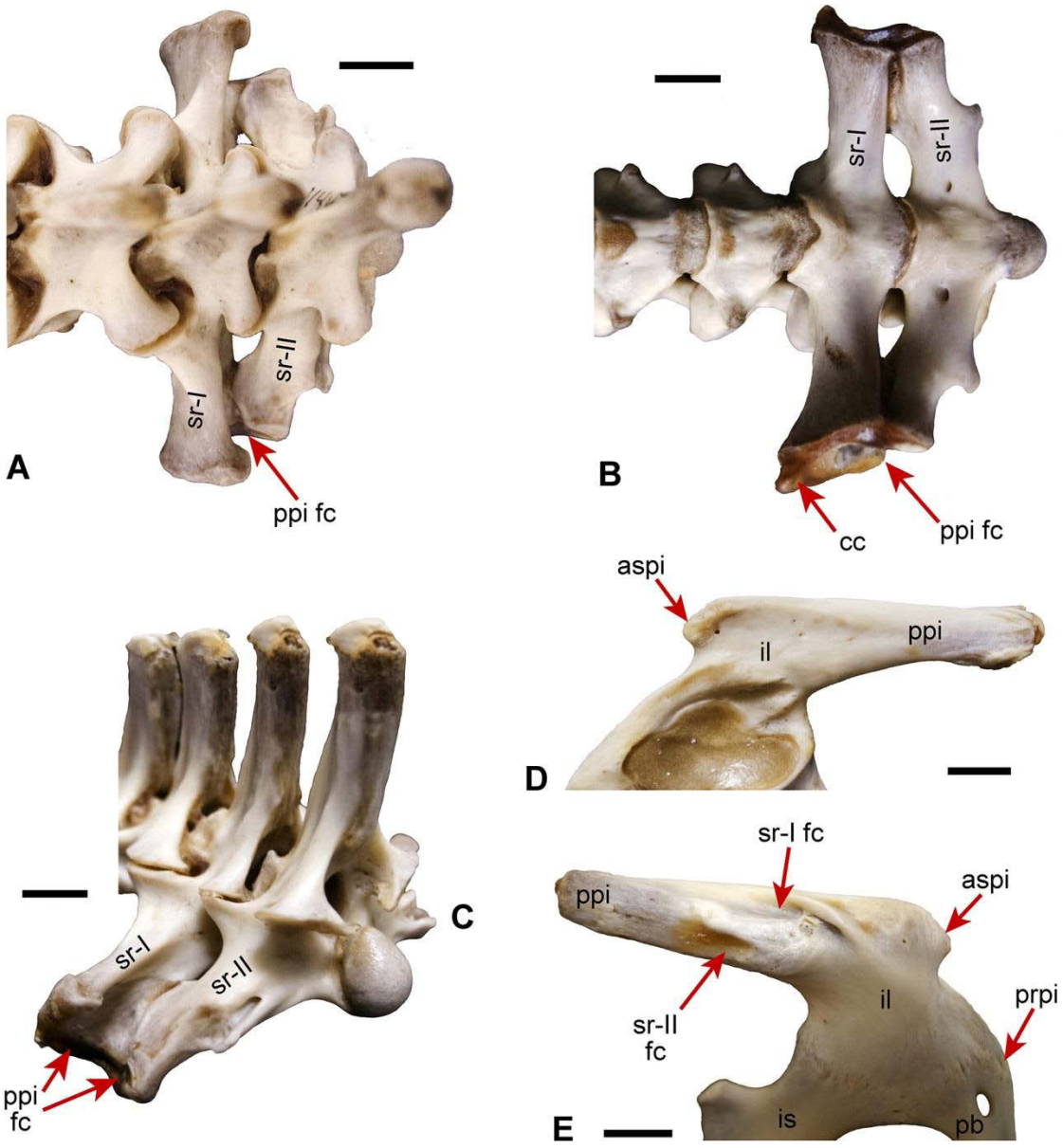

Figure 4.10. Osteology of the ISJ of *Amblyrhynchus cristatus* (AMNH R-114492). (A) Sacrals in dorsal view. (B) Sacrals in ventral view. (C) Left sacral ribs in posterolateral view showing the joint surface of articulation for the posterior process of the ilium. (D) Left ilium in lateral view. (E) Left ilium in medial view with emphasis on the position of the facets for the two sacral ribs on the posterior process. Scale bars: 1 cm. **aspi**, anterior supracetabular process of the ilium; **car**, cartilage; **fc**, facet; **il**, ilium; **is**, ischium; **pb**, pubis; **ppi**, posterior process of the ilium; **prpi**, preacetabular process of the ilium; **sr-I**, first sacral rib; **sr-II**, second sacral rib.

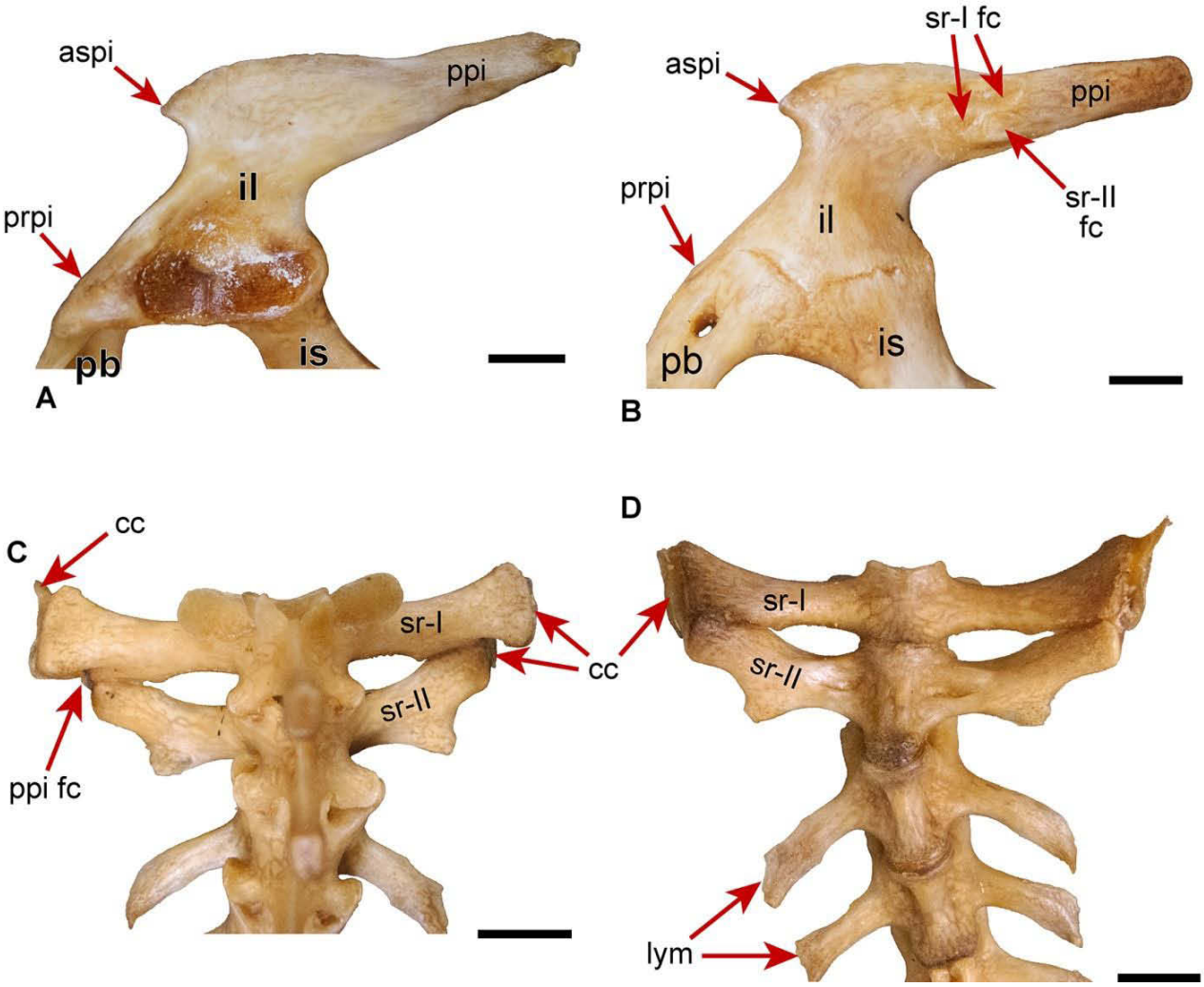

Figure 4.11. Osteology of the ISJ of *Conolophus pallidus* (AMNH R-147848). (A) Left pelvic girdle in lateral view. (B) Right pelvic girdle in medial view, showing the position of the facet for the two sacral ribs on the posterior process. (C) Sacral and post-sacral vertebrae in dorsal view. (D) Sacral and post-sacral vertebrae in ventral view. In (C) and (D), two vertebrae bearing distally grooved ribs (or lymphapophyses) are present posterior to the second sacral vertebra. Scale bars: 1 cm. **aspi**, anterior supracetabular process of the ilium; **car**, cartilage; **fc**, facet; **il**, ilium; **is**, ischium; **lym**, lymphapophysis; **pb**, pubis; **ppi**, posterior process of the ilium; **prpi**, preacetabular process of the ilium; **sr-I**, first sacral rib; **sr-II**, second sacral rib.

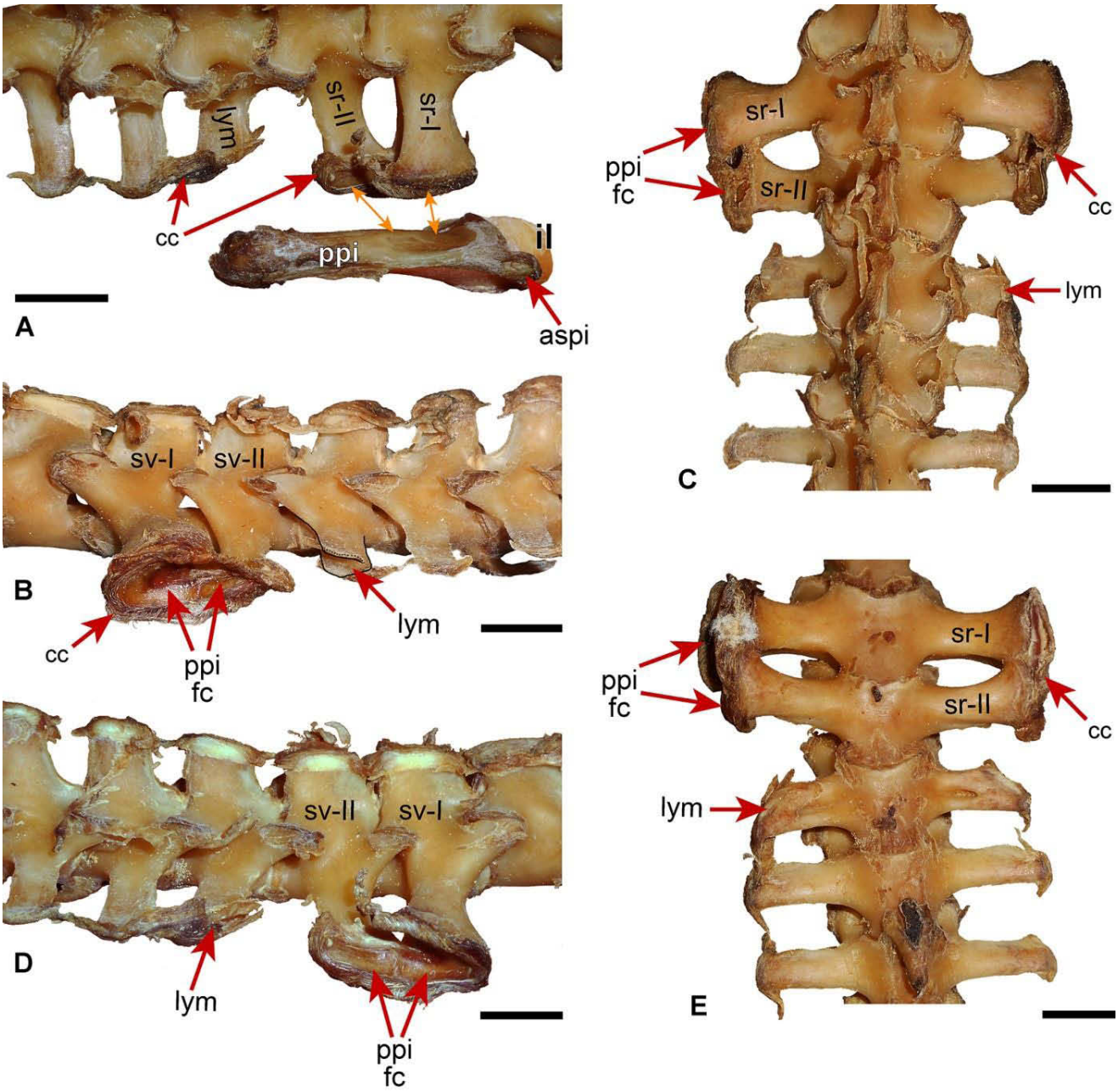

Figure 4.12. Osteology of the ISJ of *Varanus albigularis* (UAMZ R947). (A) Right sacrum, post-sacral vertebrae, and ilium in dorsal view showing the presence of abundant cartilage at the distal ends of the sacral ribs and single lymphapophysis as well as on the ilium. (B) Sacrals and post-sacrals in left lateral view showing the joint articular facet formed by the two sacral ribs for the contact with the posterior process of the ilium, and the distally grooved lymphapophysis. (C) Sacral and postsacral region of the vertebral column in dorsal view. (D) Sacrals and post-sacrals

in right lateral view. (E) Sacral and postsacral region of the vertebral column in ventral view. The orange arrows in (A) indicate the position of the articulation between the sacral ribs and the posterior process of the ilium. Scale bars: 1 cm. **aspi**, anterior supracetabular process of the ilium; **cc**, calcified cartilage; **fc**, facet; **il**, ilium; **lym**, lymphapophysis; **ppi**, posterior process of the ilium; **prpi**, preacetabular process of the ilium; **sr-I**, first sacral rib; **sr-II**, second sacral rib; **sv-I**, first sacral vertebra; **sv-II**, second sacral vertebra.

Appendix 4.1 – Staining protocol: Masson‘s trichrome technique.

Procedure takes about 1.5 hours including the cover-slipping of 8 slides with DPX

PPE: Fume hood, gloves, glasses

1. TOLUENE 1 and TOLUENE 2 (Top Shelf) 5 minutes each
2. Ethanol Series: 100%, 100%, 90%, 70%, 50% ethanol - 2 minutes each
3. Water - 2min.

4. Stain nuclei with Hematoxylin Gill III (Surgipath) 1 min

5. Wash well in cold running tap water in sink 15 min

6. Rinse in distilled water. 1 min total

7. Stain in Ponceau-acid **fuchsin** – did not filter 2 min

8. Rinse in distilled water 1 min total
Three Pots of d. water rinses best and less contamination for next solution

9. Differentiate in **1% Phosphomolybdic Acid-1** 5 min

10. Do **not** Rinse. Transfer to Acetic **Aniline Blue** 3 min

11. Rinse in distilled water 1 min total
Three Pots of d. water rinses best and less contamination for next solution

12. **1% Phosphomolybdic Acid-2** – use fresh solution 5 min

13. Place in 1% aqueous acetic acid 3 min

14. Dehydrate in 95% alcohol (discard after use) 2 min

15. 100% Ethanol Lower Shelf 2 min

16. 100% Ethanol Lower Shelf 2 min

17. Toluene Lower Shelf 2 min

18. Toluene Lower Shelf 2 min plus cover-slipping time

19. Coverslip with DPX in the Fume Hood. Wear Nitrile gloves. The slides stay in Toluene while cover-slipping.

Appendix 4.2 – Supplementary figures.

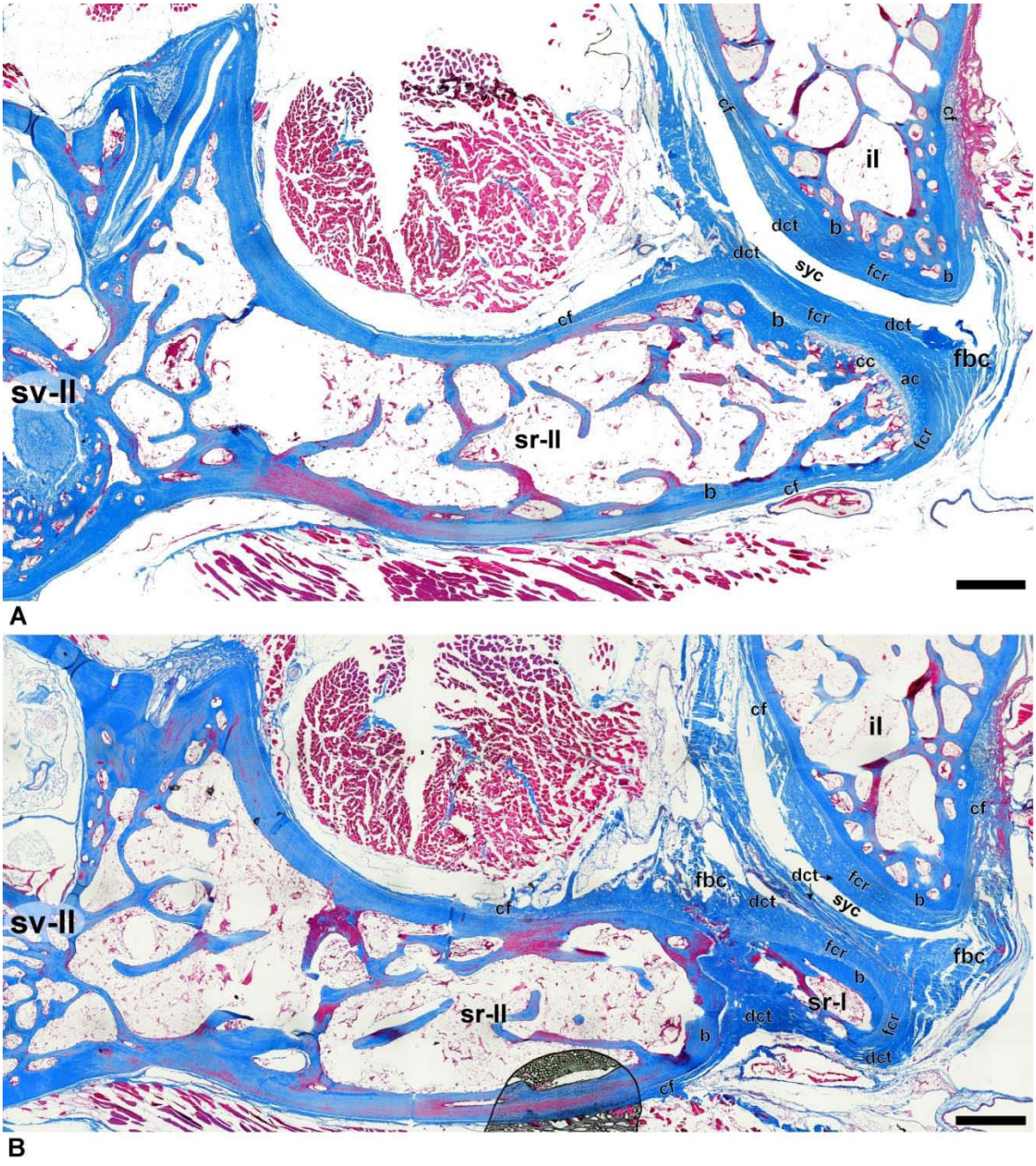

Figure A4.1. *Iguana iguana* UAMZ R951, ISJ serial histology, transverse sections at plane-polarized light. Scale bars: 1 mm. **ac**, articular cartilage; **b**, bone; **cc**, calcified cartilage; **cf**, collagen fibres; **dct**, dense connective tissue; **fbc**, fibrous capsule; **fcr**, fibrocartilage; **il**, ilium; **Shf**, Sharpey‘s fibres; **sr-II**, second sacral rib; **sv-II**, second sacral vertebra; **syc**, synovial cavity.

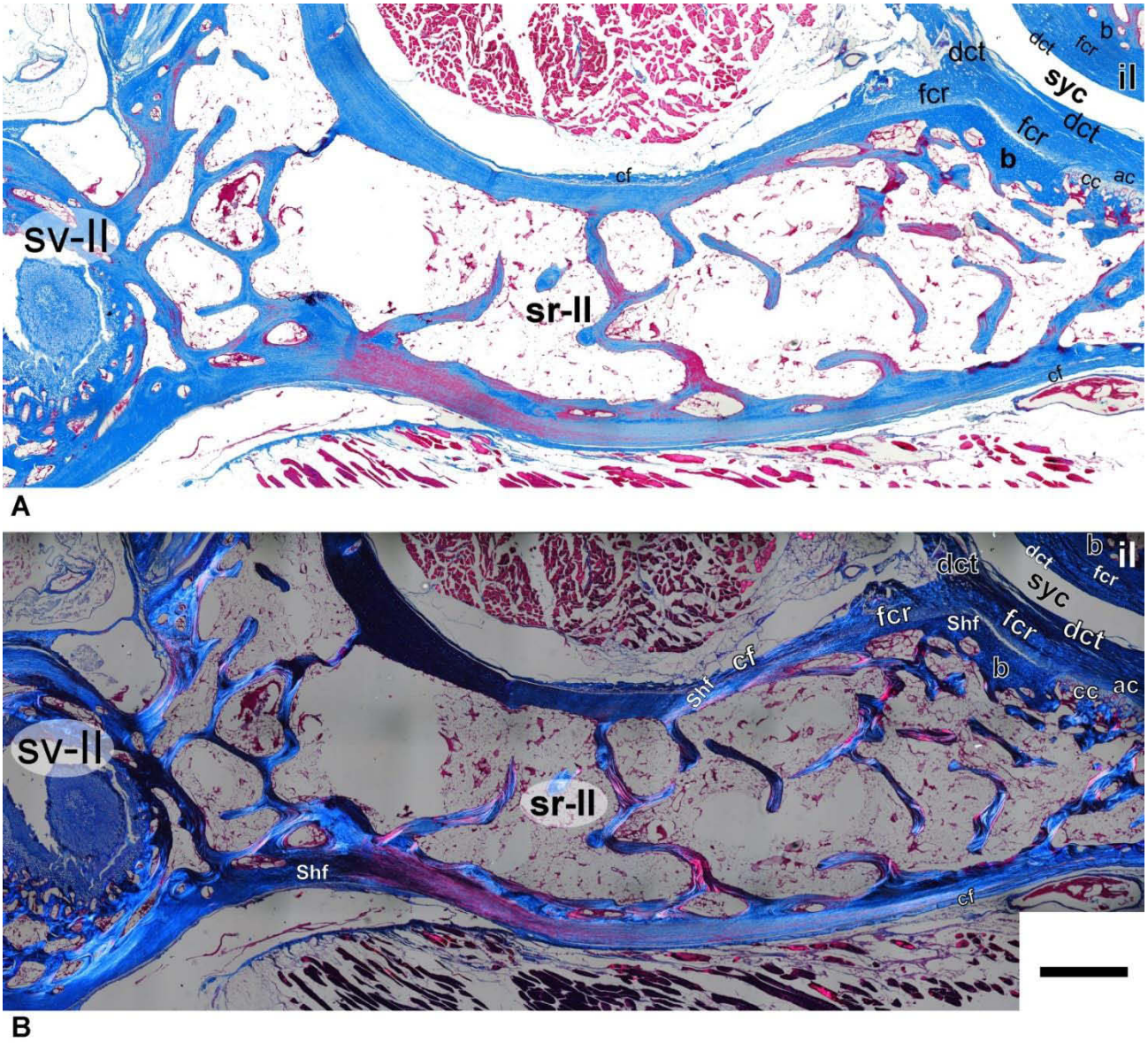

Figure A4.2. *Iguana iguana* UAMZ R951, ISJ serial histology, transverse section at plane-polarized (A) and cross polarized (B) light. Scale bar: 1 mm. **ac**, articular cartilage; **b**, bone; **cc**, calcified cartilage; **cf**, collagen fibres; **dct**, dense connective tissue; **fbc**, fibrous capsule; **fcr**, fibrocartilage; **il**, ilium; **Shf**, Sharpey‘s fibres; **sr-II**, second sacral rib; **sv-II**, second sacral vertebra; **syc**, synovial cavity.

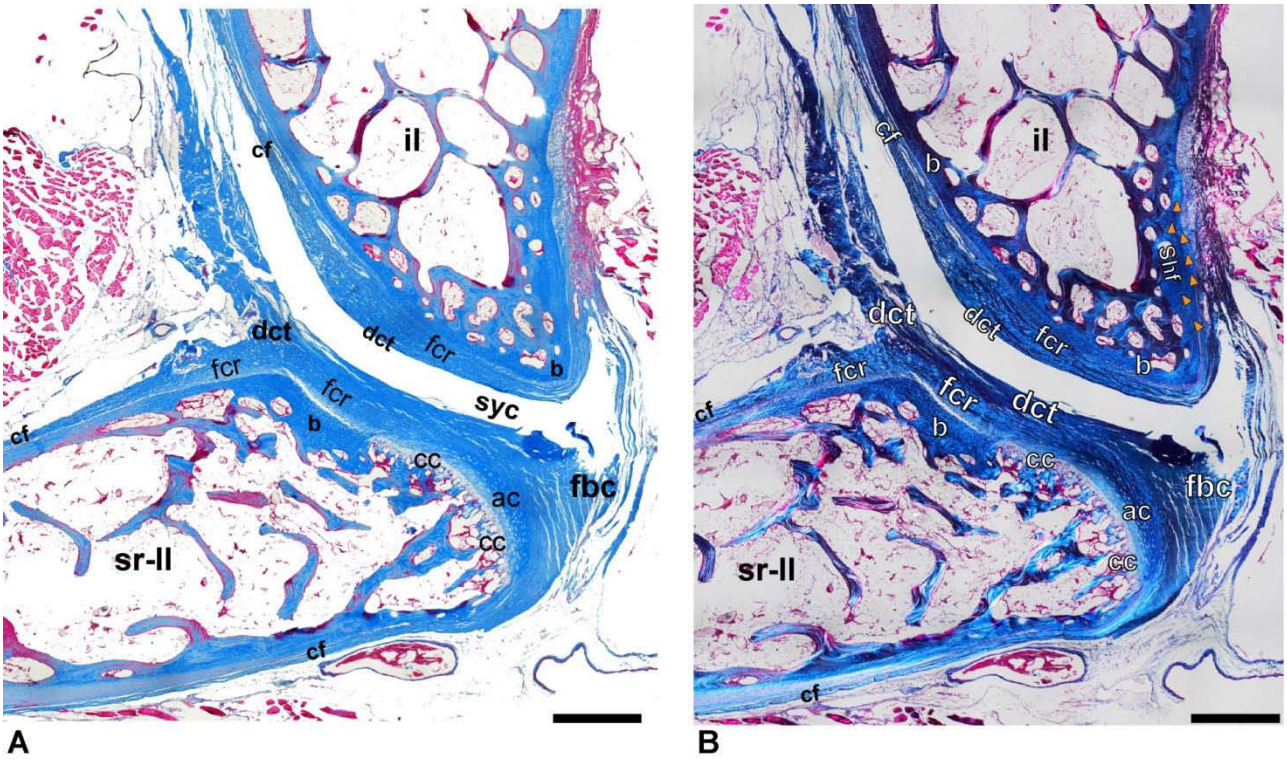

Figure A4.3. *Iguana iguana* UAMZ R951, ISJ serial histology, transverse section at plane-polarized (A) and cross-polarized (B) light. Scale bars: 1 mm. **ac**, articular cartilage; **b**, bone; **cc**, calcified cartilage; **cf**, collagen fibres; **dct**, dense connective tissue; **fbc**, fibrous capsule; **fcr**, fibrocartilage; **il**, ilium; **Shf**, Sharpey‘s fibres; **sr-II**, second sacral rib; **sv-II**, second sacral vertebra; **syc**, synovial cavity.

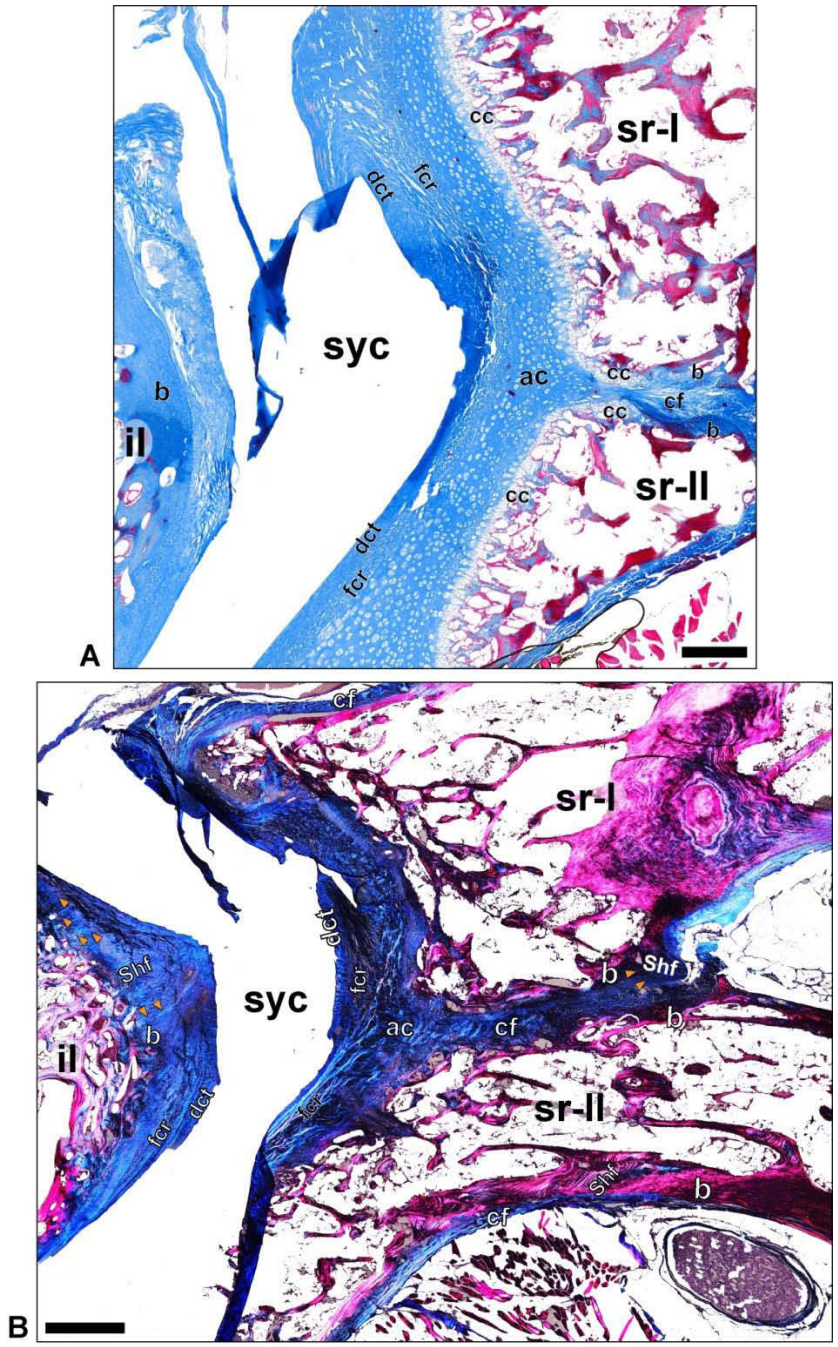

Figure A4.4. *Iguana iguana* UAMZ R951, ISJ serial histology, longitudinal section at plane-polarized (A) and cross-polarized (B) light. Scale bars: 500 µm. **ac**, articular cartilage; **b**, bone; **cc**, calcified cartilage; **cf**, collagen fibres; **dct**, dense connective tissue; **fbc**, fibrous capsule; **fcr**, fibrocartilage; **il**, ilium; **Shf**, Sharpey‘s fibres; **sr-I**, first sacral rib; **sr-II**, second sacral rib; **syc**, synovial cavity.

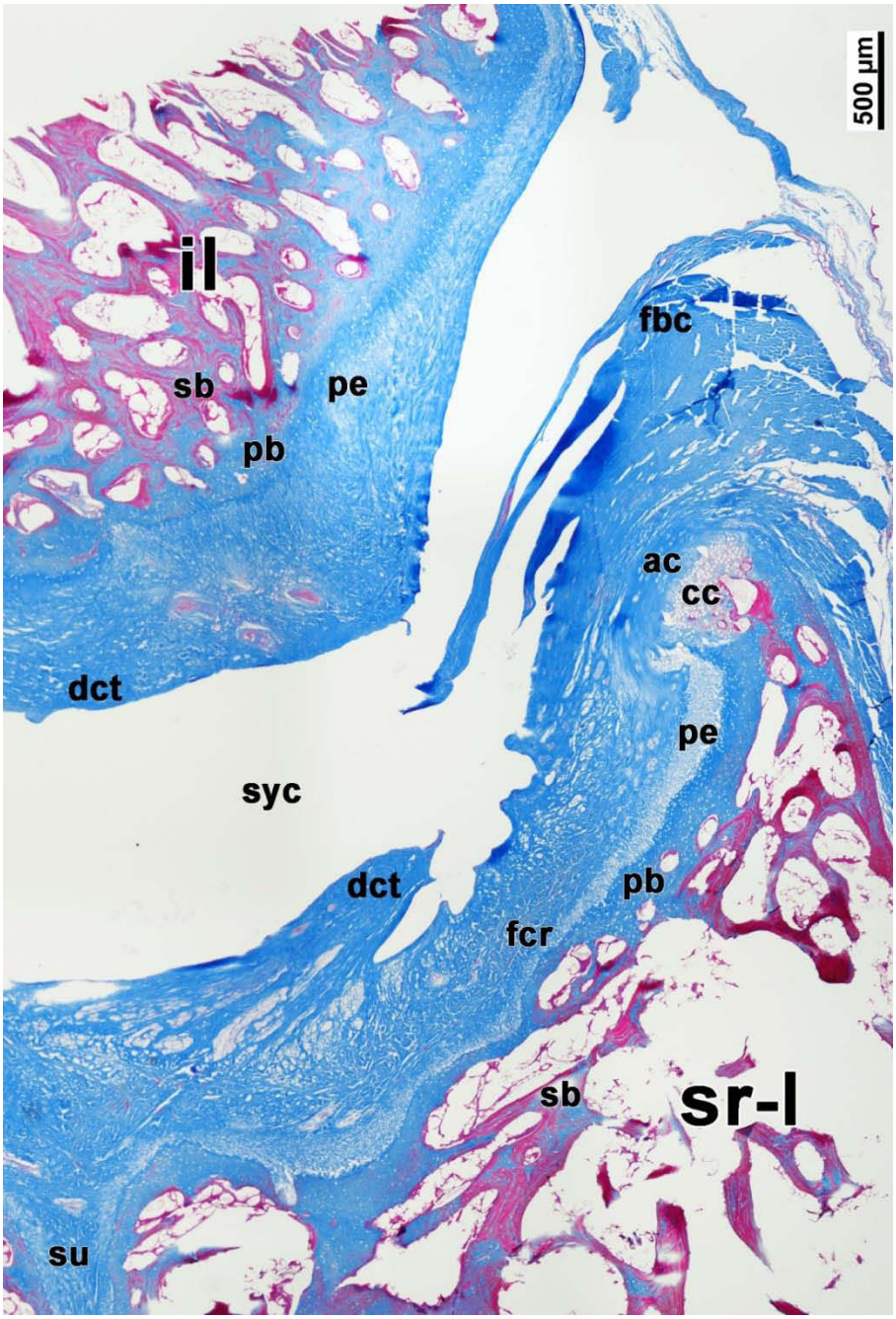

Figure A4.5. *Iguana iguana* UAMZ R951, ISJ serial histology, longitudinal section at plane-polarized (A) and cross-polarized (B) light. **ac**, articular cartilage; **cc**, calcified cartilage; **dct**, dense connective tissue; **fbc**, fibrous capsule; **fcr**, fibrocartilage; **il**, ilium; **sr-I**, first sacral rib; **sr-II**, second sacral rib; **syc**, synovial cavity. **fcr**, fibrocartilage; **pe**, periosteum; **pb**, primary bone; **sb**, secondary bone.

CHAPTER 5

New phylogeny of Iguania and origins of the modern iguanian clades

5.1 Introduction

Iguania is a diverse group of squamates represented by over 2000 living species (Uetz et al. 2020). Modern iguanians are roughly divided into two main lineages: the Pleurodonta, with a New World distribution, and the Acrodonta, spread across the Old World (Evans 2003; Frost & Etheridge 1989; Frost et al. 2001; Myers et al. 2021). There are few noticeable exceptions to this biogeographic picture, represented by pleurodontan oplurids in Madagascar and pleurodontan iguanids inhabiting several South Pacific islands. Evolutionary relationships within Iguania have been and still are highly debated amongst researchers, a fact that is reflected in the complicated taxonomic history of the group.

Traditionally, Iguania has been divided into three main families: Agamidae, Chamaeleonidae, and Iguanidae (Estes et al. 1988; McDowell & Bogert 1954). This taxonomic scheme has been widely accepted for living iguanians for a long time, however, past authors had already provided alternative classifications to encompass the greater complexity and diversity of these lizards. Cope (1864) Latinized the words Acrodonta and Pleurodonta from the French names Acrodontes and Pleurodontes as originally coined by Duméril & Bibron (1837). The terms refer to the macroscopic difference in position of the teeth relative to the jaw bone that is observed among iguanians: 1) _Acrodonta‘ from the dental condition defined as *acrodont*, meaning literally _tooth at the top‘, and composed of the Latinized forms *acr-* (_atthe end, at the

top‘) plus -*odont* (_tooth‘); 2) _Pleurodonta‘ from the dental condition defined as *pleurodont* meaning literally _tooth to the side‘, and composed of the Latinized forms *pleuro-* (_to the side, lateral‘) plus -*odont* (_tooth‘) (Online Etymology Dictionary, retrieved 15 March 2021). When they were first used, these taxonomic categories contained very different taxa than today. For instance, the modern tuatara *Sphenodon* was included in Acrodonta together with chamaeleons, while Pleurodonta included other lizard groups, like varanids, helodermatids, anguids, and more. (Cope 1864; Duméril & Bibron 1837). In time, these categories were slowly refined and, with the advent of cladistics, they were narrowed down to their modern use (Frost et al. 2001). However, the use of Acrodonta and Pleurodonta is not broadly accepted or at least not always applied by iguanian taxonomists, and a proper revised definition of these categories is certainly needed to reach a greater consensus about their inclusivity.

The taxonomic category Iguanidae has an even more problematic history. Coined by Oppel (1811) at the family rank, the term was initially use to include iguanians that resemble *Iguana* more than *Agama* or *Chamaelo*. The more our knowledge about these lizards grew, the more difficult it became to apply the term. Iguanidae became a metataxon when the three-family classification system (Agamidae, Chamaeleonidae, Iguanidae) was established and is occasionally still in use in more recent phylogenetic studies (Estes et al. 1988; Etheridge & de Queiroz 1988; Gauthier et al. 2012). A step forward towards a better-defined taxonomic scheme was given by Frost & Etheridge (1989) who recognized the limitations of the three-family system for Iguania; in doing so they accounted for their great diversity and elevated all the subgroups in the metataxon Iguanidae from the rank of subfamilies to families. This of course caused an overlap between the former subfamily Iguaninae, as defined by Etheridge & de Queiroz (1988), and the newly redefined Iguanidae *sensu* Frost & Etheridge (1989). Moreover, a

higher category including all the former subfamilies (now families), which still formed a monophyletic meta-group was not proposed.

It was not until the total evidence phylogeny of Frost et al. (2001) that both Acrodonta (including Chamaeleonidae and Agamidae) and Pleurodonta (including Corytophanidae, Crotaphytidae, Hoplocercidae, Iguanidae, Leiocephalidae, Leiosauridae, Liolaemidae, Opluridae, Phrynosomatidae, Polychrotidae, and Tropiduridae) were introduced into the classification of iguanians more consistently. Following phylogenetic studies tend to follow these categories in broad terms (Conrad 2008; Conrad & Norell 2007; Schulte et al. 2003; Sites et al. 2011; Townsend et al. 2011). Pleurodonta became essentially a replacement for the former concept of Iguanidae *sensu* Estes et al. (1988), and the new Iguanidae *sensu* Frost & Etheridge (1989) was limited to the clade including the modern genera *Iguana*, *Sauromalus*, *Dipsosaurus*, *Brachylophus*, *Cyclura*, *Ctenosaura*, *Amblyrhynchus*, and *Conolophus*. Conrad (2008) provided further support for this new classification scheme, at least at the higher taxonomic level, though he only formally adopted the use of Acrodonta and not Pleurodonta. The same author also acknowledged the general lack of inclusivity in Acrodonta for stem fossil forms such as the priscagamids from the Late Cretaceous of the Gobi Desert (e.g., Alifanov 1989; Alifanov 1996; Alifanov 2000; Alifanov 2013; Borsuk-Bialynicka 1996; Borsuk-Bialynicka & Moody 1984; Estes et al. 1988; Gao & Hou 1995). The clade Chamaeleontiformes was formalised to include Priscagamidae + Acrodonta, thus enforcing the use of the latter for mostly crown lineages (Conrad 2008).

Pleurodonta as formalised by Frost et al. (2001) continued to be largely ignored, and studies such as Gauthier et al. (2012) preferred to maintain the older concept of Iguanidae *sensu* Estes et al. (1988) with subfamily-level subgroups, thus perpetrating a reductive view of the

diversity of the iguanian lineages. Things were further complicated by the phylogenetic analysis based on morphological data as given by Daza et al. (2012), where the use of Pleurodonta *sensu* Frost et al. (2001) was ignored for no clear reasons, and a series of brand new taxonomic names were created for several node-based clades of non-chamaeleontiform iguanians that have typically been unstable across different phylogenetic studies based on either morphological, molecular, or combined evidence (e.g., Conrad 2008; Conrad & Norell 2007; Estes et al. 1988; Etheridge & de Queiroz 1988; Frost & Etheridge 1989; Frost et al. 2001; Gauthier et al. 2012; Schulte et al. 2003; Sites et al. 2011; Townsend et al. 2011; Wiens et al. 2010).

In this study, I present the results of a new phylogenetic analysis based on a combined dataset of morphological and molecular data that includes representatives of all modern lineages as well as a large fossil sampling of Iguania. All the operational taxonomic units are at the species-level. I revised morphological characters from the literature as well as formulated new ones, and scored all the taxa based on personal observations. I compiled a molecular dataset of 15 nuclear and 5 mitochondrial loci with data retrieved from the GenBank online database. I analysed the data primarily using Bayesian inference methods and performing both calibrated and uncalibrated analyses of the combined and separate data matrices. I tested the new morphological dataset also under equal and implied weighting maximum parsimony to allow for comparisons with my Bayesian results and previous studies, especially as concerns the relationships of the fossil taxa. I then used my newly formulated phylogenetic hypothesis to address questions about the origins and radiation of the modern and fossil clades as well as discuss the possible scenarios that can explain the disjointed distribution of several iguanian groups today. I also redefined some of the higher taxonomic categories that have been traditionally problematic for this group of lizards, proposing for instance to limit the use of

Pleurodonta and Acrodonta to crown iguanian lineages, and defining three new taxa to encompass the greater complexity of iguanian evolution when more fossil lineages are considered. Finally, I discuss the issues with the traditional interpretation of iguanians within the limits of the acrodont *versus* pleurodont paradigm, and the need to revise this simplistic view in light of the new developmental, histological, and osteological knowledge that has been produced in the last decade on amniote dental anatomy (e.g., Bertin et al. 2018; Buchtová et al. 2013; Caldwell 2007; Dosedělová et al. 2016; Haridy 2018; LeBlanc et al. 2017; LeBlanc et al. 2020b; Maxwell et al. 2011; Zahradnicek et al. 2014).

5.2 Material and Methods

5.2.1 Operational taxonomic units (OTUs)

The new dataset presented in this study is composed of a large number of extant species, sampling members from all modern families of acrodontan and pleurodontan iguanians, and the largest number of fossil species ever included in a phylogenetic study of Iguania to date. The fossil record of these lizards is particularly rich, however, numerous species described in the last three decades have never been included in a phylogenetic analysis. This is the case for the Middle Eocene chanjiangosaurids, some Late Cretaceous priscagamids (*Chamaeleognathus iordanskyi*, *Morunasius modestus*, *Gladidenagama semiplena*, *Mimeosaurus tugrikinensis*) and *Desertiguana gobiensis*, the Middle Eocene taxa *Tinosaurus stenodon* and *Pseudotinosaurus asiaticus*, and the more recent *Brachylophus gibbonsi* from late Holocene deposits of Tonga (Alifanov 1993a; Alifanov 2012; Alifanov 1996; Alifanov 2009; Alifanov 2013; Gilmore 1928; Gilmore 1943; Pregill & Steadman 2004). The final dataset for the combined evidence Bayesian inference consists of 99 OTUs of which 31 are fossils and 68 are modern species. All the OTUs

are at the species-level and most of the specimens used for the scoring of the morphological characters were personally analysed by myself, with the exception of the three fossil outgroups (*Megachirella wachtleri*, *Gephyrosaurus bridensis*, and *Eichstaettisaurus schroederi*), which are mostly based on personal observations from the literature; I also consulted CT scan data openly available through the Digital Morphology online library (DigiMorph: http://www.digimorph.org) and the Morphosource database (https://www.morphosource.org/). A complete list of fossil taxa with information on the age, locality, specimens, and references (Table A5.1) as well as a list of the extant specimens used for scoring, are provided in Appendix 5.3-5.4.

Six taxa were selected as outgroups, including three fossil (*Megachirella wachtleri*, *Gephyrosaurus bridensis*, and *Eichstaettisaurus schroederi*) and three extant (*Sphenodon punctatus*, *Gekko gecko*, and *Varanus salvator*) species. The inclusion of both *Varanus* and *Gekko* as outgroup was guided by the most recent phylogenetic studies of Squamata that show an increased support for a closer relationship of iguanians to anguimorphs based on molecular and combined evidence (Reeder et al. 2015; Simões et al. 2018; Vidal & Hedges 2005), as opposed to the more traditional view based only on morphological data that iguanians are the most basal squamates and are more closely related to gekkonomorphs (Conrad 2008; Estes et al. 1988; Gauthier et al. 2012). For one of the Galápagos land iguanas, *Conolophus marthae*, only molecular data were available for the phylogenetic analyses. This species was described more recently and it is considered at high risk of extinction due to the low number of individuals alive today (Gentile et al. 2009). No skeletal specimens were available for study in any collections for scoring the morphological characters.

5.2.2 Morphological dataset construction

The morphological dataset was compiled with characters revised from the literature as well as with the addition of new characters. Characters were constructed following guidelines in Patterson (1982), Sereno (2007), and Simões et al. (2016). The list of morphological characters with detailed remarks is provided in Appendix 5.1. The final dataset consists of 293 characters: 153 characters addressing skull features, 39 characters focused on the mandible, 10 dentition characters, 7 characters for the hyoid apparatus, 37 characters focused on the axial skeleton, and 47 characters for the appendicular elements. The data matrix was generated with Mesquite 3.6 (Maddison & Maddison 2018). Characters were coded considering Bayesian likelihood requirements; autapomorphic features, which are typically uninformative in parsimony analyses, were therefore also included. However, I limited the number of autapomorphic characters to about 5% of the morphological dataset as studies on what can be considered an adequate number of autapomorphies to assess phylogenetic relationships using Bayesian inference are yet to be performed.

5.2.3 Molecular dataset construction

The molecular dataset includes 15 nuclear and 5 mitochondrial loci for 68 extant species (3 outgroup and 65 ingroup OTUs). The sequence data for the selected genetic markers were retrieved from GenBank and the accession numbers are provided in Tables 5.2-5.5, Appendix 5.5. For the alignment of the sequences, I used BioEdit 7.2.5 (Hall 1999) to generate consensus sequences and then performed the multiple sequence alignment with MAFFT 7.380 online server (http://mafft.cbrc.jp/alignment/server/) (Katoh et al. 2019; Kuraku et al. 2013). All the sequences were concatenated and manually adjusted in Mesquite 3.6 (Maddison & Maddison 2018).

Finally, the molecular sequences were analysed with PartitionFinder 2.1.1 (Lanfear et al. 2012; Lanfear et al. 2016) to find the best partitioning scheme and best-fit model for each partition. Information about the genetic markers, final aligned sequences, and partitioning scheme are included in Appendix 5.5.

5.2.4 Phylogenetic analyses

Bayesian inference – To reconstruct the phylogenetic relationships of living and fossil iguanians, I used Bayesian inference (BI) implemented in MrBayes 3.2.7a (Ronquist et al. 2012b) on the CIPRES Science Gateway 3.3 (Miller et al. 2012; Miller et al. 2015), enabling the application of the BEAGLE package (Ayres et al. 2011). The choice of BI as the preferred method to reconstruct phylogenetic relationships based on combined molecular and morphological evidence was dictated by the increased number of studies showing its better performance over other statistical as well as parsimony methods (Huelsenbeck et al. 2000; O'Reilly et al. 2016; Puttick et al. 2017; Puttick et al. 2019; Wright & Hillis 2014; Yang & Rannala 2012). This consideration is based both on an *a posteriori* consistency of the inferred relationships with other analyses in this and previous studies, and on an *a priori* assessment of the currently available phylogenetic methods based on previous literature. BI offers important advantages when combining molecular and morphological data to reconstruct phylogenetic relationships. Morphological and molecular characters have different rates of variation, frequency, construction, coding, etc., and treating them under the same parameters is hardly acceptable from both a methodological and biologically significant standpoint. BI allows one to apply different priors and models of evolution to different partitions of molecular and morphological data, thus increasing both the accuracy and efficiency of the resulting topologies.

For comparison, I also performed an uncalibrated BI of the combined evidence (UcBI), as well as an uncalibrated (UmBI) and time-calibrated (TmBI) analysis of the morphological data, and an uncalibrated (UgBI) analysis of the molecular data. The nexus files of all five analyses formatted with the MrBayes block are provided as digital supplementary material (Supplementary Data 5.1-5.5). To combine the molecular and morphological matrices into a single dataset I used the text editor EmEditor Free 19.3.0 (https://www.emeditor.com/) by Emurasoft Inc., while the separate matrices were constructed using Mesquite 3.6 (Maddison & Maddison 2018) (as explained above for each dataset). Each molecular partition was analysed under the best-fit model of evolution obtained from PartitionFinder and the single morphological partition was analysed using the MkV model of evolution (Lewis 2001). To find optimality of the parameters, I ran the UcBI analysis multiple times and used Tracer 1.7.1 (Rambaut et al. 2014) to check for convergence to stationary phase and effective sample size (ESS) for each parameter to be greater than 200. Each analysis was run for 40 million generations with trees sampled every 500 generations. Rate heterogeneity distribution among morphological characters was determined through a comparison of Bayes factors after running the UmBI analysis under both a lognormal and gamma distribution (cf. Huelsenbeck & Ronquist 2001; Ronquist et al. 2011; Ronquist & Huelsenbeck 2003; Ronquist et al. 2012b). Based on Kass & Raftery (1995), I recovered no significant difference between the two distributions, with the gamma model being about 2 log units worse than the lognormal model. Hence, I used the gamma distribution of rate heterogeneity for the morphological data in all the BI analyses. The posterior maximum clade credibility trees (MCCTs) were estimated with TreeAnnotator 2.4.3 (Rambaut & Drummond 2016b) and formatted with FigTree 1.4.2 (Rambaut 2007). The TcBI and TmBI analyses were performed using the fossilized birth-death model under the relaxed clock model (Gavryushkina

et al. 2014; Heath et al. 2014; Ronquist et al. 2012a). The clock rate prior for the calibrated analyses was calculated from the uncalibrated analyses, following the steps explicated in Simões et al. (2018). Considering the large number of fossil species included in the dataset, fossil tip-dating was considered favourable over node-age calibrations. Increasing the number of fossil OTUs in calibrated phylogenetic analyses has been shown to improve precision of clade divergence times by previous works (e.g., Arcila et al. 2015; Ronquist et al. 2012a); however, there are concerns about unlikely older node age estimates using only tip-dating implementation (Arcila et al. 2015; O'Reilly et al. 2015). A possible solution to this problem is to implement both tip-dating and node-dating in the same analysis, when the oldest known fossils for the clades are well established (O'Reilly & Donoghue 2016; Simões et al. 2018). In my dataset, many fossil species are tested in a phylogenetic framework for the first time and it would be premature to use them for a priori calibration of their clade age. Moreover, some fossil OTUs have known discordant positions in previous studies (e.g., *Isodontosaurus*, *Aciprion*, and *Geiseltaliellus*), making it quite difficult to argue in favour of any particular bound for node-age calibration of any clade at this stage. Ages for the OTUs were derived from the primary literature and, when not explicitly indicated, the numerical age of the corresponding stages was derived from the International Stratigraphic Chart (Cohen et al. 2013). The age of the tree was set to a minimum of 245 Ma and a maximum of 260 Ma (corresponding to a 252.5 Ma mean root age) based on Simões et al. (2018), considering the age of the oldest OTU *Megachirella* (243.5, 244.5 Ma) and the divergence of Squamata (about 260 Ma). The MCCT with estimated mean divergence times for the combined evidence analysis is presented in Figure 5.1, while the topology with age estimates based on morphology-only is presented in Figure 5.2. The

differences for the age estimates of the main clades between the two calibrated analyses (TcBI and TmBI) are summarized in Table 5.1.

Parsimony – To further test the newly constructed morphological dataset, I also performed an equal-weight (EW) and implied-weighting (IW) maximum parsimony (MP) analysis, recognizing that some of the characters included in my dataset are uninformative under parsimony standards (e.g., autapomorphies) (cf. Strong & Lipscomb 1999). The MP analyses were performed in TNT 1.5 (Goloboff et al. 2003) using the tree bisection reconnection (TBR) algorithm, which is recommended for small datasets with less than 100 OTUs (Goloboff et al. 2008b). All the characters were processed as unordered in both the EWMP and IWMP analyses. The number of maximum trees was set to 99.999 and the number of replicates to 1.000. The trees resulting from the first TBR run were used as starting trees for subsequent runs of TBR and this step was repeated twice to increase chances of sampling the shortest trees. The recovered suboptimal trees were finally filtered to leave only the most parsimonious trees (MPTs). Settings for the IWMP analysis follow Goloboff et al. (2008a; 2017). The concavity value was set to 12 (K =12) which has been shown to act more mildly against homoplastic characters and in general to be more accurate in recovering the model trees in simulation studies (Goloboff et al. 2017). The resulting topologies were formatted and analysed for consistency and retention index in Mesquite 3.6 (Maddison & Maddison 2018). The 50% majority rule consensus trees of the EWMP and IWMP analyses are included in Figures 5.6-5.7, and the relative strict consensus trees can be found in Appendix 5.6 (Figs. A5.2-A5.3). The matrix file is provided as digital supplementary materials (Supplementary Data 5.6).

5.3 Results

The topology resulting from the time-calibrated Bayesian analysis of the combined evidence (TcBI) represents the preferred phylogenetic hypothesis (Fig. 5.1). I refer to the other resulting topologies (UcBI, TmBI, UmBI, UgBI, EWMP, IWMP) for comparisons and to discuss possible alternative hypotheses (Figs. 5.2-5.7).

Based on the TcBI results, the following new clades are defined here: 1) Iguaniformes, including Pleurodonta and Gobiguania; 2) Dracosauria, including agamids, leiolepids, and uromastycids; 3) Uromastyoidea, including leiolepids and uromastycids (Fig. 5.1; see Appendix 5.2 for synapomorphies and definitions). Historically, Acrodonta and Pleurodonta have been applied to crown iguanian lineages (e.g., Conrad 2008; Frost et al. 2001; Reeder et al. 2015; Schulte et al. 2003; Sites et al. 2011; Wiens et al. 2012). Chamaeleontiformes (‗chameleon-like forms') was defined by Conrad (2008) as the clade formed by Priscagamidae + Acrodonta, thus including both stem and crown acrodontan-like iguanians. In line with this rationale, the name Iguaniformes (‗iguana-like forms') is proposed here for the clade formed by ―Gobiguania s.l." + Pleurodonta, including both stem lineages and crown pleurodontans.

5.3.1 Early evolution of Iguania

Earliest branching of Iguania is estimated at 160-170 Ma (Late Jurassic) in the combined evidence analysis and 126-134 (Early Cretaceous) based on morphology (Table 5.1; Figs. 5.1-5.2). Both ranges and the discrepancy between them are in line with values recovered in previous studies (Burbrink et al. 2020; Irisarri et al. 2017; Pyron 2017; Simões et al. 2018; Simões & Pyron 2021; Simões et al. 2020). The pattern of diversification into two main lineages (Chamaeleontiformes and Iguaniformes) is recovered in the TcBI, TmBI, and UgBI topologies

but not in the morphology-only EWMP, IWMP, and UmBI results. In the UmBI (Fig. 5.4), Chamaeleontiformes branches from within Pleurodonta, as the sister-group to *Polychrus* + *Geiseltaliellus*. However, posterior probability support for all basal branches is extremely low (Fig. 5.4). In the two MP trees (Fig. 5.6-5.7), priscagamids do not form a monophyletic group: *Mimeosaurus* and *Arretosaurus* form a basal clade of iguanians together with Chamaeleonidae, while most priscagamids are recovered as stem iguaniforms. In this case, Dracosauria is retained as the sister-group to ―priscagamids" + Iguaniformes though there are variations in sister-group relationships within the clades.

5.3.2 Chamaeleontiformes

Chamaeleontiforms, including Priscagamidae + Acrodonta, diverged around 148 Ma (latest Jurassic) according to the TcBI analysis or 123 Ma (late Early Cretaceous) according to the TmBI analysis (Table 5.1; Figs. 5.1-5.2). My dataset includes a greater number of fossil species from the Late Cretaceous and Paleogene deposits of Mongolia in comparison to any previous studies, and Priscagamidae appears much more diverse and long-lived. For example, the late Eocene – early Oligocene taxon *Arretosaurus* from Mongolia is nested in Priscagamidae as the sister-taxon to *Pleurodontagama* (BI topologies: Figs. 5.1-5.4) or *Mimeosaurus* (MP topologies: Figs. 5.6-5.7). The branch formed by *Arretosaurus* is relatively long, covering a 40 My gap, but its position is consistent across all the analyses. The two *Mimeosaurus* species (*M. crassus*, *M. tugrikinensis*) form a clade basal to all other priscagamids and are not consistently recovered as sister-taxa.

Flaviagama represents the next diverging group of priscagamids in the TcBI topology (Fig. 5.1), though in contrast it is nested in a clade with the two *Mimeosaurus* species in the

TmBI tree as sister-taxon to *M. crassus* (Fig. 5.2). Amongst priscagamids, *Flaviagama* shows the greatest variability in phylogenetic position: in the UcBI topology (Fig. 5.3) is recovered as the most basal chamaeleontiform (and Priscagamidae as defined here is non-monophyletic); in the UmBI and EWMP topologies (Figs. 5.4, 5.6) it is recovered as the most basal priscagamid, and in the IWMP tree (Fig. 5.7) as a stem iguaniform. *Priscagama*, *Pleurodontagama*, and *Arretosaurus* are more deeply nested in Priscagamidae and tend to be closer to each other than other priscagamids.

Chamaeleognathus, *Morunasius*, *Gladidenagama*, and *Phrynosomimus* also typically form a monophyletic group, as sister-group to the *Priscagama*-clade, with some variations in sister-group relationships across the four taxa in some of the topologies (Figs. 5.1-5.3). The divergence of Priscagamidae is estimated at 141 Ma (earliest Cretaceous) in the TcBI analysis, and 117 Ma (latest Early Cretaceous) in the TmBI analysis (Table 5.1; Figs. 5.1-5.2). Several fossil taxa are nested with crown acrodontans. This is not surprising considering that most higher clades have been defined based on living taxa, and as more fossils are added to phylogenetic datasets, relationships and groupings become more intricate.

Acrodonta consists of two main lineages: the Chamaeleonoidea, comprised of Changjiangosauridae and Chamaeleonidae, and the Dracosauria, comprised of Uromastyoidea and Agamidae. Changjiangosaurids represent one of the principal novelties of this dataset. None of these fossil species have ever been assessed before in a phylogenetic framework. In my results, they are recovered as the sister-clade to chamaeleonids (Figs. 5.1-5.2), or alternatively nested as either basal or derived chamaeleonids (Figs. 5.3-5.4). In the MP topologies, they are placed as the sister-group to uromastycids (Figs. 5.6-5.7). The TcBI and TmBI results fairly agree in the divergence time estimate for changjiangosaurids, place at 62-64 Ma, slightly after

the K/Pg boundary (Table 5.1; Figs. 5.1-5.2). *Tinosaurus* and *Pseudotinosaurus* are nested with crown chamaeleonids: the former as sister to *Rieppeleon*, and the latter to *Rhampholeon*, two modern species from eastern-central Africa (Fig. 5.1) (Uetz et al. 2020). In the TmBI and UmBI results, both fossil taxa are recovered instead as basal chamaeleonids (Fig. 5.2). The only exception for the positioning of *Tinosaurus* and *Pseudotinosaurus* is offered by the IWMP analysis, where they are nested within Changjiangosauridae (as sister-clade to Uromastycidae: Fig. 5.7).

Relationships among living chamaeleonids vary slightly between the different topologies, with overall agreement between the combined evidence and molecular BI analyses (Figs. 5.1, 5.3, 5.4). In the UgBI topology, *Rhampholeon* is basal to a clade composed of *Furcifer* + (*Bradypodion* + *Trioceros*), separated by a quite long branch with medium posterior probability support (Fig. 5.5). The same long branch in the TcBI analysis is shortened by the addition of *Pseudotinosaurus* (sister-taxon to *Rhampholeon*) but posterior probability values are lower (Fig. 5.1; Appendix 5.6, Fig. A5.1). The appearance of Chamaeleonidae is estimated at 76 Ma based on combined evidence and 54 Ma based on morphology, potentially extending the evolutionary history of modern chamaeleons back to the Late Cretaceous, or at least to the early Eocene (Figs. 5.1-5.2, 5.8).

For the clade Dracosauria, the estimated age ranges from 112 Ma to 119 Ma (late-Early Cretaceous) (Table 5.1). The taxon as defined here is non-monophyletic only in the TmBI topology (Fig. 5.2), while supported in all other analyses. The two fossil taxa *Jeddaherdan* and *Gueragama* are found to be basal Uromastycidae, separated by a fairly long branch from modern *Uromastyx* , corresponding to a time lapse of about 60 My (Fig. 5.1). The same relationships for Uromastycidae are recovered in the calibrate morphological analysis, but the branch separating

Jeddaherdan and *Gueragama* are found as basal Uromastycidae, separated by a fairly long branch from modern *Uromastyx*. In both TcBI and TmBI results though, fairly high posterior probability values support this grouping (Fig. 5.2; Appendix 5.6, Fig. A5.1). Based on these findings, the lineage leading to *Uromastyx* is estimated to have diverged around 98 Ma (TcBI) or 106 Ma (TmBI), with less discrepancy inferred by the two calibrated analyses in comparison to other clades. This would place the origin of Uromastycidae at the beginning of the Late Cretaceous. Combined evidence and molecular BI analyses as well as the MP analyses recover *Leiolepis* as the sister-taxon to uromastycids (Figs. 5.1, 5.5-5.7). However, in the TcBI topology, a fairly long branch separates *Leiolepis* from Uromastycidae, with their branching estimated to have happened around 109 Ma (Fig. 5.1). This may represent a case of the long-branch attraction artefact that tends to affect primarily molecular data and consequently combined datasets (e.g., Bergsten 2005; Philippe et al. 2005; Wiens & Hollingsworth 2000). Generally, both statistical and parsimony methods are shown to be affected by long-branch attraction and increasing taxon sampling seems to be the best strategy to contrast this effect (Bergsten 2005; Brinkmann et al. 2005; Felsenstein 1978; Philippe et al. 2005; Wiens 2005).

In the morphology-only BI analyses (TmBI and UmBI), *Leiolepis* is nested within Agamidae as the sister taxon to *Physignathus* + *Calotes*, but is poorly supported by posterior probability values (Fig. 5.2). In this analysis, *Leiolepis* is the only representative of Leiolepidae – or Leiolepidinae depending on the adopted taxonomic scheme – and increasing the relative taxon sampling in the future may help to break up the long branch and solidify the phylogenetic resolution of the taxa involved. Leiolepidae and Uromastycidae are typically recovered as sister taxa in most previous phylogenetic studies, and traditionally the two modern genera *Uromastyx* and *Leiolepis* have been grouped together either both as Leiolepidinae Fitzinger, 1843 (Frost &

Etheridge 1989; Frost et al. 2001) or as two separate subfamilies (Leiolepidinae and Uromastycinae) (Macey et al. 2000; Schulte et al. 2003). Agamidae in my results consists of all extant taxa, with similar internal relationships as generally recovered by previous phylogenetic studies (e.g., Townsend et al. 2011; Zheng & Wiens 2016) (Fig. 5.1). The family is non-monophyletic only in the MP analyses and there are differences in sister-group relationships when comparing molecular and combined evidence *versus* morphological evidence (see Figs. 5.1-5.5).

Divergence time estimates for Agamidae are quite different between the TcBI, at 98 Ma, and the TmBI analysis, at 34 Ma (Figs. 5.1-5.2; Table 5.1). This discrepancy means that the evolutionary history of this clade may have started in the Early Cretaceous or much more recently in the Eocene, though posterior probability gives low branch support for the morphology-based BI (Fig. 5.2), while fairly robust values are recovered for the combined evidence BI (Appendix 5.6, Fig. A5.1).

5.3.3 Iguaniformes

Iguaniformes (‗Gobiguania s.l.' + Pleurodonta) diverged from other iguanians around 140 Ma (earliest Cretaceous) according to the TcBI analysis, or 114 Ma (late-Early Cretaceous) based on the TmBI analysis (Table 5.1; Figs. 5.1-5.2). In most results, either *Isodontosaurus*, *Isodontosaurus* + *Desertiguana*, or *Polrussia* are recovered as the most basal iguaniforms. In the TcBI and TmBI analyses, *Desertiguana* and *Isodontosaurus* are sister-taxa (Figs. 5.1-5.2). In the TcBI topology, they are separated by two fairly long branches, with divergence time estimated around 119 Ma, so approximately 40 My before their occurrence in the fossil record (70.6–84.9 Ma) (Alifanov 2013; Gao & Norell 2000; Gilmore 1943). *Desertiguana* was never assessed in a

phylogenetic analysis before and it was assigned to the modern family Phrynosomatidae in its original description (Alifanov 2013). *Isodontosaurus* has been interpreted in previous studies as either more acrodontan-like (Conrad 2008; Conrad & Norell 2007) or as having affinities to pleurodontans (Daza et al. 2012; DeMar et al. 2017; Gauthier et al. 2012). Gobiguania *sensu stricto*, as originally defined by Conrad & Norell (2007), is recovered as monophyletic in all analyses performed here (Figs. 5.1-5.4, 5.6-5.7). Other authors have implied the inclusion in Gobiguania of other Mongolian Late Cretaceous taxa such as *Polrussia* and *Isodontosaurus*, a grouping referred to here as Gobiguania *sensu lato* (Daza et al. 2012). ‗Gobiguania s.l.' is non-monophyletic in all results, hence reported in quotation marks. Either *Polrussia* (TmBI: Fig. 5.2; UcBI: Fig. 5.3) or *Isodontosaurus* (UmBI: Fig. 5.4) are recovered as the sister-taxon to Gobiguania s.s. in some topologies, but never together. In the TcBI tree, *Polrussia* is the sister-taxon to Pleurodonta, with a mean divergence age between the two branches estimated to 114 Ma (Aptian, Early Cretaceous) (Fig. 5.1). In the TmBI, *Polrussia* + Gobiguania s.s. represents the sister-clade to all Pleurodonta, with a mean divergence estimate of 108 Ma (Albian, Early Cretaceous) (Fig. 2). This sets the potential origin of Pleurodonta at 92 Ma (Turonian, Late Cretaceous) based on combined evidence, and 71 Ma (Maastrichtian, Late Cretaceous) based on morphological data (Table 5.1). In general, support by posterior probability values for the relationships among crown pleurodontan groups are quite low in the TmBI, UmBI, and UcBI topologies (Figs. 5.2-5.4). Relationships inferred by the TcBI analyses are far better supported (Appendix 5.6, Fig. A5.1). Results for Pleurodonta are mostly in agreement for the TcBI and molecular evidence analyses, with the fossil OTUs *Aciprion* and *Geiseltaliellus* nesting in a clade with Corytophanidae and Crotaphytidae, and with a difference in order of divergence among oplurids (Figs. 5.1-5.2). The MP topologies fail to recover a monophyletic Pleurodonta as

separate from Iguaniformes, due to the nesting of modern *Phrynosoma* and *Anolis* with basal fossil lineages (Figs. 5.6-5.7; Appendix 5.6, Figs. A5.2-A5.3). When removing these two OTUs from the dataset, results of the MP analyses tend to align more closely with the BI results based on morphological evidence, with a basal ‗Gobiguania s.l.' as sister-group to pleurodonts. The combined evidence and molecular BI find three main lineages of iguaniforms: 1) Corytophanidae + Crotaphytidae as the earliest diverging groups; 2) Hoplocercidae + Iguanidae as sister-group to 3) a clade including all other living families (Tropiduridae, Leiosauridae, Opluridae, Polychrotidae, Liolaemidae, Leiocephalidae, Phrynosomatidae).

Virtually, no previous phylogenetic studies agree on the relationships across modern iguaniform clades (Conrad 2008; Daza et al. 2012; Etheridge & de Queiroz 1988; Frost & Etheridge 1989; Frost et al. 2001; Gauthier et al. 2012; Scarpetta 2020; Smith 2009). This is the main reason why new combinations are not proposed for these clades, as was done previously (Daza et al. 2012). The resolution of these relationships remains unstable and at this stage it is undesireable to further complicate the current taxonomic nomenclature (see de Queiroz & Donoghue 2011).

Based on the TcBI results, the Corytophanidae + Crotaphytidae clade is estimated to have diverged from other iguaniforms around 88 Ma (mid-Late Cretaceous), while crown Corytophanidae and crown Crotaphytidae originated respectively around 34 Ma (late Eocene) and 23 Ma (Oligo-Miocene boundary) (Fig. 5.1). The other two main iguaniform lineages branched around 83 Ma (Campanian, Late Cretaceous). Node mean age estimates for the remaining extant iguaniform families are: 23 My for Hoplocercidae, 54 My for Iguanidae, 69 My for Tropiduridae, 26 My for Leiosauridae, 22 My for Opluridae, 63 My for Polychrotidae, 45 My for Liolaemidae, 44 My for Phrynosomatidae (Fig. 5.1).

Aciprion and *Geiseltaliellus* are recovered as stem crotaphytids in the TcBI analysis, but their positions change significantly across all my results, and posterior probability values are low for these OTUs in all the BI topologies. In previous studies, both fossils have been suggested as being closer to Corytophanidae (e.g., Conrad 2015; Smith 2009), however, this placement is not supported in any of the topologies recovered here. *Aciprion* is alternatively basal to the two more derived lineages of iguaniforms (TmBI: Fig. 5.2), to all Pleurodonta (UmBI: Fig. 5.4), or to the lineage including Tropiduridae and Phrynosomatidae (UcBI: Fig. 5.3). *Geiseltaliellus*, if not sister-taxon to crotaphytids (TcBI: Fig. 5.1; TmBI: Fig. 5.2), is found as more closely related to phrynosomatids (UcBI: Fig. 5.3), or sister-taxon to *Polychrus* (UmBI: Fig. 5.4) or *Uta* (EWMP: Fig. 5.6; IWMP: Fig. 5.7).

Hoplocercids are supported as the sister-group to Iguanidae by molecular and combined evidence (Figs. 5.1, 5.3, 5.5), while corytophanids are the sister-clade to iguanids based on morphological data (Figs. 5.2, 5.4, 5.6-5.7). Morphological data supports Hoplocercidae as more deeply nested in the topology, as sister-group to *Stenocercus* (TmBI: Fig. 5.2; MP: Figs. 5.6-5.7) or *Leiocephalus* (Fig. UmBI: Fig. 5.4). Iguanidae is well-supported and monophyletic in every analyses. The only unusual result is represented by the nesting of the fossil *Desertiguana* from the Late Cretaceous of the Gobi Desert within this family of extant New World iguaniforms in the uncalibrated BI analyses based on combined and morphological evidence (Figs. 5.3-5.4). However, the branch supporting this placement of *Desertiguana* has quite low posterior probability in both topologies. In the combined evidence and molecular BI analyses, *Dipsosaurus* represents the earliest diverging iguanid, sister-taxon to all other iguanids (Figs. 5.1, 5.3, 5.5), while in the morphology-based analyses (MP and BI) it forms a basal clade with *Sauromalus* (Figs. 5.6-5.7).

The living and subfossil *Brachylophus* species (*B. fasciatus* and *B. gibbonsi*) from the Fiji-Tonga archipelagos are recovered as sister-taxa in the TcBI and TmBI topologies, and represent the second diverging group of iguanids (Figs. 5.1-5.2). Their relationships have lower resolution in the MP analyses but still in a basal position within the clade (Figs. 5.6-5.7).

In the combined evidence and molecular BI, *Iguana*, *Cyclura*, and *Sauromalus* form one of the more derived clades of iguanids, while the other consists of *Ctenosaura* and the two Galápagos taxa *Amblyrhynchus* and *Conolophus* (Figs. 5.1, 5.3, 5.5). Alternatively, *Sauromalus* is more basal and sister to *Dipsosaurus* based on morphological evidence (Figs. 5.2, 5.4, 5.6-5.7). *Iguana* is either the sister-taxon to *Cyclura* or *Sauromalus*, forming a clade of derived iguanids that branched off around 34 Ma (late Eocene) or 17 Ma (early Miocene) from the *Ctenosaura*-group (Figs. 5.1-5.2). *Ctenosaura* as sister-taxon to *Amblyrhynchus* + *Conolophus* is consistent across all BI topologies (Figs. 5.1-5.5); the MP analyses, instead, support a closer relationship with *Iguana* and *Cyclura* (Figs. 5.6-5.7), however, in these trees relationships among iguanids are overall poorly resolved. *Amblyrhynchus* and *Conolophus* from the Galápagos islands form a monophyletic clade in all the resulting topologies. Based on combined evidence age estimates, the two lineages split around 21 Ma (early Miocene), while based on morphological data the timing is far more recent, about 7.8 Ma (late Miocene)(Figs. 5.1-5.2). The split between *Ctenosaura* and the Galápagos iguanids is estimated at 16 Ma (early Miocene) in the TmBI and 27 Ma (mid-Oligocene) in the TcBI.

All the other extant iguaniform families that are part of the third main lineage, including Tropiduridae, Leiosauridae, Opluridae, Polychrotidae, Liolaemidae, Leiocephalidae, Phrynosomatidae, are recovered as monophyletic based on combined and molecular evidence, with relatively high posterior probability support (Figs. 5.1, 5.3, 5.5; Appendix 5.6, Fig. A5.1); in

contrast, morphology alone results in far less consistency for these relationships and the topologies are overall poorly supported (Figs. 5.2, 5.4, 5.6-5.7; Appendix 5.6, Figs. A5.2-A5.3).

The TcBI, UcBI, and UgBI analyses recover *Stenocercus* as the most basal tropidurid and *Plica* + *Tropidurus* as the most derived, with *Uranoscodon* and *Microlophus* nested in between (Figs. 5.1, 5.3, 5.5). Node age for this clade is estimated around 69 Ma (Maastrichtian, Late Cretaceous). Leiosauridae and Opluridae are sister-groups in the combined evidence and molecular results. Opluridae remains monophyletic in all analyses. *Chalarodon* is the sister-taxon to the clade form by *Oplurus* species in the combined evidence and morphological BI (Figs. 5.1-5.4), while sister-taxon to *O. cyclurus* in the molecular analysis, with *O. cuvieri* as basal branch (Fig. 5.5). This latter reconstruction seems quite inconsistent with previous studies based on larger taxon sampling for oplurids (Vences et al. 2008). Divergence between *Chalarodon* and *Oplurus* is estimated around 22 Ma in the TcBI and 13 Ma in the TmBI (Figs. 5.1-5.2). Leiosaurids, based on the TcBI divergence estimates, appeared around 26 Ma (late Oligocene) and split from oplurids around 65 Ma (earliest Paleocene).

Polychrotidae, here represented by *Anolis* and *Polychrus*, forms the basal branch of a more deeply nested group of iguaniforms, including Liolaemidae, Leiocephalidae, and Phrynosomatidae (Fig. 5.1). The four families diverged from Leiosauridae + Opluridae around 77 Ma (Campanian, Late Cretaceous) and age for polychrotids is estimated at 63 Ma (early Paleocene). Liolaemidae, including here *Liolaemus* and *Phymaturus*, are the sister-group to Leiocephalidae + Phrynosomatidae, with an age estimate of 45 Ma (mid-Eocene) in the TcBI results (Fig. 5.1). *Leiocephalus* is recovered as sister-taxon to Phrynosomatidae in the combined evidence and molecular analyses, and it is the only representative of the family Leiocephalidae in

this dataset (cf. Frost & Etheridge 1989; Frost et al. 2001). Based on morphology, instead, *Leiocephalus* is grouped with *Stenocercus* and Hoplocercidae (Figs. 5.2, 5.4, 5.6-5.7).

For Phrynosomatidae, the TcBI, UcBI, and UgBI topologies recovered similar results to previous authors (Frost & Etheridge 1989; Wiens et al. 2010): Sceloporinae includes *Petrosaurus*, *Sceloporus*, and *Uta*; Phrynosomatinae includes *Phrynosoma*, *Uma*, *Holbrookia*, and *Callisaurus* (Figs. 5.1, 5.3, 5.5). Based on combined evidence node estimates, Phrynosomatidae split around 44 Ma (mid-Eocene) and diverged from other iguaniforms (Leiocephalidae) around 57 Ma (late Paleocene) (Fig. 5.1). *Phrynosoma* is one of the most unstable OTUs in the morphological analyses, likely due to its extremely derived features and convergences with some chamaeleontiforms, in particular priscagamids and modern chamaeleonids (see description of morphological characters in Appendix 5.1 for examples). In the TmBI and MP trees, *Phrynosoma* is recovered as the most basal iguaniform, which in the calibrated analysis results in a fairly long branch and a divergence time estimate of 71 My (Fig. 5.2). The uncalibrated BI based on morphology recovers at least *Phrynosoma* nested with the other members of the subfamily Phrynosomatinae (Fig. 5.4).

One last observation concerning these results is the abundance of long branches for some of the inferred phylogenetic relationships. This is particularly evident in the calibrated analyses (TcBI and TmBI), where the length of the branches can be evaluated also in terms of estimated time interval between nodes (Figs. 5.1-5.2). Only in a few cases do these long branches show poor statistical support (posterior probability), e.g., *Tinosaurus* + *Rieppeleon* and *Rhampholeon* + *Pseudotinosaurus* among chamaeleonids, or *Aciprion* and *Geiseltaliellus* among iguaniforms. Undoubtedly, some of these may well represent examples of long-branch attraction, which is the tendency for OTUs supported by long branches to be clustered together despite not being truly

phylogenetically related (Bergsten 2005; Brinkmann et al. 2005; Philippe et al. 2005; Wiens & Hollingsworth 2000). Further testing after increasing taxon sampling will be required to determine if this is affecting the dataset and to what extent. As shown in both simulation and real-life studies, and for both statistical and parsimony methods, increasing the number of OTUs (especially fossils) can help break up long branches, providing better resolutions and support in phylogenetic results (Bergsten 2005; Brinkmann et al. 2005; Simões et al. 2015; Wiens 2005). Sampling for living non-iguanid iguaniforms is still limited and hopefully in the future these results can be improved by accounting for this shortage.

5.4 Discussions

Based on the new phylogenetic hypothesis presented here, a revised classification of Iguania can be summarized as follows:

Iguania Cope, 1864
- Chamaeleontiformes Conrad, 2008
  - Priscagamidae Borsuk-Białynicka and Moody, 1984
  - Acrodonta Cope, 1864 *sensu* Frost et al. (2001)
    - Chamaeleonoidea Fitzinger, 1826
      - Changjiangosauridae (Hou 1976) *sensu* Alifanov (2009)
      - Chamaeleonidae Rafinesque, 1815 *sensu* Frost & Etheridge (1989)
    - Dracosauria comb. nov.
      - Agamidae Gray, 1827 *sensu* Frost & Etheridge (1989)
        - Hydrosaurinae Kaup, 1828
        - Amphibolurinae Wagler, 1830
        - Agaminae Spix, 1825
        - Draconinae Fitzinger, 1826
      - Uromasyoidea comb. nov.
        - Uromastycidae Theobald, 1868

Leiolepidae (Fitzinger 1843)

Iguaniformes comb. nov.

Gobiguania Conrad & Norell, 2007

Pleurodonta Cope, 1864 *sensu* Frost et al. (2001)

Corytophanidae Fitzinger, 1843

Crotaphytidae Smith and Brodie, 1982

Hoplocercidae Frost and Etheridge, 1989

Iguanidae Oppel, 1811 *sensu* Frost & Etheridge (1989)

Tropiduridae Bell, 1843 *sensu* Frost & Etheridge (1989)

Leiosauridae Frost et al., 2001

Opluridae Moody, 1983

Polychrotidae Fitzinger, 1843 *sensu* Frost & Etheridge (1989)

Liolaemidae Frost and Etheridge, 1989

Leiocephalidae Frost and Etheridge, 1989

Phrynosomatidae Fitzinger, 1843

Sceloporinae Wiens et al., 2010

Phrynosomatinae Wiens et al., 2010

This new phylogenetic analysis of Iguania based on combined evidence provides important insights into the origin and evolution of modern iguanian lineages, and a more complex taxonomic scheme than previously thought. The traditional view of iguanians differentiated in two main groups based on the gross interpretation of dental features (acrodont *versus* pleurodont) is challenged here as being too simplistic. A re-interpretation of these morphological features is necessary in order to clarify important new information on iguanian evolution (see section 5.4.1). The new dataset presented here includes the largest number of fossil species ever sampled before in a phylogeny of Iguania, as well as a sampling of all modern iguanian clades. The inclusion of so many fossil taxa helped break up some of the long branches that potentially affected results in previous analyses, and provides a better picture of the

relationships among the earliest iguanians found in the fossil record (see section 5.4.2). Moreover, the inferred relationships offer new hypotheses for the divergence and biogeographic history of acrodontan chamaeleonids in the Old World (see section 5.4.3), the presence of pleurodontan oplurids in Madagascar (see section 5.4.4), and the colonization of South Pacific islands by pleurodontan iguanids (see section 5.4.5).

5.4.1 The acrodont *versus* pleurodont paradigm in iguanians

Existing vertebrate geometries of tooth implantation can be summarised in three main types: 1) apicolingual, where the growing teeth are set on the lingual side of the jaw wall and attach to its crest and base; 2) apical, where the teeth attach along the top of the jaw; 3) lingual, where the teeth are set along the lingual side of the jaw wall (in so-called ‗sockets'), without attaching to the apex of the jaw but only to its base (Bertin et al. 2018; Owen 1840-1845; Peyer 1968; Tomes 1874). Overall these three conditions correspond to the traditional terms ‗pleurodonty', ‗acrodonty', and ‗thecodonty' respectively, defined and commonly used in the literature long ago (Owen 1840-1845; Peyer 1968; Tomes 1874).

For iguanians, the apparently neat separation into two major lineages based on the gross difference in geometry of tooth implantation has been a paradigm that has affected our understanding of the evolutionary trends and patterns in this diverse group of squamates. The definition of the crown groups Acrodonta and Pleurodonta is a direct expression of this simplified view of iguanian evolution and as the fossil record grows, we face the difficulty of interpreting the new material under this paradigm. However, with recent breakthroughs in our understanding of odontogenesis, tooth development, and modes of implantation in lizards as well as other reptiles, it is increasingly obvious that there are serious limitations to this dichotomous

paradigm of iguanian evolution (Bertin et al. 2018; Buchtová et al. 2013; Budney et al. 2006; Caldwell et al. 2003; Dosedělová et al. 2016; Haridy 2018; LeBlanc et al. 2017; LeBlanc et al. 2020a; LeBlanc et al. 2020b; Maxwell et al. 2011; Zaher & Rieppel 1999; Zahradnicek et al. 2014).

The main difference between most acrodontan and pleurodontan iguanians is in the timing of tooth growth, not strictly in the geometry of tooth implantation. Acrodontans such as agamids (e.g., *Pogona*) grow teeth that attach to the crest and base of the lingual side of the jaw exactly as it happens in pleurodont-type lizards (e.g., Haridy 2018; LeBlanc et al. 2020b). This apicolingual geometry of tooth implantation is shared for instance, between agamids, uromastycids, and all pleurodontan iguanians. In *Pogona*, Haridy (2018) showed how early in ontogeny the teeth are added posteriorly to the tooth row while a mineralized wall grows along the lingual side of the teeth. The teeth at some point get anchored between the jaw wall (on the labial side of the tooth) and the mineralized lingual wall (on the lingual side of the tooth) and cease to be replaced. The addition of the mineralized lingual wall gives the impression that the teeth in these lizards are positioned apically on the jaw, while their development follow the same apicolingual implantation as pleurodont lizards (*Iguana*-type or *Varanus*-type pleurodonty in LeBlanc et al. [2020]). The nature of the mineralized lingual wall present in agamids and other acrodonts, however, is yet to be determined. Haridy (2018) showed how this wall grows on the lingual side of the tooth row, but we still lack information about its composition and relation to the surrounding jaw bone and dental tissues.

Similar to the work done on tooth attachment and implantation for pleurodont-type lizards by LeBlanc et al. (2020), we need histological data that can help us understand this important difference not only between acrodontans and pleurodontans, but also among different

clades within Chamaeleontiformes. Based on this re-assessment, the only acrodontan iguanians with true apical tooth implantation seem to be chamaeleons and, possibly, changjiangosaurids, *Tinosaurus*, and *Pseudotinosaurus*. In chamaeleonids, the developing tooth buds are positioned superficially along the jaw and the tooth bases fuse together to the top of the jaw (Buchtová et al. 2013). This apical position of the teeth is set early in ontogeny and afterwards there is no tooth replacement throughout life. When comparing the studies by Haridy (2018) and Buchtová et al. (2013), it is clear that the lack of tooth replacement in agamids and chamaeleonids is achieved in two very different ways as different are the geometric relationships between their teeth and jaw.

For this study, numerous characters and state descriptors were recoded and recharacterized in order to improve the morphological characters related to jaw and dental features between acrodontan and pleurodontan iguanians. As discussed above, teeth are replaced in both acrodont and pleurodont lizards, but in a different mode and with a very different timing and duration: one-to-one with resorption pits in pleurodonts (which continues throughout life), and at the back of tooth row in acrodonts (which stops early in ontogeny) (Bertin et al. 2018; Haridy 2018; LeBlanc et al. 2020b; Owen 1840-1845; Peyer 1968; Tomes 1874).

For example, Character 197 (Appendix 5.1) concerning the presence or absence of resorption pits accounts for one of the main differences between acrodonts and pleurodonts (as tooth implantation types and not taxonomic groups). Acrodonts typically have no resorption pits because their teeth are added posteriorly to the tooth row, and this process ceases early in ontogeny (Haridy 2018). Pleurodont lizards instead tend to have visible resorption pits and their teeth continue to be replaced throughout life (e.g., Bertin et al. 2018; LeBlanc et al. 2020b; Owen 1840-1845; Peyer 1968; Tomes 1874).

Another important morphological difference between acrodontan and pleurodontan iguanians is in the different shape of the teeth (Character 199, Appendix 5.1). In pleurodontans as much as in other pleurodont lizards, the teeth tend to be strongly asymmetrical, with the labial side of the tooth being much shorter and not extending below the level of the crown that attaches to the apex of the jaw (see LeBlanc et al. 2020). This is because the tooth pulp cavity opens lingually in pleurodont-type teeth to a greater (*Iguana*-type pleurodonty) or lesser (*Varanus*-type pleurodonty) degree. Therefore the root of the tooth in pleurodonts lacks a dentine labial wall, which results in the typical asymmetrical shape of the overall tooth. In acrodonts by comparison, the teeth are fairly symmetrical and overall shorter than typical pleurodonts. The labial side of the tooth is still slightly shorter than the lingual side, but never to the extent seen in pleurodont teeth. In terms of tooth shape, acrodontan iguanians like *Uromastyx* are more pleurodont-like in having asymmetrical teeth (typical of pleurodontans) coupled with apicolingual implantation (all pleurodontans and all acrodontans except for chamaeleonoids), and a tall subdental shelf (typical of acrodontans).

In conclusion, the more we learn about dental attachment and implantation across the different iguanian groups, the more it becomes obvious that their differences cannot be categorized into two distinct categories, nor can characters for phylogenetic analyses be sensibly constructed around this false dichotomy. This picture has been too simplistic for too long and thus the complexity of the evolutionary patterns in iguanians have remained largely overlooked. By adding and re-interpreting some morphological characters commonly used in squamate phylogeny, character conceptualizations and recodings shifted the focus from an overall condition (pleurodont *versus* acrodont) to the single features that contribute to create such

conditions, which clearly vary and combine in variable ways across the different iguanian lineages.

5.4.2 The Cretaceous faunas of Laurasia and Gondwana and the early radiation of iguanians

Reconstructing the origins of iguanians based on the current fossil record and phylogenetic inference is quite complex. By the time we have enough evidence of their occurrence in the fossil record, their diversity and paleogeographic distribution are so vast that we are forced to assume a much earlier age for their origin.

The Late Cretaceous Gobi Desert fauna is generally recovered at the stem of the radiation of the two major iguanian lineages: Chamaeleontiformes and Iguaniformes. With the inclusion of several more taxa in this new dataset than in previous studies, it is clear that the diversity of this fauna seems to encompass the incipient evolutionary history of all modern iguanian clades. Most Gobi Desert taxa have unambiguous affinities to chamaeleonids, agamids, uromastycids, or iguaniforms, leading to the current interpretation of Priscagamidae and Gobiguania respectively as stem Chamaeleontiformes and Iguaniformes (Conrad 2008; Conrad & Norell 2007; Daza et al. 2012; Gauthier et al. 2012; Simões et al. 2015). The abundance of fossils from the Gobi Desert deposits provide solid evidence of a rich iguanian presence in south-eastern Laurasia by the Late Cretaceous (Alifanov 1989; Alifanov 1993b; Alifanov 2000; Alifanov 2013; Borsuk-Bialynicka 1996; Borsuk-Bialynicka & Alifanov 1991; Borsuk-Bialynicka & Moody 1984; Conrad & Norell 2007; Gao & Norell 2000; Gao & Hou 1995; Gilmore 1943). However, the presence of Late Cretaceous iguanians has also been reported from western Laurasia and Gondwana (Apesteguía et al. 2005; Apesteguia et al. 2016; DeMar et al. 2017; Estes & Price 1973; Gao & Fox 1996;

Gilmore 1928; Nava & Martinelli 2011; Simões et al. 2015). All these Late Cretaceous occurrences demonstrate that iguanians were well distributed across both Laurasia and Gondwana at that time, and their evolutionary history began earlier than has been previously predicted.

The large number of taxa reconstructed as Priscagamidae offers a better picture of the diversity of this group. With the nesting of *Arretosaurus* among priscagamids, the age of this clade is extended to the late Paleogene, well beyond the K/Pg mass. More on the potential affinities of *Arretosaurus* can be found in the next section. In my new phylogenetic hypothesis, two main clades of priscagamids are recovered: one including *Priscagama*, *Pleurodontagama*, and the Paleogene *Arretosaurus*, as sister-group to the second clade including *Chamaeleognathus*, *Morunasius*, *Gladidenagama*, and *Phrynosomimus* (Fig. 5.1). The two *Mimeosaurus* species form the basal branch, while *Flaviagama* is nested in the middle.

The validity of some of these taxa has been questioned in the past. Previous authors have excluded some of these fossil species a priori in their analyses, dismissing them as synonyms of earlier defined taxa. Conrad (2008) and Gao & Norell (2000) included *Chamaeleognathus* and *Pleurodontagama* in *Priscagama* without providing much evidence. Based on personal analysis of the material, I agree that *Pleurodontagama* specimens show important similarities to *Priscagama* and are generally less well-preserved, while *Chamaeleognathus*, which consists of a fairly complete and three-dimensional skull, has noticeable differences from *Priscagama* (some of these features are discussed in the description of the morphological characters provided in Appendix 5.1). *Gladidenagama* was also dismissed as a valid taxon and synonymized with *Mimeosaurus crassus* by Conrad (2008), but again without providing specific reasons or actually analysing the material in person. If anything, *Gladidenagama* resembles instead *Phrynosomimus*

quite closely and differences between the two are mostly taphonomic, due to the more fragmentary nature of the holotype of *Gladidenagama*. Gao & Hou (1995) argued that M. *tugrikinensis* represents a junior synonym of *M. crassus*, as Alifanov (1989) did not provide any distinguishing feature for the new species. There are certainly issues with the validity of these taxa: the holotype (AMNH 6655) of *M. crassus* is represented by a maxilla and the referred material (ZPAL MgR II-73) is a partial mandible; *M. tugrikinensis* is represented by a few more cranial elements, including two maxillae, a partial mandible, circumorbital and temporal bones, and a quadrate. When the holotype is based on a single bone, it is hard to support the attribution of different isolated elements to the same taxon. Such assignments should be treated with great caution. Based on personal examination of all the material, I find the maxilla of *M. tugrikinensis* to be much more slender and elongate, and with a more prominent supradental shelf than that of *M. crassus*. The teeth are more heavily weathered in *M. crassus* than they are in *M. tugrikinensis*, and there is no significant variation in size between the two elements; no resorption pits are visible in *M. crassus*, while they are evident for multiple teeth in *M. tugrikinensis*. I believe that a redescription of the two taxa will be necessary before drawing any conclusions, but until then *M. tugrikinensis* should be treated as a valid taxon. The same approach should be apply to all currently known priscagamids; it is possible that eventually some of these taxa will be discarded as junior synonyms of other taxa, but that must wait until all the specimens are properly re-assessed.

Another highly debated taxon from the Gobi fauna is *Isodontosaurus*, described by Gilmore (1943) as an anguid lizard and only later re-assigned to Iguania (Alifanov 1989; Conrad 2008; Gao & Norell 2000; McDowell & Bogert 1954). In the results presented here, *Isodontosaurus* is recovered as a basal member of Iguaniformes and is not related to

Chamaeleontiformes as suggested by Conrad (2008). The teeth in *Isodontosaurus* have similarities with taxa like *Jeddhardhan* and *Gueragama* but more numerous cranial features are shared for instance with *Ctenomastax* and *Saichangurvel*, and gobiguanians in general (see Appendix 5.1).

Reports of the earliest presumed iguanians can be found both from Laurasia and Gondwana (Datta & Ray 2006; Evans et al. 2002; Li et al. 2007). However, the identification of some of these fossils is quite ambiguous and should be treated with caution. The affinities of the Early Cretaceous taxon *Xianglong* from China (Li et al. 2007), as much as those of *Bharatagama* (Evans et al. 2002) from the Early-Middle Jurassic and *Tikiguana* (Datta & Ray 2006) from the Late Triassic of India, will remain dubious without a re-description of the material. *Bharatagama* was already dismissed as an iguanian by previous authors, and I generally agree with its re-attribution to sphenodontians (Jones et al. 2013). The age of *Tikiguana* was likely the result of more recent sediments (Neogene-Quaternary) encrusting Triassic rocks in the deposit where the specimen was uncovered (Hutchinson et al. 2012). For *Xianglong* there is simply not enough evidence provided in its original description to support its interpretation as an acrodontan (Li et al. 2007). Its specialized morphology as a glider and all the comparisons to the modern agamid genus *Draco* are much more likely the result of convergence rather than homology. Skull anatomy is mostly obliterated and a thorough revision of the material will be necessary before considering its taxonomic assignment as valid.

Huehuecuetzpalli from the Early Cretaceous of Mexico has been suggested as a potential iguanomorph, based on few shared derived feature such as the reduction of the postfrontal and the presence of a dorsal squamosal process (Conrad 2008; Daza et al. 2012; Evans 2003;

Gauthier et al. 2012; Reynoso 1998). However, the phylogenetic position of this taxon as a stem squamate has been revised by Simões et al. (2018), and I fully support that reassessment.

In this dataset, the oldest iguanian is represented by the uromastycid *Jeddaherdan* from the Cenomanian of North Africa (Apesteguia et al. 2016). Another fragmentary iguanian with iguaniform affinities is reported from Cenomanian-Turonian deposits of Patagonia (Apesteguía et al. 2005). In my opinion, these two latter records are the most reliable earliest iguanians described to date. The age of *Jeddaherdan* and the Patagonian iguaniform is at least 10 My older than the Cretaceous Gobi fauna of Laurasia, giving to Gondwana the record of the earliest occurrence of iguanians thus far.

In the end, the richness and diversity of the fossil fauna from the Gobi Desert (southern Laurasia), the presence of fossil iguanians in western Laurasia, and several records across Gondwana, provide evidence that iguanians were widespread across the globe by the Late Cretaceous (Alifanov 1993b; Alifanov 2000; Apesteguia et al. 2016; Evans 2003; Gao & Norell 2000; Gao & Fox 1996; Gao & Hou 1995; Simões et al. 2017a; Simões et al. 2015). This strongly support an earlier origin than the Late Cretaceous for Iguania, as inferred by most time-calibrated phylogenies (Burbrink et al. 2020; Irisarri et al. 2017; Pyron 2017; Simões et al. 2020; this study). The origin and radiation of iguanians may be more recent than the break-up of Pangaea in the Middle Jurassic, but likely happened when the two supercontinents Laurasia and Gondwana were still close enough to allow for faunal exchanges, and undoubtedly before their fragmentation in the Early Cretaceous (Chatterjee & Scotese 2007; Chatterjee & Scotese 2010; Evans 2003). The radiation would have been characterized by some degree of dispersal across both Laurasia and Gondwana at its initial stages (Jurassic/Cretaceous boundary), while subsequently driven by vicariance by the Early Cretaceous.

5.4.3 New insights into the origins of modern chamaeleons

The monophyly of chamaeleons as well as the sister-relationships between the principle modern lineages of acrodontans (chamaeleonids, uromastycids, and agamids) is well-established and supported by numerous phylogenetic studies (Conrad 2008; Daza et al. 2012; Estes et al. 1988; Frost & Etheridge 1989; Frost et al. 2001; Gauthier et al. 2012; Macey et al. 1997; Reeder et al. 2015; Tolley et al. 2013; Townsend et al. 2011; Wiens et al. 2012; this study). The origins of the group, however, remain largely unresolved due to their scarce and highly fragmentary fossil record. Based on molecular data, the biogeographic history of chamaeleons is inferred to have started in Africa (Tolley et al. 2013). This result of course is heavily affected by the modern distribution of chamaeleonids, which are abundant all across Africa and Madagascar. Moreover, the earliest definitive fossils of chamaeleonids are reported from Miocene-age deposits in Europe and Africa (Bolet & Evans 2013; Dollion et al. 2015; Georgalis et al. 2016; Hillenius 1978a; Hillenius 1978b; Rieppel et al. 1992). The identification of some Paleocene taxa from China described by Hou (1976) as chamaeleonids was mostly dismissed by other authors (Bolet & Evans 2013; Dong et al. 2016).

A reassessment of the material from China will be necessary to determine its status, but my re-interpretation of the specimens attributed to Changjiangosauridae by Alifanov (2009) tend to support the sister-relationships of the members of this clade to chamaeleonids (Figs. 5.1-5.4), at least based on the Bayesian inference results. All my analyses support the nesting of Changjiangosauridae within crown Acrodonta. In the TcBI topology, changjiangosaurids are in the sister-group to chamaeleonids (Fig. 5.1). Chamaeleonoidea is redefined here as the clade including Chamaeleonidae + Changjiangosauridae. (Gauthier et al. 2012) used Chamaeleonoidea for the combination Agaminae + Chamaeleonidae, however, their analysis was quite limited in

taxon sampling for those clades and changjiangosaurids were not included. The dentition in changjiangosaurids is quite peculiar. Not only do they display a true apical implantation of the teeth along the jaw, but some of them also have unusually tall crowns that rise above the top of the jaw (e.g., *Khaichinsaurus*). Changjiangosaurid specimens are represented mostly by jaw material, though they are quite complete and well-preserved. Apart from the apical teeth and lack of resorption pits, other features such as the expanded coronoid process of the dentary and the tall subdental shelf would suggest affinities to uromastycids, like *Jeddhardan* and the modern genus *Uromastyx*. In the morphology-only analyses under both MP and BI, uromastycids form a clade with Chamaeleonoidea instead of agamids, and changjiangosaurids are nested with chamaeleonids in all BI topologies but not in the MP results.

The new phylogenetic hypothesis presented here weakens the scenario of an African origin for chamaeleons based on the fossil record. Either changjiangosaurids (based on Bayesian inference) or some priscagamids (based on parsimony) are recovered to be closely related to chamaeleonids in my analyses. I see evidence of strong affinities between modern chamaeleons and priscagamids like *Chamaeleognathus* and *Arretosaurus*. *Chamaeleognathus* displays incipient elongation of the supraoccipital mid-sagittal crest to contact the parietal posteroventral wall, fused vomers, and a relative reduction of the basicranial elements, all of which are features that contradistinguish and become more extreme in living chamaeleons. *Arretosaurus* is less well-preserved and some features remain hard to compare, but the extreme reduction of the quadrate tympanic conch, lack of a retroarticular process, and even shortening of the metacarpals are similarities shared with chamaeleons (see also Appendix 5.1). Overall, *Arretosaurus* has numerous features that suggest affinities to chamaeleonids; however, whether these features represent convergences or homologies will need further investigation. In my analyses, the taxon

is consistently recovered with priscagamids, extending the survival of this Cretaceous lineage up to the middle Eocene – lower Oligocene (Gilmore 1943; Alifanov 1993). Conrad (2008) supported a relationship between *Arreotosaurus* and Priscagamidae, while Alifanov (1993) assigned it to Phrynosomatidae, though without performing a phylogenetic analysis. A thorough redescription of the taxon is much needed at this point in order to shed light on some of its morphological features. My scorings of *Arreotosaurus* are based on direct observation of the material, which is partially in disagreement with both the original description by Gilmore (1943) and the interpretation in Conrad (2008).

Some of the similarities I emphasized between changjiangosaurids and modern chamaeleonids were already noted by Hou (1976) in his description of *Anqingosaurus brevicephalus* and *Changjiangosaurus huananensis*. The strongest support for the close relationship between changjiangosaurids and chamaeleonids is in the shared jaw features, and particularly in the geometry of the tooth implantation, as discussed above. The same is applicable to the affinity between *Tinosaurus* and *Pseudotinosaurus* to chamaeleonids, which in this case results in the inclusion of the two fossil taxa in crown Chamaeleonidae (Figs. 5.1-5.4, 5.6). The divergence time for crown chamaeleonids is estimated to be about 76 Ma in the TcBI analysis and 54 Ma in the TmBi topology, while the splitting of chamaeleonoids (chagjiangosaurids + chamaeleonids) goes back to about 109 Ma and 88 Ma respectively, setting overall the origins of the total clade to the Late Cretaceous.

Despite the fact that some of the sister-relationships recovered in my analysis need further corroboration upon much needed redescription of the fossil material, there is a strong hint for pinning the beginning of the evolutionary history of chamaeleons in the Late Cretaceous – early Paleogene fauna of the Gobi Desert, favouring south-eastern Laurasia as a centre of origin

and dispersal for this group rather than Africa as previously suggested (Georgalis et al. 2016; Tolley et al. 2013). The lack of both extant and fossil chamaeleonids from modern India also supports this interpretation. There is only a putative chamaeleon reported so far from Miocene deposits of India (Sankhyan & Čerňanský 2016). However, the material is fragmentary and not diagnostic. The Indian Plate broke away from the rest of East Gondwana in the Early Cretaceous and separated from Madagascar around 90 Ma to collide with the Asian Plate later in the Eocene (Chatterjee & Scotese 2007; Chatterjee & Scotese 2010). For the ancestor of chamaeleonids to have arrived via vicariance from East Gondwana, we would need fossil evidence of a Mid-Late Cretaceous age from India, Madagascar, or Africa. Based on current knowledge, we simply do not have such evidence and it is more likely that chamaeleonids originated in Asia, based on their ties to changjiangosaurids and priscagamids, spreading subsequently during the late Paleogene – early Neogene to Europe, Africa, and Madagascar via dispersal. In this framework, most of Africa and Madagascar were colonised approximately when fossil chamaeleonids have already been reported (i.e., Miocene deposits: Bolet & Evans 2013; Dollion et al. 2015; Georgalis et al. 2016; Hillenius 1978a; Hillenius 1978b; Rieppel et al. 1992).

Tinosaurus from the Eocene Bridger Basin deposits of Wyoming represents the only outlier in the current reconstruction of the paleobiogeography of chamaeleonids (Gilmore 1928). My analyses support the original interpretation by Gilmore (1928), which attributed the taxon to Chamaeleonidae, recovering *Tinosaurus* as well as *Pseudotinosaurus* from Mongolia either as stem chamaeleonids or nested in the crown group (Figs. 5.1-5.4, 5.6). This is in contrast with Smith (2011a; 2011b), who re-interpreted the taxon as having closer affinities to the modern genus *Leiolepis*. *Tinosaurus* is known mostly based on fragmentary jaw material, so comparisons are currently limited. The apical implantation of the marginal teeth is the same as modern

chamaeleons and changjiangosaurids. This unique evidence of the presence of a chamaeleontiform in the New World during the Paleogene opens up the possibility that at some point western Laurasia was inhabited not just by iguaniforms, as the modern distribution of taxa and recent fossil material would suggest. Obviously, one possible explanation for the presence of *Tinosaurus* in North America is a faunal exchange via dispersal from Eurasia. This may have happened either through a Beringian land bridge or a trans-Atlantic route (cf. Burbrink & Lawson 2007; Macey et al. 2006). *Tinosaurus* is of a similar age (Eocene) to *Pseudotinosaurus*, *Arretosaurus*, and changjiangosaurids from Gobi. This makes it older than any chamaeleontiform fossil reported from Europe, which are mostly Miocene (e.g., Bolet & Evans 2013; Cernanský 2011; Čerňanský 2010; Georgalis et al. 2016). An arrival of this taxon via a crossing of Beringia would appear more likely in this case, with immigration to North America from eastern Asia, where we already have documented evidence of the presence of a coeval and phylogenetically related fauna. On the other hand, as discussed previously for the Late Cretaceous Mongolian fauna, there is increasing evidence from phylogenetic inference based on combined fossil and molecular data that the radiation of the two main lineages of iguanians (chamaeleontiforms and iguaniforms) started in the Late Jurassic (Burbrink et al. 2020; Irisarri et al. 2017; Pyron 2017; Simões et al. 2018; Simões et al. 2020; this study). Further fragmentation of the super-continents Laurasia and Gondwana is what caused the distribution of the two groups in either part of the globe (iguaniforms in the Americas and chamaeleontiforms in Eurasia, Africa, and Oceania), but their earliest relatives were likely co-existing in the different parts of the fragmenting Pangaean sub-continents. Under these circumstances, ghost taxa of both lineages may have survived without necessarily requiring secondary dispersal events and more recent intercontinental faunal exchanges. More fossil evidence is needed to hypothesize a more accurate

picture of the complex paleobiogeographic history of chamaeleonids. Overall, my new phylogenetic hypothesis and reinterpretation of some key fossil taxa from the Gobi Desert as either chamaeleonids or stem chamaeleonids offers a brand new perspective on our understanding of the origins and paleogeographic history of this group.

5.4.4 Iguaniforms in the land of chamaeleontiforms: the case of the Malagasy oplurids

The affinities of Malagasy oplurids to iguaniforms has never been questioned. Despite their unusual presence in the Old World, unlike any other iguaniform, their taxonomic identity is unambiguous from both a morphological and molecular point of view (e.g., Altmanová et al. 2016; Daza et al. 2012; Estes et al. 1988; Etheridge & de Queiroz 1988; Frost & Etheridge 1989; Macey et al. 1997; Wiens & Hollingsworth 2000; this study). However, there is currently not a straightforward explanation for the presence of iguaniform oplurids in Madagascar. Based on the phylogenetic results presented here, there are two most likely scenarios to discuss: 1) a Gondwanan dispersion via vicariance, with oplurids representing a long-lasting lineage of iguaniforms that diverged from modern South American lineages when the Indian Plate migrated north-eastward; 2) a Laurasian dispersion via dispersal, with oplurids diverging from European iguaniforms in the mid-Cenozoic and colonizing Madagascar more recently.

Gondwanan vicariance hypothesis – The first scenario is supported by the molecular and combined evidence topologies. The TcBI tree estimates the splitting of oplurids from Gondwanan iguaniforms (leiosaurids) at about 60 Ma (Figs. 5.1, 5.6). In this case, oplurids may represent what is left of a long-lasting lineage of iguaniforms that were carried over the Indian Plate after it broke up from western Gondwana to migrate north-east during the Middle-Late Jurassic (Chatterjee & Scotese 2007). It is clear that iguaniforms, as much as chamaeleontiforms,

were already wide spread in the Late Cretaceous, as supported by the numerous fossils of that age found in the Americas and Asia (see discussion above). This also means that the radiation and dispersion of iguanians started long before then and, if the age estimates in this study and other recent phylogenetic analyses are correct, as long ago as 150-160 Ma (Late Jurassic) (Burbrink et al. 2020; Irisarri et al. 2017; Pyron 2017; Simões et al. 2020).

The possibility that iguaniforms were spread across Gondwana similarly to chamaeleontiforms remains an open question, and evidence of their presence is reported in the literature. For example, *Pristiguana brasiliensis* is reported from a Maastrichtian deposit of the Bauru Basin (Estes & Price 1973; Fernandes & Ribeiro 2015). Unfortunately, the holotype is currently lost and its relationship to other iguaniforms remain unresolved. Daza et al. (2012) recovered *Pristiguana* as a basal iguanomorph *incertae sedis*, however, an affinity to teiids rather than iguanians was also recognized in the original description by Estes & Price (1973). Nava & Martinelli (2011) described another taxon from the Upper Cretaceous of the Bauru Basin, *Brasiliguana prudentis*, which they assigned to Iguania *incertae sedis*. The remains are fragmentary and not quite diagnostic, but I generally agree with the authors in their assessment. Less ambiguous is the report of an iguaniform from the Late Cretaceous deposits of Patagonia by Apesteguía et al. (2005). Despite the incompleteness of the material, which is represented by a partial frontal, iguaniform-like features are undeniable, with potential affinities to polychrotids or possibly tropidurids (pers. obs.). Based on these records, we can conclude that it is not unlikely that oplurids may be what is left of an iguaniform radiation in Gondwana, representing a long-lasting vicariant lineage now restricted to Madagascar.

Laurasian dispersal hypothesis – The results of the morphology-only analyses, both MP and BI, hint at another possible scenario (Figs. 5.2, 5.4, 5.6, 5.7). In the TmBI topology, oplurids

are the sister-group to Crotaphytidae, and together with them, they share a common ancestor with *Geiseltaliellus longicaudus*, a fossil species from the Eocene deposits of Germany. Based on this hypothesis, oplurids may have Laurasian origins and colonized Madagascar via dispersal from Europe in the late Paleogene (~Oligocene). At that time (about 30 Ma), Madagascar was already separated from India and closer to Africa and its current geographic position. If oplurids or their closest ancestors reached Madagascar from the north, we would expect the presence of iguaniforms between northeastern Africa or possibly southwestern Asia, but so far there is no fossil record from these regions to support such a hypothesis. There is also no evidence of the potential presence of iguaniforms on the Indian Plate before the separation from Madagascar, as discussed for the previous hypothesis. Fossil iguanians from India are fragmentary and thus far are limited to chamaeleontiforms. *Bharatagama rebbanensis* from Jurassic deposits of India that was originally described as potentially the oldest acrodontan/chamaeleontiform (Evans et al. 2002), it is now considered to be a sphenodontian (Jones et al. 2013), a re-interpretation that I personally find more accurate. If the presence of fossil iguaniforms was to be reported in India or elsewhere in southern Asia or northern Africa, the idea of a colonization of Madagascar via dispersal from the north may gather more support.

Unfortunately, until more data becomes available from the fossil record or the modern biodiversity, how oplurids colonized Madagascar will remain controversial. Based on the current data, both the hypotheses presented here are equally as likely and remain highly debatable. Fossil collection bias is certainly one of the main problems. We lack data from Cretaceous to recent fossil deposits of both Madagascar and Africa that could add important pieces to the disjunct distribution of this group in comparison to all other iguaniforms. There are also difficulties in exploring most areas of Central Africa and Madagascar which may prevent the discovery of

additional modern species. For instance, a new species of *Chalarodon* was just recently reported (Miralles et al. 2015), and several new species of chamaeleons were described from this area in the last decade (Branch & Tolley 2010; Crottini et al. 2012; Glaw et al. 2012). It seems possible that we are missing important information not only about the fossil taxa, but also about the modern distribution and biodiversity of the African and Malagasy iguanian fauna.

5.4.5 The colonization of the Galápagos Islands and the Pacific dispersion of iguanids

To conclude the discussion about the evolutionary and biogeographic history of iguanians around the world, I consider here the colonization of the Galápagos Archipelago and other South Pacific islands by the iguanids. Iguanidae includes the genera *Iguana*, *Dipsosaurus*, *Brachylophus*, *Cyclura*, *Sauromalus*, *Ctenosaura*, *Amblyrhynchus*, *Conolophus* that are distributed across Central and South America, and on several South Pacific islands (Galápagos, Fiji, and Tonga) (Buckley et al. 2016; Etheridge 1982; Frost & Etheridge 1989) (Fig. 5.8). This clade has one of the most disjointed distributions across all iguanians, despite their relatively recent evolutionary history. In the phylogenetic results presented in this study, the age of the clade varies substantially between the combined evidence and morphological-only analyses: 53.47 Ma mean divergence time in the TcBI and 26.88 Ma in the TmBI (Figs. 5.1-5.2; Table 5.1). This makes the reconstruction of a potential scenario for the dispersion of iguanids across the South Pacific quite difficult to trace, as both the geological history of the islands they inhabit and the plate tectonics varies substantially between 26 Ma (mid-Oligocene) and 53 Ma (early Eocene).

The oldest occurrence of a fossil iguanid is documented from the Miocene deposits (11.6-16.5 Ma) of New Mexico (Norell & de Queiroz 1991). *Armandisaurus explorator* Norell & de

Queiroz, 1991 was a small-sized iguana, recovered as sister taxon to *Dipsosaurus*. Unfortunately, the holotype and only specimen is currently lost, which prevented the inclusion of the taxon into my phylogenetic dataset. Its age is well within the estimates for Iguanidae in this and previous studies, and its locality is consistent with the modern range of distribution of most iguanids. Aside from *Armandisaurus*, the only other two fossil/subfossil iguanids were found in archaeological sites of late Quaternary age in Fiji (*Lapitiguana impensa*) and Tonga (*Brachylophus fasciatus*) (Pregill & Steadman 2004; Pregill & Worthy 2003). The uncalibrated combined and morphological analyses recover the Late Cretaceous iguaniform *Desertiguana* nested with Iguanidae, either at the stem or as sister-taxon to *Brachylophus* (Figs. 5.3-5.4). As interesting as this interpretation could be, this result is likely affected by homoplasy coupled with the incomplete nature of the holotype and only specimen of *Desertiguana*, which is represented by a broken mandible (Alifanov 2013). *Desertiguana* shares with iguanids features such as the apicolingual implantation of the marginal teeth, flaring tooth crowns, and the anterior opening of the Meckelian canal, all variably present across Iguaniformes in general. These features characterize for instance most Cretaceous gobiguanians and *Isodontosaurus*, to which *Desertiguana* is more closely related in most of the results (Figs. 5.1-5.2, 5.6-5.7).

Short-distance hopping hypothesis from the Caribbean to the ancestral Galápagos – Based on the current distribution and phylogenetic relationships of iguanids, combined with plate tectonic reconstructions, the Caribbean Plate is a likely centre of radiation for the Galápagos iguanids, *Amblyrhynchus* (marine iguana) and *Conolophus* (land iguana). The two taxa are persistently recovered as sister-groups hre and in previous studies (e.g., de Queiroz 1987; Etheridge & de Queiroz 1988; Miralles et al. 2017; Rassmann 1997; Rassmann et al. 1997b; Wiens & Hollingsworth 2000). Moreover, episodes of hybridization between male individuals of

the Galápagos marine iguana *Amblyrhynchus cristatus* and females of the Galápagos land iguana *Conolophus subcristatus* are still reported to occur, with the hybrids pursuing a marine iguana lifestyle (Rassmann et al. 1997b). For the last 5 My, the geological history of the islands has been characterized by variations in the number of emerged islands and intermittent connections between islands mostly related to sea level changes associated with the glacial-interglacial cycles (Geist et al. 2014). For instance, during the last glacio-eustatic variation, sea level dropped to approximately 120 m below the current level (Fairbanks 1989); the Galápagos platform extends for 900 m below the sea level, so larger areas would be exposed with such a sea level decrease (Glynn & Wellington 1983). The presence of larger islands and land bridges between islands would have favoured dispersal via land until disruption by a new sea level rise, creating the perfect conditions for allopatric speciation between the three modern species of land iguana (*C. subcristatus*, *C. pallidus*, *C. marthae*) (Bowman et al. 1983; Gentile et al. 2009; Gentile & Snell 2009; Harpp et al. 2014; Higgins 1978; MacLeod et al. 2015; Rassmann et al. 1997b). The habitat of the marine iguana also appears to have been affected by these cycles combined with the increased distances between islands, causing an incipient divergence between different populations of *Amblyrhynchus*, with 7 subspecies identified thus far (Miralles et al. 2017).

Previous analyses based on morphology, recovered either *Sauromalus* (Norell & de Queiroz 1991) or *Iguana* (Etheridge & de Queiroz 1988) as sister-taxon to *Amblyrhynchus* + *Conolophus*, while the results presented here agree with molecular and combined evidence phylogenies in identifying *Ctenosaura* as sharing a most recent common ancestor with the Galápagos taxa (Wiens & Hollingsworth 2000). A discussion concerning morphological comparisons among iguanids can be found in Chapter 2, where I provide a detail description of the marine iguana cranial anatomy. *Ctenosaura* species are found in several parts of Central

America, such as Mexico and the Caribbean islands (Myers et al. 2021). Based on the calibrated analyses, *Amblyrhynchus* + *Conolophus* diverged from their common ancestor with *Ctenosaura* around 15.9 Ma (TmBI: Fig. 5.2) or 26.7 Ma (TcBI: Fig. 5.1), corresponding to the late Oligocene – early Miocene.

The Galápagos volcanic arch is located on the Nazca plate, which is currently drifting away from both the Coco Plate (north) and the Pacific Plate (west), and subducting under the South America Plate (east) (Cox 1983; Eardley 1954; Geist 1996; Holden & Dietz 1972; Kelley et al. 2019; Morgan 1971; Searle & Francheteau 1986; Wyles & Sarich 1983). The modern islands are not older than 5 My, but the Galápagos Hotspot has been active since 80-90 Ma (Late Cretaceous), and older islands (19-20 My) have been discovered at the bottom of the seafloor off of the coasts of Costa Rica (Christie et al. 1992; Geist 1996; Grehan 2001; Neall & Trewick 2008; Werner et al. 1999). Slightly older islands (9-11 My) than those currently emergent are found instead closer to the Ecuadorian coasts, supporting a shift in the drifting direction of plate movements (Christie et al. 1992; Geist et al. 2014). During the range of activity of the hotspot, new Galápagos islands emerged and sank continuously, at first migrating north-east (towards the Caribbean plate) and then, after the Farallon Plate split into the Cocos and Nazca Plates around 25 Ma, the sinking islands started drifting east due to the subduction of Nazca under the South American Plate (Duncan & Hargraves 1984; Grehan 2001; Kelley et al. 2019; Neall & Trewick 2008; Orellana-Rovirosa & Richards 2018). Previous studies also support the existence of larger Galápagos Islands between the latest Cretaceous and into the Eocene, suggested by both geological and biological evidence, which may have favoured the evolution and radiation of species across the archipelago as a result of the island effect (Croizat 1952; Croizat 1958; Grehan 2001; MacArthur & Wilson 1967). Older Galápagos islands that were emerged around 20-25 Ma

were much closer to the Caribbean area and about to change drifting direction (from north-east to east) as a consequence of the break-up of the Farallon Plate (Duncan & Hargraves 1984; Grehan 2001; Neall & Trewick 2008).

It seems possible that it is during this time that the islands were colonised by the iguanids, which then continued evolving on the emerging islands through a series of ~~"s~~hort-distance hopping" dispersal events. This timing fits much better with the estimated divergence time of *Amblyrhynchus* and *Conolophus* from their common ancestor with *Ctenosaura* than the age of the modern islands (5 My). An older evolutionary age of the Galápagos iguanas in comparison to the age of the islands has been recovered also in previous studies (Rassmann 1997; Wyles & Sarich 1983), and in general marine iguanas show little genetic divergence and a fairly old evolutionary age based on both nuclear and mitochondrial evidence (Rassmann et al. 1997a). In my results, the divergence between *Amblyrhynchus* and *Conolophus* varies between 21.1 Ma in the TcBI analysis and 7.7 Ma in the TmBI analysis.

These age numbers are in disagreement with a more recent study by (MacLeod et al. 2015), where the splitting between *Amblyrhynchus* and *Conolophus* is estimated to 3.18-5.85 Ma; however, their calibration of the phylogenetic analysis is based on molecular-clocks and the age of the modern islands, while morphological data are represented only by measurements and scale counts. When constraints derived from the modern age of the Galápagos are removed, time estimates tend to be longer (Rassmann 1997; Rassmann et al. 1997a; Rassmann et al. 1997b). It is important to acknowledge that the tip-dating calibration implemented here is known to often estimate older node ages and these divergence times may be similarly exaggerated (Arcila et al. 2015; O'Reilly et al. 2015).

A slightly younger age for the divergence between the Galápagos iguanids and other iguanids, around for instance 10 Ma as suggested by previous studies (Rassmann et al. 1997a), would place the volcanic islands much closer to their current position, thus increasing the distance to cover for faunal exchanges with the mainland. At that time, the Nazca Plate had already started the subduction under the South American plate, and sinking islands were migrating east, as demonstrated by the presence of seamounts close to the coasts of Ecuador (Christie et al. 1992; Geist 1996; Geist et al. 2014). I find more compelling a scenario that takes into account simultaneously the evolutionary relationships among iguanids (*Ctenosaura* from the Caribbean-Central America more closely related to *Amblyrhynchus* + *Conolophus* than any other iguanids), the geological history of the Galápagos Hotspot, plate movements, and calibration using fossil evidence. A short-distance oceanic dispersal couple with short-distance island hopping by the ancestor of the Galápagos iguanids from the Caribbean area around 15-20 Ma (see Censky et al. 1998; Lawrence 1998), with some degree of vicariance due to plate movements, can explain the colonization of this archipelago without the need for invoking long-distance passive rafting dispersal events from South America as have been proposed in the past (Bartholomew 1987; Rassmann et al. 1997a). Iguanids, aside from *Dipsosaurus* and *Brachylophus*, are fairly large animals and a long-distance rafting on logs and debris seems more unlikely. Moreover, I showed how when trying to match the timing of divergence between Galápagos and American mainland iguanas, the distances become far less than what they are today, and the chances of a faunal migration become easier to explain (cf. Noonan & Sites Jr 2009).

Iguanids in Melanesia and Polynesia – Members of the Iguanidae are also found on several islands surrounding the Fiji and Tonga archipelagos, well-isolated from all other taxa of

the family (Buckley et al. 2016; Frost & Etheridge 1989; Gibbons 1981). *Brachylophus* is the only modern genus and includes four living (*B. fasciatus*, *B. bulabula*, *B. vitiensis*, *B. gau*) and one fossil (*B. gibbonsi*) species (Fisher et al. 2017; Gibbons 1981; Keogh et al. 2008; Pregill & Steadman 2004). Another fossil taxon, *Lapitiguana impensa*, was described from late Quaternary deposits of Fiji (Pregill & Worthy 2003). Both fossil taxa, *B. gibbonsi* and *Lapitiguana*, are interpreted as giant forms, since all modern *Brachylophus* species are much smaller in size (Pregill & Steadman 2004; Pregill & Worthy 2003).

It is a mystery as to when iguanids actually arrived in Fiji-Tonga. The size of the fossil forms is similar to that of modern adults of *Cyclura* or *Iguana* and, if invasion of Melanesia and Polynesia is fairly recent, both fossil species may have been closer in size to the original colonizer, with living *Brachylophus* being a product of island dwarfism (MacArthur & Wilson 1967). Most modern iguanids are fairly large, except for *Dipsosaurus* and *Brachylophus*. However, these two taxa are persistently recovered as the most basal iguanids, suggesting that smaller size is likely the ancestral condition for this group. The size of the Miocene-age *Armandisaurus* also supports this interpretation (Norell & de Queiroz 1991). Moreover, iguanids share a common ancestor either with hoplocercids (combined and molecular evidence) or corytophanids (morphological evidence) and both groups never grow larger than 20 cm snout-vent length (Myers et al. 2021). This corresponds to approximately the average size of a hatchling green iguana (*Iguana iguana*) that can grow up to 2 meters total length (Alberts et al. 2004; Myers et al. 2021; Oldham & Smith 1975). Increased size appears to be a more derived trait for Iguanidae based on current phylogenetic reconstructions.

How iguanids ended up inhabiting the Melanesian and Polynesian archipelagos is even more complex to explain than the already difficult case of the Galápagos iguanids. Based on the

inferred phylogenetic relationships and divergence time estimates, it remains difficult to find a reasonable explanation without assuming either a long-lasting persistence of an ancestral iguanid lineage in the area – similarly to the Gondwanan vicariance hypothesis presented for oplurids – or a more recent human-mediated dispersal. In all recovered topologies, *Brachylophus* is the second earliest diverging iguanid (after *Dipsosaurus*), branching either around 21.4 Ma (early Miocene) (TmBI: Fig. 5.2) or 47.8 Ma (early Eocene) (TcBI: Fig. 5.1). This contrast between divergence time estimates makes it difficult to narrow down the arrival of iguanids to Fiji-Tonga, assuming modest accuracy in the recovered phylogenies.

Tonga is part of the Tonga–Kermadec volcanic arc which has been active since at least 45 Ma (Neall & Trewick 2008). The Fiji platform is part of the Australian Plate and close to the Australian–Pacific Plate boundary. Both volcanic islands and atolls are part of the archipelago and the oldest known rocks are dated to the Late Eocene (Begg & Gray 2002; Neall & Trewick 2008). Based on this timing, at no point during their documented geological history do these islands seem to have been close enough to any American plates to hypothesize a reasonable oceanic dispersal event. Dispersal across the Fiji-Tonga Archipelago has thus been hypothesized to be fairly recent and most likely human-mediated (Pregill & Steadman 2004). There are records in the literature of local iguanas being used as food sources by the first human settlers and remains of both fossil Fiji-Tongan iguanids are found in archaeological sites (Pregill & Steadman 2004; Pregill & Worthy 2003). Noonan & Sites Jr (2009) put forward a different idea, that in fact iguanas may have been present in the past all across the Pacific. This is supported for instance by the unusually long evolutionary ages for modern iguanid lineages, in addition to the disrupted biogeographic distribution (Keogh et al. 2008; Macey et al. 1997; Noonan & Sites Jr 2009; Rassmann 1997; Rassmann et al. 1997a; Townsend et al. 2011). The disappearance of

iguanids on most of the modern Melanesian and Polynesian islands, as well as northern Pacific island (e.g., Hawaii) would be due to human colonization, as proved for some Fiji-Tongan islands (Pregill & Steadman 2004; Pregill & Worthy 2003). The tectonics of the Pacific Plate is of course intricate enough to assume that a series of island volcanic arcs have existed and disappeared since the earliest opening of the Pacific Ocean began, around 180-200 Ma when Pangaea broke up (Scotese 2001; Shields 1979).

Plausible or not, this suggests a scenario similar to the Caribbean-Galápagos hopping hypothesis presented above, but extending over a much longer time period. It is unlikely that fossil evidence will provide insights as materials older than the Quaternary are unlikely to be found on any of the modern Pacific islands due to the volcanic nature of the rocks, which in general have a lower potential for fossil preservation. Still, the only element that could add new insights to our understanding of the paleobiogeographic history of the Pacific iguanids lies with new fossil collections. These potential new data would corroborate or falsify Noonan & Sites Jr (2009) hypothesis that the mosaic distribution of Iguanidae today is a reflection of a much more diverse and widespread iguanid assemblage that existed possibly since the Paleogene.

Table 5.1 Age estimates of main clades obtained from the TcBI and TmBI analyses.

Clade	TcBI age (Ma)			TmBI age (Ma)		
	Max	**Mean**	**Min**	**Max**	**Mean**	**Min**
Iguania	169.85	164.95	160.05	133.96	130.09	126.23
Chamaeleontiformes	152.69	148.28	143.88	126.81	123.15	119.49
Priscagamidae	145.51	141.31	137.12	121.27	117.77	114.27
Acrodonta	129.52	125.78	122.05	123.54	119.98	116.42
Chamaeleonoidea	112.3	109.06	105.82	90.62	88.01	85.39
Changjiangosauridae	66.07	64.16	62.26	64.09	62.24	60.4
Chamaeleonidae	78.62	76.35	74.09	55.74	54.13	52.52
Dracosauria	119.08	115.64	112.21	-	-	-
Uromastyoidea	112.66	109.41	106.16	-	-	-
Agamidae	100.66	97.76	94.86	35.41	34.39	33.37
Iguaniformes	143.82	139.67	135.52	117.53	114.14	110.75
Gobiguania s.s.	99.66	96.79	93.91	99.72	96.85	93.97
Pleurodonta	94.97	92.23	89.49	73.46	71.34	69.22
Iguanidae	55.06	53.47	51.89	27.68	26.88	26.08

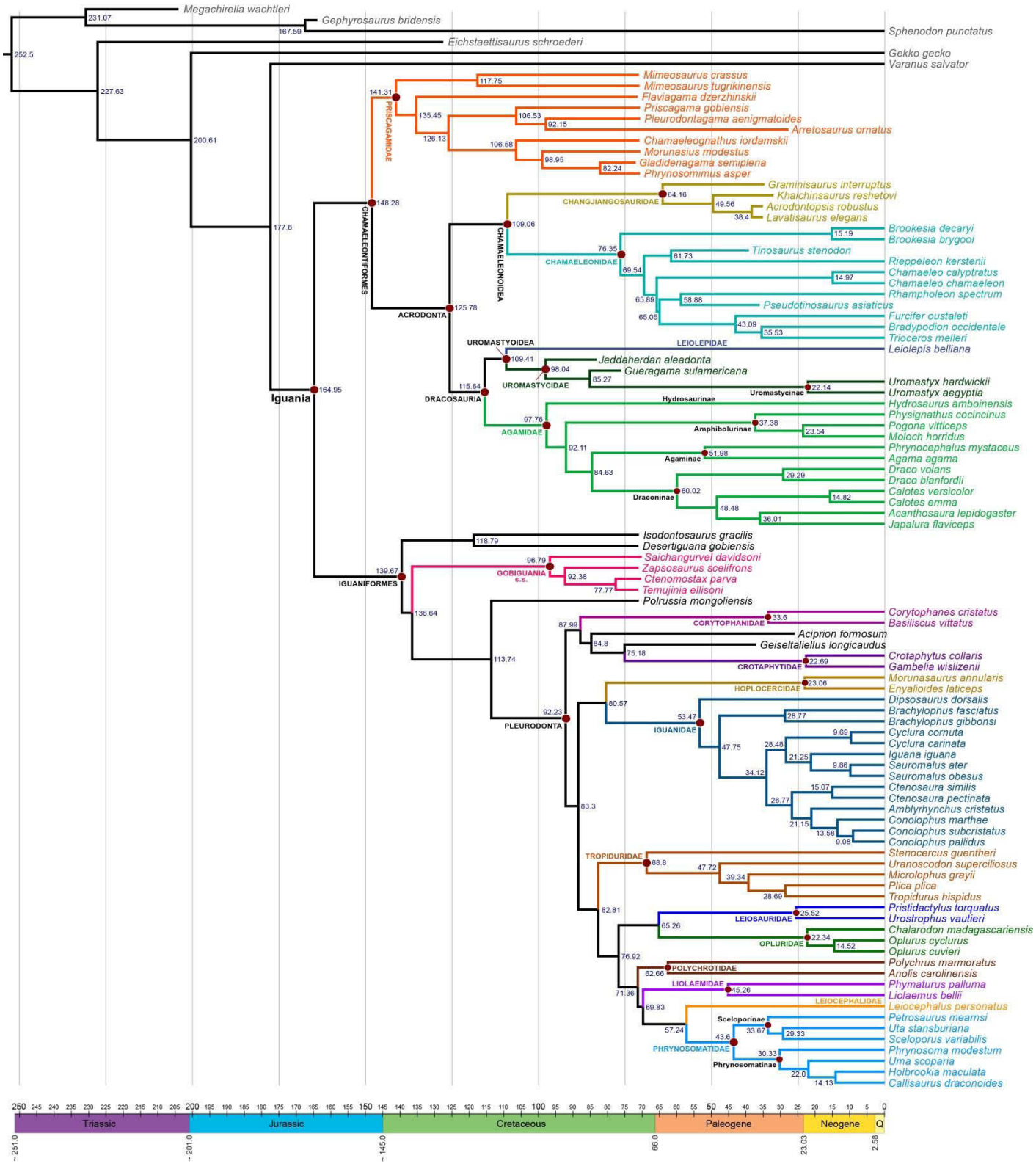

Figure 5.1. Time-calibrated maximum-clade credibility topology resulting from the Bayesian analysis of combined molecular and morphological data (TcBI). Values at nodes represents the

mean divergence time estimates for the corresponding clades. The time scale is based on the International Stratigraphic Chart (Cohen et al. 2013). The same topology with posterior probability values is provided in Appendix 5.6 (Fig. A1).

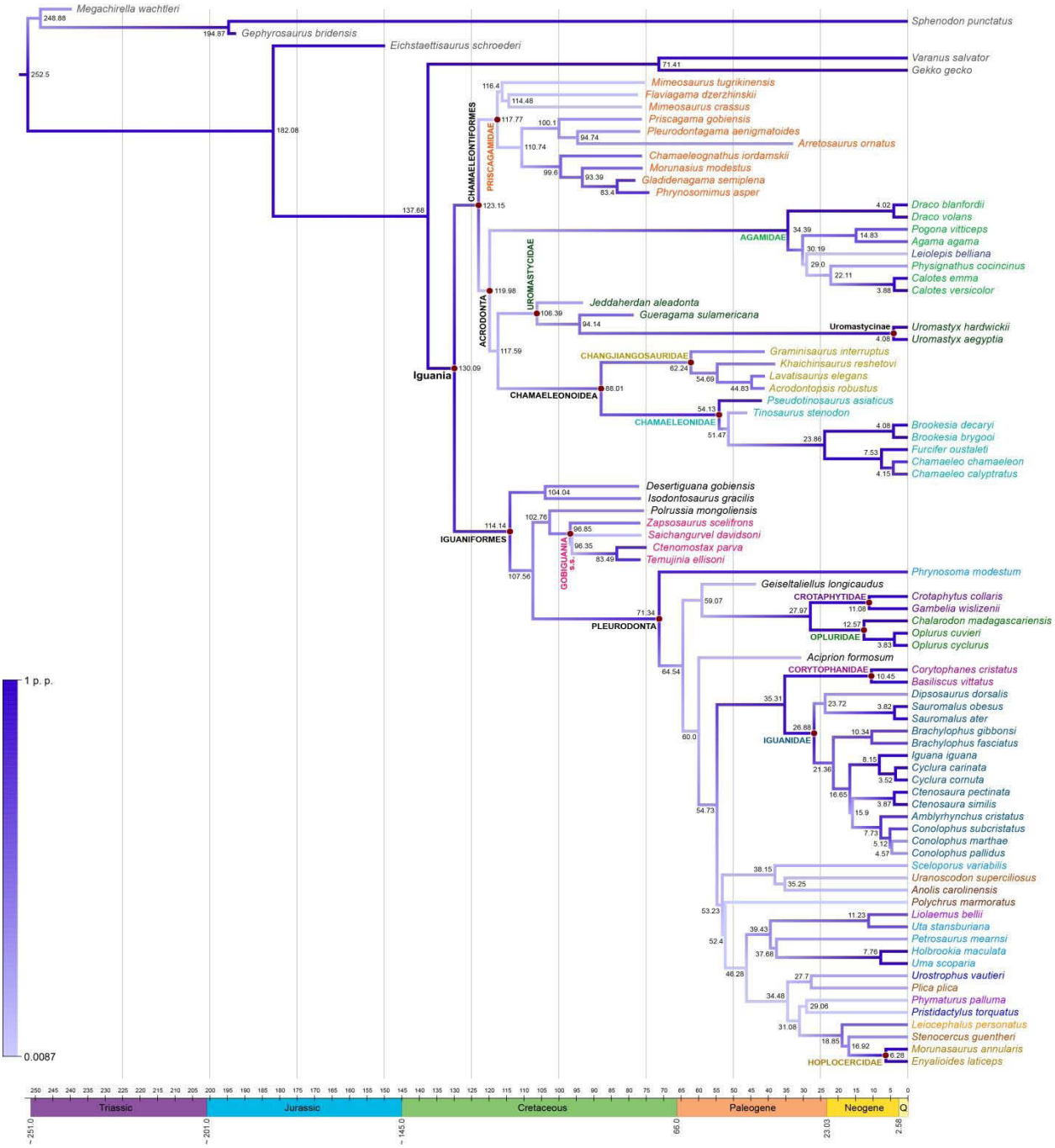

Figure 5.2. Time-calibrated maximum-clade credibility topology resulting from the Bayesian analysis of morphological data (TmBI). Branches colour gradient shows the trend in posterior probability support with scale of values reported on the left.

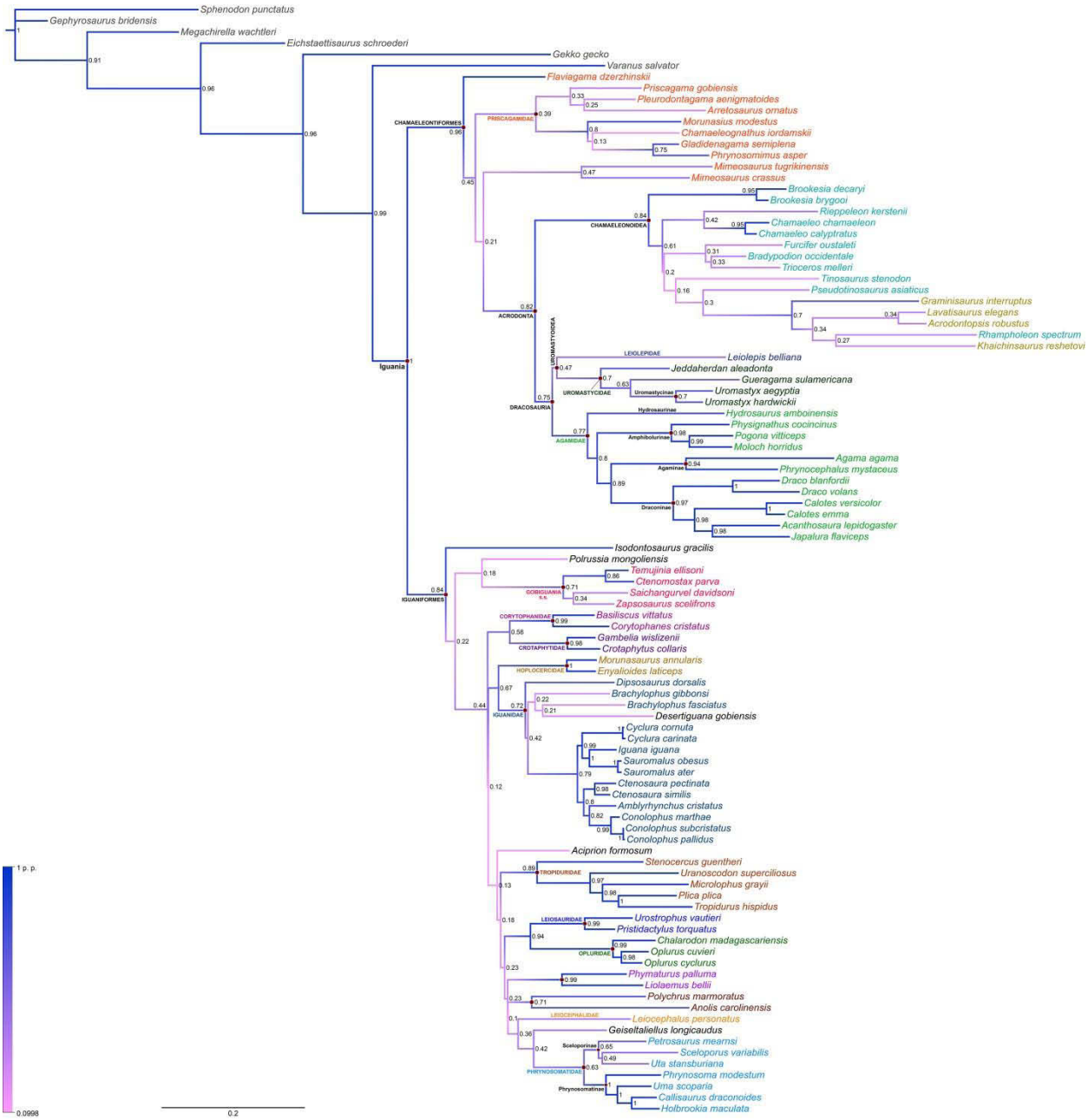

Figure 5.3. Uncalibrated maximum-clade credibility topology resulting from the Bayesian analysis of combined molecular and morphological data (UcBI). Branches colour gradient shows the trend in posterior probability support with scale of values reported on the left.

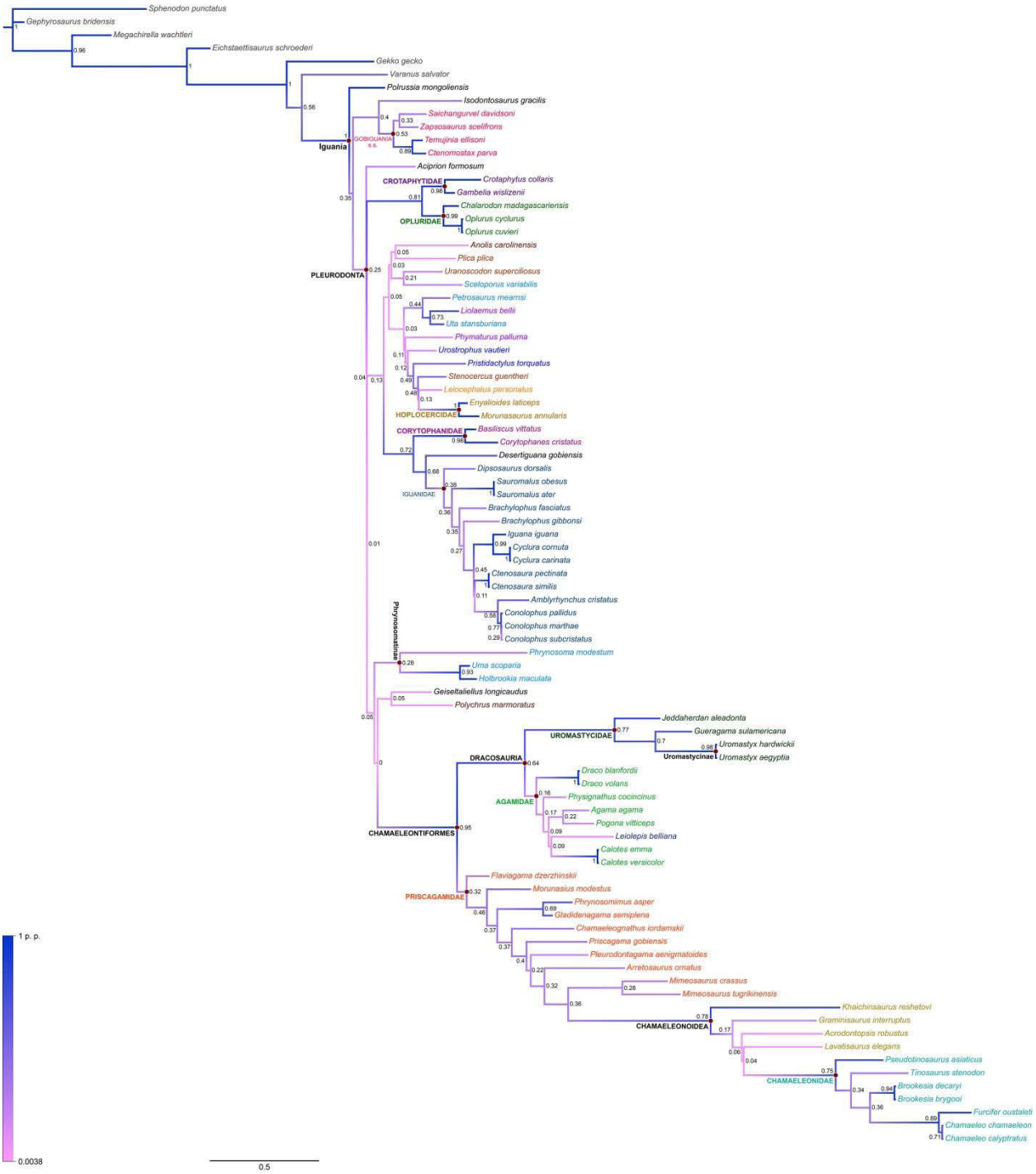

Figure 5.4. Uncalibrated maximum-clade credibility topology resulting from the Bayesian analysis of morphological data (UmBI). Branches colour gradient shows the trend in posterior probability support with scale of values reported on the left.

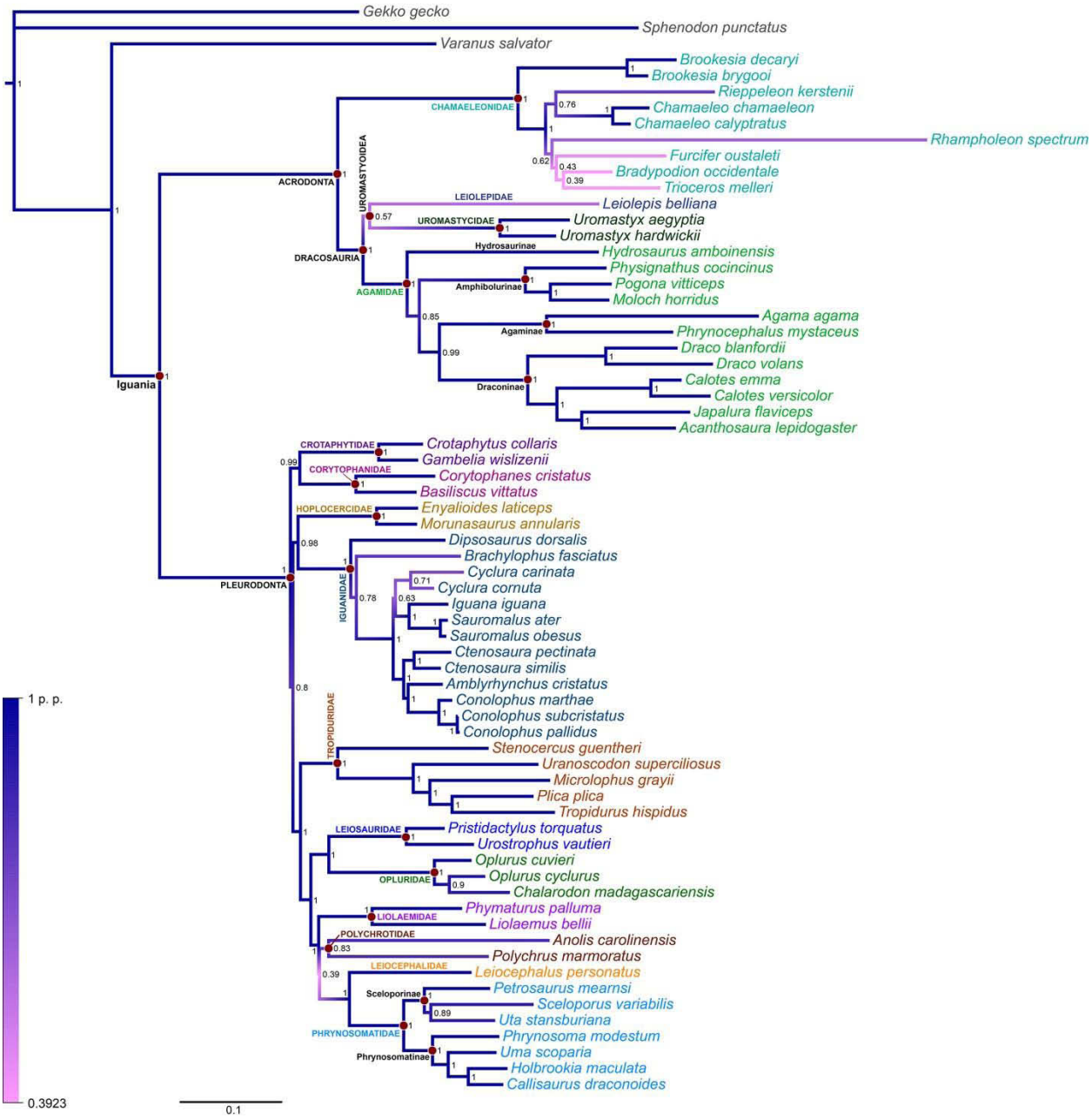

Figure 5.5. Uncalibrated maximum-clade credibility topology resulting from the Bayesian analysis of molecular data (UgBI). Branches colour gradient shows the trend in posterior probability support with scale of values reported on the left.

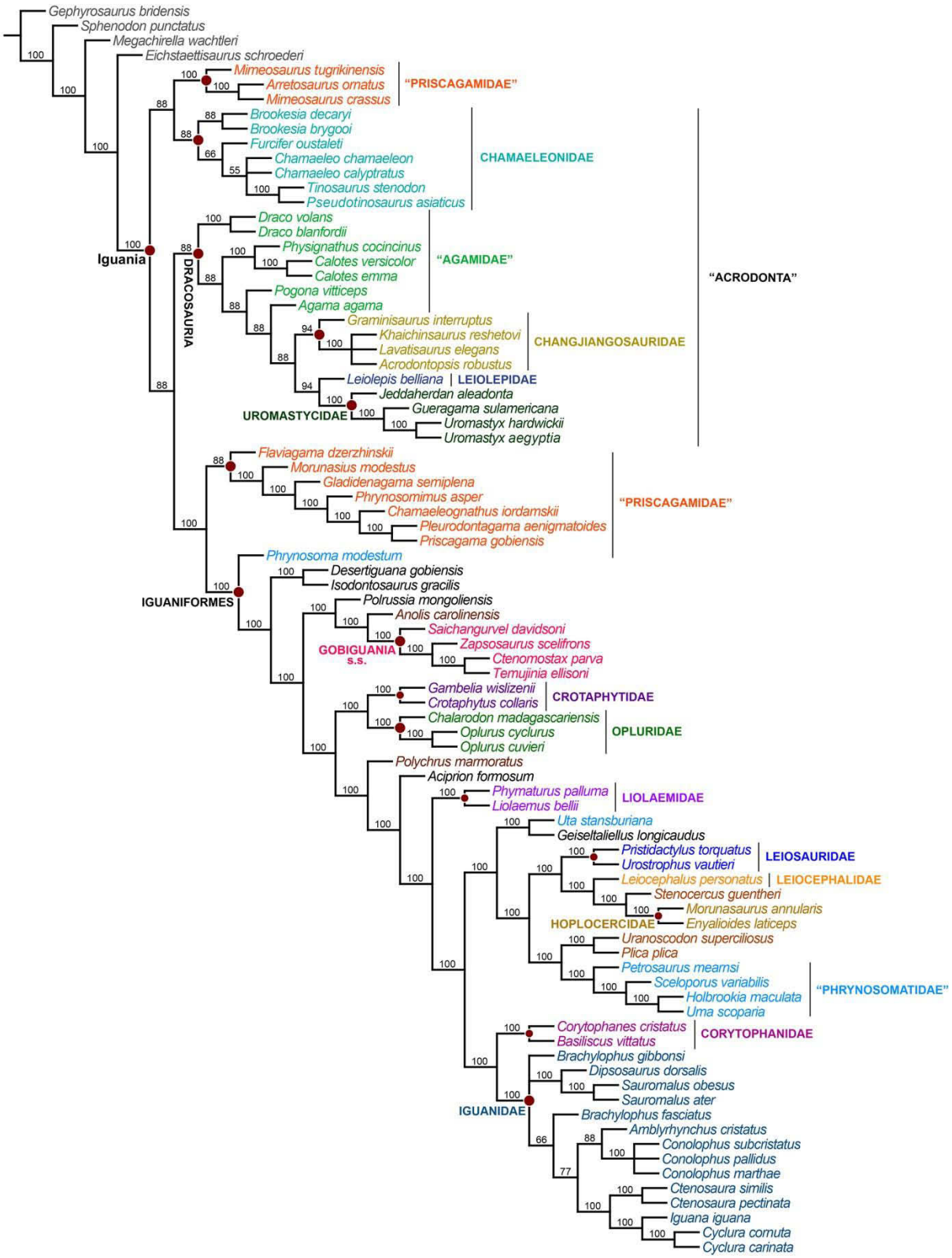
Gephyrosaurus bridensis
Sphenodon punctatus
Megachirella wachtleri
Eichstaettisaurus schroederi
Mimeosaurus tugrikinensis
Arretosaurus ornatus
Mimeosaurus crassus
"PRISCAGAMIDAE"
Brookesia decaryi
Brookesia brygooi
Furcifer oustaleti
Chamaeleo chamaeleon
Chamaeleo calyptratus
Tinosaurus stenodon
Pseudotinosaurus asiaticus
CHAMAELEONIDAE
Draco volans
Draco blanfordii
Physignathus cocincinus
Calotes versicolor
Calotes emma
Pogona vitticeps
Agama agama
"AGAMIDAE"
Iguania
DRACOSAURIA
Graminisaurus interruptus
Khaichinsaurus reshetovi
Lavatisaurus elegans
Acrodontopsis robustus
CHANGJIANGOSAURIDAE
Leiolepis belliana
LEIOLEPIDAE
Jeddaherdan aleadonta
UROMASTYCIDAE
Gueragama sulamericana
Uromastyx hardwickii
Uromastyx aegyptia
"ACRODONTA"
Flaviagama dzerzhinskii
Morunasius modestus
Gladidenagama semiplena
Phrynosomimus asper
Chamaeleognathus iordamskii
Pleurodontagama aenigmatoides
Priscagama gobiensis
"PRISCAGAMIDAE"
Phrynosoma modestum
Desertiguana gobiensis
Isodontosaurus gracilis
IGUANIFORMES
Polrussia mongoliensis
Anolis carolinensis
Saichangurvel davidsoni
GOBIGUANIA s.s.
Zapsosaurus scelifrons
Ctenomostax parva
Temujinia ellisoni
Gambelia wislizenii
Crotaphytus collaris
CROTAPHYTIDAE
Chalarodon madagascariensis
Oplurus cyclurus
Oplurus cuvieri
OPLURIDAE
Polychrus marmoratus
Aciprion formosum
Phymaturus palluma
Liolaemus bellii
LIOLAEMIDAE
Uta stansburiana
Geiseltaliellus longicaudus
Pristidactylus torquatus
Urostrophus vautieri
LEIOSAURIDAE
Leiocephalus personatus
LEIOCEPHALIDAE
Stenocercus guentheri
Morunasaurus annularis
HOPLOCERCIDAE
Enyalioides laticeps
Uranoscodon superciliosus
Plica plica
Petrosaurus mearnsi
Sceloporus variabilis
Holbrookia maculata
Uma scoparia
"PHRYNOSOMATIDAE"
Corytophanes cristatus
Basiliscus vittatus
CORYTOPHANIDAE
Brachylophus gibbonsi
Dipsosaurus dorsalis
Sauromalus obesus
Sauromalus ater
IGUANIDAE
Brachylophus fasciatus
Amblyrhynchus cristatus
Conolophus subcristatus
Conolophus pallidus
Conolophus marthae
Ctenosaura similis
Ctenosaura pectinata
Iguana iguana
Cyclura comuta
Cyclura carinata

Figure 5.6. 50% Majority-rule consensus tree resulting from the EWMP analysis. The analysis recovered 18 MPTs with tree length of 1505 steps, consistency index of 0.2173, and retention index of 0.6344. Clade names that are in quotation marks are non-monophyletic in this topology (but traditionally monophyletic in previous studies and other results in this study). The strict consensus tree is provided in Appendix 5.6 (Fig. A2).

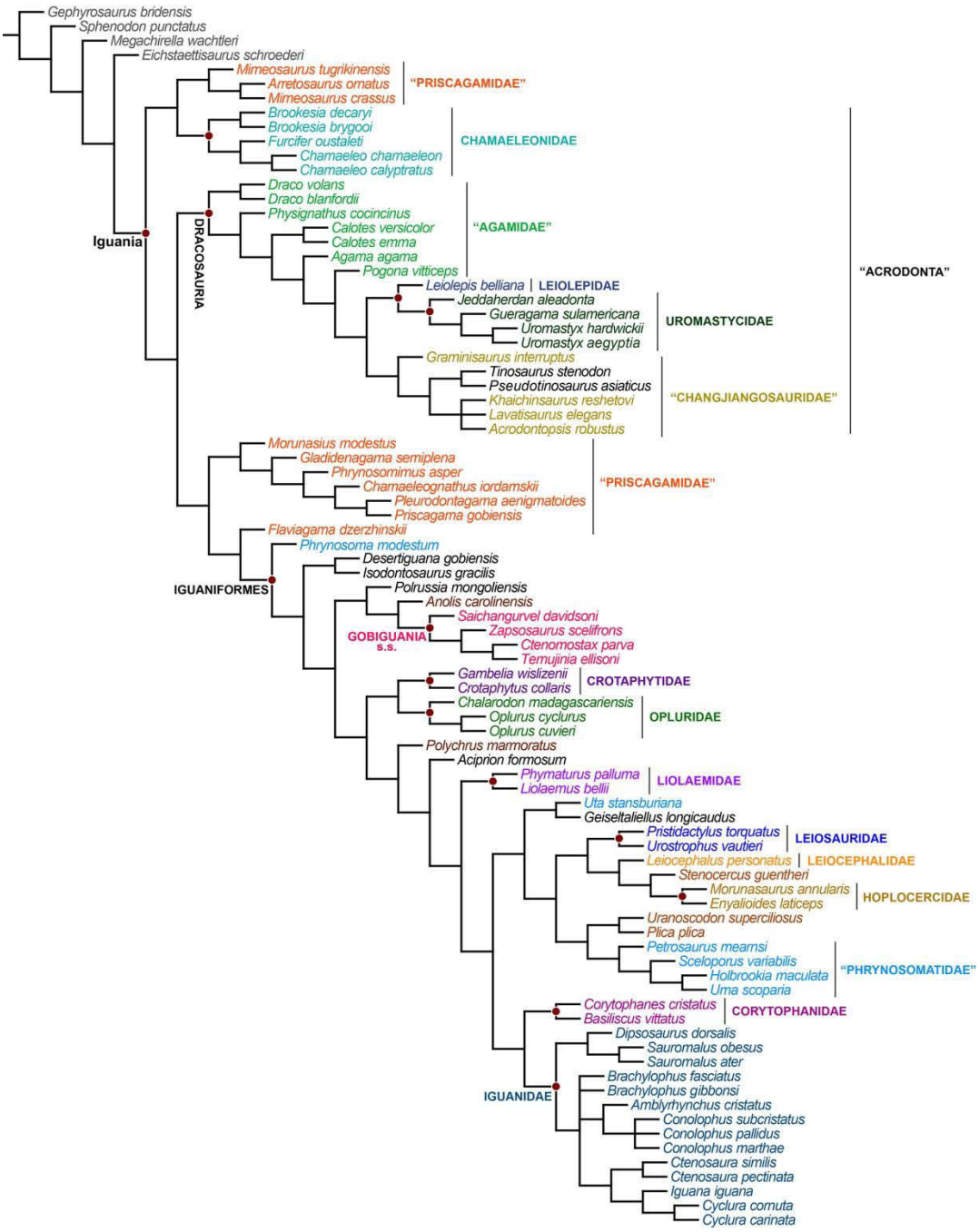

Figure 5.7. 50% Majority-rule consensus tree resulting from the IWMP analysis. The analysis recovered 7 MPTs with tree length of 1506 steps, consistency index of 0.2178, and retention index of 0.6340. Clade names that are in quotation marks are non-monophyletic in this topology (but traditionally monophyletic in previous studies and other results in this study). The strict consensus tree is provided in Appendix 5.6 (Fig. A3).

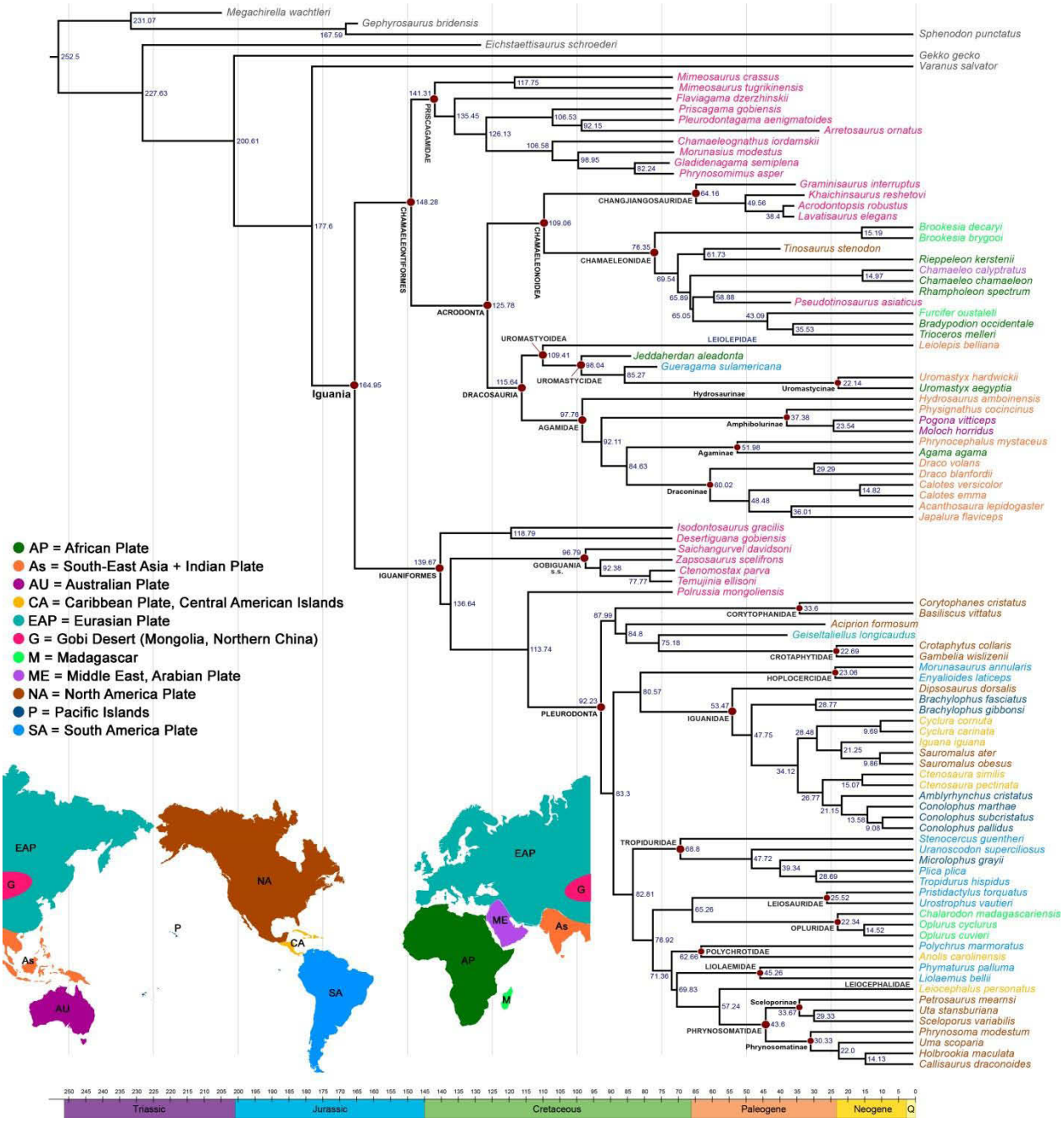

Figure 5.8. Time-calibrated maximum-clade credibility topology in Figure 5.1 with geographic distribution of living and fossil iguanians included in this study. Both stem chamaelontiforms and iguaniforms are found in Late Cretaceous deposits of the Gobi Desert, supporting the interpretation of south-eastern Laurasia as a radiation centre for both lineages in the Cretaceous.

Appendix 5.1 – List of morphological characters.

The morphological dataset used in this analysis includes characters that are revised from the literature as well as new characters. The citations for each character are not necessarily the first or only sources for the relative character but they represent the works that I have personally consulted for the character construction. When a character derived from the literature was modified, this is explicitly indicated at the end of the character statement and explained in the remarks.

Literature abbreviations: **Be97**, Bell (1997); **B85**, Benton (1985); **Co08**, Conrad (2008); **CoN06**, Conrad & Norell (2006); **C&N07**, Conrad & Norell (2007); **D&C93**, DeBraga & Carroll (1993); **deQ87**, de Queiroz (1987); **E88**, Estes *et al.* (1988); **E&dQ88**, Etheridge & de Queiroz (1988); **Ev90**, Evans (1990); **F92**, Frost (1992); **F&E89**, Frost & Etheridge (1989); **G&N98**, Gao & Norell (1998); **G88**, Gauthier *et al.* (1988); **G12**, Gauthier *et al.* (2012); **L97**, Lee (1997); **L98**, Lee (1998); **L05**, Lee (2005); **L&C00**, Lee & Caldwell (2000); **P86**, Pregill *et al.* (1986); **Pr88**, Presch (1988); **Ri80**, Rieppel (1980); **Si18**, Simões et al. (2018); **Sm09**, Smith (2009).

Skull

ROSTRAL, SKULL ROOF & CIRCUMORBITAL BONES

Premaxilla

1. **Premaxilla, fusion:** unfused (0) / fused (1) (B85, ch. Y1; E88, ch. 1; Si18, ch. 1). **Remarks:** The premaxillae are separate for instance in *Sphenodon*, while fused into a single element in all ingroup taxa.
2. **Premaxilla, nasal process, mid-shaft, shape:** tapering sides throughout (0) / parallel sides (1) / flaring (2) (F92, ch. 5; Sm09, ch. 3 - modified). **Remarks:** This process is also referred to as posterior process or internarial bar. In state 0 (e.g., *Cyclura*), the nasal process is broader at the base then keeps tapering posteriorly, appearing roughly subtriangular (and narrow in most cases). In state 1, the nasal process is wide at the base and its lateral margins remain parallel for most of its length to then taper abruptly at the end (e.g., *Ctenosaura*). In this case, the overall shape of the nasal process is more subtrapezoidal. The margins of the premaxilla nasal process gently flare posteriorly in

Isodontosaurus, where the posterior end of this process is spatulated (cf. Gao & Norell 2000).

3. **Premaxilla, nasal process, contact with frontal:** absent (0) / present (1) (D&C93, ch. 6). **Remarks:** The posterior end of the premaxillary nasal process can in some taxa reach the anterior margin of the frontals (e.g., *Furcifer*), . This should be assessed both in dorsal and ventral views, as the contact may not be exposed in dorsal view, but still happening ventrally.
4. **Premaxilla, maxillary (= anterolateral) process:** absent (0) / present (1) (G12, ch. 3 - modified). **Remarks:** The maxillary process is located laterally on each side of the premaxilla and, when present, it mediates the premaxilla-maxilla contact, giving to the premaxilla an overall T-like shape . When this process is absent, there is continuity between the margins of the premaxilla anterior body and its nasal process, with an overall triangular shape of the bone (e.g., *Polychrus*, *Furcifer*). Present in most OTUs.

Polychrus – maxillary process of premaxilla absent

5. **Premaxilla, incisive process:** absent (0) / present (1) (Si18, ch. 7). **Remarks:** This process is located on the ventral surface of the premaxilla, behind the dentigerous portion (e.g.,

Oelrich 1956). Absent in *Furcifer* and *Sphenodon*, while present in *Ctenosaura* and *Brachylophus*.

6. **Premaxilla, incisive process, shape:** single / bilobed (G&N98, ch. 46; Co08, ch. 14). **Remarks:** This process can be single or bilobed (Oelrich 1956). The incisive process is single for instance in *Iguana* and *Ctenosaura*, while bilobed in *Cyclura* and most Acrodonta. This condition is independent from the fusion of the premaxillae, as taxa with fused premaxillae can still display a bilobed incisive process, as for instance *Cyclura*.
7. **Premaxilla, ventral surface, premaxillary foramina:** absent (0) / present (1) (G12, ch. 8; Si18, ch. 8). **Remarks:** According to Oelrich 1956, on the ventral surface of the premaxilla there is one foramen on each side of the midline, just behind the dentigerous portion; these foramina represent the exits of the terminal branches of the maxillary artery. Absent in *Sphenodon* and *Gekko*, present in *Furcifer* and *Iguana*.
8. **Premaxilla, ventral surface, vomerine process (= flange):** absent (0) / present (1) (Si18, ch. 9). **Remarks:** This is a structure on the ventral surface of the premaxilla, located in median position and posterior to the premaxillary teeth. When the premaxillary incisive process is present, the vomerine process is posterior to this as well. The vomerine process extends posteriorly to contact the vomers. It is also referred to as vomerine medial flange (Si18) and sometimes merged with the palatal process (see next character) and called vomeromaxillary process (see for instance Klembara et al. 2017). However, the presence/absence of the vomerine and palatal processes of the premaxilla are independent conditions, since there are taxa with a palatal process that lack the median vomerine process (e.g., *Ctenosaura*, *Cyclura*). Because of this, these two processes are treated here as separate characters.
9. **Premaxilla, ventral surface, palatal process (= flange):** absent (0) / present (1) (NEW). **Remarks:** The palatal process or flange is a structure on the ventral surface of the premaxilla, transversely oriented and posterior to the teeth (and the incisive process, if present). It is also referred to as premaxillary shelf or premaxillary supradental shelf (e.g., Daza et al. 2012; Čerňanský et al. 2016). In some lizards, the palatal process can be constricted or grooved at the midline (e.g., Ledesma & Scarpetta 2018; Čerňanský et al. 2016). Absent for instance in *Furcifer* and *Amblyrhynchus*, present in *Ctenosaura* and *Brachylophus*.

Maxilla

10. **Maxilla, premaxillary (= anterior/anteromedial) processes, contact:** absent (0) / present (1) (F&E89, ch. 2 - modified). **Remarks:** In state 0, the maxillae are completely separated from each other by the premaxilla (e.g., *Iguana*, *Basiliscus*). In state 1, the two premaxillary processes of the maxillae meet medially, right behind the most anterior portion of the nasal process (e.g., *Ctenomastax*, *Uromastyx*).
11. **Maxilla, premaxillary (= anterior/anteromedial) process, dorsal surface, groove:** absent (0) / present (1) (S09, ch. 7; G12, ch. 112; Si18, ch. 21). **Remarks:** This is a narrow (e.g., *Dipsosaurus*, *Basiliscus*) or large (e.g., *Sauromalus*, *Iguana*) groove that can be present on the dorsal surface of the premaxillary process of the maxilla, additionally to the overall concave shape of this process. Absent for instance in *Polychrus* and *Amblyrhynchus*.
12. **Maxilla, anterodorsal process:** absent (0) / present (1) (NEW). **Remarks:** This process is not to be confused with the facial process of the maxilla (next character). It represents a dorsal projection from the anterodorsal margin of the maxilla at the contact with the premaxilla. It contributes to most of the anterior border of the external narial opening in chamaeleonids. Present, although small, also in some acrodontans (e.g., *Pogona*, *Agama*).
13. **Maxilla, anterodorsal process, orientation:** dorsoventral (0) / medially deflected (1) (NEW). **Remarks:** This process is medially deflected for instance in *Varanus*, while typically vertical in iguanians when present.
14. **Maxilla, facial process, orientation:** dorsoventral (0) / medially deflected (1) (G12, ch. 116 - modified). **Remarks:** This process is also referred to as nasal process of the maxilla (e.g., Oelrich 1956) and it is located along the mid-dorsal margin of the maxilla. In state 0, the facial process is about dorsoventrally oriented and straight throughout its height, only visible in lateral/anterolateral view (e.g., *Uromastyx*, *Dipsosaurus*). In state 1, the process is medially curved, being also largely exposed in dorsal view (e.g., *Ctenosaura*, *Amblyrhynchus*).
15. **Maxilla, facial process, anterior margin, lateral view, shape:** straight slope (0) / concave (1) (G12, ch. 118 - modified). **Remarks:** This character assesses the condition of the anterior margin of the facial process of the maxilla. In most OTUs this is the only

dorsal process of the maxilla, while in some acrodonts there is a second, more anterior process (= anterordorsal process; see ch. 13). In state 0, the anterior margin of the facial process (contributing to the narial opening) forms a straight slope, resulting in a lower angle relative to the maxillary tooth row (e.g., *Cyclura*). In state 1, this margin forms a posteriorly oriented concavity (more or less pronounced) and is almost vertical, resulting in a higher angle relative to the maxillary tooth row (e.g., *Iguana*, *Basiliscus*, *Furcifer*).

16. **Maxilla, posterodorsal process:** absent (0) / present (1) (NEW). **Remarks:** This process is found in some taxa along the posterodorsal margin of the maxilla. It is posteriorly oriented and usually gives an apparent bifurcated shape to the anterior margin of the jugal suborbital ramus (e.g., *Uromastyx*, *Agama*).

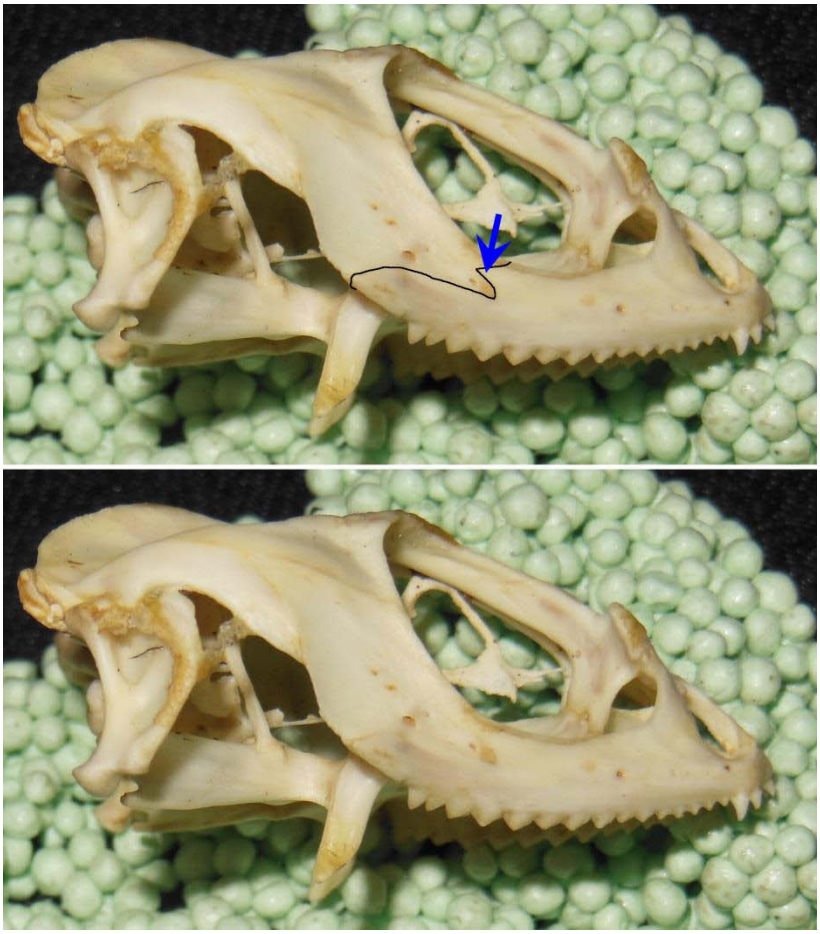

Pogona – posterodorsal process of maxilla present

Foramina of the upper jaw

17. **Anterior ethmoidal foramina:** absent (0) / piercing premaxilla (1) / notching premaxilla (2) / between premaxilla and maxilla (3) / piercing maxilla (4) (L98, ch. 2; G12, chh. 6-7 - modified). **Remarks:** These foramina serve for the passage of the medial ethmoidal nerves and the subnarial branches of the maxillary arteries (Oelrich 1956). When the foramina are absent, the medial ethmoidal nerves and the subnarial branches of the maxillary arteries exit through the external nares, either completely (state 0: e.g., *Oplurus*, *Phrynosoma*) or forming occasionally a notch on the sides of the premaxilla (state 2: e.g., *Anolis*, *Chalarodon*). The difference between state 2 (notching premaxilla) and state 3 (between premaxilla and maxilla) is that in the former the notch on the premaxilla is not bordered laterally by any bone and confluent with the narial opening, while in state 3 the notch on the premaxilla is closed laterally by the maxilla premaxillary process (e.g., *Agama*, *Physignathus*).

Septomaxilla

18. **Septomaxilla:** present (0) / absent (1) (E88; Co08, ch. 102). **Remarks:** The septomaxillae appear absent in most chamaeleonids. However, in some taxa (e.g., *Furcifer*, *Chamaeleo*), an extra paired bone is present in the rostral region on the sides of the premaxilla nasal process and anterior to the nasals. These paired elements roof the anterior portion of the external narial openings and are well-sutured to the anterodorsal process of the maxilla, with just a faint line of suture outlining those bones. Dorsal exposure of the septomaxillae through the external nares is not unusual within Iguania (and possibly in Squamata overall): in *Cyclura*, where the external nares are particularly expanded, the septomaxillae are visible on the sides of the premaxilla nasal process, basically roofing the anterior narial openings, although remaining clearly separate from the other rostral bones (unlike in chamaeleonids). I tentatively scored this character as state 0 (presence of septomaxillae) in those chamaeleonids where additional paired elements can be clearly identified in connection with the external nares and between maxillae, premaxillae and nasals. Further analyses to determine the fate of the septomaxillae in chamaeleonids will be necessary to improve our knowledge on the matter.

19. **Septomaxilla, anterolateral margin, notch:** absent (0) / present (1) (NEW). **Remarks:** This structure is also referred to as exochoanal incisure (e.g., Klembara et al. 2016). The septomaxillae are notched anterolaterally in *Amblyrhynchus* and *Ctenosaura*, while straight in *Iguana* and *Cyclura*.
20. **Septomaxilla, anterodorsal surface, shape:** flat (0) / convex (1) / concave (2) (E88, ch. 41; Si18, ch. 12 - modified). **Remarks:** The septomaxillae contribute to the anterior and dorsal portion of the osseous capsule around the Jacobson's organ (Oelrich 1956).
21. **Septomaxilla, lateral margin, shape:** straight (0) / angled (1) (NEW). **Remarks:** The lateral margin of the septomaxilla can be straight, as in *Amblyrhynchus* and *Ctenosaura*, or forming a pointy angle, as in *Iguana* and *Cyclura*. Overall, the shape of the two articulating septomaxillae in *Cyclura* and *Iguana* appears rhomboidal, while trapezoidal in *Amblyrhynchus* and *Ctenosaura*.
22. **Septomaxilla, dorsal surface, medial crest:** absent (0) / present (1) (E88, ch. 40; G12, ch. 205; Si18, ch. 13). **Remarks:** This crest is variably present across the OTUs. Found for instance in Gekko and *Amblyrhynchus*, while absent in Cyclura and *Pogona*.
23. **Septomaxilla, ventral surface, medial crest:** absent (0) / present (1) (G12, ch. 202). **Remarks:** Present for instance in *Amblyrhynchus* and *Dipsosaurus*, while absent in *Iguana* and *Furcifer*.

Nasal

24. **Nasals, fusion:** unfused / fused (P86, ch. 1; Si18, ch. 22). **Remarks:** The nasals are fused for instance in *Furcifer* and *Chamaeleo*, while paired in *Ctenosaura* and *Pogona*.
25. **Nasal, mid-lateral process:** absent / present (G12, ch. 22 - modified). **Remarks:** This is sometimes referred to as supranial process (e.g., Gauthier et al. 2012). In state 0, the lateral margins of the nasals are straight, while in state 1 they appear angled due to the lateral projection from the mid-anterior half of the bone. Absent for instance in *Ctenosaura*, present in *Amblyrhynchus*.
26. **Nasal, mid-lateral process, shape:** single (0) / bifurcated (1) (NEW). **Remarks:** The mid-lateral process of the nasal is bifurcated in *Oplurus* and *Chalarodon*, while single in most cases.

27. **Nasal, anteromedial (= premaxillary) process:** absent (0) / present (1) (NEW). **Remarks:** When present, this process bears the facet for the articulation of the nasal process of the premaxilla, to which it is usually in contact (e.g., *Priscagama*, *Sphenodon*, *Amblyrhynchus*). This process is quite long in taxa such as *Priscagama*, *Sphenodon*, *Agama*, *Dipsosaurus*, and extremely elongated in *Cyclura*, where the anteromedian processes of the nasals wrap around the posterior process of the premaxilla and largely contribute to the medial border of quite enlarged external nares. This process is instead fairly short but still present in *Amblyrhynchus*, *Iguana*, and *Basiliscus*. Absent for instance in *Brookesia brygooi*.

Cyclura cornuta - elongated anteromedial nasal process

28. **Nasal, anterolateral process:** absent (0) / present (1) (NEW). **Remarks:** When present, in most taxa, this process bears the facet for the articulation of the maxilla to which it is in contact in dorsolateral view. Present for instance in *Sphenodon*, *Iguana*, and *Agama*, absent in *Priscagama* and *Amblyrhynchus*.
29. **Nasal, posterior process:** absent (0) / present (1) (NEW). **Remarks:** Oelrich (1956) describes this process in *Ctenosaura* as diverging from the midline of the nasal, with the anteromedian process of the frontal (when present) positioned in between the two posterior

processes of the nasals. Present for instance in *Ctenosaura*, *Sphenodon*, and *Urostrophus*; absent in *Iguana*, *Amblyrhynchus* and *Brookesia*. This feature seems to be slightly variable in *Cyclura*; however, when the posterior margin of the nasals is not fully straight (usually in larger individuals), only a mild and broad posterior convexity is visible, hence the character is scored as absent for this taxon.

30. **Nasal, dorsal surface, foramina:** absent (0) / present (1) (Si18, ch. 25 - modified). **Remarks:** One or two foramina for the passage of the cutaneous branches of the lateral trunk of the ethmoidal nerve and venous tributaries of the orbital sinus can be present in the mid-posterior half of the nasal (at the base of the posterior process, when present) (Oelrich 1956). High variability is recognized for this feature especially among iguanids (e.g., *Iguana*, *Amblyrhynchus*), where sometimes a posterior foramen is visible only on one of the two nasals or multiple foramina are present and in different numbers between right and left nasals (pers. obs.). Possibly due to the extreme elongation of its anteromedian processes of the nasals and great extension of the external nares, in *Cyclura* these foramina appear more anterior on the main body of the nasals. The character is scored as present even when the foramen(ina) frequently appear only on one side of the skull (e.g., *Amblyrhynchus*, *Cyclura*). Absent for instance in *Basiliscus* and *Furcifer*.
31. **Nasal, ventral surface, conchal ridge:** absent (0) / present (1) (NEW). **Remarks:** This ridge is oriented about anterolateral to posteromedial and serves as attachment site for the olfactory capsule (Oelrich 1956). Present for instance in *Ctenosaura* and *Cyclura*, absent in *Polychrus* and *Furcifer*.

Lacrimal

32. **Lacrimal:** present (0) / absent (1) (E88, ch. 28; F&E89, ch. 5; G12, ch. 137; Si18, ch. 27). **Remarks:** The lacrimal‘s presence/absence is quite variable across both Acrodonta and Pleurodonta. This is often not the case of a true absence, but related to the fusion of this element to the prefrontal or possibly the jugal. This character is simply coding for the lack of a distinct lacrimal, independently from the cause of its absence. Absent as a distinct element for instance in *Polychrus* and *Gekko*, while present in iguanids.

Prefrontal

33. **Prefrontal, dorsolateral surface, boss(es):** absent (0) / present (1) (Co08, ch. 34; G12, ch. 130 - modified). **Remarks:** This is equivalent to the dorsolateral tuberosity in Conrad (2008).In *Amblyrhynchus cristatus* there is a single boss on the dorsolateral surface of the prefrontal, while in *Iguana iguana* there are two bosses (one mid-dorsolateral and another other one more anterolateral) connected by a crest (see next character). It seems that the different types of ornamentations (bosses and crest) on the prefrontal can occur together, as for instance in *Iguana iguana*, so I decided to treat them as separate features (see Patterson 1982: homology test of conjunction).
34. **Prefrontal, dorsolateral surface, crest:** absent (0) / present (1) (D&C93, ch. 13; Co08, ch. 35; Si18, ch. 33). **Remarks:** Conrad (2008) refers to this crest as supraorbital ridge, and DeBraga & Carroll (1993) as supraorbital process. *Amblyrhynchus*; has for instance a large boss and no crest; *Iguana* has two smaller bosses with a crest connecting them; *Brachylophus* has two tiny bosses and no crest, as does *Furcifer*. *Dipsosaurus* and *Basiliscus* have a crest but no bosses.
35. **Prefrontal, posterodorsal process:** absent (0) / present (1) (NEW). **Remarks:** A process along the posterodorsal (antorbital) margin of the prefrontal is found for instance in *Pogona*, *Corytophanes*, and *Holbrookia*. This is different from the prefrontal boss, forming a posterior projection along the antorbital margin of the prefrontal. In *Corytophanes* this process is quite elongate and join with the expanded postfrontal boss to form a supraorbital bar.

Pogona – prefrontal posterodorsal process present

36. **Prefrontal, palatine (= posteroventral) process, contact with jugal and/or lacrimal:** absent (0) / present (1) (NEW). **Remarks:** This structure is referred to as orbitonasal flange in Evans (2008) and palatine process in Oelrich (1956) and usually contributes to the lacrimal foramen. This character accounts for the variation related to the position of the palatine process of the prefrontal. In taxa such as *Iguana* and *Amblyrhynchus*, this ventral projection of the prefrontal is closer to the anterior orbital margin, and contact the palatine (on its ventral side) and the jugal and/or lacrimal (on its lateral side). The palatine process is more medially placed for instance in *Physignathus* and *Furcifer*, where it makes contact exclusively with the palatine dorsal/dorsolateral margin and/or the maxilla, bordering a much wider and oval lacrimal foramen (unlike *Iguana* and *Amblyrhynchus*, where the foramen is very narrow).

Supraorbital

37. **Supraorbital:** absent (0) / present (1) (E88, ch. 36). **Remarks:** A supraorbital or palpebral bone is present in *Varanus*.

Jugal

38. **Jugal, posterodorsal (= postorbital) ramus:** present (0) / absent (1) (E88, ch. 32 - modified). **Remarks:** This process is absent in *Gekko*.
39. **Jugal, posterodorsal (= postorbital) ramus, bony flange:** absent (0) / present (1) (G12, ch. 153; Si18, ch. 37 - modified). **Remarks:** The postorbital ramus or posterodorsal process of the jugal is posteriorly expanded via a bony flange in taxa such as *Physignathus*, *Pogona,* and *Arretosaurus*, while mostly rod-like in other taxa (e.g., *Iguana iguana*, *Priscagama*). This bony flange makes the jugal wider in lateral view and connects the posterodorsal process to the posteroventral process, when the latter is also present, but the two features appear to be independent from each other. For instance, *Priscagama gobiensis* (ZPAL MgR III-32, holotype) has a well-developed jugal posteroventral process but not a bony flange, resulting in a rod-like jugal posterodorsal process, while *Physignathus* has both a sharp posteroventral process of the jugal and a fairly wide bony flange on the jugal posterodorsal ramus.

40. **Jugal, posterodorsal (= postorbital) ramus, contact with squamosal:** absent (0) / present (1) (G12, ch. 154 - modified). **Remarks:** The posterodorsal process of the jugal contacts the anterior ramus of the squamosal for instance in *Iguana*, *Pogona* and *Physignathus*. The two elements are not in contact for instance in *Sceloporus*.
41. **Jugal, posterodorsal (= postorbital) ramus, contact with squamosal, topology:** anterior (0) / dorsal (1) (NEW). **Remarks:** This character assesses the relative position of the jugal posterodorsal ramus when contacting the squamosal (as visible in lateral view). In state 0, the jugal posterodorsal ramus simply contacts the anterior margin of the squamosal (e.g., *Iguana iguana*), and the contact is visible in lateral and/or ventral view. In state 1, the jugal posterodorsal process overlaps the anterior ramus of the squamosal dorsally (e.g., *Pogona*, *Physignathus*), resulting in a more extensive contact between the two elements. In *Priscagama gobiensis*, the topology of this contact is visible at least in one referred specimen, IGM(MAS) 3/80, where the partial disarticulation of the squamosal exposes the extended articulatory facet on the ventral margin of the jugal dorsal tip.
42. **Jugal, anterior (= suborbital) ramus, lateral surface, shelf:** absent (0) / present (1) (NEW). **Remarks:** In some taxa, such as *Priscagama gobiensis* and *Mimeosaurus tugrikinensis*, a shelf is visible on the lateral surface of the suborbital ramus of the jugal, along its dorsal margin. The presence of this shelf results in a slightly concave appearance of the lateral surface of the jugal suborbital ramus, in contrast with the flat and smooth surface visible for instance in *Physignathus* and *Agama*. In chamaeleonids, the condition is variable: the suborbital shelf is present in *Chamaeleo* but absent in *Brookesia*.
43. **Jugal, posteroventral process:** absent (0) / present (1) (Ev88, ch. O5; Si18, ch. 36). **Remarks:** Present for instance in *Physignathus*, *Agama* and *Priscagama gobiensis*, while absent in *Iguana* and *Chamaeleo*. For *Priscagama gobiensis*, I noticed that this process is well-developed in the holotype ZPAL MgR III-32 but absent in the paratype ZPAL MgR III-72, likely due to ontogenetic variation: in fact, the two specimens are considerably different in size, and ZPAL MgR III-72 has other features that also suggest an earlier ontogenetic stage (e.g., weak sculpturing, incomplete fusion of frontals, domed-shape parietal, wide open parietal fontanelle, proportionally larger than the holotype).

Frontal

44. **Frontals, fusion:** unfused (0) / fused (1) (B85, ch. Y1; Ri80, ch. 13; E88, ch. 6; Si18, ch. 67). **Remarks:** The frontals are separate for instance in *Sphenodon*, while fused into a single element in all ingroup taxa.
45. **Frontal, dorsal surface, shape:** flat (0) / concave (1) (NEW). **Remarks:** The dorsal surface of the frontal can be either flat throughout or sagittally concave (along the midline). The frontal table is flat for instance in *Iguana*, while concave in *Physignathus*. See also relative discussion in Smith (2009).
46. **Frontal, mid-lateral margins, dorsal/ventral view, shape:** straight (0) / constricted (1) / convex (2) (E88, ch. 7; Sm09, ch. 44 - modified). **Remarks:** The lateral margins of the frontal table (at the level of the orbits) can be parallel to each other (state 0), or constricted between the orbits (state 1), as visible in dorsal or ventral view. These margins are fairly straight in *Iguana* and *Chamaeleo*, while in *Furcifer*, two mid-lateral projections at the level of the orbits give a convex shape to its frontal table. Constricted for instance in *Amblyrhynchus* and *Priscagama*.
47. **Frontal, anteromedian process (= orbitonasal projection):** absent (0) / present (1) (Si18, ch. 71). **Remarks:** In some taxa, the orbitonasal projection (or anteromedian process) of the frontal can be overlapped by the nasals, hence this condition should be assessed when the bones are disarticulated or in ct-scans (e.g., *Amblyrhynchus*). This process can also mediate the contact with the nasal process of the premaxilla, when this contact is present. Present for instance in iguanids and *Priscagama*.
48. **Frontal, anteromedian process, shape:** single (0) / bifurcated (1) (NEW). **Remarks:** Bifurcated for instance in *Gambelia* and *Priscagama*, while single in most OTUs.
49. **Frontal, anterolateral processes:** absent (0) / present (1) (NEW). **Remarks:** Present in *Iguana*, *Amblyrhynchus* and *Ctenosaura*, absent in *Cyclura*. In *Cyclura*, weak anterolateral processes are seen in young individuals on the disarticulated frontal; however, adults maintain the single anteromedial process, while the anterolateral corners of the frontal have no projections.
50. **Frontal, posterolateral processes (= parietal tabs):** absent (0) / present (1) (E88, ch. 11; Si18, Ch. 68). **Remarks:** Also referred to as _frontal tabs‘ (e.g., Estes et al. 1988) or

_parietal tabs‘ (e.g., Simoes et al. 2018). When present, these processes project posteriorly from the lateral margins of the frontal to overlap the parietal table laterally.

51. **Frontal, posteromedial processes:** absent (0) / present (1) (Be97, ch. 19 - modified). **Remarks:** When present, these processes can contribute to the bordering of the pineal opening at the fronto-parietal suture (if the pineal foramen is present), but can be present independently from the position of the pineal foramen (e.g., *Polychrus*). In *Furcifer*, this process is dorsally deflected and contributes to the parietal midsagittal crest. Present in *Phrynosoma*, but only visible in ventral view on articulated specimens.
52. **Frontal, ventral surface, ossified subolfactory processes:** absent (0) / present (1) (G12, ch. 38; Si18, ch. 69). **Remarks:** In iguanids (e.g., *Iguana*, *Ctenosaura*, *Cyclura*), the subolfactory canal bordered by the crista cranii frontalis is surrounded by a cartilaginous element and there are no ossified projections (= subolfactory processes) along the ventral surface of the frontal. Hence, ossified subolfactory processes are absent in most OTUs. Present in *Gekko*.
53. **Frontal, ventral surface, ossified subolfactory processes, contact:** absent (0) / present (1) (P86, ch. 7; Si18, ch. 70). **Remarks:** The subolfactory processes can contact each other along the midline, and even fuse to each other. These processes are fused along the midline in *Gekko*.
54. **Frontal, ventral surface, anteromedian crest (or pillar):** absent (0) / present (1) (G12, ch. 45 - modified). **Remarks:** In *Amblyrhynchus* a sharp ventral crest extends from the orbitonasal projection (or anteromedian process) of the frontal to about mid-length of the frontal table. This character is inapplicable when the anteromedian process is absent (ch. 47).

Parietal

55. **Parietals, fusion:** unfused (0) / fused (1) (B85, Ch. Y1; Si18, ch. 72). **Remarks:** Parietals are separate for instance in *Sphenodon* and *Gekko*, while fused into a single element in all ingroup taxa.
56. **Parietal, supratemporal processes:** absent (0) / present (1) (L&C00, ch. 46; Si18, ch. 74). **Remarks:** Evans (2008) refers to these processes as postparietal processes, and in mosasaurs they are known as suspensorial rami (e.g., Russell 1967). They are absent in

some chamaeleonids (e.g., *Furcifer*). Very reduced in *Phrynosoma*, but still present and contacting the squamosal to close the posterior border of the upper temporal fenestra.

57. **Parietal, supratemporal process, contact with paroccipital process:** present (0) / absent (1) (Ri80, ch. 32). **Remarks:** This character is quite variable amongst both Acrodonta and Pleurodonta. Absent for instance in *Amblyrhynchus cristatus* while present in *Iguana iguana*.
58. **Parietal, anteromedial processes (= frontal tabs):** absent (0) / present (1) (E88, ch. 22; Si18, ch. 78). **Remarks:** Estes et al. (1988) refer to these processes as ‗parietal tabs' that project anteriorly to insert into triangular fossae on the posteroventral surface of the frontals. This character is independent from the position of the pineal foramen, and it may be difficult to assess in articulated specimens, as the tabs may be hidden underneath the frontal. Assessing both dorsal and ventral views in articulated specimens is usually necessary. Present for instance in *Furcifer*., while absent in *Chamaeleo*.
59. **Parietal, mid-sagittal (= adductor) crest:** absent (0) / present (1) (E&dQ88, ch. 3; F&E89, ch. 10; Sm09, ch. 53; G12, ch. 93; Si18, ch. 85 - modified). **Remarks:** Present in most iguanids, except Dipsosaurus and Brachylophus. The crest tend to be absent in young/small size specimens of Iguana and *Amblyrhynchus* but well-developed in large individuals.
60. **Parietal, mid-sagittal crest, dorsal expansion:** absent (0) / present (1) (G12, ch. 93 - modified). **Remarks:** The parietal mid-sagittal crest is expanded for instance in *Corytophanes*, *Basiliscus*, and *Furcifer*.
61. **Parietal, posterior wall, nuchal fossa:** absent (0) / present as single (1) / present as double (2) (Co08, ch. 83; G12, ch. 94; Si18, ch. 79 - modified). **Remarks:** When present, the nuchal fossa is found along the posterior wall of the parietal table, between the two supratemporal processes. The nuchal fossa is different from the fossa parietalis (or parietal fossa) that is found instead on the ventral surface of the parietal, where the processus ascendens of the synotic tectum makes contact (cf. Oelrich 1956; Evans 2008). The nuchal fossa can be fully roofed by the posteromedial process of the parietal table or exposed in dorsal view (cf. Conrad 2008; Gauthier et al. 2012); moreover, it can be present as a single mid-fossa (e.g., *Amblyrhynchus*, *Iguana*) or two separate fossae (e.g., *Temujinia*, *Agama*). Its development is quite late during ontogeny (similarly to the ossification of the PAST), as

for instance in *Iguana* and *Amblyrhynchus* there is no nuchal fossa in small and mid-size individuals, while in larger ones the fossa is well-developed (with a dividing septum in the case of *Amblyrhynchus*). A nuchal fossa is never present for instance in specimens of various sizes of both *Ctenosaura* and *Cyclura*.

Cyclura (left-no nuchal fossa) and *Iguana* (right-with single nuchal fossa)

Amblyrhynchus - single nuchal fossa divided by a septum

Temujinia - two nuchal fossae and meridian crest along posterior wall of parietal (next character)

62. **Parietal, posterior wall, nuchal fossa, septum:** absent (0) / present (1) (NEW). **Remarks:** When a single nuchal fossa is present on the mid-posterior wall of the parietal, it can be divided by a thin mid-sagittal septum (running vertically within the fossa). This character is inapplicable when the fossa is absent or double (see also remarks in chh. 61 and 63). This condition is treated separately from the presence of a double nuchal fossa (e.g., *Agama*, *Temujinia*), as in the latter case there are two distinct fossae along the posterior wall of the parietal, divided by a flat space or a notch for the passage of the processus ascendens of the synotic tectum (PAST). This is clearly distinct from the vertical septum within a single mid-fossa (e.g., *Amblyrhynchus*). The septum is present for instance in *Amblyrhynchus* and *Brachylophus*, while no septum divides the single nuchal fossa in *Iguana*.
63. **Parietal, posterior wall, median crest:** absent (0) / present (1) (NEW). **Remarks:** A vertical crest can be present along the middle of the parietal posterior wall in some taxa. This condition is inapplicable when a single mid-nuchal fossa is present (state 1 in ch. 61) due to their topological overlap (presence of one condition excludes the other). However, the presence of a median crest along the posterior wall of the parietal appears independent

from the presence/absence of double nuchal fossae, as this crest can be found when the two nuchal fossae are either absent (e.g., *Zapsosaurus*) or present (e.g., *Ctenomastax*).

Zapsosaurus - median crest along the parietal posterior wall (but no nuchal fossae)

64. **Parietal, posteromedian process:** absent (0) / present (1) (G12, ch. 95; Si18, ch. 80 - modified). **Remarks:** This process projects posteriorly from the parietal table and roofs the parietal nuchal fossa when the latter is present. It is also referred to as postparietal projection in (G12, ch. 95) or parietal posterior flange (Si18, ch. 80). This is independent from the parietal sagittal crest, and present ventral to this structure for instance in *Furcifer* and *Basiliscus*.
65. **Parietal, posteromedian process, shape:** single (0) / bifid (1) (G12, ch. 97; Si18, ch. 84). **Remarks:** Inapplicable when the process is absent. Single for instance in *Basiliscus* and *Gekko*, while bifid in *Liolaemus*.
66. **Parietal, ventral surface, fossa:** present (0) / absent (1) (CoN06, ch. 46; Co08, ch. 78; Si18, ch. 81). **Remarks:** In Oelrich 1956, the parietal fossa (= fossa parietalis) is located posteriorly on the ventral surface of the parietal, where the processus ascendens of the synotic tectum contacts the parietal. This is what Evans (2008) calls a ventral pit for the processus ascendens of the supraoccipital.
67. **Parietal, ventral surface, fossa, posterior margin:** open (0) / closed (1) (CoN06, ch. 46; Si18, ch. 82). **Remarks:** The posterolateral margins of the parietal fossa are also called

cristae juxtafovealis (e.g., Conrad 2008; Klembara et al. 2010). These crested margins can either projects all the way posteriorly and join closing the parietal fossa (state 1: e.g., *Brachylophus fasciatus*) or never meet posteriorly, leaving the posterior border of the fossa open (state 0: e.g., *Furcifer*, *Dipsosaurus*).

68. **Parietal, crista cranii parietalis, ventral (= epipterygoid) process:** absent (0) / present (1) (E88, ch. 23; G12, ch. 108; Si18, ch. 87). **Remarks**: This is also referred to as epipterygoid process or ventrolateral crest of the crista cranii parietalis (e.g., Evans 2008; Klembara et al. 2010; Simoes et al. 2018). It usually mediates the contact with the epipterygoid when present, either directly (e.g., *Ctenosaura*) or via an extensive amount of cartilage (e.g., *Agama*). The epipterygoid contacts directly the crista cranii parietalis when the process is absent (e.g., *Brachylophus fasciatus*). A short crista cranii parietalis is visible on the reduced parietal table ventral surface in chamaeleonids, joining posteriorly with the posterolateral margins of the parietal fossa for instance in *Furcifer*. No ventral projections are found along this short segment, so I scored this character as absent in this case.

Postfrontal and Postorbital

69. **Postfrontal:** absent (0) / present (1) (E88, ch. 12). **Remarks:** The postfrontal seems to be truly absent for instance in *Polychrus*, *Uromastyx*, and *Holbrookia*. In *Phrynosoma*, the postfrontal appears to possibly fuse to the frontal (IP pers. obs.), where the posterolateral margins of the frontal table are unusually elongated and bear an anterior projection that invades the orbital opening (topologically similar to the supraorbital boss present on the postfrontal of many iguanids: see characters 73-74). However, since it is difficult to determine whether or not the postfrontal is fused to a different bone other than the postorbital without further analyses, this character accounts for the lack of a distinct postfrontal and it is scored as inapplicable when the postfrontal is clearly fused to the postorbital (forming a postorbitofrontal bone).

70. **Postfrontal-postorbital:** unfused (0) / fused (1) (E88, ch. 14; Co08, ch. 94; Si18, ch. 44). **Remarks:** The fusion between postorbital and postfrontal occurs frequently within squamates and is highly variable during ontogeny and sometimes intraspecifically (IP pers. obs.). Fused for instance in *Basiliscus vittatus*, while separate in iguanids. In *Phrynosomimus*, a faint suture between the postfrontal and postorbital is still visible on the

holotype (PIN 3142-318), while fully obliterated in a larger size specimen (IGM 3-81), hence I scored this character as state 1 for this OTU.

71. **Postfrontal, distal (= lateral) process, shape:** single (0) / bifurcated (1) (G12, ch. 64; Si18, ch. 58). **Remarks:** Inapplicable when postfrontal and postorbital are fused or postfrontal absent. Bifurcated for instance in Temujinia, while single in Uranoscodon and most OTUs.

72. **Postfrontal/postorbitofrontal, anterodorsal surface, supraorbital crest:** absent (0) / present (1) (NEW). **Remarks:** This feature is present in chamaeleonids and priscagamids, as well as *Corytophanes* among pleurodontans.

73. **Postfrontal/postorbitofrontal, anterodorsal surface, supraorbital boss:** absent (0) / present (1) (NEW). **Remarks:** A rugouse and rounded process, similar to the prefrontal boss, is present along the anterodorsal margin of the postfrontal and or postorbital in some iguanids (e.g., *Amblyrhynchus*, *Brachylophus*). This structure is located at the contact between the postfrontal and the postorbital (e.g., *Brachylophus*) or more commonly on the postorbital only.

74. **Postfrontal/postorbitofrontal, anterodorsal surface, supraorbital boss, anterior expansion:** absent (0) / present (1) (NEW). **Remarks:** An elongated anterior projection is visible on the postfrontal in *Cyclura*. This element is rugouse and rounded like the supraorbital boss in other iguanids, but extremely more elongated, partially invading the top of the orbital opening and similar to a ‗horn‘.

Cyclura - expanded supraorbital boss of postorbitofrontal

75. **Postfrontal/postorbitofrontal, anterodorsal surface, supraorbital boss, contact with prefrontal posterodorsal process:** absent (0) / present (1) (NEW). **Remarks:** The expanded anterodorsal supraorbital boss of the postfrontal/postorbitofrontal contacts the posterodorsal process of the prefrontal for instance in *Corytophanes*, forming a complete bar above the orbital opening. Inapplicable when either or both the postfrontal supraorbital boss and the posterodorsal process of the prefrontal are absent, and when the postfrontal supraorbital boss is not expanded (see previous character).

76. **Postfrontal/postorbitofrontal, dorsal/dorsomedial margin, shape:** single (0) / bifurcated (1) straight (2) (E88, ch. 13; G12, ch. 63; Si18, ch. 60). **Remarks:** This character assesses for the lunate or triangular (state 0) versus bifurcated (state 1) shape of the postfrontal dorsomedial margin. Single for instance in *Physignathus* and *Amblyrhynchus*, while bifurcated in *Sphenodon*, *Arretosaurus*, and *Priscagama*. In chameleons, this process is straight and antero-posteriorly wide (state 2). Inapplicable when a postfrontal is absent.

Arretosaurus - bifurcated dorsomedial margin of postorbitofrontal

Pogona - dorsomedial margin of postorbitofrontal single

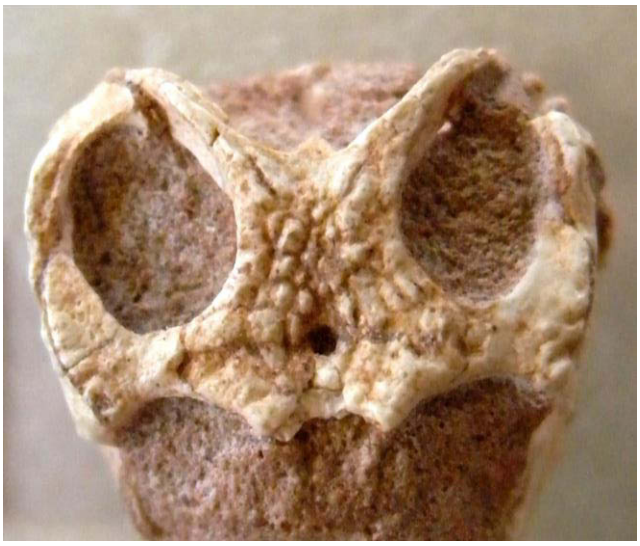

Priscagama - bifurcated dorsomedial margin of postorbitofrontal

77. **Postfrontal/postorbitofrontal, contact with parietal:** dorsal (0) / lateral (1) / anterior (2) / absent (3) (G12, ch. 65; Si18, ch. 59 – modified). **Remarks:** This character assesses the geometrical relationship between the postfrontal/postorbitofrontal dorsomedial margin relative to the parietal table. This character is inapplicable when a distinct postfrontal is missing (e.g., *Polychrus*, *Phrynosoma*). Absent for instance in *Sceloporus*, where the contact is prevented by the frontal and postorbital.
78. **Postorbital, dorsal process, contact with parietal:** absent (0) / present (1) (G12, ch. 71 - modified). **Remarks:** When postorbital and postfrontal are fused, this character is inapplicable. The anterodorsal process of the postorbital contacts the parietal for instance in *Dipsosaurus*, behind the postfrontal. Postfrontal prevents contact between postorbital and parietal for instance in *Priscagama*.
79. **Postorbital, dorsal margin, position relative to postfrontal:** lateral (0) / posterior (1) / anterior (2) (Si18, ch. 45). **Remarks:** The postorbital is lateral (or distal) to the postfrontal for instance in *Temujinia* (state 0), where the dorsal margin of the postorbital is clasped between the bifurcated distal (or lateral) margin of the postfrontal. The postorbital dorsal margin is typically posterior to the postfrontal for instance in *Amblyrhynchus*, (state 1), while the anterior condition (state 2) in our dataset is found only in the outgroup

Eichstaettisaurus. Inapplicable when postorbital and postfrontal are fused or a distinct postfrontal is missing (e.g., *Polychrus*, *Phrynosoma*).

80. **Postorbital/postorbitofrontal, anteroventral (= jugal) process:** absent (0) / present (1) (Si18, ch. 47). **Remarks:** When this process is absent, the ventral border of the postorbital is straight and flat. Absent for instance in *Priscagama* while present in most OTUs.
81. **Postorbital/postorbitofrontal, posterior process, dorsal/dorsomedial flange:** absent (0) / present (1) (NEW). **Remarks:** A dorsal/dorsomedial flange along the dorsal margin of the posterior process of the postorbital is found for instance in *Basiliscus* and *Amblyrhynchus*.
82. **Postorbital/postorbitofrontal, posterior process, dorsal fossa:** absent (0) / present (1) (NEW). **Remarks:** A large fossa is located on the dorsal/posterodorsal margin of the postorbital in *Amblyrhynchus*. The postorbital fossa seems to be an autapomorphy of *Amblyrhynchus cristatus*, as the element is absent in all other iguanids (including *Conolophus* spp.) and iguanians.

DERMAL OSSIFICATION AND SCULPTURING OF THE UPPER JAW, SKULL ROOF AND CIRCUMORBITAL BONES

These characters try to account for the variation in skull bone ornamentations that is found across iguanians. I acknowledge that the definition of dermal sculpturing is quite general and encompass potentially a variation of structures that may not be homologous. In fact, quite often with this term both simple bony ornamentaions and true integumentary ossifications are clumped together. The presence of integumentary ossifications, also known as osteoderms, as long been considered a typical feature of anguimorphs and gekkonomorphs; however, recent studies have shown their presence in chamaeleons (Schucht et al. 2020) and based on comparison, other iguanians like priscagamids and some pleurodontans most likely also possess skull osteoderms. The lack of studies on the topic across iguanians makes it difficult at this stage to justify the construction and scoring of a character on presence/absence of osteoderms, hence I kept the characters on dermal sculpturing mostly unchanged from the literature, trying to improve consistency in scoring the shape of the sculpturing across OTUs.

83. **Dermal sculpturing, frontal:** absent (0) /present (1) (C&N07, ch. 7 - modified). **Remarks:** When sculpturing on the dorsal skull roof is present, it is continuous and invariable between frontal and parietal, thus I selected a single landmark to account for this condition. The frontal is better preserved in most of the fossil OTUs used in this analysis, and because of this was preferred over other elements of the skull roof.
84. **Dermal sculpturing, frontal, shape:** vermiculated (0) / tuberculated (1) / rugose (2 / pitted (3) (E88, ch. 129; C&N07, ch. 4; Si18, ch. 76 - modified). **Remarks:** Since there is no variation in the type of sculpturing between the bones of the same OTU, I selected a single landmark to account for this condition. This character is inapplicable when sculpturing is absent.

PALATAL COMPLEX

Vomer

85. **Vomer, fusion:** unfused (0) / fused (1) (E88, ch. 38; Si18, ch. 88). **Remarks:** Fused for instance in *Chamaeleon* and *Chamaelognathus*.
86. **Vomer, anteromedial (= premaxillary) process:** absent (0) / present (1) (Si18, ch. 90). **Remarks:** Present for instance in *Cyclura* and *Conolophus*, while absent in *Amblyrhynchus* and *Sphenodon*. This character represents a case of late ontogenetic ossification. Oelrich (1956) describe this element as cartilaginous (‗rostral part of the cartilaginous nasal septum‘: Oelrich 1956, p. 24) in *Ctenosaura*, but based on personal observation, an ossified premaxillary process is found in large-sized individuals of *Ctenosaura similis*. A similar situation is found in *Cyclura* and *Iguana*: in smaller size specimens, the incisive foramen (i.e., the gap between the vomers and the incisive process of the premaxilla) is open, while the foramen is fully invaded by an ossified anterior process of the vomers in larger size specimens. Always absent for instance in *Amblyrhynchus*, *Sphenodon*, and *Gekko*.

Cyclura - anteromedial process of vomer present

Amblyrhynchus - anteromedial process of vomer absent

Conolophus - anteromedial process of vomer present

87. **Vomer, lateral margins, expansion:** absent (0) / present (1) (Ev90, ch. 8; Si18, ch. 91). **Remarks:** This represents a lateral expansion of the main body of the vomer, posterior to the lacrimal groove and fenestra vomeronasalis contribution (cf. Oelrich 1956). Absent for instance in *Amblyrhynchus* and *Chamaeleo*, where the lateral margins of the vomers are straight throughout, while present in *Conolophus* and *Iguana*.

Amblyrhynchus - expansion of vomer lateral margins absent

Conolophus - expansion of vomer lateral margins present

Iguana - expansion of vomer lateral margins present

88. **Vomer, ventral surface, mid-sagittal crest:** absent (0) / present (1) (Si18, ch. 92). **Remarks:** Also referred to as longitudinal ridge in G12 (ch. 222). Present for instance in *Dipsosaurus*, while absent in *Iguana* and *Amblyrhynchus*.
89. **Vomer, ventral surface, anterolateral crest:** absent (0) / present (1) (Si18, ch. 93). **Remarks:** Also referred to as longitudinal ridge in G12 (ch. 222), where it is combined with the medial crest (previous character). It is located on the anterior half of the vomer and represents a transverso-lateral structure that runs along the anterior constriction of the vomer and then posterolaterally to it. The medial and anterolateral crests appear to be independent, as reported in Si18 (chh. 92-93), since they can both be present at the same time (e.g., *Varanus*, *Dipsosaurus*) or only one of the two (e.g., *Amblyrhynchus* and *Ctenosaura* only have the anterolateral crest). Present in many OTUs, absent for instance in *Gephyrosaurus* and *Basiliscus*.
90. **Vomer, ventral surface, foramina:** absent (0) / present (1) (G12, Ch. 229; Si18, ch. 94). **Remarks:** The ventral surface of the vomers can be pierced by the paired ramus medialis of the palatine nerve VII, when one foramen on each vomer is visible at the level of the anterior portion of the fenestra exochoanalis (Oelrich 1956).
91. **Vomer, ventral surface, shape:** flat (0) / concave (1) (Si18, ch. 95 - modified). **Remarks:** The ventral surface of the vomer is flat for instance in *Ctenosaura* and *Chamaeleo*, while concave in *Amblyrhynchus* and *Liolaemus*.

Palatine

92. **Palatine, vomerine (= anteromedial) process, dorsal deflection:** absent (0) / present (1) (NEW). **Remarks:** The anterior process of the palatine for the contact with the vomer is present in all our ingroup and outgroup. However, in some taxa (e.g., chamaeleonids, *Dipsosaurus*) its position is abruptly deflected dorsally in comparison to the palatine shaft, creating a distinct angle between the process itself and the rest of the palatine. In most other OTUs, despite a gentle slope, this process is coplanar and continuous with the palatine shaft and other processes (e.g., *Iguana*, *Physignathus*).
93. **Palatine, vomerine (= anteromedial) process, shape:** single (0) / bifurcated (1) (NEW). **Remarks:** The anterior process of the palatine is single in most OTUs, while bifurcated for instance in *Oplurus* and *Chalarodon*.

94. **Palatine, maxillary (= lateral) process:** absent (0) / present (1) (G12, ch. 239; Si18, ch. 103). **Remarks:** This process is present for instance in Uromastyx and Furcifer, while absent in *Chamaeleo* and *Holbrookia*.

Pterygoid

95. **Pterygoid, contact at midline:** absent (0) / present (1) (E88, ch. 83; G12, ch. 257). **Remarks:** Contact present for instance in *Spheodon*, while absent in *Amblyrhynchus*.
96. **Pterygoid, main body, ventral surface, shape:** flat (0) / concave (1) (Si18, ch. 110). **Remarks:** The main body of the pterygoid is the portion surrounded by the palatine process anteriorly, the transverse process laterally, and the quadrate process posteriorly, and bearing teeth when they are present. Flat for instance in *Iguana* and *Amblyrhynchus*, concave in *Dipsosaurus* and *Cyclura*.
97. **Pterygoid, main body, ventral surface, eminence:** absent (0) / present (1) (Be97, ch. 42 - modified). **Remarks:** In some taxa, a prominent bony eminence (usually bearing teeth) can be present posteromedially on the ventral surface of the main body of the pterygoid (e.g., *Cyclura*). When the pterygoid teeth are present, the ventral eminence can be absent, and in *Anolis* for instance there is an eminence but no teeth. An example of presence of pterygoid teeth without the dentigerous eminence is *Amblyrhynchus*, where they are set in a groove. It seems to vary in *Iguana iguana*, where larger specimens bear numerous small teeth without an eminence, while small to medium size specimens tend to have one.
98. **Pterygoid, main body, posteromedial flange:** absent (0) / present (1) (Si18, ch. 111). **Remarks:** Referred to as arcuate flange in Si18. This flange is located at the contact with the basipterygoid process of the basisphenoid and projects medially from the posterior portion of the main body of the pterygoid, at the transition with the pterygoid quadrate process. When present, the flange partially overlaps the contact with the basipterygoid process of the basisphenoid and can have a blunt or tapering shape. Present for instance in *Sphenodon*, *Oplurus*, and *Chamaelognathus*.

Chamaelognathus - flange present

Oplurus - flange present

99. **Pterygoid, palatine (= anterior) process, anterior end, shape:** single (0) / bifurcated (1) (Si18, ch. 106). **Remarks:** This character is better assessed when the elements are disarticulated, as one of the two ends can be covered in ventral view by the palatine (e.g., *Ctenosaura pectinata*: in articulation the element appears single, but when looking at the disarticulated pterygoid, there is a bifurcated palatine process bearing the facets for the palatine). For the terminology, I refer to Oelrich (1956). The palatine process of the pterygoid is single for instance in *Amblyrhynchus* and *Iguana*, while bifurcated in *Ctenosaura* and *Cyclura*.
100. **Pterygoid, palatine process, anterior expansion:** absent (0) / present (1) (NEW). **Remarks:** The palatine process can extend anteriorly to border most of the medial margin of the palatine and reach up to the vomer (e.g., *Phrynosomimus*, *Gladidenagama*).
101. **Pterygoid, quadrate process, dorsal flange:** absent (0) / present (1) (NEW). **Remarks:** Found for instance in *Isodontosaurus* and *Uromastyx*, while absent in *Agama* and *Iguana*.
102. **Pterygoid, quadrate process, medial surface, groove:** absent (0) / present (1) (G12, ch. 265 - modified). **Remarks:** The medial surface of the quadrate (or posterior) process of the pterygoid can have a deep excavation or groove for the insertion of the protractor

pterygoideus muscle (e.g., Oelrich 1956), in addition to its already concave shape. Excavation is particularly pronounced for instance in *Amblyrhynchus*. Absent for instance in *Furcifer* and *Gekko*.

103. **Pterygoid, quadrate process, posteroventral notch:** absent (0) / present (1) (NEW). **Remarks:** A notch along the posteroventral margin of the pterygoid quadrate process is found for instance in *Pogona* and *Phymaturus*.
104. **Pterygoid, transverse-quadrate processes, ventral flange:** absent (0) / on transverse process only (1) / from transverse to quadrate process (2) / on quadrate process only (3) (G12, ch. 266; Si18, ch. 108 - modified). **Remarks:** A ventrally oriented flange departing from the margin of the transverse process and continuing to the quadrate process of the pterygoid is present for instance in *Chamaeleo* (state 2). The ventral flange is limited to the transverse process in *Iguana iguana* (state 1), while absent completely in *Priscagama*.

Ectopterygoid

105. **Ectopterygoid, contact with palatine:** absent (0) / present (1) (Co08, chh. 124-125 - modified). **Remarks:** Present for instance in *Uromastyx* and *Chamaeleon*, while absent in *Ctenosaura* and *Iguana*.
106. **Ectopterygoid, anterolateral process:** absent (0) / present (1) (NEW). **Remarks:** The ectopterygoid has 3 processes: a ventral more prominent one that makes up most of the bone, plus an anterolateral and a posterolateral one. While the ventral process is always present, anterolateral and a posterolateral processes show variation across the OTUs. Absent for instance in *Phrynosoma*. See also remarks for next character.
107. **Ectopterygoid, posterolateral process:** absent (0) / present (1) (G12, ch. 283; Si18, ch. 114 - modified). **Remarks:** This is referred to as posterior process in G12 and lateral process in Si18. As the ectopterygoid can have two lateral processes (one oriented anteriorly and one posteriorly), I created two separate characters and named those processes respectively as anterolateral and posterolateral (this and previous character). The posterolateral process of the ectopterygoid is absent for instance in *Oplurus* and *Chalarodon*, while both these OTUs retain an anterolateral process.

FORAMINA OF THE SKULL ROOF, CIRCUMORBITAL BONES, AND PALATAL COMPLEX

108. **Lacrimal duct, foramen:** single (0) / double (1) (P86, ch. 22; Si18, ch. 29). **Remarks:** The foramen that transmits the lacrimal duct can be single (e.g., *Ctenosaura*) or double (e.g., *Uromastyx*), resulting in two distinct foramina in the latter condition. The lacrimal foramen/foramina represent a passage for the lacrimal duct from the orbital region to the snout region, with the anterior end of the duct usually passing through a groove on the ventral surface of the vomer (e.g., Bellairs 1949; Oelrich 1956).
109. **Lacrimal duct, foramen/foramina, position:** no contribution from palatine (0) / with contribution from palatine (1) (G12, ch. 141 - modified). **Remarks:** The palatine can contribute to the ventral border of the lacrimal foramen in some taxa (e.g., *Enyalioides*)(see also Oelrich 1956; Etheridge & deQueiroz 1988; Evans 2008). There is no contribution from palatine for instance in *Iguana* and *Cyclura*. Contribution from the palatine is present in *Amblyrhynchus*, where the lacrimal duct has a double passage, and *Furcifer*, where instead there is a single foramen.
110. **Maxillo-palatine foramen:** absent (0) / perforating palatine only (1) / between palatine and maxilla (2) (G12, ch. 246; Si18, ch. 102 - modified). **Remarks:** Known also as palatine foramen or dorsal opening for the alveolar canal. When present, this foramen is located close to the palatine-prefrontal-maxilla contact, at the level of the palatine maxillary process and close to the infraorbital foramen (cf. Oelrich 1956, Evans 2008). Absent for instance in *Brookesia* and *Pogona*.
111. **Rostral foramen:** absent (0) / present as large opening (1) / present as foramen (2) (NEW). **Remarks:** This is a paired opening or foramen that can be found on both sides of the rostrum. In chamaeleonids, where this opening is relatively large, it is considered as derived from the separation of the external naris via a bony bar formed mostly by the prefrontal (Rieppel 1993). In this case, the opening is posterior and dorsal to the external narial opening and has been referred to as ‗prefrontal fontanelle' (e.g., Rieppel 1993; Evans 2008; Tolley 2013). However, a secondary opening in the same region of the skull is found in other iguanians. Rieppel (1993) showed how in embryos and hatchlings the fontanelle appears to be separated from the external nares in later stages at least in *Chamaeleo*, while it would remain confluent (i.e., fontanelle absent) with the narial

opening in *Rhampholeon* (cf. Tolley 2013). The prefrontal bone tends to contribute to most of the opening lateral/posterolateral margin, while the nasal contributes to its anterior/anteromedial margin. A variation occurs among other chamaeleonids, with either the maxilla (e.g., *Trioceros*) or the frontal (e.g., *Chamaeleo*, *Bradypodion*) also contributing to the border of this opening. A much smaller, but topologically similar, opening is present in other OTUs: in *Priscagama gobiensis* (specimen ZPAL MgR III-33) and some agamids (e.g., *Pogona*, *Agama*) between nasal, prefrontal and maxilla; in *Phrynosomimus* and *Gladidenagama* between nasal and prefrontal; in *Uromastyx* within the nasals, close to the contact with the nasal process of the premaxilla and the external nares (IP pers.obs.). In the chamaeleonids *Brookesia* there is no secondary large opening on the rostral region of the skull, but a small foramen is visible between maxilla, nasal and prefrontal (IP pers.obs.). I tentatively treated these openings as homologous and coded this character to assess the observed variation in our dataset.

112. **Rostral foramen:** paired (0) / single (1) (NEW). **Remarks:** A single sub-elliptical opening along the midline of the nasals is found in *Corytophanes*. Also referred to as naso-frontal fontanelle (e.g., Conrad 2015), I believe this opening to be homologous to the rostral foramen described in the previous characters due to topology and skull elements involved.
113. **Pineal foramen:** present (0) / absent (1) (E88 ch. 26; F92, ch. 9). **Remarks:** The pineal foramen is absent for instance in *Gekko* and *Polychrus*, as well as most chamaeleons.

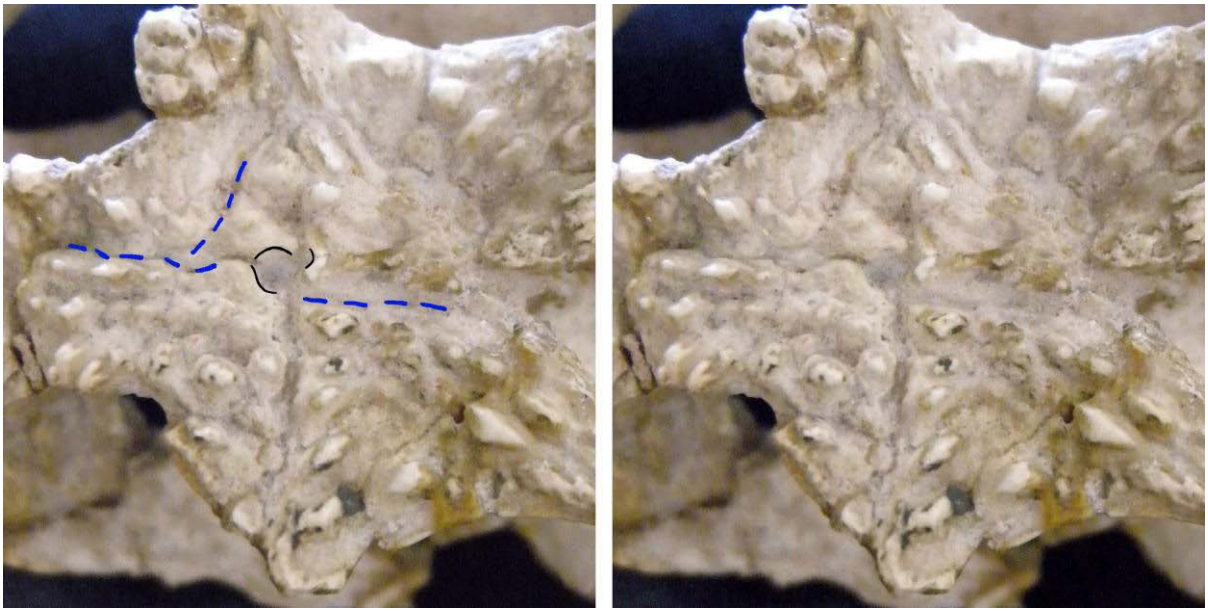

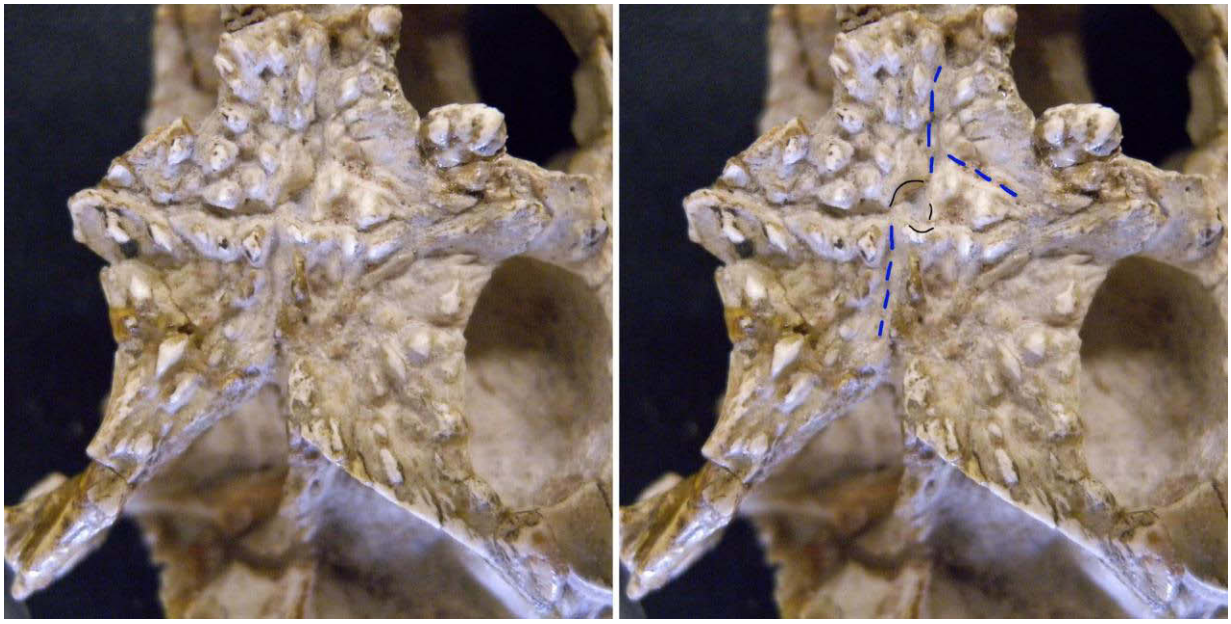

Arretosaurus - pineal foramen present between parietal and frontal

114. **Pineal foramen, position:** on parietal only (0) / on frontal only (1) / at frontoparietal contact (2) (F&E89, ch. 11 - modified). **Remarks:** The position of the pineal foramen shows some intraspecific variation within Iguania. In *Amblyrhynchus*, for instance, the pineal foramen can be fully enclosed by either the parietal or frontal, or located at the fronto-parietal suture. This variation does not seem to follow any specific pattern of ontogeny, dimorphism or population distribution. The more frequent condition in *Amblyrhynchus* is the pineal foramen located between the frontal and parietal, thus I scored this OTU as state 2.

SUSPENSORIUM

Quadrate

115. **Quadrate, foramen:** present (0) / absent (1) (Si18, ch. 118). **Remarks:** There can be multiple foramina on the quadrate, but the quadrate foramen is located just dorsally to the mandibular condyle, close to the quadrate pillar, and piercing anterior-posteriorly (e.g., Oelrich 1956). There seems to be variation in its position relative to the quadrate pillar, occurring at times on the lateral side (e.g., *Ctenosaura similis*) or on the medial side (e.g., *Cyclura*). However, the condition of this foramen appears quite variable across all Iguania

(pers. obs.) as it has been reported for geckos (Villa et al. 2018). The variation seems to be both inter- and intraspecific, with the foramen sometimes not fully piercing the quadrate, being double, and/or of variable size. Present for instance in *Amblyrhynchus cristatus* and *Ctenosaura pectinata*. Variably present in *Iguana iguana*. This foramen is mostly absent among chamaeleonids (e.g., *Chamaeleo*).

Polychrus - quadrate foramen present

116. **Quadrate, conch:** present (0) / absent (1) (Si18, ch.121). **Remarks:** The quadrate conch is absent in chamaeleonids. The conch is very weak in *Phrynosoma* and *Arretosaurus*.
117. **Quadrate, pterygoid lappet:** absent (0) / present (1) (E88, ch. 37). **Remarks:** The pterygoid lappet, if present, is located closer to the mandibular condyle(s) and along the medial crest (*sensu* Oelrich 1956) of the quadrate, where the pterygoid makes contact. Present for instance in *Ctenosaura*, absent in *Chamaeleon*. Not much prominent (but present) in *Iguana iguana*, including in larger specimens.
118. **Quadrate, suprastapedial process:** absent (0) / present (1) (D&C93, ch. 40; L97, ch. 30; G12, ch. 179; Si18, ch. 122). **Remarks:** The position of the quadrate cephalic condyle can be more or less deflected posteriorly/posteroventrally relative to the main axis of the quadrate shaft, but a suprastapedial process is present only when a lappet of bone extends posteroventrally beyond the quadrate posterior pillar (= posterior crest in Oelrich 1956). Absent for instance in *Chamaeleon* and *Phrynosoma*, while present in *Iguana*, *Agama*, and *Amblyrhynchus*.

119. **Quadrate, dorsal (= squamosal) notch:** absent (0) / present (1) (Si18, ch. 123). **Remarks:** A notch on the dorsal head of the quadrate for the articulation of the squamosal is common amongst iguanians (cf. E88, deQueiroz 1987).
120. **Quadrate, dorsal (= squamosal) notch, position:** on mid-dorsal surface (0) / along dorsolateral crest (1) (NEW). **Remarks:** The notch on the dorsal head of the quadrate can be located either in the middle of the dorsal surface of the quadrate (e.g., *Amblyrhynchus*, *Basiliscus*, *Chamaeleo*) or along the lateral margin of the dorsal head (e.g., *Iguana*, *Sauromalus*).

Epipterygoid

121. **Epipterygoid:** absent (0) / present (1) (E88, ch. 47; G12, ch. 290; Si18, ch. 115). **Remarks:** Absent for instance in *Chamaeleon*. Absent in all chamaeleonids (e.g., Estes et al. 1988).
122. **Epipterygoid, base, shape:** flared (0) / columnar (1) (Si18, ch. 116). **Remarks:** The epipterygoid base is flared for instance in *Gephyrosaurus* and *Sphenodon*, while columnar for all the ingroup.

TEMPORAL BONES

Quadratojugal

123. **Quadratojugal:** present (0) / absent (1) (Si18, ch. 38). **Remarks:** Present in the outgroup (e.g., *Sphenodon*, *Megachirella*).

Squamosal

124. **Squamosal:** present (0) / absent (1) (E88, ch. 33). **Remarks:** Absent in some geckos, like *Gekko gecko* included here as an outgroup (e.g., Estes et al. 1988). Present in all other OTUs.
125. **Squamosal, anterodorsal process:** present (0) / absent (1) (NEW). **Remarks:** This process contributes to the tetraradiate shape of the squamosal found for instance in rhynchocephalians, where it contacts the dorsal margin of the postorbital. Present in *Sphenodon*, *Gephyrosaurus*, and some agamids.

126. **Squamosal, posterolateral flange:** present (0) / absent (1) (NEW). **Remarks:** A ventral flange developing from the posterolateral margin of the squamosal is found in *Sphenodon*, where it extends to contact the lower temporal bar made by the posteroventral process of the jugal. This is different from the quadrate process of the squamosal that is found in most OTUs (see next character).
127. **Squamosal, posteroventral (= quadrate) process:** present (0) / absent (1) (Si18, ch. 51). **Remarks:** When present, this process can insert into the quadrate dorsal notch in squamates and contacts the quadrate and/or quadratojugal in rhynchocephalians (e.g., Evans 2008). Present in most iguanians, absent for instance in *Sphenodon*.
128. **Squamosal, posterodorsal process:** present (0) / absent (1) (E88, ch. 34; Si18, ch. 52). **Remarks:** Present in most OTUs (cf. Estes et al. 1988); absent for instance in *Ctenomastax* and *Morunasius*.
129. **Squamosal, contact with parietal:** absent (0) / present (1) (Ri80, ch. 37 - modified). **Remarks:** The squamosal contacts the supratemporal process of the parietal in most cases. In chamaeleonids, the contact between the parietal and squamosal is present between the mid-sagittal dorsal expansion of the parietal and the elongate posterodorsal process of the squamosal. The supratemporal processes of the parietal are in fact absent in most chamaeleonids (see character 56). The supratemporal prevents this contact for instance in *Physignathus*.

Supratemporal

130. **Supratemporal:** absent (0) / present (1) (E88, ch. 35; G12, ch. 166; Si18, ch. 62). **Remarks:** Absent in some agamids (e.g., *Moloch*) and *Sphenodon*., while present in most OTUs.
131. **Supratemporal, contact with parietal:** present (0) / absent (1) (NEW). **Remarks:** Present in most OTUs, and absent for instance in *Furcifer* and *Priscagama*.
132. **Supratemporal, contact with parietal, topology relative to parietal supratemporal process:** medioventrolateral (0) / ventrolateral (1) / ventromedial (2) / only ventral (3) (F&E89, ch. 12; G12, ch. 170 - modified). **Remarks:** This character assesses the geometry of the contact between the parietal supratemporal processes and the supratemporal bone, as well as the shape of the supratemporal. In many iguanians (e.g., *Cyclura*, *Iguana*), the

supratemporal wraps around the supratemporal process of the parietal, being exposed on its medial, ventral and lateral surfaces at the same time (state 0). Alternatively, the supratemporal contact the parietal just along its ventral+lateral margins (state 1, as in *Priscagama*) or its ventral+medial margins (state 2, as in *Sauromalus*). In *Sauromalus*, the supratemporal contacts extensively the medial surface of the parietal supratemporal process, slightly invading the ventral surface. This character is inapplicable when the supratemporal does not contact the parietal, as for instance in *Furcifer*. The contact is limited to the posteroventral margin of the parietal supratemporal processes for instance in *Uma* and *Holbrookia* (state 3), where the supratemporal is sandwiched between the squamosals and paroccipital processes.

BRAINCASE

Supraoccipital

133. **Supraoccipital, ossified processus ascendens of the synotic tectum (PAST):** absent (0) / present (1) (G12, Ch. 297; Si18, ch. 126). **Remarks:** This process is also called processus ascendens of the supraoccipital (e.g., Oelrich 1956; Rieppel & Zaher 2000) or medial ascending process (Simoes et al. 2018). When present, this process contacts the parietal usually via the parietal fossa on the ventral/posteroventral surface of the parietal bone. This character codes for the presence of an ossified PAST and as a cartilaginous element. For instance, in small to large size individuals of *Ctenosaura* and *Cyclura*, this element is always cartilaginous, while in taxa such as *Iguana* and *Amblyrhynchus*, the PAST becomes ossified only in fairly large size specimens (IP pers. obs.). This is a clear example of late ontogenetic development and scorings should be based on skeletally mature individuals only.
134. **Supraoccipital, ossified PAST, anterodorsal flange:** absent (0) / present (1) (NEW). **Remarks:** An expanded anterodorsal flange of the PAST is found amongst chamaeleonids. Inapplicable when an ossified PAST is absent.
135. **Supraoccipital, median (= mid-sagittal) crest:** absent (0) / present (1) (Co08, ch. 135; Si18, ch. 128). **Remarks:** The same as the supraoccipital crest in Oelrich (1956), this structure is widely present amongst iguanians. The crest is often blunt and/or incomplete in smaller size/younger individuals and it gets sharper and/or complete in larger size/adult

individuals (e.g., *Iguana*, *Cyclura*, *Ctenosaura*, and *Amblyrhynchus*: pers.obs.). The crest is particularly expanded for instance in *Furcifer*, where it contacts the expanded parietal mid-sagittal crest (next character).

136. **Supraoccipital, median (= mid-sagittal) crest, contact with parietal mid-sagittal crest:** absent (0) / present (1) (G12, ch. 301 - modified). **Remarks:** The supraoccipital mid-sagittal crest expands in some chamaeleonids to contact the ventral margin of the expanded parietal mid-sagittal crest. This contact is absent for instance in *Basiliscus*, despite the presence of a mid-sagittal crest on both parietal and supraoccipital. Inapplicable if either of the crests is absent.
137. **Supraoccipital, dorsolateral ridges:** absent (0) / present (1) (NEW). **Remarks:** Two lateral ridges, projecting dorsally, on each side of the mid-sagittal crest are present for instance in *Chamaeleo* and *Physignathus*. These structures are usually visible in both dorsal and posterior views and not always reach the ventral margin of the supraoccipital (e.g., *Dipsosaurus*, *Brachylophus*). Absent for instance in *Furcifer* and *Sauromalus*.

Basioccipital

138. **Basioccipital, dorsal surface:** smooth (0) / with mid-sagittal groove (1) / with mid-sagittal crest (2) (Bell 1997, ch. 67 - modified). **Remarks:** The dorsal surface of the basioccipital is concave but smooth in *Cyclura* and *Ctenosaura*, while a distinct groove is visible in *Furcifer*, *Amblyrhynchus*, and *Uromastyx*. In *Calotes* and *Petrosaurus* there is instead a median crest dividing the slightly concave dorsal surface of the basioccipital.
139. **Basioccipital, ventral surface, concavity:** absent (0) / single (1) / divided (2) (Si18, ch. 134). **Remarks:** The ventral surface of the basioccipital can be either flat or concave. When present, this concavity is single or separated by a longitudinal crest. This condition seems to be independent from the concavity sometimes present on the ventral surface of the basisphenoid (see ch. 142). In *Furcifer*, the basioccipital is flat, while the basisphenoid is concave. Present and divided for instance in *Gekko*, while single in *Basiliscus*.
140. **Basioccipital, ventral surface, transverse crest:** absent (0) / present (1) (NEW). **Remarks:** A horizontal/transverse crest can be present on the ventral surface of the basioccipital, right anterior to the occipital condyle, as seen in *Pogona* and *Arretosaurus*.

Basisphenoid

141. **Basisphenoid, crista trabecularis, ossified cultriform process:** absent (0) / present (1) (G12, ch. 328 - modified). **Remarks:** The crista trabecularis is also referred to as parasphenoid process (e.g., Oelrich 1956). This is an anteromedian projection of the basisphenoid, at the contact with the parasphenoid, that can bear an additional median process (i.e, the cultriform process) (cf. Oelrich 1956; G12). When present, this element is usually discernable even if basisphenoid and parasphenoid are fused, or should be scored as inapplicable when this fusion prevents a clear assessment. Contra to G12, I found that an ossified cultriform process is absent in *Dipsosaurus*. Present for instance in *Furcifer* and *Uma*.
142. **Basisphenoid, ventral surface, concavity:** absent (0) / single (1) / divided (2) (Si18, ch. 138). **Remarks:** The ventral surface of the basisphenoid can be flat or concave, and when a concavity is present, this can be divided by a median crest. I scored the division of the concavity as present (state 2) also when the median crest is not running throughout the ventral surface of the basisphenoid but only for part of it, like for instance in *Chamaeleo*. See also remarks for character 139.

Orbitosphenoid

143. **Orbitosphenoid, ossification:** absent (0) / present (1) (Si18, ch. 158). **Remarks:** The orbitosphenoid is not ossified in *Sphenodon* and *Gekko* (cf. Evans 2008).
144. **Orbitosphenoid, dorsal margin, shape:** convex (0) / concave (1) (NEW). **Remarks:** The dorsal end of the orbitosphenoid in most lizards bears two processes: the superior (or anteromedian) process and the posterior (or posterolateral) process (cf. Oelrich 1956). These two processes are well-distinct when the dorsal margin is deeply concave (state 1), as in *Agama*. To a lesser degree, but concave in *Iguana* as well, while a convex bony flange between the superior and posterior processes of the orbitosphenoid (state 0) is found in *Physignathus*, *Cyclura*, and *Amblyrhynchus*.

Prootic

145. **Prootic, crista prootica:** absent (0) / present (1) (Si18, ch. 140). **Remarks:** A crista prootica is absent for instance in *Polychrus*, where exit foramen for facial nerve VII is fully

exposed in lateral view. The crista is poorly developed but still present in *Anolis*, similarly to *Agama*.

146. **Prootic, crista prootica, shape:** straight (0) / with mid-ventral flange (1) (Si18, ch. 141 - modified). **Remarks:** A ventral flange is present along the margin of the crista prootica for instance in *Gekko*, giving to its margin a triangular/angled shape. The crest is a straight slope in *Amblyrhynchus*. Fundamentally, the shape of the crista prootica varies by having or not a triangular apex in anterior and lateral view. In *Iguana iguana* the prootic crest in anterior view is broader, descending, and triangular with the apex pointing ventrally. In *Amblyrhynchus* the prootic crest is sharper but there is no mid-ventral projection. In chameleons (e.g., *Furcifer*), the crista is shorter and does not reach the anterior margin of prootic.
147. **Prootic, crista alaris:** absent (0) / present (1) (E88, ch. 49; G12, ch. 305; Si18, ch. 142). **Remarks:** The prootic alar process can have an extension along its anterior margin which is known as crista alaris (Oelrich 1956). When present, the crista alaris extends dorsolaterally reaching as far as the trigeminal notch, and it is anterior to the anterior semicircular canal, which runs through the prootic. Absent in *Pogona* and *Physignathus*, while present for instance in *Ctenosaura* and *Gekko*.
148. **Prootic, supratrigeminal process:** absent (0) / present (1) (E88, ch. 5; G12, ch. 306; Si18, ch. 143). **Remarks:** When present, the supratrigeminal process is located on the anteromedial margin of the prootic (e.g., Oelrich 1956). Absent for instance in *Furcifer* and *Dipsosaurus*, present in *Cyclura* and *Amblyrhynchus*.
149. **Prootic, lateral wall, medial view, facial foramen:** absent (0) / present (1) (L98, ch. 68; G12, ch. 313; Si18, ch. 145). **Remarks:** The facial foramen can fully pierce the prootic lateral wall or just be visible in medial view (e.g., *Gekko*: cf. Villa et al. 2018). Absent for instance in *Brookesia*.

Opisthotic + Exoccipital (= Otoccipital)

150. **Opisthotic-exoccipital:** unfused (0) / fused (1) (E88, ch. 51; G12, ch. 352; Si18, ch. 151 - modified). **Remarks:** The fusion of the opisthotic and exoccipital to form the otoccipital is prevalent among squamates. State 0 is found for instance in *Sphenodon*, while all iguanians have state 1.

151. **Exoccipital/otoccipital, occipital condyle processes, contact:** absent (0) / present (1) (NEW). **Remarks:** The occipital condyle processes of the exoccipitals contact each other medially for instance in *Chamaeleo* and *Furcifer* (visible dorsally but not always in posterior view). This contact is visible in dorsal view, while it may appear absent in posterior view (e.g., *Furcifer*). This character is difficult to assess when the basicranial bones are fully fused, as frequently amongst squamates, and should be scored as unknown if the two processes cannot be discerned.
152. **Exoccipital/otoccipital, crista interfenestralis:** present (0) / absent (1) (G12, ch. 311; Si18, ch. 149). **Remarks:** The crista interfenestralis borders and usually covers the anterior margin of the occipital recess (= lateral aperture of the recessus scalae tympani, LARST) (e.g., Oelrich 1956; Evans 2008). When the crista is absent, the LARST is well-exposed in lateral and anterior view. The element is present in *Iguana* and *Conolophus*, while absent for instance in *Amblyrhynchus*, *Chamaeleo*, and *Furcifer*.
153. **Exoccipital/otoccipital, crista tuberalis:** absent (0) / present (1) (G12, ch. 312; Si18, ch. 153). **Remarks:** The crista tuberalis makes up the posterior margin of the occipital recess, where is located the lateral aperture of the recessus scalae tympani (LARST) (e.g., Oelrich 1956; Evans 2008). Present for instance in *Ctenosaura*.

Mandible

Subdental shelf and lingual wall are different structures. The subdental shelf is the structure underneath the teeth, made of an about horizontal shelf plus a ventrally projecting flange (here referred to as ventrolingual flange of the dentary). While the horizontal portion of the subdental shelf is always present, the extension/height of its ventral component (= ventrolingual flange) varies. The lingual wall, instead, is the structure that can be present along the lingual side of the tooth row, representing a dorsal projection of the subdental shelf on the lingual side of the dentary. The subdental shelf is tight to the Meckelian canal (and/or alveolar canal) and always below the teeth, while the lingual wall is tight to the teeth and always medial/lingual to them. The dentary lingual wall can be variably high relative to the dentary labial wall, and in some cases even higher than the latter (e.g., *Furcifer*).

Dentary

154. **Dentary, symphyseal surface, anterior view, shape:** flat (0) / rounded (1) (L98, ch. 110; G12, ch. 355; Si18, ch. 166). **Remarks:** This character assesses the shape of the articular portion of the anterior margin of the dentary (i.e., symphysis). In most iguanids the symphyseal surfaces are well-rounded with a fair amount of cartilage in between. In *Amblyrhynchus* especially, the layer of cartilage leaves the bony surfaces of the two symphyses quite spaced up (pers.obs.). In chamaeleons (e.g., *Furcifer*) the symphyseal surfaces are more greatly extended along the anterior margin of the dentary and also flatter, with a relatively smaller amount of cartilage in between (pers.obs.). In *Physignathus* for instance the symphyseal surfaces of the dentaries are quite flat, with the contact limited to the dorsal portion (see following character).
155. **Dentary, symphyseal articulatory facet, position:** only dorsal (0) / dorsoventral (1) (Si18, ch. 168 - modified). **Remarks:** The contact between the two dentaries at the symphysis can be limited to the most dorsal portion of the anterior margin of the dentaries, as in *Amblyrhynchus*, *Iguana*, and *Physignathus*, or extended dorsal-to-ventral (sometimes excluding just the most dorsal tip), as in *Sphenodon*, *Holbrookia*, and *Furcifer*.
156. **Dentary, Meckel's canal opening:** absent (0) / present as anterior fenestra (1) / open throughout the dentary (2) (E88, ch. 55; G12, chh. 371-372; Si18, ch. 167 - modified). **Remarks:** The Meckel's canal can open medially or ventrally on the dentary, either throughout the length of the dentary (state 2) or as simple fenestra on its anterior end (state 1). An anterior fenestra is found for instance in *Brachylophus* and *Ctenosaura*, while the canal is opened throughout the dentary in *Brookesia* (ventrally) and *Callopistes* (medially). The anterior opening is extremely reduced (but still present) in *Amblyrhynchus*. Absent in *Leiocephalus*.
157. **Dentary, subdental shelf, ventrolingual flange:** absent (0) / present (1) (E88, ch. 59; Si18, ch. 169 - modified). **Remarks:** The subdental shelf is made of the dentary tooth shelf plus a ventral projection (here called ventrolingual flange) from its medial/lingual margin. The subdental shelf is more or less developed but always present at least for most of the dentary, and is located above and medially to the Meckel's canal. The ventrolingual flange can be expanded in some OTUs (e.g., chamaeleonids, *Uromastyx*, agamids), where it creates a particularly tall subdental shelf. The extension of the dentary ventrolingual flange

and its relationship with the dentary ventrolabial flange determines whether the Meckel's canal is open or enclosed (see previous character).

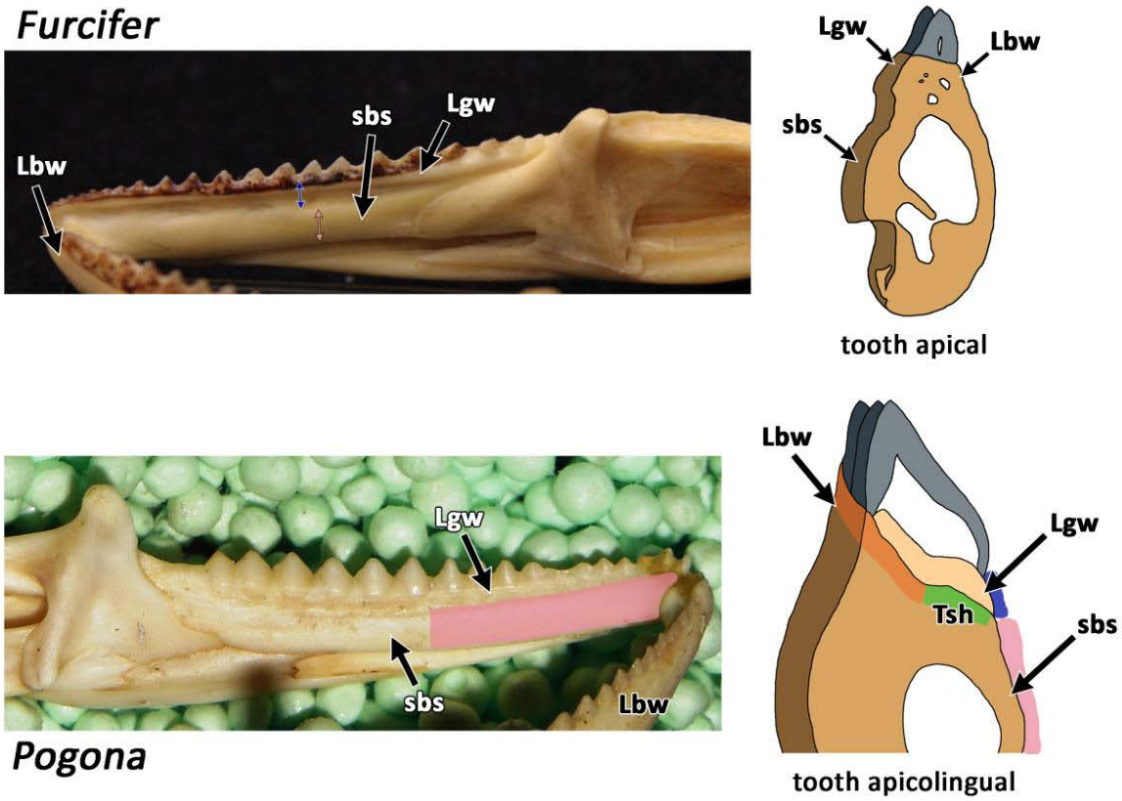

Difference between subdental shelf and lingual wall in *Furcifer* (top) and *Pogona* (bottom). For additional information on tooth implantation in *Pogona* and chamaeleons see respectively Haridy (2018), and Dosedělová et al. (2016) and Buchtová et al. (2013).

158. **Dentary, lingual wall:** present (0) / absent (1) (NEW). **Remarks:** The lingual wall of the dentary extends along the lingual side of the teeth. This structure basically represents a dorsal projection from the medial/lingual margin of the subdental shelf, in contrast to the ventrolingual flange which extends ventrally (see also remarks for previous character). A dentary lingual wall is found for instance in chamaeleonids, where it is usually as high or higher than the labial wall of the dentary (see next character).
159. **Dentary, lingual wall, height relative to labial wall:** same height (0) / shorter (1) / higher (2) (NEW). **Remarks:** Inapplicable when the lingual wall is absent. The lingual wall is as high as the labial wall for instance in *Acrodontopsis*, shorter than the labial wall for

instance in *Priscagama* and *Gekko*, while taller than the labial wall for instance in *Furcifer*. See also remarks for previous character.

160. **Dentary, ventrolingual flange contact to ventrolabial wall:** separate (0) / in contact (1) / fused (2) (F&E89, ch. 20; Sm09, ch. 94; G12, ch. 372; Si18, chh. 170-171 - modified). **Remarks:** The ventrolingual flange of the dentary borders the Meckel's canal and/or alveolar canal together with the ventrolabial wall of the dentary to various degrees: never contacting the dentary ventrolabial wall (state 0), as in *Pogona* and *Brookesia*; simply contacting the dentary ventrolabial wall (state 1), as in *Uma* and *Desertiguana*; or fusing to the ventrolabial wall of the dentary (state 2), as in iguanids and *Holbrookia*.
161. **Dentary, coronoid process:** absent (0) / present (1) (Si18, ch. 172). **Remarks:** The coronoid process represents a posterior dorsal projection of the dentary, behind the tooth row. Its presence can be assessed either in lateral or dorsal view. It is largely present amongst iguanians, but absent in some OTUs. More variability is found for the presence or lack of its expansion (see following character). Present for instance in *Iguana* and *Uromastyx*; absent in *Amblyrhynchus* and *Brookesia*. Reduced (but still present) in *Ctenosaura* and *Conolophus*.
162. **Dentary, coronoid process, dorsal expansion:** absent (0) / present (1) (E88, ch. 60; G12, ch. 367; Si18, ch. 173). **Remarks:** When the coronoid process of the dentary has a dorsal expansion, this extends to invade the dorsal process of the coronoid. Present for instance in *Uromastyx* and *Sphenodon*; absent in *Brookesia* and *Iguana*.
163. **Dentary, coronoid process, shape:** single (0) / bifurcated (1) (Si18, ch. 174). **Remarks:** The coronoid process of the dentary can be bifurcated posteriorly to wrap around the anterior and/or lateral margin of the coronoid (cf. Simões et al. 2015). The coronoid process is single for instance in *Furcifer*, while bifurcated in *Gueragama*.
164. **Dentary, posterolateral process:** absent (0) / present (1) (NEW). **Remarks:** A posterolateral process of the dentary is absent for instance in *Lavatisaurus* and other changjiangosaurids, as well as the outgroups *Varanus* and *Gekko*.
165. **Dentary, posterolateral process, expansion:** absent (0) / present (0) (NEW). **Remarks:** The dentary posterolateral process can extend posteriorly to the level of or beyond the coronoid posterodorsomedial process in some taxa (e.g., *Anolis*, *Pogona*, *Arretosaurus*, *Furcifer*). This can happen either when the process is single or bifid (see next character). In

Anolis, the posterolateral process overlaps most of the surangular, similarly to the condition seen in Pogona and many acrodontans, where it can reach up to the retroarticular process.

166. **Dentary, posterolateral process, shape:** single (0) / bifid (1) (NEW). **Remarks:** This process is bifid for instance in Leiolepis and Pristidactylus, while single in the majority of OTUs.
167. **Dentary, posteroventral (or posteroventrolateral) process:** absent (0) / present (0) (G12, ch. 370 - modified). **Remarks:** When present, this process is about parallel or diverging from the posteroventral (here posterolateral) process accounted for in Si18 (ch. 175), which instead is exposed on the mid-lateral side of the mandible (along the posterior margin of the dentary). This process can be exposed in either ventral or ventrolateral views. Absent for instance in *Furcifer* and *Sphenodon*, while commonly present in iguanids. G12 addresses this condition as the presence of a bifid or single angular process.

Coronoid

168. **Coronoid, dorsal process, position relative to terminal dentary teeth:** posterior (0) / medial (1) (NEW). **Remarks:** The coronoid is located posterior to the dentary tooth row in most lizards. In chameleons, however, the coronoid contacts with the medial surface of the dentigerous portion of the dentary, with the last dentary teeth reaching as far as the posterior border of the coronoid dorsal process (which is selected as a landmark for this character).
169. **Coronoid, anterolateral process:** absent (0) / present (1) (E88, ch. 68; G12, ch. 394; Si18, ch. 198). **Remarks:** Absent for instance in *Stenocercus* and *Uromastyx*, present in *Ctenosaura* and *Morunasaurus*.
170. **Coronoid, posterodorsomedial process:** present (0) / absent (1) (Si18, ch. 200). **Remarks:** This process is bifid in Conolophus, but single in all other iguanids, including *Amblyrhynchus*. It is quite elongate in chamaeleons. Absent for instance in *Basiliscus*.
171. **Coronoid, posterodorsomedial process, shape:** single (0) / bifid (1) (NEW). **Remarks:** Single in most OTUs; bifid for instance in *Conolophus* and *Furcifer*.
172. **Coronoid, posteroventromedial process:** present (0) / absent (1) (G12, ch. 393; Si18, ch. 201). **Remarks:** A posteroventromedial process is absend in *Sphenodon*.

173. **Coronoid, posterodorsomedial-posteroventromedial process, flange:** absent (0) / present (1) (NEW). **Remarks:** A flange connecting the two posteromedial processes of the coronoid is found for instance in *Furcifer* and *Arretosaurus*, while the two processes are distinctly separate in most OTUs. Inapplicable when one of the two processes is absent.

Arretosaurus - flange present

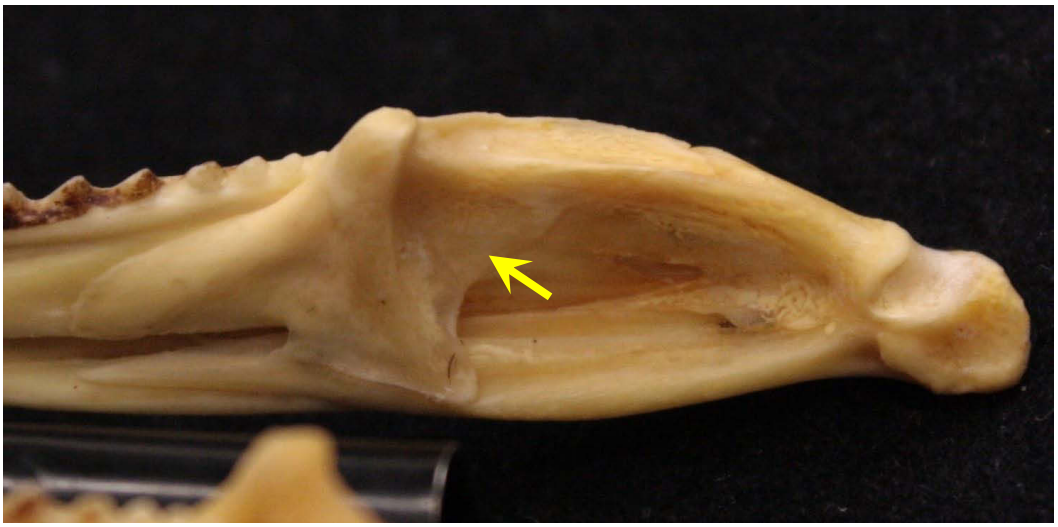

Furcifer - flange present

Splenial

174. **Splenial:** absent (0) / present (1) (E88, ch. 65; G12, ch. 374; Si18, ch. 176). **Remarks:** Absent for instance in *Sphenodon* and *Brookesia*, while present in all iguanids.
175. **Splenial, anterior border, shape:** tapering (0) / notched (1) (Si18, ch. 179 - modified). **Remarks:** The anterior margin of the splenial tapers in most OTUs, while is notched for instance in *Physignathus* and *Uma*. The position of the anterior inferior alveolar foramen during skeletal growth affects the shape of the splenial anterior end, as variation is found between specimens of different size for instance in *Physignathus*: small size (young) individuals tend to have a flat or slightly tapering anterior margin of the splenial, while in more skeletally mature individuals this margin is notched by the anterior inferior alveolar foramen. Our scorings are based exclusively on skeletally mature specimens.

Angular

176. **Angular:** present (0) / absent (1) (E88, ch. 72; Si18, ch. 180). **Remarks:** This character assesses the presence of a distinct angular whose absence is consistent throughout the ontogenetic stages of a species. For instance, the angular fuses to the prearticular and surangular in *Gekko* but a suture is still often visible in many individuals, hence the element cannot be scored as absent (cf. Si18). In *Anolis* and *Phrynosoma* instead, a distinct angular is consistently lacking and so accordingly with previous authors (e.g., E88, Si18), I scored the element as absent in these OTUs.

Surangular

177. **Surangular, coronoid process:** absent (0) / present (1) (Si18, ch. 182). **Remarks:** The dorsal margin of the surangular can bear an anterior projection rising towards the coronoid posterior margin. This condition has to be assessed on the disarticulated bone, as the process can be covered by the coronoid (e.g., *Amblyrhynchus*, *Cyclura*), especially when not as prominent as in *Sphenodon*. Absent for instance in *Dipsosaurus* and *Iguana*, where the dorsal margin of the surangular is straight.
178. **Surangular, lateral adductor crest (= lateral shelf):** absent (0) / present (1) (Si18, ch. 183). **Remarks:** A crest bordering the lateral adductor fossa can be present on the lateral margin of the surangular, where the *m. adductor mandibularis externus* inserts (Oelrich

1956). This crest is quite blunt but present in *Iguana*, *Cyclura* and *Ctenosaura* while sharp and prominent in *Amblyrhynchus* and *Conolophus*. Absent for instance in chamaeleonids and *Sphenodon*.

179. **Surangular, anterior foramen:** absent (0) / present (1) (Co08, ch. 172; Si18, ch. 184). **Remarks:** An anterior surangular foramen is absent in *Polychrus* and *Anolis*, while present in most OTUs. In some OTUs such as *Furcifer* and *Pogona*, where the dentary is posteriorly expanded, its position is usually lower on the surangular and at the contact with the dentary, which partially contributes to its anterior border (see next character).
180. **Surangular, anterior foramen, position relative to posterolateral process of dentary:** posterior (0) / ventral (1) / dorsal (2) (F&E89, ch. 19 - modified). **Remarks:** The anterior foramen of the surangular is posterior in all iguanids, dorsal for instance in chamaeleons and *Uromastyx*, while ventral in *Zapsosaurus* and *Priscagama*.

Articular and prearticular

181. **Articular, foramen chorda tympani:** absent (0) / present (1) (Si18, ch. 189). **Remarks:** A foramen for the chorda tympani nerve can be present on the dorsal surface of the articular, approximately at the level of the anterior margin of the retroarticular process (visible in dorsal and medial views). The foramen is absent for instance in *Uma* and *Holbrookia*.
182. **Articular, retroarticular process:** present (0) / absent (1) (G88, ch. 73; Si18, ch. 190). **Remarks:** A retroarticular process is absent in *Phrynosoma* and chamaeleons too, as well as *Arretosaurus*. Present in most OTUs.
183. **Articular, retroarticular process, shape:** tapering posteriorly (0) / with parallel lateral and medial margins (1) / flaring posteriorly (2) (E88, ch. 78 - modified). **Remarks:** The retroarticular process is fairly triangular and tapering posteriorly for instance in *Ctenosaura*; its margins flare posteriorly in *Dipsosaurus* and *Polychrus*, while parallel in *Anolis*.
184. **Articular, retroarticular process, dorsal surface, shape:** flat (0) / concave (1) (E88, ch. 74; Si18, ch. 191). **Remarks:** Referred to as dorsal fossa (Simoes et al. 2018), sulcus or pit (Estes et al. 1988; Conrad 2008), and articular fossa (Oelrich 1956). There are three conditions for the dorsal surface of the retroarticular process: 1) flat (e.g., *Uromastyx*); 2)

homogeneously concave (*Cyclura*, *Amblyrhynchus*, *Conolophus*); 3) overall concave with an additional fossa on the most anterior portion (e.g., *Iguana iguana*). However, conditions 2) and 3) are heavily dependent on skeletal maturity of the specimens and may be challenging to distinguish unambiguously, so I decided to code this character for the two most obvious different conditions (flat *versus* concave).

185. **Articular, retroarticular process, lateral notch:** absent (0) / present (1) (E88, ch. 77; G12, ch. 409; Si18, ch. 192). **Remarks:** A notch on the lateral side of the retroarticular process is present in *Gekko* and *Phrynosoma*.
186. **Articular-prearticular, angular (= medial) process:** absent (0) / present (1) (E88, chh. 73, 80; Co08, ch. 209; Si18, ch. 193). **Remarks:** Also referred to as pterygoideus process in G12, and medial process in Si18. I adopted the terminology used by Oelrich (1956) and Evans (2008). The angular process projects from the ventral/ventromedial surface of the medial margin of the quadrate articular condyle of the articular, often reaching as far posteriorly as the retroarticular process (cf. Oelrich 1956). However, it can still be present if the retroarticular process is absent (e.g., chamaeleons).
187. **Articular-prearticular, angular (= medial) process, orientation:** ventromedial (0) / medial (1) (NEW). **Remarks:** The angular process of the articular can be simply medially oriented (e.g., *Sauromalus*, *Amblyrhynchus*) or ventrally deflected (e.g., *Iguana*, *Basiliscus*). There is some variability in smaller *Iguana* and *Cyclura* specimens, but in larger individuals is strongly ventrally deflected in both cases.
188. **Articular-prearticular, angular (= medial) process, prearticular crest:** absent (0) / present (1) (E88, ch. 73; Si18, ch. 194). **Remarks:** This is not the same as the lateral crest of the angular process in Evans (2008), or the tympanic crest of the articular in Oelrich (1956). The prearticular crest as described in Si18 is on the dorsomedial surface of the angular process. A short crest on the dorsal surface of the angular process is present in *Conolophus*, *Amblyrhynchus*, and *Ctenosaura*, while absent in *Cyclura* and *Iguana*. The presence of this crest gives to the angular process a thick, sub-square or sub-trapezoidal shape in medial view, while when absent the angular process is fairly thin and triangular in the same view. In *Furcifer*, where the angular process is ventrally deflected, a blunt crest is visible on its medial surface.

189. **Articular-prearticular, lateral process:** absent (0) / present (1) (NEW). **Remarks:** This process projects from the lateral surface of the articular (beside the articular-quadrate contact), reflecting the angular process on the medial side. Particularly prominent and projecting laterally in *Arretosaurus*; much smaller in *Furcifer* and projecting ventrolaterally; in *Crotaphytus* is also much smaller than *Arretosaurus* and projecting laterally.

Arretosaurus - lateral process of the articular present.

Foramina of the lower jaw

190. **Anterior inferior alveolar foramen:** absent (0) / present (1) (Si18, ch. 164). **Remarks:** Present in most OTUs, while absent for instance in *Uma* and *Furcifer*. In taxa where the Meckel‘s canal is open throughout, a dedicated foramen for the inferior alveolar canal is usually absent or making a notch on the anterior margin of the splenial (e.g., *Uromastyx*).
191. **Anterior mylohyoid foramen:** absent (0) / present (1) (Si18, ch. 162). **Remarks:** The anterior mylohyoid foramen transmits the anterior branch of the mylohyoid nerve (Oelrich 1956). It is usually quite smaller than the anterior inferior alveolar foramen. In some taxa, as *Sphenodon* and *Uromastyx*, the mylohyoid nerve is transmitted via the Meckel‘s canal, so dedicated foramina for this nerve are in fact absent.
192. **Posterior mylohyoid foramen:** absent (0) / present (1) (Co08, ch. 175; Si18, ch. 163). **Remarks:** The posterior mylohyoid foramen represents the passage for the posterior branch of the mylohyoid nerve, and its ventral margin is a site of attachment for the *m.*

mandibulohyoideus (Oelrich 1956). It can be visible in medial or ventral view in articulated jaws. This foramen is open on the posterior end of the ventral margin of the dentary in *Anolis*, where the dentary is extended to almost reach the retroarticular process.

DENTITION

Marginal teeth

I set two landmarks to best assess dentition characters in our ingroup. The anterior marginal dentition landmark is set to the most anterior (circumsymphyseal) dentary teeth, or teeth at the premaxilla-maxilla contact. The posterior marginal dentition landmark is set to the most posterior dentary teeth (at the end of the tooth row). Many iguanians show important differences between anterior and posterior marginal dentition in several aspects: from a different geometry of tooth implantation (mostly acrodontans), to a variation in number of crown cusps (both acrodontans and pleurodontans), and/or to the extent and position of the opening of the pulp cavity (see Haridy (2018) and LeBlanc et al. (2020) for further details). For example, in *Conolophus* the anterior marginal teeth are tricuspid, but about halfway through the dentary and maxillary tooth rows, another cusp is added anteriorly on the crown apex (consistently across all the specimens examined here). This implies that the use of two separate landmarks for the marginal dentition is necessary to best encompass the variability found in our ingroup. Polycuspid anterior marginal teeth are found for instance in *Cyclura* and *Iguana*; tricuspid anterior marginal teeth are found in *Amblyrhynchus* and *Conolophus*. The number of cusps remains constant (three) in *Amblyrhynchus* throughout the tooth row, while it changes in *Conolophus*, as explained above.

193. **Anterior marginal teeth, crown shaft, shape of mesio-distal margins:** tapering throughout (0) / parallel-sided (1) / flaring (2) (NEW). **Remarks:** The tooth crown shaft can have margins homogeneously tapering towards its apex (state 0), resulting in a conical tooth shape, with the margins remaining parallel up to the apex (state 1), or diverging towards the apex (state 2). Although state 0 encompasses mostly conical, non-cuspate teeth, in some cases, while the margins of the crown shaft keeps tapering throughout, an abrupt convergence of the two margins at the apex is still possible (i.e., tapering-sided teeth with a monocusp and not simply conical). Hence, this feature is independent from the

cuspate or non-cuspate shape of the apex of the crown (next character), as the cuspate condition can be present in any of these states.

194. **Anterior marginal teeth, crown apex, shape:** conical (0) / monocuspid (1) / tricuspid (2) / polycuspid (3) / spatulate (4) (NEW). **Remarks:** State 0 accounts for a simple conical tooth shape, as seen for some acrodontans. The tooth crown can have a single cusp, where the apical margins of the crown abruptly converge to form a monocusp (state 1), or also have accessory anterior and posterior cusps (state 2 if only three cusps; state 3 if more than three cusps). State 4 accounts for the slightly flat to rounded, spatulate condition seen for instance in *Isodontosaurus*, *Jeddhardhan* and *Gueragama*. In this taxa, the shape of the crown apex changes along the row from fairly round to flat. This is likely related to the tooth life cycle, with crowns getting flatter due to increased wearing. This would suggest a slow to none replacement rate of the teeth, considering that at least in *Isodontosaurus* and *Gueragama* resorption pits are present (while they appear absent in *Jeddhardhan*).
195. **Posterior marginal teeth, crown shaft, shape of mesio-distal margins:** tapering throughout (0) / parallel-sided (1) / flaring (2) (NEW). **Remarks:** See remarks for character 193.
196. **Posterior marginal teeth, crown apex, shape:** conical (0) / monocuspid (1) / tricuspid (2) / polycuspid (3) / spatulate (4) (NEW). **Remarks:** See remarks for character 194.
197. **Posterior marginal teeth, resorption pits:** absent (0) / present (1) (E88, ch. 85; G12, ch. 431; Si18, ch. 207). **Remarks:** This character accounts for one of the major differences between acrodonts and pleurodonts (as tooth implantation types and not taxonomic groups). Acrodonts have no pits and teeth are added posteriorly, stopping early in ontogeny (see Haridy 2018), while pleurodonts have resorption pits and keep replacing teeth throughout life. The character on ‗replacement mode' in Si18, in addition to this character, is not included here because in my dataset, when resorption pits are absent, the alternative replacement mode is always by adding teeth posteriorly (at least until a certain stage in ontogeny). In Si18, the character on replacement mode makes sense because snakes for instance have no (visible) resorption pits, but teeth are still replaced continuously (but from within the pulp cavity). None of the dentary fragments available for *Arretosaurus* show the presence of pits. *Mimeosaurus tugrikinensis* has resorption pits, which are well-exposed for the maxillary teeth.

198. **Posterior dentary teeth, position relative to jaw labial wall:** apicolingual (0) / apical (1) (Si18, ch. 210 - modified). **Remarks:** This character accounts for the geometrical relationships between teeth and jaw bone. In state 0, the teeth attach to the apex and base of the jaw (e.g., *Iguana*, *Pogona*), independently from the presence (e.g., *Pogona*) or absence (e.g., *Iguana*) of a mineralized wall on the lingual side of the tooth. This roughly corresponds to the so-called pleurodont-type tooth implantation (e.g., Owen 1840-1845; Peyer 1968; Tomes 1874; LeBlanc et al. 2017; 2020; Bertin et al. 2018). State 1 describes the condition where teeth are implanted along the top of the jaw bone (e.g., *Chamaeleo*, *Furcifer*), referred to as acrodont implantation (se.g., Owen 1840-1845; Peyer 1968; Tomes 1874; Haridy 2018; Bertin et al. 2018). I interpreted these character states differently from Si18, based on recent studies on tooth implantation in acrodontan and pleurodontan iguanians (Buchtová et al. 2013; Haridy 2018; LeBlanc et al. 2020). A third state could be added to this character, accounting for a full lingual implantation, where the teeth lack any contact with the apex of the jaw bone and are set in grooves or sockets along the top of the subdental shelf (i.e., thecodont implantation1: e.g., Owen 1840-1845; Peyer 1968; Tomes 1874; Bertin et al. 2018; LeBlanc et al. 2020). This last condition is not included here because does not characterize any of my OTUs. See also discussions in the main manuscript. The image below exemplify state 0 and 1 adopted in this study.

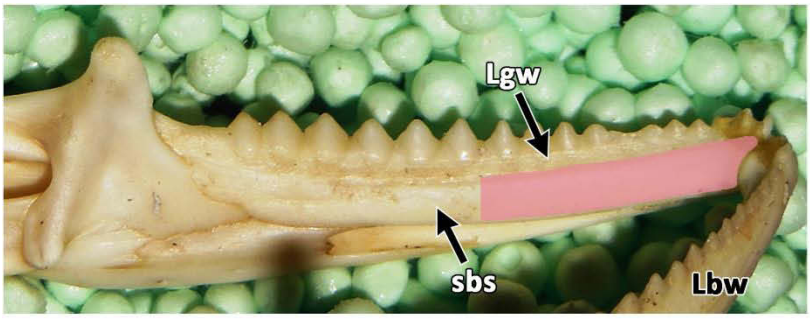

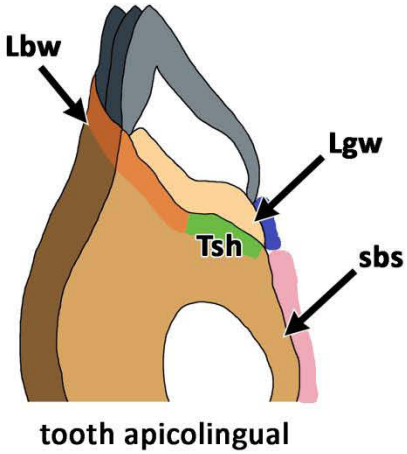

State 0 - apicolingual

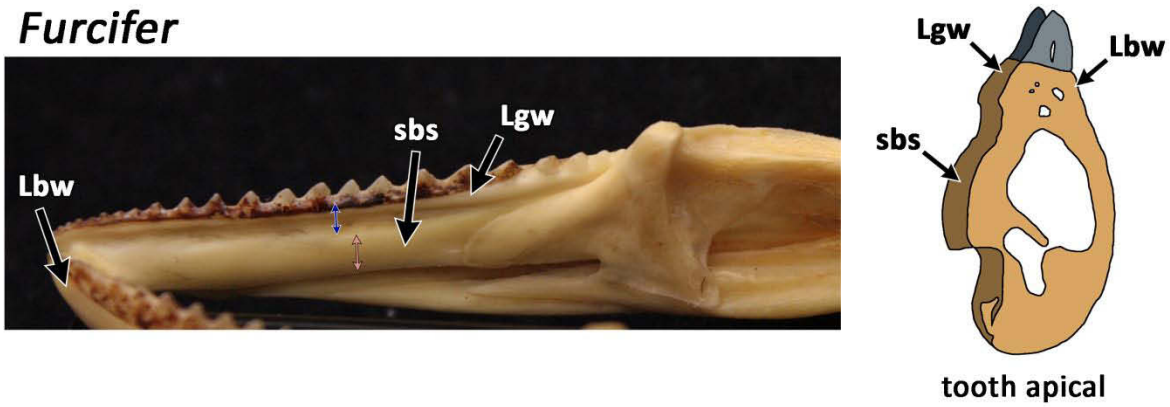

State 1 – apical

199. **Posterior dentary teeth, root, dentine labial wall:** present (0) / absent (1). **Remarks:** When the dentine wall of the tooth root is absent, the teeth are highly asymmetrical, as seen for instance in *Iguana* and *Amblyrhynchus*. When the teeth are more symmetrical, labial and lingual walls of the teeth are both present (e.g., *Sphenodon*, *Furcifer*). For more information see LeBlanc et al. (2020).

Palatal teeth

200. **Palatine teeth:** absent (0) / present (1) (E88, ch. 82). **Remarks:** Present in *Sphenodon*, while absent in the ingroup.
201. **Pterygoid teeth:** absent (0) / present (1) (E88, ch. 83). **Remarks:** Pterygoid teeth are typically absent in Acrodontans, but also for instance in *Dipsosaurus* and *Conolophus*. In *Amblyrhynchus*, there is a small number of pterygoid teeth, sometimes only on one side of the skull, or fully absent in some specimens. This is in contrast with *Iguana* for instance, where the teeth are microscopic, numerous, and always present.
202. **Pterygoid teeth, crown apex, shape:** non-cuspate (0) / monocuspid (1) / tricuspid (2) / polycuspid (3) (NEW). **Remarks:** See remarks for character 194.

HYOID

For the hyoid, I adopted the terminology used by Tanner & Avery (1982).

203. **Epihyal:** absent (0) / present (1) (NEW). **Remarks:** Absent in some chamaeleonids.

204. **Epihyal, anteromedial process:** absent (0) / present (1) (G12, ch. 452 - modified). **Remarks:** Anteromedial bulge or flange of the epihyal found for instance in *Pristidactylus* and *Cyclura*; absent in *Sauromalus*.
205. **Epihyal, anterolateral process:** absent (0) / present (1) (G12, ch. 452 - modified). **Remarks:** Anterolateral flange of the epihyal found for instance in *Gekko*, while absent in *Brachylophus* and *Sauromalus*.
206. **Epihyal, posterolateral process:** absent (0) / present (1) (G12, ch. 453 - modified). **Remarks:** Posterolateral flange of the epihyal found for instance in *Varanus*, but absent in most OTUs.
207. **Ceratobranchial-I, posteroventral flange:** absent (0) / present (1) (NEW). **Remarks:** This flange is present for instance in *Phrynosoma*. Absent in most OTUs.
208. **Ceratobranchial-II:** absent (0) / present (1) (E88, ch. 91). **Remarks:** The second ceratobranchial is absent for instance in *Chamaeleo* while present in *Cyclura* and *Brachylophus*.
209. **Ceratobranchials-II, shape:** diverging (0) / parallel (1) (NEW). **Remarks:** The two second ceratobranchials are parallel for instance in *Anolis carolinensis*, *Agama* and *Brachylophus*, while diverging in *Sauromalus* and *Pristidactylus*. When parallel, the two ceratobranchials sometimes contact each other for most of their length.

Postcranium

AXIAL SKELETON

Atlas and axis

210. **Atlas, neural arches:** separate (0) / sutured to each other (1) / sutured to axis neural spine (2) (Si18, ch. 220). **Remarks:** The character refers to the relationships between the two atlas neural arches, which remain separate in most lizards, and also to the axis neural spine that in few cases is sutured to the two atlas neural arches (see character remarks in Si18 for further details).

Iguana iguana - cervicals I to IV. The atlas arches are sutured to the axis neural spine.

Amblyrhynchus - cervicals I to V. The atlas arches are sutured to each other but not to the axis neural spine.

211. **Atlas, neural arch, postzygapophyses:** absent (0) / present (1) (L97, ch. 106; Si18, ch. 221). **Remarks:** Absent for instance in *Spheonodon* and *Oplurus*, while present in iguanids.
212. **Atlas, neural arch, synapophyses, orientation:** posterior (0) / posteroventral (1) (NEW). **Remarks:** The synapophyses of the atlas neural arches are posteriorly oriented for instance in *Ctenosaura* and *Furcifer*, while posteroventral in *Phrynosoma* and *Sphenodon*.
213. **Axis, connection to intercentrum(a):** to intercentrum 2 only (0) / to intercentra 2 and 3 (1) (Si18, ch. 225). **Remarks:** The axis contacts both intercentra 2 and 3 for instance in *Cyclura* and *Iguana*, while the contact is limited to intercentrum 2 in *Furcifer* and *Chamaeleo*.
214. **Axis, intercentrum, fusion to axial pleurocentrum:** unfused (0) / fused (1) (Si18, ch. 226). **Remarks:** Unfused for instance in *Sphenodon* and *Gephyrosaurus*, while fused in most other OTUs. This character is deeply affected by late ontogeny. In medium-size specimens of *Cyclura* and *Iguana* the two elements are separate, while they are clearly fused in large size individuals of both taxa. In *Ctenosaura*, axis intercentrum and pleurocentrum are fused also in fairly small specimens. There is also variation in fusion
215. **Axis, ribs:** present (0) / absent (1) (Si18, ch. 227). **Remarks:** Present for instance in Megachirella, while absent in most OTUs.

Postaxial presacral vertebrae (cervicals + dorsals)

The limit cervical-dorsal series is set at the first anterior presacral vertebra with ribs that articulate to the sternum (i.e., first dorsal), following Hoffstetter & Gasc (1969). Anterior presacral region refers to the most posterior cervical vertebrae and most anterior dorsal vertebrae, at the transition between cervical and dorsal region. In this part, most vertebral features are not easily discernable between cervical and dorsal vertebrae, and more differences are actually found with the posterior dorsal region (= posterior presacral vertebrae). Some characteristics, like the margo ventralis and lateralis, tend to be present in the anterior presacral region and then disappear more posteriorly along the column in some taxa. Hence, the necessity to set different landmarks throughout the vertebral column, where traditional regionalization in cervical, dorsal, etc. can be more ambiguous. Each specific case is addressed in the different characters with relative examples.

216. **Cervical vertebrae, intercentrum, articulation:** intervertebral (0) / to preceding corresponding pleurocentrum (1) (E88, chh. 97-98; Si18, ch. 238 - modified). **Remarks:** In state 0, the intercentra articulate between consecutive vertebrae, at the level of the condyles. In state 1, the intercentra articulate to their matching vertebral centrum, which is anterior (preceding) to the intercentrum in question.
217. **Cervical vertebrae, pleurocentrum, midventral ridge:** absent (0) / present (1) (Si18, ch. 231). **Remarks:** A median ridge, with a more or less pointed apex, between the hypapophysis and the cotyle (almost reaching the cotyle) can be present on the ventral surface of the cervical pleurocentra (e.g., Hoffstetter & Gasc 1969). Present for instance in *Physignathus*, absent in *Furcifer*.
218. **Dorsal vertebrae, intercentrum:** absent (0) / present (1) (B85, ch. L5; Si18, ch. 239). **Remarks:** Present in *Gekko* and *Sphenodon*; absent in most OTUs.
219. **Posterior dorsal vertebrae, pleurocentrum, midventral ridge:** absent (0) / present (1) (Si18, ch. 232). **Remarks:** A blunt ridge (with two well-developed grooves on the sides) can be visible on the ventral surface of the dorsal vertebrae. Present for instance in *Iguana* and *Ctenosaura*, while absent in *Cyclura* and *Furcifer*.
220. **Presacral vertebrae, pleurocentrum, shape:** amphicoelous (0) / procoelous (1) (Si18, ch. 228 - modified). **Remarks:** Lack of condyles (i.e., amphicoelous condition of presacral pleurocentra) is found for instance in *Sphenodon* and *Gekko*, while most OTUs have procoelic presacrals.
221. **Presacral vertebrae, pleurocentrum, precondylar constriction:** absent (0) / present (1) (E88, ch. 94; Si18, ch. 233). **Remarks:** A constriction can be present anterior to the condyle in some taxa, like *Physignathus* and *Uromastyx*. The character is inapplicable when there are no condyles (i.e., presacral pleurocentra are amphicoelous; see Si18 for further remarks).
222. **Anterior presacral vertebrae, pleurocentrum, cotyle-synapophysis crest:** absent (0) / present (1) (NEW). **Remarks:** This is a crest that can be present between the synapophysis and the lateral/ventrolateral margin of the cotyle, and usually at the cervical-dorsal vertebrae transition. The crest tends to disappear posteriorly in all taxa, so I set the landmark to the most anterior presacrals. Present in *Ctenosaura*, absent in *Furcifer*. In *Ctenosaura*, this crest is present for all the cervicals and most of the anterior dorsal series

but not in the most posterior presacrals. In *Iguana*, the crest disappears almost right after the cervical series (i.e., the first one or two dorsals can have a crest but most of the dorsals do not have this crest).

223. **Posterior presacral vertebrae, pleurocentrum, cotyle-synapophysis crest:** absent (0) / present (1) (NEW). **Remarks:** See remarks for previous character.
224. **Posterior presacral vertebrae, pleurocentrum, synapophysis-condyle crest (= margo ventralis):** absent (0) / present (1) (Si18, ch. 234 - modified). **Remarks:** This is a crest that can be present between the synapophysis and the lateral/lateroventral margin of the condyle: see Hoffstetter & Gasc (1969). This character is best assessed in the dorsal series, as the crest is too variable in the cervical series, affected by the variation in size of the synapophyses which increases posteriorly. Absent for instance in *Furcifer*, present in *Iguana* and *Ctenosaura*. In *Cyclura* this crest is quite blunt but still visible.
225. **Presacral vertebrae, neural arch, zygosphenes and zygantra:** absent (0) / present (1) (LC00, Ch. 186; Si18, ch. 248). **Remarks:** Absent for instance in *Furcifer*, present in *Iguana*.
226. **Presacral vertebrae, neural arch, zygosphenes, orientation:** facing dorsolaterally (0) / facing ventrolaterally (1) (LC00, ch. 187; Si18, ch. 249). **Remarks:** Considering the position in articulation of the vertebrae, the zygosphene articular facet faces either dorsolaterally (transversal to the prezygapophysis articular facet) or ventrolaterally (facing the prezygapophysis articular facet). This character can be also scored if only the zygantra on the posterior surface of the vertebra are visible: to match the states of the current character, the zygantra facing ventromedially correspond to state 0 (dorsolaterally facing zygosphenes), while the zygantra facing dorsomedially correspond to state 1 (ventrolaterally facing zygosphenes).
227. **Mid-anterior presacral vertebrae, neural arch, prezygapophysis-synapophysis crest:** absent (0) / present (1) (Be97, ch. 103 - modified). **Remarks:** Present in *Ctenosaura*, *Iguana* and *Furcifer*. In some taxa this crest easily disappears more posteriorly (e.g., *Iguana*, *Furcifer*), while is more consistent throughout the presacral series in others (e.g., *Ctenosaura*). Absent for instance in *Gekko* and *Leiocephalus*.
228. **Mid-anterior presacral vertebrae, neural arch, prezygapophysis-postzygapophysis crest (= margo lateralis):** absent (0) / present (1) (Si18, ch. 251). **Remarks:** This crest

connects the prezygapophysis to the postzygapophysis, as shown in Hoffstetter & Gasc (1969; Fig. 69). Present in *Ctenosaura*, *Iguana*, and *Stenocercus*, while absent in *Furcifer*. This crest tends to disappear more posteriorly in the presacral series, with the most posterior dorsals consistently lacking a margo lateralis (e.g., *Iguana*). The crest also seems more prominent in younger/smaller size individuals and more blunt in more skeletally mature/larger individuals of the same species (e.g., *Cyclura cornuta*, *Ctenosaura similis*). The margo lateralis appears incomplete on most vertebrae that display this crest in *Cyclura*: an evident crest starts at the prezygapophysis but does not reach all the way posterior to the postzygapophyses, interrupting before the anterior margin of the neural spine; the terminal cervicals have a complete crest, but all the dorsals have an incomplete one, that tend to disappear posteriorly in the series.

229. **Posterior presacral vertebrae, neural spine:** present (0) / absent (1) (Si18, ch. 255). **Remarks:** Absent for instance in *Sauromalus*, where weak neural spines are visible on the most anterior cervicals, then disappear through the rest of the presacral series, and reappear behind the sacral vertebrae, (although never prominent).

230. **Mid-posterior presacral vertebrae, neural spine, anterior midline flange:** absent (0) / present (1) (NEW). **Remarks:** This fairly thin, midline flange extends from the top of the neural spines, all along its anterior margin, and reaches the dorsal margin of the zygosphenes. Found for instance in most iguanids (*Iguana*, *Ctenosaura*, *Cyclura*, etc.). This midline extension of the anterior margin of the neural spines tends to reduce or disappear more posteriorly along the vertebral column (post-sacral to caudal region), and sometimes is also quite reduced in the cervical region (e.g., *Ctenosaura*), while prominent throughout the dorsal series. Because of this, I set the landmark to the posterior presacral vertebrae, or mid-posterior dorsals. Absent for instance in *Furcifer*. Inapplicable in *Sauromalus*, where the dorsal neural spines are absent.

231. **Anterior-to-posterior presacral vertebrae, neural spine, height increase:** absent (0) / present (1) (NEW). **Remarks:** This accounts for the increase in height along the vertebral column of the neural spines in some taxa (e.g., *Pogona*). The elongation of the neural spines is usually more apparent in the mid-posterior region of the presacral series and in the intermediate caudal (post-sacral) series.

Sacral/cloacal vertebrae

232. **Sacral vertebrae, ribs, distal contact:** present (0) / absent (1) (NEW). **Remarks:** The ribs fused to the two sacral vertebrae tend to converge distally in most limbed-lizards to form the articular facet for the contact with the posterior process of the ilium (Hoffstetter & Gasc 1969; Paparella et al. 2020). As reported by Hoffstetter & Gasc (1969) the contacting ribs can also fuse in some lizards (e.g., geckos), and I observed this to be the case for instance in *Basiliscus* (pers. obs.). In some iguanians, the two sacral ribs never meet distally and contact the ilium separately, like for instance in *Furcifer*.
233. **Sacral vertebra II, ribs, mid-distal posterior process:** absent (0) / present (1) (NEW). **Remarks:** Two vertebrae with ribs articulating with the ilium are present in all ingroup-outgroup (i.e., presence of two sacral vertebrae). On the ribs of the second sacral vertebra, approximately halfway along the posterior margin of the rib, or more distally, a process projecting posterolaterally can be present, as for instance in *Iguana* and *Pogona*. Present also in *Chamaeleo* and *Gekko*, while absent in *Furcifer* and *Brachylophus fasciatus*.

Post-sacral/caudal vertebrae

234. **Intermediate-to-posterior caudal vertebrae, transverse processes:** present as single (0) / present as double (1) / absent (2) (F&E89, ch. 34 - modified). **Remarks:** Independently from the presence or absence of fracture planes, amongst our OTUs there is variation in the number of transverse processes present in the mid/intermediate caudal series. I define this region as the portion of the tail posterior to the anteriormost post-sacral vertebrae with fused ribs (*sensu* Malashichev 2001 and Paparella et al. 2020). Previous authors (Etheridge, 1967; Etheridge and de Queiroz, 1988; Frost & Etheridge 1989) have recognised that paired transverse processes can be present and usually (but not always) with fracture planes in between, as for instance in *Iguana*. In other taxa, the fracture planes are present and single transverse processes are located either anteriorly or posteriorly to them. This character should be assessed on complete tails only, since the number of intermediate caudals with double transverse processes can be very limited (as low as three throughout the tail in some specimens). The character is scored as unknown in most fossil taxa.

235. **Intermediate-to-posterior caudal vertebrae, intravertebral autotomic septa (= fracture planes):** absent (0) / present (1) (P86, ch. 52; Pr88, ch. 30; F&E89, ch. 41; Si18, ch. 236). **Remarks:** Transverse fracture planes usually associated with caudal autotomy can be present on the caudal vertebrae of several iguanians (and lizards in general), and their presence is highly variable within each subgroup (e.g., Etheridge 1967; Hoffstetter & Gasc 1969; Frost & Etheridge 1989). Moreover, few taxa have been described to possess a single autotomic vertebra, but most squamates have multiple intermediate caudals with intravertebral fracture planes (e.g., Etheridge 1967; Hoffstetter & Gasc 1969). As many lizards can shed their tail through intervertebral autotomy, the absence of transversal fracture planes on the caudals does not necessarily translate in the lack of the ability to autotomize their tails (Etheridge 1967; Arnold 1984). Similarly, not all the taxa with fracture planes actually shed their tails (see Etheridge 1967). In *Amblyrhynchus* and *Conolophus*, smaller size individuals can have septa on some intermediate caudals, but in larger size specimens the septa are usually sutured and a faint line can be seen sometimes on part of the vertebra, usually at the pleurocentrum-neural arch transition and between the double transverse processes.

236. **Anterior-to-intermediate caudal vertebrae, haemal arches (= chevrons), articulation:** between pleurocentra (0) / with posterior pleurocentrum via articulatory facet (1) / with posterior pleurocentrum via haemapophyses (2) (P86, ch. 54; Si18, ch. 243). **Remarks:** The chevrons articulate between pleurocentra for instance in *Furcifer* and *Sauromalus*. There is some overlapping for these character states. In *Amblyrhynchus* the chevrons are suspended between pleurocentra contacting the condyle of the preceding vertebra, while few vertebrae actually show weak facets along the posteroventral margin of the centrum. In *Conolophus* there are actual facets for most intermediates. Haemapophyses are present in *Uma* and *Holbrookia*. The haemapophyses are known in the literature also as pedicels or pedestals.

Amblyrhynchus - chevrons articulating between pleurocentra, with weak facets present in some vertebrae.

Polychrus - chevron facets present along the posteroventral margin of the pleurocentrum.

Ribs

237. **Mid-anterior presacral ribs, anteroventral process at rib head:** absent (0) / present (1) (L98, ch. 187; Si18, ch. 263). **Remarks:** A preaxial/anteroventral tuberculum can be present close to the head of the ribs in some taxa (e.g., Hoffstetter & Gasc 1969). In most cases, this process can be prominent for some ribs along the trunk and then fade away

posteriorly (e.g., *Amblyrhynchus*). The position is slightly variable: in *Basiliscus* for instance, this process is often at the same level of the rib head, while in *Amblyrhynchus* is clearly behind it.

238. **Posteriormost presacral ribs:** present (0) / absent (1) (Si18, ch. 265). **Remarks:** Some taxa lack ribs on the posteriormost dorsal vertebrae, right before the sacral region (e.g., Hofstetter & Gasc 1969).

239. **Sacral vertebrae, ribs, distal forking:** absent (0) / on first sacral rib only (1) / on first and second sacral ribs (2) / on second sacral rib only (3) (Lee98, ch. 189; Si18, ch. 267). **Remarks:** There is no distal forking of sacral ribs for instance in *Furcifer*; both sacral ribs are grooved in *Amblyrhynchus* and *Pogona*; only the first sacral rib is forked in *Basiliscus* and *Brachylophus*; in *Gekko*, the first sacral rib is expanded but not forked, while the second one is forked.

240. **Anteriormost post-sacral (= caudal) ribs, lymphapophyses:** absent (0) / present (1) (NEW). **Remarks:** Many iguanians have one or more vertebrae bearing distally grooved or forked ribs following the two sacrals. These grooved ribs are for the support of the lymph hearts, as for the cloacal vertebrae in snakes (e.g., Hoffstetter & Gasc 1969). This shows that the presence of vertebrae with lymphapophyses is independent from the presence/absence of sacral vertebrae and from the presence/absence of distal forking in the sacral ribs (Hoffstetter & Gasc 1969; Paparella et al. 2020). For these reasons, I treated the conditions as separate.

Amblyrhynchus - lymphapophysis (i.e., forked postsacral vertebra).

Gastralia

241. **Gastralia:** present (0) / absent (1) (Si18, ch. 342). **Remarks:** Present in *Sphenodon* and *Megachirella* (Simoes et al. 2018). Gastralia are absent in all the other OTUs and are not to be confused with inscriptional ribs (see Si18, ch. 342 for further details).

Sternum

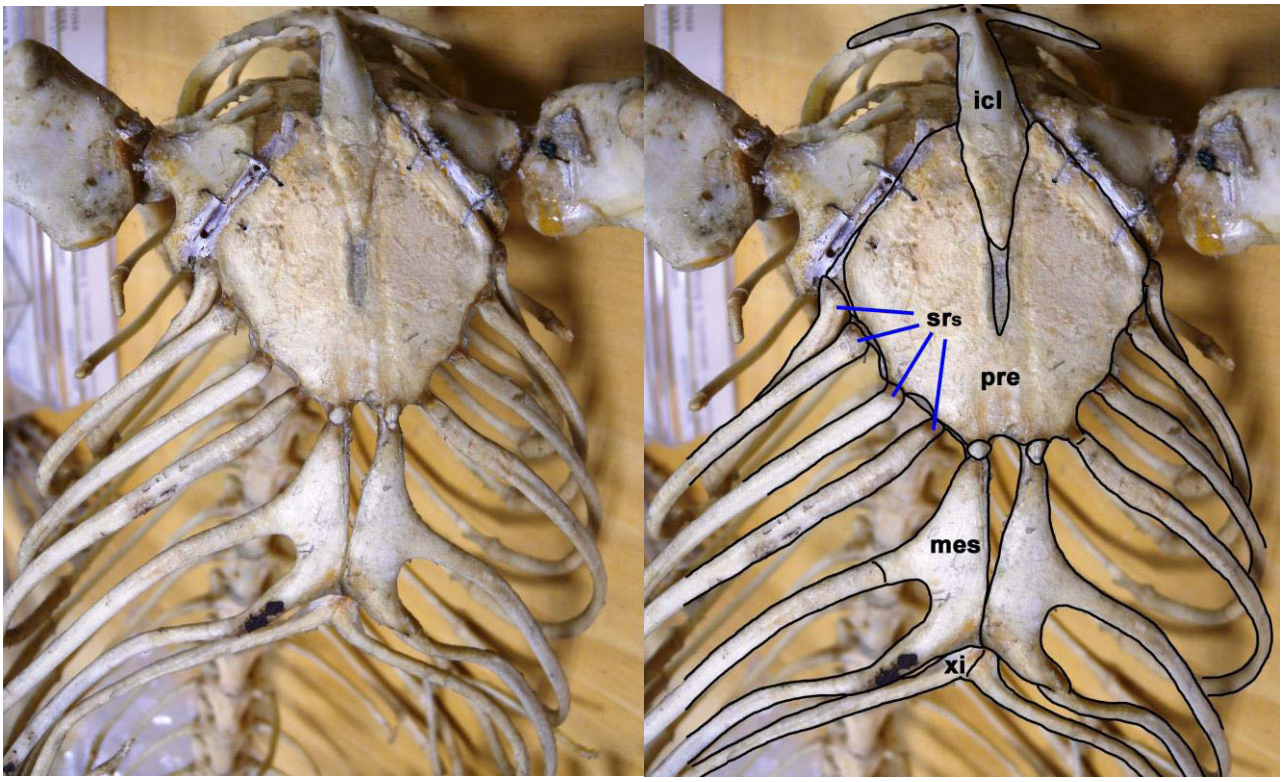

Conolophus - complete sternum (presternum + mesosternum + xiphisternum). The presternum has 4 ribs attached on each side.

242. **Presternum, ribs:** present (0) / absent (1) (NEW). **Remarks:** There are no sternal ribs on the presternum or presternum + mesosternum in some chamaeleonids. Sternal ribs in this case attach to the expanded xiphisternum.
243. **Preternum, number of rib attachments:** five (0) / four (1) / three (2) / two (3) / one (4) (G12, ch. 483 - modified). **Remarks:** This character accounts for how many ribs attach to one side of the presternum. Inapplicable when presternal ribs are absent.

244. **Presternum, fontanelle:** absent (0) / present (1) (E88, ch. 121; G12, ch. 481). **Remarks:** The sternum of squamates consists of a presternum, a mesosternum and a xiphisternum (cf. Estes et al. 1988; Russell & Bauer 2008; see figure above). Absent in *Iguana* and *Ctenosaura*, present in *Pogona*.
245. **Presternum, fontanelle, number:** single (0) / double (1) (G12, ch. 482). **Remarks:** Double for instance in *Pogona* and *Leiolepis*, while single in *Leiocephalus*.
246. **Xiphisternum:** present (0) / absent (1) (G12, ch. 484; Si18, ch. 272). **Remarks:** When present, the xiphisternum represents a posterior projection from the mesosternum (see figure above). Absent for instance in *Leiolepis*; present and expanded chamaeleons.

APPENDICULAR SKELETON

Pectoral girdle

Scapula

247. **Scapula, glenoid-shaft transition, constriction:** absent (0) / present (1) (G12, ch. 489 - modified). **Remarks:** The margins of the scapula tend to vary from fairly straight and continuous (e.g., *Sauromalus*, *Iguana*) to constricted (e.g., *Furcifer*, *Uranoscodon*) at the glenoid-shaft transition, forming in the latter case an evident neck behind the glenoid head.
248. **Scapula, supraglenoid foramen:** absent (0) / present (1) (Si18, ch. 275). **Remarks:** Foramen located posterodorsal to the glenoid region of the scapula. Widely present amongst iguanians; absent for instance in *Sceloporus*.
249. **Scapula, scapular ray:** absent (0) / present (1) (E88, ch. 111; Si18, ch. 277). **Remarks:** Presence/absence of the scapular ray determines whether or not there is a scapular fenestra (cf. Russell & Bauer 2008; Estes et al. 1988). Present for instance in *Iguana* and *Uranoscodon*, while absent in *Sauromalus* and *Furcifer*. Present and expanded in *Amblyrhynchus*, leaving between the main scapular shaft and the scapular ray a foramen rather than a large fenestra. Present but reduced in *Anolis*.
250. **Scapula, acromion (= anterodorsal) process:** absent (0) / present (1) (Si18, ch. 278). **Remarks:** In many squamates, an anterior expansion can be present on the preaxial margin of the scapula main shaft (usually involving also the suprascapular cartilage) and pointing towards the scapular ray (when this is present) or clavicle. Present for instance in *Iguana* and *Cyclura*, absent in *Furcifer*.

Coracoid

251. **Coracoid, emargination(s):** absent (0) / anterior emargination only (1) / anterior and ventral emarginations (2) (P86, chh. 56-57; Estes et al. 1988, ch. 112-113; Si18, ch. 284-modified). **Remarks:** Considering the pectoral elements in their articulated position, the emargination(s) of the coracoid can be present along the anterior-to-ventral margin of the bone (e.g., Russell & Bauer 2008). Two emarginations are present for instance in *Cyclura* and *Ctenosaura*, a single emargination is found in *Polychrus* and *Phrynosoma*, while no emargination in *Furcifer*.
252. **Epicoracoid cartilage:** present (0) / absent (1) (Si18, ch. 286). **Remarks:** The epicoracoid is present as calcified cartilage in most lepidosaurs, but can be absent in some iguanians (e.g., *Furcifer*, *Trioceros*).
253. **Epicoracoid cartilage, contact with mesoscapula-suprascapula:** absent (0) / present (1) (E88, ch. 114; L05, ch. 271; G12, ch. 498 - modified). **Remarks:** The epicoracoid cartilage shows some variation in extension amongst lepidosaurs. This element can reach up to contact the mesoscapula-suprascapula (i.e., the most dorsal portion of the scapula, away from the glenoid region) in some taxa (state 1), while being more reduced in others (state 0) (cf. Russell & Bauer 2008; Estes et al. 1988). This character is inapplicable when the epicoracoids are absent.

Interclavicle

254. **Interclavicle:** absent (0) / present (1) (E88, ch. 118). **Remarks:** An ossified interclavicle between the cartilaginous sternum is absent for instance in *Furcifer* and *Trioceros*. Present in most other OTUs.
255. **Interclavicle, anterior process:** absent (0) / present (1) (P86, ch. 59; E88, ch. 120; G12, ch. 507; Si18, ch. 293). **Remarks:** Absent for instance in *Iguana* and *Cyclura*, present in *Ctenosaura similis* and *Uromastyx*. When present, this process is more commonly just an anterior tubercle rather than a well-developed and elongated projection, with the exception of *Gekko* amongst our OTUs.
256. **Interclavicle, posterior process:** present (0) / absent (1) (Si18, ch. 294). **Remarks:** Absent in *Phrynosoma*.

Clavicle

257. **Clavicle:** present (0) / absent (1) (E88, ch. 115; L05, ch. 207). **Remarks:** Absent for instance in *Furcifer* and *Chamaeleo*, present in *Iguana* and *Agama*.
258. **Clavicle, proximoventral fenestra:** absent (0) / present (1) (LC00, ch. 218; L05, ch. 209; G12, ch. 500; Si18, ch. 288). **Remarks:** When there is no fenestration in the proximal region of the clavicle, the bone is simply rod-like throughout its extension (e.g., *Uromastyx*, *Sauromalus*), or poorly expanded proximally. In state 1 (e.g., *Pristidactylus*, *Gekko*), a fenestra is usually associated with a greatly expanded proximal region of the clavicles, bearing a single opening on each side (cf. Lee 2005).
259. **Clavicle, posterolateral flange:** absent (0) / present (1) (Si18, ch. 289). **Remarks:** A flange along the mid-posterior margin of the clavicle is visible for instance in *Leiocephalus* and *Amblyrhynchus*, while absent in *Iguana* and *Conolophus*.
260. **Clavicle, ventral process:** absent (0) / present (1) (NEW). **Remarks:** A pointed process is present on the proximoventral margin of the clavicle in *Basiliscus*.

Basiliscus basiliscus - clavicle fenestra and ventral process.

261. **Clavicle, distal end, contact:** with scapula and suprascapula (0) / with suprascapula only (1) / with scapula only (2) (G12, ch. 503 - modified). **Remarks:** The distal articulation of

the clavicle is directly with the scapula for instance in *Physignathus*, while for instance in *Iguana* and *Uranoscodon* the clavicle insert into a notch along the anterior margin of the suprascapular cartilage. When the articulation is with the suprascapula, a notch is evident along the anterior margin of this element (close to its contact with the scapula), allowing to score for this character even if the elements are disarticulated.

Ctenosaura similis - contact of clavicle to suprascapular cartilage only.

Pelvic girdle

Ilium

262. **Ilium, preacetabular process:** present (0) / absent (1) (B85, ch. J12; Si18, ch. 298).
Remarks: This process extends anteroventrally from the anterior margin of the ilium to partially overlap the pubis. Also referred to as anterior pubic process of the ilium (e.g., Russell & Bauer 2008; Simoes et al. 2018). Absent for instance in *Furcifer* and *Chamaeleo*, while present in most OTUs. In fossils, to be scored as unknown when the degree of fusion between the three elements of the pelvic girdle prevents a clear assessment.

263. **Ilium, supracetabular process:** absent (0) / present (1) (L98, ch.208; G12, ch. 521).
Remarks: This process project anterodorsally from the main shaft of the ilium, as opposed to the anteroventral preacetabular process (previous character). It is also referred to as iliac

tubercle or spine. See Paparella et al. (2020) for further details. Absent for instance in *Furcifer* and *Polychrus*.

264. **Ilium, supracetabular process, shape:** tapering throughout (0) / blunt (1) (NEW). **Remarks:** Rounded and blunt as in *Amblyrhynchus*, or tapering into a pointed/conical process as in *Conolophus* and *Basiliscus*. See Paparella et al. (2020) for further details.
265. **Ilium, sacral process, orientation:** posterior (0) / dorsal (1) (G12, ch. 522 - modified). **Remarks:** This is usually referred to as the posterior process of the ilium and it is the process that mediates the contact with the sacral ribs (e.g., Hoffstetter & Gasc 1969; Paparella et al. 2020). While having usually a posterior or posterodorsal orientation relative to the vertebral column, in some taxa this process can be vertical (e.g., *Sphenodon*) or about anterodorsally oriented (*Chamaeleo calyptratus*: cf. Molnar et al. 2017). The variation is particularly evident when looking at the geometrical relationship between the main process of the ilium and the ischium or pubis. The dorsal-anterodorsal condition seems to be associated with strong lateral body compression and consequent downward shifting of the pelvic girdle and hindlimb relative to the vertebral column. In state 1, the sacral ribs contact the most dorsal region of the sacral process of the ilium, either conjunctly or separately (see character 237 for further details). This is in contrast with the position of the ilium-sacrals contact when state 0 is present, which is typically mid-to-proximal along the iliac sacral process (cf. Paparella et al. 2020).
266. **Ilium, sacral process, medial view, shape:** cylindrical (0) / compressed (1) (G12, ch. 523 - modified). **Remarks:** This condition has to be assessed behind the articulation with the sacral ribs and in medial view, as the lateral surface is overall flat throughout in all OTUs. This also allows to score for this condition in articulated as well as disarticulated specimens. Laterally compressed as in *Furcifer* and *Saichangurvel*, or cylindrical as in *Cyclura* and *Iguana*. See Paparella et al. (2020) for further details.

Pubis

267. **Pubis, anterior process:** absent (0) / present (1) (B85, ch. J11; Si18, ch. 301). **Remarks:** Also known as pubic tubercle or anterior tubercle of the pubis (e.g., Russell & Bauer 2008; Si18). Absent for instance in chamaeleons, while present in *Sphenodon*. *Holbrookia* has no anterior process but the anterior flange is present (see next character).

268. **Pubis, anterior flange:** absent (0) / present (1) (NEW). **Remarks:** The anterior margin of the pubis can bear a simple projection, as in *Phrynosoma*, or also a flange connecting this projection to the symphyseal end of the pubis, as in most OTUs. This condition appears independent from the presence or absence of the anterior process of the pubis.
269. **Pubis, distal end (= symphyseal process), shape:** flaring (0) / columnar (1) (D&C93, ch. 125 ; G12, ch. 513). **Remarks:** In state 0, the pubic dorsal end is expanded, as for instance in *Furcifer*, while in state 1, the pubic shaft is straight or slightly tapers distally, as for instance in *Iguana* and *Sauromalus*. This condition has to be assessed on the pubic shaft and independently from the anterior pubic process and its flange (when these are present).

Ischium

270. **Ischium, posterior process:** absent (0) / present (1) (G12, ch. 517; Si18, ch. 304). **Remarks:** Also known as posterior tubercle of the ischium or ischiadic/ischial tuberosity (e.g., Russell & Bauer 2008; Si18). Absent in *Chamaeleo* and *Furcifer*.
271. **Ischium, posterior flange:** absent (0) / present (1) (NEW). **Remarks:** A bony flange can be present between the posterior process and the symphyseal end of the ischium, as in *Iguana*, *Cyclura* and *Ctenosaura*. This condition appears independent from the presence or absence of the posterior process of the ischium. Absent for instance in *Sauromalus*.
272. **Hypoischium, foramen:** absent (0) / present (1) (G12, ch. 519). **Remarks:** This foramen can be present on the hypoischial cartilage, posteriorly to the contact between the two ischia. Present for instance in *Pristidactylus* and *Anolis*, while absent in *Ctenosaura* and *Cyclura*.

Anterior stylopodium

Humerus

273. **Humerus, ectepicondylar foramen:** notch or groove (0) / complete foramen (1) (E88, ch. 122; Si18, ch. 307 - modified). **Remarks:** State 1 encompasses any form of incomplete, not-fully-open foramen. The ectepicondylar foramen is represented by a groove on the anteroventral margin of the distal humeral end in *Furcifer* and *Iguana*, while fully open in *Ctenosaura* and *Cyclura*. In E88, chamaeleontids are described as lacking completely this

foramen, but I found it present as a notch or complete in all the chamaeleonids included in this analysis.

274. **Humerus, dorso-distal flange:** absent (0) / present (1) (NEW). **Remarks:** A flange along the dorsal margin of the humerus is present distally (from the level of the ectepicondylar foramen to about mid-shaft) in *Gekko* and *Varanus*.

Polychrus (left) and *Gekko* (right) showing respectively absence and presence of the humerus dorsodistal flange.

275. **Humerus, entepicondylar foramen:** absent (0) / notch or groove (1) / complete foramen (2) (Si18, ch. 309 - modified). **Remarks:** State 1 encompasses any form of incomplete, not-fully-open foramen. This foramen is located on the posterior/posterodorsal surface of the distal end of the humerus. Present and fully open in *Iguana*, *Ctenosaura*, and *Furcifer*. Present as a shallow notch in *Sauromalus*. Absent for instance in *Varanus*.
276. **Humerus, expanded radial condyle (= capitellum):** present (0) / absent (1) (Si18, ch. 310). **Remarks:** The radial condyle is expanded for instance in *Sphenodon* and *Arretosaurus*.

Arretosaurus - expanded radial condyle.

277. **Humerus, expanded entepicondyle:** present (0) / absent (1) (NEW). **Remarks:** An expanded entepicondyle is commonly present amongst our OTUs (and squamates in general). Absent for instance in *Furcifer*.

Anterior zeugopodium

Radius

278. **Radius, distal epiphysis, styloid process:** absent (0) / present (1) (G88, ch. 59; G12, ch. 534; Si18, ch. 316). **Remarks:** The main contribution to this process is from the epiphysis, and an asymmetrical margin of the distal end of the radius is visible on the diaphysis to a minor extent when this process is present. In absence of articulated epiphyses, this character should be scored as unknown. Present in most OTUs. Absent in *Sphenodon* and *Megachirella*.

Ulna

279. **Ulna, olecranon process:** absent (0) / present (1) (G88, ch. 107; G12, ch. 532; Si18, ch. 318). **Remarks:** Formed on the proximal epiphysis of the ulna. If the epiphyses are missing, this character should be scored as unknown. Absent for instance in *Furcifer*.

280. **Ulna, distal epiphysis, expansion:** absent (0) / present (1) (G88, ch. 58; Si18, ch. 319). **Remarks:** A ball-like expansion of the distal epiphysis of the ulna is present in *Furcifer* and most OTUs, while absent in *Sphenodon* and *Megachirella*.

Anterior mesopodium (= carpals)

For carpals and tarsals terminology and homology, I followed Russel & Bauer (2008), Table 1.7.

PROXIMAL CARPAL ROW

Intermedium

When present, the intermedium is located along the most proximal carpal row, at the level of the radiale-ulnare-pisiform, or sometimes more proximally in comparison to radiale and ulnare. The central, instead, is part of the middle row. According to Russel & Bauer (2008), the intermedium is variably present amongst lizards, with variability found across individuals of the same species. Some authors attribute this to the fact that the intermedium fuses early in ontogeny to the ulnare, but this fusion is not always complete (e.g., Presch 1969; Lang 1991; Fisher & Tanner 1970; Camp 1923; Sewertzoff 1908; Holmgren 1933). A different hypothesis is given by Born (1876; 1880), Mohammed (1991), and Mathur (1977), for which the intermedium develops in the embryo but then degenerates via necrosis before hatching (see also Russel & Bauer 2008).

281. **Carpal intermedium:** present (0) / absent (1) (G12, ch. 535; Si18, ch. 321). **Remarks:** Rather than truly absent, the intermedium is argued to fuse to the ulnare or occasionally present in adults. Absent for instance in *Iguana iguana* (see also Russel & Bauer 2008). The intermedium is present and large in *Sphenodon*. A survey about the presence/absence of carpal elements in iguanians can be found in Avery & Tanner (1964).

DISTAL CARPAL ROW

Anterior autopodium (= metacarpals + phalanges)

Metacarpal I (Mc-I)

282. **Mc-I, proximal epiphysis, expansion:** present (0) / absent (1) (NEW). **Remarks:** This character accounts for the expansion of the proximal epiphysis of the first metacarpal relative to the shaft. In Si18 (ch. 324) this condition is treated as presence/absence of distal carpal I that fuses to the mc-I thus resulting in an apparent expansion of the mc-I epiphysis.

However, it is hard to argue for such a fusion in absence of developmental proofs. I believe that addressing the shape of the proximal epiphysis of mc-I is easier than assuming the presence of a fused dc-I when mc-I has an expanded epiphysis. Expanded for instance in *Iguana* and *Furcifer*. This character should be scored as unknown when the epiphyses are missing (especially in fossils).

283. **Mc-I, mid-shaft, expansion:** absent (0) / present (1) (NEW). **Remarks:** This character addresses the modified shape of mc-I and all metacarpals and metatarsals seen for instance in chamaeleonids. *Arretosaurus* also displays an expansion and shortening of mc-I (together with the proximal phalanges in this case). In state 1, the mc-I is shorter and broader, lacking a mid-shaft constriction, unlike the typical rod-like shape of both metacarpals and metatarsals in most other OTUs.

Arretosaurus - short mc-I and proximal phalanges.

Posterior stylopodium

Femur

284. **Femur, internal trochanter:** present (0) / absent (1) (G12, ch. 550; Si18, ch. 327). **Remarks:** The lack of the internal trochanter is listed as potential synapomorphy of chamaeleontids in Estes et al. (1988), however this feature is not used in that dataset. Present for instance in *Iguana*, absent in *Chamaeleo*.

Posterior zeugopodium

Tibia

285. **Tibia, distal epiphysis, notch:** absent (0) / present (1) (E88, ch. 123; G12, ch. 555; Si18, ch. 330). **Remarks:** When the notch is present, the distal epiphysis of the tibia appears saddle-shaped at the joint with the astragalocalcaneum. If the epiphyses are not preserved (either in fossils or skeletonized specimens that may have been affected by preparation), the character must be scored as missing data. Present for instance in *Gekko*, absent in most OTUs.

Posterior mesopodium (= tarsals)

Tarsals in lizards are divided in proximal (astragalus-calcaneum) and distal (distal tarsal II, III, IV) rows: see Russel & Bauer (2008).

PROXIMAL TARSAL ROW

Astragalus-calcaneum

286. **Astragalus-calcaneum:** separate (0) / fused (1) (B85, ch. X10; Si18, ch. 331). **Remarks:** The degree of fusion between the astragalus and calcaneum amongst iguanians is highly variable during late ontogeny/skeletal maturity. The elements however remain truly separate only in *Uromastyx*.
287. **Astragalus, dorsal margin, notch:** absent (0) / present (1) (Be97, ch. 140 - modified). **Remarks:** The dorsal margin of the astragalus represents the distal border of the crurotarsal foramen. A concavity or notch along this margin is found for instance in *Sphenodon*, while absent in *Iguana* and *Furcifer*, where the dorsal margin is straight.
288. **Calcaneum, posterolateral process:** present (0) / absent (1) (Si18, ch. 333). **Remarks:** The lateral process of the calcaneum is best assessed in proximal view, while usually less

prominent in dorsal view (cf. Russell & Bauer 2008). When present, a sub-squared projection is visible along the lateral margin of the calcaneum, just besides the deflected fibular facet. Present for instance in *Sauromalus* and *Iguana*, absent in *Basiliscus* and *Furcifer*.

289. **Astragalus-calcaneum, distal surface, tarsal facet:** double (0) / single (1) (NEW). **Remarks:** The contact with distal tarsal IV can be present via two notches (e.g., *Ctenosaura*, *Iguana*) or via a single notch (e.g., *Chamaeleo*, *Sphenodon*) along the distal surface of the astragalocalcaneum (fused or not fused). When the contact is double, one notch is only on the astragalus, while the second notch is close to the astragalus-calcaneum contact, although usually mainly on the calcaneum. This character is best assessed in posterior view.

Posterior autopodium (= metatarsals + phalanges)

Metatarsals

290. **Mt-V, proximal end, hooked expansion:** absent (0) / present (1) (B85, ch. C14; Si18, ch. 340). **Remarks:** The proximal end of metatarsal V is typically expanded in most lizards, assuming a hooked shape in preaxial/postaxial view (e.g., Snyder 1954; Russell & Bauer 2008). Absent for instance in chameleons, where all metatarsals have the same shape.
291. **Mt-V, proximal end, plantar (= preaxial) tubercle:** present (0) / absent (1) (Si18, ch. 341 - modified). **Remarks:** There are two plantar tubercles that can be present on the ventral surface of the expanded proximal end of the fifth metatarsal: one tubercle is located preaxially and referred to as mesial or plantar tubercle; the other tubercle is located postaxially (or laterally) (e.g., Russell & Bauer 2008, Fig. 1.20; see next character).
292. **Mt-V, proximal end, postaxial tubercle:** present (0) / absent (1) (Si18, ch. 341 - modified). **Remarks:** See remarks for previous character.
293. **Digits, zygodactyly:** absent (0) / present (1) (G12, chh. 545, 568 - modified). **Remarks:** Zygodactyly is the condition of the autopodium where opposing sets of digits are present (usually with digits 1 to 3 opposing digits 4 and 5). This is typical of chamaeleonids, and as opposing digits are never found only either on manus or pes, I constructed a single character and treated this condition as a serial homologue.

Appendix 5.2 – List of synapomorphies for key clades based on the time-calibrated analysis of combined data (TcBI). An asterisk (*) was added to denote clades which composition in my analysis is re-defined in comparison to previous studies. For most families of extant iguaniforms, synapomorphies are not provided as the taxon sampling is too low to be meaningful. Iguanidae is the only exception as one of the main focus of this study.

CHAMAELEONTIFORMES Conrad, 2008

(Priscagamidae + Acrodonta)

Char. 9: 1 --> 0 - Palatal flange of the premaxilla absent.

Char. 10: 0 --> 1 - Premaxillary processes of the maxilla contacting each other.

Char. 36: 1 --> 0 - Palatine process of the prefrontal does not contact the jugal and/or lacrimal.

Char. 43: 0 --> 1 - Posteroventral process of jugal present.

Char. 111: 0 --> 2 - Rostral foramen present.

Char. 133: 0 --> 1 - Ossified processus ascendens of the supraoccipital present.

Char. 157: 0 --> 1 - Dentary subdental shelf with ventrolingual flange.

Char. 158: 1 --> 0 - Dentary lingual wall present.

Char. 277: 0 --> 1 - Radius distal epiphysis with styloid process.

Definition: All taxa sharing a more recent common ancestor with *Priscagama gobiensis*, *Chamaeleo calyptratus*, *Agama agama*, and *Uromastyx hardwickii* than with *Iguana iguana*, *Corytophanes cristatus*, and *Stenocercus guentheri*.

PRISCAGAMIDAE Borsuk-Białynicka and Moody, 1984

Char. 81: 1 --> 0 - Postorbital jugal process absent.

Char. 165: 1 --> 0 - Dentary posterolateral process expanded.

Definition: All taxa sharing a more recent common ancestor with *Priscagama gobiensis*, *Phrynosomimus asper*, and *Mimeosaurus crassus* than with *Graminisaurus interruptus*, *Agama agama*, and *Uromastyx hardwickii*.

ACRODONTA Cope, 1864 *sensu* Frost et al. (2001)

(Chamaeleonoidea + Dracosauria)

Char. 4: 1 --> 0 - Maxillary process of the premaxilla absent.

Char. 12: 0 --> 1 - Anterodorsal process of the maxilla present.

Char. 109: 0 --> 1 - Lacrimal duct foramen with contribution from the palatine.

Char. 190: 1 --> 0 - Anterior inferior alveolar foramen absent.

Definition: All taxa sharing a more recent common ancestor with *Chamaeleo calyptratus*, *Agama agama*, and *Uromastyx hardwickii* than with *Priscagama gobiensis*, *Varanus salvator*, *Gekko gecko*, and *Iguana iguana*.

CHAMAELEONOIDEA* Fitzinger, 1826

(Changjiangosauridae + Chamaeleonidae)

Char. 198: 0 --> 1 - Posterior dentary teeth with apical position relative to jaw labial wall.

Definition: All taxa sharing a more recent common ancestor with *Graminisaurus interruptus* and *Chamaeleo calyptratus* than with *Leiolepis belliana*, *Agama agama*, and *Uromastyx hardwickii*.

CHANGJIANGOSAURIDAE* (Hou 1976)

Char. 162: 0 --> 1 - Dentary coronoid process with dorsal expansion.

Char. 164: 1 --> 0 - Dentary posterolateral process absent.

Definition: All taxa sharing a more recent common ancestor with *Graminisaurus interruptus* and *Lavatisaurus elegans* than with *Chamaeleo calyptratus* and *Furcifer oustaleti*.

Notes: The original name for the family coined by Hou (1976) was „Changjiangidae“; this was changed to „Changjiangosauridae“ by Estes (1983) and the clade was re-defined by Alifanov (2009).

CHAMAELEONIDAE* Rafinesque, 1815 *sensu* Frost and Etheridge (1989)

Char. 159: 1 --> 0 - Dentary lingual wall with same height as the labial wall.

Char. 180: 1 --> 2 - Surangular anterior foramen dorsal relative to posterolateral process of dentary.

Char. 196: 1 --> 2 - Posterior marginal teeth with tricuspid crown apex.

Definition: All taxa sharing a more recent common ancestor with *Chamaeleo calyptratus* and *Furcifer oustaleti* than with *Graminisaurus interruptus* and *Lavatisaurus elegans*.

DRACOSAURIA comb. nov.

(Uromastyoidea + Agamidae)

Char. 140: 0 --> 1 - Basioccipital with transverse crest on ventral surface.

Definition: All taxa sharing a more recent common ancestor with *Uromastyx hardwickii*, *Agama agama*, and *Leiolepis belliana* than with *Graminisaurus interruptus* and *Furcifer oustaleti*.

Etymology: *Dracosauria* meaning "dragon-like lizards", a reference to agamids being commonly called "dragon lizards"; from the Latin word *draco* meaning "huge serpent or dragon", and the Latinized form of Greek *sauros* meaning "lizard" (Online Etymology Dictionary, retrieved 15 March 2021).

UROMASTYOIDEA comb. nov.

(Leiolepidae + Uromastycidae)

Char. 21: 0 --> 1 - Septomaxilla with angled lateral margin.

Char. 33: 0 --> 1 - Prefrontal with dorsolateral boss.

Char. 80: 1 --> 0 - Anteroventral process of postorbital absent.

Char. 99: 0 --> 1 - Pterygoid palatine process with bifurcated anterior end.

Char. 107: 1 --> 0 - Ectopterygoid posterolateral process absent.

Char. 137: 0 --> 1 - Supraoccipital with dorsolateral ridges.

Char. 139: 0 --> 1 - Basioccipital with single concavity on ventral surface.

Char. 144: 0 --> 1 - Orbitosphenoid with concave dorsal margin.

Definition: All taxa sharing a more recent common ancestor with *Leiolepis belliana* and *Uromastyx hardwickii* than with *Agama agama* and *Hydrosaurus amboinensis*.

Etymology: *Uromasty-* referring to the genus *Uromastyx*, from the Greek word *ourá* meaning "tail" and *mastix* meaning "whip", and *–oidea* to indicate a clade above the rank of family-level (Online Etymology Dictionary, retrieved 15 March 2021).

IGUANIFORMES comb. nov.

(Gobiguania s.l. + Pleurodonta)

Char. 30: 0 --> 1 - Foramina present on nasal dorsal surface.

Char. 165: 1 --> 0 - Dentary posterolateral process not expanded.

Char. 178: 0 --> 1 – Surangular with lateral adductor crest.

Char. 195: 0 --> 2 - Posterior marginal teeth with flaring mesio-distal margins.

Char. 196: 0 --> 2 - Posterior marginal teeth with tricuspid crown apex.

Char. 197: 0 --> 1 - Posterior marginal teeth with resorption pits.

Char. 199: 0 --> 1 - Posterior dentary tooth root without a dentine labial wall.

Definition: All taxa sharing a more recent common ancestor with *Isodontosaurus gracilis*, *Iguana iguana*, *Corytophanes cristatus*, and *Stenocercus guentheri* than with *Priscagama gobiensis*, *Chamaeleo calyptratus*, *Agama agama*, and *Uromastyx hardwickii*.

Etymology: *Iguaniformes* meaning "iguana-like forms"; *Iguani-* referring to the genus *Iguana*, from the Arawakan (West Indies) word *iwana* meaning "lizard" in the local language, and *-formes* from the Latin word *forma* meaning "shape, appearance" (Online Etymology Dictionary, retrieved 15 March 2021).

GOBIGUANIA Conrad & Norell, 2007

Char. 10: 0 --> 1 - Premaxillary processes of maxilla contacting each other.

Char. 71: 0 --> 1 - Postfrontal distal process single.

Char. 128: 0 --> 1 - Squamosal posterodorsal process absent.

Char. 227: 1 --> 0 - Mid-anterior presacral vertebrae lacking a prezygapophysis-synapophysis crest.

Definition: All taxa sharing a more recent common ancestor with *Saichangurvel davidsoni* and *Temujinia ellisoni* than with *Corytophanes cristatus* and *Iguana iguana*.

PLEURODONTA Cope, 1864 *sensu* Frost et al. (2001)

Char. 180: 1 --> 02 - Surangular anterior foramen dorsal to posterolateral process of dentary.

Char. 201: 0 --> 1 - Pterygoid teeth present.

Definition: All taxa sharing a more recent common ancestor with *Corytophanes cristatus* and *Iguana iguana* than with *Saichangurvel davidsoni* and *Isodontosaurus gracilis*.

IGUANIDAE Oppel, 1811 *sensu* Frost and Etheridge (1989) [former Iguaninae *sensu* Etheridge & de Queiroz (1988)]

Char. 23: 0 --> 1 - Septomaxilla with ventral medial crest.

Char. 118: 0 --> 1 - Quadrate suprastapedial process present.

Char. 137: 0 --> 1 - Supraoccipital dorsolateral ridges present.

Char. 139: 0 --> 2 - Basioccipital with divided ventral concavity.

Char. 161: 0 --> 1 - Dentary coronoid process present (without expansion).

Char. 193: 1 --> 2 - Anterior marginal teeth with flaring mesio-distal margins.

Char. 194: 1 --> 2 - Anterior marginal teeth with tricuspid crown apex.

Char. 195: 1 --> 2 - Posterior marginal teeth with flaring mesio-distal margins.

Char. 209: 1 --> 0 - Hyoid ceratobranchials-II diverging from each other.

Definition: All taxa sharing a more recent common ancestor with *Dipsosaurus dorsalis*, *Iguana iguana*, and *Amblyrhynchus cristatus* than with *Corytophanes cristatus*, *Stenocercus guentheri*, and *Enyalioides laticeps*.

Appendix 5.3 – Data on iguanian fossil record.

Table A5.1. Comprehensive list of fossil iguanians with relative information on specimens, locality, stratigraphic range, and references.

Mesozoic

TAXON	SPECIMENS	AGE & LOCALITY	REFERENCES
Polrussia mongoliensis	holotype ZPAL MgR-I/119; referred specimen: IGM 3/73 (MAE 219/92-45)	Khulsan, Nemegt Basin, Mongolia; Barun Goyot Formation, Late Cretaceous (?middle Campanian)	Borsuk-Bialynicka M, and Alifanov V. 1991. First Asiatic 'iguanid' lizards in the Late Cretaceous of Mongolia. Acta Palaeontologica Polonica 36:325-342; Gao K, and Norell MA. 2000. Taxonomic composition and systematics of Late Cretaceous lizard assemblages from Ukhaa Tolgod and adjacent localities, Mongolian Gobi Desert. Bulletin of the American Museum of Natural History 249:1-118; Alifanov VR. 2013. Desertiguana gobiensis gen. et sp. nov., a new lizard (Phrynosomatidae, Iguanomorpha) from the Upper Cretaceous of Mongolia. Paleontological Journal 47:417-424.
Desertiguana gobiensis	holotype PIN no. 4487/9	Mongolia, Ömnögov Aimag, Khulsan locality; Upper Cretaceous, Barun Goyot Fm, ?Santonian–Campanian	Alifanov VR. 2013. Desertiguana gobiensis gen. et sp. nov., a new lizard (Phrynosomatidae, Iguanomorpha) from the Upper Cretaceous of Mongolia. Paleontological Journal 47:417-424.
Igua minuta	holotype ZPAL MgR-I/60; referred: PIN no. 4487/8, PIN 4487/9	Barun Goyot Formation, Late Cretaceous (?middle Campanian); Khulsan, Nemegt Basin of the Gobi Desert, Mongolia	Borsuk-Bialynicka M, and Alifanov V. 1991. First Asiatic ‗iguanid' lizards in the Late Cretaceous of Mongolia. Acta Palaeontologica Polonica 36:325-342.
Anchaurosaurus gilmorei	IVPP V10028	SCDP surface collections, North Canyon area, (Bayan Mandahu region), which is in a Campanian eolian sandstone in the Djadokhta Formation of China; 84.9 to 70.6 Ma	Gao and Hou 1995. Iguanians from the Upper Cretaceous Djadochta Formation, Gobi Desert, China. Journal of Vertebrate Paleontology 15(1):57-78; Gao K, and Norell MA. 2000. Taxonomic composition and systematics of Late Cretaceous lizard assemblages from Ukhaa Tolgod and adjacent localities, Mongolian Gobi Desert. Bulletin of the American Museum of Natural History 249:1-118.
Xihaina aquilonia	IVPP V10030	SCDP surface collections, Bayan Mandahu/near Bayan Mandahu, which is in a Campanian eolian	Gao and Hou 1995. Iguanians from the Upper Cretaceous Djadochta Formation, Gobi Desert, China. Journal of Vertebrate Paleontology 15(1):57-79

		sandstone/mudstone in the Djadokhta Formation of China; 84.9 to 70.6 Ma	
Mimeosaurus crassus	holotype AMNH 6655; referred material: IVPP V10031-36, IVPP V10037; IGM 3/74 (MAE 83/93-89), IGM 3/75 (MAE 63/93-153), IGM 3/76 (MAE 96-105)	Bayn Dzak (Shabarakh Usu), Mongolian Gobi Desert; Upper Cretaceous Djadokhta Fm (see Gilmore, 1943); Campanian on International StratChart: 72.1-83.6	Gao and Hou 1995. Iguanians from the Upper Cretaceous Djadochta Formation, Gobi Desert, China. Journal of Vertebrate Paleontology 15(1):57-80; Gao K, and Norell MA. 2000. Taxonomic composition and systematics of Late Cretaceous lizard assemblages from Ukhaa Tolgod and adjacent localities, Mongolian Gobi Desert. Bulletin of the American Museum of Natural History 249:1-118; Borsuk-Bialynicka and S. M. Moody. 1984. Priscagaminae, a new subfamily of the Agamidae (Sauria) from the Late Cretaceous of the Gobi Desert. Acta Palaeontologica Polonica 29:51-81; Gilmore CW. 1943. Fossil lizards of Mongolia. Bulletin of the American Museum of Natural History 81:361-384.
Mimeosaurus tugrikinensis	holotype PIN 3143/102	Tugrikin-Shire locality, Upper Cretaceous, Dzhadokht Fm, Mongolia, Southern Gobi Desert	Alifanov V. 1989. New Priscagamida (Lacertilia) from the Upper Cretaceous of Mongolia and their systematic position among Iguania. Paleontological Journal 4:68-80.
Priscagama gobiensis	holotype ZPAL MgR-III/32; referred material: IVPP V10038; ZPAL MgR-I/69; ZPAL MgR-II/77; ZPAL MgR-II/101; ZPAL MgR-III/31-33; ZPAL MgR-III/72; ZPAL MgR-III/83; IGM 3/77 (MAE 62/93-153), IGM 3/78 (120/93-93), IGM 3/79 (MAE 130)	Khermeen Tsav, Mongolian Gobi Desert; Upper Cretaceous Barun Goyot Fm	Gao and Hou 1995. Iguanians from the Upper Cretaceous Djadochta Formation, Gobi Desert, China. Journal of Vertebrate Paleontology 15(1):57-80; Gao K, and Norell MA. 2000. Taxonomic composition and systematics of Late Cretaceous lizard assemblages from Ukhaa Tolgod and adjacent localities, Mongolian Gobi Desert. Bulletin of the American Museum of Natural History 249:1-118; Borsuk-Bialynicka and S. M. Moody. 1984. Priscagaminae, a new subfamily of the Agamidae (Sauria) from the Late Cretaceous of the Gobi Desert. Acta Palaeontologica Polonica 29:51-81.
Pleurodontagama aenigmatodes	holotype ZPAL MgR-III/35; referred: IVPP V10039		Gao and Hou 1995. Iguanians from the Upper Cretaceous Djadochta Formation, Gobi Desert, China. Journal of Vertebrate Paleontology 15(1):57-80; Borsuk-Bialynicka and S. M. Moody. 1984. Priscagaminae, a new subfamily of the

			Agamidae (Sauria) from the Late Cretaceous of the Gobi Desert. Acta Palaeontologica Polonica 29:51-81
Zapsosaurus scelifrons	holotype IGM 3/71 (MAE 255/92-10); IGM 3/72 (MAE 20/93-15) left upper and lower jaws (topotypic)	Tögrögiin Shiree, Campanian eolian sandstone in the Djadokhta Formation of Mongolia	Gao and M. A. Norell. 2000. Taxonomic composition and systematics of Late Cretaceous lizard assemblages from Ukhaa Tolgod and adjacent localities, Mongolian Gobi Desert. Bulletin of the American Museum of Natural History 249:1-118; D. G. DeMar, J. L. Conrad, J. J. Head, D. J. Varricchio, and G. P. Wilson. 2017. A new Late Cretaceous iguanomorph from North America and the origin of New World Pleurodonta (Squamata, Iguania). Proceedings of the Royal Society of London B 284:20161902:1-7; Conrad and M. A. Norell. 2007. A complete Late Cretaceous iguanian (Squamata, Reptilia) from the Gobi and identification of a new iguanian clade. American Museum Novitates 3584:1-47.
Isodontosaurus gracilis	holotype AMNH 6647; referred material: Ukhaa Tolgod—IGM 3/84 (MAE 96-113), IGM 3/85–3/89 (MAE 27/93-192, 42/93, 49/93-163, 161/93-40, and 94-16-1); Zos—IGM 3/90 (MAE 94-54); Tugrugeen Shireh—IGM 3/91 (MAE 261/92-123), IGM 3/92 (MAE 23/93-28), IGM 3/93, 3/94 (MAE 221/93-8, 88/93-19)	Bayn Dzak (Shabarakh Usu), Mongolian Gobi Desert; Upper Cretaceous Djadokhta Fm; Bayn Dzak, Bayan Mandahu, Ukhaa Tolgod, Zos, and Tugrugeen Shireh localities (Gilmore, 1943; Alifanov, 1993a; Gao and Hou, 1996; Gao & Norell 2000)	Gilmore. 1943. Fossil lizards of Mongolia. Bulletin of the American Museum of Natural History 81(4):361-384; Gao and M. A. Norell. 2000. Taxonomic composition and systematics of Late Cretaceous lizard assemblages from Ukhaa Tolgod and adjacent localities, Mongolian Gobi Desert. Bulletin of the American Museum of Natural History 249:1-118.
Saichangurvel davidsoni	holotype IGM 3/858	Ukhaa Tolgod, Campanian/Maastrichtian eolian sandstone/mudstone in the Djadokhta Formation of Mongolia; 84.9 to 66.043 Ma	Conrad and M. A. Norell. 2007. A complete Late Cretaceous iguanian (Squamata, Reptilia) from the Gobi and identification of a new iguanian clade. American Museum Novitates 3584:1-47; DeMar, J. L. Conrad, J. J. Head, D.

			J. Varricchio, and G. P. Wilson. 2017. A new Late Cretaceous iguanomorph from North America and the origin of New World Pleurodonta (Squamata, Iguania).
Pristiguana brasiliensis	holotype DGM 552 Divisao de Geologia e Mineralogia no. 552 (DGM, Museu de Ciencias da Terra, Companhia de Pesquisa de Recursos Minerais, Rio de Janeiro, Rio de Janeiro State, Brazil) The specimen is lost: see Simoes et al. 2017, Table 1.	Minas Gerais, Brazil; Price Quarry 1 (Caieira quarry), which is in a Maastrichtian fluvial sandstone in the Marília Formation of Brazil; 70.6 to 66.043 Ma	Estes and L. I. Price. 1973. Iguanid lizard from the Upper Cretaceous of Brazil. Science 180:748-751. Borsuk-Bialynicka, M. & Moody, S.M. 1984. Priscagaminae. A new subfamily of the Agamidae (Sauria) from the Late Cretaceous of the Gobi Desert. Acta Palaeontologica Polonica, 29(1-2): 51-81. Daza, J.D., Abdala, V., Arias, J.S., García-López, D. & Ortiz, P. 2012. Cladistic analysis of Iguania and a fossil lizard from the Late Pliocene of northwestern Argentina. Journal of Herpetology, 46(1): 104-119.
Temujinia ellisoni	holotype IGM 3/63 (MAE 121/93-93); referred specimens: IGM 3/64–3/69 (MAE 145/94-40, 75/93-89, 235/93-130, 319/93-147, 39/93-90, MAE 94-37), IGM 3/70 (MAE 19/93-6)	Ukhaa Tolgod (AMNH), which is in a Campanian/Maastrichtian eolian sandstone/mudstone in the Djadokhta Formation of Mongolia; 84.9 to 70.6 Ma	Gao and M. A. Norell. 2000. Taxonomic composition and systematics of Late Cretaceous lizard assemblages from Ukhaa Tolgod and adjacent localities, Mongolian Gobi Desert. Bulletin of the American Museum of Natural History 249:1-118
Ctenomastax parva	holotype IGM 3/61 (MAE 89/93-70); referred specimens IGM 3/62 (MAE 131)	Zos, Nemegt Basin, Mongolian Gobi Desert; Upper Cretaceous Djadokhta Fm	Gao and M. A. Norell. 2000. Taxonomic composition and systematics of Late Cretaceous lizard assemblages from Ukhaa Tolgod and adjacent localities, Mongolian Gobi Desert. Bulletin of the American Museum of Natural History 249:1-118
Flaviagama dzerzhinskii	holotype PIN 3143/101	Dzhadokht Fm, Tugrik (Tugrikin-Shire) locality, Upper Cretaceous, Mongolia, Southern Gobi Desert	Alifanov V. 1989. New Priscagamida (Lacertilia) from the Upper Cretaceous of Mongolia and their systematic position among Iguania. Paleontological Journal 4:68-80.
Phrynosomimus asper	holotype PIN No. 3142/318;	Khermeen Tsav locality; Upper Cretaceous Barun	Gao and M. A. Norell. 2000. Taxonomic composition and systematics of Late

	referred material: IGM 3/81 (MAE 258/92-63), IGM 3/82 (MAE 96-31), IGM 3/83 (MAE 152/93-40)	Goyot Fm, Mongolian Gobi Desert; Barun Goyot Formation Khermeen Tsav and Khulsan localities; Djadokhta Formation Ukhaa Tolgod	Cretaceous lizard assemblages from Ukhaa Tolgod and adjacent localities, Mongolian Gobi Desert. Bulletin of the American Museum of Natural History 249:1-118.
Jeddaherdan aleadonta	holotype MNHN.F.MRS51.1	Cenomanian (Late Cretaceous) beds fromthe Kem Kem region of Southeastern Morocco, Gara Tabroumit	Apesteguia S, Daza JD, Simoes TR, and Rage JC. 2016. The first iguanian lizard from the Mesozoic of Africa. Royal Society Open Science 3:160462. 10.1098/rsos.160462
Gueragama sulamericana	holotype CP.V 2187 (CENPALEO, Universidade do Contestado, Mafra, Santa Catarina State, Brazil)	Cruzeiro do Oeste, Paranà State, Brazil; Goio-Ere Fm, Caiua´ Group, Bauru Basin; Turonian-Campanian, Late Cretaceous	Simões TR, Wilner E, Caldwell MW, Weinschütz LC, and Kellner AWA. 2015. A stem acrodontan lizard in the Cretaceous of Brazil revises early lizard evolution in Gondwana. Nature Communications 6:1-8. DOI: 10.1038/ncomms9149
Tikiguania estesi	holotype GSI type Pal/CHQ-010 (Geological Survey of India Central Palaeontological Repository Unit, Kolkata, India)	original: Late Triassic (Carnian) Tiki Fm of the South Rewa Gondwana basin near the village of Tiki (23º 64.15‘ N, 81° 22‘ E), Shadol district, Madhya Pradesh, India; current: Quaternary, Late Tertiary (Hutchinson et al. 2012)	Datta and S. Ray. 2006. Earliest lizard from the Late Triassic (Carnian) of India. Journal of Vertebrate Paleontology 26(4):795-800; Hutchinson MN, Skinner A, and Lee MSY. 2012. Tikiguania and the antiquity of squamate reptiles (lizards and snakes). Biology Letters 8:665-669. 10.1098/rsbl.2011.1216.
Magnuviator ovimonsensis	holotype MOR 6627 (Museum of the Rockies)	type locality Egg Mountain, Teton County, MT, USA; Upper Cretaceous (Campanian; ca 75.5+0.40 Ma; Two Medicine Fm, Teton County, northwestern Montana, USA	DeMar DG, Conrad JL, Head JJ, Varricchio DJ, and Wilson GP. 2017. A new Late Cretaceous iguanomorph from North America and the origin of New World Pleurodonta (Squamata, Iguania). Proc R Soc B: The Royal Society. p 20161902.
Parauromastyx gilmorei	holotype ZPAL 5/301 (lost)	Bayan Zag (= Bayn Dzak, Shabarakh Usu GILMORE, 1943), Ömnögov (South Gobi), Mongolia; Djadochta Fm, Middle Campanian Stage, Senonian Subepoch, Gulf Epoch, Late Cretaceous	Alifanov V. 2004. Parauromastyx gilmorei gen. et sp. nov. (Isodontosauridae, Iguania), a new lizard from the Upper Cretaceous of Mongolia. PALEONTOLOGICAL JOURNAL C/C OF PALEONTOLOGICHESKII ZHURNAL 38:206-210.
Brasiliguana prudentis	holotype MN 7230-V (Coleção de Paleovertebrados,	Adamantina Formation, Bauru Group, Turonian-Santonian, Upper Cretaceous; Presidente Prudente Municipality, west São Paulo State, southeast	Nava WR, and Martinelli AG. 2011. A new squamate lizard from the Upper Cretaceous Adamantina Formation (Bauru Group), São Paulo State, Brazil. Anais da Academia Brasileira de Ciencias 83:291-299.

	Museu Nacional, Rio de Janeiro, Brazil)	Brazil	Albino, A.M. & Brizuela, S. 2014. First record of squamate reptiles from the Oligocene of South America. Alcheringa, 38(3): 412-421.
Pariguana lancensis	holotype AMNH 22208	Lance Formation (Maastrichtian) of Wyoming; Type locality is Bushy Tailed Blowout, which is in a Lancian terrestrial shale in the Lance Formation of Wyoming. Age range: 70.6 to 66.043 Ma	Longrich NR, Bhullar BAS, Gauthier JA (2012a) Mass extinction of lizards and snakes at the Cretaceous–Paleogene boundary. Proc Natl Acad Sci USA 109(52):21396–21401; Nydam RL. 2013. Squamates from the Jurassic and Cretaceous of North America. Palaeobiodiversity and Palaeoenvironments 93:535-565; Simões TR, Caldwell MW, Weinschütz LC, Wilner E, and Kellner AWA. 2017. Mesozoic Lizards from Brazil and Their Role in Early Squamate Evolution in South America. Journal of Herpetology:307-315. 10.1670/16-007.
Conicodontosaurus kanhsienensis	holotype IVPP V.4021	?	Young. 1973. [On a Mesozoic lizard from Kanhsien, Kiangsi]. Vertebrata PalAsiatica 11(1):44-45.
Conicodontosaurus djadochtaensis	holotype AMNH 6519	Shabarakh Usu (AMNH loc. 12049), Campanian eolian sandstone in the Djadokhta Fm of Mongolia	Gilmore CW. 1943. Fossil lizards of Mongolia. Bulletin of the American Museum of Natural History 81:361-384; Gao KQ, and Hou LH. 1996. Systematics and taxonomic diversity of squamates from the Upper Cretaceous Djadochta Formation, Bayan Mandahu, Gobi Desert, People's Republic of China. Canadian Journal of Earth Sciences 33:578-598.
Chamaeleognathus iordansky	holotype PIN 3142/345	Its type locality is Khermeen Tsav, Red Beds [SMPE] (PIN coll. 3142), which is in a Campanian terrestrial horizon in the Barun Goyot Formation of Mongolia. Age range: 84.9 to 70.6 Ma	Alifanov. 1996. Lizards of the families Priscagamidae and Hoplocercidae (Sauria, Iguania): phylogenetic position and new representatives from the Late Cretaceous of Mongolia. Paleontological Journal 30(4):466-483.
Gladidenagama semiplena	holotype PIN 3142/319	Its type locality is Khermeen Tsav, Red Beds [SMPE] (PIN coll. 3142), which is in a Campanian terrestrial horizon in the Barun Goyot Formation of Mongolia. Age range: 84.9 to 70.6 Ma	Alifanov. 1996. Lizards of the families Priscagamidae and Hoplocercidae (Sauria, Iguania): phylogenetic position and new representatives from the Late Cretaceous of Mongolia. Paleontological Journal 30(4):466-483.
Morunasius modestus	holotype PIN 3142/317	Its type locality is Khermeen Tsav, Red Beds [SMPE] (PIN	Alifanov. 1996. Lizards of the families Priscagamidae and Hoplocercidae (Sauria,

		coll. 3142), which is in a Campanian terrestrial horizon in the Barun Goyot Formation of Mongolia.	Iguania): phylogenetic position and new representatives from the Late Cretaceous of Mongolia. Paleontological Journal 30(4):466-483.
Xianglong zhaoi	holotype LPM 000666 (Liaoning Paleontological Museum, China)	Zhuanchengzi locality, near Yizhou, Liaoning Province, China. The horizon of the find is the Lower Cretaceous Zhuanchengzi Bed of the Yixian Formation	Li, P.-P., Gao, K.-Q., Hou, L.-H. & Xu, X. A gliding lizard from the Early Cretaceous of China. Proc. Natl. Acad. Sci. USA 104, 5507-5509 (2007).

Cenozoic

TAXON	SPECIMENS	AGE & LOCALITY	REFERENCES
Babibasiliscus alxi	holotype UWBM 89090 UWBM, Burke Museum of the University of Washington (Seattle, WA)	Lucky Lizard Locality (UWBM C1046), Uinta County, Wyoming. Blacks Fork Member of Bridger Formation (Bridger B), Green River Basin, late Early Eocene, approximately 48 Ma	Conrad JL (2015) A New Eocene Casquehead Lizard (Reptilia, Corytophanidae) from North America. PLoS ONE 10(7): e0127900. doi:10.1371/journal.pone.0127900
Khaichinsaurus reshetovi	holotype PIN no. 3107/227; 3107/229 (maxillary fragment without teeth), 230–232 (dentary fragments)	Mongolia, Umnegov Aimag, Khaichin Uul 2 locality; Middle Eocene, Khaichin FM, Khaich Member	Alifanov VR. 2009. New acrodont lizards (Lacertilia) from the Middle Eocene of southern Mongolia. Paleontological Journal 43:675-685. 10.1134/S0031030109060124
Changjiangosaurus huananensis	holotype IVPP V4451	Upper Paleocene terrestrial horizon in the Wanghudun Fm of China; 66.043 to 61.7 Ma; Fossil pit 71001, about 150 m southeast of Wangdawu, Huangpu Village, Qianshan County, Anhui; Lower Member, Wanghudun Formation (Early Paleocene)(Dong et al. 2016)	Hou. 1976. New materials of Palaeocene lizards of Anhui. Vertebrata PalAsiatica 14(1):44-52; Dong L, Evans S, and Wang Y. 2016. Taxonomic revision of lizards from the Paleocene deposits of the Qianshan Basin, Anhui, China. Vertebrata PalAsiatica 54:243-268.
Lentisaurus giganteus	PIN no. 3107/226	Mongolia, Umnegov Aimag, Khaichin Uul 2 locality; Middle Eocene, Khaichin Formation, Khaich Member Age: (33.9,47.8)	Alifanov VR. 2009. New acrodont lizards (Lacertilia) from the Middle Eocene of southern Mongolia. Paleontological Journal 43:675-685. 10.1134/S0031030109060124

Graminisaurus interruptus	PIN no. 3107/234	Mongolia, Umnegov Aimag, Khaichin Uul 2 locality; Middle Eocene, Khaichin Fm, Khaich Member	Alifanov VR. 2009. New acrodont lizards (Lacertilia) from the Middle Eocene of southern Mongolia. Paleontological Journal 43:675-685. 10.1134/S0031030109060124
Agamimus gracilis	holotype PIN no. 3107/280; 3107/276–279 (maxillae) and 281–306 (dentaries)	Mongolia, Umnegov Aimag, Khaichin Uul 2 locality; Middle Eocene, Khaichin Fm, Khaich Member	Alifanov VR. 2009. New acrodont lizards (Lacertilia) from the Middle Eocene of southern Mongolia. Paleontological Journal 43:675-685. 10.1134/S0031030109060124
Lavatisaurus elegans	holotype PIN no. 3107/257; PIN 3107/252–256, 258–275 (dentaries)	Mongolia, Umnegov Aimag, Khaichin Uul 2 locality; Middle Eocene, Khaichin Fm, Khaich Member	Alifanov VR. 2009. New acrodont lizards (Lacertilia) from the Middle Eocene of southern Mongolia. Paleontological Journal 43:675-685. 10.1134/S0031030109060124.
Acrodontopsis robustus	holotype PIN no. 3107/246; PIN 3107/235–245 and 247–251 (dentary fragments)	Mongolia, Umnegov Aimag, Khaichin Uul 2 locality; Middle Eocene, Khaichin Fm, Khaich Member	Alifanov VR. 2009. New acrodont lizards (Lacertilia) from the Middle Eocene of southern Mongolia. Paleontological Journal 43:675-685. 10.1134/S0031030109060124.
Dornosaurus gobiensis	holotype PIN, no. 3107/321; specimens PIN, nos. 3107/322, 323; PIN, nos. 3107/307, 314–320	Mongolia, Ömnögovi Aimag, Khaychin Ula 2 locality; Middle Eocene, Khaychin Formation, Khaych Member	Alifanov. 2012. Lizards of the family Arretosauridae Gilmore, 1943 (Iguanomorpha, Iguania) from the Paleogene of Mongolia. Paleontological Journal 46(4):412-420.
Khaichinguana eocaenica	holotype PIN, no. 3107/308; specimens PIN, nos. 3107/309–313, 3107/324–328	Mongolia, Ömnögovi Aimag, Khaychin Ula 2 locality; Middle Eocene, Khaychin Formation, Khaych Member	Alifanov. 2012. Lizards of the family Arretosauridae Gilmore, 1943 (Iguanomorpha, Iguania) from the Paleogene of Mongolia. Paleontological Journal 46(4):412-420.
Ergiliinsaurus postumus	holotype PIN, no. 4751/3	Mongolia, Doronogov Aimag, Khoer Dzan locality; Lower Oligocene**,** Ergiliin Zoo Formation (upper alluvial member)	Alifanov. 2012. Lizards of the family Arretosauridae Gilmore, 1943 (Iguanomorpha, Iguania) from the Paleogene of Mongolia. Paleontological Journal 46(4):412-420.
Arretosaurus ornatus	holotype AMNH 6706 referred: AMNH 6708, 6716	Twin Obo (Ulan Gochu horizon), Oligocene terrestrial horizon in the Ulan Gochu Formation of China; up.Eocene-lw.Oligocene	Gilmore. 1943. Fossil lizards of Mongolia. Bulletin of the American Museum of Natural History 81(4):361-384. Alifanov. 2012. Lizards of the family Arretosauridae Gilmore, 1943 (Iguanomorpha, Iguania) from the Paleogene of Mongolia. Paleontological Journal 46(4):412-420.
Hemishinisaurus latifrons	holotype IVPP V9595.1	Yuanqu, Eocene terrestrial horizon in the Hedi Formation of China	Li. 1991. Fossil reptiles from Zhaili member, Hedi Formation, Yuanqu, Shanxi. Vertebrata PalAsiatica 29(4):276-285; Alifanov. 2012. Lizards of the family Arretosauridae Gilmore, 1943 (Iguanomorpha, Iguania) from the Paleogene of Mongolia. Paleontological Journal 46(4):412-420.

Tinosaurus stenodon	holotype YPM 615; referred: AMNH 3822, 3823, 9000, 15776, 15777	type locality is Henry's Fork Hill (Bridger C), Bridgerian terrestrial horizon in the Bridger Fm of Wyoming Eocene: see Murphey et al. 2011 for the stratigraphic age	Marsh 1872; see also Gilmore 1943 and Prasad & Bajpai 2008 Gilmore CW. 1943. Fossil lizards of Mongolia. Bulletin of the American Museum of Natural History 81:361-384; Prasad GVR, and Bajpai S. 2008. Agamid Lizards From The Early Eocene of Western India: Oldest Cenozoic Lizards From South Asia. Palaeontologia Electronica 11:1-20. Murphey PC, Townsend KEB, Friscia AR, Evanoff E, Lee J, and Evans JP. 2011. Paleontology and stratigraphy of middle Eocene rock units in the Bridger and Uinta Basins, Wyoming and Utah. Geologic Field Trips to the Basin and Range, Rocky Mountains, Snake River Plain, and Terranes of the US Cordillera: Geological Society of America, 125-166.
Tinosaurus indicus	holotype IITR/SB/VLM/ 904; referred: IITR/SB/VLM 1051, IITR/SB/VLM 748, IITR/SB/VLM 820, IITR/SB/VLM 1040 Referred material: GU/RSR/VAS-2008, 2015, 2037-2039, 2051-2052, GU/RSR/VAS-2016-18, 2022-2023, 2025-2026	Lower Eocene Cambay Shale of Vastan Lignite Mine, District, Surat, Gujarat state, India Cambay Shale Formation, early to middle Ypresian, Early Eocene, Vastan Lignite Mine, Surat District, Gujarat, India	Prasad GVR, and Bajpai S. 2008. Agamid Lizards From The Early Eocene of Western India: Oldest Cenozoic Lizards From South Asia. Palaeontologia Electronica 11:1-20; Rana RS, Augé M, Folie A, Rose KD, Kumar K, Singh L, Sahni A, and Smith T. 2013. High diversity of acrodontan lizards in the early Eocene Vastan lignite mine of India. Geologica Belgica 16:290-301.
Tinosaurus asiaticus	holotype AMNH 6717	type locality is Chimney Butte, North Mesa, Eocene terrestrial horizon in the Ulan Shireh Formation of Mongolia Age range: 48.6 to 37.2 Ma	Gilmore CW. 1943. Fossil lizards of Mongolia. Bulletin of the American Museum of Natural History 81:361-384.
Uromastyx europaeus	holotype MNHN No. QU 17160	Type locality is Phosphorites du Quercy (for taxa with non-specific locality data), Eocene/Miocene terrestrial phosphorite in the Quercy Phosphorites Formation of France; 33.9 to 28.4 Ma	Augé. 2005. Evolution des lézards du Paléogène en Europe. *Mémoires du Muséum national d'histoire naturelle* **192**:1-369.
Barbaturex	holotype UCMP	Paleogene; type locality is	Head JJ, Barrett PM, and Rayfield EJ. 2009.

morrisoni	142227 (University of California Museum of Paleontology); referred material: UCMP 128388, 128410, 130290, 130291, 130292; NMMP-KU 0092, 1923, 1924–1926	UCMP V96009; Thandaung kyitchaung, Pondaung Formation, northwest of Mogaung village, Sagaing District, Myanmar; Fossil-bearing beds of the Pondaung Formation near the village of Bahin have been dated to 37.2 ± 1.3 Ma	Neurocranial osteology and systematic relationships of Varanus (Megalania) prisca Owen, 1859 (Squamata: Varanidae). Zoological Journal of the Linnean Society 155:445-457. 10.1111/j.1096-3642.2008.00448.x.
Vastanagama susani (*susanae*)	holotype IITR/ SB/ VLM 1050; referred: IITR/SB/VLM/793, IITR//SB/VLM/ 886; Vastanagama susanae Prasad and Bajpai, 2008 Holotype: IIT-1050; Referred material: GU/RSR/VAS-2001-2002, GU/RSR/VAS-2003, GU/RSR/VAS-2007, GU/RSR/VAS-2031	Lower Eocene Cambay Shale of Vastan Lignite Mine, District Surat, Gujarat state, India; Cambay Shale Formation, early to middle Ypresian, Early Eocene, Vastan Lignite Mine, Surat District, Gujarat, India	Prasad GVR, and Bajpai S. 2008. Agamid Lizards From The Early Eocene of Western India: Oldest Cenozoic Lizards From South Asia. Palaeontologia Electronica 11:1-20; Rana RS, Augé M, Folie A, Rose KD, Kumar K, Singh L, Sahni A, and Smith T. 2013. High diversity of acrodontan lizards in the early Eocene Vastan lignite mine of India. Geologica Belgica 16:290-301.
Armandisaurus explorator	holotype AMNH-FAM 8799	Tesuque Fm, Skull Ridge Member, White Operation Ridge, Santa Fe County, New Mexico, USA; 11.6-16.5 Ma, Miocene	Norell MA, and Queiroz Kd. 1991. The earliest iguanine lizard (Reptilia: Squamata) and its bearing on iguanine phylogeny. Amer museum novitates 2997.
Geiseltaliellus longicaudus	holotype GM 4043	early to late Eocene of Europe (MP7-19:Augé 2005); type locality is Geiseltal, Ce III, Grube "Cecilie", which is in a Lutetian lacustrine coal in Germany; 48.6 to 40.4 Ma	Kuhn 1944; Augé 2005; Smith KT. 2009. Eocene lizards of the clade Geiseltaliellus from Messel and Geiseltal, Germany, and the early radiation of Iguanidae (Reptilia: Squamata). Bulletin of the Peabody Museum of Natural History 50:219-306.
Geiseltaliellus grisolli	holotype MNHN GRI 17405	early to late Eocene of Europe (MP7-19:Augé 2005); type locality is Grisolles, which is in a Bartonian mire/swamp limestone in the Calcaire de Saint-Ouen Formation of France; 40.4 to 37.2 Ma	Augé. 2005. Evolution des lézards du Paléogène en Europe. Mémoires du Muséum national d'histoire naturelle 192:1-369. Smith KT. 2009. Eocene lizards of the clade Geiseltaliellus from Messel and Geiseltal, Germany, and the early radiation of Iguanidae (Reptilia: Squamata). Bulletin of the Peabody Museum of Natural History 50:219-306.
Geiseltaliellus lamandini	holotype MNHN No. QU 17739	early to late Eocene of Europe (MP7-19:Augé 2005); Type locality is	Filhol, H. 1877. Recherches sur les Phosphorites du Quercy. Pt. II. Annales Sciences Géologiques, 8:1-338.

		Phosphorites du Quercy (for taxa with non-specific locality data), which is in an Eocene/Miocene terrestrial phosphorite in the Quercy Phosphorites Formation of France; 37.2 to 33.9 Ma	Smith KT. 2009. Eocene lizards of the clade Geiseltaliellus from Messel and Geiseltal, Germany, and the early radiation of Iguanidae (Reptilia: Squamata). Bulletin of the Peabody Museum of Natural History 50:219-306.
Geiseltaliellus pradiguensis	holotype referred: IPS 56093, IPS 56094, IPS 59521, IPS 59523	Sossis (Eocene of Spain), 37.2 to 33.9 Ma	Augé, M. 2007. Past and present distribution of iguanid lizards. Arquivos do Museu Nacional, Rio de Janeiro, 65:403-416. Bolet A, and Evans SE. 2013. Lizards and amphisbaenians (Reptilia, Squamata) from the late Eocene of Sossís (Catalonia, Spain). Palaeontologia Electronica 16:8A.
Geiseltaliellus maarius	holotype HLMD-Me 10207; referred: SMF ME 2, 1769, 2684, 2938	early to late Eocene of Europe (MP7-19:Augé 2005); HLMD pit 14, middle Messel Fm, middle Eocene (MP 11); temporal range of pit is 160 Kyr;	Smith KT. 2009. Eocene lizards of the clade Geiseltaliellus from Messel and Geiseltal, Germany, and the early radiation of Iguanidae (Reptilia: Squamata). Bulletin of the Peabody Museum of Natural History 50:219-306.
Capitolacerta dubia	holotype GM 4005; referred: GM 4001, GM 4002; (synonymized with G. longicaudus by Estes 1983a, also confirmed by Rossmann 2000 and Smith 2009)	Geiseltal Ce IV	Smith KT. 2009. Eocene lizards of the clade Geiseltaliellus from Messel and Geiseltal, Germany, and the early radiation of Iguanidae (Reptilia: Squamata). Bulletin of the Peabody Museum of Natural History 50:219-306.
Cadurciguana hoffstetteri	holotype USTL, ECC 2502; referred: USTL, SND625 USTL Université Montpellier 2, Sciences et Techniques du Languedoc	type locality is Escamps C, which is in a MP 19 karst phosphorite in France; 37.2 to 33.9 Ma	Augé, M. 1987. Confirmation de la présence d'Iguanidae (Reptilia, Lacertilia) dans l'Eocène européen. Comptes Rendus de l'Académie des Sciences, Paris, 305:633-636. Bolet A, Daza JD, Auge M, and Bauer AM. 2015. New genus and species names for the Eocene lizard Cadurcogekko rugosus Augé, 2005. Zootaxa 3985:265-274.
Pseudolacerta mucronata	holotype presumed lost, MNHN	type locality is Phosphorites du Quercy (for taxa with non-specific locality data), which is in an Eocene/Miocene terrestrial phosphorite in the Quercy Phosphorites Formation of France; Eocene to Miocene, 37.2 to 33.9 Ma	Rage. 1988. Le gisement du Bretou (Phosphorites du Quercy, Tarn-et-Garonne, France) et sa faune des vertebres de l'Eocene superieur; 1. Amphibiens et reptiles. Palaeontographica Abteilung A 205(1-6):3-27.

Pseudolacerta quercyini	holotype MNHN BRT 1413	type locality is Le Bretou, which is in a Bartonian karst phosphorite in France; Eocene to Miocene of France, 37.2 to 33.9 Ma	Augé. 2005. Evolution des lézards du Paléogène en Europe. Mémoires du Muséum national d'histoire naturelle 192:1-369.
Heterodontagama borsukae	holotype GU/RSR/VAS-2035; Paratype: GU/RSR/VAS-2036; Referred material: GU/RSR/VAS-2046, GU/RSR/VAS-2050	Early Eocene, Vastan Lignite Mine, Gujarat, India; Cambay Shale Formation, early to middle Ypresian, Early Eocene, Vastan Lignite Mine, Surat District, Gujarat, India	Rana RS, Augé M, Folie A, Rose KD, Kumar K, Singh L, Sahni A, and Smith T. 2013. High diversity of acrodontan lizards in the early Eocene Vastan lignite mine of India. Geologica Belgica 16:290-301.
Suratagama neeraae	Holotype: GU/RSR/VAS-2030; Referred material: GU/RSR/VAS-2033, GU/RSR/VAS-2040	Cambay Shale Formation, early to middle Ypresian, Early Eocene, Vastan Lignite Mine, Surat District, Gujarat, India	Rana RS, Augé M, Folie A, Rose KD, Kumar K, Singh L, Sahni A, and Smith T. 2013. High diversity of acrodontan lizards in the early Eocene Vastan lignite mine of India. Geologica Belgica 16:290-301.
Indiagama gujarata	holotype GU/RSR/VAS-2009	Cambay Shale Formation, early to middle Ypresian, Early Eocene, Vastan Lignite Mine, Surat District, Gujarat, India	Rana RS, Augé M, Folie A, Rose KD, Kumar K, Singh L, Sahni A, and Smith T. 2013. High diversity of acrodontan lizards in the early Eocene Vastan lignite mine of India. Geologica Belgica 16:290-301.
Lapitiguana impensa	holotype MNZ 37015 (Museum of New Zealand Te Papa Tongarewa)	Voli Voli Cave (Qara-ni-vokai Site) near Sigatoka, Viti Levu, Fiji, Southwest Pacific. Late Quaternary	Pregill GK, and Worthy TH. 2003. A new iguanid lizard (Squamata, Iguanidae) from the late Quaternary of Fiji, Southwest Pacific. Herpetologica 59:57-67.
Brachylophus gibbonsi	holotype UF 212300 UF, Florida Museum of Natural History	Excavation unit 17, level 11, Faleloa Archaeological Site, Foa Island, Ha'apai Group, Kingdom of Tonga; Late Holocene, approximately 2800 years B.P.	Pregill GK, and Steadman DW. 2004. South Pacific iguanas: human impacts and a new species. Journal of Herpetology:15-21.
Tinosaurus doumuensis	holotype IVPP V 4453	Fossil pit 71018, 150 m southwest of Chongliwu, Huangpu Village, Qianshan County, Anhui; Upper Member, Doumu Formation (Middle Paleocene)	Hou L H, 1974. Paleocene lizards from Anhui, China. Vert PalAsiat, 12(3): 193–202; Dong L, Evans S, and Wang Y. 2016. Taxonomic revision of lizards from the Paleocene deposits of the Qianshan Basin, Anhui, China. Vertebrata PalAsiatica 54:243-268.
Agama sinensis	holotype IVPP V 4454	Fossil pit 71079(72), 300 m south of Hanlaowu (Hanhuawu), Huangpu Village, Qianshan County; Lower Member, Doumu Formation (Middle Paleocene)	Hou L H, 1974. Paleocene lizards from Anhui, China. Vert PalAsiat, 12(3): 193–202; Dong L, Evans S, and Wang Y. 2016. Taxonomic revision of lizards from the Paleocene deposits of the Qianshan Basin, Anhui, China. Vertebrata PalAsiatica 54:243-268.

Qianshanosaurus huangpuensis	Holotype IVPP V 4448 Paratype IVPP V 4449 Referred material: IVPP V 22768 ; V 22769	Type locality and Fossil pit 71002 (about 100 m northwest of Haixingdi, Huangpu Village, Qianshan County); Fossil pit 70021, about 300 m east of Lijialaowu, Huangpu Village, Qianshan County, Anhui; Upper Member, Wanghudun Formation (Early–Middle Paleocene)	Hou L H, 1974. Paleocene lizards from Anhui, China. Vert PalAsiat, 12(3): 193–202; Dong L, Evans S, and Wang Y. 2016. Taxonomic revision of lizards from the Paleocene deposits of the Qianshan Basin, Anhui, China. Vertebrata PalAsiatica 54:243-268.
Anqingosaurus brevicephalus	Holotype IVPP V 4452	Fossil pit 71001, about 150 m southeast of Wangdawu, Huangpu Village, Qianshan County, Anhui; Lower Member, Wanghudun Formation (Early Paleocene)	Hou L H, 1976. New materials of Palaeocene lizards of Anhui. Vert PalAsiat, 14(1): 45–52. Dong L, Evans S, and Wang Y. 2016. Taxonomic revision of lizards from the Paleocene deposits of the Qianshan Basin, Anhui, China. Vertebrata PalAsiatica 54:243-268.
Aciprion formosum	AMNH 1609, 3663, 8715, 8716, 8717, 8722, 11400, 21444	Oligocene Type locality Cedar Creek, Logan County, Colorado; Horizon Oreodon beds, White River formation, Oligocene. (Gilmore 1928)	see Estes 1983 for diagnosis and definition; Cope 1873. Synopsis of new Vertebrata from the Tertiary of Colorado obtained during the summer of 1873. Seventh Annual Report of the United States Geological Survey of the Territories. Conrad JL, Rieppel O, and Grande L. 2007. A Green River (Eocene) polychrotid (Squamata: Reptilia) and a re-examination of iguanian systematics. Journal of Paleontology 81:1365-1373. Smith KT. 2009. Eocene lizards of the clade Geiseltaliellus from Messel and Geiseltal, Germany, and the early radiation of Iguanidae (Reptilia: Squamata). Bulletin of the Peabody Museum of Natural History 50:219-306.
Aciprion majus	Princeton Univ. Mus. No. 10015	Gilmore 1928: Collected by the Princeton scientific expedition of 1882. Type locality.—Chalk Bluffs, Logan County, Colo.Horizon.—Oreodon beds?, White River formation, Oligocene.	Gilmore. 1928. Fossil lizards of North America. Memoirs of the National Academy of Sciences 22(3):1-201.
Afairiguana avius	FMNH PR 2379 (Field Museum of Natural History)	Early Eocene-aged Green River Formation of Wyoming Age range: 55.8 to 50.3 Ma	Conrad JL, Rieppel O, and Grande L. 2007. A Green River (Eocene) polychrotid (Squamata: Reptilia) and a re-examination of iguanian systematics. Journal of Paleontology 81:1365-1373.

Parasauromalus olseni [Note: *not an iguanian based on personal observation]	AMNH 1620	early Eocene Type locality is Alkali Creek (AMNH), which is in an Eocene terrestrial horizon in the Wind River Formation of Wyoming. Age range: 46.2 to 40.4 Ma	Gilmore, C.W. 1928. Fossil lizards of North America. Memoirs of the National Academy of Sciences, 22:1-201. Smith KT. 2006. A diverse new assemblage of Late Eocene squamates (Reptilia) from the Chadron Formation of North Dakota, USA. Palaeontologia Electronica 9:1-44. Zonneveld, G. F. Gunnell, and W. S. Bartels. 2000. Early Eocene fossil vertebrates from the southwestern Green River Basin, Lincoln and Uinta counties, Wyoming. Journal of Vertebrate Paleontology 20(2):369-386. Bolet A. 2017. First early Eocene lizards from Spain and a study of the compositional changes between late Mesozoic and early Cenozoic Iberian lizard assemblages. Palaeontologia Electronica 20:1-22.
Suzanniwana patriciana	UCMP 167664	UCMP locality V99019, earliest Eocene (zone Wa0), Willwood Formation, Bighorn Basin, Wyoming, USA	Smith KT. 2009. A new lizard assemblage from the earliest Eocene (zone Wa0) of the Bighorn Basin, Wyoming, USA: biogeography during the warmest interval of the Cenozoic. Journal of Systematic Palaeontology 7:299-358. Bolet A. 2017. First early Eocene lizards from Spain and a study of the compositional changes between late Mesozoic and early Cenozoic Iberian lizard assemblages. Palaeontologia Electronica 20:1-22.
Anolbanolis banalis	holotype UCMP 400150	UCMP locality V99019, earliest Eocene (zone Wa0), Willwood Formation, Bighorn Basin, Wyoming, USA	Smith KT. 2009. A new lizard assemblage from the earliest Eocene (zone Wa0) of the Bighorn Basin, Wyoming, USA: biogeography during the warmest interval of the Cenozoic. Journal of Systematic Palaeontology 7:299-358;
Crotaphytus wislizeni	LACM 35177, LACM not numbered; UALP 7343:6456	Upper Pleistocene, California; Holocene, Great Basin southward into Mexico, west to San Joaquin Valley, California.	Estes R. 1983. Handbuch der Paläoherpetologie: Sauria terrestria, Amphisbaenia, part 10A. Munich: Gustav Fischer Verlag.
Crotaphytus? oligocenicus	SMNH 1444 + others	Lower Oligocene, Cypress Hills Formation, Saskatchewan, Canada.	Estes R. 1983. Handbuch der Paläoherpetologie: Sauria terrestria, Amphisbaenia, part 10A. Munich: Gustav Fischer Verlag.
Ctenosaura premaxillaris	AMNH, premaxilla (type of Deltatmema premaxillaris)	subfossil, Actun Spukil, Hacienda Calcehtok, Yucatan, Mexico	Estes R. 1983. Handbuch der Paläoherpetologie: Sauria terrestria, Amphisbaenia, part 10A. Munich: Gustav Fischer Verlag.

Cyclura pinguis	USNM 59358, MCZ 12460, USNM, abundant material representing most of the major skeletal elements.	Upper Pleistocene (15-18 thousand years B.P.) Holocene, Puerto Rico; Holocene, Anegada I., British Virgin Islands.	Estes R. 1983. Handbuch der Paläoherpetologie: Sauria terrestria, Amphisbaenia, part 10A. Munich: Gustav Fischer Verlag.
Cypressaurus hypsodontus	SMNH 1442	Lower Oligocene, Cypress Hills Formation, Saskatchewan, Canada.	Estes R. 1983. Handbuch der Paläoherpetologie: Sauria terrestria, Amphisbaenia, part 10A. Munich: Gustav Fischer Verlag.
Erichosaurus diminutus	MACN specimen, now **lost**	Lower Miocene, Santa Cruz beds, Argentina.	Estes R. 1983. Handbuch der Paläoherpetologie: Sauria terrestria, Amphisbaenia, part 10A. Munich: Gustav Fischer Verlag.
Erichosaurus bombimaxilla	lost?	Lower Miocene, Santa Cruz beds, Argentina.	Estes R. 1983. Handbuch der Paläoherpetologie: Sauria terrestria, Amphisbaenia, part 10A. Munich: Gustav Fischer Verlag.
Erichosaurus debilis	lost?	Lower Miocene, Santa Cruz beds, Argentina.	Estes R. 1983. Handbuch der Paläoherpetologie: Sauria terrestria, Amphisbaenia, part 10A. Munich: Gustav Fischer Verlag.
Harrisonsaurus fossilis	MSU 1029	Lower Miocene, Harrison Formation, Cherry County, Nebraska.	Estes R. 1983. Handbuch der Paläoherpetologie: Sauria terrestria, Amphisbaenia, part 10A. Munich: Gustav Fischer Verlag.
Holbrookia maculata	UMMP no number UTEP, UALP, no number	Pleistocene, Kansas; Holocene, Great Plains, southwestward to the Colorado Desert and southward into northern Mexico.	Estes R. 1983. Handbuch der Paläoherpetologie: Sauria terrestria, Amphisbaenia, part 10A. Munich: Gustav Fischer Verlag.
Holbrookia texana	UMMP 34171, 33832, 34168, 34172-34176, 34167-34168, 34178, 34166-34167; 34451-34152,34556. UT 40450-1659.	Pleistocene, Kansas; Pleistocene-Holocene, Texas; Holocene, Arizona, New Mexico, Texas and northern Mexico.	Estes R. 1983. Handbuch der Paläoherpetologie: Sauria terrestria, Amphisbaenia, part 10A. Munich: Gustav Fischer Verlag.
Leiocephalus carinatus	UF 10175, 10173-10176, 10177, 10178, 10174.	Upper Pleistocene, Banana Hole, New Providence, Bahamas; Upper Pleistocene-Holocene, Bahamas; Holocene, Cuba, Florida.	Estes R. 1983. Handbuch der Paläoherpetologie: Sauria terrestria, Amphisbaenia, part 10A. Munich: Gustav Fischer Verlag.
Leiocephaills apertosulcus	Holotype MCZ 3404.	Upper Pleistocene, Stratum 2, Cueva Cerro de San	Estes R. 1983. Handbuch der Paläoherpetologie: Sauria terrestria,

	Referred specimens: UF 10088, 10090- 9, 10092, 10093, 10094, 10095, 10096, 10097, 10098, 10099, 10100, 10101.	Francisco, San Rafael, Dominican Republic.	Amphisbaenia, part 10A. Munich: Gustav Fischer Verlag.
Leiocephalus cuneus	Holotype: UF 8226, dentary. Upper Pleistocene, Cave V, Two Foot Bay, Barbuda, British West Indies. Referred specimens: UF 8227-8233, dentaries; 8234-8235, premaxillae; 8236- 8240, maxillae; 8241, articular-surangular; 8242, articular; 8249, interclavicle; 8251, scapulocoracoid; 8252, scapula; 8253-8254, pelves; 8255-8256, ilia; 8257, presacral vertebrae; 8258, sacral vertebrae; 8259- 8261, caudal vertebrae; 8262, limb bones; all from the type locality. Cave I: 8469, dentaries;.8263, 8270, premaxillae; 8264-8265, 8468, maxillae; 8266- 8267, quadrates; 8268, pterygoids; 8269-8270, frontals; 8271, parietal; 8444, postorbital; 8250, jugal; 8271, pelvis. Cave II; 8334, pelvis. Cave III: 8317, dentary; 8395, ilium. All from Barbuda, British West Indies.		Estes R. 1983. Handbuch der Paläoherpetologie: Sauria terrestria, Amphisbaenia, part 10A. Munich: Gustav Fischer Verlag.
Leiocephalus etheridgei	Holotype: USNM 259190, dentary; Upper Pleistocene, Blackbone I Cave, Barahona (Morovis), Puerto Rico. Referred specimens: USNM dentaries, maxillae, frontals, basicrania, pterygoids, vertebrae; topotypic specimens. Also KU 11473, dentaries; Cuevo del Perro, Barahona (Morovis), Puerto Rico.		Estes R. 1983. Handbuch der Paläoherpetologie: Sauria terrestria, Amphisbaenia, part 10A. Munich: Gustav Fischer Verlag.
Leiocephalus jamaicensis	Holotype: AMNH 2311, dentary. Upper Pleistocene, Dairy Cave, Dry Harbour, Jamaica. Referred specimens: Dairy Cave, Loe. E: AMNH 2312--2313, maxillae; 2314, parietal; 2315, caudal vertebrae. Dairy Cave, Loc. D: UF 8503- 8504. Dairy Cave, Loe. G: UF 8502, dentary. Montego Bay Airport Cave: UF 8505, dentary; 8506, parietal; 8508, frontal; 8509, pterygoid; 8510, caudal vertebrae. Portland Cave r, Loc. E: UF 8511 - 8512, dentaries, !l513, maxilla; 8514, pterygoid; 8516, 8518, vertebrae. Portland Cave III: UF 8489-8490, dentaries; 8491 - 8493, maxillae; 8494, articular-surangular; 8495, premaxillae; 8496, frontal; 8497, 8500, 8501, vertebrae.		Estes R. 1983. Handbuch der Paläoherpetologie: Sauria terrestria, Amphisbaenia, part 10A. Munich: Gustav Fischer Verlag.
Leiocephalus partitus	Holotype: USNM 259203, dentary; Upper PleistoceneSlibreeent, Glianica Bat Cave, Reserv<l		Estes R. 1983. Handbuch der Paläoherpetologie: Sauria terrestria,

	Forestal Glianica (Cuayanilla), Puerto Rico. Referred specimens: KU, USNM, two dentaries, one topotypic, the other from Cueva d el Perro, Barahona (Morovis), Puerto Rico.	Amphisbaenia, part 10A. Munich: Gustav Fischer Verlag.
Leiocephalus personatus	Referred specimens: UF 10102, dentaries; 10103, maxillae; 10104, frontals; 10105, parietals. Uppermost Pleistocene-4000 years B.P., Cueva Cerro de San Francisco, San Rafael, Dominican Republic.	Estes R. 1983. Handbuch der Paläoherpetologie: Sauria terrestria, Amphisbaenia, part 10A. Munich: Gustav Fischer Verlag.
Leiocephaltts septentrionalis	Holotype: UNSM 56085, dentary; Upper Miocene (Barstovian), Valentine Formation, Knox County, Nebraska. Referred specimens: UNSM, numerous topotypic dentaries and maxillae.	Estes R. 1983. Handbuch der Paläoherpetologie: Sauria terrestria, Amphisbaenia, part 10A. Munich: Gustav Fischer Verlag.
Leiosaums bellii	Holotype: MACN?/(Col. Paleo. RUSCONI 1215), vertebral column with 16 articulated vertebrae and ribs. Middle Pleistocene (Ensenadense), Est. Anchorena, Prov. Buenos Aires, Argentina	Estes R. 1983. Handbuch der Paläoherpetologie: Sauria terrestria, Amphisbaenia, part 10A. Munich: Gustav Fischer Verlag.
Paradipsosaurus mexicanus	Holotype: USNM 20667, skull and mandibles, posterior and anterior ends damaged. Eocene or Oligocene, Red Conglomerate, Guanajuato, Mexico Where: Guanajuato, Mexico (21.0° N, 101.3° W: paleocoordinates 24.2° N, 90.4° W) When: lower Member (Guanjuato Red Conglomerate Formation), Bridgerian (50.3 - 46.2 Ma)	Estes R. 1983. Handbuch der Paläoherpetologie: Sauria terrestria, Amphisbaenia, part 10A. Munich: Gustav Fischer Verlag.
Phrynosoma orbiculare	Referred specimens: LACM, fragment with three temporal spines; Pleistocene, San Josecito Cavern, Nuevo Leon, Mexico.	Estes R. 1983. Handbuch der Paläoherpetologie: Sauria terrestria, Amphisbaenia, part 10A. Munich: Gustav Fischer Verlag.
Phrynosoma adinognathus	Holotype: KUMVP 25258, dentary; Lower Pleistocene, Borchers locality, Meade County, Kansas. Referred specimens: KUMVP 25259, dentary; 25260, dentary; both topotypic specimens.	Estes R. 1983. Handbuch der Paläoherpetologie: Sauria terrestria, Amphisbaenia, part 10A. Munich: Gustav Fischer Verlag.
Phrynosoma cornutum	Referred specimens Upper Pliocene: UMMP, many specimens, Rexroad Formation, Meade County, Kansas (TWENTE 1952; OELRICH 1954; ETHERIDGE 1958); KU 5099, 5115, delltaries (types of EHmecoicles hibbardi and E. mylocoelus), Rexroad Formation, Seward County, Kansas (TAYLOR 1941; ETHERIDGE 1958, 1960a). MU 9279, dentaries, maxillae, frontals, parietal; Ogalalla Formation, Scurry County, Texas (ROGERS 1976). Lower Pleistocene: UMMP, occipital horns, Keim	Estes R. 1983. Handbuch der Paläoherpetologie: Sauria terrestria, Amphisbaenia, part 10A. Munich: Gustav Fischer Verlag.

	Formation, Brown County, Nebraska; UMMP dentaries, Crooked Creek formation, Meade County, Kansas (Hol.MAN 1972a, 1979a). Upper Pleistocene: MU 8051, squamosal, Slaton Quarry, Lubbock County, Texas (Illinoianj HOLMAN 1969b, c); UMM]> 34126, squamosal, Cragin Quarry, Meade County, Kansas (Sangamonian; ETHERIDGE (958); UT 40450--1663, Cave Without-a-Name, Kendall County, Texas (Wisconsi nianj HOLMAN 1968); UTEP 4- 631, dentary, Dry Cave, Eddy County, New Mexico (HOLMAN 1970b); AMNH 6405, maxillae, dentary, and mandibular fragment, Conard Fissure, Newton County, Arkansas (GILMORE 1928; ETHERIDGE 1958). UNSM, dentary; Burnet Cavc, Eddy County, New Mexico (RICKART 1977). Holocene: LACM, parietals, frontal, scapula, maxilla; Shelter Cave, Dona Ana County, New Mexico (BRATTSTROM 1964); UTEP, UAL]>, many skull bones, Howells Ridge Cave, Grant County, New Mexico (VAN DEVENDER and WORTHINGTON 1977).	
Phrynosoma coronatum	Referred specimens: LACM, temporal spines. Upper Pleistocene, Rancho La Brea, Los Angeles County, California.	Estes R. 1983. Handbuch der Paläoherpetologie: Sauria terrestria, Amphisbaenia, part 10A. Munich: Gustav Fischer Verlag.
Phrynosoma douglassi	Referred specimens SDSM 8578, maxill a, dentary, vertebra; Upper Pleistocene (Kansan), Java, Walworth County, South Dakota (HOLIVIAN 1977a). UTE]>, maxillae, frontals, parietals, squamosals, occipital, 35 dcntaries, scapulocoracoids, humeri, pelves; Upper Pleistocene, Dry Cave, Eddy County, New Mexico (HOLMAN 1970b). UNSM, dentaries, frontals , sq uamosals; Upper PleistoceneHolocene, Burnet and Dark Canyon Caves, Eddy County, New Mexico (RICKART 1977). LACM frontals, maxillae, dentaries; Upper Pleistocene (Wisconsin ian) or Holocene, Smith Creek Cave, White Pine County, Nevada (MEAD, THOMPSON and VAN DEVENDER 1982). UTE]>, UALP, many skull bones; Holocene, Howells Ridge Cave, Grant COllIllY, New Mexico (VAN DEVENDER and WORTHINGTON 1977). MSU VP 258, parietal; Pratt Cave, Culberso County,	Estes R. 1983. Handbuch der Paläoherpetologie: Sauria terrestria, Amphisbaenia, part 10A. Munich: Gustav Fischer Verlag.

	Texas (GEHLBACH and HOLMAN 1974).	
Phrynosoma holmani	Holotype: UMMP V61389, d entary; Upper Pliocene, Belleville Formation, Republic County, Kansas. Referred specimen: UMMP V61390, dentary; topotypic specImen.	Estes R. 1983. Handbuch der Paläoherpetologie: Sauria terrestria, Amphisbaenia, part 10A. Munich: Gustav Fischer Verlag.
Phrynosoma josecitensis	Holotype: LACM, sk ull fragment with four temporal spines. Pleistocene, San Josecito Cavern, Nuevo Leon, Mexico.	Estes R. 1983. Handbuch der Paläoherpetologie: Sauria terrestria, Amphisbaenia, part 10A. Munich: Gustav Fischer Verlag.
Phrynosoma modestum	Referred specimens: UMMP 34146, 34145, dentaries; 33827, parietal; 34144, 34143, maxillae; 34140- 34142, squamosals. Upper Pleistocene (Sangamonian), Kingsdown Formation, Meade County, Kansas. UTEP, UALP, many skull bones; Holocene, Howells Ridge Cave, Grant County, New Mexico.	Estes R. 1983. Handbuch der Paläoherpetologie: Sauria terrestria, Amphisbaenia, part 10A. Munich: Gustav Fischer Verlag.
Phrynosoma platyrhinos	Referred specimens: LACM, frontal, occipital spine, temporal spines. Upper Pleistocene or Holocene, Gypsum Cave, C lark County, Nevada. LACM, parietal; Upper Pleistocene or Holocene, Smith Creek Cave, White Pine County, Nevada.	Estes R. 1983. Handbuch der Paläoherpetologie: Sauria terrestria, Amphisbaenia, part 10A. Munich: Gustav Fischer Verlag.
Sauromalus obesus	Referred specimens: UALP 7235:5612, 5767, vertebrae; Upper Pleistocene, Wolcott Peak, Pima County, Arizona. UALP 7449:7460, denrary; Upper Pleistocene, Fallen Arches, San Bernardino County, California. UALP 7312:6184-6185, 7204:6518, 7315:6194, 7446:7415, vertebrae; 7512:8083, dentary; NPSB B404, B406, B407, B429, B430, two skulls and three mandibles; Lower Pleistocene, Rampart Cave, Grand Canyon, Arizona. LACM 1979, vertebrae; Pleistocene, Schuiling Cave, San Bernardino County, California. LACM, dcntaries, parietals, vertebrae, skin, footbones, twO skulls, one with mandible; Subfossil (8000- 10,000 years B.P.) Gypsum Cave, Clark County, Nevada.	Estes R. 1983. Handbuch der Paläoherpetologie: Sauria terrestria, Amphisbaenia, part 10A. Munich: Gustav Fischer Verlag.
Sceloporus graciosus	Referred specimens; LACM, dentary. Pleistocene, Hawver Cave, El Dorado County, California . LACM, mummified skeleton; Upper Pleistocene-Holocene, Smith Cave, White Pine County, Nevada.	Estes R. 1983. Handbuch der Paläoherpetologie: Sauria terrestria, Amphisbaenia, part 10A. Munich: Gustav Fischer Verlag.
Sceloporus jarrovi	Referred specimens: LACM, vertebrae; Upper Pleistocene, Barranca cle Rio Grande, Texuixquiac, Zumpango, Mexico.	Estes R. 1983. Handbuch der Paläoherpetologie: Sauria terrestria, Amphisbaenia, part 10A. Munich: Gustav Fischer Verlag.
Sceloporus magister	Referred specimens: LACM dentaries, maxillae, quadrate, frontals, occipital, parietals; Upper Pleistocene, Rancho la Brea, Los Angeles County, California. LACM, frontal; Upper Pleistocene or	Estes R. 1983. Handbuch der Paläoherpetologie: Sauria terrestria, Amphisbaenia, part 10A. Munich: Gustav Fischer Verlag.

	Holocene, Smith Creek Cave, White Pine County, Nevada.		
Sceloporus occidentalis	Referred specimens: Upper Pleistocene: LACM, vertebrae, McKittrick Asphalt, Kern County, California (BRATTSTROM 1953b); LACM, 40 dentaries, maxillae, parietals, frontals, occipitals, scapulae, femur, Rancho La Brea, Los Angeles County, California (BRATTSTROM 1953b); LACM, dentaries, Carpinteria, Santa Barbara County, California (BRATTsTRoM 1955c); LACM, dentaries, mandible, maxillae, Mescal Cave, San Bernardino County, California (BRAHSTROM 1958a). LACM dentaries, maxillae, frontal, scale; Smith Creek Cave (may be Holocene), White Pine County, Nevada (MEAD, THOMPSON and VAN DEVENDER 1982).		Estes R. 1983. Handbuch der Paläoherpetologie: Sauria terrestria, Amphisbaenia, part 10A. Munich: Gustav Fischer Verlag.
Uquiasaurus heptanodonta	holotype PVL 6388 referred: PVL 6395, 6387, 6391, 6394, 6389, 6392, 6393.	San Roque (23°14'32.9"S, 65°21'55.5"W; 2,940 m elevation), Humahuaca, Jujuy Province, Argentina. Late Pliocene**,** middle unit of Uquia Formation.	Daza JD, Abdala V, Arias JS, García-López D, and Ortiz P. 2012. Cladistic analysis of Iguania and a fossil lizard from the Late Pliocene of northwestern Argentina. Journal of Herpetology 46:104-119.
Sauropithecoides charisticus	Holotype. PTRM 1841	Chadron Formation of the Medicine Pole Hills of southwestern North Dakota; late Eocene age	Smith, K. T. The Evolution of Mid-latitude Faunas during the Eocene: Late Eocene Lizards of the Medicine Pole Hills Reconsidered. Bull. Peabody Mus. Nat. Hist. 52, 3-105 (2011). Smith, K. T. A diverse new assemblage of Late Eocene squamates (Reptilia) from the Chadron Formation of North Dakota, USA. Palaeontol. Electron. 9, 1-44 (2006).
Queironius praelapsus	Holotype. PTRM 19499	Chadron Formation of the Medicine Pole Hills of southwestern North Dakota; late Eocene age	Smith, K. T. The Evolution of Mid-latitude Faunas during the Eocene: Late Eocene Lizards of the Medicine Pole Hills Reconsidered. Bull. Peabody Mus. Nat. Hist. 52, 3-105 (2011).
Cypressaurus sp.		Chadron Formation of the Medicine Pole Hills of southwestern North Dakota; late Eocene age	Smith, K. T. The Evolution of Mid-latitude Faunas during the Eocene: Late Eocene Lizards of the Medicine Pole Hills Reconsidered. Bull. Peabody Mus. Nat. Hist. 52, 3-105 (2011). Smith, K. T. A diverse new assemblage of Late Eocene squamates (Reptilia) from the Chadron Formation of North Dakota, USA. Palaeontol. Electron. 9, 1-44 (2006).
Oreithyia oaklandi	PTRM 5198	Chadron Formation of the Medicine Pole Hills of southwestern North Dakota;	Smith KT. 2011. The Evolution of Mid-latitude Faunas during the Eocene: Late Eocene Lizards of the Medicine Pole Hills

		late Eocene age	Reconsidered. Bulletin of the Peabody Museum of Natural History 52:3-105; Smith. 2011. Oreithyia, a replacement name for Orithyis Smith, 2011, nec Orithyia Fabricus, 1798. Bulletin of the Peabody Museum of Natural History 52(2):273. Bolet A. 2017. First early Eocene lizards from Spain and a study of the compositional changes between late Mesozoic and early Cenozoic Iberian lizard assemblages. Palaeontologia Electronica 20:1-22.
Tuberculacerta pearsoni	Holotype. PTRM 5296	Chadron Formation of the Medicine Pole Hills of southwestern North Dakota; late Eocene age	Smith, K. T. The Evolution of Mid-latitude Faunas during the Eocene: Late Eocene Lizards of the Medicine Pole Hills Reconsidered. Bull. Peabody Mus. Nat. Hist. 52, 3-105 (2011). Smith, K. T. A diverse new assemblage of Late Eocene squamates (Reptilia) from the Chadron Formation of North Dakota, USA. Palaeontol. Electron. 9, 1-44 (2006).
Swainiguanoides milleri	holotype AMNH 12082 referred: AMNH 5190, 5191, 7264, 15902, 15933, 12048, 12081	Fort Union Formation in Wyoming (Sullivan 1982); Paleocene.	Smith KT (2009) A new lizard assemblage from the earliest Eocene (zoneWa0) of the Bighorn Basin, Wyoming, USA: biogeography during the warmest interval of the cenozoic. J Syst Palaeontol 7(3):299–358. Sullivan RM (1982) Fossil Lizards from Swain Quarry "Fort UnionFormation," Middle Paleocene (Torrejonian), Carbon County, Wyoming. J Paleont 56(4):996–1010. Nydam RL. 2013. Squamates from the Jurassic and Cretaceous of North America. Palaeobiodiversity and Palaeoenvironments 93:535-565.

Appendix 5.4 – List of specimens of extant iguanians that were examined for the coding and scoring of the morphological characters.

Agama agama: AMNH 141129; UF 62562; http://www.digimorph.org/specimens/Agama_agama/ (FMNH 47531). *Amblyrhynchus cristatus*: AMNH 29937; AMNH 29938; AMNH 36230; AMNH 36231; AMNH 43228; AMNH 46270; AMNH 75942; AMNH 76197; AMNH 78979; AMNH 89841; AMNH 114491; AMNH 114492; AMNH 123309; AMNH 147810; UAMZ 384; UF 41424; UF 41558 (http://www.morphosource.org/Detail/MediaDetail/Show/media_id/20786); UF 49137; UF 49138; UF 54782; UF 57134; http://www.morphosource.org/Detail/MediaDetail/Show/media_id/9055 (MVZ 67721); http://www.morphosource.org/Detail/MediaDetail/Show/media_id/9056 (UCMP 137167). *Anolis carolinensis*: ROM 2476; UF 162758; http://digimorph.org/specimens/Anolis_carolinensis/ (FMNH 242298). *Basiliscus vittatus* : ROM 283; ROM 312; UF 11486; UF 11490; UF 11491. *Basiliscus basiliscus*: ROM 441; ROM 5539; ROM 5583; UF 140835; http://www.digimorph.org/specimens/Basiliscus_basiliscus/ (FMNH 165622). *Brachylophus fasciatus*: AMNH 29033; AMNH 29034; AMNH 121274; UF 37578; http://www.digimorph.org/specimens/Brachylophus_fasciatus/ (FMNH 210158). *Brookesia brygooi*: http://www.digimorph.org/specimens/Brookesia_brygooi/ (FMNH 260015). *Calotes emma*: http://www.digimorph.org/specimens/Calotes_emma/ (FMNH 252264). *Calotes versicolor*: UF 68490; UF 99258. *Chalarodon madagascariensis*: AMNH 12841; http://www.digimorph.org/specimens/Chalarodon_madagascariensis/ (YPM 12866). *Chamaeleo calyptratus*: http://www.digimorph.org/specimens/Chamaeleo_calyptratus/whole/ (TNHC 62768). *Chamaeleo chamaeleon*: UF 40629; UF 42415. *Conolophus pallidus*: AMNH 147847;

AMNH 147848; AMNH 147849. *Conolophus subcristatus*: AMNH 50797; AMNH 50798; AMNH 89845; AMNH 110168; AMNH 114493; AMNH 131308; ROM 112; UF 11583. *Corytophanes cristatus*: UF 57739; http://digimorph.org/specimens/Corytophanes_cristatus/ (FMNH 69227). *Crotaphytus collaris*: ROM 7711; http://www.digimorph.org/specimens/Crotaphytus_collaris/ (FMNH 48667). *Ctenosaura pectinata*: ROM 1046; ROM 6709; UF 48333; UF 55461; UF 56553; UF 56619; http://digimorph.org/specimens/Ctenosaura_pectinata/. *Ctenosaura similis*: AMNH 147860; AMNH 147861; UF 48750; UF 67496; UF 67525; UF 67707. *Cyclura carinata*: UF 30425; UF 67232. *Cyclura cornuta*: AMNH 93182; AMNH 147865; AMNH 147865: UF 52004; UF 57134; UF 99016; UF 99017; UF 99056. *Dipsosaurus dorsalis*: AMNH 73058; AMNH 75603; AMNH 141110; AMNH141115; ROM 875; ROM 4279; UF 42777; http://digimorph.org/specimens/Dipsosaurus_dorsalis/ (YPM 14376). *Draco volans*: UF 53599; UF 63233. *Enyalioides laticeps*: http://www.digimorph.org/specimens/Enyalioides_laticeps/ (FMNH 206132). *Furcifer oustaleti*: UF 166103; UF 166109. *Gambelia wislizenii*: AMNH 154776; AMNH 154788; AMNH 154789; http://www.digimorph.org/specimens/Gambelia_wislizenii/ (YPM 14380). *Gekko gecko*: TMP 1990.007.0021; TMP 1997.030.0327; TMP 1997.030.0333; http://digimorph.org/specimens/Gekko_gecko/ (FMNH 186818). *Holbrookia maculata*: http://www.morphosource.org/Detail/MediaDetail/Show/media_id/42812 (LSUMZ 84795); http://www.morphosource.org/Detail/MediaDetail/Show/media_id/42815 (LSUMZ 84795). *Iguana iguana*: AMNH 81871; AMNH 88423; AMNH 94167; AMNH 154811; ROM 294; ROM 346; ROM 373; ROM 401; ROM 426; ROM 428; ROM 441; 7716; UAMZ 951; UF 142724; UF 146560; UF 149744. *Leiocephalus personatus*: UF 99140; UF 99376. *Leiolepis*

belliana: UF 62046; http://digimorph.org/specimens/Leiolepis_belliana/ (USNM 205722). *Liolaemus bellii*: http://www.digimorph.org/specimens/Liolaemus_bellii/ (MVZ 125659). *Morunasaurus annularis*: http://www.digimorph.org/specimens/Morunasaurus_annularis/ (USNM 200767). *Oplurus cuvieri*: AMNH 47944. *Oplurus cyclurus*: AMNH 71462; AMNH 138120; http://www.digimorph.org/specimens/Oplurus_cyclurus/ (YPM 12861). *Petrosaurus mearnsi*: AMNH 141107; AMNH 154916; AMNH 154853; ROM 6760. *Physignathus cocincinus*: TMP 1990.007.0347; UF 71685; http://www.digimorph.org/specimens/Physignathus_cocincinus/ (YPM 14378). *Phrynosoma cornutum*: UF 41530; http://www.digimorph.org/specimens/Phrynosoma_cornutum/whole/; (TNHC 1930) *Phrynosoma modestum*: TMP1990.007.0161; TMP1997.030.0318; TMP1997.030.0321; TMP1997.030.0324. *Phymaturus palluma*: http://www.digimorph.org/specimens/Phymaturus_palluma/ (FMNH 209123). *Plica plica*: ROM 70; UF 56616; UF 67979. *Pogona vitticeps*: ROM 8514; ROM 22699; UAMZ 952; http://www.digimorph.org/specimens/Pogona_vitticeps/ (ROM 22699). *Polychrus marmoratus*: UF 56851; UF 57019; UF 60914; UF 61608; UF 71671. *Pristidactylus torquatus*: http://www.digimorph.org/specimens/Pristidactylus_torquatus/ (FMNH 206964). *Sauromalus obesus*: ROM R 335; ROM R 9335; UF 11691. *Sceloporus variabilis*: ROM 8788; UF 53687; http://www.digimorph.org/specimens/Sceloporus_variabilis/ (FMNH 122866). *Sphenodon punctatus*: UAMZ 405; http://digimorph.org/specimens/Sphenodon_punctatus/adult/ (YPM 9194). *Stenocercus guentheri*: UF 83601; UF 83603; http://www.digimorph.org/specimens/Stenocercus_guentheri/ (FMNH 27674). *Uma scoparia*: UF 49376; http://www.digimorph.org/specimens/Uma_scoparia/ (FMNH 1203). *Uranoscodon superciliosus*: UF 62540; http://www.digimorph.org/specimens/Uranoscodon_superciliosus/

(YPM 12871). *Uromastyx hardwickii*: http://www.digimorph.org/specimens/Uromastyx_hardwickii/ (UCL.5); *Uromastyx aegyptia*: UF 90273; http://www.digimorph.org/specimens/Uromastyx_aegyptius/ (FMNH 78661). *Urostrophus vautieri*: http://www.digimorph.org/specimens/Urostrophus_vautieri/ (FMNH 83576). *Uta stansburiana*: UF 42344; UF 87986. http://www.digimorph.org/specimens/Uta_stansburiana/ (FMNH 213914). *Varanus salvator*: TMP 1990.007.0036; TMP 1990.007.0037; TMP 1990.007.0270; http://digimorph.org/specimens/Varanus_salvator/ (FMNH 35144).

Appendix 5.5 – Molecular data: access, alignment, and partitions.

Table A5.2. GenBank accession numbers for the 15 nuclear loci.

Species	AKAP9	BDNF	BMP2	CAND1	CARD4
Sphenodon punctatus	JF805808.1	GU457846.1	GU457880.1	GU432592.1	JN702010.1
Gekko gecko	JF805798.1	EU402614.1	EU402669.1	GU432614.1	JN702049.1
Varanus salvator	JN654786.1	EU402618.1	EU402673.1	GU432610.1	JN702045.1
Acanthosaura lepidogaster	JF805815.1	JF806003.1	JF806037.1	JF818533.1	JN702101.1
Agama agama	JF805816.1	DQ340698.1	EU402670.1	GU432593.1	JN702015.1
Amblyrhynchus cristatus		KR350716.1			
Anolis carolinensis	JF805835.1	EU402616.1	EU402671.1	GU432598.1	JN702122.1
Basiliscus vittatus					
Brachylophus fasciatus	JF805837.1	AY987980.1	JF806054.1	JF818555.1	JN702091.1
Bradypodion occidentale	KC507556.1	KC507645.1			
Brookesia brygooi	JF805817.1	JF806004.1	JF806038.1	JF818548.1	JN702073.1
Brookesia decaryi					
Callisaurus draconoides	KP820597.1	KP820847.1	KP820736.1	KP820774.1	KP820719.1
Calotes emma	JF805818.1		JF806039.1	JF818534.1	JN702078.1

Calotes versicolor		DQ340705.1			
Chalarodon madagascariensis	JF805838.1	AY987972.1	JF806055.1	JF818563.1	JN702130.1
Chamaeleo calyptratus	JF805819.1	GU457847.1	GU457881.1	GU432594.1	JN702072.1
Chamaeleo chamaeleon					
Conolophus marthae					
Conolophus pallidus					
Conolophus subcristatus		KR350715.1			
Corytophanes cristatus	JF805839.1	JF806020.1		JF818551.1	JN702099.1
Crotaphytus collaris	JF805840.1	JF806021.1	JF806056.1	JF818552.1	JN702103.1
Ctenosaura pectinata					
Ctenosaura similis		KR350714.1			
Cyclura carinata					
Cyclura cornuta		KR350712.1			
Dipsosaurus dorsalis	JF805841.1	GQ853275.1	JF806057.1	JF818556.1	JN702104.1
Draco blanfordii	JF805824.1	JF806010.1	JF806043.1	JF818538.1	JN702063.1
Draco volans					
Enyalioides laticeps	JF805842.1	GU457848.1	GU457882.1	GU432595.1	JN702044.1
Furcifer oustaleti					
Gambelia wislizenii	JF805843.1	KP820845.1	KP820735.1	JF818553.1	JN702009.1
Holbrookia maculata	KP820592.1	KP820844.1	KP820733.1	KP820770.1	
Hydrosaurus amboinensis					
Iguana iguana		KR350713.1			
Japalura (Diploderma) flaviceps		MK001544.1			
Leiocephalus personatus					
Leiolepis belliana	JF805827.1	AY987965.1	JF806046.1	JF818549.1	JN702111.1
Liolaemus bellii	JF805846.1	HQ876220.1	JF806061.1	JF818561.1	JN702065.1
Microlophus grayii					
Moloch horridus	JF805828.1	DQ340734.1	JF806047.1	JF818541.1	JN702127.1

Morunasaurus annularis	JF805847.1	HQ876218.1	JF806062.1	JF818554.1	JN702155.1
Oplurus cuvieri		AY987971.1			
Oplurus cyclurus	JF805848.1		GU457884.1	GU432597.1	JN702120.1
Petrosaurus mearnsi	JF805849.1	JN648396.1	JF806063.1	JF818564.1	JN702154.1
Phrynocephalus mystaceus	JF805829.1	DQ340735.1	JF806048.1	JF818542.1	
Phrynosoma modestum	KR360025.1	DQ385325.1	KR360258.1	KR360318.1	KR360227.1
Phymaturus palluma	JF805851.1	JF806024.1	JF806065.1	JF818562.1	JN702043.1
Physignathus cocincinus	JF805830.1	DQ340736.1	JF806049.1	JF818543.1	JN702109.1
Plica plica	JF805857.1	JF806028.1	JF806071.1	JF818572.1	JN702097.1
Pogona vitticeps	JF805832.1	DQ340739.1	JF806051.1	JF818545.1	JN702087.1
Polychrus marmoratus	JF805852.1	AY987966.1	JF806066.1	JF818569.1	JN702129.1
Pristidactylus torquatus	JF805853.1	JF806025.1	JF806067.1	JF818559.1	JN702117.1
Rhampholeon spectrum	KC507575.1	JQ073091.1			
Rieppeleon kerstenii					
Sauromalus ater	JF805854.1	JF806026.1	JF806068.1	JF818557.1	JN702012.1
Sauromalus obesus					
Sceloporus variabilis	JF805855.1	GQ464464.1	JF806069.1	JF818566.1	JN702157.1
Stenocercus guentheri	JF805856.1	HQ876224.1	JF806070.1	JF818571.1	JN702141.1
Trioceros melleri					
Tropidurus hispidus		AY987967.1			
Uma scoparia	JF805858.1	JF806029.1	JF806072.1	JF818567.1	JN702042.1
Uranoscodon superciliosus	JF805859.1	JF806030.1	JF806073.1	JF818573.1	JN702150.1
Uromastyx aegyptia					
Uromastyx (Saara) hardwickii	JF805834.1		GU457883.1	GU432596.1	JN702085.1
Urostrophus vautieri	JF805860.1	HQ876219.1	JF806074.1	JF818560.1	JN702090.1
Uta stansburiana	JF805861.1	GQ464466.1	JF806075.1	KP820771.1	JN702061.1
Species	**C-mos**	**CXCR4**	**ENC1**	**HLCS**	**NTF3 (= NT3)**
Sphenodon punctatus	AF039483.1	JN702443.1	GU432510.1	JN702715.1	GU456002.1

Gekko gecko	EU366455.1	JN702441.1	GU432530.1	JN702635.1	EU390898.1
Varanus salvator	AF435017.1	JN702430.1	GU432526.1	JN702669.1	EU390902.1
Acanthosaura lepidogaster		JN702311.1		JN702685.1	JF804531.1
Agama agama	AF137530.1	JN702406.1	GU432511.1	JN702737.1	EU390899.1
Amblyrhynchus cristatus	KX610480.1				KX610521.1
Anolis carolinensis		JN702390.1	GU432515.1	JN702732.1	EU390900.1
Basiliscus vittatus					
Brachylophus fasciatus	AY987993.1	JN702323.1	JF818189.1	JN702663.1	JF804533.1
Bradypodion occidentale	FJ984260.1				
Brookesia brygooi	FJ984305.1		JF818182.1	JN702646.1	JF804534.1
Brookesia decaryi	FJ984307.1				
Callisaurus draconoides	AF315401.1	KP820522.1		KP820572.1	KP820629.1
Calotes emma		JN702379.1	JF818168.1	JN702666.1	JF804535.1
Calotes versicolor	AF137525.1				JX839246.1
Chalarodon madagascariensis	AY987987.1	JN702360.1	JF818197.1	JN702653.1	JF804536.1
Chamaeleo calyptratus		JN702417.1	GU432512.1	JN702693.1	GU456003.1
Chamaeleo chamaeleon					
Conolophus marthae					
Conolophus pallidus	HM352531.1				HM352521.1
Conolophus subcristatus	HM352532.1				HM352522.1
Corytophanes cristatus	AF315390.1	JN702338.1	JF818185.1	JN702657.1	JF804541.1
Crotaphytus collaris	AY987985.1	JN702405.1	JF818186.1	JN702656.1	JF804542.1
Ctenosaura pectinata					KX610536.1
Ctenosaura similis	GU332022.1				KX610539.1
Cyclura carinata	HM352534.1				HM352524.1
Cyclura cornuta					
Dipsosaurus dorsalis	EU116680.1	JN702334.1	JF818190.1	JN702696.1	KX578910.1

Draco blanfordii		JN702374.1	JF818172.1	JN702610.1	JF804546.1
Draco volans					
Enyalioides laticeps		JN702377.1	GU432513.1	JN702664.1	GU456004.1
Furcifer oustaleti	FJ984271.1				
Gambelia wislizenii	EU116682.1	JN702414.1	JF818187.1	JN702733.1	KP820626.1
Holbrookia maculata		KP820520.1		KP820567.1	KP820625.1
Hydrosaurus amboinensis					
Iguana iguana	AF148708.1				HM352530.1
Japalura (Diploderma) flaviceps					
Leiocephalus personatus					
Leiolepis belliana	FJ984253.1	JN702402.1	JF818183.1	JN702638.1	JF804552.1
Liolaemus bellii		JN702328.1	JF818195.1	JN702690.1	JF804554.1
Microlophus grayii	EF615759.1				
Moloch horridus	DQ340697.1	JN702455.1	JF818175.1	JN702708.1	JF804555.1
Morunasaurus annularis		JN702363.1	JF818188.1	JN702655.1	JF804556.1
Oplurus cuvieri	EU099664.1				
Oplurus cyclurus	EU099671.1	JN702378.1	GU432514.1	JN702614.1	GU456006.1
Petrosaurus mearnsi		JN702387.1	JF818198.1	JN702747.1	JF804557.1
Phrynocephalus mystaceus	AF137527.1	JN702404.1	JF818176.1	JN702702.1	JF804558.1
Phrynosoma modestum		KR359901.1		KR359982.1	KR360083.1
Phymaturus palluma	JX969520.1	JN702352.1	JF818196.1	JN702745.1	JF804560.1
Physignathus cocincinus	DQ340688.1	JN702421.1	JF818177.1	JN702662.1	JF804561.1
Plica plica	EF615737.1	JN702445.1	JF818206.1	JN702726.1	KU245152.1
Pogona vitticeps	DQ340691.1	JN702388.1	JF818179.1	XM_020789322.1	JF804563.1
Polychrus marmoratus	AY987983.1	JN702359.1	JF818203.1	JN702697.1	JF804564.1
Pristidactylus torquatus	KT342956.1	JN702459.1	JF818193.1	JN702728.1	JF804565.1
Rhampholeon spectrum	FJ984254.1				
Rieppeleon kerstenii					

Sauromalus ater	HM352537.1	JN702333.1	JF818191.1	JN702722.1	JF804568.1
Sauromalus obesus	AF315400.1				
Sceloporus variabilis		JN702330.1	JF818200.1	JN702707.1	KU767979.1
Stenocercus guentheri		JN702380.1	JF818205.1	JN702649.1	JF804570.1
Trioceros melleri	JN090149.1				
Tropidurus hispidus	AY987984.1				KU245142.1
Uma scoparia		JN702371.1	JF818201.1	JN702748.1	JF804574.1
Uranoscodon superciliosus		JN702342.1	JF818207.1	JN702612.1	KU245150.1
Uromastyx aegyptia	AF137531.1				MF960421.1
Uromastyx (Saara) hardwickii				JN702629.1	MF960472.1
Urostrophus vautieri	KT342957.1	JN702451.1	JF818194.1	JN702647.1	JF804576.1
Uta stansburiana	AF315389.1	JN702401.1	JF818202.1	KP820568.1	JF804577.1
Species	**R35 (= GPR149)**	**SLC8A1**	**TRAF6**	**VCPIP1**	**ZEB2**
Sphenodon punctatus	HQ876320.1	GU456070.1	GU456147.1	GU456182.1	GU456224.1
Gekko gecko	HQ876378.1	GU456093.1	EU391048.1	GU456204.1	EU390847.1
Varanus salvator	JN568500.1	GU456088.1	EU391052.1	GU456199.1	EU390851.1
Acanthosaura lepidogaster	JF804578.1	JF804160.1	JF804334.1	JN702936.1	JF804612.1
Agama agama	HQ876321.1	GU456071.1	EU391049.1	GU456183.1	EU390848.1
Amblyrhynchus cristatus	KR350703.1	GU456088.1			
Anolis carolinensis	HQ876334.1	GU456076.1	EU391050.1	GU456187.1	EU390849.1
Basiliscus vittatus					
Brachylophus fasciatus	JF804579.1	JF804163.1	JF804336.1		JF804614.1
Bradypodion occidentale					
Brookesia brygooi	JF804580.1	JF804164.1	JF804337.1	JN702935.1	JF804615.1
Brookesia decaryi					
Callisaurus draconoides	KP820532.1	KP820829.1	KP820645.1	KP820562.1	KP820754.1
Calotes emma	JF804581.1	JF804165.1	JF804338.1	JN702891.1	JF804616.1

Calotes versicolor	MK001440.1				
Chalarodon madagascariensis	JF804582.1	JF804166.1	JF804339.1	JN702907.1	JF804617.1
Chamaeleo calyptratus	HQ876323.1	GU456072.1	GU456148.1	GU456184.1	GU456225.1
Chamaeleo chamaeleon					
Conolophus marthae					
Conolophus pallidus					
Conolophus subcristatus	KR350701.1				
Corytophanes cristatus	JF804585.1	JF804170.1	JF804344.1	JN702939.1	JF804622.1
Crotaphytus collaris	JF804586.1	JF804171.1	JF804345.1	JN702940.1	JF804623.1
Ctenosaura pectinata					
Ctenosaura similis	KR350700.1				
Cyclura carinata					
Cyclura cornuta	KR350698.1				
Dipsosaurus dorsalis	HQ876329.1	JF804174.1	JF804347.1	JN702903.1	JF804625.1
Draco blanfordii	JF804589.1	JF804175.1	JF804348.1	JN702912.1	JF804626.1
Draco volans					
Enyalioides laticeps	JF804590.1	GU456073.1	GU456149.1	GU456185.1	GU456226.1
Furcifer oustaleti					
Gambelia wislizenii	HQ876327.1	JF804177.1	JF804350.1	JN702913.1	JF804628.1
Holbrookia maculata	KP820528.1		KP820641.1	KP820558.1	KP820749.1
Hydrosaurus amboinensis					
Iguana iguana	KR350699.1				
Japalura (Diploderma) flaviceps	MK001472.1				
Leiocephalus personatus					
Leiolepis belliana	HQ876324.1	JF804181.1	JF804354.1	JN568538.1	JF804632.1
Liolaemus bellii	HQ876331.1	JF804184.1	JF804356.1	JN702934.1	JF804634.1
Microlophus grayii					
Moloch horridus	JF804595.1		JF804357.1	JN702955.1	JF804635.1

Morunasaurus annularis	HQ876328.1		JF804358.1	JN702931.1	JF804636.1
Oplurus cuvieri					
Oplurus cyclurus	HQ876332.1	GU456075.1	GU456151.1	GU456186.1	GU456228.1
Petrosaurus mearnsi	HQ876333.1	JF804187.1	JF804359.1	JN702922.1	JF804637.1
Phrynocephalus mystaceus	JF804596.1	JF804188.1	JF804360.1	JN702924.1	JF804638.1
Phrynosoma modestum	KJ124012.1	KR360430.1	KR360111.1		KR360287.1
Phymaturus palluma	JF804598.1	JF804190.1	JF804362.1	JN702899.1	JF804640.1
Physignathus cocincinus	HQ876322.1	JF804191.1	JF804363.1	JN702938.1	JF804641.1
Plica plica	JF804607.1	JF804204.1	JF804376.1	JN702926.1	JF804653.1
Pogona vitticeps	JF804600.1	JF804193.1	JF804365.1	JN702947.1	JF804643.1
Polychrus marmoratus	HQ876335.1	JF804194.1	JF804366.1	JN702906.1	JF804644.1
Pristidactylus torquatus	JF804601.1	JF804195.1	JF804367.1	JN702950.1	JF804645.1
Rhampholeon spectrum					
Rieppeleon kerstenii					
Sauromalus ater	JF804603.1	JF804198.1	JF804370.1	JN702909.1	JF804648.1
Sauromalus obesus					
Sceloporus variabilis	JF804604.1	JF804199.1	JF804371.1	JN702923.1	JF804649.1
Stenocercus guentheri	HQ876337.1	JF804200.1	JF804372.1	JN702951.1	JF804650.1
Trioceros melleri					
Tropidurus hispidus					
Uma scoparia	JF804608.1	JF804205.1	JF804377.1	JN702920.1	JF804654.1
Uranoscodon superciliosus	JF804609.1	JF804206.1	JF804378.1	JN702945.1	JF804655.1
Uromastyx aegyptia					
Uromastyx (Saara) hardwickii	HQ876325.1	GU456074.1	GU456150.1		GU456227.1
Urostrophus vautieri	HQ876330.1	JF804207.1	JF804379.1	JN702921.1	JF804656.1
Uta stansburiana	JF804610.1	JF804208.1	JF804380.1	JN702946.1	JF804657.1

Table A5.3. GenBank accession numbers for the 5 mitochondrial loci.

Species	12S	16S	CO1 (= COX1, COI)	Cytb	ND2
Sphenodon punctatus	AF534390.1	AF534390.1	NC_004815.1	NC_004815.1	NC_004815.1
Gekko gecko	NC_007627.1	NC_007627.1	NC_007627.1	NC_007627.1	NC_007627.1
Varanus salvator	NC_010974.1	NC_010974.1	NC_010974.1	NC_010974.1	NC_010974.1
Acanthosaura lepidogaster	KR092427.1	KR092427.1	KR092427.1	KR092427.1	KR092427.1
Agama agama		JF520680.1	KF604749.1		AF128504.1
Amblyrhynchus cristatus	NC_028031.1	NC_028031.1	NC_028031.1	NC_028031.1	NC_028031.1
Anolis carolinensis	NC_010972.2	NC_010972.2	EU747728.2	NC_010972.2	NC_010972.2
Basiliscus vittatus	NC_012829.1	NC_012829.1	NC_012829.1	NC_012829.1	NC_012829.1
Brachylophus fasciatus				KX610572.1	AF528721.1
Bradypodion occidentale		HQ130519.1			AF448728.1
Brookesia brygooi		JN674044.1	JQ909275.1		AF448774.1
Brookesia decaryi	NC_014174.1	NC_014174.1	NC_014174.1	NC_014174.1	
Callisaurus draconoides	AF194257.1	L41441.1	KP899449.1	DQ001780.1	AY297492.1
Calotes emma			MG935448.1	AB263942.1	
Calotes versicolor	NC_009683.1	NC_009683.1	NC_009683.1	NC_009683.1	NC_009683.1
Chalarodon madagascariensis	NC_012836.1	NC_012836.1	NC_012836.1	NC_012836.1	NC_012836.1
Chamaeleo calyptratus			NC_012420.1	NC_012420.1	
Chamaeleo chamaeleon	NC_012427.1	NC_012427.1	NC_012427.1	NC_012427.1	NC_012427.1
Conolophus marthae	KR350838.1	KR350861.1	KR350813.1	FJ535989.1	KR350767.1
Conolophus pallidus	KR350821.1		KR350796.1	KX610586.1	KR350750.1
Conolophus subcristatus	NC_028030.1	NC_028030.1	NC_028030.1	NC_028030.1	NC_028030.1
Corytophanes cristatus			MH140109.1		AF528717.1
Crotaphytus collaris	L40439.1	L41443.1	KU985978.1	EU037439.1	EU038488.1
Ctenosaura pectinata				KX610597.1	
Ctenosaura similis				KU664598.1	
Cyclura carinata				KX610601.1	

Cyclura cornuta					
Dipsosaurus dorsalis		KC621331.1	KU985572.1	KX610605.1	AF049857.1
Draco blanfordii	AB023733.1	MG935759.1	MG935463.1		AF128477.1
Draco volans	AB023730.1	AB023770.1	KU986311.1		AF288267.1
Enyalioides laticeps	KY982512.1	KY982408.1			AF528719.1
Furcifer oustaleti	NC_008777.1	NC_008777.1	JQ909374.1	NC_008777.1	NC_008777.1
Gambelia wislizenii	NC_012831.1	NC_012831.1	KU985618.1	NC_012831.1	NC_012831.1
Holbrookia maculata			KU985569.1	EU543769.1	
Hydrosaurus amboinensis	NC_014178.1	NC_014178.1	NC_014178.1	NC_014178.1	NC_014178.1
Iguana iguana	NC_002793.1	NC_002793.1	NC_002793.1	NC_002793.1	NC_002793.1
Japalura (Diploderma) flaviceps	NC_039541.1	NC_039541.1	NC_039541.1	NC_039541.1	NC_039541.1
Leiocephalus personatus	NC_012834.1	NC_012834.1	NC_012834.1	NC_012834.1	NC_012834.1
Leiolepis belliana	AB537554.1	AB537554.1	AB537554.1	AB537554.1	AB537554.1
Liolaemus bellii	AY662069.1			MH178576.1	AF099223.1
Microlophus grayii	EF615617.1	FJ458502.1		FJ458894.1	AY625170.1
Moloch horridus					AF128467.1
Morunasaurus annularis					AF528720.1
Oplurus cuvieri	U39587.1	AF215260.1	JQ909483.1	KY942063.1	U82685.1
Oplurus cyclurus			JQ909484.1	KY942064.1	
Petrosaurus mearnsi	L40444.1	L41450.1	KU985580.1	GQ272777.1	GQ502768.1
Phrynocephalus mystaceus	NC_021131.1	NC_021131.1	MG257706.1	NC_021131.1	NC_021131.1
Phrynosoma modestum	DQ385397.1	L41455.1	KU986259.1	AY141091.1	DQ385350.1
Phymaturus palluma	KT203839.1			KT203834.1	AF099216.1
Physignathus cocincinus	KM272197.1	KM272197.1	KM272197.1	AB263945.1	U82690.1
Plica plica	AB218961.1	AB218961.1	AB218961.1	AB218961.1	AB218961.1
Pogona vitticeps	NC_006922.1	NC_006922.1	NC_006922.1	NC_006922.1	NC_006922.1
Polychrus marmoratus	NC_012839.1	NC_012839.1	NC_012839.1	NC_012839.1	NC_012839.1
Pristidactylus torquatus	KT342933.1	L41456.1		KT342906.1	
Rhampholeon spectrum	AM055682.1	AJ609599.1			

Rieppeleon kerstenii	AB474918.1	AB474918.1	AB474918.1	AB474918.1	
Sauromalus ater			KU985584.1	KX610612.1	
Sauromalus obesus				AF020223.1	U82687.1
Sceloporus variabilis	GQ464573.1	L41479.1	KU985786.1		AY297507.1
Stenocercus guentheri		L41481.1	JQ687071.1		JQ687071.1
Trioceros melleri	NC_014176.1	NC_014176.1	NC_014176.1	NC_014176.1	NC_014176.1
Tropidurus hispidus	KU245279.1	KU245305.1	KM588056.1	KU245065.1	AY625153.1
Uma scoparia	AF194260.1		MH274758.1	EU543750.1	EU543782.1
Uranoscodon superciliosus	KU245288.1	KU245315.1	KU245105.1	KU245082.1	AF528749.1
Uromastyx aegyptia	FJ639656.1	FJ639620.1		AB116942.1	AB113805.1
Uromastyx (Saara) hardwickii				AB474757.1	
Urostrophus vautieri				KT342907.1	AF528734.1
Uta stansburiana	NC_027261.1	NC_027261.1	NC_027261.1	NC_027261.1	NC_027261.1

Table A5.4. Information on aligned gene sequences used in the phylogenetic analyses. Data about the genes where retrieved from the GenBank online database (Coordinators 2016) (https://www.ncbi.nlm.nih.gov/genbank/).

Gene code	Full gene name	Aligned sequence length
AKAP9	A-kinase anchoring protein 9	1463
BDNF	Brain derived neurotrophic factor	669
BMP2	Bone morphogenetic protein 2	633
CAND1	Cullin associated and neddylation dissociated 1	759
CARD4	Caspase recruitment domain family, member 4	912
C-mos	Moloney sarcoma oncogene	729
CXCR4	C-X-C motif chemokine receptor 4	669
ENC1	Ectodermal-neural cortex 1	879

HLCS	Holocarboxylase synthetase	585
NTF3	Neurotrophin 3	588
R35 (= GPR149)	G protein-coupled receptor 149	708
SLC8A1	Solute carrier family 8, member A1	996
TRAF6	TNF (Tumor necrosis factor) receptor associated factor 6	627
VCPIP1	Valosin containing protein interacting protein 1	789
ZEB2	Zinc finger E-box binding homeobox 2	879
12S	Segment 12S(Svedberg), ribosomal RNA	537
16S	Segment 16S(Svedberg), ribosomal RNA	906
CO1 (= COX1, COI)	Mitochondrially encoded cytochrome c oxidase I	1521
Cytb	Mitochondrially encoded cytochrome b	1053
ND2	Mitochondrially encoded NADH (nicotinamide adenine dinucleotide, reduced form) dehydrogenase 2	966

Table A5.5. Best partitioning scheme and best-fit models for the aligned gene sequences generated with PartitionFinder 2.1.1 (Lanfear et al. 2012; Lanfear et al. 2016).

Subset	**Partition**	**Length**	**Model of evolution**
1	12S	537	GTR+I+G
2	16S	906	GTR+G
3	CO1	1521	GTR+I+G
4	Cytb	1053	GTR+I+G
5	ND2	966	GTR+I+G
6	AKAP9	1463	GTR+I+G
7	BDNF	669	GTR+I+G
8	CXCR4, BMP2	1302	SYM+I+G
9	ZEB2, CAND1	1638	GTR+I+G

10	CARD4	912	HKY+I+G
11	TRAF6, C-mos	1356	GTR+I+G
12	ENC1	879	GTR+G
13	HLCS	585	GTR+G
14	NTF3	588	GTR+I+G
15	R35	708	GTR+I+G
16	SLC8A1	996	SYM+I+G
17	VCPIP1	789	SYM+I+G

Appendix 5.6 – Supplementary figures.

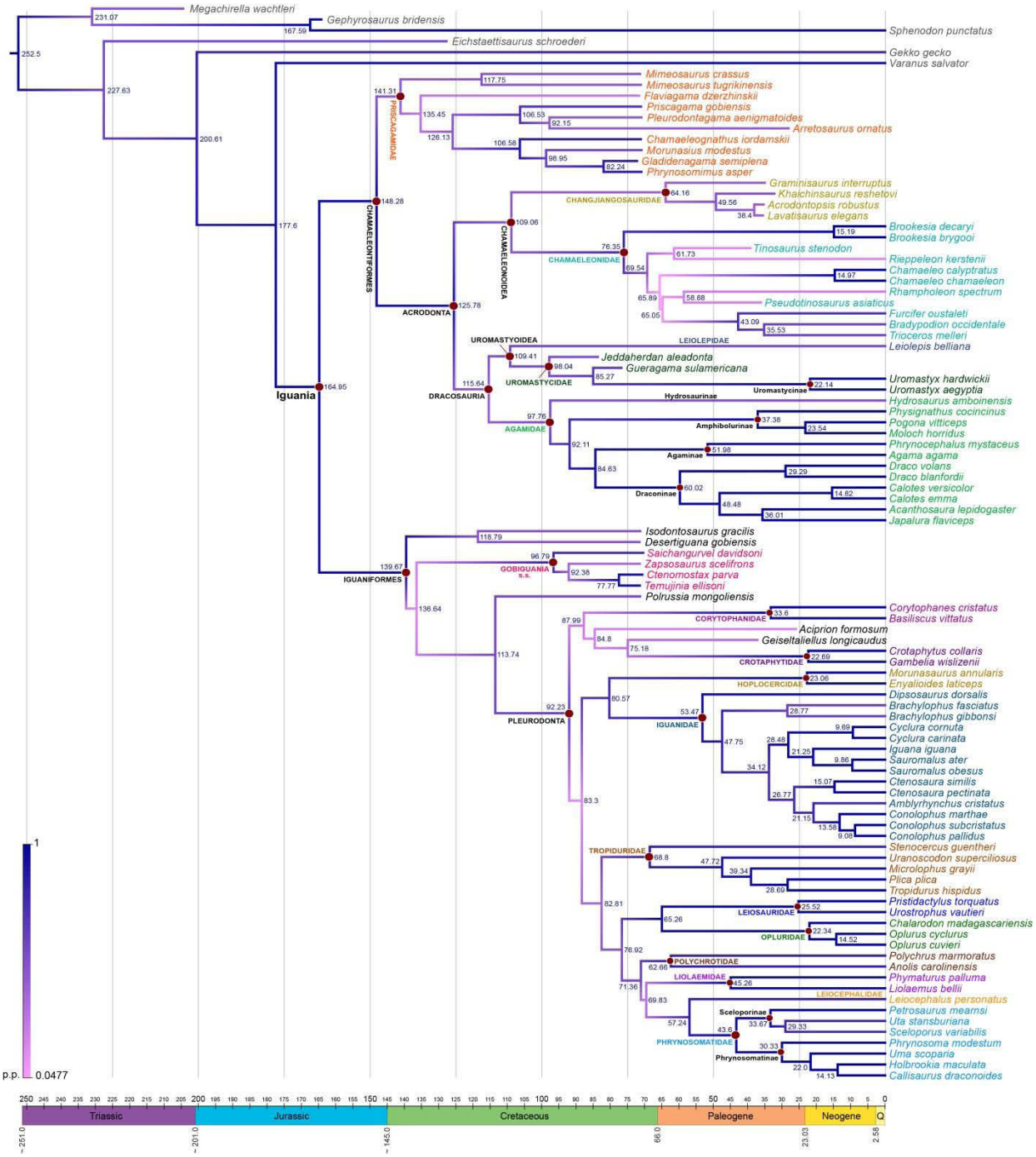

Figure A5.1. Time-calibrated maximum-clade credibility topology resulting from the Bayesian analysis of combined molecular and morphological data with posterior probability gradient of values illustrated on branches.

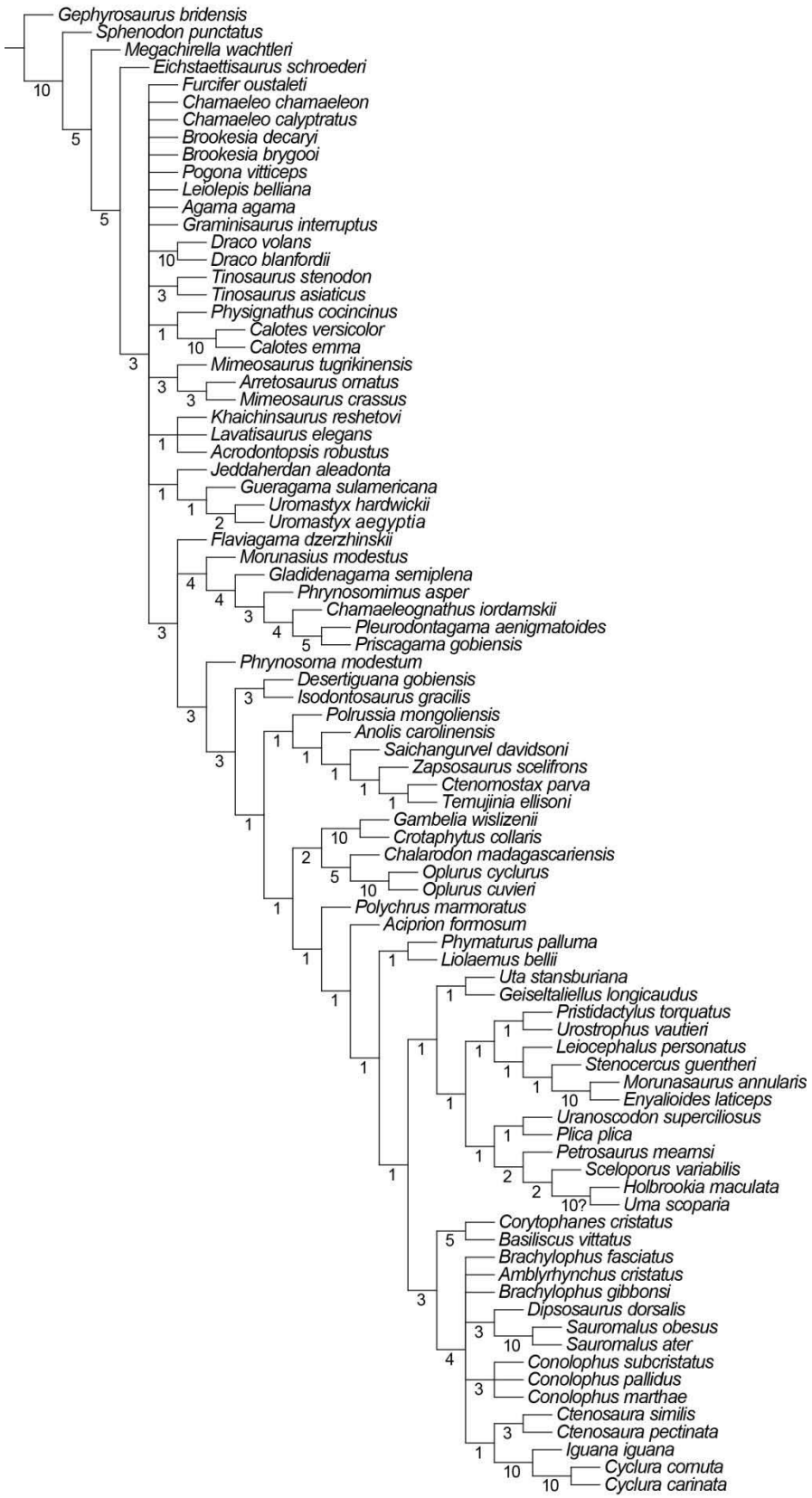

Figure A5.2. Strict consensus tree resulting from the EWMP analysis of morphological data.

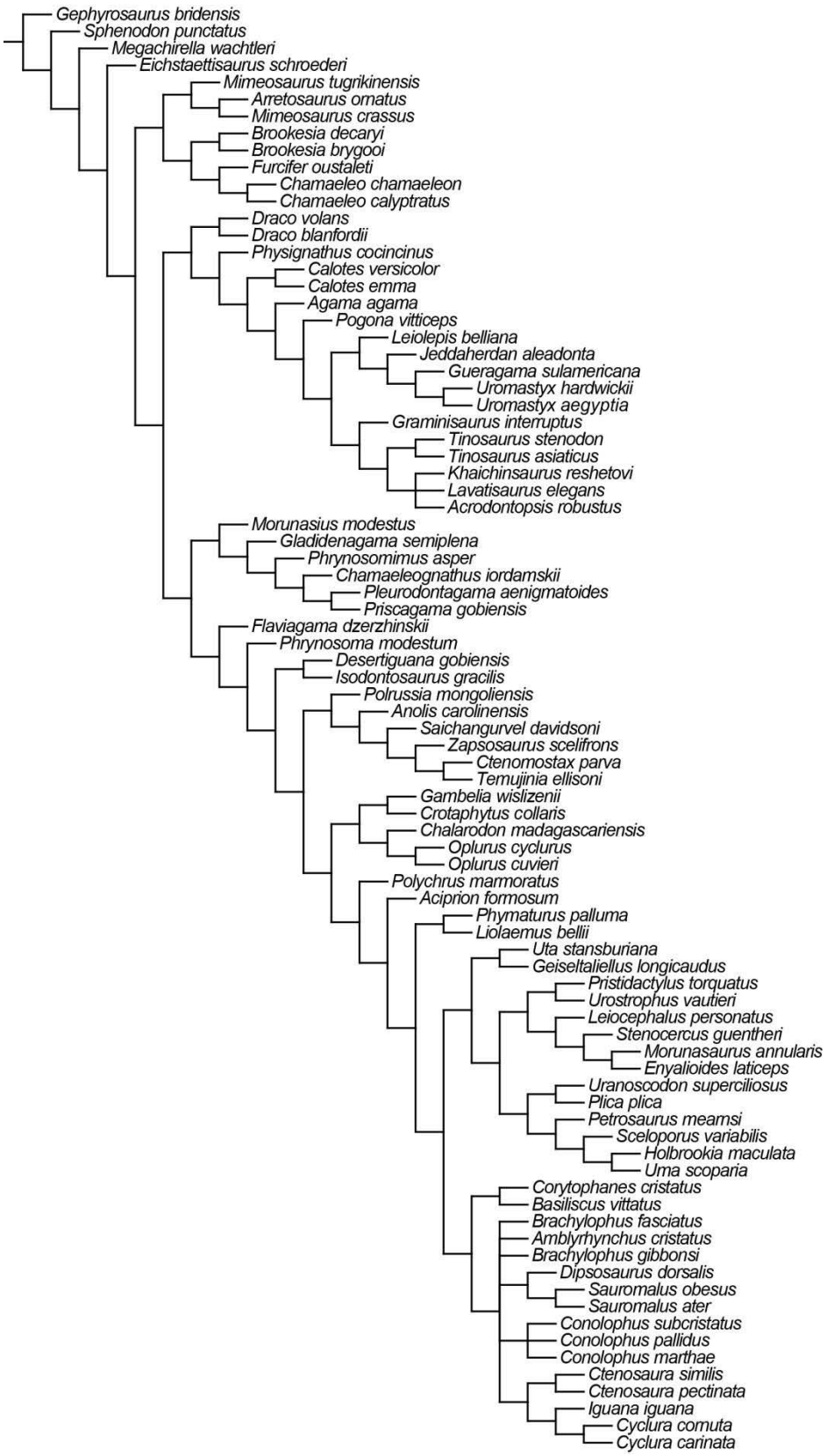

Figure A5.3. Strict consensus tree resulting from the IWMP analysis of morphological data.

CHAPTER 6

General Conclusions

In my dissertation, I analysed the modern marine iguana *Amblyrhynchus cristatu*s Bell, 1825, to provide a detailed description of its anatomy and revised the morphological characters that are used to assess the phylogenetic relationships of all iguanians. I used *Amblyrhynchus* as a source of novel morphological characters and as a model for comparison of functional adaptations between living and fossil marine lizards.

Chapter 1 includes a general introduction to the taxonomy and overview of the fossil record of Iguania, with a more detailed review of the clade including the marine iguana, the family Iguanidae. In Chapter 2, I presented a detailed description of the cranial anatomy of *Amblyrhynchus*. In my study, I examined several specimens of marine iguana, including skeletal, wet, and ct-scanned material, and individuals at different ontogenetic stages. I also analyzed specimens of all other modern iguanid genera (*Conolophus*, *Iguana*, *Ctenosaura*, *Cyclura*, *Dipsosaurus*, *Brachylophus*, *Sauromalus*) in order to make comparisons between *Amblyrhynchus* and its closest relatives. I was able to identify several autapomorphic features that distinguish the marine iguana from all other iguanids. These unique morphologies are mostly associated with the modified configuration of the snout (nasal chamber), increased muscle attachments in the temporal-postorbital region of the skull, and dentition. Some of the new cranial features described for *Amblyrhynchus* also represent a source of novel morphological characters that I used in my phylogenetic analyses to assess the relationships of all iguanians (Chapter 5). As the

marine iguana is the only modern limb-bearing squamate adapted to a partially marine lifestyle, comparisons with fossil marine lizards proved particularly insightful to discuss and identify some functional adaptations.

On the other hand, the anatomy of the marine iguana provides an excellent model to interpret fossil lizards showing a less derived aquatic body plan. This is the case for instance for some basal mosasauroids and their close relatives, the dolichosaurids. In Chapter 3 I describe a new dolichosaur (Squamata, Pythonomorpha) from Late Cretaceous deposits of the Apulian Platform, Southern Italy. *Primitivus manduriensis* gen. et sp. nov. fills an important paleogeographic gap in the range of distribution of dolichosaurs in the Mediterranean Tethys, and extends the stratigraphic range of these marine lizards to the upper Campanian–lower Maastrichtian. The new specimen shows exceptional preservation of the soft tissues (muscles and scales) and possess a combination of aquatic and terrestrial features, more similar to the modern marine iguana than to the fully aquatic and closely related mosasauroids. In fact, *Primitivus* displays a fairly conservative morphology in terms of both axial elongation of the trunk and limb reduction, and the coexistence of aquatic adaptations, together with features hinting at the retention of the ability to move on land, suggests a semi-aquatic lifestyle that was likely similar to that of the modern marine iguana.

Further comparisons across aquatic and terrestrial lizards regarding the anatomy of the articulation between the pelvic girdle and sacral vertebrae via a sacral rib – also known as iliosacral joint (ISJ) – led directly to the topic treated in Chapter 4. Here, I explore the anatomy of this articulation from an osteological and histological perspectives, providing data from several limb-bearing lizards and comparing both fossil and living species. I performed a survey of the variability of the structures associated with the iliosacral joint, i.e., sacral ribs and ilium,

and showed how such features can be directly correlated to specific lifestyles. The marine iguana, for instance, shares with both dolichosaurids and basal mosasauroids the reduction of the anterior supracetabular process of the ilium. This process is still functional as site of ligament attachment in *Amblyrhynchus*, but quite blunt in comparison to all terrestrial limbed lizards. In dolichosaurids and basal mosasaurids (i.e., aigialosaurs), the reduction of these process is even more extreme, usually with a weak spur left in its place. Osteologically, I recorded consistent variability in all three processes of the ilium (preacetabular, supracetabular and posterior) and the two sacral ribs typically present in limbed squamates (e.g., Snyder 1954, Hoffstetter & Gasc 1969). Based on my observations and comparisons with previous studies, I determined that this variability in lizards correlates directly with posture and type of locomotion. The presence of a cavity between the ilium and sacral ribs, abundant articular cartilage and fibrocartilage, and a surrounding membrane of dense fibrous connective tissue allowed me to define this contact as a synovial joint. By comparison, the two sacral ribs are connected to each other mostly by dense fibrous tissue, with some cartilage found more distally along the margins of the two ribs, defining this joint as a combination of a syndesmosis and synchondrosis. Considering the intermediary position of the ISJ between the axial and appendicular skeletons, the shape of the articular surfaces of the sacral ribs and ilium, and the characteristics of the muscles associated with this structure, I argue that the mobility of the ISJ is primarily driven by the movements of the hindlimb during locomotion. I hypothesize that limited torsion of the ilium at the ISJ happens when the hip is abducted, and the joint is likely able to absorb the compressional and extensional forces related to the protraction and retraction of the femur. The mix of fibres and cartilage between the two sacral ribs instead serves primarily as a shock absorber, with the potential for limited vertical translation during locomotion.

Finally, In Chapter 5 I present a revised phylogenetic analysis of Iguania based on combined morphological and molecular evidence. My new dataset includes the largest sampling of fossil taxa ever tested in a phylogeny of iguanians before. In fact, several of the fossil species that I was able to examine in person, were never assessed phylogenetically and their classification was based solely on anatomical comparisons. A detailed description of all the morphological characters that I revised from the literature or formulated anew is also provided in an appendix to this chapter, with explicit examples from the scorings and some illustrations. With the results of my analysis, I provide a new framework for the internal classification of iguanians that is more inclusive of the great diversity and complexity of these long-lasting squamate lineage, accounting for both extant and fossil taxa. Assembling a comprehensive phylogenetic dataset of iguanian lizards had important implications associated with multiple aspects of iguanian evolution that could not go unnoticed. Nor I could limit the discussion of my results to the origins and evolution of the marine iguana as originally intended.

6.1 A revised taxonomy of Iguania

Thanks to the new phylogenetic hypothesis, I was able to provide a revised classification of Iguania that hopefully will clarify the use of some taxonomic categories. I suggested to limit the use of Acrodonta and Pleurodonta to the two main iguanian crown groups, each branching from a common ancestor shared with a different fossil group. This is generally more consistent with the previous use of both taxa in the literature. To account for the sister-group relationship between Pleurodonta and its closest fossil relatives, I established the new clade Iguaniformes. This reflects the formalisation of Chamaeleontiformes by Conrad (2008) to include Acrodonta + Priscagamidae.

Encompassing the diversity of the iguanian fossil record is probably one of the highest achievements of my phylogenetic analysis. Priscagamidae, recovered as stem chamaeleontiforms, appears much more diverse than previously thought and has an extended temporal range. In fact, with the inclusion of the Oligo-Eocene fossil taxon *Arretosaurus*, priscagamids are inferred to survive the K/Pg extinction and are no longer restricted to the Late Cretaceous. Fossil taxa recovered as basal iguaniforms do not form a single monophyletic clade like the priscagamids on the chamaeleontiform side of the tree. The Late Cretaceous gobiguanians, as originally defined by Conrad & Norell (2007), form a monophyletic group, while other fossil iguaniforms of the same age from Gobi – *Isodontosaurus*, *Desertiguana*, *Polrussia* – branch separately, either as most basal or as sister to all Pleurodonta. Other fossil taxa are recovered as nested within either Acrodonta or Pleurodonta. The Eocene changjiangosaurids from Gobi represent the sister-group to modern chamaeleonids, while *Tinosaurus* and *Pseudotinosaurus* are recovered within Chamaeleonidae. The two Late Cretaceous fossil taxa *Jeddaherdan* and *Gueragama* are nested within this group and recognized as members of the Uromastycidae, together with modern *Uromastyx*. Two fossil iguaniforms are nested with crown pleurodontans: the Eocene *Geiseltaliellus* from Messel, and *Aciprion* from the Oligocene of North America. However, their sister relationships remain poorly resolved, as their positions are the least stable across all my analyses, and so a more accurate classification for these two taxa is not possible at this stage.

With the nesting of fossil taxa within the crown groups, some adjustments to the traditional classification of modern iguanians were necessary. *Leiolepis* and Uromastycidae fall outside of Agamidae and form their own clade – that I formalised as Uromastyoidea – representing together the sister-group to modern agamids. This is not unexpected as the former

Agamidae *sensu* Estes et al. (1988) or Frost & Etheridge (1989) was already recognized as paraphyletic. This becomes even more obvious when taxon sampling is increased and fossils are also involved. Some of the subfamilies typically used to divide Agamidae are recovered in the combined evidence analysis and no major changes are found in comparison to previous studies. I formalised the clade including agamids, leiolepids, and uromastycids as the Dracosauria (meaning ‗dragon-like lizards') which represents the sister-taxon to Chamaelonoidea (stem + crown chamaeleonids).

The origins and biogeographic history of modern chamaeleons change substantially with the new phylogenetic hypothesis presented here. With the re-interpretation of the Paleogene changjiangosaurids as stem-chamaeleonoids and the nesting of *Tinosaurus* and *Pseudotinosaurus* in crown Chamaeleonidae, the original range of distribution of these lizards become suddenly much broader and ancient than previously thought (see Georgalis et al. 2016; Tolley et al. 2013). Like most iguanian lineages, the evolutionary history of chamaeleons seems to have started in the Late Cretaceous and in my opininon is strongly tied to the evolution of priscagamids, for reasons that I explain extensively in Chapter 5.

Changes in the classification of chamaeleontiforms in particular are affected by my re-interpretation of the acrodont *versus* pleurodont conditions in iguanians. The separation of iguanians into the two taxonomic categories Acrodonta and Pleurodonta reflects the differences in tooth-jaw geometries found between most of the members of the two groups. Traditionally, acrodont implantation has been used to indicate that the teeth are positioned apically on the jaw bone, as it appears in most crown chamaeleontiforms, while pleurodont implantation refers to the teeth being located on the lingual side of the jaw, as in all iguaniforms and some chamaeleontiforms (e.g., Bertin et al. 2018; Haridy 2018; LeBlanc et al. 2020b; Owen 1840-

1845; Peyer 1968; Tomes 1874). As more fossils of iguanians emerged, several intermediate conditions have been described and quite often tooth geometries are masked by macroscopic and superficial observations. There are several new studies available on dental attachment and implantation in lizards as well as other amniotes, and I believe that this new knowledge can bring new insights into the evolutionary patterns associated with dental morphologies in iguanians. With my revised morphological characters, I addressed the single features that can contribute to determine an overall acrodont or pleurodont appearance separately, and used the results of some recent studies to update the common interpretation of these conditions in iguanians (Bertin et al. 2018; Buchtová et al. 2013; Dosedělová et al. 2016; Haridy 2018; LeBlanc et al. 2017; LeBlanc et al. 2020b; Zahradnicek et al. 2014).

6.2 The colonization of the Galápagos Islands and other cases of disjointed distribution

With a more complete picture of the relationships of iguanians over time and a new phylogenetic framework to rely on, I was able to discuss some of the widespread theories currently available in the literature to explain the modern distribution of chamaeleontiforms and iguaniforms across the world. In particular, I focused on the most evident examples of disjointed biogeographic history, such as the oplurids in Madagascar and the iguanids that are spread across the Americas and the Pacific islands.

In Chapter 5 I argue that iguanids may have colonized the ancient Galápagos Islands as long as 20-25 Ma via a dispersal event from the Caribbean area. The activity of the Galápagos Hotspot that is producing these islands became active at least 80-90 Ma and former islands as old as 19-20 Ma have been found at the bottom of the ocean close to Costa Rica (Christie et al. 1992; Geist 1996; Grehan 2001; Neall & Trewick 2008; Werner et al. 1999). Before the splitting of the

Farallon Plate into the Cocos and Nazca Plates – where the modern Galápagos are located – the islands were closer to the Caribbean. After the break-up of the Farallon Plate around 25 Ma, the Nazca Plate rotated and started drifting east (instead of north-east) and its subduction under the South American Plate is still ongoing (Duncan & Hargraves 1984; Grehan 2001; Kelley et al. 2019; Neall & Trewick 2008; Orellana-Rovirosa & Richards 2018). This is why more recent Galápagos islands (9-11 My) are found instead off of the cost of Ecuador (Christie et al. 1992; Geist et al. 2014). The iguanas would have undergone an initial dispersal event from the region of the Caribbean plate, which would then have been followed by constant short-range hopping from older to newer islands that were continually being produced by the activity of the Galápagos Hotspot. This, coupled with a certain degree of vicariance associated with plate movements, finally caused the iguanas to inhabit the modern Galápagos archipelago. This scenario is also consistent with the fact that the Galápagos iguanas share a more recent common ancestor with *Ctenosaura* from Central America and with the unusually old divergence time estimates that are persistently inferred in phylogenetic studies, especially those based on molecular (mitochondrial and nuclear) data (Noonan & Sites Jr 2009; Rassmann 1997; Rassmann et al. 1997a; Townsend et al. 2011; Wyles & Sarich 1983; this study).

The presence of iguanids across several Melanesian and Polynesian islands is possibly more difficult to explain, considering the greater distance between the majority of modern iguanids and *Brachylophus*, the only living genus currently known from the Fiji-Tonga. However, if we apply the mechanism described for the colonization of the Galápagos over a longer period of time, starting at least in the Late Cretaceous, we may have a reasonable explanation for the colonization of multiple South Pacific islands, without the need of one or more recent long-range rafting events from the Americas (cf. Noonan & Sites Jr 2009). In the

case of the Fiji and Tonga archipelagos, there is greater complexity added by documented evidence of human settlers carrying the iguanas from islands to islands as food source, thus introducing these lizards in islands where they were not present before (Pregill & Steadman 2004; Pregill & Worthy 2003). However, this human-mediated dispersal can only explain the larger spreading of iguanids across Melanesia and Polynesia but not their overall presence in this area of the Pacific. I still find it to be more likely that as Noonan & Sites Jr (2009) suggested, the mosaic distribution of modern Iguanidae is simply what is left of a much larger and widespread iguanid group that was present across the Pacific since possibly the Paleogene, or even earlier. Unfortunately, it is highly unlikely that we will ever find fossil evidence in support of this scenario, as most Pacific islands are short-lived and volcanic rocks are not ideal for fossil preservation.

Persistence of a long-lasting lineage of Gondwanan iguaniforms is also my preferred hypothesis to explain the presence of oplurids in Madagascar. These are the only pleurodontan iguanians currently found outside of the Americas and Pacific islands, in the midst of what is considered to be the area of distribution of acrodontan iguanians. We have no fossil evidence in either Madagascar or on the African mainland that can help to reconstruct the biogeographic history of pleurodontans in this area of the world and the more closely related fossil iguaniforms are either from the Late Cretaceous of South America (e.g., *Pristiguana*, *Brasiliguana*) or the Eocene of Europe (e.g., *Geiseltaliellus*) (Apesteguía et al. 2005; Estes & Price 1973; Nava & Martinelli 2011; Smith 2009). Oplurids are more often recovered as more closely related to South American pleurodontans in phylogenetic analyses, and in my results the age estimates for their divergence is fairly old based on combined evidence (65 Ma). The alternative to this hypothesis would require a more recent dispersal event from either Eurasia or South America;

however, the lack of oplurids or any pleurodontans in general anywhere near Madagascar, makes this scenario less likely. This could obviously change if new fossil evidence become available.

In conclusion, my research provides the first comprehensive phylogenetic analysis of fossil and living iguanian lizards, based on combined morphological and molecular evidence. I focused on the study of the anatomy of the Galápagos iguanid *Amblyrhynchus cristatus* to perform a revision of the morphological characters used to assess phylogenetic relationships across iguanians and presented a new phylogenetic hypothesis of iguanian evolution.

The results of my work have important implications for the manner in which we interpret the evolutionary patterns and biogeographic history of the clades that are part of Iguania. They also offer another clear example of how the inclusion of fossils in phylogenetic analyses has major impacts in the reconstruction of the evolutionary history of long-lasting groups of organisms, as many authors have argued previously (e.g., Gauthier et al. 1988; Gauthier et al. 2012; Caldwell 2007; Simões et al. 2015; Lee 1998; Wiens 2004; 2005; Wiens et al. 2010; Reeder et al. 2015; Mongiardino Koch et al. 2021). My revised classification of iguanians relies heavily on the reconstruction of the relationships of some key fossil iguanians. I hope that the results presented here will help clarify the use of some historically problematic taxonomic categories as well as provide a better framework for future phylogenetic and systematic studies on this highly diverse squamate lineage.

REFERENCES

Alberts AC, Carter RL, Hayes WK, and Martins EP. 2004. *Iguanas: biology and conservation*. Berkeley and Los Angeles, California: University of California Press.

Ali S. 1948. Studies on the anatomy of the tail in Sauria and Rhynchocephalia. Part II. *Chameleon zeylanicus*. *Proceedings: Plant Sciences* 28:151-165. 10.1007/bf03049956

Alifanov V. 1989. New Priscagamida (Lacertilia) from the Upper Cretaceous of Mongolia and their systematic position among Iguania. *Paleontological Journal* 4:68-80.

Alifanov V. 1993a. Revision of *Tinosaurus asiaticus* Gilmore (Agamidae). *Paleontological Journal* 27:148-154.

Alifanov V. 2012. Lizards of the family Arretosauridae Gilmore, 1943 (Iguanomorpha, Iguania) from the Paleogene of Mongolia. *Paleontological Journal* 46:412-420.

Alifanov VR. 1993b. The Upper Cretaceous lizard fauna from Mongolia and the problem of the first inter-american contact. *Paleontological Journal* 27:100-107.

Alifanov VR. 1996. Lizards of the families Priscagamidae and Hoplocercidae (Sauria, Iguania): phylogenetic position and new representatives from the Late Cretaceous of Mongolia. *Paleontological Journal* 30:466-483.

Alifanov VR. 2000. The fossil record of Cretaceous lizards from Mongolia. *The age of dinosaurs in Russia and Mongolia*:368-389.

Alifanov VR. 2009. New acrodont lizards (Lacertilia) from the Middle Eocene of southern Mongolia. *Paleontological Journal* 43:675-685. 10.1134/S0031030109060124

Alifanov VR. 2013. *Desertiguana gobiensis* gen. et sp. nov., a new lizard (Phrynosomatidae, Iguanomorpha) from the Upper Cretaceous of Mongolia. *Paleontological Journal* 47:417-424.

Altmanová M, Rovatsos M, Kratochvíl L, and Johnson Pokorná M. 2016. Minute Y chromosomes and karyotype evolution in Madagascan iguanas (Squamata: Iguania: Opluridae). *Biological Journal of the Linnean Society* 118:618-633. 10.1111/bij.12751

An YH, and Martin KL. 2003. *Handbook of histology methods for bone and cartilage*. Totowa, NJ: Humana Press, Totowa, NJ.

Apesteguía S, Agnolin FL, and Lio GL. 2005. An early Late Cretaceous lizard from Patagonia, Argentina. *Comptes Rendus Palevol* 4:311-315. 10.1016/j.crpv.2005.03.003

Apesteguia S, Daza JD, Simoes TR, and Rage JC. 2016. The first iguanian lizard from the Mesozoic of Africa. *Royal Society Open Science* 3:160462. 10.1098/rsos.160462

Archer CW, Dowthwaite GP, and Francis-West P. 2003. Development of synovial joints. *Birth Defects Research Part C: Embryo Today: Reviews* 69:144-155.

Arcila D, Pyron RA, Tyler JC, Ortí G, and Betancur-R R. 2015. An evaluation of fossil tip-dating versus node-age calibrations in tetraodontiform fishes (Teleostei: Percomorphaceae). *Molecular Phylogenetics and Evolution* 82:131-145.

Arnold P, Fischer MS, and Nyakatura JA. 2014. Soft tissue influence on ex vivo mobility in the hip of Iguana: comparison with in vivo movement and its bearing on joint motion of fossil sprawling tetrapods. *Journal of Anatomy* 225:31-41. 10.1111/joa.12187

Ayres DL, Darling A, Zwickl DJ, Beerli P, Holder MT, Lewis PO, Huelsenbeck JP, Ronquist F, Swofford DL, and Cummings MP. 2011. BEAGLE: an application programming interface and high-performance computing library for statistical phylogenetics. *Systematic Biology*:syr100.

Bailleul AM, and Holliday CM. 2017. Joint histology in *Alligator mississippiensis* challenges the identification of synovial joints in fossil archosaurs and inferences of cranial kinesis. Proc R Soc B: The Royal Society. p 20170038.

Bardet N, Houssaye A, Rage J-C, and Suberbiola XP. 2008. The Cenomanian-Turonian (late Cretaceous) radiation of marine squamates (Reptilia): the role of the Mediterranean Tethys. *Bulletin de la Societe Geologique de France* 179:605-622.

Bardet N, Suberbiola XP, and Jalil N-E. 2003. A new mosasauroid (Squamata) from the Late Cretaceous (Turonian) of Morocco. *Comptes Rendus Palevol* 2:607-616. http://dx.doi.org/10.1016/j.crpv.2003.09.006

Barnett CH, Davies D, and MacConaill M. 1961. *Synovial joints: their structure and mechanics*. Springfield, IL: Thomas.

Bartholomew GA. 1987. Living in two worlds: The marine iguana, *Amblyrhynchus cristatus*. *Comparative physiology: Life in water and on land* 9:389.

Bartholomew GA, Bennett AF, and Dawson WR. 1976. Swimming, diving and lactate production of the marine iguana, *Amblyrhynchus cristatus*. *Copeia*:709-720.

Bartholomew GA, and Lasiewski RC. 1965. Heating and cooling rates, heart rate and simulated diving in the Galápagos marine iguana. *Comparative Biochemistry and Physiology* 16:573-582.

Begg G, and Gray DR. 2002. Arc dynamics and tectonic history of Fiji based on stress and kinematic analysis of dikes and faults of the Tavua Volcano, Viti Levu Island, Fiji. *Tectonics* 21:5-1-5-14.

Bejder L, and Hall BK. 2002. Limbs in whales and limblessness in other vertebrates: mechanisms of evolutionary and developmental transformation and loss. *Evolution & Development* 4:445-458.

Bell BA, Murry PA, and Osten LW. 1982. *Coniasaurus* Owen, 1850 from North America. *Journal of Paleontology*:520-524.

Bell T. 1825. On a new genus of Iguanidae. W. Phillips.

Bennett SP, Barrett PM, Collinson ME, Moore-Fay S, Davis PG, and Palmer CP. 2012. A new specimen of Ichthyosaurus communis from Dorset, UK, and its bearing on the stratigraphical range of the species. *Proceedings of the Geologists' Association* 123:146-154. 10.1016/j.pgeola.2011.07.001

Bergsten J. 2005. A review of long-branch attraction. *Cladistics* 21:163-193. 10.1111/j.1096-0031.2005.00059.x

Bertin TJC, Thivichon-Prince B, LeBlanc ARH, Caldwell MW, and Viriot L. 2018. Current Perspectives on Tooth Implantation, Attachment, and Replacement in Amniota. *Frontiers in Physiology* 9. 10.3389/fphys.2018.01630

Bever GS, Bell CJ, and Maisano JA. 2005. The ossified braincase and cephalic osteoderms of *Shinisaurus crocodilurus* (Squamata, Shinisauridae). *Palaeontologia Electronica* 8:1-36.

Bhullar BAS. 2009. A reevaluation of the unusual abdominal musculature of squamate reptiles (Reptilia: Squamata). *The Anatomical Record* 292:1154-1161.

Bilezikian JP, Raisz LG, and Martin TJ. 2008. *Principles of bone biology*. Orlando, FL: Academic Press.

Boersma P. 1983. An ecological study of the Galápagos marine iguana. *Patterns of evolution in Galápagos organisms*:157-176.

Boisvert CA. 2005. The pelvic fin and girdle of *Panderichthys* and the origin of tetrapod locomotion. *Nature* 438:1145.

Bolet A, and Evans SE. 2013. Fossil History of Chameleons. In: Tolley K, and Herrel A, eds. *The biology of chameleons*. Berkeley: University of California Press, 175-192.

Borsuk-Bialynicka M. 1996. The Late Cretaceous lizard *Pleurodontagama* and the origin of tooth permanency in Lepidosauria. *Acta Palaeontologica Polonica* 41:231.

Borsuk-Białynicka M. 2008. Evolution of the iliosacral joint in diapsid phylogeny. *Neues Jahrbuch für Geologie und Paläontologie - Abhandlungen* 249:297-311. 10.1127/0077-7749/2008/0249-0297

Borsuk-Bialynicka M, and Alifanov V. 1991. First Asiatic 'iguanid' lizards in the Late Cretaceous of Mongolia. *Acta Palaeontologica Polonica* 36:325-342.

Borsuk-Bialynicka M, and Moody SM. 1984. Priscagaminae. A new subfamily of the Agamidae (Sauria) from the Late Cretaceous of the Gobi Desert. *Acta Palaeontologica Polonica* 29:51-81.

Bossio A, Foresi LM, Margiotta S, Mazzei R, Salvatorini G, and Donia F. 2006. Stratigrafia neogenico-quaternaria del settore nord-orientale della Provincia di Lecce (con rilevamento geologico alla scala 1: 25.000). *Geologica Romana* 39:63-88.

Bowman RI, Berson M, and Leviton AE. 1983. *Patterns of evolution in Galápagos organisms*: Pacific Division, AAAS.

Branch WR, and Tolley KA. 2010. A new species of chameleon (Sauria: Chamaeleonidae: *Nadzikambia*) from Mount Mabu, central Mozambique. *African Journal of Herpetology* 59:157-172. 10.1080/21564574.2010.516275

Briggs D, Kear A, Martill D, and Wilby P. 1993. Phosphatization of soft-tissue in experiments and fossils. *Journal of the Geological Society* 150:1035-1038.

Briggs DE. 2003. The role of decay and mineralization in the preservation of soft-bodied fossils. *Annual Review of Earth and Planetary Sciences* 31:275-301.

Briggs DEG, and Kear AJ. 1993. Fossilization of Soft Tissue in the Laboratory. *Science* 259:1439-1442. 10.1126/science.259.5100.1439

Brinkmann H, van der Giezen M, Zhou Y, de Raucourt GP, and Philippe H. 2005. An Empirical Assessment of Long-Branch Attraction Artefacts in Deep Eukaryotic Phylogenomics. *Systematic Biology* 54:743-757. 10.1080/10635150500234609

Buchtová M, Zahradníček O, Balková S, and Tucker AS. 2013. Odontogenesis in the veiled chameleon (*Chamaeleo calyptratus*). *archives of oral biology* 58:118-133.

Buckley LJ, de Queiroz K, Grant TD, Hollingsworth BD, Iverson JB, Pasachnik SA, Stephen CL, and Group ITW. 2016. A checklist of the iguanas of the world (Iguanidae; Iguaninae).

Budney LA, Caldwell MW, and Albino AM. 2006. Tooth socket histology in the Cretaceous snake *Dinilysia*, with a review of amniote dental attachment tissues. *Journal of Vertebrate Paleontology* 26:138-145. 10.1671/0272-4634(2006)26[138:TSHITC]2.0.CO;2

Burbrink FT, Grazziotin FG, Pyron RA, Cundall D, Donnellan S, Irish F, Keogh JS, Kraus F, Murphy RW, and Noonan B. 2020. Interrogating genomic-scale data for Squamata (lizards, snakes, and amphisbaenians) shows no support for key traditional morphological relationships. *Systematic Biology* 69:502-520.

Burbrink FT, and Lawson R. 2007. How and when did Old World ratsnakes disperse into the New World? *Molecular Phylogenetics and Evolution* 43:173-189.

Butler AD, Cunningham JA, Budd GE, and Donoghue PC. 2015. Experimental taphonomy of *Artemia* reveals the role of endogenous microbes in mediating decay and fossilization. *Proc R Soc B* 282:20150476.

Caldwell MW. 1999. Description and phylogenetic relationships of a new species of *Coniasaurus* Owen, 1850 (Squamata). *Journal of Vertebrate Paleontology* 19:438-455.

Caldwell MW. 2000. On the aquatic squamate *Dolichosaurus longicollis* owen, 1850 (Cenomanian, Upper Cretaceous), and the evolution of elongate necks in squamates. *Journal of Vertebrate Paleontology* 20:720-735. 10.1671/0272-4634(2000)020[0720:otasdl]2.0.co;2

Caldwell MW. 2002. From fins to limbs to fins: limb evolution in fossil marine reptiles. *Am J Med Genet* 112:236-249. 10.1002/ajmg.10773

Caldwell MW. 2003. "Without a leg to stand on": on the evolution and development of axial elongation and limblessness in tetrapods. *Canadian Journal of Earth Sciences* 40:573-588. 10.1139/e02-081

Caldwell MW. 2006. A new species of *Pontosaurus* (Squamata, Pythonomorpha) from the Upper Cretaceous of Lebanon and a phylogenetic analysis of Pythonomorpha. *Memorie della Società italiana di scienze naturali e Museo civico di storia naturale di Milano* 34:1-43.

Caldwell MW, Budney LA, and Lamoureux DO. 2003. Histology of tooth attachment tissues in the Late Cretaceous mosasaurid *Platecarpus*. *Journal of Vertebrate Paleontology* 23:622-630. 10.1671/0272-4634(2003)023[0622:HOTATI]2.0.CO;2

Caldwell MW, Carroll RL, and Kaiser H. 1995. The pectoral girdle and forelimb of *Carsosaurus marchesetti* (Aigialosauridae), with a preliminary phylogenetic analysis of mosasauroids and varanoids. *Journal of Vertebrate Paleontology* 15:516-531. 10.1080/02724634.1995.10011245

Caldwell MW, and Dal Sasso C. 2004. Soft-Tissue Preservation in a 95 Million Year Old Marine Lizard: Form, Function, and Aquatic Adaptation. *Journal of Vertebrate Paleontology* 24:980-985.

Caldwell MW, Nydam RL, Palci A, and Apesteguía S. 2015. The oldest known snakes from the Middle Jurassic-Lower Cretaceous provide insights on snake evolution. *Nature Communications* 6. 10.1038/ncomms6996

Caldwell MW, and Palci A. 2007. A new basal mosasauroid from the Cenomanian (U. Cretaceous) of Slovenia with a review of mosasauroid phylogeny and evolution. *Journal of Vertebrate Paleontology* 27:863-880. 10.1671/0272-4634(2007)27[863:anbmft]2.0.co;2

Caldwell MW, and Palci A. 2010. A new species of marine ophidiomorph lizard, *Adriosaurus skrbinensis*, from the Upper Cretaceous of Slovenia. *Journal of Vertebrate Paleontology* 30:747-755. 10.1080/02724631003762963

Camp CL. 1923. Classification of the lizards. *Bulletin of the American Museum of Natural History* 48:289-481.

Carey EJ. 1922. Direct observations on the transformation of the mesenchyme in the thigh of the pig embryo (*Sus scrofa*), with especial reference to the genesis of the thigh muscles, of the knee- and hip-joints, and of the primary bone of the femur. *Journal of Morphology* 37:1-77. 10.1002/jmor.1050370102

Carpenter CC. 1966. The marine iguana of the Galápagos Islands: its behavior and ecology. *Proceedings of the California Academy of Sciences, 4th series*. San Francisco: California Academy of Sciences, 329-376.

Carrier DR. 1989. Ventilatory action of the hypaxial muscles of the lizard Iguana iguana: a function of slow muscle. *Journal of Experimental Biology* 143:435-457.

Carroll RL. 1988. *Vertebrate Paleontology and Evolution*. New York: W. H. Freeman and Companay.

Carroll RL, and de Braga M. 1992. Aigialosaurs: Mid-Cretaceous Varanoid Lizards. *Journal of Vertebrate Paleontology* 12:66-86.

Carroll RL, Irwin J, and Green DM. 2005. Thermal physiology and the origin of terrestriality in vertebrates. *Zoological Journal of the Linnean Society* 143:345-358.

Censky EJ, Hodge K, and Dudley J. 1998. Over-water dispersal of lizards due to hurricanes. *Nature* 395:556-556. 10.1038/26886

Cernanský A. 2011. A revision of the chameleon species *Chamaeleo pfeili* Schleich (Squamata; Chamaeleonidae) with description of a new material of chamaeleonids from the Miocene deposits of southern Germany. *Bulletin of Geosciences* 86:2.

Čerňanský A. 2010. A revision of chamaeleonids from the Lower Miocene of the Czech Republic with description of a new species of Chamaeleo (Squamata, Chamaeleonidae). *Geobios* 43:605-613.

Cestari R, and Sirna G. 1987. Rudist fauna in the Maastrichtian deposits of southern Salento (Southern Italy). *Memorie della Societa Geologica Italiana* 40:133-147.

Chatterjee S, and Scotese C. 2007. Biogeography of the Mesozoic lepidosaurs on the wandering Indian plate. Paleontologia: Cenários de Vida. Rio de Janeiro, Brazil: Editora Interciência. p 551-579.

Chatterjee S, and Scotese C. 2010. The Wandering Indian Plate and Its Changing Biogeography During the Late Cretaceous-Early Tertiary Period. *New Aspects of Mesozoic Biodiversity*. Berlin, Heidelberg: Springer Berlin Heidelberg, 105-126.

Cheng Y-n, Wu X-c, and Ji Q. 2004. Triassic marine reptiles gave birth to live young. *Nature* 432:383.

Christie D, Duncan R, McBirney A, Richards M, White WM, Harpp K, and Fox C. 1992. Drowned islands downstream from the Galápagos Hotspot imply extended speciation times. *Nature* 355:246-248.

Citton P, Nicosia U, and Sacchi E. 2015. Updating and reinterpreting the dinosaur track record of Italy. *Palaeogeography, Palaeoclimatology, Palaeoecology* 439:117-125. 10.1016/j.palaeo.2015.01.018

Coates MI, Jeffery JE, and Ruta M. 2002. Fins to limbs: what the fossils say. *Evolution & Development* 4:390-401.

Cohen KM, Finney SC, Gibbard PL, and Fan J-X. 2013. The ICS international chronostratigraphic chart. *Episodes* 36:199-204.

Conrad JL. 2008. Phylogeny and systematics of Squamata (Reptilia) based on morphology. *Bulletin of the American Museum of Natural History* 310:1-182. 10.1206/310.1

Conrad JL. 2015. A New Eocene Casquehead Lizard (Reptilia, Corytophanidae) from North America. *PLoS ONE* 10:e0127900. 10.1371/journal.pone.0127900

Conrad JL, and Norell MA. 2007. A complete Late Cretaceous iguanian (Squamata, Reptilia) from the Gobi and identification of a new iguanian clade. *American Museum Novitates* 3584:1-47.

Coordinators NR. 2016. Database resources of the national center for biotechnology information. *(https://wwwncbinlmnihgov/genbank/)*.

Cope ED. 1864. On the Characters of the Higher Groups of Reptilia Squamata: And Especially of the Diploglossa. *Proceedings of the Academy of Natural Sciences of Philadelphia* 16:224-231.

Cope ED. 1886. On the Species of Iguaninœ. *Proceedings of the American Philosophical Society*:261-271.

Cormack DH. 2001. *Essential histology*. Philadelphia: Lippincott Williams & Wilkins.

Cosmidis J, Benzerara K, Gheerbrant E, Estève I, Bouya B, and Amaghzaz M. 2013. Nanometer-scale characterization of exceptionally preserved bacterial fossils in Paleocene phosphorites from Ouled Abdoun (Morocco). *Geobiology* 11:139-153. doi:10.1111/gbi.12022

Cox A. 1983. Ages of the Galápagos islands. *Patterns of evolution in Galápagos organisms* 1:1-23.

Croizat L. 1952. *Manual of phytogeography*: Uitgeverij Dr. W. Junk; Hague.

Croizat L. 1958. Panbiogeography. 3 vols. *Published by the author, Caracas*.

Crottini A, Miralles A, Glaw F, Harris DJ, Lima A, and Vences M. 2012. Description of a new pygmy chameleon (Chamaeleonidae: Brookesia) from central Madagascar. *Zootaxa* 3490:63-74.

Cuthbertson RS, Maddin HC, Holmes RB, and Anderson JS. 2015. The Braincase and Endosseous Labyrinth of *Plioplatecarpus peckensis* (Mosasauridae, Plioplatecarpinae), With Functional Implications for Locomotor Behavior. *The Anatomical Record* 298:1597-1611. https://doi.org/10.1002/ar.23180

Cuvier G. 1829.

. Paris: Chez Déterville.

Darwin CR. 1845. *Journal of researches into the natural history and geology of the countries visited during the voyage of H.M.S. Beagle round the world, under the Command of Capt. Fitz Roy, R.N.* London: John Murray.

Datta PM, and Ray S. 2006. Earliest lizard from the Late Triassic (Carnian) of China. *Journal of Vertebrate Paleontology* 26:795-800. 10.1671/0272-4634(2006)26[795:elftlt]2.0.co;2

Dawson WR, Bartholomew GA, and Bennett AF. 1977. A reappraisal of the aquatic specializations of the Galápagos marine iguana (*Amblyrhynchus cristatus*). *Evolution* 31:891-897.

Daza JD, Abdala V, Arias JS, García-López D, and Ortiz P. 2012. Cladistic analysis of Iguania and a fossil lizard from the Late Pliocene of northwestern Argentina. *Journal of Herpetology* 46:104-119. 10.1670/10-112

Daza JD, Abdala V, Thomas R, and Bauer AM. 2008. Skull anatomy of the miniaturized gecko *Sphaerodactylus roosevelti* (Squamata: Gekkota). *Journal of Morphology* 269:1340-1364. doi:10.1002/jmor.10664

de Queiroz K. 1987. *Phylogenetic systematics of iguanine lizards: a comparative osteological study*: University of California Press.

de Queiroz K, and Donoghue MJ. 2011. Phylogenetic nomenclature, three-taxon statements, and unnecessary name changes. *Systematic Biology* 60:887-892.

DeMar DG, Conrad JL, Head JJ, Varricchio DJ, and Wilson GP. 2017. A new Late Cretaceous iguanomorph from North America and the origin of New World Pleurodonta (Squamata, Iguania). Proc R Soc B: The Royal Society. p 20161902.

Dollion AY, Cornette R, Tolley KA, Boistel R, Euriat A, Boller E, Fernandez V, Stynder D, and Herrel A. 2015. Morphometric analysis of chameleon fossil fragments from the Early Pliocene of South Africa: a new piece of the chamaeleonid history. *The Science of Nature* 102:1-14.

Dong L, Evans S, and Wang Y. 2016. Taxonomic revision of lizards from the Paleocene deposits of the Qianshan Basin, Anhui, China. *Vertebrata PalAsiatica* 54:243-268.

Dornbos SQ. 2010. Phosphatization Through the Phanerozoic. In: Allison PA, and Bottjer DJ, eds. *Taphonomy: Process and Bias Through Time*. Dordrecht: Springer Netherlands, 435-456.

Dosedělová H, Štěpánková K, Zikmund T, Lesot H, Kaiser J, Novotný K, Štembírek J, Knotek Z, Zahradníček O, and Buchtová M. 2016. Age-related changes in the tooth–bone interface area of acrodont dentition in the chameleon. *Journal of Anatomy* 229:356-368.

Drachman DB, and Sokoloff L. 1966. The role of movement in embryonic joint development. *Developmental Biology* 14:401-420.

Duméril AHA. 1856. *Description des reptiles nouveaux ou imparfaictement connus de la M 'H N rques sur la classification et les . D M . T q f ' des Sauriens (Geckotiens, Varaniens et Iguaniens)*. Paris.

Duméril AMC, and Bibron G. 1837. *Erpétologie générale ou histoire naturelle complète des reptiles: Contenant l'histoire de quarante-six genres et de cent quarante-six espèces de la famille des iguaniens, de l'ordre des sauriens*: Librairie encyclopédique de Roret.

Duncan R, and Hargraves R. 1984. Plate tectonic evolution of the Caribbean region in the mantle reference frame. *Geological Society of America Memoirs* 162:81-94.

Dunson WA. 1969. Electrolyte excretion by the salt gland of the Galápagos marine iguana. *American Journal of Physiology-Legacy Content* 216:995-1002.

Dutchak AR, and Caldwell MW. 2006. Redescription of *Aigialosaurus dalmaticus* Kramberger, 1892, a Cenomanian mosasauroid lizard from Hvar Island, Croatia. *Canadian Journal of Earth Sciences* 43:1821-1834. 10.1139/e06-086

Dutchak AR, and Caldwell MW. 2009. A redescription of *Aigialosaurus* (= *Opetiosaurus*) *bucchichi* (Kornhuber, 1901)(Squamata: Aigialosauridae) with comments on mosasauroid systematics. *Journal of Vertebrate Paleontology* 29:437-452.

Eardley A. 1954. Tectonic relations of North and South America. *AAPG Bulletin* 38:707-773.

Estes R, de Queiroz K, and Gauthier JA. 1988. Phylogenetic relationships within Squamata. In: Estes R, and Pregill G, eds. *Phylogenetic relationships of the lizard families*. Stanford: Stanford University Press, 119-281.

Estes R, and Price LI. 1973. Iguanid lizard from the Upper Cretaceous of Brazil. *Science* 180:748-751.

Etheridge R. 1982. Checklist of the iguanine and Malagasy iguanid lizards,(pp. 7-37). la: Iguanas of the World. Their behavior, ecology, and conservation. GM Burghardt and A. S. Rand. Noyes Publications, Park Ridge, New Jersey.

Etheridge R, and de Queiroz K. 1988. A phylogeny of the Iguanidae. In: Estes R, and Pregill G, eds. *Phylogenetic relationships of the lizard families*. Stanford: Stanford University Press, 283 - 367.

Evans SE. 2003. At the feet of the dinosaurs: the early history and radiation of lizards. *Biological Reviews* 78:513 - 551.

Evans SE. 2008. The Skull of Lizards and Tuatara. In: Gans C, Gaunt A, and Adler K, eds. *Biology of the Reptilia - The Skull of Lepidosauria*. Ithaca: Society for the Study of Amphibians and Reptiles, 1 - 347.

Evans SE, Manabe M, Noro M, Isaji S, and Yamaguchi M. 2006. A Long-Bodied Lizard from the Lower Cretaceous of Japan. *Palaeontology* 49:1143-1165.

Evans SE, Prasad GVR, and Manhas BK. 2002. Fossil lizards from the Jurassic Kota Formation of India. *Journal of Vertebrate Paleontology* 22:299-312.

Fairbanks RG. 1989. A 17,000-year glacio-eustatic sea level record: influence of glacial melting rates on the Younger Dryas event and deep-ocean circulation. *Nature* 342:637-642. 10.1038/342637a0

Felsenstein J. 1978. Cases in which parsimony or compatibility methods will be positively misleading. *Systematic Zoology* 27:401-410.

Fernandes LA, and Ribeiro CMM. 2015. Evolution and palaeoenvironment of the Bauru Basin (upper Cretaceous, Brazil). *Journal of South American Earth Sciences* 61:71-90.

Fisher RN, Niukula J, Watling D, and Harlow PS. 2017. A new species of iguana *Brachylophus* Cuvier 1829 (Sauria: Iguania: Iguanidae) from Gau Island, Fiji Islands. *Zootaxa* 4273:407-422.

Fitzinger LJFJ. 1843. *Systema reptilium: Fasc. primus. Amblygolssae*: Braumüller et Seidel.

Forst SL, Wheeler MT, Fortin JD, and Vilensky JA. 2006. The sacroiliac joint: anatomy, physiology and clinical significance. *Pain physician* 9:61-67.

Fortin JD. 1993. Sacroiliac Joint Dysfunction. *Journal of back and musculoskeletal rehabilitation* 3:31-43.

Frost DR, and Etheridge R. 1989. A phylogenetic analysis and taxonomy of iguanian lizards (Reptilia: Squamata). *University of Kansas Natural History Museum Miscellaneous Publication* 81:1-65.

Frost DR, Etheridge R, Janies D, and Titus TA. 2001. Total evidence, sequence alignment, evolution of polychrotid lizards, and a reclassification of the Iguania (Squamata: Iguania). *American Museum Novitates*:1-39.

Gans C, Gaunt A, and Adler K. 2008. *Biology of the Reptilia. Volume 21. Morphology I. The Skull and Appendicular Locomotor Apparatus of Lepidosauria*. Ithaca, New York: Society for the Study of Amphibians and Reptiles.

Gao K, and Norell MA. 2000. Taxonomic composition and systematics of Late Cretaceous lizard assemblages from Ukhaa Tolgod and adjacent localities, Mongolian Gobi Desert. *Bulletin of the American Museum of Natural History* 249:1-118.

Gao KQ, and Fox RC. 1996. Taxonomy and evolution of Late Cretaceous lizards (Reptilia: Squamata) from western Canada. *Bulletin of the Carnegie Museum of Natural History* 33:1-107.

Gao KQ, and Hou LH. 1995. Iguanians from the Upper Cretaceous Djadochta Formation, Gobi Desert, China. *Journal of Vertebrate Paleontology* 15:57-78. 10.1080/02724634.1995.10011207

Gauthier JA, Estes R, and de Queiroz ET. 1988. A phylogenetic analysis of Lepidosauromorpha. In: Estes R, and Pregill G, eds. *Phylogenetic relationships of the lizard families*. Stanford: Stanford University Press, 15-98.

Gauthier JA, Kearney M, Maisano JA, Rieppel O, and Behlke ADB. 2012. Assembling the squamate tree of life: perspectives from the phenotype and the fossil record. *Bulletin of the Peabody Museum of Natural History* 53:3-308.

Gavryushkina A, Welch D, Stadler T, and Drummond AJ. 2014. Bayesian inference of sampled ancestor trees for epidemiology and fossil calibration. *PLoS Comput Biol* 10:e1003919.

Geist D. 1996. On the emergence and submergence of the Galápagos Islands. *Noticias de Galápagos* 56:5-9.

Geist DJ, Snell H, Snell H, Goddard C, and Kurz MD. 2014. A paleogeographic model of the Galápagos Islands and biogeographical and evolutionary implications. *The Galápagos: a natural laboratory for the Earth Sciences American Geophysical Union, Washington DC, USA*:145-166.

Gentile G, Fabiani A, Marquez C, Snell HL, Snell HM, Tapia W, and Sbordoni V. 2009. An overlooked pink species of land iguana in the Galápagos. *Proceedings of the National Academy of Sciences* 106:507-511.

Gentile G, and Snell H. 2009. *Conolophus marthae* sp. nov.(Squamata, Iguanidae), a new species of land iguana from the Galápagos archipelago. *Zootaxa* 2201:1-10.

Georgalis GL, Villa A, and Delfino M. 2016. First description of a fossil chamaeleonid from Greece and its relevance for the European biogeographic history of the group. *The Science of Nature* 103:1-12.

Gibbons JR. 1981. The biogeography of *Brachylophus* (Iguanidae) including the description of a new species, B. vitiensis, from Fiji. *Journal of Herpetology* 15:255-273.

Gilmore CW. 1928. Fossil lizards of North America. *Memoirs of the National Academy of Sciences* 22:1-201.

Gilmore CW. 1943. Fossil lizards of Mongolia. *Bulletin of the American Museum of Natural History* 81:361-384.

Gingerich PD, Raza SM, Arif M, Anwar M, and Zhou X. 1994. New whale from the Eocene of Pakistan and the origin of cetacean swimming. *Nature* 368:844.

Glaw F, Köhler J, Townsend TM, and Vences M. 2012. Rivaling the world's smallest reptiles: discovery of miniaturized and microendemic new species of leaf chameleons (Brookesia) from northern Madagascar. *PLoS ONE* 7:e31314.

Glynn PW, and Wellington GM. 1983. *Corals and coral reefs of the Galápagos Islands*: Univ of California Press.

Goloboff P, Farris J, and Nixon K. 2003. TNT: Tree Analysis Using New Technology. Program and documentation, available from the authors, at www.lillo.org.ar/phylogeny/tnt.

Goloboff PA, Carpenter JM, Arias JS, and Esquivel DRM. 2008a. Weighting against homoplasy improves phylogenetic analysis of morphological data sets. *Cladistics* 24:758-773.

Goloboff PA, Farris JS, and Nixon KC. 2008b. TNT, a free program for phylogenetic analysis. *Cladistics* 24:774-786. 10.1111/j.1096-0031.2008.00217.x

Goloboff PA, Torres A, and Arias JS. 2017. Weighted parsimony outperforms other methods of phylogenetic inference under models appropriate for morphology. *Cladistics*:1-31. 10.1111/cla.12205

Gray H. 1878. *Anatomy of the human body*: Lea & Febiger.

Grehan J. 2001. Biogeography and evolution of the Galapagos: integration of the biological and geological evidence. *Biological Journal of the Linnean Society* 74:267-287.

Guidotti G, Landini W, Sorbini L, and Varola A. 1993. Le ittiofaune del Cretaceo di Alessano e Nardò. Guida alle escursioni. In: Conte, editor. XII Convegno della Società Paleontologica Italiana. Terra d'Otranto, Lecce, Puglia, Italy. p 45-49.

Hall-Stoodley L, Costerton JW, and Stoodley P. 2004. Bacterial biofilms: from the natural environment to infectious diseases. *Nature reviews microbiology* 2:95.

Hall BK. 2005. *Bones and cartilage: developmental and evolutionary skeletal biology*. New York: Academic Press.

Hall TA. 1999. BioEdit: a user-friendly biological sequence alignment editor and analysis program for Windows 95/98/NT. Nucleic acids symposium series: [London]: Information Retrieval Ltd., c1979-c2000. p 95-98.

Hallowell E. 1854. Description of new reptiles from California. *Proceedings of the Academy of Natural Sciences of Philadelphia* 7:91–97.

Handschuh S, Natchev N, Kummer S, Beisser CJ, Lemell P, Herrel A, and Vergilov V. 2019. Cranial kinesis in the miniaturised lizard *Ablepharus kitaibelii* (Squamata: Scincidae). *The Journal of Experimental Biology* 222:jeb198291. 10.1242/jeb.198291

Haridy Y. 2018. Histological analysis of post-eruption tooth wear adaptations, and ontogenetic changes in tooth implantation in the acrodontan squamate *Pogona vitticeps*. *PeerJ* 6:e5923. 10.7717/peerj.5923

Harlan R. 1824. Description of two species of Linnaean Lacerta not before described, and construction of the new genus *Cyclura*. *Journal of the Academy of Natural Sciences of Philadelphia* 4:242-251.

Harpp KS, Mittelstaedt E, d'Ozouville N, and Graham DW. 2014. *The Galápagos: A Natural Laboratory for the Earth Sciences*: John Wiley & Sons.

Head JJ, Barrett PM, and Rayfield EJ. 2009. Neurocranial osteology and systematic relationships of *Varanus* (*Megalania*) *prisca* Owen, 1859 (Squamata: Varanidae). *Zoological Journal of the Linnean Society* 155:445-457. 10.1111/j.1096-3642.2008.00448.x

Heath TA, Huelsenbeck JP, and Stadler T. 2014. The fossilized birth–death process for coherent calibration of divergence-time estimates. *Proceedings of the National Academy of Sciences* 111:E2957-E2966.

Hetherington T. 2008. Comparative anatomy and function of hearing in aquatic amphibians, reptiles, and birds. *Sensory evolution on the threshold: adaptations in secondarily aquatic vertebrates*:183-209.

Higgins PJ. 1978. The Galápagos Iguanas: Models of Reptilian Differentiation. *Bioscience* 28:512-515. 10.2307/1307298

Hillenius D. 1978a. Notes on Chameleons IV. A New Chameleon, from the Miocene of Fort Ternan, Kenya (Chamaeleonidae, Reptilia). *Beaufortia* 28:9-15.

Hillenius D. 1978b. Notes on chameleons V. The chameleons of North Africa and adjacent countries, Chamaeleo chamaeleon (Linnaeus)(Sauria: Chamaeleonidae). *Beaufortia* 28:37-55.

Hoffstetter R, and Gasc J-P. 1969. Vertebrae and ribs of modern reptiles. *Biology of the Reptilia* 1:201-310.

Holden JC, and Dietz RS. 1972. Galápagos gore, NazCoPac triple junction and Carnegie/Cocos ridges. *Nature* 235:266-269.

Hou L. 1976. New materials of Palaeocene lizards of Anhui. *Vertebrata PalAsiatica* 14:48-52.

Houssaye A. 2009. "Pachyostosis" in aquatic amniotes: a review. *Integr Zool* 4:325-340. 10.1111/j.1749-4877.2009.00146.x

Houssaye A. 2010. A new aquatic pythonomorph (Reptilia, Squamata) from the Turonian (Late Cretaceous) of France. *Comptes Rendus Palevol* 9:39-45. 10.1016/j.crpv.2009.09.002

Houssaye A, Bardet N, Narváez I, and Ortega F. 2013. Squamate finding in “Lo Hueco” (Late Campanian-Early Maastrichtian, Cuenca Province, Spain): the second non-marine pythonomorph lizard. *Paläontologische Zeitschrift* 87:415-422. 10.1007/s12542-013-0164-6

Houssaye A, De Buffrenil V, Rage J-C, and Bardet N. 2008. An analysis of vertebral ‗pachyostosis‘ in *Carentonosaurus mineaui* (Mosasauroidea, Squamata) from the Cenomanian (early Late Cretaceous) of France, with comments on its phylogenetic and functional significance. *Journal of Vertebrate Paleontology* 28:685-691. 10.1671/0272-4634(2008)28[685:aaovpi]2.0.co;2

Houssaye A, Sander PM, and Klein N. 2016. Adaptive Patterns in Aquatic Amniote Bone Microanatomy—More Complex than Previously Thought. *Integrative and Comparative Biology* 56:1349-1369. https://doi.org/10.1093/icb/icw120

Huelsenbeck JP, Rannala B, and Masly JP. 2000. Accommodating phylogenetic uncertainty in evolutionary studies. *Science* 288:2349-2350.

Huelsenbeck JP, and Ronquist F. 2001. MrBayes: Bayesian inference of phylogenetic trees. *Bioinformatics* 17:754-755.

Hugi J, and Sánchez-Villagra MR. 2012. Life History and Skeletal Adaptations in the Galápagos Marine Iguana (*Amblyrhynchus cristatus*) as Reconstructed with Bone Histological Data—A Comparative Study of Iguanines. *Journal of Herpetology* 46:312-324. 10.1670/11-071

Hutchinson MN, Skinner A, and Lee MSY. 2012. *Tikiguania* and the antiquity of squamate reptiles (lizards and snakes). *Biology Letters* 8:665-669. 10.1098/rsbl.2011.1216

Inc ORSO. 2016. Dragonfly 2.0 for Windows. 2.0 ed. Montreal, Canada.

Inc ORSO. 2020. Dragonfly 2020.2 for Windows. 2020.2 ed. Montreal, Canada.

Irisarri I, Baurain D, Brinkmann H, Delsuc F, Sire J-Y, Kupfer A, Petersen J, Jarek M, Meyer A, and Vences M. 2017. Phylotranscriptomic consolidation of the jawed vertebrate timetree. *Nature Ecology & Evolution* 1:1370-1378.

Irschick DJ, and Jayne BC. 1999. Comparative three-dimensional kinematics of the hindlimb for high-speed bipedal and quadrupedal locomotion of lizards. *Journal of Experimental Biology* 202:1047-1065.

Jiménez-Huidobro P, Caldwell MW, Paparella I, and Bullard TS. 2018. A new species of tylosaurine mosasaur from the upper Campanian Bearpaw Formation of Saskatchewan, Canada. *Journal of Systematic Palaeontology*:1-16. 10.1080/14772019.2018.1471744

John KO. 1971. Caudal Musculature of the South Indian Flying Lizard *Draco dussumieri* Dum. and Bibr. *Acta Zoologica* 52:249-255. doi:10.1111/j.1463-6395.1971.tb00561.x

Jones ME, Anderson CL, Hipsley CA, Müller J, Evans SE, and Schoch RR. 2013. Integration of molecules and new fossils supports a Triassic origin for Lepidosauria (lizards, snakes, and tuatara). *BMC Evolutionary Biology* 13. 10.1186/1471-2148-13-208

Kardong KV. 2006. *Vertebrates: comparative anatomy, function, evolution*: McGraw-Hill Boston.

Kass RE, and Raftery AE. 1995. Bayes factors. *Journal of the American Statistical Association* 90:773-795. 10.1080/01621459.1995.10476572

Katoh K, Rozewicki J, and Yamada KD. 2019. MAFFT online service: multiple sequence alignment, interactive sequence choice and visualization. *Briefings in bioinformatics* 20:1160-1166.

Kelley D, Page K, Quiroga D, and Salazar R. 2019. *In the Footsteps of Darwin: Geoheritage, Geotourism and Conservation in the Galápagos Islands*. Cham: Springer International Publishing.

Keogh JS, Edwards DL, Fisher RN, and Harlow PS. 2008. Molecular and morphological analysis of the critically endangered Fijian iguanas reveals cryptic diversity and a complex biogeographic history. *Philosophical Transactions of the Royal Society B: Biological Sciences* 363:3413-3426.

Konishi T, Caldwell MW, Nishimura T, Sakurai K, and Tanoue K. 2015. A new halisaurine mosasaur (Squamata: Halisaurinae) from Japan: the first record in the western Pacific realm and the first documented insights into binocular vision in mosasaurs. *Journal of Systematic Palaeontology*:1-31. 10.1080/14772019.2015.1113447

Konishi T, Lindgren J, Caldwell MW, and Chiappe L. 2012. *Platecarpus tympaniticus* (Squamata, Mosasauridae): osteology of an exceptionally preserved specimen and its insights into the acquisition of a streamlined body shape in mosasaurs. *Journal of Vertebrate Paleontology* 32:1313-1327. 10.1080/02724634.2012.699811

Kornhuber A. 1901. Opetiosaurus Bucchichi. Eine neue fossile Eidechse aus der unteren Kreide von Lesina in Dalmatien. *Abhandlungen der kk (kaiserlich-königlichen) geologischen Reichsanstalt* 17:1-24.

Kuraku S, Zmasek CM, Nishimura O, and Katoh K. 2013. aLeaves facilitates on-demand exploration of metazoan gene family trees on MAFFT sequence alignment server with enhanced interactivity. *Nucleic Acids Research* 41:W22-W28.

Lambert AE. 1938. Introduction and Guide to the Study of Histology.

Lanfear R, Calcott B, Ho SY, and Guindon S. 2012. PartitionFinder: combined selection of partitioning schemes and substitution models for phylogenetic analyses. *Molecular Biology and Evolution* 29:1695-1701.

Lanfear R, Frandsen PB, Wright AM, Senfeld T, and Calcott B. 2016. PartitionFinder 2: new methods for selecting partitioned models of evolution for molecular and morphological phylogenetic analyses. *Molecular Biology and Evolution* 34:772-773.

Laurie WA. 1989. Effects of the 1982-83 El Niño-Southern Oscillation event on marine iguana (Amblyrhynchus cristatus Bell, 1825) populations on Galápagos. *Elsevier Oceanography Series*. New York: Elsevier, 361-380.

Lawrence E. 1998. Iguanas ride the waves. *Nature*. 10.1038/news981015-3

LeBlanc AR, Lamoureux DO, and Caldwell MW. 2017. Mosasaurs and snakes have a periodontal ligament: timing and extent of calcification, not tissue complexity, determines tooth attachment mode in reptiles. *Journal of Anatomy* 231:869-885.

LeBlanc ARH, Apesteguía S, Larsson HCE, and Caldwell MW. 2020a. Unique Tooth Morphology and Prismatic Enamel in Late Cretaceous Sphenodontians from Argentina. *Current Biology*. 10.1016/j.cub.2020.02.071

LeBlanc ARH, Paparella I, Lamoureux DO, Doschak MR, and Caldwell MW. 2020b. Tooth attachment and pleurodont implantation in lizards: Histology, development, and evolution. *Journal of Anatomy*:1-23. https://doi.org/10.1111/joa.13371

Lee MS, Palci A, Jones ME, Caldwell MW, Holmes JD, and Reisz RR. 2016. Aquatic adaptations in the four limbs of the snake-like reptile *Tetrapodophis* from the Lower Cretaceous of Brazil. *Cretaceous Research* 66:194-199.

Lee MS, and Scanlon JD. 2002a. The Cretaceous marine squamate *Mesoleptos* and the origin of snakes. *Bulletin of the Natural History Museum: Zoology* 68:131-142.

Lee MSY. 2005. Squamate phylogeny, taxon sampling, and data congruence. *Organisms Diversity & Evolution* 5:25-45. 10.1016/j.ode.2004.05.003

Lee MSY, and Caldwell MW. 2000. *Adriosaurus* and the affinities of mosasaurs, dolichosaurs and snakes. *Journal of Paleontology* 74:915-937. 10.1666/0022-3360(2000)074<0915:aataom>2.0.co;2

Lee MSY, and Scanlon JD. 2002b. Snake phylogeny based on osteology, soft anatomy and ecology. *Biological Reviews of the Cambridge Philosophical Society* 77:333-401. 10.1017/s1464793102005924

Levangie P, and Norkin C. 2005. *Joint structure and function: a comprehensive analysis*. Philadelphia: F.A. Davis Company.

Lewis PO. 2001. A Likelihood Approach to Estimating Phylogeny from Discrete Morphological Character Data. *Systematic Biology* 50:913-925. 10.1080/106351501753462876

Li P-P, Gao K-Q, Hou L-H, and Xu X. 2007. A gliding lizard from the Early Cretaceous of China. *Proceedings of the National Academy of Sciences* 104:5507-5509.

Lindgren J, Everhart MJ, and Caldwell MW. 2011. Three-dimensionally preserved integument reveals hydrodynamic adaptations in the extinct marine lizard *Ectenosaurus* (Reptilia, Mosasauridae). *PLoS ONE* 6:e27343.

Linnaeus C. 1758. *Systema naturae per regna tria naturae*. Stockholm (Sweden): Impensis Direct. Laurentii Salvii.

MacArthur RH, and Wilson EO. 1967. *The theory of Island Biogeography/by Roberth Mac Arthur and Edwar O. Wilson*. Princeton, NJ: Princeton University Press.

Macey JR, Larson A, Ananjeva NB, and Papenfuss TJ. 1997. Evolutionary shifts in three major structural features of the mitochondrial genome among iguanian lizards. *Journal of Molecular Evolution* 44:660-674. https://doi.org/10.1007/PL00006190

Macey JR, Schulte JA, Larson A, Ananjeva NB, Wang Y, Pethiyagoda R, Rastegar-Pouyani N, and Papenfuss TJ. 2000. Evaluating Trans-Tethys Migration: An Example Using Acrodont Lizard Phylogenetics. *Systematic Biology* 49:233-256. 10.1093/sysbio/49.2.233

Macey RJ, Schulte JA, Strasburg JL, Brisson JA, Larson A, Ananjeva NB, Wang Y, Parham JF, and Papenfuss TJ. 2006. Assembly of the eastern North American herpetofauna: new evidence from lizards and frogs. *Biology Letters* 2:388-392.

Mackie RI, Rycyk M, Ruemmler RL, Aminov RI, and Wikelski M. 2004. Biochemical and microbiological evidence for fermentative digestion in free-living land iguanas (*Conolophus pallidus*) and marine iguanas (*Amblyrhynchus cristatus*) on the Galápagos archipelago. *Physiological and Biochemical Zoology* 77:127-138.

MacLeod A, Rodríguez A, Vences M, Orozco-terWengel P, García C, Trillmich F, Gentile G, Caccone A, Quezada G, and Steinfartz S. 2015. Hybridization masks speciation in the evolutionary history of the Galápagos marine iguana. *Proceedings of the Royal Society B* 282:20150425.

Maddison WP, and Maddison DR. 2018. Mesquite: A Modular System for Evolutionary Analysis. Version 3.6. *http://wwwmesquiteprojectorg*.

Maisano JA. 2002. Terminal fusions of skeletal elements as indicators of maturity in squamates. *Journal of Vertebrate Paleontology* 22:268-275. 10.1671/0272-4634(2002)022[0268:tfosea]2.0.co;2

Maisano JA, Laduc TJ, Bell CJ, and Barber D. 2019. The Cephalic Osteoderms of *Varanus komodoensis* as Revealed by High-Resolution X-Ray Computed Tomography. *Anat Rec (Hoboken)* 302:1675-1680. 10.1002/ar.24197

Makádi L, Caldwell MW, and Ősi A. 2012. The first freshwater mosasauroid (Upper Cretaceous, Hungary) and a new clade of basal mosasauroids. *PLoS ONE* 7:e51781.

Malashichev YB. 2001. Sacrum and pelvic girdle development in Lacertidae. *Russian Journal of Herpetology* 8:1-16.

Manley GA. 1972. A review of some current concepts of the functional evolution of the ear in terrestrial vertebrates. *Evolution* 26:608-621.

Martin RB, Burr DB, and Sharkey NA. 1998a. *Skeletal tissue mechanics*. New York: Springer.
Martin RB, Burr DB, Sharkey NA, and Fyhrie DP. 1998b. Synovial Joint Mechanics. *Skeletal Tissue Mechanics*. New York: Springer, 227-273.
Maxwell EE, Caldwell MW, Lamoureux DO, and Budney LA. 2011. Histology of tooth attachment tissues and plicidentine in *Varanus* (Reptilia: Squamata), and a discussion of the evolution of amniote tooth attachment. *Journal of Morphology* 272:1170-1181. 10.1002/jmor.10972
McDowell SB, and Bogert CM. 1954. The systematic position of *Lanthanotus* and the affinities of the anguinomorphan lizards. *Bulletin of the American Museum of Natural History* 105.
Medizza F, and Sorbini L. 1980. Il giacimento del Salento (Lecce). In: Verona MdSNd, editor. I vertebrati fossili italiani. Verona: Museo di Storia Naturale di Verona. p 131-134.
Merlen G. 2014. Plate tectonics, evolution, and the survival of species. *The Galápagos: a natural laboratory for the Earth sciences*:119-144.
Miller MA, Pfeiffer W, and Schwartz T. 2012. The CIPRES science gateway: enabling high-impact science for phylogenetics researchers with limited resources. Proceedings of the 1st Conference of the Extreme Science and Engineering Discovery Environment: Bridging from the extreme to the campus and beyond. p 1-8.
Miller MA, Schwartz T, Pickett BE, He S, Klem EB, Scheuermann RH, Passarotti M, Kaufman S, and O'Leary MA. 2015. A RESTful API for access to phylogenetic tools via the CIPRES science gateway. *Evolutionary Bioinformatics* 11:EBO. S21501.
Miralles A, Glaw F, Ratsoavina FM, and Vences M. 2015. A likely microendemic new species of terrestrial iguana, genus *Chalarodon*, from Madagascar. *Zootaxa* 3946:201-220.
Miralles A, Macleod A, Rodríguez A, Ibáñez A, Jiménez-Uzcategui G, Quezada G, Vences M, and Steinfartz S. 2017. Shedding light on the Imps of Darkness: an integrative taxonomic revision of the Galápagos marine iguanas (genus *Amblyrhynchus*). *Zoological Journal of the Linnean Society*.
Morgan WJ. 1971. Convection plumes in the lower mantle. *Nature* 230:42-43.
Moritz S, and Schilling N. 2013. Fiber-type composition in the perivertebral musculature of lizards: Implications for the evolution of the diapsid trunk muscles. *Journal of Morphology* 274:294-306.
Motani R. 2009. The evolution of marine reptiles. *Evolution: Education and Outreach* 2:224-235.
Motani R, Minoura N, and Ando T. 1998. Ichthyosaurian relationships illuminated by new primitive skeletons from Japan. *Nature* 393:255 - 257.
Motani R, and Vermeij GJ. 2021. Ecophysiological steps of marine adaptation in extant and extinct non-avian tetrapods. *Biological Reviews of the Cambridge Philosophical Society*. 10.1111/brv.12724
Motani R, You H, and McGowan C. 1996. Eel-like swimming in the earliest ichthyosaurs. *Nature* 382:347 - 348.

Myers P, Espinosa R, Parr C, Jones T, Hammond G, and Dewey T. 2021. The Animal Diversity Web (online). Accessed at https://animaldiversity.org.

Nagy KA, and Shoemaker VH. 1984. Field Energetics and Food Consumption of the Galápagos Marine Iguana, *Amblyrhynchus cristatus*. *Physiological Zoology* 57:281-290.

Nava WR, and Martinelli AG. 2011. A new squamate lizard from the Upper Cretaceous Adamantina Formation (Bauru Group), São Paulo State, Brazil. *Anais da Academia Brasileira de Ciencias* 83:291-299.

Neall VE, and Trewick SA. 2008. The age and origin of the Pacific islands: a geological overview. *Philosophical Transactions of the Royal Society B: Biological Sciences* 363:3293-3308.

Noonan BP, and Sites Jr JW. 2009. Tracing the origins of iguanid lizards and boine snakes of the Pacific. *The American Naturalist* 175:61-72.

Nopcsa FB. 1903. Über Die Varanusartigen Lacerten Istriens. *Beitr z Pal & Geol OestrUng* 15:31-42.

Norell MA, and de Queiroz K. 1991. The earliest iguanine lizard (Reptilia: Squamata) and its bearing on iguanine phylogeny. *American Museum Novitates* 2997.

O'Reilly JE, and Donoghue PC. 2016. Tips and nodes are complementary not competing approaches to the calibration of molecular clocks. *Biology Letters* 12:20150975.

O'Reilly JE, Puttick MN, Parry L, Tanner AR, Tarver JE, Fleming J, Pisani D, and Donoghue PC. 2016. Bayesian methods outperform parsimony but at the expense of precision in the estimation of phylogeny from discrete morphological data. *Biology Letters* 12:20160081.

O'Reilly JE, Dos Reis M, and Donoghue PC. 2015. Dating tips for divergence-time estimation. *Trends in Genetics* 31:637-650.

Oelrich TM. 1956. The anatomy of the head of *Ctenosaura pectinata* (Iguanidae). *Miscellaneous Publications - Museum of Zoology, University of Michigan* 94:1-172.

Oldham JC, and Smith HM. 1975. *Laboratory anatomy of the iguana*: Dubuque, Iowa: Wm. C. Brown.

Oppel M. 1811. *Die ordnungen, familien und gattungen der reptilien als prodrom einer naturgeschichte derselben*. Munich: Joseph Lindauer.

Orellana-Rovirosa F, and Richards M. 2018. Emergence/subsidence histories along the Carnegie and Cocos Ridges and their bearing upon biological speciation in the Galápagos. *Geochemistry, Geophysics, Geosystems*. doi:10.1029/2018GC007608

Owen R. 1840-1845. *Odontography, or, a treatise on the comparative anatomy of the teeth, their physiological relations, mode of developement, and microscipic structure, in the vertebrate animals*. London: Hippolyte Bailliere.

Palci A, and Caldwell MW. 2007. Vestigial forelimbs and axial elongation in a 95 million-year-old non-snake squamate. *Journal of Vertebrate Paleontology* 27:1-7.

Palci A, and Caldwell MW. 2010. Redescription of *Acteosaurus tommasinii* von Meyer, 1860, and a discussion of evolutionary trends within the clade Ophidiomorpha. *Journal of Vertebrate Paleontology* 30:94-108. 10.1080/02724630903409139

Palci A, Lee MS, and Hutchinson MN. 2016. Patterns of postnatal ontogeny of the skull and lower jaw of snakes as revealed by micro-CT scan data and three-dimensional geometric morphometrics. *Journal of Anatomy*.

Panzer S, Mc Coy MR, Hitzl W, Piombino-Mascali D, Jankauskas R, Zink AR, and Augat P. 2015. Checklist and Scoring System for the Assessment of Soft Tissue Preservation in CT Examinations of Human Mummies. *PLoS ONE* 10:e0133364. 10.1371/journal.pone.0133364

Paparella I, LeBlanc ARH, Doschak MR, and Caldwell MW. 2020. The iliosacral joint in lizards: an osteological and histological analysis. *Journal of Anatomy* 236:668-687. 10.1111/joa.13132

Paparella I, Palci A, Nicosia U, and Caldwell MW. 2018. A new fossil marine lizard with soft tissues from the Late Cretaceous of southern Italy. *Royal Society Open Science* 5:172411. 10.1098/rsos.172411

Patterson C. 1982. Morphological characters and homology. In: Joysey KA, and Friday AE, eds. *Systematics Association Special Volume: "Problems of phylogenetic reconstruction"*. London and New York: Academic Press, 21-74.

Peck S. 1996. Origin and development of an insect fauna on a remote archipelago: The Galápagos Islands, Ecuador. *Keast A, Miller SE (eds): The origin and evolution of Pacific Island biotas, New Guinea to eastern Polynesia: patterns and processes*:91-122.

Pees M, Kiefer I, Thielebein J, Oechtering G, and Krautwald-Junghanns M-E. 2009. Computed Tomography of the Lung of Healthy Snakes of the Speciespython Regius, Boa Constrictor, Python Reticulatus, Morelia Viridis, Epicrates Cenchria, Andmorelia Spilota. *Veterinary Radiology & Ultrasound* 50:487-491. 10.1111/j.1740-8261.2009.01569.x

Peyer B. 1968. *Comparative odontology*. Chicago: The University of Chicago Press.

Philippe H, Zhou Y, Brinkmann H, Rodrigue N, and Delsuc F. 2005. Heterotachy and long-branch attraction in phylogenetics. *BMC Evolutionary Biology* 5:50. 10.1186/1471-2148-5-50

Pierce SE, and Caldwell MW. 2004. Redescription and phylogenetic position of the Adriatic (Upper Cretaceous; Cenomanian) dolichosaur *Pontosaurus lesinensis* (Kornhuber, 1873). *Journal of Vertebrate Paleontology* 24:373-386.

Pierce SE, Clack JA, and Hutchinson JR. 2012. Three-dimensional limb joint mobility in the early tetrapod *Ichthyostega*. *Nature* 486:523. 10.1038/nature11124

Pregill GK, and Steadman DW. 2004. South Pacific iguanas: human impacts and a new species. *Journal of Herpetology*:15-21.

Pregill GK, and Worthy TH. 2003. A new iguanid lizard (Squamata, Iguanidae) from the late Quaternary of Fiji, Southwest Pacific. *Herpetologica* 59:57-67.

Puttick MN, O'Reilly JE, Oakley D, Tanner AR, Fleming JF, Clark J, Holloway L, Lozano-Fernandez J, Parry LA, and Tarver JE. 2017. Parsimony and maximum-likelihood phylogenetic analyses of morphology do not generally integrate uncertainty in inferring

evolutionary history: a response to Brown et al. *Proceedings of the Royal Society B: Biological Sciences* 284:20171636.

Puttick MN, O'Reilly JE, Pisani D, and Donoghue PC. 2019. Probabilistic methods outperform parsimony in the phylogenetic analysis of data simulated without a probabilistic model. *Palaeontology* 62:1-17.

Pyron RA. 2017. Novel approaches for phylogenetic inference from morphological data and total-evidence dating in squamate reptiles (lizards, snakes, and amphisbaenians). *Systematic Biology* 66:38-56.

Rage J-C, Vullo R, and Néraudeau D. 2016. The mid-Cretaceous snake Simoliophis rochebrunei Sauvage, 1880 (Squamata: Ophidia) from its type area (Charentes, southwestern France): Redescription, distribution, and palaeoecology. *Cretaceous Research* 58:234-253. 10.1016/j.cretres.2015.10.010

Rambaut A. 2007. FigTree, a graphical viewer of phylogenetic trees. *Available at http://tree.bio.ed.ac.uk/software/figtree*.

Rambaut A, and Drummond A. 2016a. LogCombiner 2.4.3. *Available at http://beast.bio.ed.ac.uk/LogCombiner*.

Rambaut A, and Drummond A. 2016b. TreeAnnotator 2.4.3. *Available at http://beast.bio.ed.ac.uk/TreeAnnotator*.

Rambaut A, Suchard M, Xie D, and Drummond A. 2014. Tracer 1.6. *Available at http://beast.bio.ed.ac.uk/Tracer*.

Rassmann K. 1997. Evolutionary age of the Galápagos iguanas predates the age of the present Galápagos Islands. *Molecular Phylogenetics and Evolution* 7:158-172.

Rassmann K, Tautz D, Trillmich F, and Gliddon C. 1997a. The microevolution of the Galápagos marine iguana *Amblyrhynchus cristatus* assessed by nuclear and mitochondrial genetic analyses. *Molecular Ecology* 6:437-452.

Rassmann K, Trillmich F, and Tautz D. 1997b. Hybridization between the Galápagos land and marine iguana (*Conolophus subcristatus* and *Amblyrhynchus cristatus*) on Plaza Sur. *Journal of Zoology* 242:729-739.

Reeder TW, Townsend TM, Mulcahy DG, Noonan BP, Wood PL, Jr., Sites JW, Jr., and Wiens JJ. 2015. Integrated Analyses Resolve Conflicts over Squamate Reptile Phylogeny and Reveal Unexpected Placements for Fossil Taxa. *PLoS ONE* 10:e0118199. 10.1371/journal.pone.0118199

Reynoso V-H. 1998. *Huehuecuetzpalli mixtecus gen. et sp. nov: a basal squamate (Reptilia) from the Early Cretaceous of Tepexi de Rodríguez, Central México*.

Ricqlès Ad, and Buffrénil Vd. 2001. Bone histology, heterochronies and the return of tetrapods to life in water: where are we? *Secondary adaptation of tetrapods to life in water*:289-310.

Rieppel O. 1989. *Helveticosaurus zollingeri* Peyer (Reptilia, Diapsida) skeletal paedomorphosis, functional anatomy and systematic affinities. *Palaeontographica Abteilung A*:123-152.

Rieppel O, Li C, and Fraser NC. 2008. The skeletal anatomy of the Triassic protorosaur *Dinocephalosaurus orientalis* Li, from the Middle Triassic of Guizhou Province, southern China. *Journal of Vertebrate Paleontology* 28:95-110.

Rieppel O, Walker A, and Odhiambo I. 1992. A preliminary report on a fossil chamaeleonine (Reptilia: Chamaeleoninae) skull from the Miocene of Kenya. *Journal of Herpetology* 26:77-80.

Rieppel O, and Zaher H. 2000. The braincases of mosasaurs and *Varanus*, and the relationships of snakes. *Zoological Journal of the Linnean Society* 129:489-514.

Ritter D. 1996. Axial muscle function during lizard locomotion. *Journal of Experimental Biology* 199:2499-2510.

Romer AS. 1956. *Osteology of the Reptiles*. Chicago: University of Chicago Press.

Ronquist F, Huelsenbeck J, and Teslenko M. 2011. Draft MrBayes version 3.2 manual: tutorials and model summaries. *Distributed with the software from http://brahms biology rochester edu/software html*.

Ronquist F, and Huelsenbeck JP. 2003. MrBayes 3: Bayesian phylogenetic inference under mixed models. *Bioinformatics* 19:1572-1574.

Ronquist F, Klopfstein S, Vilhelmsen L, Schulmeister S, Murray DL, and Rasnitsyn AP. 2012a. A total-evidence approach to dating with fossils, applied to the early radiation of the Hymenoptera. *Systematic Biology* 61:973-999.

Ronquist F, Teslenko M, van der Mark P, Ayres DL, Darling A, Hohna S, Larget B, Liu L, Suchard MA, and Huelsenbeck JP. 2012b. MrBayes 3.2: efficient Bayesian phylogenetic inference and model choice across a large model space. *Systematic Biology* 61:539-542. 10.1093/sysbio/sys029

Ronquist F, Teslenko M, Van Der Mark P, Ayres DL, Darling A, Höhna S, Larget B, Liu L, Suchard MA, and Huelsenbeck JP. 2012c. MrBayes 3.2: efficient Bayesian phylogenetic inference and model choice across a large model space. *Systematic Biology* 61:539-542.

Rupert M, Lee M, Manchikanti L, Datta S, and Cohen S. 2009. Evaluation of sacroiliac joint interventions: A systematic appraisal of the literature. *Pain physician* 12:399-418.

Russell DA. 1967. *Systematics and morphology of American mosasaurs (Reptilia, Sauria)*: Peabody Museum of Natural History, Yale University.

Salle O. 1880. Untersuchungen über die Lymphapophysen von Schlangen und schlangenähnlichen Sauriern. Georg-August-Universität zu Göttingen.

Sankhyan AR, and Čerňanský A. 2016. A first possible chameleon from the late Miocene of India (the hominoid site of Haritalyangar): a tentative evidence for an Asian dispersal of chameleons. *The Science of Nature* 103:94.

Saunders JC, Duncan RK, Doan DE, and Werner YL. 2000. The Middle Ear of Reptiles and Birds. In: Dooling RJ, Fay RR, and Popper AN, eds. *Comparative Hearing: Birds and Reptiles*. New York, NY: Springer New York, 13-69.

Scanlon JD. 2006. Skull of the large non-macrostomatan snake *Yurlunggur* from the Australian Oligo-Miocene. *Nature* 439:839-842. 10.1038/nature04137

Scanlon JD, and Hocknull SA. 2007. A dolichosaurid lizard from the latest Albian (mid-Cretaceous) Winton Formation, Queensland, Australia. Second Mosasaur Meeting (May 3-6, 2007). Hays, Kansas, USA: Transactions of the Kansas Academy of Science, Fort Hays Studies Special Issue, Proceedings of the Second Mosasaur Meeting. p 131-136.

Scarpetta SG. 2020. Combined-evidence analyses of ultraconserved elements and morphological data: an empirical example in iguanian lizards. *Biology Letters* 16:20200356. doi:10.1098/rsbl.2020.0356

Schlüter M, Steuber T, and Parente M. 2008. Chronostratigraphy of Campanian–Maastrichtian platform carbonates and rudist associations of Salento (Apulia, Italy). *Cretaceous Research* 29:100-114.

Schmidt-Nielsen K, and Fange R. 1958. Salt glands in marine reptiles. *Nature* 182:783-785.

Schulte JA, Valladares JP, and Larson A. 2003. Phylogenetic relationships within Iguanidae inferred using molecular and morphological data and a phylogenetic taxonomy of iguanian lizards. *Herpetologica* 59:399-419.

Scotese CR. 2001. *Atlas of earth history*: PALEOMAP project.

Searle R, and Francheteau J. 1986. Morphology and tectonics of the Galápagos triple junction. *Marine geophysical researches* 8:95-129.

Sereno PC. 2007. Logical basis for morphological characters in phylogenetics. *Cladistics* 23:565-587. 10.1111/j.1096-0031.2007.00161.x

Shields O. 1979. Evidence for initial opening of the Pacific Ocean in the Jurassic. *Palaeogeography, Palaeoclimatology, Palaeoecology* 26:181-220.

Shoemaker VH, and Nagy KA. 1984. Osmoregulation in the Galápagos marine iguana, *Amblyrhynchus cristatus*. *Physiological Zoology* 57:291-300.

Simões TR, Caldwell MW, Palci A, and Nydam RL. 2016. Giant taxon-character matrices: quality of character constructions remains critical regardless of size. *Cladistics*.

Simões TR, Caldwell MW, Tałanda M, Bernardi M, Palci A, Vernygora O, Bernardini F, Mancini L, and Nydam RL. 2018. The origin of squamates revealed by a Middle Triassic lizard from the Italian Alps. *Nature* 557:706-709. 10.1038/s41586-018-0093-3

Simões TR, Caldwell MW, Weinschütz LC, Wilner E, and Kellner AWA. 2017a. Mesozoic Lizards from Brazil and Their Role in Early Squamate Evolution in South America. *Journal of Herpetology*:307-315. 10.1670/16-007

Simões TR, and Pyron RA. 2021. The squamate tree of life. *Bulletin of the Museum of Comparative Zoology* 163:47-95, 49.

Simões TR, Vernygora O, Caldwell MW, and Pierce SE. 2020. Megaevolutionary dynamics in reptiles and the role of adaptive radiations in evolutionary innovation. *bioRxiv*:2020.2004.2022.055061. 10.1101/2020.04.22.055061

Simões TR, Vernygora O, Paparella I, Jimenez-Huidobro P, and Caldwell MW. 2017b. Mosasauroid phylogeny under multiple phylogenetic methods provides new insights on the evolution of aquatic adaptations in the group. *PLoS ONE* 12:e0176773. 10.1371/journal.pone.0176773

Simões TR, Wilner E, Caldwell MW, Weinschütz LC, and Kellner AWA. 2015. A stem acrodontan lizard in the Cretaceous of Brazil revises early lizard evolution in Gondwana. *Nature Communications* 6:1-8. DOI: 10.1038/ncomms9149

Sites JW, Reeder TW, and Wiens JJ. 2011. Phylogenetic Insights on Evolutionary Novelties in Lizards and Snakes: Sex, Birth, Bodies, Niches, and Venom. *Annual Review of Ecology, Evolution, and Systematics* 42:227-244. 10.1146/annurev-ecolsys-102710-145051

Smith K. 2011a. On the phylogenetic affinity of the extinct acrodontan lizard *Tinosaurus*. *Tropical vertebrates in a changing world*:9-27.

Smith KT. 2009. Eocene lizards of the clade *Geiseltaliellus* from Messel and Geiseltal, Germany, and the early radiation of Iguanidae (Reptilia: Squamata). *Bulletin of the Peabody Museum of Natural History* 50:219-306.

Smith KT. 2011b. Acrodont iguanians (Squamata) from the middle Eocene of the Huadian Basin of Jilin Province, China, with a critique of the taxon "Tinosaurus". *Vertebrata PalAsiatica* 49:69-84.

Snow FH. 1878. On the dermal covering of a mosasauroid reptile. *Transactions of the Kansas Academy of Science (1872-1880)* 6:54-58.

Snyder RC. 1954. The anatomy and function of the pelvic girdle and hindlimb in lizard locomotion. *American Journal of Anatomy* 95:1-45. 10.1002/aja.1000950102

Snyder RC. 1962. Adaptations for Bipedal Locomotion of Lizards. *American Zoologist* 2:191-203. 10.2307/3881209

Sood MS. 1948. The anatomy of the vertebral column in serpentes. Proceedings of the Indian Academy of Sciences-Section B. New Delhi: Springer India. p 1-26.

Sorbini L. 1978. New fish bed localities of latest Campanian age. *Bollettino del Museo Civico di Storia Naturale di Verona* V:607-608.

Sorbini L. 1981. The Cretaceous fishes of Nardò. I. Order Gasterosteiformes (Pisces). *Bollettino del Museo Civico di Storia Naturale di Verona* VIII:1-27.

Street HP, and Caldwell MW. 2017. Rediagnosis and redescription of *Mosasaurus hoffmannii* (Squamata: Mosasauridae) and an assessment of species assigned to the genus *Mosasaurus*. *Geological Magazine* 154:521-557.

Strong EE, and Lipscomb D. 1999. Character Coding and Inapplicable Data. *Cladistics* 15:363-371. 10.1111/j.1096-0031.1999.tb00272.x

Theobald W. 1868. Catalogue of the Reptiles of British Birma, embracing the Provinces of Pegu, Martaban, and Tenasserim; with descriptions of new or little-known species. *Zoological Journal of the Linnean Society* 10:4-67.

Tolley KA, Townsend TM, and Vences M. 2013. Large-scale phylogeny of chameleons suggests African origins and Eocene diversification. *Proceedings of the Royal Society of London B: Biological Sciences* 280:20130184.

Tomes CS. 1874. Studies upon the attachment of teeth. *Transactions of the Odontological Society of Great Britain* 7:41-58.

Townsend TM, Mulcahy DG, Noonan BP, Sites JW, Kuczynski CA, Wiens JJ, and Reeder TW. 2011. Phylogeny of iguanian lizards inferred from 29 nuclear loci, and a comparison of concatenated and species-tree approaches for an ancient, rapid radiation. *Molecular Phylogenetics and Evolution* 61:363-380.

Trillmich KGK, and Trillmich F. 1986. Foraging strategies of the marine iguana, *Amblyrhynchus cristatus*. *Behavioral Ecology and Sociobiology* 18:259-266. 10.1007/bf00300002

Trinajstic K, Marshall C, Long J, and Bifield K. 2007. Exceptional preservation of nerve and muscle tissues in Late Devonian placoderm fish and their evolutionary implications. *Biology Letters* 3:197-200.

Tsai HP, and Holliday CM. 2015. Articular soft tissue anatomy of the archosaur hip joint: structural homology and functional implications. *Journal of Morphology* 276:601-630.

Tsai HP, Middleton KM, Hutchinson JR, and Holliday CM. 2018. Hip joint articular soft tissues of non-dinosaurian Dinosauromorpha and early Dinosauria: evolutionary and biomechanical implications for Saurischia. *Journal of Vertebrate Paleontology*:e1427593. 10.1080/02724634.2017.1427593

Uetz P, Freed P, and Hošek J. 2020. The Reptile Database, http://www.reptile-database.org. 17 December 2020 ed.

Vences M, Glaw F, Wollenberg K, and Münchenberg T. 2008. Molecular phylogeny and geographic variation of Malagasy iguanas (*Oplurus* and *Chalarodon*). *Amphibia-Reptilia* 29:319-327.

Vidal N, and Hedges BS. 2005. The phylogeny of squamate reptiles (lizards, snakes, and amphisbaenians) inferred from nine nuclear protein-coding genes. *Comptes Rendus Biologies* 328:1000-1008. 10.1016/j.crvi.2005.10.001

Vidal N, and Hedges SB. 2009. The molecular evolutionary tree of lizards, snakes, and amphisbaenians. *Comptes Rendus Biologies* 332:129-139. 10.1016/j.crvi.2008.07.010

Vleeming A, Schuenke MD, Masi AT, Carreiro JE, Danneels L, and Willard FH. 2012. The sacroiliac joint: an overview of its anatomy, function and potential clinical implications. *Journal of Anatomy* 221:537-567. doi:10.1111/j.1469-7580.2012.01564.x

Werner R, Hoernle K, van den Bogaard P, Ranero C, von Huene R, and Korich D. 1999. Drowned 14-my-old Galápagos archipelago off the coast of Costa Rica: implications for tectonic and evolutionary models. *Geology* 27:499-502.

Wiegmann AFA. 1828. *Ctenosaura*. In: Oken L, ed. *Isis von Oken*. Jena, Germany: Expedition der Isis, 371-377.

Wiens JJ. 2005. Can incomplete taxa rescue phylogenetic analyses from long-branch attraction? *Systematic Biology* 54:731-742. 10.1080/10635150500234583

Wiens JJ, and Hollingsworth BD. 2000. War of the iguanas: conflicting molecular and morphological phylogenies and long-branch attraction in iguanid lizards. *Systematic Biology* 49:143-159.

Wiens JJ, Hutter CR, Mulcahy DG, Noonan BP, Townsend TM, Sites JW, and Reeder TW. 2012. Resolving the phylogeny of lizards and snakes (Squamata) with extensive sampling of genes and species. *Biology Letters* 8:1043-1046. 10.1098/rsbl.2012.0703

Wiens JJ, Kuczynski CA, Arif S, and Reeder TW. 2010. Phylogenetic relationships of phrynosomatid lizards based on nuclear and mitochondrial data, and a revised phylogeny for *Sceloporus*. *Molecular Phylogenetics and Evolution* 54:150-161. https://doi.org/10.1016/j.ympev.2009.09.008

Wikelski M, and Trillmich F. 1994. Foraging strategies of the Galápagos marine iguana (*Amblyrhynchus cristatus*): adapting behavioral rules to ontogenetic size change. *Behaviour* 128:255-279.

Wikelski M, and Wrege PH. 2000. Niche expansion, body size, and survival in Galápagos marine iguanas. *Oecologia* 124:107-115. 10.1007/s004420050030

Wilby PR, and Briggs DE. 1997. Taxonomic trends in the resolution of detail preserved in fossil phosphatized soft tissues. *Geobios* 30:493-502.

Wilby PR, Briggs DE, Bernier P, and Gaillard C. 1996. Role of microbial mats in the fossilization of soft tissues. *Geology* 24:787-790.

Wilken AT, Middleton KM, Sellers KC, Cost IN, and Holliday CM. 2019. The roles of joint tissues and jaw muscles in palatal biomechanics of the savannah monitor (*Varanus exanthematicus*) and their significance for cranial kinesis. *The Journal of Experimental Biology* 222:jeb201459. 10.1242/jeb.201459

Wilson P, Parry LA, Vinther J, and Edgecombe GD. 2016. Unveiling biases in soft-tissue phosphatization: extensive preservation of musculature in the Cretaceous (Cenomanian) polychaete Rollinschaeta myoplena (Annelida: Amphinomidae). *Palaeontology* 59:463-479.

Winchester L, and Bellairs AdA. 1977. Aspects of vertebral development in lizards and snakes. *Journal of Zoology* 181:495-525.

Wolff H-D. 1990. Comments on the evolution of the sacroiliac joint. In: Paterson JK, and Burn L, eds. *Back Pain: An International Review*. Dordrecht: Springer Netherlands, 175-185.

Woltering JM. 2012. From lizard to snake; behind the evolution of an extreme body plan. *Current Genomics* 13:289-299.

Wright AM, and Hillis DM. 2014. Bayesian Analysis Using a Simple Likelihood Model Outperforms Parsimony for Estimation of Phylogeny from Discrete Morphological Data. *PLoS ONE* 9:e109210. 10.1371/journal.pone.0109210

Wyles J, and Sarich V. 1983. Are the Galápagos iguanas older than the Galápagos? Molecular evolution and colonization models for the archipelago. *Patterns of Evolution in Galápagos Organisms (eds RI Bowman, M Berson & AE Levinton)*:177-185.

Yang Z, and Rannala B. 2012. Molecular phylogenetics: principles and practice. *Nature Reviews Genetics* 13:303-314.

Zaaf A, Herrel A, Aerts P, and De Vree F. 1999. Morphology and morphometrics of the appendicular musculature in geckoes with different locomotor habits (Lepidosauria). *Zoomorphology* 119:9-22.

Zaher H, and Rieppel O. 1999. Tooth implantation and replacement in squamates, with special reference to mosasaur lizards and snakes. *American Museum Novitates* 3271:1.

Zahradnicek O, Buchtova M, Dosedelova H, and Tucker A. 2014. The development of complex tooth shape in reptiles. *Frontiers in Physiology* 5. 10.3389/fphys.2014.00074

Zheng Y, and Wiens JJ. 2016. Combining phylogenomic and supermatrix approaches, and a time-calibrated phylogeny for squamate reptiles (lizards and snakes) based on 52 genes and 4162 species. *Molecular Phylogenetics and Evolution* 94:537-547. 10.1016/j.ympev.2015.10.009